HETEROBIMETALLIC POLYPHOSPHIDO COMPLEXES AS USEFUL SYNTHONS FOR THE ACTIVATION AND FUNCTIONALIZATION OF WHITE PHOSPHORUS

vorgelegt von

CHRISTOPH GERMAN PETER ZIEGLER

aus Tirschenreuth

Regensburg 2021

Der experimentelle Teil der vorliegenden Arbeit wurde in der Zeit zwischen November 2017 und Februar 2021 unter Anleitung von Prof. Dr. Robert Wolf am Institut für Anorganische Chemie der Universität Regensburg angefertigt.

Prologue

This thesis reports on the synthesis and characterization of novel heterodinuclear polyphosphido complexes and in particular their application in the functionalisation of white phosphorus (P_4). *Chapter 1* defines heterobimetallic also termed heterodinuclear activation and functionalization of P_4 and gives an overview of the current state of this research field. *Chapter 2* addresses the synthesis of cobalt-gallium heterobimetallic tetraphosphido complexes and represents a rare example of their subsequent functionalization resulting in novel organo-substituted pentaphosphido complexes. The synthesis and characterization of iron-gallium and cobalt-gallium tetraphosphido complexes featuring reduced P_4 units and labile ligands is described in *chapter 3*. In c*hapter 4* the benefits of heterodinuclear P_4 activation were further explored in the synthesis of single source precursors for phosphorus-base materials and the unusual $Ni_2Si_2P_8$ cluster was synthesized under mild conditions. *Chapter 5* deals with the targeted synthesis of new heterodinuclear inorganic sandwich complexes, which have proven to be suitable precursors for the construction of polyphosphido complexes such as a "carbon-free" homoleptic bis(tetraphosphacyclobutadiene) cobaltate. The synthetic mythology developed and presented in this chapter might pave the way to a variety of novel polyphosphorus compounds. The final *chapter 6* summarizes the results of this thesis and gives a brief outlook for future projects.

Prolog

Diese Dissertation behandelt die Synthese und Charakterisierung von neuartigen, heterodinuklearen Polyphosphidokomplexen und insbesondere deren Anwendung in der Funktionalisierung von weißem Phosphor (P_4). *Kapitel 1* definiert das Konzept der heterobimetallischen oder auch heterodinuklearen Aktivierung und Funktionalisierung von P_4 und setzt sich mit dem aktuellen Stand der Forschung auf diesem Gebiet auseinander. *Kapitel 2* beschreibt die Synthese von Cobalt-Gallium heterobimetallischen tetraphosphido Komplexen und zeigt ein seltenes Beispiel für die anschließende Funktionalisierung dieser Verbindungen zu neuartigen, organo-substituierten pentaphosphiod Komplexen. *Kapitel 3* beschreibt die Synthese und Charakterisierung von Eisen-Gallium und Cobalt-Gallium Tetraphosphidokomplexen mit hochreduzierten P_4-Einheiten und labilen Anthracenliganden. Der Nutzen der heterobinuklearen Aktivierung von weißem Phosphor für die gezielte Synthese von Vorläuferverbindungen für phosphorhaltige Grundmaterialien wird in *Kapitel 4* diskutiert. Dabei wurde ein ungewöhnlicher $Ni_2Si_2P_8$ Cluster unter milden Bedingungen hergestellt und charakterisiert. Das *fünfte Kapitel* befasst sich mit der Synthese neuer heterodinuklearer anorganischer Sandwichkomplexe, welche sich als hervorragende Ausgangsverbindungen für den Aufbau von polyphosphido Komplexen herausgestellt haben. So konnte beispielsweise ein Komplex von Cobalt mit vollständig aus Phosphoratomen aufgebauten Tetraphosphaycyclobutadienliganden erstmals nachgewiesen werden. Das letzte *Kapitel 6* fasst die Ergebnisse dieser Arbeit zusammen und gibt einen kurzen Ausblick.

Table of Contents

Chapter 1   Heterobimetallic Activation and Functionalization of White Phosphorus

1.1   Introduction

Phosphorus, element 15 in the periodic table, plays a fundamental role in modern human society as one of the six most important chemical elements necessary for any living organism on earth.[1],[2],[3],[4],[5] The elemental form was discovered in 1669 by the German alchemist Hennig Brandt who first obtained phosphorus by heating human urine.[1],[4] It then took over 150 years until phosphorus was realized as a valuable plant nutrient.[1],[6] Since then, the agriculture and food industries concentrate on phosphorus containing fertilizers to ensure the global food supply for the continuously expanding human population.[1],[6] Today, modern society relies on (organo)phosphorus compounds such as fertilizers, insecticides, herbicides, nutritional supplements and additives, flame retardants, battery electrolytes, and pharmaceuticals.[3],[7] For the vast majority of these synthetic compounds chemical industry depends on white phosphorus (P_4) − the most reactive allotrope.[2],[3],[5],[7] It is synthesized by the reduction of mineral apatite $Ca_5(PO_4)_3(OH, F, Cl)$ with coke in presence of quartz sand (SiO_2; for $CaSiO_3$ slag formation) in an electric arc furnace at 1500−1600 °C (Scheme 1a).[1],[2],[3]
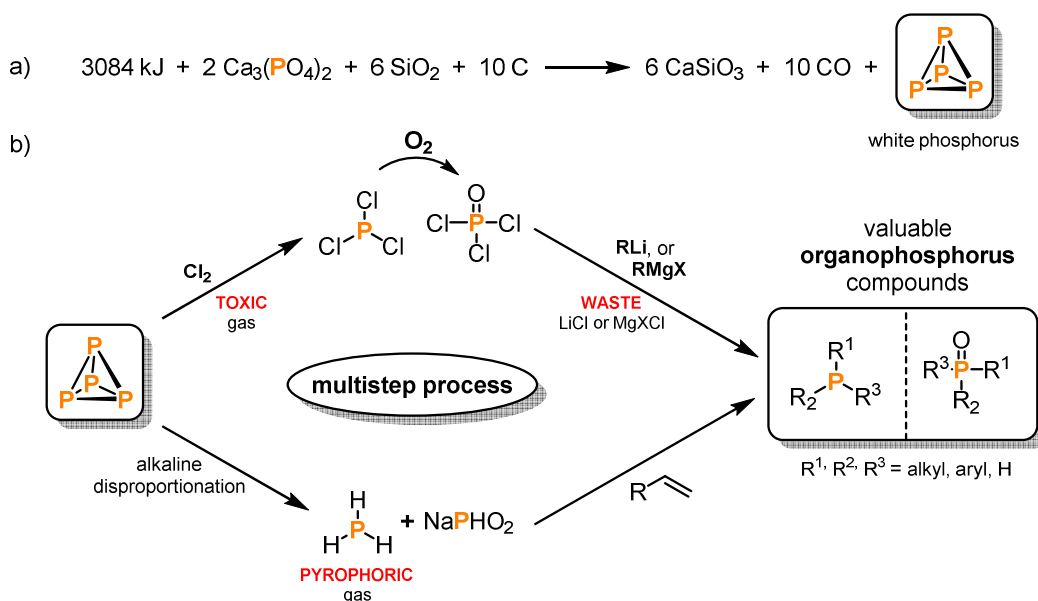
Scheme 1. a) production of white phosphorus (P_4) from calcium phosphate part of apatite minerals. b) schematic representation of the state-of-the-art multistep synthesis of organophosphorus compounds.

Most of the relevant organophosphorus compounds are then synthesized starting from P_4 in a multistep process.[3],[8],[9] This process is based on the initial halogenation of P_4 with Cl_2 gas, forming intermediates such as PCl_3, PCl_5, and $POCl_3$. In the subsequent step, these corrosive key derivatives are functionalized to the valuable organophosphorus compounds *via* salt elimination reactions with suitable Grignard or organolithium reagents (Scheme 1b).[2],[3],[8]

1

It is a current subject of academia and industry to improve or even replace this unsustainable and environmentally harmful process.[5] To achieve such a goal, one of the strategies has been to study the activation of white phosphorus with main group[9],[10] and transition metal elements.[8] Over decades of research, a plethora of unique and impressive structural motifs have been reported. From an academic point of view, these phosphorus compounds provide fundamental insights into the reactivity, structure, and bonding of phosphorus and (metal)polyphosphides.[5],[11] Even though a multitude of different approaches for the synthesis of polyphosphorus compounds are known the development of new protocols for the activation and transformation of P_4 is still an important subject in phosphorus chemistry.[3],[5],[8],[9] Nevertheless, the heterobimetallic activation of white phosphorus remains overlooked although it has the potential to form novel metal-phosphorus/polyphosphorus species otherwise inaccessible.

1.2   Heterobimetallic activation and functionalization of P_4

One underexplored strategy for the activation and functionalization of white phosphorus is with the use of heterobimetallic compounds. This is the formation of highly reduced ("activated") P_n units by the cooperative action of two electronically distinct metal atoms. In most cases, the P_4 tetrahedron has already been pre-activated by one of the employed metal atoms. The choice of the incorporated metals and ligands is crucial as the obtained results are strongly dependent on the stereo-electronic nature of the reagents. While the activation of P_4 with transition metals has received considerable attraction and has led to a manifold of fascinating (poly)phosphorus complexes, reviewed several times in literature,[3],[5],[8] the concept of heterobimetallic activation and transformation has remained significantly less explored.

In this chapter, the concept of heterobimetallic activation and functionalization of P_4 will be reviewed. As outlined by the definition, only systems that involve the activation or transformation of a P_n unit will be discussed here. Thus, the pure coordination of e.g. transition metal carbonyl complexes to already activated (poly)phosphorus ligands as well as the coordination chemistry of coinage metals giving access to intriguing supramolecular frameworks or 1D and 2D coordination polymers are beyond the scope of this short review and won't be discussed.[12]

1.2.1   Heterobimetallic transition metal mediated activation and functionalization of P_4

The activation of white phosphorus using transition metal complexes is one of the most investigated concepts in this field of research. This is mainly due to the beneficial properties of the d-block elements such as the Lewis acidity, the coordinative unsaturation, and the availability of d-electrons.[8] The idea of activating the P_4 tetrahedron through two chemically distinct transition metal atoms dates back to the early 1990s. At this time, Scherer and co-workers investigated the reactivity of the ferrocene analogue, pentamethylpentaphosphaferrocene [Cp*Fe(η^5-P_5)] (**1**, Cp* = η^5-Me$_5$C$_5$) toward early and late transition metal carbonyl complexes

(Scheme 2).[13] Thermolysis of the iridium binuclear complex [{Cp*Ir(CO)$_2$}$_2$] in presence of **1** in refluxing toluene gives the heterodinuclear complex [Cp*Fe(μ_3-η^5:η^1:η^1-P$_5$){Cp*Ir(CO)$_2$}$_2$] (**2**) in good yield. The single-crystal X-ray diffraction (XRD) analysis revealed a *cyclo*-P$_5$ ligand in an envelope conformation which is perpendicularly coordinated to the iridium atoms forming a spirocyclic structure.[13]

Addition of another equivalent [{Cp*Ir(CO)$_2$}$_2$] to complex **2** yields compound [Cp*Fe(μ_5-η^5:η^2:η^1:η^1:η^1-P$_5$){Cp*Ir(CO)$_2$}$_2${Cp*Ir(CO)$_2$}{Cp*Ir(CO)$_2$}] (**3**). During the reaction, the Ir−Ir bond of the starting material is cleaved and inserted into a P−P bond of the *cyclo*-P$_5$ ligand resulting in an IrP$_5$ ring in a strongly distorted chair conformation.[13]

Likewise, the reaction of **1** with the early transition metal carbonyl complex [Cp″Ta(CO)$_4$] (Cp″ = η^5-1,3-*t*Bu$_2$C$_5$H$_3$) at 190 °C affords a mixture of products. In addition to minor amounts of the homonuclear complexes [(Cp″Ta)$_3$(P$_4$)(P$_2$)] and [(Cp″Ta)$_4$(P$_3$)$_2$], the heterobimetallic compounds [Cp*Fe(μ-P$_5$)TaCp″] (**4**) and the FeTa$_2$P$_4$ cubanes (**5a,b**) were isolated as the major products.[14] The molecular structure of **4** is best described as an iron-coordinated TaP$_5$ unit forming a Dewar benzene like framework. The authors suggest the presence of an Fe−Ir bond leading to an 18 valence electron configuration. The P$_5$ ligand of **4** might be considered as either a triradical pentaphospha-1,4-pentadiene-1,3,5-triyl or as trianion P$_5^{3-}$.[13] The isomers **5a,b** were isolated from the reaction mixture by column chromatography in a yield of 42%. Variable temperature NMR studies on a mixture of **5a,b** revealed an equilibrium between the two isomers. At room temperature this equilibrium is slightly shifted toward **5b**. However, it can be shifted fully by further coordination of [Mo(CO)$_5$], leading to compound **6**. The ^{31}P NMR spectrum of **5a** gives rise to an AA′MXX′ spin system, which is typical for *catena*-P$_5$ ligands. Isomer **5b** shows four multiplets assigned to an AMN$_2$X spin system with signals ranging from 778.8 ppm to −313.3 ppm. According to Scherer and co-workers the low field shifted resonance is assigned to the single phosphorus atom connected to one [Cp*Fe] and to two [Cp″Ta] fragments.[14]

The reaction of **4** with [Cp″Ta(CO)$_2$(cod)] (cod = 1,5-cyclooctadiene) affords complex [(Cp*Fe)(Cp″Ta{Cp″(CO)$_2$Ta})(P$_3$)P$_2$)] (**7**) in excellent yields. Compound **7** features an asymmetric FeTa$_2$P$_5$ core which can be subdivided into a P$_3$ and a P$_2$ unit both coordinated to iron and additionally bridged by two Ta metal fragments. The ^{31}P NMR spectrum of **7** gives rise to an AMNXY spin system reflected by the asymmetric arrangement of the atoms.[14]
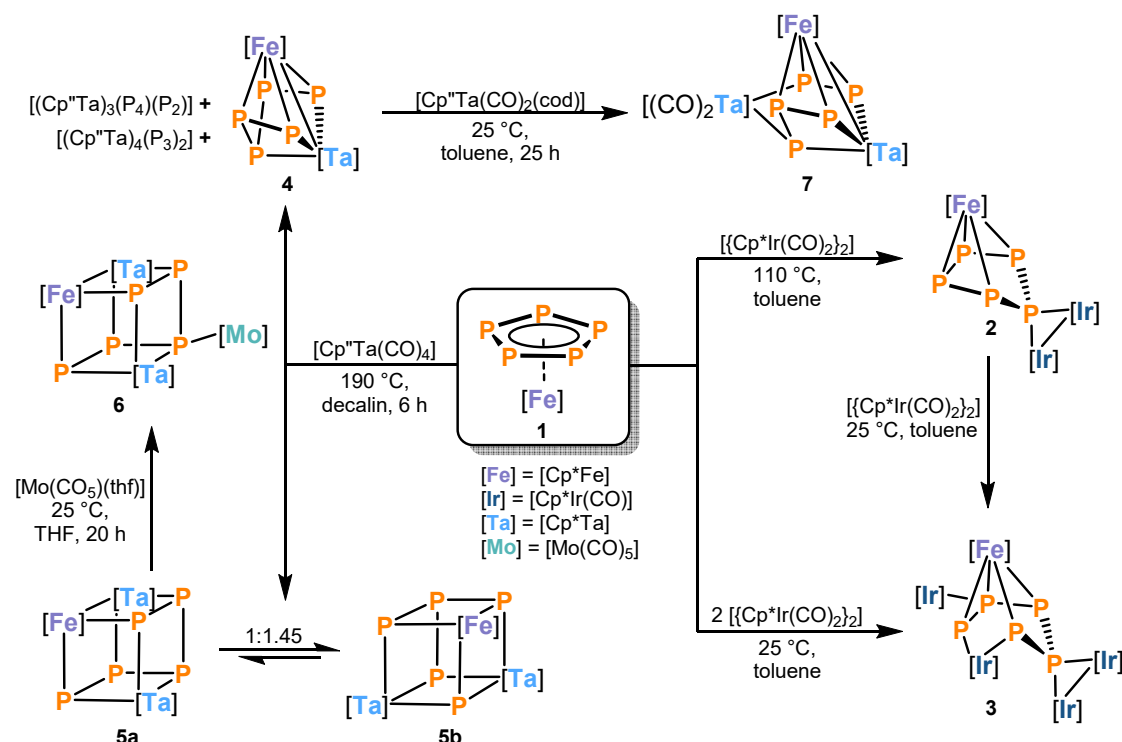
Scheme 2. Synthesis of heterodinuclear transition metal complexes *via* co-thermolysis of the P_4-activated sandwich complex $[Cp*Fe(\eta^5-P_5)]$ ($Cp* = C_5Me_5$) with early and late transition metal carbonyl complexes.

The same group explored the reactivity of the *cyclo*-P_4 sandwich complex $[Cp''(CO)_2Ta(\eta^4-P_4)]$ (**8**) prepared by photolysis of a thallium tetracarbonyl precursor $[Cp''Ta(CO)_4]$ in the presence of white phosphorus (Scheme 3). Reaction of **8** with the late transition metal complex $[Cp*Co(\eta^2-C_2H_4)_2]$ yielded quantitatively the heterobimetallic compound $[Cp*Co(\mu-\eta^2:\eta^2-P_2)_2Cp''Ta(CO)]$ (**9**) upon loss of the labile ethylene ligands.[15] A single-crystal XRD analysis of amber-colored crystals of **9** revealed the cleavage of two P−P bonds of the starting material forming a dumbbell-like structural motif. The two P_2 units in **9** are coordinated in a $\mu-\eta^2:\eta^2-P_2$ fashion to the bridged early and late transition metal atoms.[15] In contrast, photolysis of the early transition metal carbonyl complex $[Cp*Nb(CO)_4]$ in the presence of **8** is less selective yielding a mixture of two products $[\{Cp*(CO)_2Nb\}\{Cp*Nb\}\{Cp''(CO)Ta\}(\mu_3-\eta^2:\eta^1:\eta^1-P_2)_2]$ (**10**) and $[Cp*Nb(\mu-\eta^2:\eta^2-P_2)_2Cp''Ta(CO)]$ (**11**) which were successfully separated using column chromatography.[15] While compound **10** crystallizes as brownish crystals which were characterized by XRD, the by-product **11** could only be isolated as a red-violet powder. Notwithstanding the lack of the solid-state molecular structure, the authors suggest based on the ^{31}P NMR spectroscopic data that **11** is structurally related to complex **9**. The solid-state molecular structure of **10** reveals a novel coordination mode of a P_2 ligand. The authors propose the $\mu_3-\eta^2:\eta^1:\eta^1-P_2$ unit is best described as a formally $4e^-$ donor, π-side-on coordinated to the tantalum metal center and two times σ-coordinated to the niobium fragments.[15]
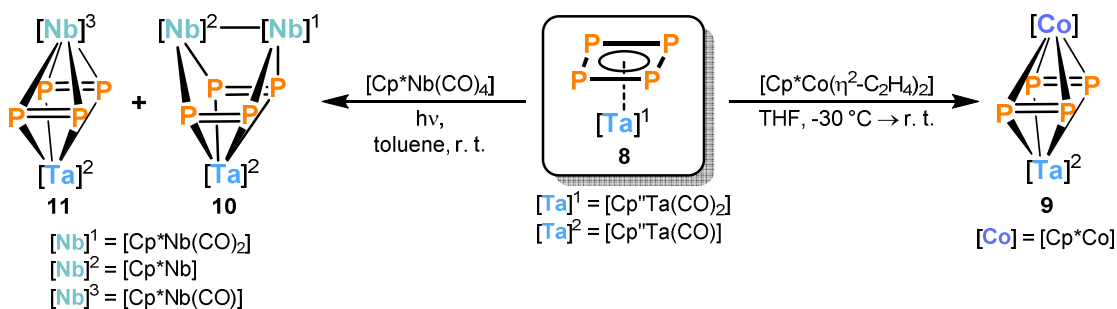
Scheme 3. Synthesis of heterodinuclear transition metal complexes *via* co-thermolysis and photolysis of the P_4-activated sandwich complex $[Cp''Ta(\eta^4\text{-}P_4)]$.

In 1992, Scheer and co-workers reported on a three-component reaction in which the P_4 tetrahedron is directly transformed by transition metal carbonyl complexes in presence of the Lewis acid $[Cr(CO)_5(thf)]$ (thf = tetrahydrofuran) which stabilizes the obtained polyphosphido frameworks (Scheme 4).[16],[17],[18] Even though the pure coordination chemistry of P_4 with transition metal carbonyl complexes was not envisaged to be covered by this short review, these selected examples show the benefits of heterobimetallic P_4 activation. Without the cooperative action of two distinct metal centers, the polyphosphorus compounds could not have been isolated. The reaction of white phosphorus with $[Cp''Rh(CO)_2]$ or $[Cp''Co(CO)_2]_2$ in presence of five equivalents of $[Cr(CO)_5(thf)]$ results in a mixture of products which were separated by column chromatography. Complexes $[M(\mu\text{-}\eta^2{:}\eta^1{:}\eta^1{:}\eta^1{:}\eta^1\text{-}P_4)\{Cr(CO)_5\}_4]$ (M = Cp''Rh(CO) (**12a**), Cp''Co(CO) (**12b**)) and the *cyclo*-P_4 complexes $[M(\eta^4{:}\eta^1{:}\eta^1{:}\eta^1\text{-}P_4)\{Cr(CO)_5\}_3]$ (M = Cp''Rh(CO) (**13a**), Cp''Co(CO) (**13b**)) were isolated, however in very low yields (approx. < 15%).[17] The molecular structures of these complexes feature tetraphosphabicyclo[1.1.0]butane ligands – often termed as "P_4 butterfly".[3],[5],[17] When performing the reaction in an analogue manner using $[Cp^*Ir(CO)_2]$ as the reagent a different outcome is observed. After chromatographic work-up the butterfly complex $[Cp^*Ir(CO)(\mu_4\text{-}\eta^2{:}\eta^1{:}\eta^1{:}\eta^1\text{-}P_4)\{Cr(CO)_5\}_3]$ (**14**), as well as the CO insertion product of **14**, complex $[Cp^*Ir(CO)(\mu_4\text{-}\eta^1{:}\eta^1{:}\eta^1{:}\eta^1\text{-}P_4)\{Cr(CO)_5\}_3]$ (**15**) were isolated. The molecular structure of **15** shows a distorted bicyclotetraphosphane framework. In addition, a few crystals of the octaphosphane cuneane-like complex $[\{Cp^*Ir(CO)\}_2(P_8)\{Cr(CO)_5\}_3]$ (**16**) were isolated and characterized by a single-crystal XRD experiment, showing that the dimerization of the P_4 ligand is also feasible under such conditions.[18]
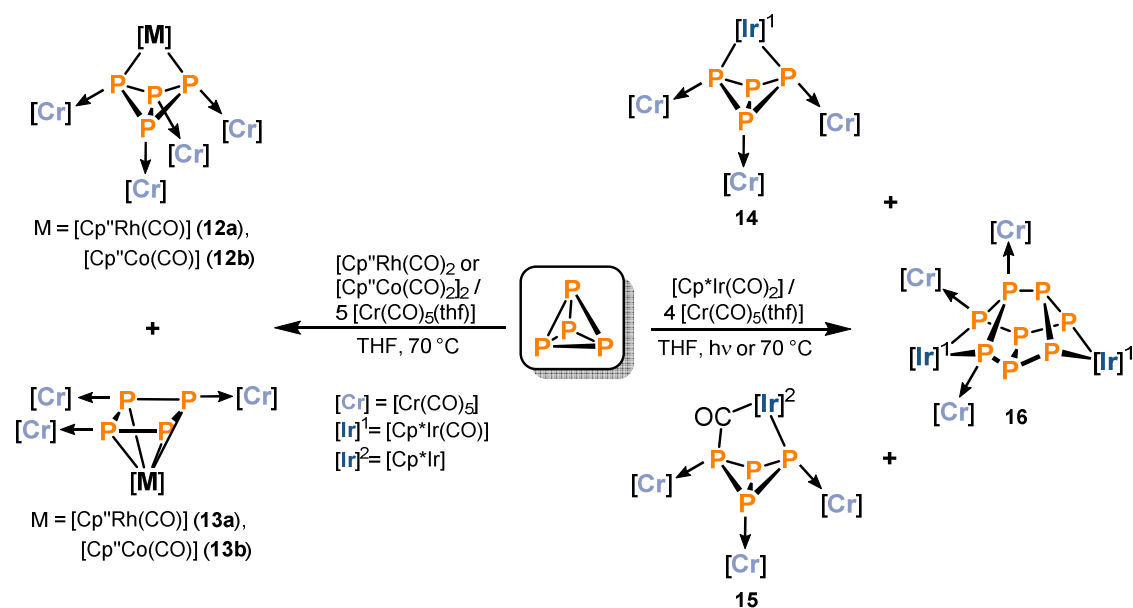
Scheme 4. Selected examples of three-component reaction of transition metal carbonyl precursors in presence of the Lewis acidic [Cr(CO)$_5$(thf)] and P$_4$.

In the period of 2011 to 2015 Ruiz and co-workers reported on tetranuclear phosphide- and phosphinidene bridged derivatives of the diphosphenyl complex [Mo$_2$Cp$_2$(μ-PCy$_2$)(μ-κ^2: κ^2-P$_2$Me)(CO)$_2$] (**17**).[19],[20],[21] This was obtained by reacting P$_4$ with the anionic complex [Mo$_2$Cp$_2$(μ-PCy$_2$)(μ-CO)$_2$]$^-$ and a subsequent methylation reaction with methyl iodide (MeI).[19] The reaction of the P$_4$ activation product **17** toward several 16 or 14 valence electron metal carbonyl fragments was investigated, forming different heteronuclear compounds (Scheme 5).[20],[21] The reported reactions are highly dependent on stoichiometry and often form metastable intermediates. In general, the detailed investigations of Ruiz and co-workers can be summarized as the coordination and subsequent bond cleavage of the diphosphenyl ligand by the Lewis acidic metal fragments.[20],[21] For instance, the stoichiometric reaction of [Fe$_2$(CO)$_9$] or [W(CO)$_4$(thf)$_2$] with complex **17** led to the facile cleavage of the P−P bond by the formal insertion of an [Fe(CO)$_3$] or [W(CO)$_4$] fragment resulting in the trinuclear complexes [FeMo$_2$Cp$_2$(μ_3-P)(μ-PCy$_2$)(μ_3-PMe)(CO)$_5$] (**18a**) and [Mo$_2$WCp$_2$(μ_3-P)(μ-PCy$_2$)(μ_3-PMe)(CO)$_6$](**18b**), respectively.[20] Compound **18a** further reacts with another equivalent of [Fe$_2$(CO)$_9$] to the tetranuclear phosphide- and phosphinidene bridged complex [Fe$_2$Mo$_2$Cp$_2$(μ_4-P)(μ-PCy$_2$)(μ_3-PMe)(CO)$_9$] (**19**).[21] In contrast, the stoichiometric reaction of **17** with the tetrahydrofuran adducts [Cp′Mn(CO)$_2$(thf)] (Cp′ = η^5-C$_5$H$_4$Me) and [W(CO)$_5$(thf)] gave [Mo$_2$MCp$_2$(μ-PCy$_2$)(μ_3-κ^2:κ^2:κ^1-P$_2$Me)(CO)$_2$L$_n$] (ML$_n$ = Cp′Mn(CO)$_2$ (**20a**), W(CO)$_5$ (**20b**)). Complexes **20a,b** are formed by the coordination of a 16 valence electron metal carbonyl fragment to the lone pair of the bridging phosphide. Both compounds are unstable and decompose at room temperature or under mild heating upon loss of methylphosphinidene (PMe) to the corresponding derivatives [Mo$_2$MCp$_2$(μ_3-P)(μ-PCy$_2$)(CO)$_2$L$_n$] (ML$_n$ = Cp′Mn(CO)$_2$ (**21a**), W(CO)$_5$ (**21b**)).[20] XRD analysis of **21a,b** revealed trigonal-planar phosphide ligands side-on coordinated to the unsaturated Mo$_2$

center and the ^{31}P NMR spectroscopy gives rise to strongly deshielded resonances ($\delta \approx 1000$ ppm) of the phosphide ligands. Based on these data and supported by computations, the authors suggest an isolobal analogy of the P→ML$_n$ fragments and a carbyne ligand (CR).[20]

In 2015, the same group reinvestigated the previously described reactions and found that different tetranuclear diphosphenyl-bridged complexes [M$_2$Mo$_2$Cp$_2$(μ-PCy$_2$)(μ-κ^2:κ^1:κ^1:κ^1-P$_2$Me)(CO)$_2$L$_{2n}$] (ML$_n$ = Cp′Mn(CO)$_2$ (**22a**), W(CO)$_5$ (**22b**)) are obtained using an excess of the metal carbonyl precursors. The formation of **22a,b** includes the cleavage of one Mo−PMe bond and the formation of a Mo−Mo double bond. Interestingly, in case of the tungsten carbonyl thf adduct a second species is observed and identified as [Mo$_2$W$_2$Cp$_2$(μ_3-P)(μ-PCy$_2$)(μ_3-PMe)(CO)$_{10}$] (**23**), featuring a Mo−Mo triple bond and a trigonal planar phosphide ligand.[21]

Moreover, the cluster compound, [Mo$_4$Cp$_2$(μ_4-P)(μ-PCy$_2$)(μ_3-PMe)(CO)$_9$] (**24a**) was synthesized by reacting **17** with excess of [Mo(CO)$_4$(thf)$_2$]. It is assembled on a Mo$_3$ triangular core bridged by phosphinidene and phosphide ligands and additionally stabilized by a 16 valence electron coordinated metal carbonyl [Mo(CO)$_5$] fragment. The tungsten analogue, [Mo$_2$W$_2$Cp$_2$(μ_3-P)(μ-PCy$_2$)(μ_3-PMe)(CO)$_9$] (**24b**) was obtained starting with the trinuclear tungsten complex **18b**.[21]

The reaction of **17** with metal carbonyl dimers [M$_2$(CO)$_n$] (M = Mn, Re, n = 10; M = Co, n = 8) was also examined. The result of these reactions was the cleavage of the P−P bond in the diphosphenyl ligand forming tetranuclear phosphide- and phosphinidene-bridged clusters with partially decarbonylated dimetal fragments. The reaction of **17** with the manganese and rhenium carbonyl dimers [M$_2$(CO)$_{10}$] (M = Mn, Rh) only proceeds under irradiation of UV light and resulted in the formation of open chain tetranuclear clusters [M$_2$Mo$_2$Cp$_2$(μ_4-P)(μ-PCy$_2$)(μ_3-PMe)(CO)$_9$] (M = Mn (**25a**), Rh (**25b**)). In addition, the reaction of **17** with a slight excess of [Co$_2$(CO)$_8$] at room temperature yielded the square-planar cluster compound [Co$_2$Mo$_2$Cp$_2$(μ_4-P)(μ-PCy$_2$)(μ_4-PMe)(μ-CO)(CO)$_6$] (**26**) formed by the P−P bond cleavage of the diphosphenyl ligand through the partially decarbonylated [Co$_2$(CO)$_8$] dimer.[21]
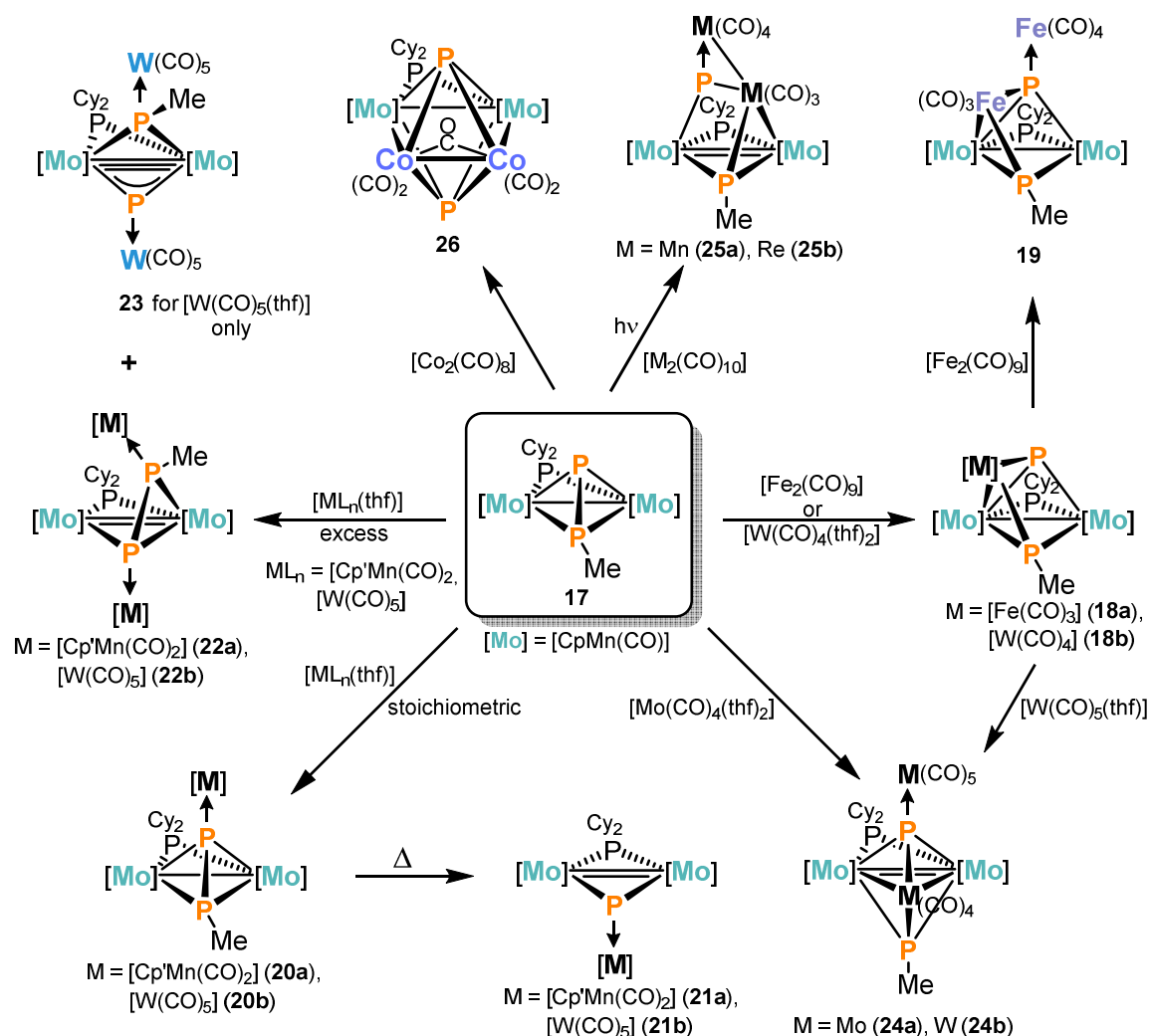
Scheme 5. Synthesis of heteronuclear transition metal complexes starting from the P_4-activated complex **17** with different transition metal carbonyl precursors.

A very recent example of the heterobimetallic activation and fragmentation of P_4 with transition metal carbonyl complexes was reported by Scheer and co-workers. They utilized the P_4 butterfly complex $[\{Cp*Cr(CO)_3\}_2(\mu-\eta^1:\eta^1-P_4)]$ (**27**) obtained by the reduction of white phosphorus using $[Cp*Cr(CO)_3]_2$ as a starting point.[22] Subsequent reactions of **27** with $[M(CO)_4(nbd)]$ (M = Cr, Mo; nbd = norbonadiene) did not lead to the expected Lewis adduct but yielded the mono-substituted $[\{Cp*Cr(CO)_2\}_2(\mu_3-\eta^3:\eta^1:\eta^1-P_4)\{M(CO)_5\}]$ (M = Cr (**28a**), Mo (**28b**)) and the bis-substituted tetraphosphido complexes $[\{Cp*Cr(CO)_2\}_2(\mu_3-\eta^3:\eta^1:\eta^1-P_4)\{M(CO)_5\}_2]$ (M = Cr (**29a**), Mo (**29b**)) (Scheme 6). Both complexes **28a,b** and **29a,b** feature a deltoid *cyclo*-P_4 ligand resulting from a P−P bond cleavage and an initial CO migration from the $[Cp*Cr(CO)_3]$ substituent of **27** to the $[M(CO)_4]$ fragment. The authors suggest that the electron deficient wing tip P atom coordinated by a $[Cp*Cr(CO)_2]$ substituent in **28a,b** and **29a,b** is stabilized by the formation of a formal Cr=P double bond which agrees with the 18 valence electron rule. Compounds **29a,b** are metastable and decompose slowly to the *cyclo*-P_3 complex $[Cp*Cr(CO)_2(\eta^3-P_3)]$ (**30**) and the phosphinidene complex $[\{Cp*Cr(CO)_2\}(\mu_3-P)\{Cr(CO)_5\}_2]$ (**31**). The latter compound could not be crystallized or fully characterized.[23] However, the ^{31}P

NMR resonance of **31** is extremely low-field shifted (δ = 1123 ppm), which is characteristic of such a planar phosphinidene-type structure. In summary, this reaction can be considered as [3+1] fragmentation induced by transition metal carbonyl complexes.[23]
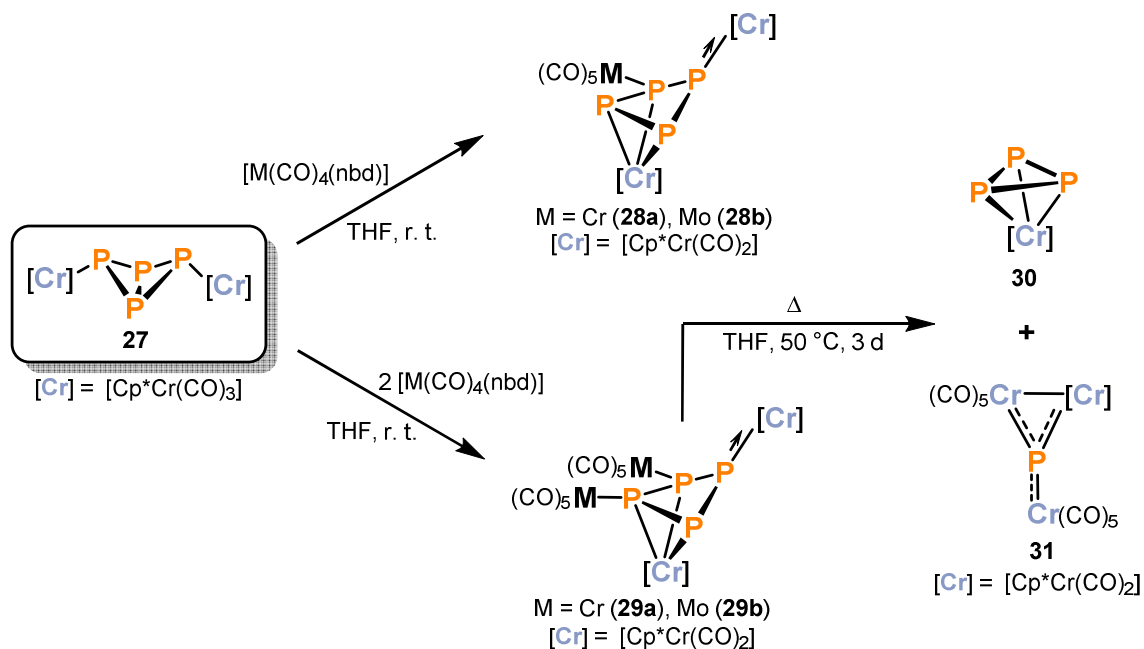

Scheme 6. Reaction of P-activated butterfly complex **27** with Lewis acidic [M(CO)$_4$(nbd)] (M = Cr, Mo) and subsequent [3+1] fragmentation.

Moving away from the formation of heterobimetallic polyphosphorus complexes from metal carbonyl compounds, Stoppioni investigated the reaction of the cationic nickel and cobalt complexes [(triphos)Ni(η^3-P$_3$)][BF$_4$] (**32**, triphos = bis(diphenylphosphinoethyl)-phenylphosphine) and [(triphos)Co(H)(η^3-P$_3$)][CF$_3$SO$_3$] (**33**) toward the neutral carbene analogue [(PPh$_3$)$_2$Pt(η^2-C$_2$H$_4$)] (Scheme 7).[24] This led to a new heterobimetallic complex [(triphos)Ni(μ-η^3:η^2-P$_3$)Pt(PPh$_3$)$_2$][BF$_4$] (**34**), which could be isolated in an excellent yield of 90%. Multinuclear NMR spectroscopy confirmed that the [Pt(PPh$_3$)$_2$] fragment selectively inserts into the *cyclo*-P$_3$ unit present in the starting material **32**, and this was corroborated by a single-crystal XRD analysis. The reaction of the closely related cobalt hydride complex **33** was conducted in a similar manner.[24] However, this resulted in an unexpected platinum-induced dimerization of the starting material, yielding [{(triphos)Co(H)}$_2$(μ_3-η^3:η^3:η^3-P$_6$){Pt(PPh$_3$)}][(CF$_3$SO$_3$)$_2$] (**35**). Compound **35** was isolated in a good yield of 65% and an XRD analysis revealed a chain of six P atoms connected to a [Pt(PPh$_3$)] fragment as the central structural motif. It is noteworthy that the skeletal hydrogen atoms in **35** could not be located by the structural investigations, presumably because they are disordered over the atoms of the *catena*-P$_6$ backbone. In line with such an observation, the ^{31}P{^{1}H} NMR spectrum of **35** in deuterated acetone shows eight resonances over a large chemical shift range, which are assigned to the P$_6$H$_2$ ligand and the P atoms of the triphos ligand. Some of the signals are rather broad, which may indicate a fluxional behavior of the complex in solution.[24]
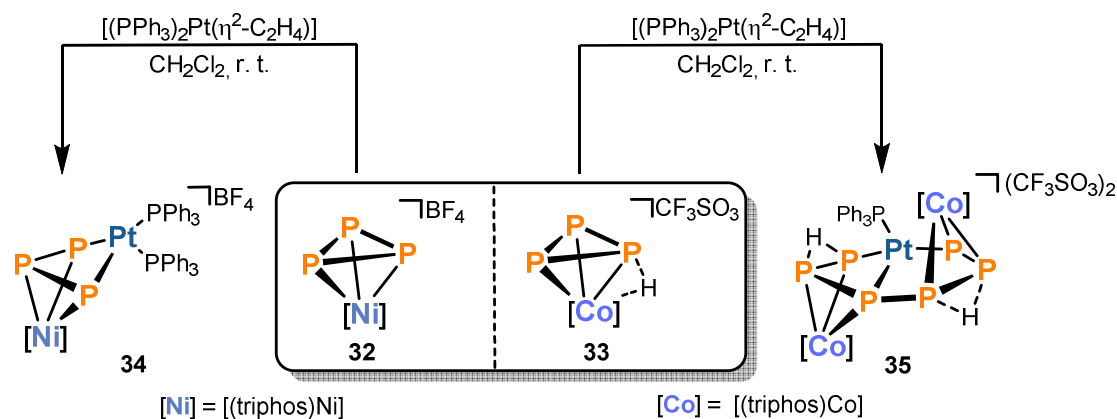
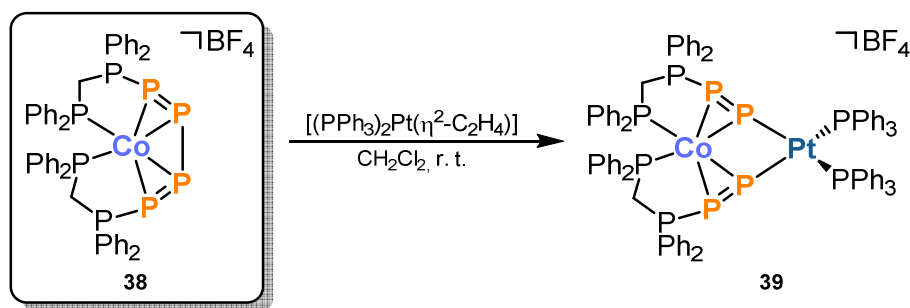**Scheme 7.** Heterodinuclear complexes synthesized by insertion of a carbene analogue [Pt(PPh₃)₂] fragment.

A similar approach was investigated by the research groups of Akbayeva and Perruzini. Both independently studied the insertion of the carbene analogue [Pt(PPh₃)₂] fragment into several η^1-coordinated *tetrahedro*-P₄ ligands (Schema 8).[25],[26] The obtained insertion products could not be crystallized and thus their formation and behavior in solution was extensively investigated by NMR spectroscopy and DFT calculations. While Akbayeva and co-workers reacted the η^1-P₄ coordinated complexes [(η^5-C₅R₅)(L)₂M(η^1-P₄)]X (**36a**; M = Fe, Ru; X = PF₆, CF₃SO₃, BPh₄; R = H, Me) with the platinum complex [(PPh₃)₂Pt(η^2-C₂H₄)], Peruzzini and co-workers focused on the hydride complex *trans*-[Ru(dppm)₂(H)(η^1-P₄)]BF₄ (**37a**, dppm = bis(diphenylphosphino)methane) as a starting material. Based on NMR spectroscopy both groups suggest the selective formation of the heterobimetallic complexes [(η^5-C₅R₅)(L)₂M(μ-η^1:η^2-P₄){Pt(PPh₃)₂}]X (**36b**; M = Fe, Ru; X = PF₆, CF₃SO₃, BPh₄; R = H, Me) and *trans*-[Ru(dppm)₂(H)(μ-η^1:η^2-P₄){Pt(PPh₃)₂}]BF₄ (**37b**), respectively. These compounds all show a fluxional behavior in solution which was further investigated by variable-temperature NMR experiments. Akbayeva and co-workers suggested the migration of the [Pt(PPh₃)₂] fragment between the atoms of the μ-η^1:η^2-P₄ bridging unit while Peruzzini and co-workers proposed the fluxional coordination of the [Ru(dppm)₂(H)] moiety in either an η^1-coordinated or in a bridging μ-η^2-coordination mode.[25],[26] The latter was further confirmed by theoretical calculations.[26]
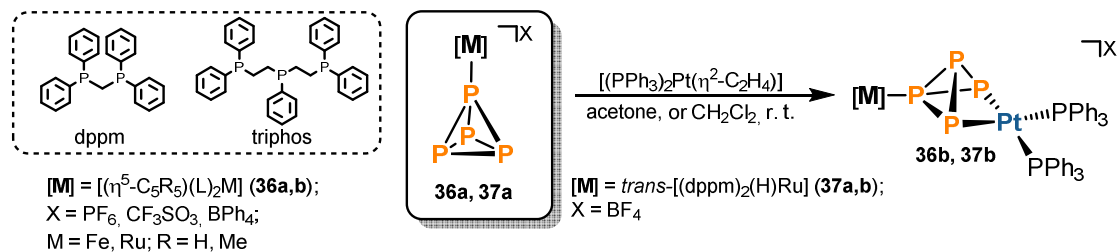
Scheme 8. Synthesis of heterobimetallic transition metal complexes containing a μ-η^1:η^2-P₄ bridging unit.

Another example of the consecutive insertion of a [Pt(PPh₃)₂] unit into a P₄-framework was presented by Peruzzini and co-workers in 2008. The authors started with the P₄-activation product [Co(Ph₂PCH₂PPh₂*PPPP*Ph₂PCH₂PPh₂)][BF₄] (**38**) which was obtained by reacting Co(BF₄)₂·H₂O, dppm (dppm = bis(diphenylphosphino)methane) and P₄ in a refluxing

THF/butanol mixture (Scheme 9).[27] Cation **38** is comprised of an unusual P_8-ligand incorporating a *catena*-P_6 unit, which is built out of a tetraphosphabutadiene moiety obtained after reaction with the P_4 tetrahedron and a subsequent nucleophilic attack by the PPh_2 moieties of the coordinated dppm ligands. Upon reacting **38** with $[(PPh_3)_2Pt(\eta^2-C_2H_4)]$ the heterobimetallic complex $[Co(\mu-\eta^1:\eta^2:\eta^1-P=PPh_2CH_2PPh_2)_2\{Pt(PPh_3)_2\}]$ (**39**) is obtained nearly quantitatively. During this reaction, the labile ethene ligand is released and a consecutive insertion of the $[Pt(PPh_3)_2]$ fragment into the central P−P bond of **38** takes place. The electronic structure of the P_3 ligands bridging the metal atoms in **39** is extraordinary. According to the authors, the ligand can be described as a zwitterionic diphenyl(alkyl)phosphonium(+)diphosphenide(−) fragment, in which the negative charge is located on the μ-Co, Pt-bridging P atom and the positive charge on the PPh_2R phosphonium P atom resulting in a formal $RPh_2P^{(+)}-P=P^{(-)}$ (R=Ph_2PCH_2) unit.[27]


Scheme 9. Synthesis of the heterodinuclear complex **39** *via* insertion of a $[Pt(PPh_3)_2]$ fragment featuring diphenyl(alkyl)phosphonium(+)diphosphenide(−) ligands.

In a recent collaboration between Peruzzini and Scheer, ruthenium and manganese complexes with a coordinated P_4 tetrahedron were reacted with the low-valent transition metal compound $[\{Cp'''Co\}_2(\mu-C_7H_8)]$ ($Cp''' = \eta^5$-1,2,4-$tBu_3C_5H_2$) and the β-diketiminato complex $[LM(\mu-C_7H_8)]$ (M = Fe, Co; L = $CH\{CHN(2,6-Me_2C_6H_3)\}_2$, C_7H_8 = toluene) (Scheme 10).[28] The reaction of the 14 valence electron precursor $[\{Cp'''Co\}_2(\mu-C_7H_8)]$ with P_4 has previously led to a mixture of aggregated polyphosphorus frameworks.[29] In contrast, the heterobimetallic approach is more selective and results in a single species. For instance, the reaction of $[CpRu(PPh_3)_2(\eta^1-P_4)][CF_3SO_3]$ (**40**) with $[\{Cp'''Co\}_2(\mu-C_7H_8)]$ yields the heterobimetallic complex $[\{CpRu(PPh_3)_2\}\{Cp'''Co\}(\mu-\eta^1:\eta^4-P_4)][CF_3SO_3]$ (**41**) in a very good yield of 82%. The structural analysis of complex **41** reveals a *cyclo*-P_4 ligand η^4-coordinated to the cobalt center, which is stabilized by an η^1-coordination to the $[CpRu(PPh_3)_2]$ unit. A similar outcome was observed when the neutral species $[\{Cp^{Big}Mn(CO)_2\}_2(\mu-\eta^1:\eta^1-P_4)]$ (**42**, $Cp^{Big} = C_5(C_6H_4nBu)_5$) was reacted with the triple-decker complex $[\{Cp'''Co\}_2(\mu-C_7H_8)]$. In this case, the trinuclear complex $[\{Cp^{Big}Mn(CO)_2\}_2\{CoCp'''\}(\mu-\eta^1:\eta^1:\eta^4-P_4)]$ (**43**) containing a planar *cyclo*-P_4 ligand was isolated. The reaction of **42** with the low-valent β-diketiminato iron or cobalt precursors $[LM(\mu-C_7H_8)]$ (M = Fe, Co) led to a similar heterotrinuclear *cyclo*-P_4 species $[\{Cp^{Big}Mn(CO)_2\}_2\{ML\}(\mu-\eta^1:\eta^1:\eta^4-P_4)]$ (M = Fe (**44a**), Co (**44b**)). Based on DFT calculations, it is likely that the *cyclo*-P_4 ligand in complexes **41**, **43**, and **44a,b** can be regarded as a π-delocalized P_4^{2-} dianion.[28]
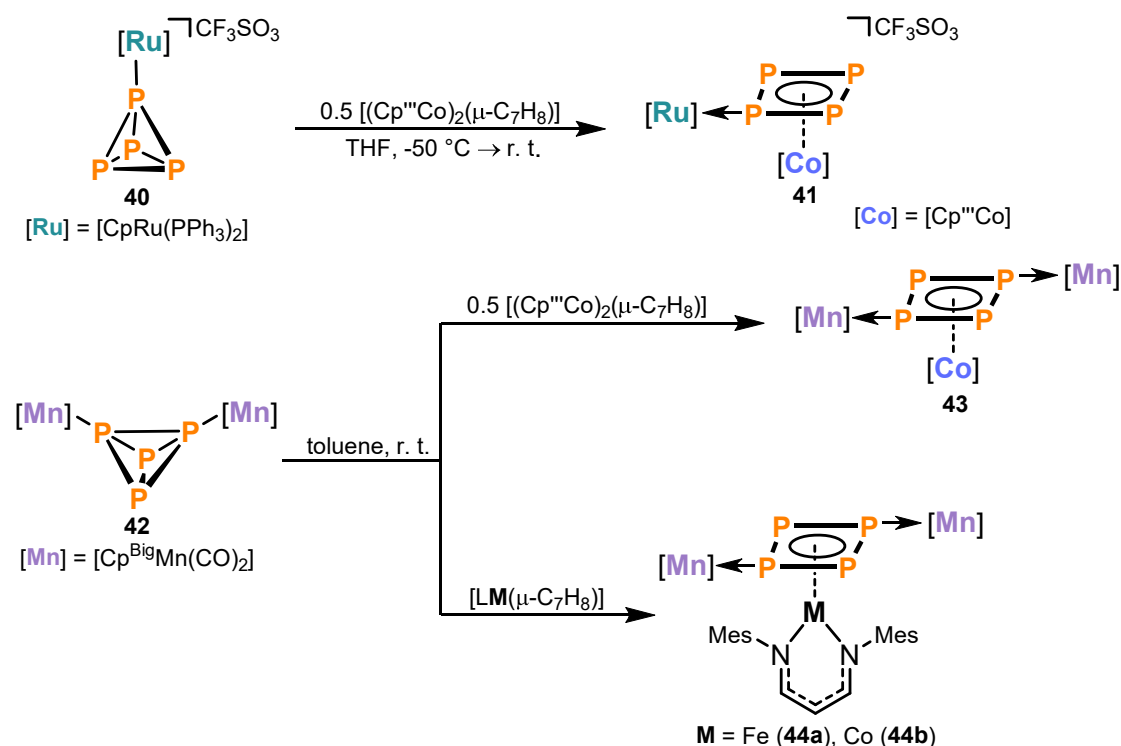
Scheme 10. Synthesis of heteronuclear *cyclo*-P_4 transition metal complexes stabilized by the cooperative action of two distinct metal fragments.

Very recently, Scheer and co-workers reported on the second example of an octaphospha-bis(cyclobutadiene)sandwich complex [{(Cp'''Fe(CO)$_2$)$_2$(μ_3-η^4:η^1:η^1-P_4)}$_2$Co][SbF$_6$]$_3$ (**47**).[30] The reaction of the P_4 activation product [{Cp'''Fe(CO)$_2$}$_2$(μ-$\eta^{1:1}$-P_4)] (**45**) with the Co^{II} salts [Co(NCCH$_3$)$_6$][X]$_2$ (X = PF$_6$, SbF$_6$) resulted in a mixture of different para- and diamagnetic products (Scheme 11), which included **47**. Halogen abstraction with Tl[PF]$_6$ from the heterobimetallic complex [{Cp'''Fe(CO)$_2$}$_2$(μ_3-η^2:$\eta^{1:1}$-P_4){CoBr$_2$}] (**46**) in the presence of **45** did not increase the selectivity and resulted in the same products. Nonetheless, using the less soluble hexafluoroantimonate anion enabled the characterization of two new heterobimetallic species **47** and [{Cp'''Fe(CO)$_2$}$_4$(μ_5-η^4:η^1:η^1:η^1:η^1-P_8){Co(CO)$_2$}][SbF$_6$] (**48**). Both complexes were obtained in a very low yield of only 3% for **47** and a few crystals of **48**. The XRD analysis of sandwich complex **47** revealed two *cyclo*-P_4[Fe]$_2$ units that are η^4-coordinated to the central cobalt atom. The *cyclo*-P_4 ligands in **47** are best described as a formal 6π-electron donor to the central Co^{III} ion. Thus, the authors assume that two *cyclo*-P_4^{2-} units are present. The solid-state molecular structure of by-product **48** shows the formation of a monocationic complex that is comprised of an octaphosphabicyclo[3.3.0]octane cage. This central structural motif can be rationalized as two connected *cyclo*-P_5 rings which are bent and coordinated to the [Co(CO)$_2$]$^{3+}$ fragment.[30]
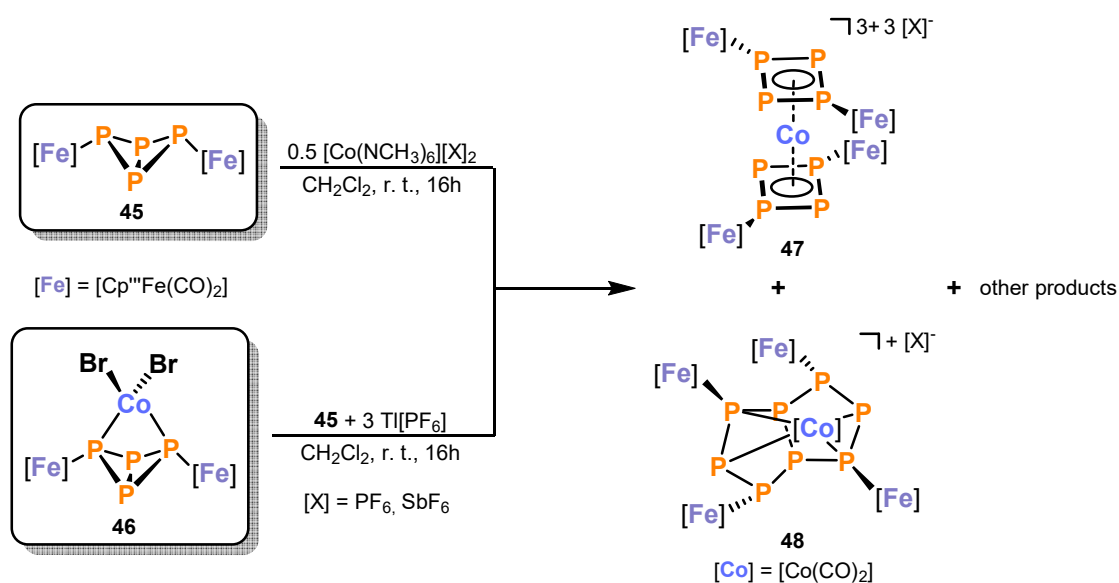
Scheme 11. Heterobimetallic complexes derived from **45**. Labile ligands at cobalt centers enable an isomerization of the phosphorus ligand.

These selected examples have shown that the heterobimetallic activation of P_4 with two distinct transition metal complexes can lead to (poly)phosphido complexes bearing novel structural motifs amenable for further derivatization or functionalization reactions. Nevertheless, the functionalization of such heteronuclear transition metal complexes remains underexplored, and this was an important part of this Ph.D. thesis.

1.2.2 Heterobimetallic activation and functionalization of P_4 involving lanthanide complexes

While the activation and functionalization of white phosphorus with d-block metal complexes is well studied and has been the subject of several reviews,[8] the reactivity of lanthanides toward P_4 is less well established. The first example of a molecular lanthanide polyphosphido complex $[(Cp*Sm)_4P_8]$ was reported by Roesky and co-workers in 2009. This landmark complex was obtained by the direct reaction of white phosphorus with samarocene $[(Cp*)_2Sm]$. The molecular structure comprises a realgar-shaped P_8^{4-} ligand stabilized by four samarocene units.[31] Subsequently, rare earth polyphosphorus chemistry began to flourish.[32] However, the concept of heterobimetallic d/f-block metal activation of white phosphorus is still limited to a handful of examples, which are mainly due to the collaborative work of the groups of Scheer and Roesky. Similar to the seminal work of heterobimetallic transition metal mediated P_4 activation pentamethylpentaphosphaferrocene $[Cp*Fe(\eta^5-P_5)]$ (**1**) was utilized for initial studies. The reduction of **1** with $[(Dipp_2pyr)SmI(thf)_3]$ ($Dipp_2pyr$ = 2,5-bis{N-(2,6-diisopropylphenyl)iminomethyl}pyrrolyl) in the presence of potassium naphthalenide yielded the monomeric tetrahydrofuran adduct $[Cp*Fe(\mu-\eta^4:\eta^3-P_5)Sm(thf)_2(Dip_2pyr)]$ (**49**) or the dimeric species $[Cp*Fe(P_5)Sm(Dipp_2pyr)]_2$ (**50**), depending on the crystallization method (Scheme 12).[33] Complex **50** is also formed when **1** is treated with two equivalents of $[(Dip_2pyr)SmI(thf)_3]$, with

13

the dimeric samarium Sm^{III} complex [(Dipp$_2$pyr)SmI$_2$(thf)]$_2$ being formed as a by-product. The solid-state molecular structures of both complexes **49** and **50** reveal a *cyclo*-P$_5$ ligand in an envelope conformation sandwiched between the 3d transition metal iron and the 4f element samarium. In the monomeric **49**, two THF solvate molecules are additionally coordinated to samarium atom, which prevents dimerization. In non-coordinating solvents, the samarium atom is coordinated in an η^2-coordination mode to second *cyclo*-P$_5$ moiety, which affords the dimer **50**. Magnetic (SQUID) measurements and near-infrared spectroscopy (NIR) gave further insight into the electronic structure of complexes **49** and **50** and suggest that samarium is present in its formal oxidation state +III in both cases.[33]

Compounds **49** and **50** represent the first examples of mixed d/f metal triple-decker complexes featuring a purely inorganic middle deck.[33] However, no P−P bond formation was achieved, and thus Scheer and co-workers extended their collaboration studying the reactivity of **1** towards other divalent samarocenes.[34] The reaction of samarocenes [(C$_5$Me$_4$R)Sm(thf)$_2$] (R = Me, *n*-propyl) with **1** at 60 °C afford P$_{10}$-bridged tetranuclear complexes [(Cp*Fe)$_2$(μ-η^4:η^4:η^2:η^2-P$_{10}${Sm(η^5-C$_5$Me$_4$R)$_2$}$_2$](R=Me (**51a**), *n*-propyl (**51b**)) (Scheme 12). An XRD analysis clearly shows the presence of the desired new 2-center-2-electron P−P bond. It is plausible that a one electron reduction of the *cyclo*-P$_5$ unit of **1** affords a formal 19 valence electron species which subsequently dimerizes forming a new P−P bond. In order to confirm this hypothesis, the oxidation state assignment of the samarium atom complexes **51a,b** was examined by NIR spectroscopy. The NIR spectra reveal that the Sm atom is present in its formal oxidation state +III which was derived by the characteristic absorption pattern. Compounds **51a,b** represent the first known complexes where the reductive coupling of polyphosphido precursors with divalent samarocenes yielded heteronuclear 3d/4f polyphosphido complexes.[34]
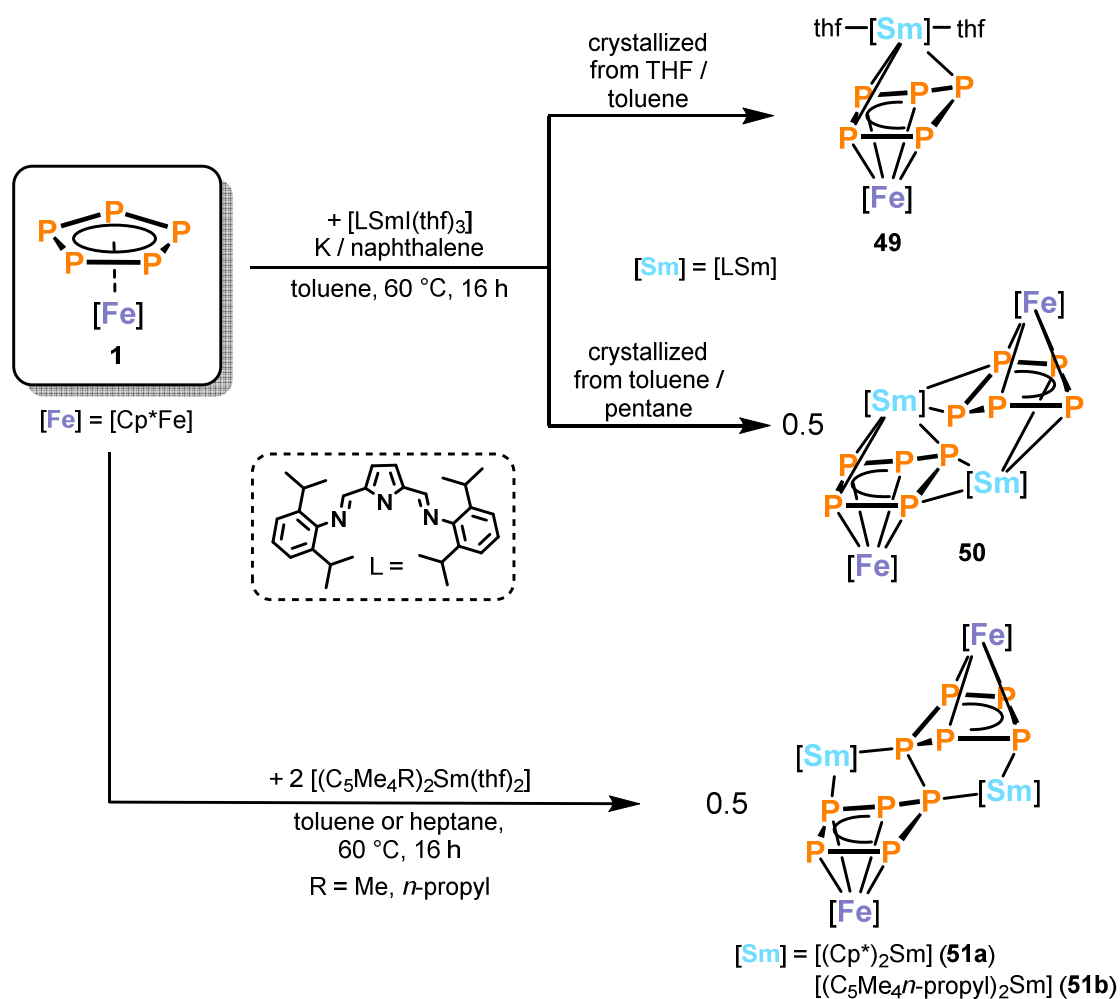
Scheme 12. Synthesis of 3d/4f heterodinuclear polyphosphido complexes.

Interested in the idea of P−P bond formation by samarocene induced single electron reduction processes, Scheer and Roesky further investigated the reactivity of the homoleptic complex [{Cp′′′Co(μ-η^2:η^2-P$_2$)}$_2$] (**52**) (Scheme 13).[35] Compound **52** can be easily synthesized in a high yield by the direct reaction of white phosphorus with [(Cp′′′Co)$_2$(μ-η^4:η^4-C$_7$H$_8$)] in toluene.[36] The single electron reduction of **52** by divalent samarocenes [(C$_5$Me$_4$R)Sm(thf)$_2$] (R = Me, *n*-propyl) resulted in the selective formation of the trinuclear complexes [(Cp′′′Co)$_2$(μ-η^3:η^2-P$_4$)Sm(η^5-C$_5$Me$_4$R)$_2$] (R=Me (**53a**), *n*-propyl (**53b**)). XRD analysis of dark brown crystals of **53a,b** revealed an acyclic *catena*-P$_4$ fragment sandwiched between two cobalt atoms and capped by a single samarium atom. The bond distances of the terminal P−P bonds are slightly longer than typical P−P double bonds while the distance of the formed samarocene-bridged internal P−P bond is in the range of P−P single bonds. Supported by NIR spectroscopy, the authors suggest that the samarium atom in **53a,b** is present in its formal oxidation +III reminiscent of the heteronuclear iron-samarium polyphosphido complexes discussed above.[35]
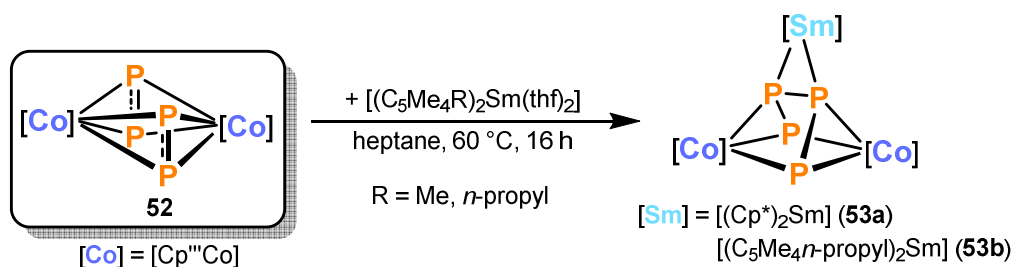
Scheme 13. Intermolecular P−P coupling induced by divalent samarium complexes yielding heteronuclear 3d/4f polyphosphorus complexes.

Another example of lanthanide induced aggregation of P_n units was published by Scheer and Roesky in 2015. In this report, they explored the reactivity of the P_4 activation product [{CpMo(CO)$_2$}$_2$(μ-η^2:η^2-P_2)] (**54**) toward the lanthanide metallocenes [Cp*$_2$Ln(thf)$_2$] (Ln = Sm, Yb).[37] These reactions yield a mixture of products (Scheme 14). The authors identified the 16-membered bicyclic compounds [(Cp*$_2$Ln)$_2$P$_2$(CpMo(CO)$_2$)$_4$] (Ln = Sm (**55a**), Yb (**55b**)) as the major products. When performing the reaction with samarocene, two by-products [(Cp*$_2$Sm)$_2$P$_4$(CpMo(CO)$_2$)$_2$] (**56**) and [(Cp*$_2$Sm)$_3$P$_5$(CpMo(CO)$_2$)$_3$] (**57**) were identified by single-crystal XRD analysis. NIR spectroscopy and magnetic measurements indicate that the lanthanide atoms in [Cp*$_2$Ln(thf)$_2$] are oxidized to the +III oxidation state. A P_2^{2-} unit is end-on coordinated to two metal-metal bonded [CpMo(CO)$_2$]$_2$ fragments in complexes **55a,b**. In addition, the central [P$_2${CpMo(CO)$_2$}$_4$]$^{2-}$ unit is coordinated by two carbonyl bridging ligands which are bound to [Cp*$_2$Ln]$^+$ (Ln = Sm, Yb) fragments. The minor product **56** shows a planar, rectangular P_4 ring η^2-coordinated to two [CpMo(CO)$_2$] units. [Cp*$_2$Sm]$^+$ fragments are connected to these units by carbonyl ligands.[37] A similar *cyclo*-tetraphosphabutadiene ligand was observed in a Co^I complex [(LCo)$_2$(μ-η^4:η^4-P_4)] (L = CH[C(Me)N(2,6-Et$_2$C$_6$H$_3$)]$_2$) after the direct reaction of white phosphorus with [(LCo)$_2$].[37],[38] The solid-state molecular structure of the minor by-product **57** reveals a planar *cyclo*-P_5 unit connected to three [CpMo(CO)$_2$] moieties. The molybdenum atoms are each η^2-coordinated by the *cyclo*-P_5 unit. In addition, three [Cp*$_2$Sm]$^+$ moieties are bound to the [CpMo(CO)$_2$] units by bridging carbonyl ligands as observed for **55a,b** and **56**.[37]

In order to further explore the reduction chemistry of molybdenum polyphosphides, Scheer and Roesky reduced the molybdenum complex [Cp*Mo(CO)$_2$(η^3-P_3)] (**58**), bearing a triangular P_3 unit, with the single electron reducing agents [Cp*$_2$Ln(thf)$_2$] (Ln = Sm, Yb). As expected, a single electron reduction led to the formation of a new P−P bond and isostructural 4d/4f hexaphosphides [(Cp*$_2$Ln)$_2$P$_6${Cp*Mo(CO)$_2$}$_2$] (Ln = Sm (**59a**), Yb (**59b**)) were isolated. The authors suggest that one Mo−P bond is cleaved upon the one electron reduction of **58**, and a new P−P bond is established between two 18 valence electron [Cp*Mo(CO)$_2$P$_3$]$^-$ fragments. In addition, two [Cp*$_2$Ln]$^+$ moieties are coordinated to the P_6 framework and each of them is bound to one [CpMo(CO)$_2$] unit by the carbonyl bridging ligands. Furthermore, the [CpMo(CO)$_2$] units are coordinated in an η^2-fashion to the phosphorus scaffold.[37]

16
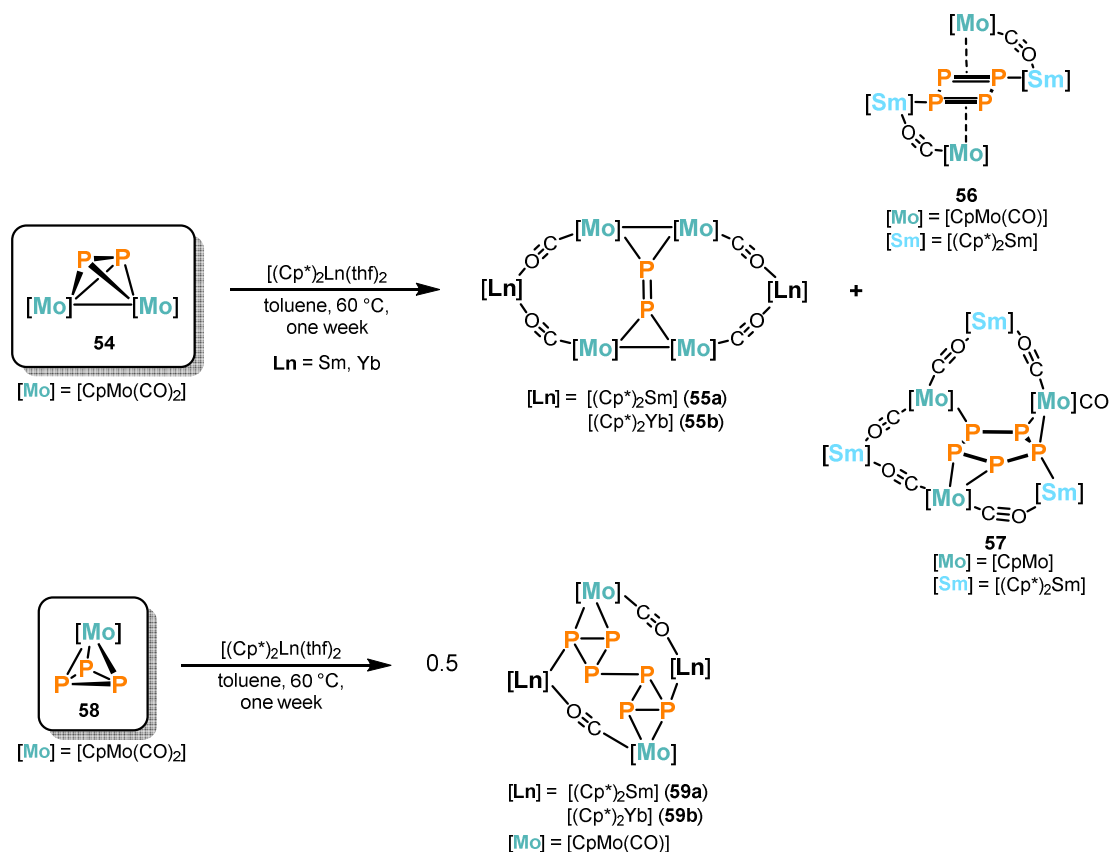
Scheme 14. Synthesis of heteronuclear 4d/4f polyphosphido complexes by single electron reduction induced by divalent f-block metallocenes.

The collaborative work of Scheer and Roesky shows that the concept of heterobimetallic lanthanide mediated activation of white phosphorus holds a lot of potentials. The incorporation of f-block elements gives rise to unprecedented (poly)phosphorus frameworks which in turn might be amenable to innovative functionalization reactions in the future, which utilize the cooperative action of P_4 with d-block and f-block elements.

1.2.3 Activation and functionalization of P_4 mediated by p-block elements in combination with d-block elements

Besides the ongoing research of transition metal mediated activation and functionalization of white phosphorus, the use of main group element compounds for the activation and fragmentation of P_4 has seen increasing academic interest in recent times.[9] In history, white phosphorus was mostly transformed by nucleophilic s/p-block elements such as organolithium compounds. Today, this strategy is more and more superseded by examples of the activation of P_4 using low-oxidation main group species, including carbenes and carbene analogue heavier group 13 and group 14 compounds.[9] However, the use of heterobimetallic p-block / d-block element compounds has only started to develop during the last decades.

One of the first examples of this strategy was reported by Driess and co-workers in 2009.[39] They studied the P_4 activation product $[(^{Dipp}nacnac')Si(\eta^2\text{-}P_4)]$ (**60**, $^{Dipp}nacnac'$ = $CH[C(Me)N(Dipp)][C(CH_2)N(2,6\text{-}iPr_2C_6H_3)])$ obtained by the direct reaction of white

phosphorus with silylene [(^{Dipp}nacnac′)Si]. A second silylene molecule can be inserted into a P−P bond of **60** to give [(^{Dipp}nacnac′)Si)$_2$(μ-η$^{2:2}$-P$_4$)].[40] Inspired by this Driess and co-workers studied the reaction of **60** toward low-valent transition metal complexes which would lead to similar heterodinuclear tetraphosphido compounds.[39] The authors chose the β-diketiminato nickel(I) complexes [(LNi)$_2$(μ-C$_7$H$_9$)] (L = CH[CMeN(2,6-iPr$_2$C$_6$H$_3$)]$_2$ or CH[CMeN(2,6-Et$_2$C$_6$H$_3$)]$_2$) as a starting material to study the coordination behavior of **60** (Scheme 15). After work-up of the reactions performed at low temperatures in a 1:1 stoichiometry the paramagnetic complexes [(^{Dipp}nacnac′)Si(μ-η$^{2:2}$-P$_4$)NiL] (L = CH[CMeN(2,6-iPr$_2$C$_6$H$_3$)]$_2$ (**61a**), CH[CMeN(2,6-Et$_2$C$_6$H$_3$)]$_2$ (**61b**)) were obtained in good yields. The molecular structures of both complexes feature a [Si(μ-η$^{2:2}$-P$_4$)Ni] core which is comprised of an intact SiP$_4$ unit side-on coordinated to a Ni^I center. According to the XRD analysis, the desired insertion of the Ni^I fragment into a P−P bond of the starting material did not occur. However, the Ni coordinated P−P bond is elongated at about 0.1 Å which can be attributed to the coordination of the Ni^I fragment.[39]
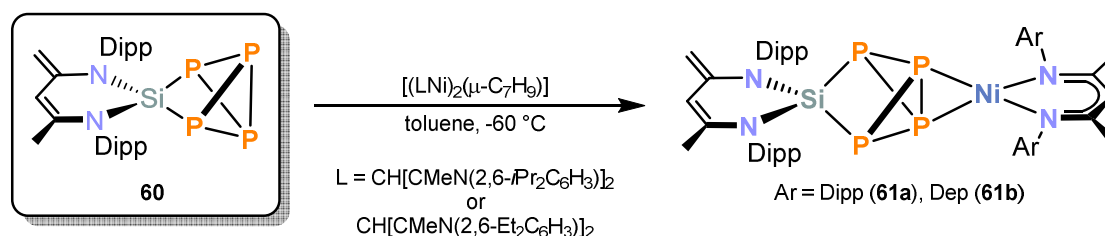
Scheme 15. Synthesis of heterodinuclear tetraphosphido complexes starting from [(^{Dipp}nacnac′)Si(η^2-P$_4$)] (**60**) and low-valent β-diketiminatonickel(I) precursors.

A cooperative study by Power, Wolf and co-workers showed that the white phosphorus is selectively activated by the heterobimetallic cobalt-tin cluster [Ar′SnCo]$_2$ (**62**, Ar′ = C$_6$H$_3$-2,6{C$_6$H$_3$-2,6-iPr$_2$}$_2$, Scheme 16) forming complex [Ar′$_2$Sn$_2$Co$_2$P$_4$] (**63**) in 76% yield.[3],[41] In this reaction, the P$_4$ molecule is inserted into the Co$_2$Sn$_2$ core of the starting material and a terphenyl substituent migrates to one of the terminal P atoms of the newly formed *catena*-P$_4$ unit. The XRD analysis of **63** shows a terphenyl-substituted *catena*-P$_4$ ligand coordinated by two cobalt and tin atoms. The P−P bond lengths of the P$_4$ unit in **63** lie in between 2.2005(8) Å and 2.1621(8) Å and are therefore in the range of P−P single bonds. The Sn−P bonds (2.6587(6) Å and 2.5716(6) Å) behave similarly with typical distances of Sn−P single bonds. Looking more closely at the Co−P distances of cluster **63** reveals that the terminal P atoms coordinated to the bridging cobalt atom are shorter (2.1864(6) Å and 2.2289(7) Å) than those of the P atoms coordinated to the cobalt atom in an η^2-fashion (2.3350(6) Å and 2.3501(6) Å). The collaborative work of Power, Wolf and co-workers has generated the first heterobimetallic tetraphosphido complex comprised of cobalt and tin.[3],[41]
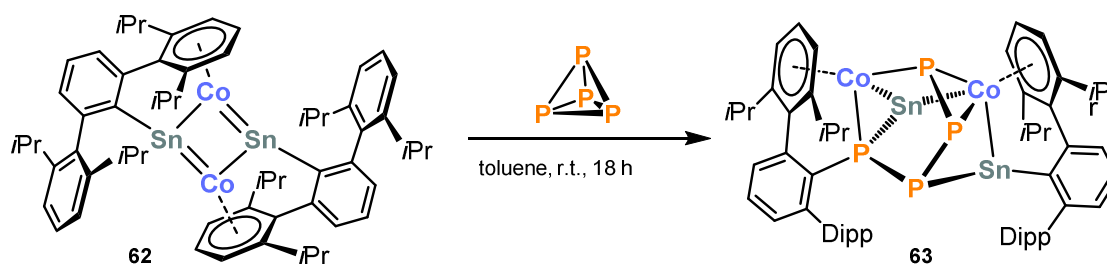
**Scheme 16.** Arylation of P_4 by a low coordinate heterobimetallic cobalt-tin cluster.

Roesky and co-workers recently reported on the synthesis of mixed Al-Fe polyphosphides.[42] They started their investigations again utilizing pentamethylpentaphosphaferrocene **1** (Scheme 17). Neutral Al-Fe based triple-decker polyphosphido complexes were synthesized using two aluminum(I) complexes. The stoichiometric reaction of **1** with the carbene analogue [(^{Dipp}nacanc)Al] afforded the heterodinuclear complex [(^{Dipp}nacnac)Al(μ-η^3:η^4-P_5)FeCp*] (**64a**) in yields of 35%. The solid-state molecular structure of **64a** shows a triple-decker type complex with an envelope *cyclo*-P_5 ring sandwiched between the η^4-coordinated iron center and aluminum coordinated to the polyphosphido ligand in an η^3-binding mode. The authors suggest that a redox reaction takes place in which the aluminum species is oxidized to the formal oxidation state +III while starting material **1** is reduced leading to a conformational change of the P_5 ligand. In line with the solid-state molecular structure, the ^{31}P NMR spectrum of **64** recorded at room temperature shows three broad resonances which decoalesce at −40 °C to an AA′MXX′ spin system. Interestingly, a different outcome is observed when reacting **1** with the Al^I tetramer [(Cp*Al)$_4$]. This reaction afforded the unexpected insertion of [Cp*Al] moieties into the P_5 unit of **1** yielding the heterobimetallic complex [(μ_3-P)(AlCp*)$_2${P_4(AlCp*)}(FeCp*)] (**65**). The molecular structure of the mixed Al-Fe polyphosphido compound **65** is described as a complex of the [Cp*Fe]$^+$ fragment with an η^4-coordinated *cyclo*-P_4(AlCp*) ligand, which is additionally η^2-coordinated to two [Cp*Al]$^{2+}$ moieties. This arrangement is capped by a single P atom binding to all three aluminum atoms. The authors rationalize this reaction as the formal six-fold reduction of the *cyclo*-P_5 ring of the starting material resulting in a P_4^{4-} and in a P^{3-} fragment. The ^{1}H NMR spectrum recorded at room temperature reveals only two signals in the aliphatic region despite three inequivalent aluminum centers are observed in the solid-state molecular structure. The authors propose a fluxional behavior of the Cp* ligand in solution. Likewise, two singlet resonances were detected in the ^{31}P NMR spectrum of **65** however a J(^{31}P,^{31}P) coupling even at low temperatures could not be observed. It is plausible that complex **64b** is an intermediate en route to **65**. Presumably, the formation of the latter species includes the insertion of [Cp*Al] units into the P_5 ligand of **64b**. This was supported by NMR spectroscopic investigations, which showed that an intermediate **64c** stabilized by dimethoxymethane (DME) can be observed by ^{31}P NMR spectroscopy when the reaction is performed in DME as solvent.[3],[42] In order to further support this hypothesis, the plausible intermediate was trapped with 1,3,4,5-tetramethylimidazol-

2-ylidene (NHC), giving the NHC-stabilized complex $[(Cp^*)Al(NHC)(\mu-\eta^3:\eta^4-P_5)FeCp^*]$ (**64d**).[3],[42]
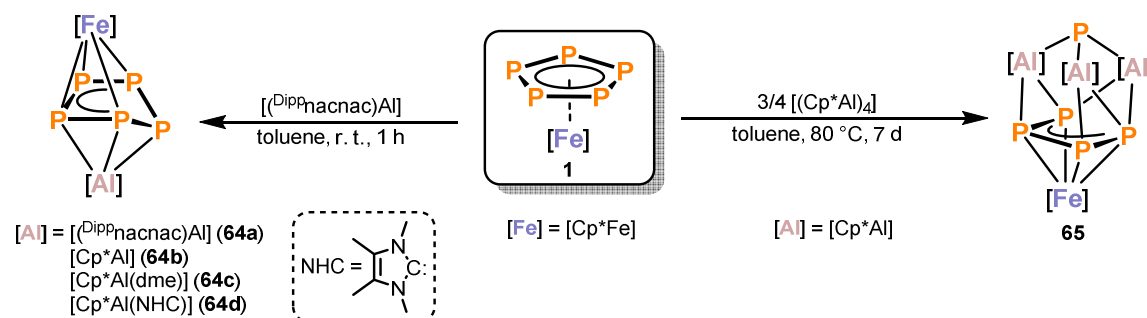
Scheme 17. Synthesis of heterobimetallic complexes by reaction of $[Cp^*Fe(\eta^5-P_5)]$ (**1**) with two different low-valent aluminum compounds.

Further exploring the use of carbene analogue p-block element species, the groups of Roesky and Scheer studied the reactivity of **1** toward silylenes (Scheme 18).[43] Reaction of **1** with three equivalents of silylene, [LSi(Cl)] (L = [PhC(NtBu)$_2$]) resulted in the phosphasilene species **67** and $[Cp^*Fe(\eta^4-P_4SiL)]$ (**66**) in 40% yield. The nature of the *catena*-P$_4$ unit in **66** is described as a *cyclo*-LSiP$_4^{4-}$ ligand coordinated to the $[Cp^*Fe]^+$ cation in an η^4-mode. The authors suggest that the reaction presumably proceeds *via* an intermediary formed *cyclo*-P$_5$ species $[\{LSiCl\}\{(\eta^4-P_5)FeCp^*\}]$ (**65a**), which was detected in $^{31}P\{^1H\}$ VT-NMR studies. The mechanism for the formation of the silylphosphacyclopentadienyl complex **66** was further investigated. The reaction of **1** with one equivalent of the sterically more demanding silylene [LSi{N(SiMe$_3$)$_2$}] led to the Si-substituted η^4-P$_5$ complex $[\{LSi(N(SiMe_3)_2)\}\{(\eta^4-P_5)FeCp^*\}]$ (**65b**), which resembled the proposed intermediate, **65a**. In addition, treatment of **1** with the Si^I compound [LSi−SiL] in a 1:1 ratio resulted in the ring expansion and incorporation of two [LSi] fragments in the *cyclo*-P$_5$ ligand of **1** affording complex $[Cp^*Fe\{\eta^4-P_5(SiL)_2\}]$ (**68**). However, $^{31}P\{^1H\}$ VT-NMR monitoring of this reaction has shown that the formation of **68** is unselective and traces of [L$_2$Si$_2$P$_2$] (**69**), compound **66**, and two unstable species were detected as by-products.[3],[43]
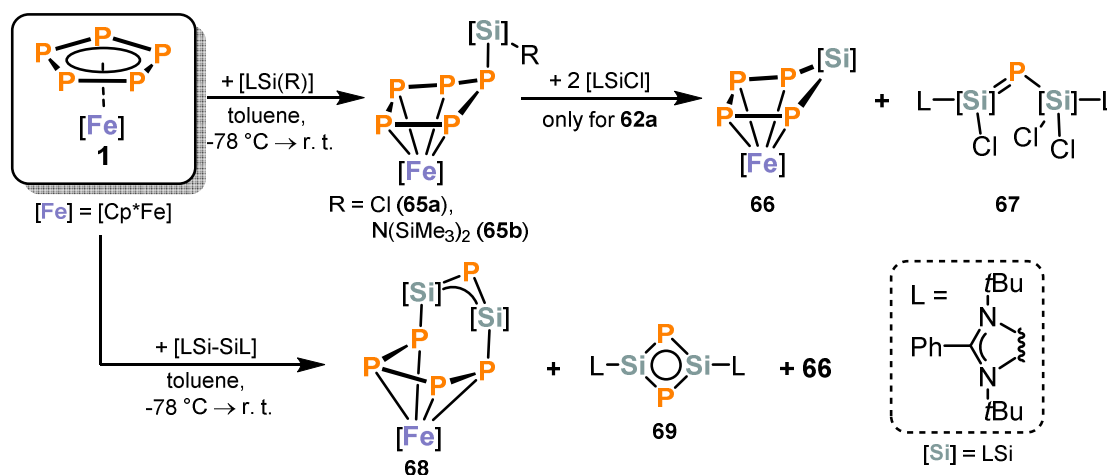
Scheme 18. Functionalization of the *cyclo*-P$_5$ ligand in $[Cp^*Fe(\eta^5-P_5)]$ (**1**) by silicon carbene analogues.

Inspired by these results, Scheer and Roesky investigated the reactivity of **1** toward the mono- and digermylenes [LGeCl] and [LGe−GeL] (L = [PhC(N*t*Bu)$_2$], Scheme 19).[44] Unlike [LSiCl], complex **1** does not react with the analogue chloro-germylene, [LGeCl] even at elevated temperatures. This might be a result of the different oxidation potentials of the two related homologs.[44] As described previously by Scheer and Roesky[43] and mentioned earlier in this chapter the disilylene [LSi−SiL] is more reactive than the corresponding monosilylene [LSiCl]. Therefore the two groups focused on the corresponding digermylene [LGe−GeL].[44] The ^{31}P{^{1}H} NMR monitoring of the equimolar reaction of **1** with [LGe−GeL] at room temperature resulted in a mixture of different polyphosphorus species. However, at low temperature, one of these compounds [(LGe)$_2${(μ-η^4-P$_5$)FeCp*}] (**71**) was successfully isolated in 60% yield. It is worth noting that the reaction of anion [{K(dme)}$_2$][Cp*Fe(η^4-P$_5$)] (**70**) with [LGeCl] in a 1:2 ratio led to the same product **71** (Scheme 19). An XRD analysis of **71** reveals a *cyclo*-P$_5$ ligand in an envelope conformation coordinated in an η^4-fashion to the transition metal center. In line with the solid-state structure, the ^{31}P{^{1}H} NMR spectrum of **71** shows an AMM′XX′ spin system which is typical for such a coordinated *cyclo*-P$_5$ ligand. Compound **71** is not stable in solution and slowly decomposes at room temperature to the starting material **1** and other species over the course of more than a month. Performing the targeted degradation at higher temperatures allowed the characterization of [(LGe){(μ-η^3-P$_5$)(η^1-GeL)FeCp*}] (**72**). The XRD analysis of crystals of **72** revealed a 1,2-migration followed by a subsequent insertion of a [LGe]$^+$ substituent into an Fe−P bond. Hence, **72** can be considered as an isomer of complex **71**. The isolation of the isomer **72** might help to understand the formation of plausible intermediates which were observed, but not conclusively characterized in the analogue reactions with the silicon derivatives[43] [LSiCl] and [LSi−SiL] (*vide supra*, Scheme 18).[44]
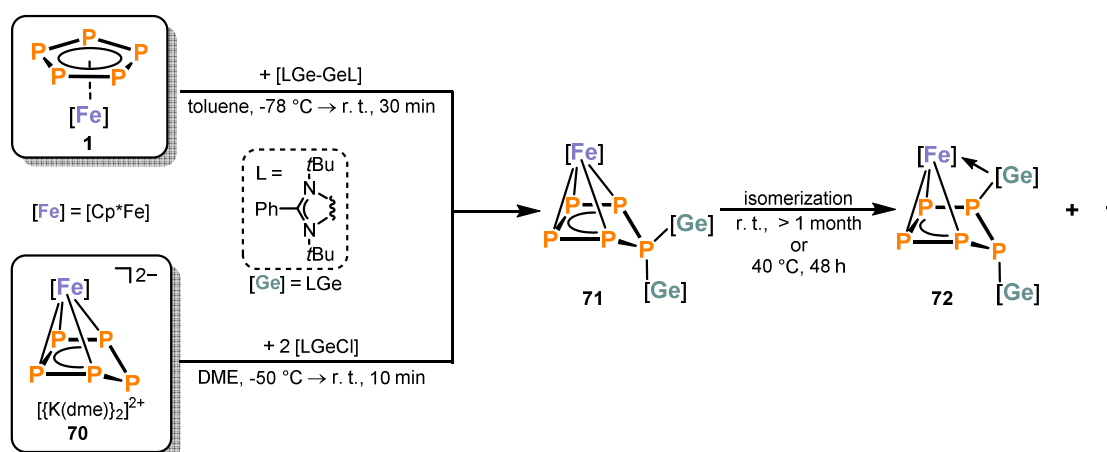
Scheme 19. Functionalization of the *cyclo*-P$_5$ ligand in [Cp*Fe(η^5-P$_5$)] (**1**) and [{K(dme)}$_2$][Cp*Fe(η^4-P$_5$)] (**70**) by germanium carbene analogues.

1.3 Conclusion

The development of different approaches for the synthetic and catalytic activation and transformation of P_4 into organophosphorus compounds remains an important topic for researchers around the globe.

One potential strategy is the heterobimetallic activation and functionalization of white phosphorus, which has been the focus of review in this chapter. This concept combines two chemically distinct metal atoms leading to highly reduced P_n units that are potentially amenable for further derivatization reactions (see section 1.2). First examples of such heterobimetallic P_4 activation were reported by Scherer and co-workers, who investigated the reactivity of white phosphorus toward different transition metal carbonyl complexes. Insertion of carbene analogue platinum complexes have been studied by Akbayeva, Stoppioni and Peruzzini. Scheer and co-workers demonstrated the heterobimetallic opening of intact P_4 tetrahedra (see section 1.2.1). Although such transition metal mediated heterobimetallic activation of P_4 led to novel and impressive polyphosphorus frameworks the subsequent functionalization to valuable and useful organophosphorus compounds remains unexplored. Similarly, the lanthanide mediated heteronuclear activation of white phosphorus is even less studied (see section 1.2.2). Seminal work of Scheer and Roesky mainly focused on single electron reduction of transition metal polyphosphido complexes with samarium. Nonetheless, these few examples demonstrate the potential of f-block elements in the heterobimetallic activation and transformation of P_4. Another promising approach is employing both transition metals and p-block elements to mediate the activation of white phosphorus (see section 1.2.3). The combination of a p- and d-block element was pioneered by Driess and co-workers. The benefit of main group-mediated heterobimetallic activation of P_4 was further demonstrated by our group for a cobalt-tin cluster, which is able to activate and functionalize the P_4 molecule in one step. Pursuing a different approach, Scheer and Roesky reported on extrusion and insertion processes in pentamethylpentaphosphaferrocene with low-valent aluminum and silicon species, which simultaneously generate P_1 and P_4 units.

The results described in this introduction impressively demonstrate that the use of two electronically different metals enable P_4 activation pathways that are inaccessible for homobimetallic or mononuclear species. Motivated by these insights, this thesis aims at further exploring heterobimetallic P_4 functionalization as a strategy for the synthesis of novel polyphosphorus frameworks and in particular rare, organosubstituted polyphosphido complexes. In particular, there have been few investigations into subsequent transformations of the obtained heterobimetallic polyphosphorus species. The present thesis, therefore, aims at improving our understanding of the activation of P_4 and the functionalization of the resulting heteronuclear polyphosphorus frameworks.
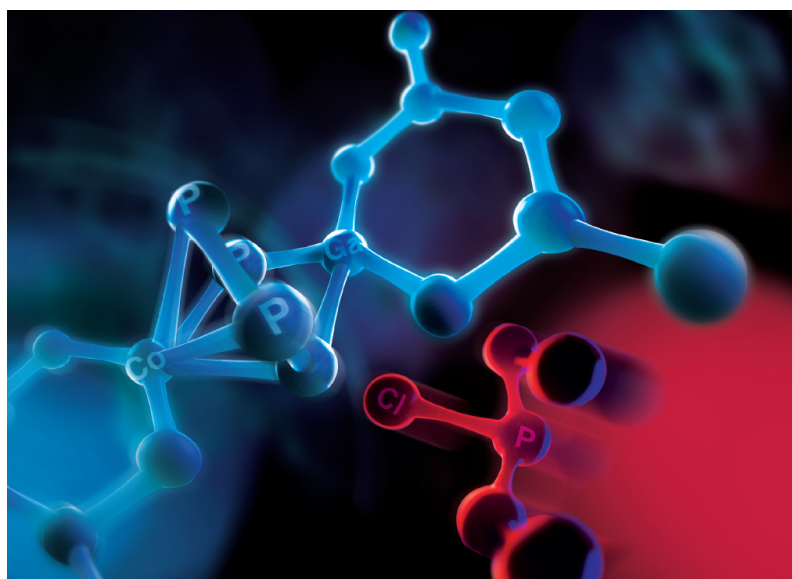
1.4 References

[1]   K. Ashley, D. Cordell, D. Mavinic, *Chemosphere* **2011**, *84*, 737.

[2]   A. F. Holleman, E. Wiberg, N. Wiberg, *Lehrbuch der Anorganischen Chemie,* 102. Aufl., de Gruyter, Berlin, **2007**, 743.

[3]   C. M. Hoidn, D. J. Scott, R. Wolf, *Chem. Eur. J.* **2020**, *27*, 1886.

[4]   J. Emsley, *The 13th element. The sordid tale of murder, fire, and Phosphorus*, John Wiley and sons, Inc, New York, **2000**.

[5]   L. Giusti, V. R. Landaeta, M. Vanni, J. A. Kelly, R. Wolf, M. Caporali, *Coord. Chem. Rev.* **2021**, *441*, 213927.

[6]   P. J. A. Withers, *Nat. Sustain.* **2019**, *2*, 1001.

[7]   J. C. Slootweg, *Angew. Chem. Int. Ed.* **2018**, *57*, 6386; *Angew. Chem.* **2018**, *130*, 6494.

[8]   (a) M. Peruzzini, L. Gonsalvi, A. Romerosa, *Chem. Soc. Rev.* **2005**, *34*, 1038; (b) B. M. Cossairt, N. A. Piro, C. C. Cummins, *Chem. Rev.* **2010**, *110*, 4164.

[9]   (a) M. Scheer, G. Balázs, A. Seitz, *Chem. Rev.* **2010**, *110*, 4236; (b) N. A. Giffin, J. D. Masuda, *Coord. Chem. Rev.* **2011**, *255*, 1342; (c) J. E. Borger, A. W. Ehlers, J. C. Slootweg, K. Lammertsma, *Chem. Eur. J.* **2017**, *49*, 11738-11746.

[10] S. Khan, S. S. Sen, H. W. Roesky, *Chem. Commun.* **2012**, *48*, 2169.

[11] (a) H. G. von Schnering, W. Hoenle, *Chem. Rev.* **1988**, *88*, 243; (b) S. Carenco, D. Portehault, C. Boissière, N. Mézailles, C. Sanchez, *Chem. Rev.* **2013**, *113*, 7981; (c) Y. Shi, B. Zhang, *Chem. Soc. Rev.* **2016**, *45*, 1529.

[12] selected examples: (a) H. Brake, E. Peresypkina, C. Heindl, A. V. Virovets, W. Kremer, M. Scheer, *Chem. Sci.* **2019**, *10*, 2940; (b) E. Peresypkina, C. Heindl, A. Virovets, H. Brake, E. Mädl, M. Scheer, *Chem. Eur. J.* **2018**, *24*, 2503; (c) F. Dielmann, E. V. Peresypkina, B. Krämer, F. Hastreiter, B. P. Johnson, M. Zabel, C. Heindl, M. Scheer, *Angew. Chem. Int. Ed.* **2016**, *55*, 14833; *Angew. Chem.* **2016**, *128*, 15053; (d) C. Heindl, E. V. Peresypkina, A. V. Virovets, W. Kremer, M. Scheer, *J. Am. Chem. Soc.* **2015**, *137*, 10938; (e) J. Bai , A. V. Virovets and M. Scheer , *Science*, **2003**, *300* , 781.

[13] M. Detzel, T. Mohr, O. J. Scherer, G. Wolmershäuser, *Angew. Chem. Int. Ed. Engl.* **1994**, *33*, 1110; *Angew. Chem.* **1994**, *106*, 1142.

[14] O. J. Scherer, T. Mohr, G. Wolmershäuser, *J. Organomet. Chem.* **1997**, *529*, 379.

[15] O. J. Scherer, R. Winter, G. Wolmershäuser, *Z. Anorg. Allg. Chem.* **1993**, *619*, 827.

[16] (a) M. Scheer, C. Troitzsch, P. G. Jones, *Angew. Chem. Int. Ed.* **1992**, *31*, 1377; *Angew. Chem.* **1992**, *104*, 1395; (b) M. Scheer, U. Becker, J. Magull, *Polyhedron* **1998**, *17*, 1983.

[17] (a) M. Scheer, U. Becker, J. C. Huffman, M. H. Chisholm, *J. Organomet. Chem.* **1993**, *461*, C1-C3; (b) M. Scheer, C. Troitzsch, L. Hilfert, M. Dargatz, E. Kleinpeter, P. G. Jones, J. Sieler, *Chem. Ber.* **1995**, *128*, 251.

[18] M. Scheer, U. Becker, E. Matern, *Chem. Ber.* **1996**, *129*, 721.

[19]   M. A. Alvarez, M. E. García, D. García-Vivó, A. Ramos, M. A. Ruiz, *Inorg. Chem.* **2011**, *50*, 2064.

[20]   M. A. Alvarez, M. E. García, D. García-Vivó, R. Lozano, A. Ramos, M. A. Ruiz, *Inorg. Chem.* **2014**, *53*, 11261.

[21]   M. A. Alvarez, M. E. García, R. Lozano, A. Ramos, M. A. Ruiz, *Inorg. Chem.* **2015**, *54*, 2455.

[22]   C. Schwarzmaier, A. Y. Timoshkin, G. Balázs, M. Scheer, *Angew. Chem. Int. Ed.* **2014**, *53*, 9077; *Angew. Chem.* **2017**, *126*, 9223.

[23]   R. Grünbauer, G. Balázs, M. Scheer, *Chem. Eur. J.* **2020**, *26*, 11722.

[24]   M. Di Vaira, P. Stoppioni, *Polyhedron* **1994**, *13*, 3045.

[25]   D. N. Akbayeva, *Russ. J. Coord. Chem.* **2007**, *33*, 661.

[26]   V. Mirabello, M. Caporali, V. Gallo, L. Gonsalvi, A. Ienco, M. Latronico, P. Mastrorilli, M. Peruzzini, *Dalton Trans.* **2011**, *40*, 9668.

[27]   M. Caporali, P. Barbaro, L. Gonsalvi, A. Ienco, D. Yakhvarov, M. Peruzzini, *Angew. Chem. Int. Ed.* **2008**, *47*, 3766; *Angew. Chem.* **2008**, *120*, 3826.

[28]   M. Modl, S. Heinl, G. Balázs, F. Delgado Calvo, M. Caporali, G. Manca, M. Keilwerth, K. Meyer, M. Peruzzini, M. Scheer, *Chem. Eur. J.* **2019**, *25*, 6300.

[29]   F. Dielmann, M. Sierka, A. V. Virovets, M. Scheer, *Angew. Chem. Int. Ed.* **2010**, *49*, 6860; *Angew. Chem.* **2010**, *38*, 7012.

[30]   J. Müller, M. Scheer, *Chem. Eur. J.* **2020**, *27*, 3675.

[31]   S. N. Konchenko, N. A. Pushkarevsky, M. T. Gamer, R. Köppe, H. Schnöckel, P. W. Roesky, *J. Am. Chem. Soc.* **2009**, *131*, 5740.

[32]   Selected examples: (a) A. S. P. Frey, F. G. N. Cloke, P. B. Hitchcock, J. C. Green, *New J. Chem.* **2011**, *35*, 2022; (b) W. Huang, P. L. Diaconescu, *Chem. Commun.* **2012**, *48*, 2216; (c) W. Huang, P. L. Diaconescu, *Eur. J. Inorg. Chem.* **2013**, *2013*, 4090; (d) B. M. Gardner, F. Tuna, E. J. L. McInnes, J. McMaster, W. Lewis, A. J. Blake, S. T. Liddle, *Angew. Chem. Int. Ed.* **2015**, *54*, 7068; *Angew. Chem.* **2015**, *127*, 7174; (e) A. Formanuik, F. Ortu, R. Beekmeyer, A. Kerridge, R. W. Adams, D. P. Mills, *Dalton Trans.* **2016**, *45*, 2390; (f) S. Du, J. Yin, Y. Chi, L. Xu, W.-X. Zhang, *Angew. Chem. Int. Ed.* **2017**, *56*, 15886; *Angew. Chem.* **2017**, *129*, 16102; (g) C. Schoo, S. Bestgen, R. Köppe, S. N. Konchenko, P. W. Roesky, *Chem. Commun.* **2018**.

[33]   T. Li, J. Wiecko, N. A. Pushkarevsky, M. T. Gamer, R. Köppe, S. N. Konchenko, M. Scheer, P. W. Roesky, *Angew. Chem. Int. Ed.* **2011**, *50*, 9491; *Angew. Chem.* **2011**, *123*, 9663.

[34]   T. Li, M. T. Gamer, M. Scheer, S. N. Konchenko, P. W. Roesky, *Chem. Commun.* **2013**, *49*, 2183.

[35]   T. Li, N. Arleth, M. T. Gamer, R. Köppe, T. Augenstein, F. Dielmann, M. Scheer, S. N. Konchenko, P. W. Roesky, *Inorg. Chem.* **2013**, *52*, 14231.

[36]   F. Dielmann, M. Sierka, A. V. Virovets, M. Scheer, *Angew. Chem. Int. Ed.* **2010**, *49*, 6860; *Angew. Chem.* **2010**, *38*, 7012.

[37]   N. Arleth, M. T. Gamer, R. Köppe, N. A. Pushkarevsky, S. N. Konchenko, M. Fleischmann, M. Bodensteiner, M. Scheer, P. W. Roesky, *Chem. Sci.* **2015**, *6*, 7179.

[38]   S. Yao, N. Lindenmaier, Y. Xiong, S. Inoue, T. Szilvási, M. Adelhardt, J. Sutter, K. Meyer and M. Driess, *Angew. Chem., Int. Ed.* **2015**, *54*, 1250; *Angew. Chem.* **2015**, *127*, 1266.

[39]   Y. Xiong, S. Yao, E. Bill, M. Driess, *Inorg. Chem.* **2009**, *48*, 7522.

[40]   Y. Xiong, S. Yao, M. Brym, M. Driess, *Angew. Chem. Int. Ed.* **2007**, *46*, 4511; *Angew. Chem.* **2007**, *119*, 4595.

[41]   C. M. Hoidn, C. Rödl, M. L. McCrea-Hendrick, T. Block, R. Pöttgen, A. W. Ehlers, P. P. Power, R. Wolf, *J. Am. Chem. Soc.* **2018**, *140*, 13195.

[42]   R. Yadav, T. Simler, B. Goswami, C. Schoo, R. Köppe, S. Dey, P. W. Roesky, *Angew. Chem. Int. Ed.* **2020**, *59*, 9443; *Angew. Chem.* **2020**, *132*, 9530.

[43]   R. Yadav, T. Simler, S. Reichl, B. Goswami, C. Schoo, R. Köppe, M. Scheer, P. W. Roesky, *J. Am. Chem. Soc.* **2020**, *142*, 1190.

[44]   R. Yadav, B. Goswami, T. Simler, C. Schoo, S. Reichl, M. Scheer, P. W. Roesky, *Chem. Commun.* **2020**, *56*, 10207.

Chapter 2   Construction of alkyl-substituted pentaphosphido ligands in the coordination sphere of cobalt

Abstract: Rare mono- and diorganopentaphosphido cobalt complexes are accessible by P–P condensation using the unprecedented, reactive cobalt-gallium tetraphosphido complex [K(dme)$_2${(^{Mes}BIAN)Co(μ-η^4:η^2-P$_4$)Ga(nacnac)}] (**2**). Compound **2** was prepared in good yield by reaction of [K(Et$_2$O){(^{Mes}BIAN)Co(η^4-1,5cod)}] (**1**, BIAN = bis(mesitylimino)acenaphthene diimine, cod = 1,5-cyclooctadiene) with [(nacnac)Ga(η^2-P$_4$)] (nacnac = CH[CMeN(2,6-iPr$_2$C$_6$H$_3$)]$_2$). Reactions with R$_2$PCl (R = iPr, tBu, and Cy) selectively afford [(^{Mes}BIAN)Co(*cyclo*-P$_5$R$_2$)] (**3a–c**), which feature η^4-coordinated 1,1-diorganopentaphosphido ligands. The mechanism of formation of these species has been studied by ^{31}P{^{1}H} NMR spectroscopy and DFT calculations. In the case of **3a** (R = iPr), it was possible to identify the intermediate [(^{Mes}BIAN)Co(μ-η^4:η^2-P$_5i$Pr$_2$)Ga(nacnac)] (**4**) by single-crystal X-ray diffraction. A related, monosubstituted organopentaphosphido cobalt complex [(^{Mes}BIAN)Co(μ-η^4:η^1-P$_5t$Bu)GaCl(nacnac)] (**5**) was isolated by reacting dichloroalkylphosphane tBuPCl$_2$ with **2**. Heterobimetallic complexes such as **2** thus may enable the targeted construction of a range of new metal-coordinated polyphosphorus frameworks by P–P condensation.

2.1   Introduction

Over the past decades, much effort has been invested into the synthesis of transition metal polyphosphido complexes. An impressive and structurally diverse array of early and late transition metal polyphosphorus species has become accessible. Most commonly, such species have been prepared by reaction of low-valent transition metal precursors with white phosphorus.[1],[2] While the functionalization of the polyphosphorus units derived from P_4 and in particular the construction of new polyphosphorus ligands, is an attractive target, successful examples of such transformations are surprisingly scarce. This paucity is largely due to the sluggish reactivity of known complexes with electrophiles such as halophosphanes. Seminal reports by Cummins and co-workers have demonstrated the synthetic potential of some early polyphosphido transition metalate anions.[2],[3],[4] The $[Nb(OAr)_3(\eta^3\text{-}P_3)]^-$ anion (**A**, Ar = 2,6-iPr$_2$C$_6$H$_3$) was used for generating a coordinated diphosphorus molecule *in situ* under mild conditions to access diphosphanes (Scheme 1a).[5] Cummins and co-workers also devised a synthetic cycle to yield useful phosphaalkynes, and they have been using their niobium phosphido complexes to access several further unprecedented P compounds, including the previously unknown AsP$_3$ molecule obtained by reacting **A** with arsenic trichloride.[3],[4],[6],[7]

While these results indicate that anionic polyphosphido complexes are attractive precursors for functionalization reactions, there have only been scattered examples with other metals.[8],[9],[10],[11] Peruzzini and Stoppioni reported the alkylation and hydrolysis of group 8 and 9 complexes, for example using ruthenium phosphido compounds (Scheme 1b).[8] Moreover, Scheer described the functionalization of *cyclo*-P$_5$ and *cyclo*-P$_3$ units in iron and nickel complexes by main group element nucleophiles such as amides, phosphanides, and hydrocarbyl anions (Scheme 1c).[9],[10] The same group recently reported the synthesis of the first triarsa- and the triphosphatrisilabenzenes by a successful metathesis reaction of a tetraphosphido zirconium complex with a chlorosilylene.[11]
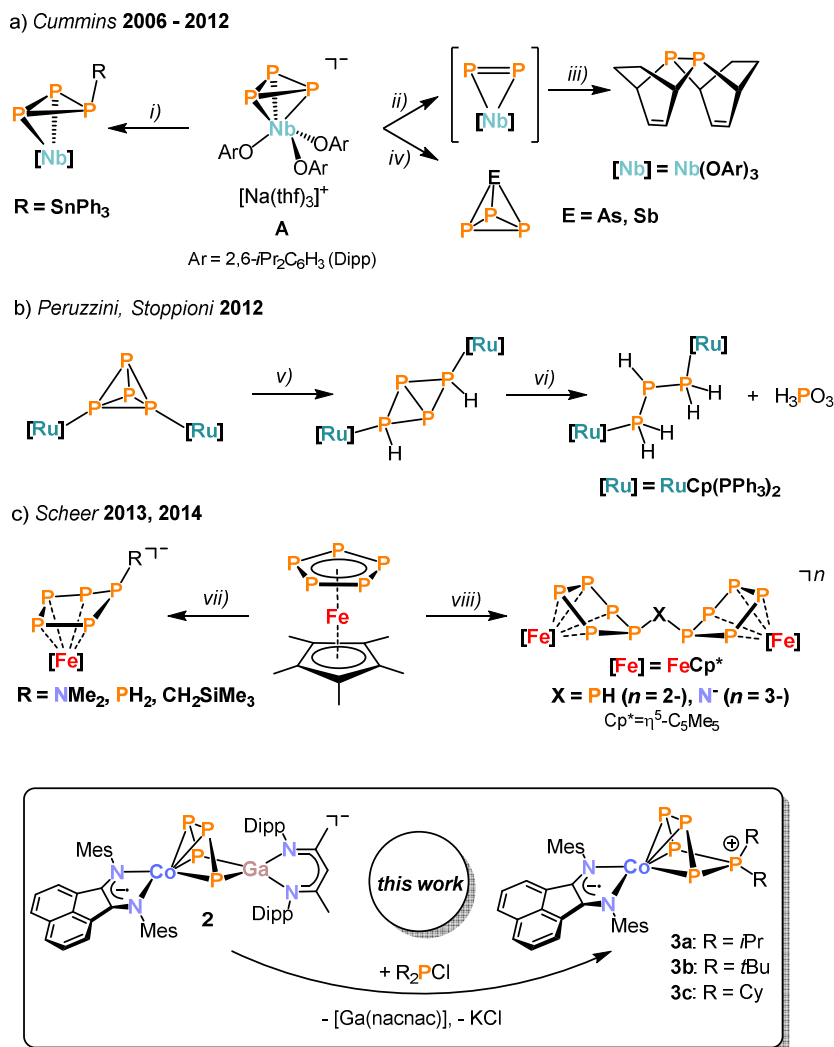
Scheme 1. Functionalization of activated phosphorus units; reagents and products: i) +Ph$_3$SnCl/−NaCl; ii) +IMo(N[tBu]Ar)$_3$/−NaI, −PMo(N{tBu}Ar)$_3$; iii) +1,3-cyclohexadiene, +C$_5$H$_5$NO/−C$_5$H$_5$N, −([Nb]O)$_2$; iv) +ECl$_3$/−NaCl, −[Nb]Cl$_2$; v) +I$_2$, +H$_2$O, +NaOTf; vi) +H$_2$O; vii) +LiCH$_2$SiMe$_3$ or +LiNMe$_2$ or +LiPH$_2$; viii) +NaNH$_2$; +LiPH$_2$. (top). Functionalization of anionic heterodinuclear tetraphosphido complexes by P–P condensation (bottom).

Here, we describe a new strategy for the synthesis of unprecedented polyphosphido complexes, which uses heterobimetallic complexes derived from P$_4$ as a tool for the construction of more extended P$_n$ units. As a proof of principle, we have synthesized the new CoGaP$_4$ complex [K(dme)$_2${(^{Mes}BIAN)Co(µ-η^4:η^2-P$_4$)Ga(nacnac)}] (**2**, ^{Mes}BIAN = 1,2-bis(2,4,6-trimethylphenylimino)acenaphthene, nacnac = CH[CMeN(2,6-iPr$_2$C$_6$H$_3$)]$_2$). This complex is a useful precursor for the targeted synthesis of the first diorganopentaphosphido complexes [(^{Mes}BIAN)Co(*cyclo*-P$_5$R$_2$)] (**3a**, R = iPr; **3b**, R = tBu; **3c**, R = Cy). ^{31}P NMR monitoring and the structural characterization of a presumed intermediate [(^{Mes}BIAN)Co(µ-η^4:η^2-P$_5i$Pr$_2$)Ga(nacnac)] (**4**) shed light on the reaction mechanism. Moreover, we report the synthesis of [(^{Mes}BIAN)Co(µ-η^4:η^1-P$_5t$Bu)GaCl(nacnac)] (**5**). The molecular structure of **5** is unusual in that it contains a disubstituted P$_5$ ligand with a single tBu moiety and a gallyl-substituent [GaCl(nacnac)].

2.2. Results and Discussion

Reaction of $[K(Et_2O)\{(^{Mes}BIAN)Co(\eta^4\text{-}1,5\text{-cod})\}]$ (**1**)[12],[13] with $[(nacnac)Ga(\eta^2\text{-}P_4)]$, obtained from white phosphorus and [Ga(nacnac)] according to a literature procedure,[14] in THF affords the heterodinuclear complex **2** (Scheme 2).
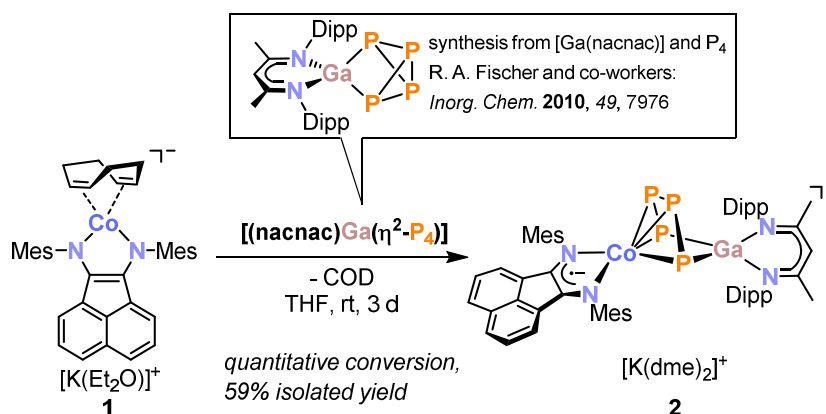
Scheme 2. Synthesis of $[K(dme)_2\{(^{Mes}BIAN)Co(\mu\text{-}\eta^4\text{:}\eta^2\text{-}P_4)Ga(nacnac)\}]$ (**2**).

$^{31}P\{^1H\}$ NMR monitoring indicates that the reaction is very selective and affords **2** as the sole P-containing product. After work-up, **2** was isolated in 59% yield by crystallization from DME/*n*-hexane. It is noteworthy that the 2,6-diisopropylphenyl-substituted complex $[K(thf)_2\{(^{Dipp}BIAN)Co(\mu\text{-}\eta^4\text{:}\eta^2\text{-}P_4)Ga(nacnac)\}]$ (**2'**) can be synthesized and isolated in an analogue manner in 53% yield by recrystallization from THF/*n*-hexane.[13] Both complexes are very similar, therefore subsequent reactivity studies focused exclusively on the Mes-substituted complex **2**. The molecular structure of **2** shows a chain of four P atoms sandwiched between cobalt and gallium. The terminal P–P bonds (P1–P2 2.1198(7) Å, P3–P4 2.1286(7) Å) are shorter than the internal P–P bond (P2–P3 2.1755(8) Å) and the distance between the terminal P atoms (P1–P4 3.3073(6) Å) is large. The dihedral angle P1, P2, P3, P4 with a value of 1.3° indicates that the P_4 chain is nearly planar. The C−C and C−N bond distances of the BIAN moiety suggest that it is present in its radical anionic form.[12] The coordination sphere of the potassium cation contains two DME molecules and two P atoms of the P_4 chain (K1–P4 3.3430(6) Å, K1–P3 3.7168(7) Å, cf. the sum of the van-der-Waals radii of K and P: 4.63 Å).[15]
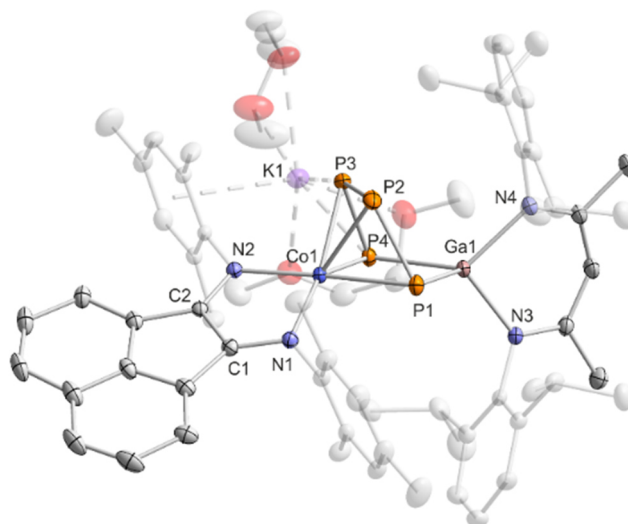
Figure 1. Solid-state molecular structure of $[K(dme)_2\{(^{Mes}BIAN)Co(\mu-\eta^4:\eta^2-P_4)Ga(nacnac)\}]$ **(2)** hydrogen atoms are omitted for clarity and thermal ellipsoids are drawn at the 40% probability level; selected bond lengths [Å] and angles [°]: P1–P2 2.1198(7), P2–P3 2.1755(8), P3–P4 2.1286(7), P1···P4 3.3073(6), P4–Ga1 2.3328(5), P1–Ga1 2.3179(5), Ga1–N3 1.991(1), Ga1–N4 2.014(2), Co1–P1 2.3514(6), Co1–P2 2.3098(6), Co1–P3 2.3117(5), Co1–P4 2.3961(6), Co1–N1 1.918(2), Co1–N2 1.948(2), N1–C1 1.337(2), N2–C2 1.334(2), C1–C2 1.411(3), K1–P3 3.7168(7); K1–P4 3.33073(6), Ga1–P4–P3 94.85(2), P4–P3–P2 106.97(3), P3–P2–P1 103.92(3), P2–P1–Ga1 97.31(2), P1–Ga1–P4 90.66(2); bond distances and angles of derivative **2'** are presented in the SI (see Figure S39, SI).[13]

A few transition metal complexes with structures related to **2** are known. For example, Driess and co-workers synthesized the heterobinuclear complex $[LSi(\mu-\eta^2:\eta^2-P_4)Ni(nacnac)]$ $(L = CH[(C=CH_2)CMe][N(2,6-iPr_2C_6H_3)]_2)$. In contrast to **2**, this complex features a more weakly activated, "butterfly"-P_4 ligand (P1–P4 = 2.335(4) Å).[16] Scherer's dirhodium complex $[(Cp^RRh)(\mu-\eta^4:\eta^2)P_4\{Rh(CO)Cp^R\}]$ $(Cp^R = \eta^5-C_5Me_4Et)$ shows a very similar motif with a P_4 chain (P–P 2.150(3) Å – 2.160(3) Å) coordinating to two rhodium centers in an η^2- and an η^4-fashion, respectively.[17] A dizirconium complex with a similar alternating short-long-short P_4 unit (2.137(1) Å – 2.152(1) Å) was described by Fryzuk and co-workers.[18] Further examples of transition metal complexes with bridging *catena*-P_4 units are diiron species reported by Scherer,[19] Miluykov,[20] and Walter.[21] Moreover, Konchenko, Scheer, and Roesky synthesized $[(Cp'''Co)_2(\mu-\eta^2:\eta^2-P_2)_2]$ $(Cp''' = \eta^5-1,2,4-tBu_3C_5H_2)$ *via* an unusual intramolecular P–P coupling process.[22]

In agreement with the solid-state structure, the $^{31}P\{^1H\}$ NMR spectrum of **2** in THF-d_8 (Figure 2 and Figure S6, SI) shows an AA'XX' spin system.[13] DFT calculations indicate that the multiplet at low frequency ($\delta = -125.4$ ppm) can be assigned to the terminal P atoms ($P_{xx'}$), while the multiplet at high frequency can be assigned to the internal P atoms ($P_{AA'}$, see the SI for details).[13] Iterative fitting of the $^{31}P\{^1H\}$ NMR spectrum revealed a $^1J_{AX'}$ coupling constant of -450.5 Hz, which is 70 Hz larger in magnitude than the $^1J_{AA'}$ coupling constant ($^1J_{AA'} = -380.5$ Hz). The $^2J_{AX'}$ (6.6 Hz) and $^3J_{XX'}$ (-7.2 Hz) couplings are rather small which is in line with the constrained alignment of the P atoms in the P_4 chain observed in the solid-state structure, causing an antiparallel orientation of the lone pairs.[23]
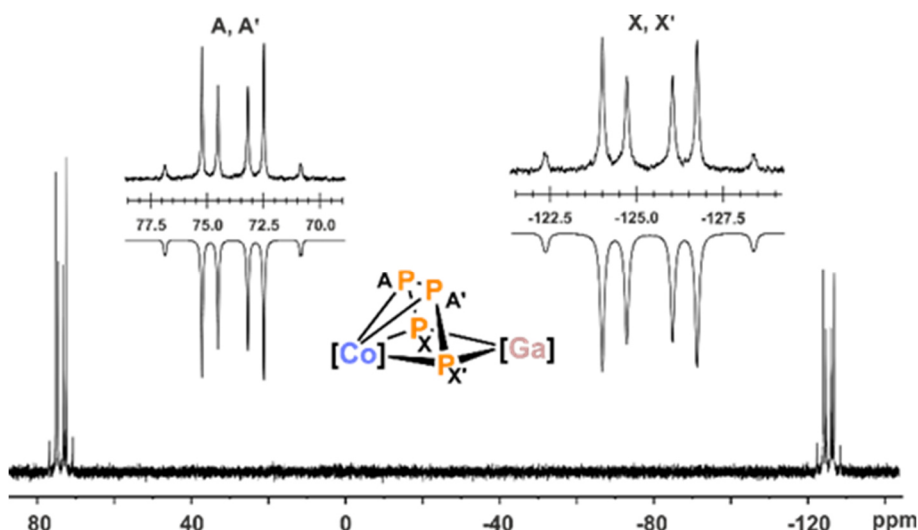
Figure 2. $^{31}P\{^1H\}$ NMR spectrum of compound **2** with nuclei assigned to an AA'XX' spin system; insets: extended signals (upwards) and simulations (downwards); $\delta(P_{AA'}) = 74.0$ ppm, $\delta(P_{XX'}) = -125.4$ ppm, $^1J_{AA'} = {}^1J_{A'A} = -380.5$ Hz, $^1J_{AX} = {}^1J_{A'X'} = -450.5$ Hz, $^2J_{AX'} = {}^2J_{A'X} = 6.6$ Hz, $^3J_{XX'} = {}^3J_{X'X} = -7.2$ Hz; the spectrum of **2'** is very similar (see Figure S11, SI);[13] [Co] = (^{Mes}BIAN)Co, [Ga] = (nacnac)Ga.

Initial reactivity studies of **2** focused on reactions with dialkylchlorophosphanes. $^{31}P\{^1H\}$ NMR monitoring of the reactions of **2** with R_2PCl (R = *i*Pr, *t*Bu, and Cy) suggests the formation of pentaphosphido complexes $[(^{Mes}BIAN)Co(\eta^4-P_5R_2)]$ (**3a**, R = *i*Pr; **3b**, R = *t*Bu; **3c**, R = Cy, Scheme 3). Chromatographic work-up is necessary to remove the by-product [Ga(nacnac)]. Recrystallization from *n*-hexane (**3a,b**) or *n*-hexane/toluene (**3c**) gave analytically pure, cyan-colored crystals of the products **3a-c** in moderate yields (26% to 31%).
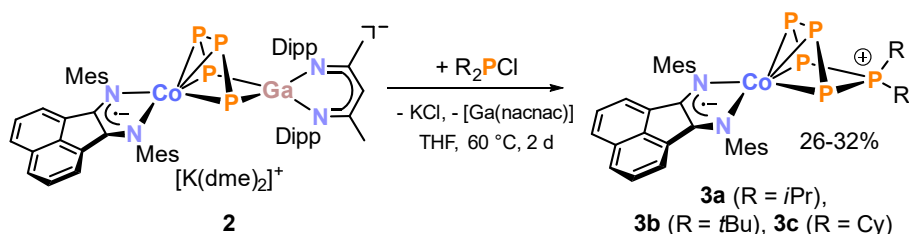
Scheme 3. Synthesis of $[(^{Mes}BIAN)Co(\eta^4-P_5R_2)]$ [R = *i*Pr (**3a**), R = *t*Bu (**3b**), R = Cy (**3c**)].

According to single-crystal XRD studies, compounds **3a-c** are isostructural and feature an unprecedented η^4-coordinated *cyclo*-P_5R_2 ligand in an envelope conformation. Interestingly, **3a-c** may be regarded as transition metal complexes of the corresponding $[P_5R_2]^+$ cage cations,[24],[25],[26],[27] but in fact they show structural isomers of these cations previously prepared by phosphenium ion insertion into P_4. The molecular structure of **3a** is shown in Figure 3, while those of **3b** and **3c** are presented in the SI (Figures S40 and S41, SI).[13] The structural parameters of the BIAN ligand are similar to those of **2** (*vide supra*). The coordinating phosphorus atoms P1, P2, P3, and P4 form an almost planar arrangement (Co−P 2.3442(1) Å − 2.3720(1) Å for **3a**). The coordinated P−P bonds show a short-long-short pattern (**3a**: P1–P2 2.12969(2) Å, P2–P3 2.1576(2) Å, P3–P4 2.1297(2) Å), which indicates a diene-like arrangement. Scheer's salts $[Li(Et_2O)][Cp^*Fe(\eta^4-P_5CH_2SiMe_3)]$, $[Na_3(dme)_5][\{Cp^*Fe(\eta^4-P_5)\}_2N]$ and

[Li$_2$(dme)$_6$][{Cp*Fe(η^4-P$_5$)}$_2$PH] (*vide supra*, Figure 1c) display a similar envelope conformation of the monosubstituted *cyclo*-P$_5$R units.[10]

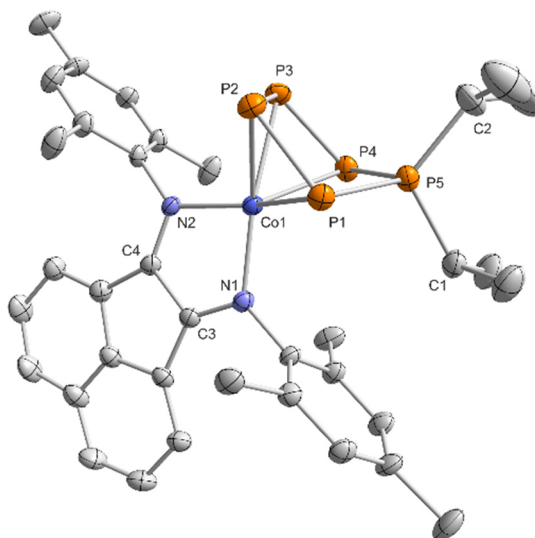**Figure 3.** Solid-state molecular structure of [(^{Mes}BIAN)Co(η^4-P$_5$*i*Pr$_2$)] (**3a**); hydrogen atoms are omitted for clarity and thermal ellipsoids are drawn at the 40% probability level; selected bond lengths [Å] and angles [°]: P1–P2 2.1297(2), P2–P3 2.1576(2), P3–P4 2.1297(2), P4–P5 2.1347(2), P5–P1 2.1506(1), P5–C1 1.8423(1), P5–C2 1.8458(1), Co1–P1 2.3720(1), Co1–P2 2.3442(1), Co1–P3 2.3447(2), Co1–P4 2.3595(2), Co1–N1 1.9104(1), Co1–N2 1.9480(1), N1–C3 1.32559(8), N2–C4 1.32069(8), C3–C4 1.4366(1); P1–P2–P3 103.926(5), P2–P3–P4 107.049(5), P3–P4–P5 98.104(6), P4–P5–P1 99.966(5), P5–P1–P2 100.689(5), C1–P5–C2 113.0644(5); bond distances and angles of derivatives **3b,c** are presented in the SI (see Figure S40 and S41, SI).[13]

The ^{31}P{^{1}H} NMR spectra of **3a-c** in C$_6$D$_6$ (Figure 4 and Figures S16, S21, and S26, SI)[13] show very similar AMM'XX' spin systems that are consistent with molecular structures observed in the solid-state. The spectrum of **3a** will be discussed in more detail here. The tetracoordinate, diorganosubstituted phosphorus nucleus (P$_A$) resonates at higher frequency (δ = 161.0 ppm for **3a**) compared to the resonances of the metal-coordinated P atoms (δ = 88.6 ppm and 111.4 ppm, respectively, for **3a**). The J_{PP} coupling constants for the derivatives **3a-c** were obtained by the iterative simulation of the ^{31}P{^{1}H} NMR spectra.[13] The one-bond P–P coupling constants of the coordinated P atoms ($^1J_{MM'}$ = −380.6 Hz and $^1J_{MX}$ = −414.2 Hz for **3a**) are comparable to those reported for [Li(Et$_2$O)][Cp*Fe(η^4-P$_5$CH$_2$SiMe$_3$)] ($^1J_{MM'}$ = −409.7 Hz, $^1J_{MX}$ = −382.6 Hz), but the $^1J_{AX}$ coupling constant (−392.9 Hz) is substantially larger (−275.3 Hz for [Li(Et$_2$O)][Cp*Fe(η^4-P$_5$CH$_2$SiMe$_3$)]).[10] The values of the $^2J_{PP}$ ($^2J_{MX'}$ = 39.9 Hz, $^2J_{AM}$ = 10.4 Hz, and $^2J_{XX'}$ = 9.2 Hz for **3a**) are in the usual range.
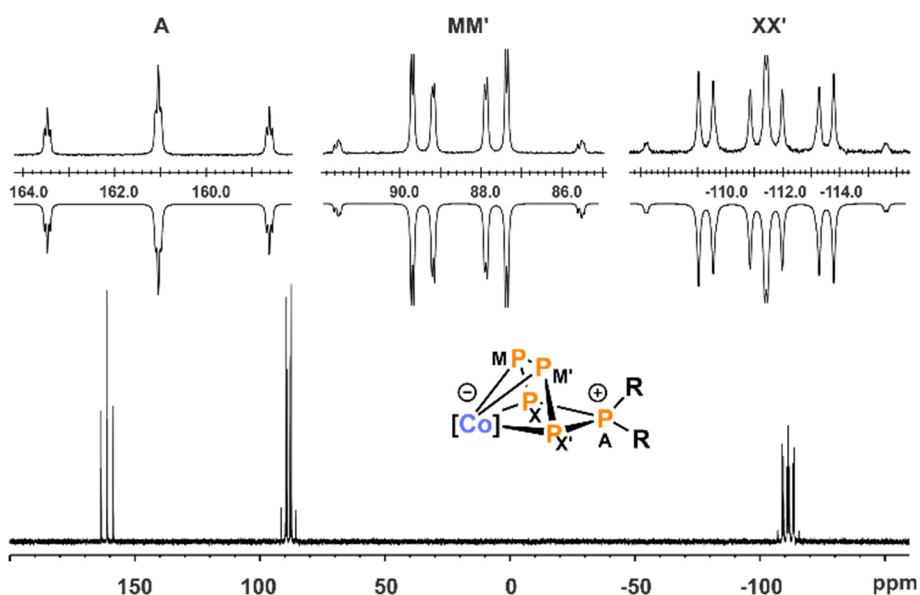
Figure 4. ^{31}P{^{1}H} NMR spectrum of compound **3a** with nuclei assigned to AMM'XX' spin system; insets: extended signals (upwards) and simulations (downwards); $\delta(P_A) = 161.0$ ppm, $\delta(P_{MM'}) = 88.6$ ppm, $\delta(P_{XX'}) = -111.4$ ppm, $^1J_{AX} = {}^1J_{AX'} = -392.9$ Hz, $^1J_{MM'} = -380.6$ Hz, $^1J_{MX} = {}^1J_{M'X'} = -414.2$ Hz, $^2J_{MX'} = {}^2J_{M'X} = 39.9$ Hz, $^2J_{AM} = {}^2J_{AM'} = 10.4$ Hz, $^2J_{XX'} = 9.2$ Hz; the spectra of **3b,c** are very similar (see Figure S21, S26, SI);[13] [Co] = (^{Mes}BIAN)Co.

In order to gain more insight in the mechanism of formation of the diorganopentaphosphido ligands in **3a-c**, we monitored the reactions of **2** with R$_2$PCl (R = *t*Bu and *i*Pr) by ^{31}P{^{1}H} NMR spectroscopy. While we did not detect any intermediate in the reaction with *t*Bu$_2$PCl, we observed two intermediate species in case of *i*Pr$_2$PCl (Figure 5). The starting materials are consumed within ten minutes, while two similar ABCDE spin systems arise that are presumably assigned to the two intermediates **Int-A** and **Int-B**. Monitoring the reaction by ^{31}P{^{1}H} VT NMR spectroscopy initially shows the exclusive formation of intermediate **Int-A** at −30 °C. Upon warming the reaction mixture above 0 °C signals of **Int-B** arise in the ^{31}P{^{1}H} NMR spectra. According to ^{31}P{^{1}H} NMR integration, **Int-A** and **Int-B** are present in a 4:1 ratio at room temperature independent of the reaction time (see Figure S36, SI).[13] It is difficult to determine the precise molecular structures of **Int-A** and **Int-B** only from ^{31}P NMR investigation, but fortunately one of the intermediates crystallized from the reaction mixture and was characterized as [(^{Mes}BIAN)Co(μ-η^4:η^2-P$_5$*i*Pr$_2$)Ga(nacnac)] (**4**, Figure 6).[13]
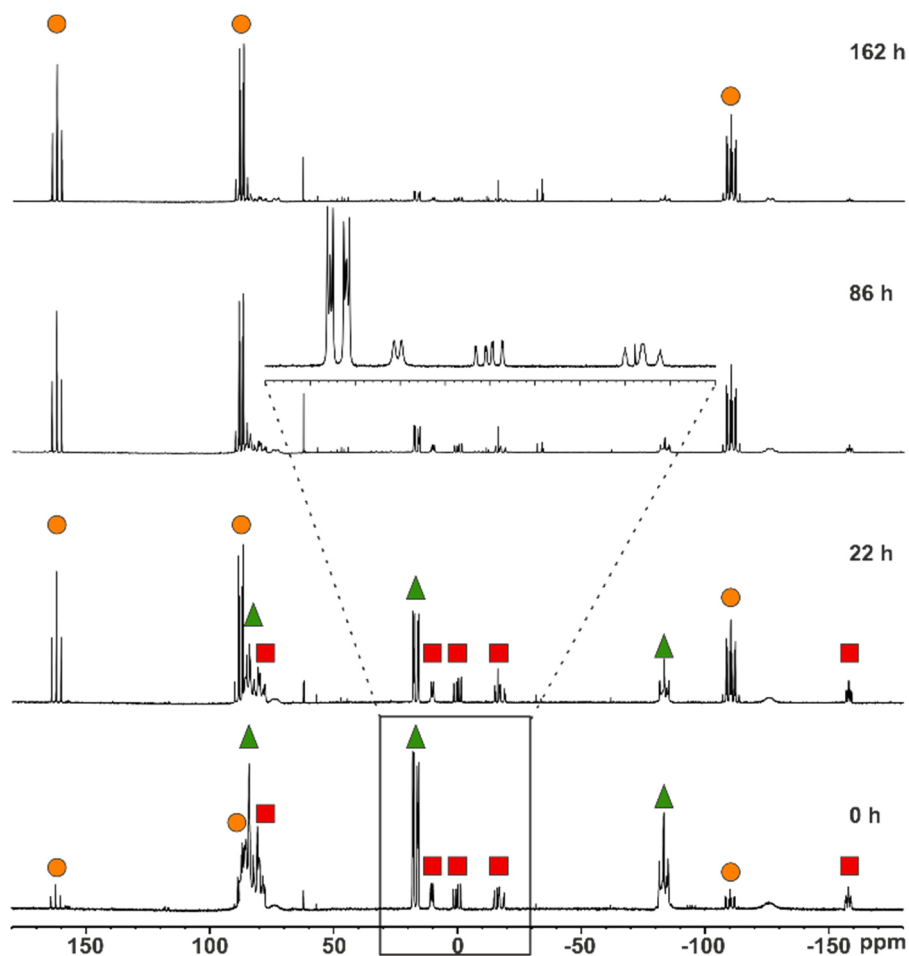
Figure 5. $^{31}P\{^1H\}$ NMR monitoring of the reaction of **2** dissolved in THF-d_8 with iPr$_2$PCl in a 1:1 ratio at room temperature over seven days; resonances marked with ● are assigned to product $[(^{Mes}BIAN)Co(\eta^4-P_5iPr_2)]$ (**3a**) whereas those marked with ▲ (**Int-A**) and ■ (**Int-B**) are assigned to intermediates; inset: section from 25 ppm to −25 ppm.

The $^{31}P\{^1H\}$ NMR spectrum of crystalline **4** in C$_6$D$_6$ recorded at room temperature after 10 minutes showed two sets of resonances which were identified as **Int-A** and **Int-B** in the same ratio as observed in the reaction mixture. Based on our calculated ^{31}P NMR chemical shieldings of **4**, it seems plausible that intermediate **Int-A** can be assigned to **4** (see the SI for details).[13] Although the exact structure of **Int-B** remains presently obscure, it seems plausible that **Int-B** is an isomer of **Int-A**. Solid **4**, when stored under an inert atmosphere, is stable for several weeks without decomposition, but it irreversibly converts to **3a** when dissolved in C$_6$D$_6$ at ambient temperature over the course of five days as indicated by $^{31}P\{^1H\}$ NMR monitoring. Based on these data, a mechanism of formation can be proposed for **3a** (Scheme 4), which involves a pre-equilibrium between **Int-A** and **Int-B**. The latter species slowly converts into **3a** by dissociation of [Ga(nacnac)]; this process appears to be irreversible. The molecular structure of **4** confirms that P–P bond formation has already occurred in this intermediate (Figure 6). The structure is in line with the $^{31}P\{^1H\}$ NMR data (ABCDE spin system, *vide infra*) and shows an almost planar P$_5$ chain which coordinates to cobalt *via* the four unsubstituted P atoms (P1–P2 2.122(1) Å, P2−P3

2.159(2) Å, and P3−P4 2.164(1) Å). The PiPr$_2$ unit adopts the terminal position (P4–P5 2.239(1) Å) and does not show close contacts to cobalt or gallium.

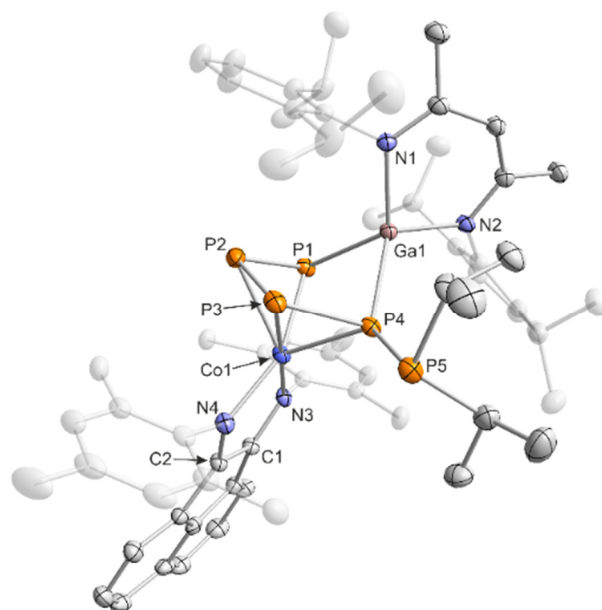**Figure 6.** Solid-state molecular structure of [(^{Mes}BIAN)Co(µ-η^4:η^2-P$_5i$Pr$_2$)Ga(nacnac)] (**4**); hydrogen atoms are omitted for clarity and thermal ellipsoids are drawn at the 40% probability level; selected bond lengths [Å] and angles [°]: P1–P2 2.122(1), P2–P3 2.159(2), P3–P4 2.164(1), P4–P5 2.239(1), P1–Ga1 2.3320(9), P4–Ga1 2.418(1), Ga1–N1 1.992(3), Ga1–N2 1.974(3), Co1–P1 2.348(2), Co1–P2 2.337(1), Co1–P3 2.306(1), Co1–P4 2.353(1), Co1–N3 1.919(3), Co1–N4 1.963(3), C1–N3 1.335(4), C2–N4 1.323(4), C1–C2 1.422(5), P1–P2–P3 103.59(5); P2–P3–P4 102.46(5), P3–P4–P5 93.59(5), P5–P4–Ga1 133.22(5), P1–Ga1–P5 82.28(3), Ga1–P1–P2 97.13(4).

The [Ga(nacnac)] moiety is η^2-coordinated to the 1,4-positions of the P$_5$ chain (P1–Ga1 2.3320(9) Å, P4–Ga1 2.418(1) Å) and the C–N and C–C bond lengths of the BIAN moiety are again comparable to **2** and **3a-c**, suggesting that the ligand is present in its radical monoanionic form.
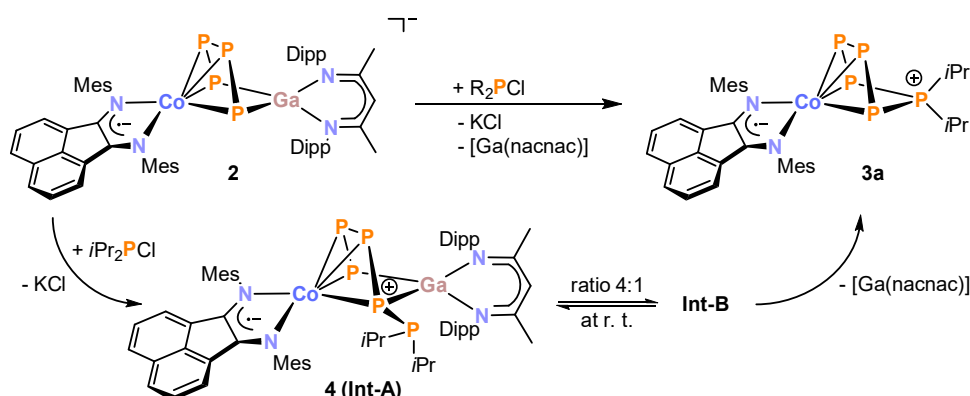
Scheme 4. Proposed mechanism of the condensation of iPr$_2$PCl with **2** leading to product **3a**. ^{31}P{^{1}H} NMR monitoring revealed two intermediates **Int-A** and **Int-B** in a 4:1 integral ratio at room temperature.

While dialkylchlorophosphanes smoothly react with **2** to form a pentaphosphido framework, reactions with mono- and diarylchlorophosphanes result in the formation of intractable products. By contrast, the reaction with tBuPCl$_2$ (Scheme 5) readily affords tBu-substituted [(^{Mes}BIAN)Co(µ-η^4:η^1-P$_5t$Bu)GaCl(nacnac)] (**5**) as the sole P-containing

species detected by $^{31}P\{^1H\}$ NMR. An unidentified paramagnetic by-product was detected in the ^1H NMR spectrum of the crude reaction mixture. This undesired species can be completely removed by several recrystallization steps from toluene. This work-up procedure is the reason for the relatively low yield (6%) for the spectroscopically and analytically pure isolated compound **5**.
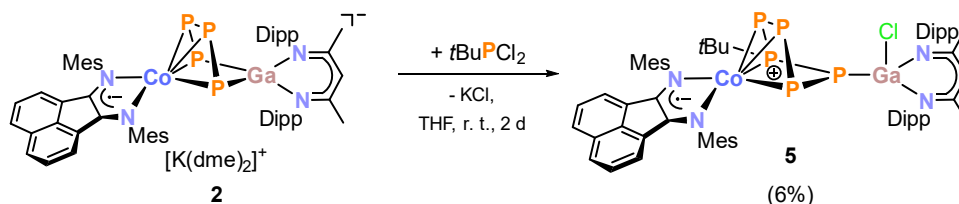
Scheme 5. Synthesis of [(^{Mes}BIAN)Co(μ-η^4:η^1-P$_5$tBu)GaCl(nacnac)] (**5**).

The synthesis of **5** nevertheless is remarkable because it shows that P–P condensations also occur with monoalkyldichlorophanes. The molecular structure of **5** determined by single-crystal XRD (Figure 7) features an η^4:η^1-coordinated *cyclo*-P$_5$tBu ligand similar to the dialkyl-substituted ligands in **3a-c**. The phosphorus atoms P2, P3, P4, and P5 coordinated to cobalt form an almost planar arrangement (Co−P 2.33156(7) Å − 2.37439(6) Å). Notably, the P atom at the tip of the *cyclo*-P$_5$ envelope is coordinated to the gallium atom of [GaCl(nacnac)] (P1–Ga1–P5 82.28(3)°, Ga1–P1–P5 115.834(2)°, and Ga1–P1–P2 112.634(2)°). The structural parameters of the BIAN ligand are close to **2** and **3a-c** (*vide supra*). The P–P bond distances (P1–P5 2.14148(6) Å, P2–P3 2.14129(5) Å, P3–P4 2.13102(7) Å, and P4–P5 2.13310(5) Å) are in a very close range except for the P1−P2 bond (2.19903(6) Å).
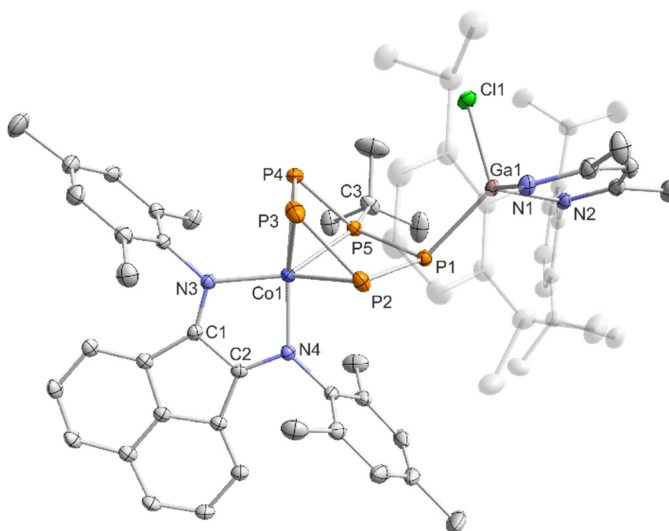

Figure 7. Solid-state molecular structure of [(^{Mes}BIAN)Co(μ-η^4:η^1-P$_5$tBu)GaCl(nacnac)] (**5**); hydrogen atoms are omitted for clarity and thermal ellipsoids are drawn at the 40% probability level; selected bond lengths [Å] and angles [°]: P1–P2 2.19903(6), P2–P3 2.14129(5), P3–P4 2.13102(7), P4–P5 2.13310(5), P5–P1 2.14148(6), P1–Ga1 2.34200(6), P5–C3 1.89094(6), Ga1–N1 1.94202(6), Ga1–N2 1.96271(5), Ga1–Cl1 2.20080(5), Co1–P2 2.33156(7), Co1–P3 2.33788(6), Co1–P4 2.37439(6), Co1–P5 2.23375(6), Co1–N3 1.95761(5), Co1–N4 1.90519(4), C1–N3 1.31832(3), C2–N4 1.32622(3), C1–C2 1.42740(3); P1–P2–P3 113.062(2), P2–P3–P4 103.661(2), P3–P4–P5 97.566(2), P4–P5–P1 118.046(2), P5–P1–P2 84.471(2), P4–P5–C3 112.065(2), P4–P5–C3 115.399(2), Ga1–P1–P5 115.834(2), Ga1–P1–P2 112.634(2).

Compound **5** gives rise to an ABEMX spin system in the ^{31}P{^{1}H} NMR spectrum, which was simulated using an iterative fitting procedure (Figure 8). Based on the observed P–P couplings and an additional ^{31}P-^{1}H HMBC spectrum, the resonance at 70.3 ppm (P$_A$) can be assigned to *t*Bu-substituted phosphorus atom. At room temperature, this resonance is broad; hence, the simulation was carried out for the spectrum recorded at –60 °C. The resulting ^{31}P NMR data suggest that the signals at 12.0 ppm (P$_M$) and –66.8 ppm (P$_X$) can be assigned to the P atoms adjacent to the *t*Bu-substituted P atom (P$_A$, Figure S34, SI).[13]
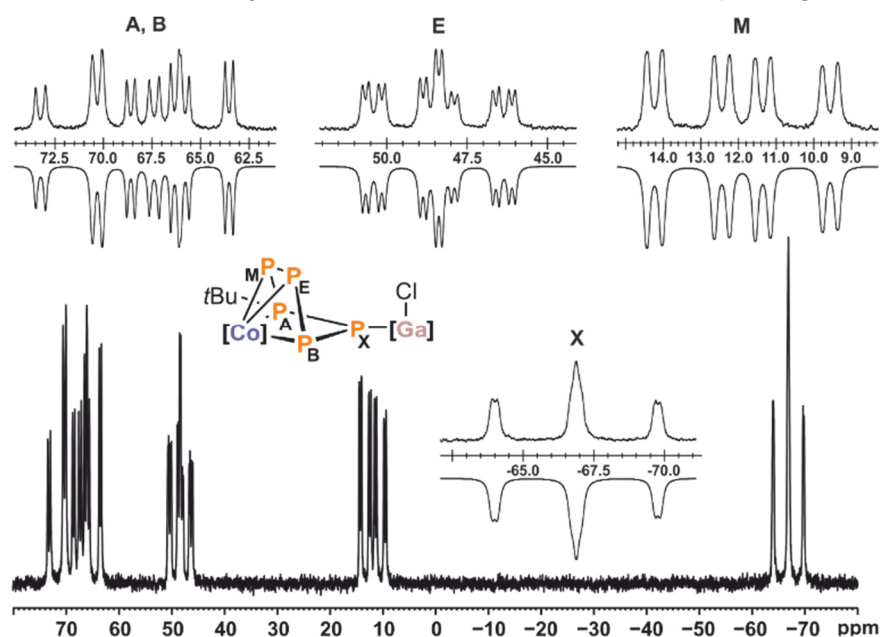

Figure 8. ^{31}P{^{1}H} NMR spectrum of compound **5** at −60°C with nuclei assigned to ABEMX spin system; insets: extended signals (upwards) and simulations (downwards); δ(P$_A$) = 70.3 ppm, δ(P$_B$) = 66.0 ppm, δ(P$_E$) = 48.4 ppm, δ(P$_M$) = 12.0 ppm, δ(P$_X$) = −66.8 ppm, ^{1}J$_{AM}$ = −466.3 Hz, ^{1}J$_{AX}$ = −481.4 Hz, ^{1}J$_{BX}$ = −455.1 Hz, ^{1}J$_{BE}$ = −367.0 Hz, ^{1}J$_{EM}$ = −291.6 Hz, ^{2}J$_{AE}$ = 81.8 Hz, ^{2}J$_{AB}$ = 8.2 Hz, ^{2}J$_{BM}$ = 67.7 Hz, ^{2}J$_{EX}$ = 33.7 Hz, ^{2}J$_{MX}$ = 12.2 Hz; [Co] = (^{Mes}BIAN)Co, [Ga] = (nacnac)Ga.

2.3 Conclusion

The anionic cobalt-gallium tetraphosphido complex **2** is readily accessible by reaction of [K(Et$_2$O){(^{Mes}BIAN)Co(η^4-1,5-cod)}] (**1**) with [(nacnac)Ga(η^2-P$_4$)]. This unique heterobimetallic complex features an activated *catena*-P$_4$ unit amenable to P–P condensation reactions. Remarkably, **2** readily forms unprecedented organosubstituted pentaphosphido complexes **3a-c**, **4**, and **5** with R$_2$PCl (R = *i*Pr, *t*Bu, and Cy) and *t*BuPCl$_2$. Related metal-free [P$_5$R$_2$]$^+$, [P$_6$R$_4$]$^{2+}$, and [P$_7$R$_6$]$^{2+}$ cations have been prepared by phosphenium cation insertion into P$_4$;[24],[25],[26],[27] metal complexes with monosubstituted P$_n$R ligands were accessed by reaction of nucleophiles, e.g. alkali metal alkyls, amides and phosphides, on pentaphosphaferrocene and related complexes.[9],[10] Notwithstanding these previous examples, the results reported in this study show that P–P condensation reactions of anionic polyphosphido complexes and halophosphane are a potentially powerful synthetic approach which can give rise to unusual new polyphosphorus species. NMR and

single-crystal XRD experiments have revealed that P–P bond formation is facile as shown by the formation of intermediate **4** characterized by X-ray crystallography. By contrast, the subsequent elimination of the [Ga(nacnac)] building block from **4** seems to be associated with a considerable barrier. The reaction properties of **3a-c** and **5** are currently under investigation. Moreover, efforts are underway to extend and fine tune the P–P condensation approach for the synthesis of further unprecedented polyphosphorus compounds.

2.4   Notes and References

[1]   (a) M. Caporali, L. Gonsalvi, A. Rossin and M. Peruzzini, *Chem. Rev.* **2010**, *110*, 4178; (b) M. Scheer, G. Balázs and A. Seitz, *Chem. Rev.* **2010**, *110*, 4236; (c) M. Peruzzini, L. Gonsalvi and A. Romerosa, *Chem. Soc. Rev.* **2005**, *34*, 1038; (d) N. A. Giffin and J. D. Masuda, *Coord. Chem. Rev.* **2011**, *255*, 1342.

[2]   B. M. Cossairt, N. A. Piro and C. C. Cummins, *Chem. Rev.* **2010**, *110*, 4164.

[3]   J. S. Figueroa and C. C. Cummins, *Dalton Trans.* **2006**, 2161.

[4]   J. S. Figueroa and C. C. Cummins, *J. Am. Chem. Soc.* **2004**, *126*, 13916.

[5]   (a) N. A. Piro, J. S. Figueroa, J. T. McKellar and C. C. Cummins, *Science* **2006**, *313*, 1276. (b) B. M. Cossairt and C. C. Cummins, *Angew. Chem. Int. Ed.* **2010**, *49*, 1595; *Angew. Chem.*, **2010**, *122*, 1639; (c) A. Velian and C. C. Cummins, *Chem. Sci.* **2012**, *3*, 1003.

[6]   B. M. Cossairt, M.-C. Diawara and C. C. Cummins, *Science* **2009**, *323*, 602.

[7]   (a) J. S. Figueroa and C. C. Cummins, *Angew. Chem. Int. Ed.* **2004**, *43*, 984; *Angew. Chem.* **2004**, *116*, 1002; (b) D. Tofan, B. M. Cossairt and C. C. Cummins, *Inorg. Chem.* **2011**, *50*, 12349.

[8]   (a) P. Barbaro, C. Bazzicalupi, M. Peruzzini, S. Seniori Costantini and P. Stoppioni, *Angew. Chem. Int. Ed.* **2012**, *51*, 8628; *Angew. Chem.* **2012**, *124*, 8756; (b) P. Barbaro, M. Di Vaira, M. Peruzzini, S. Seniori Costantini and P. Stoppioni, *Chem. Eur. J.*, **2007**, *13*, 6682; (c) M. Di Vaira, P. Frediani, S. S. Costantini, M. Peruzzini and P. Stoppioni, *Dalton Trans.* **2005**, 2234; (d) M. Di Vaira, M. Peruzzini, S. Seniori Costantini and P. Stoppioni, *J. Organomet. Chem.* **2006**, *691*, 3931; (e) P. Barbaro, M. Peruzzini, J. A. Ramirez and F. Vizza, *Organometallics* **1999**, *18*, 4237; (f) P. Barbaro, A. Ienco, C. Mealli, M. Peruzzini, O. J. Scherer, G. Schmitt, F. Vizza, G. Wolmershäuser, *Chem. Eur. J.* **2003**, *9*, 5196; (g) M. Peruzzini, J. A. Ramirez and F. Vizza, *Angew. Chem. Int. Ed.* **1998**, *37*, 2255; *Angew. Chem.* **1998**, *110*, 2376.

[9]   (a) E. Mädl, G. Balázs, E. V. Peresypkina and M. Scheer, *Angew. Chem. Int. Ed.* **2016**, *55*, 7702; *Angew. Chem.* **2016**, *128*, 7833; (b) M. V. Butovskiy, G. Balázs, M. Bodensteiner, E. V. Peresypkina, A. V. Virovets, J. Sutter and M. Scheer, *Angew. Chem. Int. Ed.* **2013**, *52*, 2972; *Angew. Chem.* **2013**, *125*, 3045; (c) R. F. Winter and W. E. Geiger, *Organometallics* **1999**, *18*, 1827.

[10]   E. Mädl, M. V. Butovskii, G. Balázs, E. V. Peresypkina, A. V. Virovets, M. Seidl and M. Scheer, *Angew. Chem. Int. Ed.* **2014**, *53*, 7643; *Angew. Chem.* **2014**, *126*, 7774.

[11]   A. E. Seitz, M. Eckhardt, A. Erlebach, E. V. Peresypkina, M. Sierka and M. Scheer, *J. Am. Chem. Soc.* **2016**, *138*, 10433.

[12]   S. Pelties, T. Maier, D. Herrmann, B. d. Bruin, C. Rebreyend, S. Gärtner, I. G. Shenderovich and R. Wolf, *Chem. Eur. J.* **2017**, *23*, 6094.

[13]   See the Supporting Information for further details.

[14]   (a) G. Prabusankar, A. Doddi, C. Gemel, M. Winter and R. A. Fischer, *Inorg. Chem.* **2010**, *49*, 7976; (b) F. Hennersdorf, J. Frötschel and J. J. Weigand, *J. Am. Chem. Soc.* **2017**, *139*, 14592; (c) F. Hennersdorf and J. J. Weigand, *Angew. Chem. Int. Ed.* **2017**, *56*, 7858; *Angew. Chem.* **2017**, *129*, 7966.

[15]   (a) S. Alvarez, *Dalton Trans.* **2013**, *42*, 8617; (b) B. Cordero, V. Gómez, A. E. Platero-Prats, M. Revés, J. Echeverría, E. Cremades, F. Barragán and S. Alvarez, *Dalton Trans.* **2008**, 2832.

[16]   Y. Xiong, S. Yao, E. Bill and M. Driess, *Inorg. Chem.* **2009**, *8*, 7522.

[17]   O. J. Scherer, M. Swarowsky, H. Swarowsky and G. Wolmershäuser, *Angew. Chem. Int. Ed. Engl.* **1988**, *27*, 694; *Angew. Chem.* **1988**, *100*, 728.

[18]   W. W. Seidel, O. T. Summerscales, B. O. Patrick and M. D. Fryzuk, *Angew. Chem. Int. Ed.* **2009**, *48*, 115; *Angew. Chem.* **2009**, *121*, 121.

[19]   O. J. Scherer, T. Hilt and G. Wolmershäuser, *Organometallics* **1998**, *17*, 4110.

[20]   V. A. Miluykov, O. G. Sinyashin, P. Lönnecke and E. Hey-Hawkins, *Mendeleev Commun.* **2003**, *13*, 212.

[21]   M. D. Walter, J. Grunenberg and P. S. White, *Chem. Sci.* **2011**, *2*, 2120.

[22]   T. Li, N. Arleth, M. T. Gamer, R. Köppe, T. Augenstein, F. Dielmann, M. Scheer, S. N. Konchenko and P. W. Roesky, *Inorg. Chem.* **2013**, *52*, 14231.

[23]   M. Baudler, Y. Aktalay, K.-F. Tebbe and T. Heinlein, *Angew. Chem. Int. Ed. Engl.* **1981**, *20*, 967; *Angew. Chem.* **1981**, *93*, 1020.

[24]   I. Krossing and I. Raabe, *Angew. Chem. Int. Ed.* **2001**, *40*, 4406; *Angew. Chem.* **2001**, *113*, 4544.

[25]   M. H. Holthausen, S. K. Surmiak, P. Jerabek, G. Frenking and J. J. Weigand, *Angew. Chem. Int. Ed.* **2013**, *52*, 11078; *Angew. Chem.* **2013**, *125*, 11285.

[26]   M. H. Holthausen, A. Hepp and J. J. Weigand, *Chem. Eur. J.* **2013**, *19*, 9895.

[27]   M. H. Holthausen, K.-O. Feldmann, S. Schulz, A. Hepp and J. J. Weigand, *Inorg. Chem.* **2012**, *51*, 3374.

2.5 Supporting Information (SI)

2.5.1   General Procedures

All manipulations were performed under an atmosphere of dry argon using standard Schlenk techniques or a MBraun UniLab glovebox.

Chemicals and Solvents: Solvents were dried and degassed with a MBraun SPS800 solvent-purification system. THF, diehtylether, and toluene were stored over molecular sieves (3 Å). *n*-Hexane was stored over a potassium mirror. 1,2-Dimethoxyethane was stirred over K/benzophenone, distilled and stored over molecular sieves (3 Å). *n*-Pentane was stirred over sodium, distilled and stored over a potassium mirror. Deuterated solvents (C_6D_6, tol-d_8, THF-d_8) were stirred over potassium, distilled, degassed, and stored over molecular sieves (3 Å). The starting materials $[K(thf)_{0.2}\{Co(\eta^4\text{-}1,5\text{-cod})_2\}]$,[1] $[K(thf)_{1.5}\{Co(^{Dipp}BIAN)(\eta^4\text{-}1,5\text{-cod})\}]$,[2] $[(nacnac)Ga(\eta^2\text{-}P_4)]$[3] and $^{Mes}BIAN$[4] were prepared according to previously reported procedures. iPr_2PCl was purchased from Sigma-Aldrich and used as delivered. Cy_2PCl,[5] tBu_2PCl,[6] $tBuPCl_2$[7] were prepared according to literature procedures.

NMR Spectroscopy: NMR spectra were measured on a Bruker AVANCE III HD Nanobay (^1H (400.13 MHz), ^{13}C (100.61 MHz), ^{19}F (376.50 MHz), ^{29}Si (79.50 MHz), ^{31}P (161.98 MHz)) 400 MHz UltraShield or on a Bruker AVANCE III HDX, 500 MHz Ascend (^1H (500.13 MHz), ^{13}C (125.75 MHz), ^{19}F (470.59 MHz), ^{29}Si (99.36 MHz), ^{31}P (202.45 MHz)). All ^{13}C NMR spectra were exclusively recorded with composite pulse decoupling. Reported numbers assigning atoms in the ^{13}C spectra were indirectly deduced from the cross-peaks in 2D correlation experiments (HMBC, HSQC). Chemical shifts were referenced to $\delta_{TMS} = 0.00$ ppm (^1H, ^{13}C), $\delta_{CFCl3} = 0.00$ ppm (^{19}F), $\delta_{TMS} = 0.00$ ppm (^{29}Si) and $\delta_{H3PO4(85\%)} = 0.00$ ppm (^{31}P). Chemical shifts (δ) are reported in ppm. Coupling constants (J) are reported in Hz. ^{31}P NMR reaction monitoring was performed on a Bruker AVANCE III HDX, 500 MHz Ascend (^{31}P(202.45 MHz)). PH-HMBC NMR spectra of compound **5** were recorded on a Bruker Avance III 600 spectrometer with a 5 mm TBI-F probe. ^1H chemical shifts were referenced to the THF-d_8 signal at 3.58 ppm. The heteronuclei ^{31}P was referenced, employing $n(X) = n(THF\text{-}d_8) \cdot X_{reference} / 100\ \%$ according to Harris et al.[8] The following frequency ratio and reference compound was used: $X(^{31}P) = 40.480742$ (H_3PO_4).

For compounds, which give rise to a higher order spin system in the $^{31}P\{^1H\}$ NMR spectrum, the resolution enhanced $^{31}P\{^1H\}$ NMR spectrum was transferred to the software gNMR, version 5.0, by Cherwell Scientific.[9] The full line shape iteration procedure of gNMR was applied to obtain the best match of the fitted to the experimental spectrum. $^1J(^{31}P^{31}P)$ coupling constants were set to negative values and all other signs of the coupling constants were obtained accordingly.

Elemental analysis: Elemental analyses were determined by the analytical department of the University of Regensburg with a Micro Vario Cube (Elementar).

UV/vis spectra: UV/vis spectra were recorded on an Ocean Optics Flame spectrometer.

Melting points: Melting points were measured on samples in sealed capillaries on a Stuart SMP10 melting point apparatus.

2.5.2 Synthesis of [K(Et$_2$O){Co(^{Mes}BIAN)(η^4-1,5-cod)}] (1)
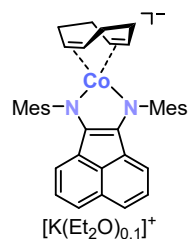
An orange THF solution (20 mL) of ^{Mes}BIAN (839 mg, 2.0 mmol, 1.0 equiv.) was added to a yellow THF solution (10 mL) of [K(thf)$_{0.2}${Co(η^4-1,5-cod)$_2$}] (663 mg, 2.02 mmol, 1.0 equiv.). The reaction mixture was stirred at room temperature for 6 h, whereupon the color changed to green. Volatiles were removed in *vacuo* and the remaining green solid was extracted with 200 mL diethyl ether and filtered through a glass frit. Dark green needles were obtained from the concentrated filtrate after 3 days at room temperature. According to the ^{1}H NMR spectroscopy, the isolated sample still contained 0.1 equiv. of diethyl ether after drying under vacuum (10^{-3} mbar). Crystals suitable for single X-ray diffraction were obtained by diffusion of *n*-hexane into a concentrated DME solution of [K(dme)$_4${Co(^{Mes}BIAN)(η^4-1,5-cod)}] (**1-dme**).

Yield: 558 mg (44%).

m.p. >250 °C (decomposition to a black oil).

UV/vis: (THF, λ$_{max}$ / nm, ε$_{max}$ / L·mol^{-1}·cm^{-1}): 303 (20000), 442 (10500), 642 (6500).

^{1}H NMR (400.13 MHz, 300 K, THF-d_8): δ / ppm = 6.81 (s, 4H, *m*-CH$_{(Mes)}$), 6.40 (br, m, 2H, CH$_{(BIAN)}$), 6.35 (br, m, 2H, CH$_{(BIAN)}$), 5.21 (d, $^3J_{HH}$ = 6.0 Hz, 2H, CH$_{(BIAN)}$), 3.64 (br, THF), 2.67 (s, 4H, CH$_{(cod)}$), 2.46 (s, 12H, *o*-CH$_{3(Mes)}$), 2.34 (s, 4H, CH$_{2(cod)}$), 2.25 (s, 6H, *p*-C*H*$_{3(Mes)}$), 1.78 (br, THF), 1.01 (br m, 4H, CH$_{2(cod)}$).

^{13}C{^{1}H} (100.61 MHz, 300 K, THF-d_8): δ / ppm = 153.0 (*ipso*-C$_{Mes}$), 137.2 (C$_{BIAN}$), 134.4 (C$_{BIAN}$), 130.5 (C$_{Mes}$), 128.6 (CH$_{Mes}$), 127.8 (CH$_{BIAN}$), 127.3 (C$_{Mes}$) 119.2 (CH$_{BIAN}$), 112.6 (CH$_{BIAN}$), 65.6 (cod-CH), 32.5 (cod-CH$_2$), 21.2 (*p*-CH$_{3(Mes)}$), 19.3 (*o*-CH$_{3(Mes)}$), resonances of two quaternary carbon atoms were not detected.

Elemental analysis calcd. for C$_{38}$H$_{40}$CoKN$_2$ · (C$_4$H$_{10}$O)$_{0.x}$ (x = 1-4) (Mw = 630.20 g·mol^{-1}): C 73.19, H 6.56, N 4.45; found C 72.58, H 6.32; N 4.34; the deviation in the carbon content is explained by a varying amount of solvate molecules present in isolated sample of **1**.
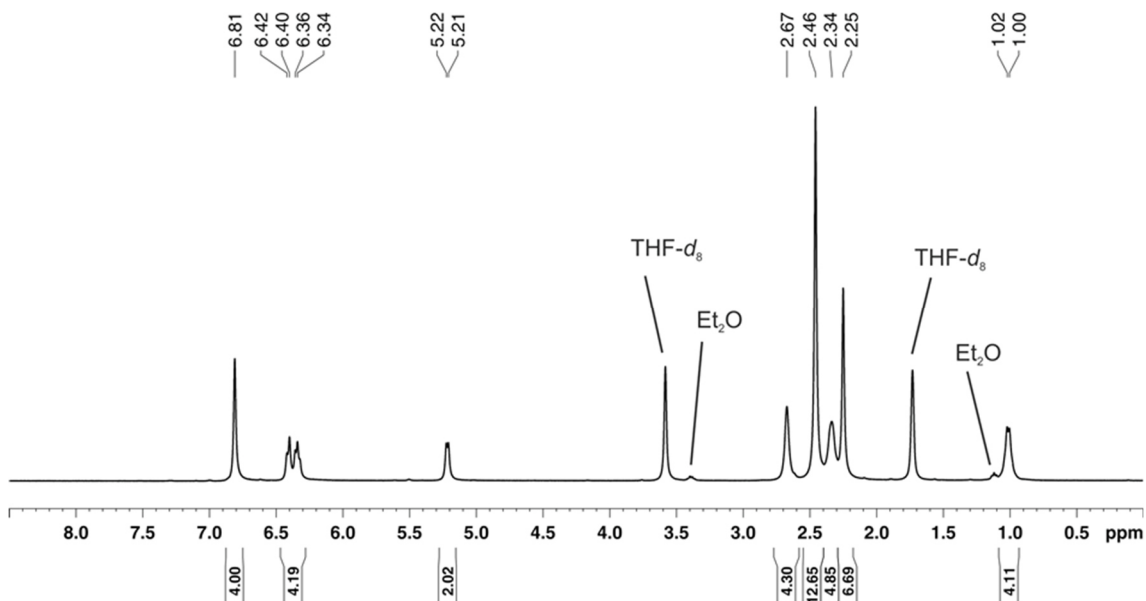

Figure S1. ^{1}H NMR spectrum (400.13 MHz, 300 K, THF-d_8) of [K(Et$_2$O){Co(^{Mes}BIAN)(η^4-1,5-cod)}] (**1**).
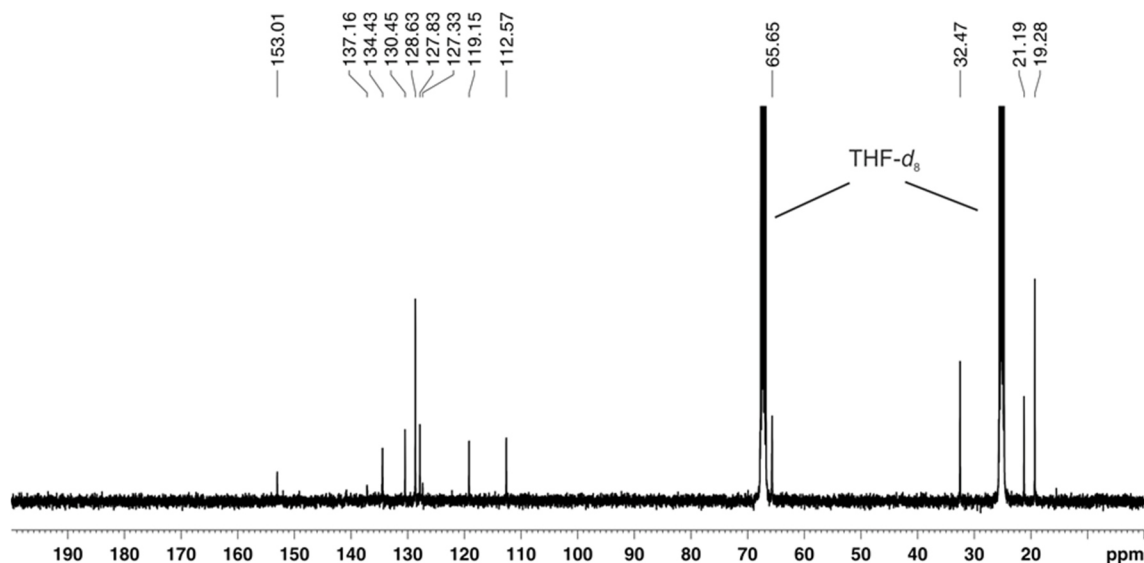
Figure S2. $^{13}C\{^1H\}$ NMR spectrum (100.61 MHz, 300 K, THF-d_8) of [K(Et$_2$O){Co(^{Mes}BIAN)(η^4-1,5-cod)}] (**1**).
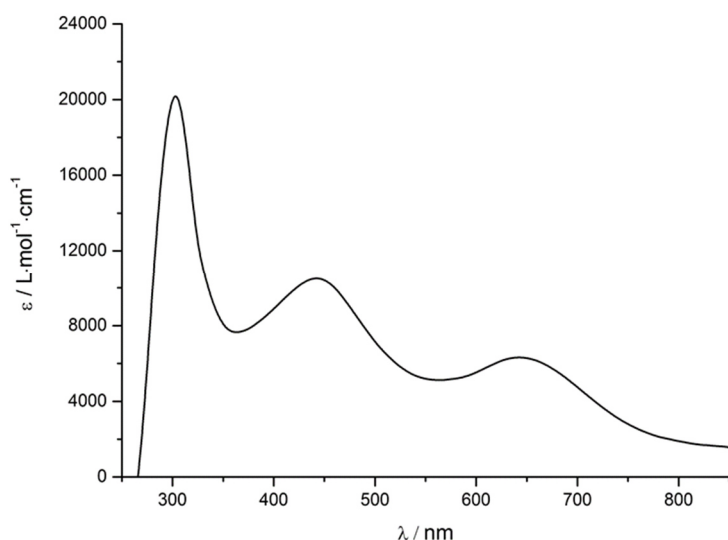
Figure S3. UV/vis spectrum of [K(Et$_2$O){Co(^{Mes}BIAN)(η^4-1,5-cod)}] (**1**) recorded in THF.

2.5.3 Synthesis of [K(dme)$_2${(^{Mes}BIAN)Co(μ-η^4:η^2-P$_4$)Ga(nacnac)}] (2)
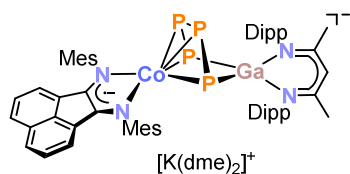
A green THF solution (15 mL) of [K(Et$_2$O)$_{0.1}${Co(^{Mes}BIAN)(1,5-cod)}] (**1**) (479 mg, 0.761 mmol, 1.0 equiv.) was added to a yellow THF solution (25 mL) of [(nacnac)Ga(η^2-P$_4$)] (500 mg, 0.761 mmol, 1.0 equiv.). The resulting green reaction mixture turned dark violet upon vigorous stirring for 3 days at room temperature. Volatiles were removed in *vacuo* and the remaining violet solid was washed with 20 mL *n*-hexane. The crude product was redissolved in 30 mL DME, filtered through a glass frit and concentrated. Dark violet needles were obtained by layering the DME solution with *n*-hexane (1:2) after storage for 3 days at room temperature. The isolated product contains 2 DME molecules and 0.1 *n*-hexane solvate molecules per formula unit after drying in *vacuo* (10^{-3} mbar) according to the ^{1}H NMR spectrum.

Yield: 566 mg (59%).

m.p. >250 °C (decomposition to black oil).

UV/vis: (THF, λ_{max} / nm, ε_{max} / L·mol^{-1}·cm^{-1}): 321 (44500), 400 (16000), 553(21000), 658 (21000).

^{1}H NMR (400.13 MHz, 300 K, THF-d_8): δ / ppm = 7.37 (m, 1H, CH$_{Dipp}$), 7.28 (d, J = 7.4 Hz, 2H, CH$_{Dipp}$), 7.03 (m, 1H, CH$_{Dipp}$), 6.95 (d, $^3J_{HH}$ = 7.4 Hz, 2H, CH$_{Mes}$), 6.73 (s, 4H, CH$_{Mes}$), 6.54 (dd, $^3J_{HH}$ = 7.1 Hz, 8.0 Hz, 2H, CH$_{BIAN}$), 5.43 (d, $^3J_{HH}$ = 7.0 Hz, 2H, CH$_{BIAN}$), 4.70 (s, 1H, CH$_{nacnac}$), 3.78 (sept, $^3J_{HH}$ = 6.8 Hz, 2H, CH(CH$_3$)$_2$), 3.43 (s, DME), 3.28 (s, DME), 2.73 (sept, $^3J_{HH}$ = 6.8 Hz, 2H, CH(CH$_3$)$_2$), 2.34 (s, 6H, p-CH$_{3(Mes)}$), 1.87 (s, 12H, o-CH$_{3(Mes)}$), 1.54 (s, 3H, CH$_{3(nacnac)}$), 1.48 (d, $^3J_{HH}$ = 6.8 Hz, 6H, CH(CH_3)$_2$), 1.42 (s, 3H, CH$_{3(nacnac)}$), 1.37 (d, $^3J_{HH}$ = 6.8 Hz, 6H, CH(CH_3)$_2$), 1.18 (d, $^3J_{HH}$ = 6.8 Hz, 6H, CH(CH_3)$_2$), 0.86 (d, $^3J_{HH}$ = 6.8 Hz, 6H, CH(CH_3)$_2$).

^{13}C{^{1}H} (100.61 MHz, 300 K, THF-d_8): δ / ppm = 167.9 (CN$_{nacnac}$), 165.9 (CN$_{nacnac}$), 154.9 (C$_{Mes}$), 147.8 (CN$_{BIAN}$), 145.2 (CN$_{Dipp}$), 145.0 (CN$_{Dipp}$), 143.9 (C$_{Dipp}$), 143.0 (C$_{Dipp}$), 137.5 (C$_{BIAN}$), 135.7 (C$_{BIAN}$), 132.1 (C$_{Mes}$), 131.6 (C$_{Mes}$), 130.8 (C$_{BIAN}$), 128.7 (CH$_{BIAN}$), 128.3 (CH$_{Mes}$), 127.4 (CH$_{Dipp}$), 126.5 (CH$_{Dipp}$), 125.2 (CH$_{Dipp}$), 124.4 (CH$_{Dipp}$), 121.5 (CH$_{BIAN}$), 115.7 (CH$_{BIAN}$), 95.8 (CH$_{nacnac}$), 29.5 (CH(CH$_3$)$_2$), 29.0 (CH(CH$_3$)$_2$), 26.6 (CH(CH$_3$)$_2$), 26.5 (CH(CH$_3$)$_2$), 24.6 (CH$_{3(nacnac)}$), 24.5(CH$_{3(nacnac)}$), 21.3 (p-CH$_{3(Mes)}$), 19.6 (o-CH$_{3(Mes)}$).

^{31}P{^{1}H} NMR (161.98 MHz, 300 K, THF-d_8): (AA'XX') spin system δ / ppm = 74.0 (m, 2P$_P$), −125.4 (m, 2P$_{Ga}$).

Elemental analysis calcd. for C$_{59}$H$_{69}$CoGaN$_4$P$_4$K · (C$_4$H$_{10}$O$_2$)$_2$ · (C$_6$H$_{14}$)$_{0.1}$ (Mw = 1314.7 g·mol^{-1}): C 61.76, H 6.93, N 4.26; found C 61.66, H 6.69; N 4.35.
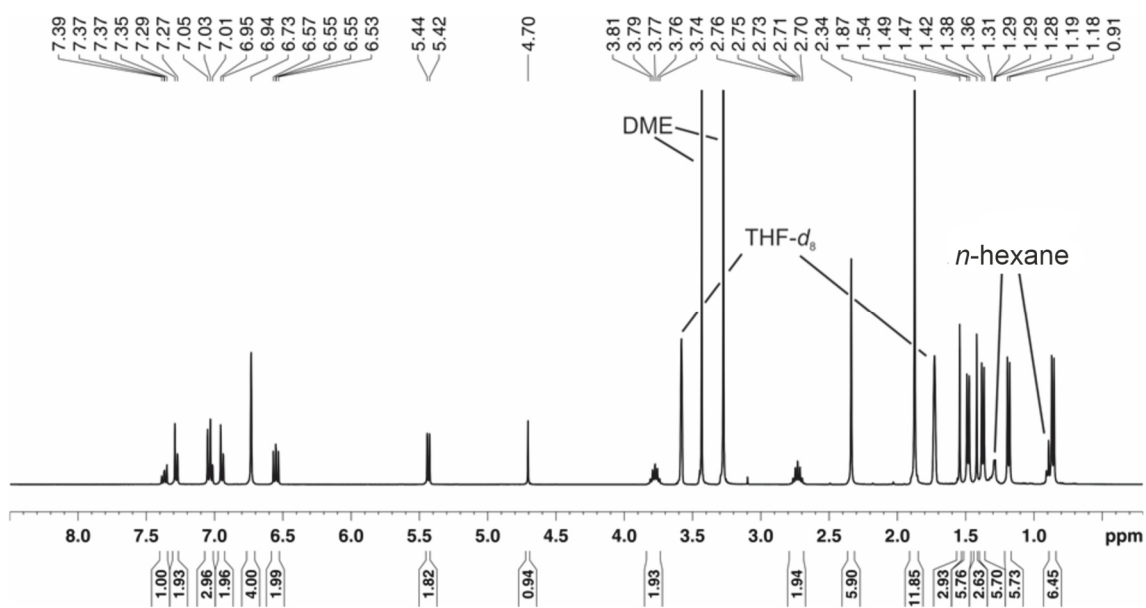
Figure S4. ^{1}H NMR spectrum (400.13 MHz, 300 K, THF-d_8) of [K(dme)$_2${(^{Mes}BIAN)Co(μ-η^4:η^2-P$_4$)Ga(nacnac)}] (**2**).
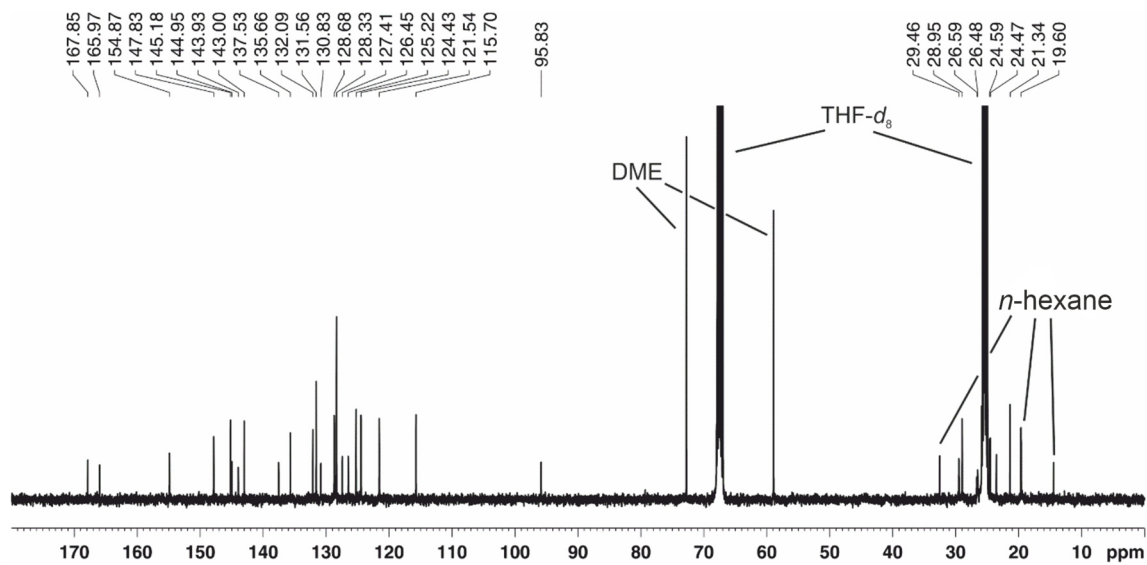
Figure S5. $^{13}C\{^{1}H\}$ NMR spectrum (100.61 MHz, 300 K, THF-d_8) of [K(dme)$_2$\{(^{Mes}BIAN)Co(μ-η^4:η^2-P$_4$)Ga(nacnac)\}] (**2**).
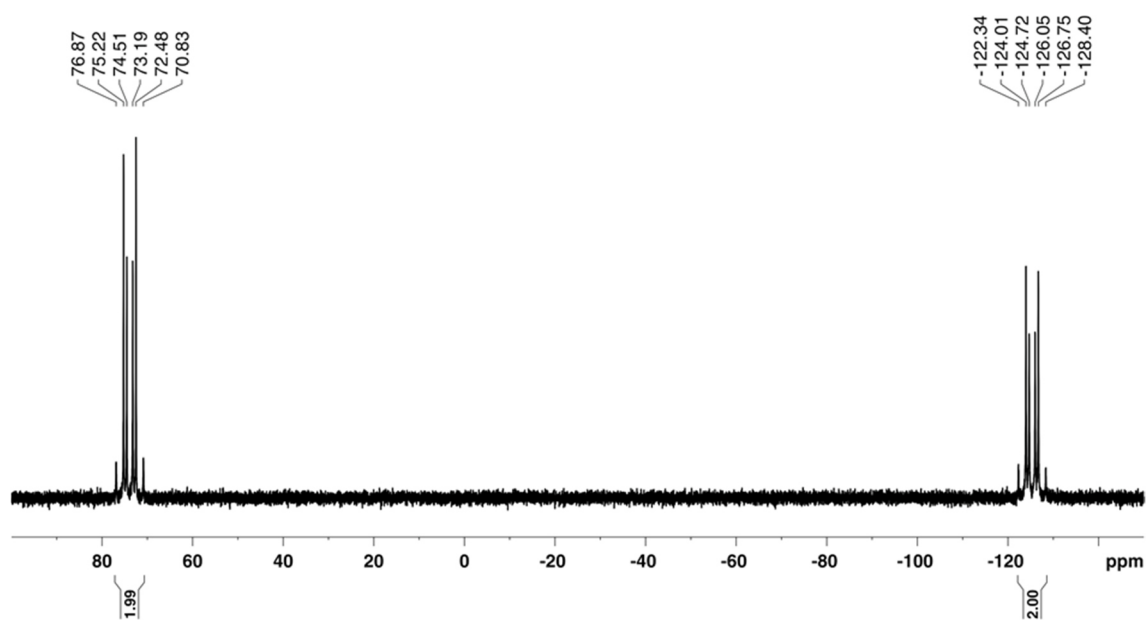
Figure S6. $^{31}P\{^{1}H\}$ NMR spectrum (161.98 MHz, 300 K, THF-d_8) of [K(dme)$_2$\{(^{Mes}BIAN)Co(μ-η^4:η^2-P$_4$)Ga(nacnac)\}] (**2**).
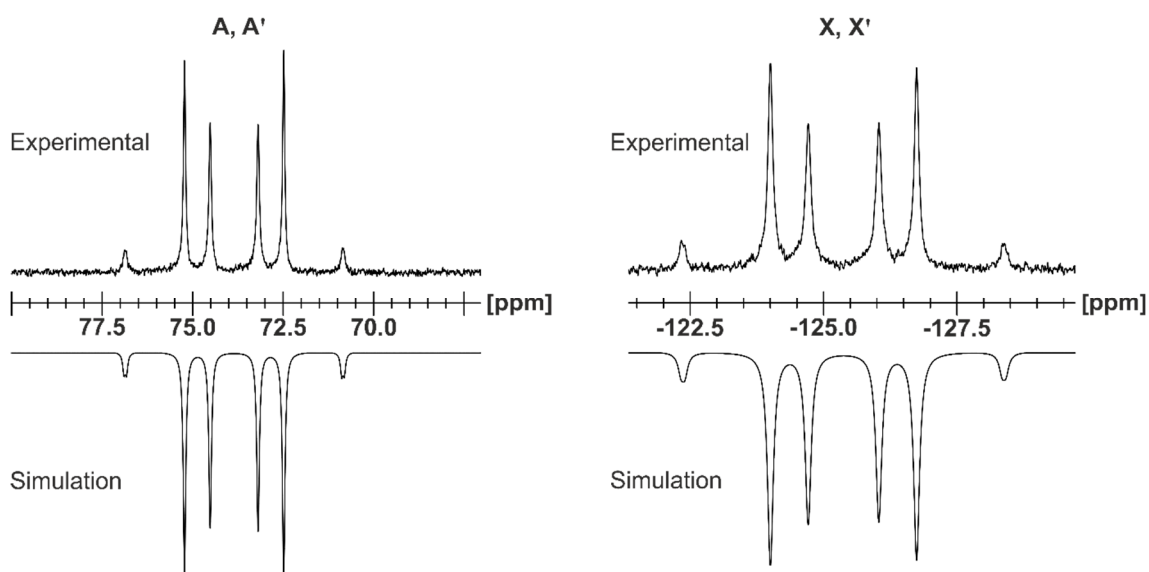
Figure S7. Section of the $^{31}P\{^1H\}$ NMR (400.13 MHz, 300 K, THF-d_8) of [K(dme)$_2${(^{Mes}BIAN)Co(μ-η^4:η^2-P$_4$)Ga(nacnac)}] (**2**); experimental (upwards) and simulation (downwards).

Table S1. Coupling constants from the iterative fit of the AA'XX' spin system and schematic representation of the CoP$_4$Ga core of [K(dme)$_2${(^{Mes}BIAN)Co(μ-η^4:η^2-P$_4$)Ga(nacnac)}] (**2**); [Co] = (^{Mes}BIAN)Co, [Ga] = (nacnac)Ga.

$^1J_{AA'} = {}^1J_{A'A}$	−380.5 Hz	$^2J_{AX'} = {}^2J_{A'X}$	6.6 Hz	
$^1J_{AX} = {}^1J_{A'X'}$	−450.5 Hz	$^3J_{XX'} = {}^3J_{X'X}$	−7.2 Hz	
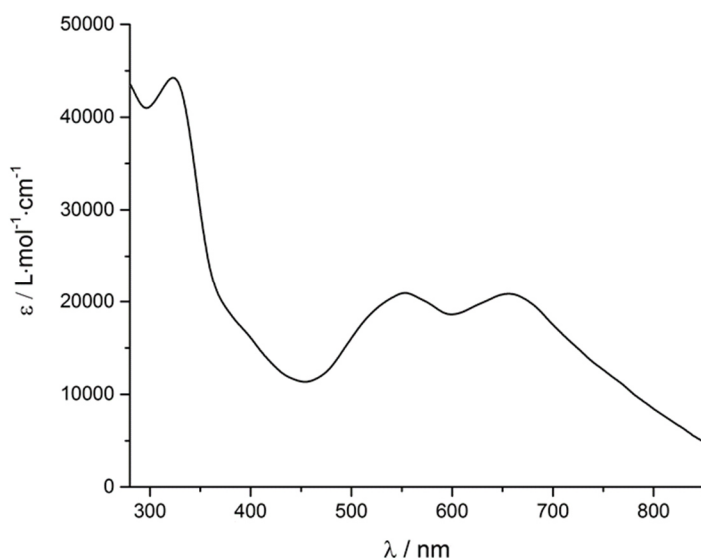
Figure S8. UV/vis spectrum of [K(dme)$_2${(^{Mes}BIAN)Co(μ-η^4:η^2-P$_4$)Ga(nacnac)}] (**2**) recorded in THF.

2.5.4 Synthesis of [K(thf)$_2${(^{Dipp}BIAN)Co(μ-η^4:η^2-P$_4$)Ga(nacnac)}] (2')
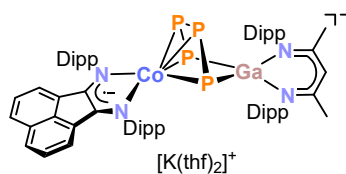
A green THF solution (2 mL) of [K(thf)$_{1.8}${Co(^{Dipp}BIAN)(1,5-cod)}] (72.2 mg, 0.0924 mmol, 1.0 equiv.) was added to a yellow THF solution (2 mL) of [(nacnac)Ga(P$_4$)] (56.5 mg, 0.0924 mmol, 1.0 equiv.). The resulting green reaction mixture turned dark violet upon vigorous stirring for 3 days at room temperature. Volatiles were removed in *vacuo* and the remaining violet solid was extracted with diethylether (5 mL) and filtered. After 2 days dark violet crystals were obtained by slow diffusion of *n*-pentane into a concentrated diethyl ether solution of the crude product **2'**. The isolated product contains 2 THF molecules per formula unit after drying under vaccuum (10^{-3} mbar) according to the ^{1}H NMR spectrum. Recrystallization by slow diffusion of *n*-hexane into a concentrated solution of **2'** dissolved DME afforded crystals suitable for single-crystal X-ray diffraction.

Yield: 66.1 mg (53%).

m.p. >250 °C (decomposition to black oil).

UV/vis: (THF, λ$_{max}$ / nm, ε$_{max}$ / L·mol^{-1}·cm^{-1}): 332 (32000), 538 (15500), 751 (11500).

^{1}H NMR (400.13 MHz, 300 K, THF-d_8): δ / ppm = 7.15-7.22 (m, 5H, CH$_{Dipp}$), 7.04-7.05 (m, 5H, CH$_{Dipp}$), 6.98 (d, $^3J_{HH}$ = 7.8 Hz, 2H, CH$_{BIAN}$), 6.96 (m, 2H, CH$_{Dipp}$), 6.50 (t, $^3J_{HH}$ = 7.8 Hz, 2H, CH$_{BIAN}$), 5.21 (d, $^3J_{HH}$ = 7.2 Hz, 2H, CH$_{BIAN}$), 4.78 (s, 1H, CH$_{nacnac}$), 3.73 (sept., $^3J_{HH}$ = 6.7 Hz, 2H, CH(CH$_3$)$_{2(Dipp)}$), 3.56 (sept., $^3J_{HH}$ = 6.7 Hz, 4H, CH(CH$_3$)$_{2(Dipp)}$), 2.75 (sept., $^3J_{HH}$ = 6.7 Hz, 2H, CH(CH$_3$)$_{2(Dipp)}$), 1.49 (d, $^3J_{HH}$ = 6.7 Hz, 6H, CH(CH_3)$_{2(Dipp)}$), 1.47 (s, 3H, CH$_{3(nacnac)}$), 1.42 (s, 3H, CH$_{3(nacnac)}$), 1.38 (d, $^3J_{HH}$ = 6.7 Hz, 6H, CH(CH_3)$_{2(Dipp)}$), 1.28 (d, $^3J_{HH}$ = 6.7 Hz, 12H, CH(CH_3)$_{2(Dipp)}$), 1.22 (d, $^3J_{HH}$ = 6.7 Hz, 6H, CH(CH_3)$_{2(Dipp)}$), 0.57 (d, $^3J_{HH}$ = 6.7 Hz, 6H, CH(CH_3)$_{2(Dipp)}$), 0.57 (d, $^3J_{HH}$ = 6.7 Hz, 12H, CH(CH_3)$_{2(Dipp)}$).

^{13}C{^{1}H} (100.61 MHz, 300 K, THF-d_8): δ / ppm = 167.8 (CN$_{nacnac}$), 166.5 (CN$_{nacnac}$), 154.5 (C$_{DippBIAN}$), 149.4 (C$_{BIAN}$), 145.4 (C$_{Dippnacnac}$), 144.4 (C$_{Dippnacnac}$), 143.2 (C$_{DippBIAN}$), 142.9 (C$_{Dippnacnac}$), 137.3 (C$_{BIAN}$), 136.3 (C$_{BIAN}$), 130.4 (C$_{BIAN}$), 127.8 (CH$_{BIAN}$), 127.2 (CH$_{Dipp}$), 126.5 (CH$_{Dippnacnac}$), 124.7 (CH$_{Dippnacnac}$), 124.5 (CH$_{DippBIAN}$), 124.4 (CH$_{Dippnacnac}$), 123.1 (CH$_{DippBIAN}$), 121.6 (CH$_{BIAN}$), 118.0 (CH$_{BIAN}$), 97.0 (CH_{nacnac}), 29.3 (CH(CH$_3$)$_{2(Dipp)}$), 28.9 (CH(CH$_3$)$_{2(Dipp)}$), 26.7 (CH(CH_3)$_{2(Dipp)}$), 25.6 (CH(CH_3)$_{2(Dipp)}$), 25.5 (CH(CH_3)$_{2(Dipp)}$), 25.2 (CH(CH_3)$_{2(Dipp)}$), 25.1 (CH(CH_3)$_{2(Dipp)}$), 25.0 (CH(CH_3)$_{2(Dipp)}$), 24.9 (CH$_{3(nacnac)}$), 24.7 (CH$_{3(nacnac)}$).

^{31}P{^{1}H} NMR (161.98 MHz, 300 K, THF-d_8): (AA'XX') spin system δ / ppm = 79.1 (m, 2P$_P$), −133.3 (m, 2P$_{Ga}$).

Elemental analysis calcd. for C$_{73}$H$_{97}$N$_4$CoGaKO$_2$P$_4$ (Mw = 1354.25 g·mol^{-1}): C 64.74, H 7.22, N 4.14; found C 63.85, H 6.76, N 4.05; the carbon content deviates from the calculated values; this may partly be explained by a varying amount of solvate molecules present in the isolated sample of **2'**, but the complete reasons for this deviation are presently unclear.
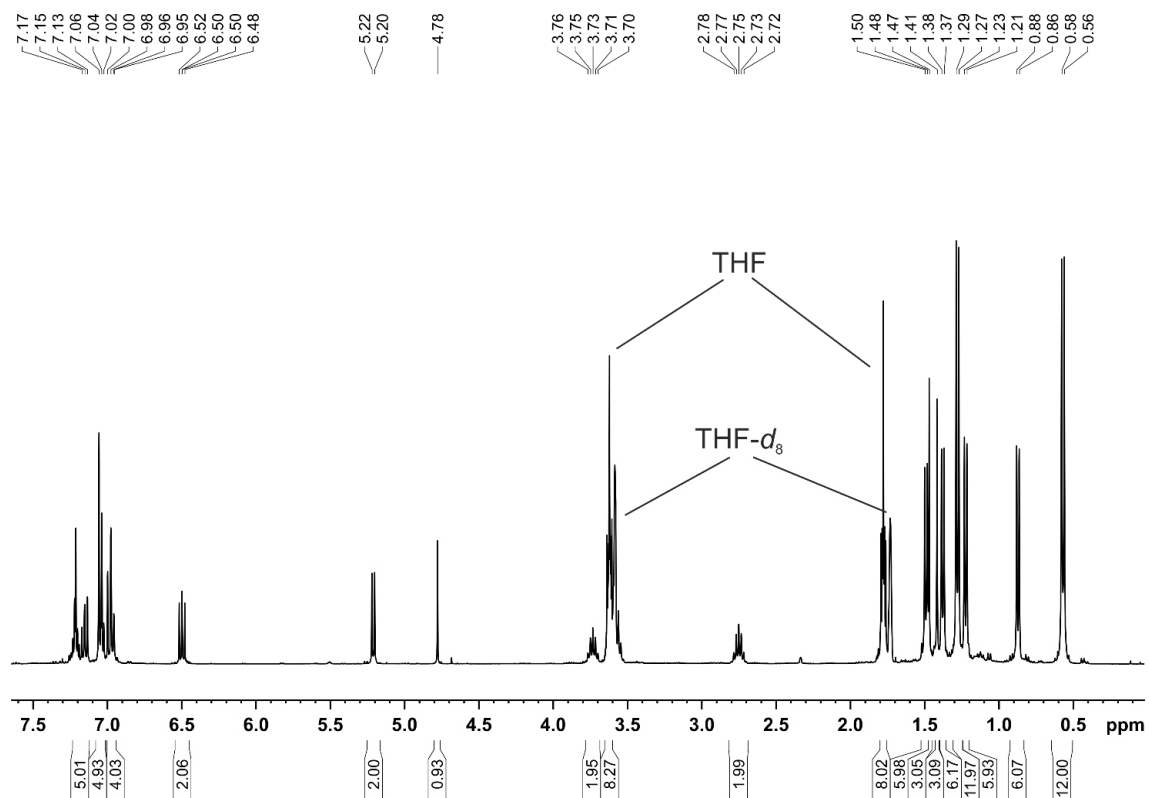
Figure S9. ^{1}H NMR spectrum (400.13 MHz, 300 K, THF-d_8) of [K(thf)$_2$\{(^{Dipp}BIAN)Co(μ-η^4:η^2-P$_4$)Ga(nacnac)\}] (**2'**).
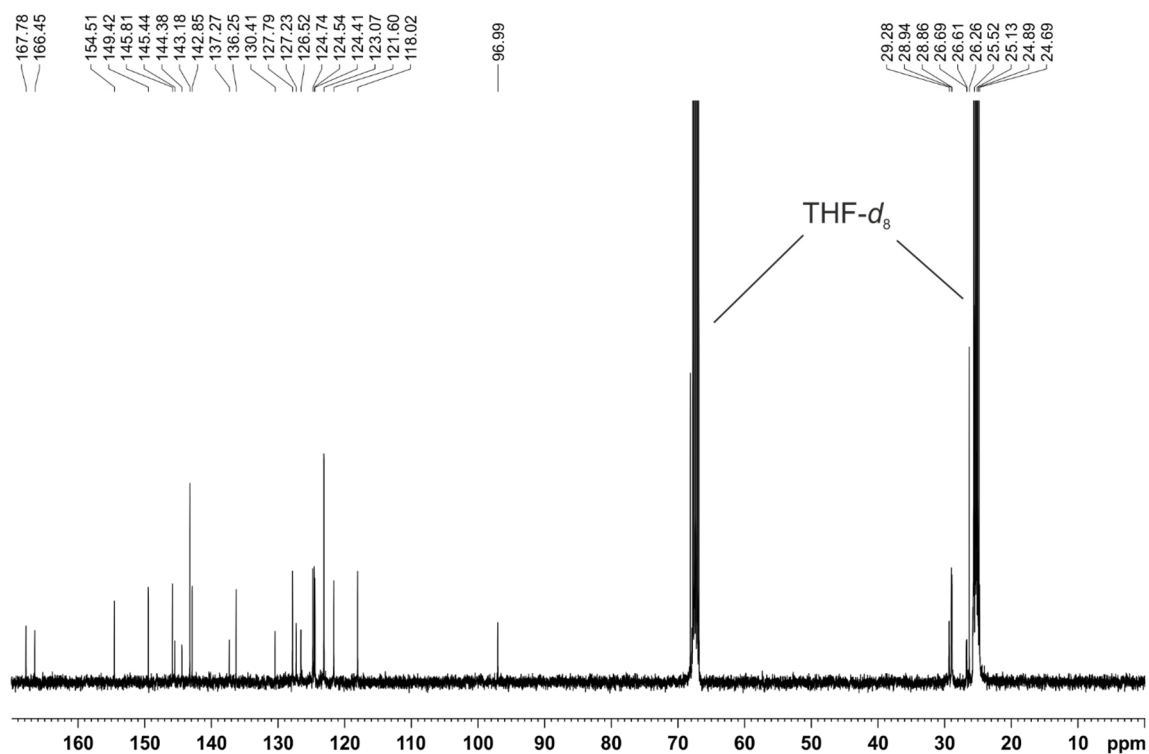
Figure S10. ^{13}C\{^{1}H\} NMR spectrum (100.61 MHz, 300 K, THF-d_8) of [K(thf)$_2$\{(^{Dipp}BIAN)Co(μ-η^4:η^2-P$_4$)Ga(nacnac)\}] (**2'**).
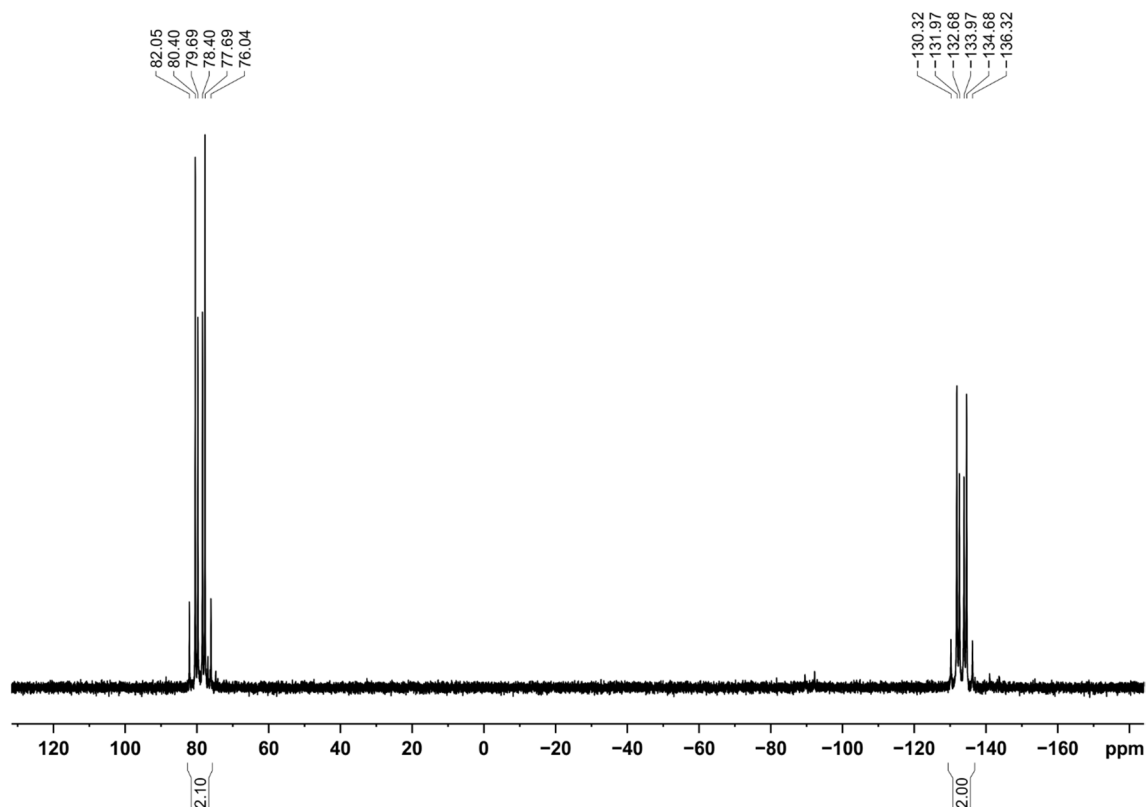
Figure S11. $^{31}P\{^1H\}$ NMR spectrum (161.98 MHz, 300 K, THF-d_8) of [K(thf)$_2$\{(^{Dipp}BIAN)Co(µ-η^4:η^2-P$_4$)Ga(nacnac)\}] (**2'**).
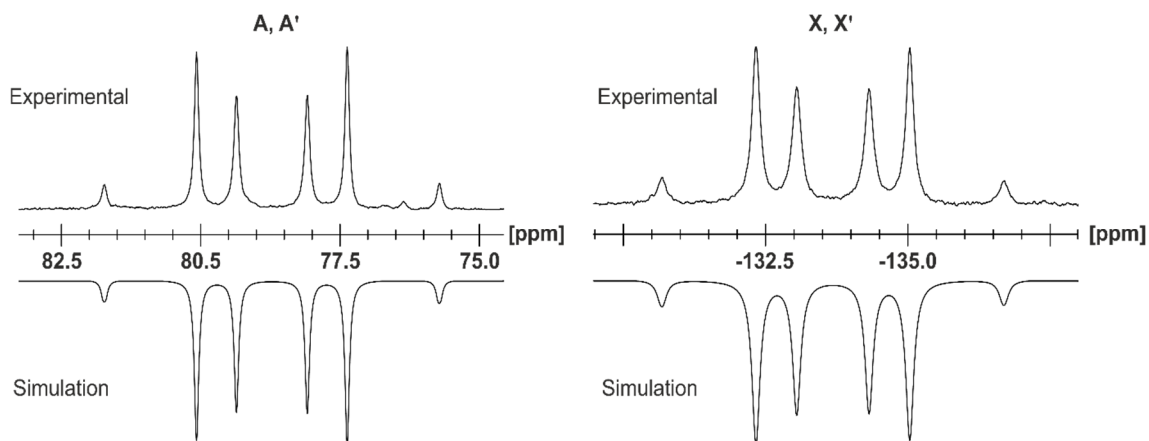
Figure S12. Section of the $^{31}P\{^1H\}$ NMR (400.13 MHz, 300 K, THF-d_8) of [K(thf)$_2$\{(^{Dipp}BIAN)Co(µ-η^4:η^2-P$_4$)Ga(nacnac)\}] (**2'**); experimental (upwards) and simulation (downwards).

Table S2. Coupling constants from the iterative fit of the AA'XX' spin and schematic representation of the CoP$_4$Ga core of [K(thf)$_2$\{(^{Dipp}BIAN)Co(µ-η^4:η^2-P$_4$)Ga(nacnac)\}] (**2'**); [Co] = (^{Dipp}BIAN)-Co, [Ga] = (nacnac)Ga.

$^1J_{AA'} = {}^1J_{A'A}$	−383.9 Hz	$^2J_{AX'} = {}^2J_{A'X}$	5.0 Hz	
$^1J_{AX} = {}^1J_{A'X'}$	−442.7 Hz	$^3J_{XX'} = {}^3J_{X'X}$	−4.8 Hz	
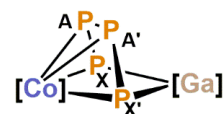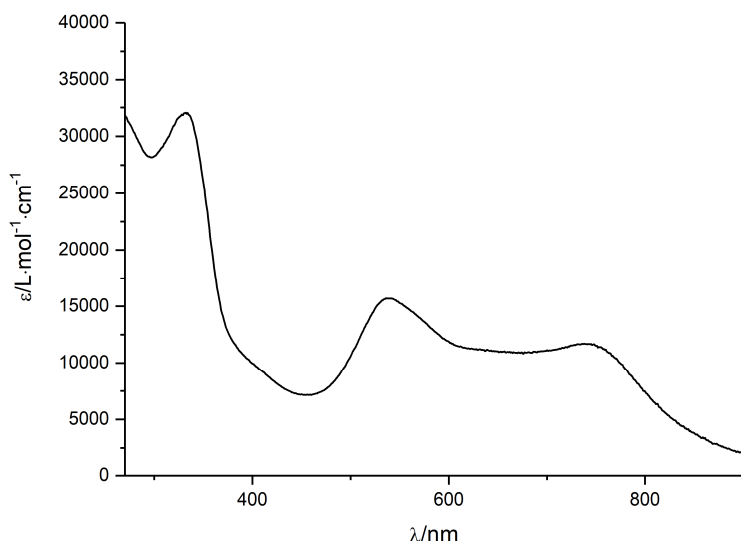
Figure S13. UV/vis spectrum of $[K(thf)_2\{(^{Dipp}BIAN)Co(\mu\text{-}\eta^4\text{:}\eta^2\text{-}P_4)Ga(nacnac)\}]$ (**2'**) recorded in THF.

2.5.5 Synthesis of $[(^{Mes}BIAN)Co(cyclo\text{-}P_5iPr_2)]$ (3a)
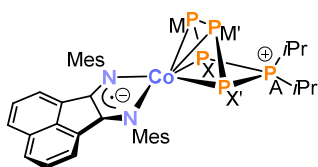
A solution of iPr_2PCl in THF (0.91 mL, $c = 0.18$ mol·L^{-1}, 1.0 equiv.) was added to a dark violet THF solution (10 mL) of $[K(dme)_2\{(^{Mes}BIAN)Co(\mu\text{-}\eta^4\text{:}\eta^2\text{-}P_4)Ga(nacnac)\}]$ (**2**) (200 mg, 0.17 mmol, 1.0 equiv.) and stirred at 60 °C for 2 days. A color change of the reaction mixture to cyan was observed. The by-product [Ga(nacnac)] was separated by column chromatography, (stationary phase: neutral aluminum oxide, activity grade: Super I, 10 x 2 cm, eluent: *n*-hexane/toluene gradient, 100/0 to 0/100). [Ga(nacnac)] hydrolyses on aluminum oxide to nacnacH, which elutes first as colorless band (R$_f$ (*n*-hexane/toluene, 7/1 = 0.6). The following blue band (R$_f$ (*n*-hexane/toluene, 7/1 = 0.2) was collected, the obtained solution concentrated in *vacuo* and crystallization by *n*-hexane diffusion gave X-ray quality crystals of **3a** after three days storage at room temperature.

Yield: 32.1 mg (27%).

m.p. 248 °C (decomposition to violet oil).

UV/vis: (THF, λ_{max} / nm, ε_{max} / L·mol^{-1}·cm^{-1}): 324sh (14500), 332 (15000), 420 (10000), 572 (16000), 578 (16500).

^{1}H NMR (400.13 MHz, 300 K, C$_6$D$_6$): δ / ppm = 7.31 (d, $^3J_{HH}$ =8.2 Hz, 2H, CH$_{(BIAN)}$), 6.95 (s, 4H. *m*-CH$_{(Mes)}$), 6.72 (dd, $^3J_{HH}$ =7.0 Hz, $^3J_{HH}$ =8.2 Hz, 2H, CH$_{(BIAN)}$), 6.54 (d, $^3J_{HH}$ =7.0 Hz, 2H, CH$_{(BIAN)}$), 2.44 (s, 12H, *o*-CH$_{3(Mes)}$) overlap with 2.44 (m, 1H, C*H*(CH$_3$)$_2$), 2.28 (s, 6H, *p*-CH$_{3(Mes)}$), 0.98 (dd, $^3J_{HP}$ = 14.6 Hz, $^3J_{HH}$ = 7.3 Hz, 6H, CH(C*H*$_3$)$_2$), 0.69 (m, 1H, C*H*(CH$_3$)$_2$), 0.22 (dd, $^3J_{HP}$ = 16.0 Hz, $^3J_{HH}$ = 7.1 Hz, 6H, CH(C*H*$_3$)$_2$).

^{13}C{^{1}H} NMR (100.61 MHz, 300 K, THF-*d*$_8$): δ / ppm = 154.5 (C$_{(BIAN)}$), 153.2 (C$_{(Mes)}$), 139.4 (C$_{(BIAN)}$), 134.9 (C$_{(Mes)}$), 133.0 (C$_{(BIAN)}$), 131.8 (C$_{(BIAN)}$), 129.5 (C$_{(Mes)}$), 129.4 (*C*H$_{(Mes)}$), 129.0 (*C*H$_{(BIAN)}$), 125.0 (*C*H$_{(BIAN)}$), 118.7 (*C*H$_{(BIAN)}$) 30.1 (br, *C*H(CH)$_2$), 27.6 (br, *C*H(CH)$_2$), 22.1 (br, CH(*C*H$_3$)$_2$), 21.2 (*p*-*C*H$_{3(Mes)}$), 19.4 (*o*-*C*H$_{3(Mes)}$), 17.6 (CH(*C*H$_3$)$_2$).

^{31}P{^{1}H} NMR (161.98 MHz, 300 K, C$_6$D$_6$): (AMM'XX') spin system δ / ppm = 161.0 (m, 1P$_A$), 88.6 (m, 2P$_{MM'}$), −111.4 (m, P$_{XX'}$).

Elemental analysis calcd. for $C_{36}H_{42}CoN_2P_5 \cdot (C_6H_{14})_{0.3}$ (Mw = 742.40 g·mol^{-1}): C 61.16, H 6.27, N 3.77; found C 62.57, H 6.58; N 3.54. According to ^{1}H NMR spectroscopy the compound contains 0.3 molecules *n*-hexane per formula unit after drying under vacuum (10^{-3} mbar). Even after two times of recrystallization, the elemental analysis showed a higher C-value than expected for this composition indicating varying concentrations of the solvate.
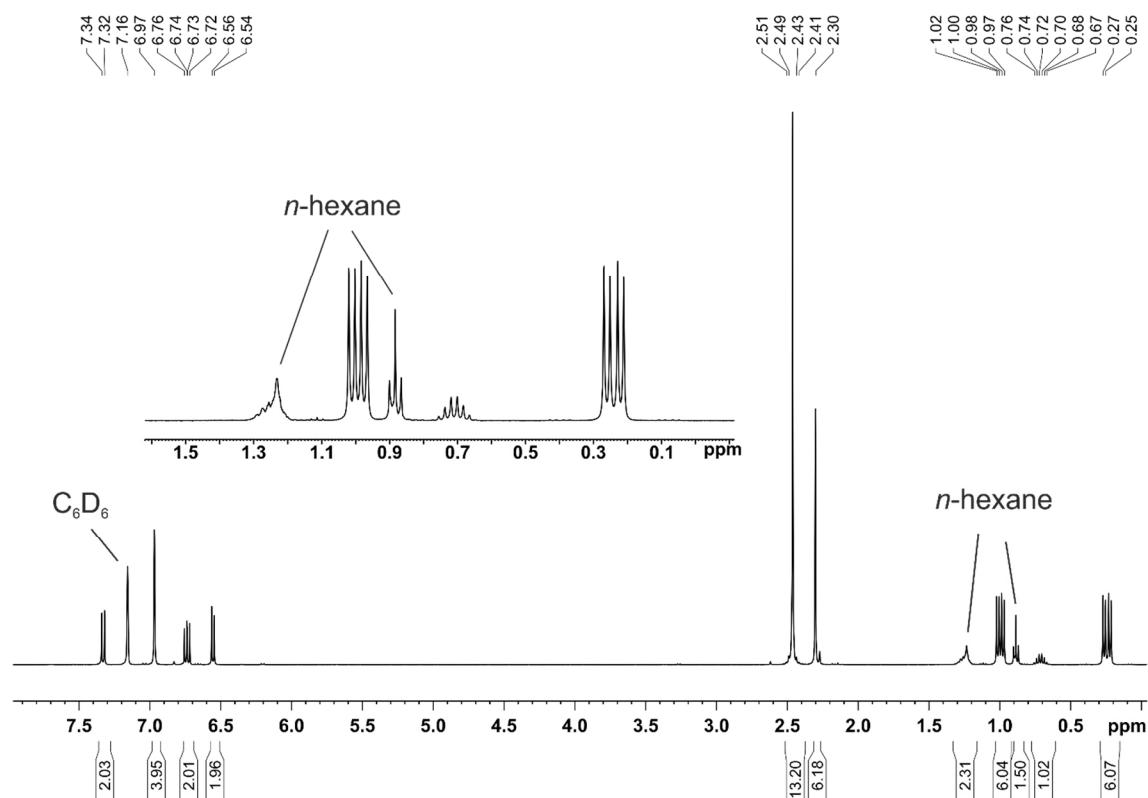
Figure S14. ^{1}H NMR spectrum (400.13 MHz, 300 K, C$_6$D$_6$) of [(^{Mes}BIAN)Co(*cyclo*-P$_5i$Pr$_2$)] (**3a**).
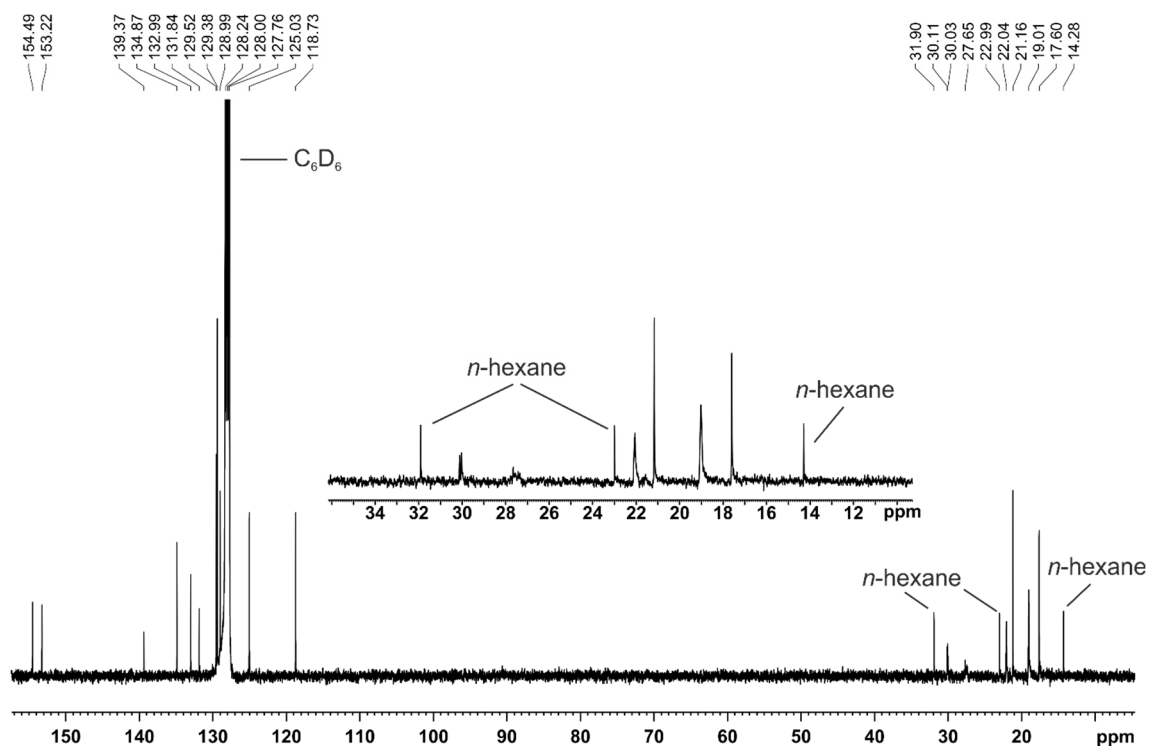
Figure S15. $^{13}C\{^1H\}$ NMR spectrum (100.61 MHz, 300 K, C_6D_6) of [(^{Mes}BIAN)Co(*cyclo*-P$_5i$Pr$_2$)] (**3a**).
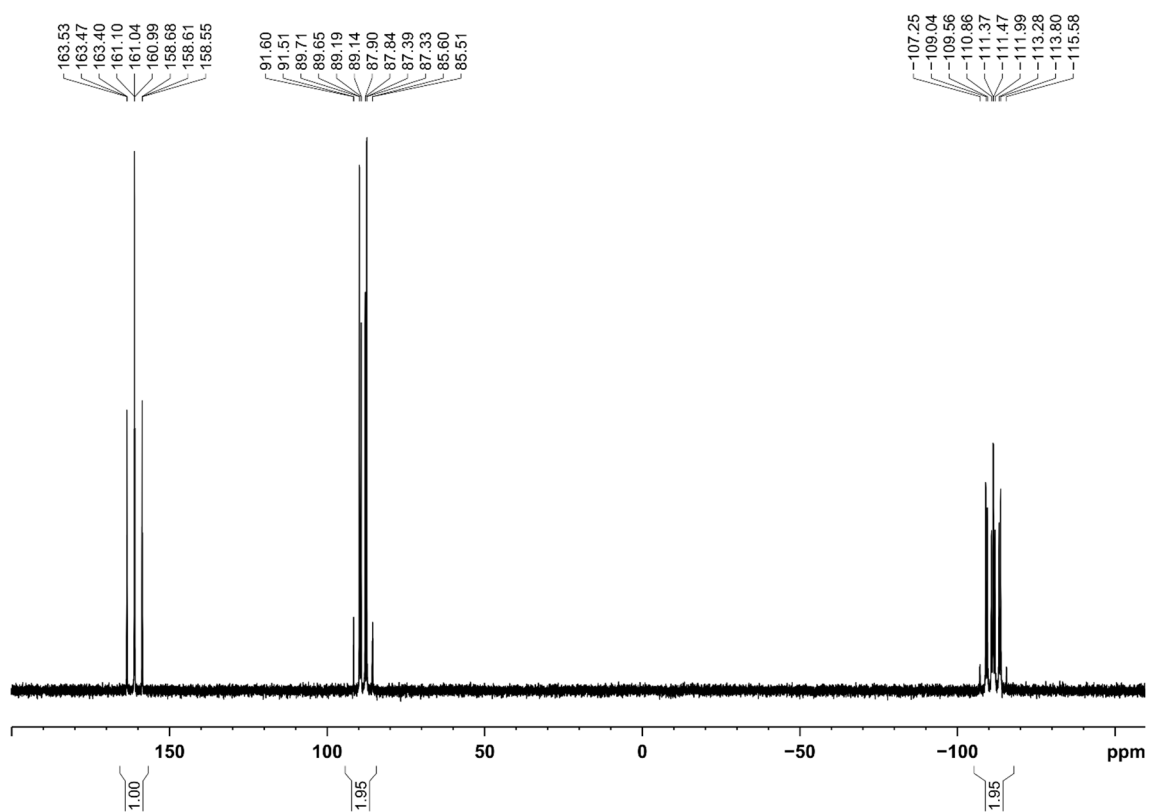
Figure S16. $^{31}P\{^1H\}$ NMR spectrum (161.98 MHz, 300 K, C_6D_6) of [(^{Mes}BIAN)Co(*cyclo*-P$_5i$Pr$_2$)] (**3a**).
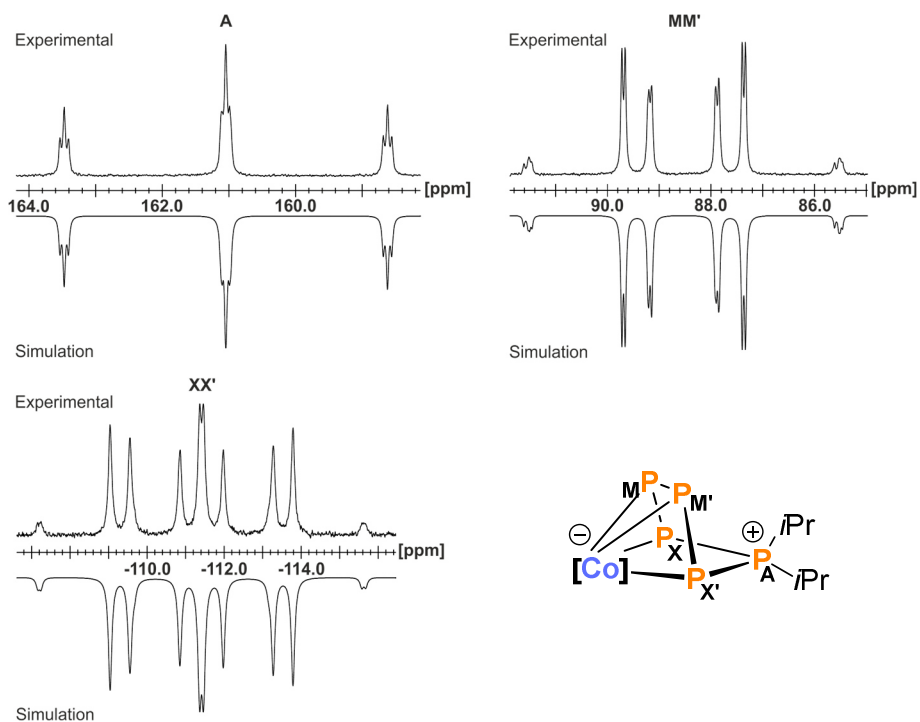
Figure S17. Section of the ^{31}P{^{1}H} NMR (400.13 MHz, 300 K, C$_6$D$_6$) of [(^{Mes}BIAN)Co(*cyclo*-P$_5$*i*Pr$_2$)] (**3a**) and schematic representation of the CoP$_5$*i*Pr$_2$ core; experimental (upwards) and simulation (downwards); [Co] = (^{Mes}BIAN)Co.

Table S3. Coupling constants from the iterative fit of the AMM'XX' spin system of [(^{Mes}BIAN)Co(*cyclo*-P$_5$*i*Pr$_2$)] (**3a**).

$^1J_{AX} = {}^1J_{AX'}$	−392.9 Hz	$^2J_{MX'} = {}^2J_{M'X}$	39.9 Hz
$^1J_{MM'}$	−380.6 Hz	$^2J_{AM} = {}^2J_{AM'}$	10.4 Hz
$^1J_{MX} = {}^1J_{M'X'}$	−414.2 Hz	$^2J_{XX'}$	9.2 Hz
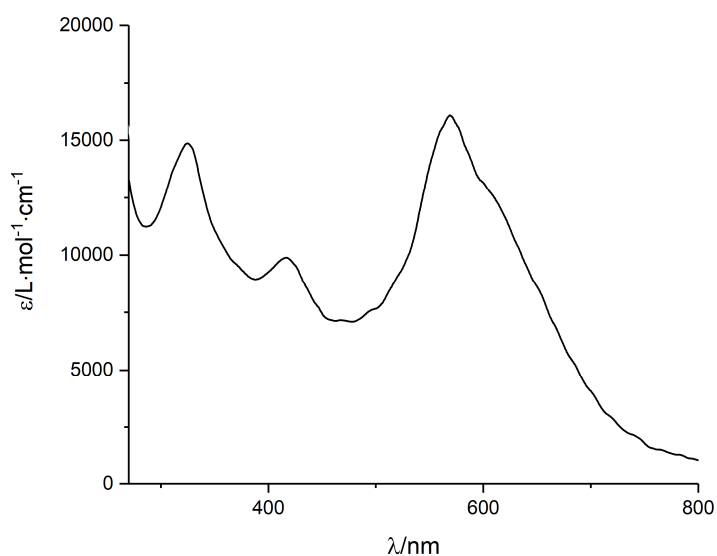
Figure S18. UV/vis spectrum of [(^{Mes}BIAN)Co(*cyclo*-P$_5$*i*Pr$_2$)] (**3a**) recorded in THF.

2.5.6 Synthesis of [(^{Mes}BIAN)Co(cyclo-P$_5$$tBu_2$)] (3b)

A solution of tBu$_2$PCl in THF (0.5 mL, c = 0.24 mol·L^{-1}, 1.0 equiv.) was added to a dark violet THF solution (15 mL) of [K(dme)$_2$\{(^{Mes}BIAN)Co(μ-η^4:η^2-P$_4$)Ga(nacnac)\}] (**2**) (150 mg, 0.12 mmol, 1.0 equiv.). The reaction mixture was stirred while heating to 60 °C for 2 days accompanied by a color change of the solution to cyan. Separation from by-product [Ga(nacnac)] was achieved by column chromatography (stationary phase: neutral aluminum oxide, activity grade: Super I, 20 x 2 cm, eluent: *n*-hexane/toluene gradient, 100/0 to 0/100). [Ga(nacnac)] hydrolyses on aluminum oxide to nacnacH, which elutes first as colorless band (R$_f$ (*n*-hexane/toluene, 7/1 = 0.6). The following blue band (R$_f$ (*n*-hexane/toluene, 7/1 = 0.2) was collected, and the solvent was removed completely under vacuum. The remaining blue solid was extracted with *n*-hexane. Pure crystalline product **3b** precipitated from a concentrated solution of *n*-hexane at room temperature in the course of three days.

Yield: 29.7 mg (32%).

m.p. 254 °C (decomposition to violet oil).

UV/vis: (THF, λ$_{max}$ / nm, ε$_{max}$ / L·mol^{-1}·cm^{-1}): 295sh (9000), 332 (13000), 393 (7400), 440 (6558), 572 (9100) 629 (9769).

^{1}H NMR (400.13 MHz, 300 K, C$_6$D$_6$): δ / ppm = 7.30 (d, $^3J_{HH}$ =8.1 Hz, 2H, CH$_{(BIAN)}$), 6.96 (s, 4H. *m*-CH$_{(Mes)}$), 6.75 (dd, $^3J_{HH}$ =7.0 Hz, $^3J_{HH}$ =8.1 Hz, 2H, CH$_{(BIAN)}$), 6.45 (d, $^3J_{HH}$ =7.0 Hz, 2H, CH$_{(BIAN)}$), 2.48 (s, 12H, *o*-CH$_{3(Mes)}$), 2.26 (s, 6H, *p*-CH$_{3(Mes)}$), 1.65 (d, $^3J_{HP}$ = 12.8 Hz, 9H, C(CH$_3$)$_3$), 0.41 (d, $^3J_{HP}$ = 13.9 Hz, 9H, C(CH$_3$)$_3$).

^{13}C\{^{1}H\} NMR (100.61 MHz, 300 K, THF-d_8): δ / ppm = 154.2 (C$_{(BIAN)}$), 148.8 (C$_{(Mes)}$), 139.5 (C$_{(BIAN)}$), 135.0 (C$_{(Mes)}$), 132.9 (C$_{(BIAN)}$), 131.5 (C$_{(BIAN)}$), 130.9 (C$_{(Mes)}$), 129.3 (CH$_{(Mes)}$), 128.8 (CH$_{(BIAN)}$), 125.1 (CH$_{(BIAN)}$), 118.9 (CH$_{(BIAN)}$) 43.7 (C(CH$_3$)), 43.6 (C(CH$_3$)), 33.3 (C(CH$_3$)$_3$), 28.3 (C(CH$_3$)$_3$), 21.2 (*p*-CH$_{3(Mes)}$), 19.4 (*o*-CH$_{3(Mes)}$).

^{31}P\{^{1}H\} NMR (161.98 MHz, 300 K, C$_6$D$_6$): (AMM'XX') spin system δ / ppm = 172.9 (m, 1P$_A$), 74.0 (m, 2P$_{MM'}$), −173.9 (m, P$_{XX'}$).

Elemental analysis calcd. for C$_{38}$H$_{46}$CoN$_2$P$_5$ (Mw = 744.60 g·mol^{-1}): C 61.30, H 6.23, N 3.76; found C 61.66, H 6.38; N 3.45.

Figure S19. ^{1}H NMR spectrum (400.13 MHz, 300 K, C_6D_6) of [(^{Mes}BIAN)Co(*cyclo*-P$_5t$Bu$_2$)] (**3b**).

Figure S20. ^{13}C{^{1}H} NMR spectrum (100.61 MHz, 300 K, C_6D_6) of [(^{Mes}BIAN)Co(*cyclo*-P$_5t$Bu$_2$)] (**3b**).

Figure S21. $^{31}P\{^1H\}$ NMR spectrum (161.98 MHz, 300 K, C_6D_6) of [(^{Mes}BIAN)Co(*cyclo*-P$_5t$Bu$_2$)] (**3b**).

Figure S22. Section of the $^{31}P\{^1H\}$ NMR (400.13 MHz, 300 K, C_6D_6) of [(^{Mes}BIAN)Co(*cyclo*-P$_5t$Bu$_2$)] (**3b**) and schematic represention of the CoP$_5t$Bu$_2$ core; experimental (upwards) and simulation (downwards); [Co] = (^{Mes}BIAN)Co.

Table S4. Coupling constants from the iterative fit of the AMM'XX' spin system of [(^{Mes}BIAN)Co(*cyclo*-P$_5$*t*Bu$_2$)] (**3b**).

$^1J_{AX} = {}^1J_{AX'}$	−411.4 Hz	$^2J_{MX'} = {}^2J_{M'X}$	38.8 Hz
$^1J_{MM'}$	−405.3 Hz	$^2J_{AM} = {}^2J_{AM'}$	13.1 Hz
$^1J_{MX} = {}^1J_{M'X'}$	−389.4 Hz	$^2J_{XX'}$	9.6 Hz

Figure S23. UV/vis spectrum of [(^{Mes}BIAN)Co(*cyclo*-P$_5$*t*Bu$_2$)] (**3b**) recorded in THF.

2.5.7 Synthesis of [(^{Mes}BIAN)Co(cyclo-P$_5$Cy$_2$)] (3c)

A solution of Cy$_2$PCl in THF (2.1 mL, c = 0.12 mol·L^{-1}, 1.0 equiv.) was added to a dark violet THF solution (10 mL) of [K(dme)$_2${(^{Mes}BIAN)Co(μ-η^4:η^2-P$_4$)Ga(nacnac)}] (**2**) (335.5 mg, 0.25 mmol, 1.0 equiv.) and stirred at 60 °C for 2 days. A color change of the reaction mixture to cyan was observed. The by-product [Ga(nacnac)] was separated by column chromatography (stationary phase: neutral aluminum oxide activity grade: Super I, 10 x 2 cm, eluent: *n*-hexane/toluene gradient, 100/0 to 0/100). [Ga(nacnac)] hydrolyses on aluminum oxide to nacnacH, which elutes first as colorless band (R$_f$ (*n*-hexane/toluene, 7/1 = 0.6). The following blue band (R$_f$ (*n*-hexane/toluene, 7/1 = 0.2) was collected, the obtained solution concentrated in *vacuo* and crystallization by *n*-hexane diffusion gave X-ray quality crystals of **3c** after three days storage at room temperature.

Yield: 54.5 mg (26%).

m.p. 252 °C (decomposition to violet oil).

UV/vis: (THF, λ$_{max}$ / nm, ε$_{max}$ / L·mol^{-1}·cm^{-1}): 332 (14000), 424 (9000), 574 (14000), 580 (14500).

^{1}H NMR (400.13 MHz, 300 K, C$_6$D$_6$): δ / ppm = 7.32 (d, $^3J_{HH}$ =8.2 Hz, 2H, CH$_{(BIAN)}$), 6.99 (s, 4H, *m*-CH$_{(Mes)}$), 6.73 (*pseudo*-t, $^3J_{HH}$ =7.4 Hz, $^3J_{HH}$ =7.8 Hz, 2H, CH$_{(BIAN)}$), 6.49 (d, $^3J_{HH}$ =6.8 Hz, 2H, CH$_{(BIAN)}$), 2.47 (s, 12H, *o*-CH$_{3(Mes)}$), 2.33 (s,6H, *p*-CH$_{3(Mes)}$), 1.94 (m, 2H, CH$_{2(cy)}$), 1.55 (m, 3H, CH$_{2(cy)}$ and CH$_{(cy)}$), 1.34 – 1.0 (m, 10H, CH$_{2(cy)}$), 0.93 – 0.64 (m, 4H, CH$_{2(cy)}$), 0.65 – 0.49 (m, 3H, CH$_{2(cy)}$ and CH$_{(cy)}$).

^{13}C{^{1}H} NMR (100.61 MHz, 300 K, C$_6$D$_6$): δ / ppm = 154.5 (C$_{(BIAN)}$), 153.6 (C$_{(Mes)}$), 139.3 (C$_{(BIAN)}$), 134.8 (C$_{(Mes)}$), 133.0 (C$_{(BIAN)}$), 131.8 (C$_{(BIAN)}$), 129.7 (C$_{(Mes)}$), 129.5 (*C*H$_{(Mes)}$), 129.0 (*C*H$_{(BIAN)}$), 125.0 (*C*H$_{(BIAN)}$), 118.7 (*C*H$_{(BIAN)}$), 40.0 (C$_{Cy}$), 39.8 (C$_{Cy}$), 32.3 (br, C$_{Cy}$), 29.3 (br, C$_{Cy}$), 26.8 (C$_{Cy}$), 26.7 (C$_{Cy}$), 26.4 (C$_{Cy}$), 26.3 (C$_{Cy}$), 25.9 (C$_{Cy}$), 25.4 (C$_{Cy}$), 21.2 (*p*-*C*H$_{3(Mes)}$), 19.0 (*o*-*C*H$_{3(Mes)}$).

^{31}P{^{1}H} NMR (161.98 MHz, 300 K, C$_6$D$_6$): (AMM'XX') spin system δ / ppm = 154.0 (m, 1P$_A$), 87.9 (m, 2P$_{MM'}$), −113.2 (m, P$_{XX'}$).

Elemental analysis calcd. for C$_{42}$H$_{50}$CoN$_2$P$_5$ · (C$_7$H$_8$)$_{0.5}$ · (C$_6$H$_{14}$)$_{0.1}$ (Mw = 851.35g·mol^{-1}): C 65.04, H 6.56, N 3.29; found C 65.48, H 6.44; N 3.22. According to ^{1}H NMR spectroscopy the compound contains 0.5 molecules toluene and approximately 0.1 molecules *n*-hexane per formula unit after drying under vacuum (10^{-3} mbar).

Figure S24. ^{1}H NMR spectrum (400.13 MHz, 300 K, C$_6$D$_6$) of [(^{Mes}BIAN)Co(*cyclo*-P$_5$Cy$_2$)] (**3c**).

Figure S25. $^{13}C\{^1H\}$ NMR spectrum (100.61 MHz, 300 K, C_6D_6) of [(^{Mes}BIAN)Co(*cyclo*-P$_5$Cy$_2$)] (**3c**).

Figure S26. $^{31}P\{^1H\}$ NMR spectrum (161.98 MHz, 300 K, C_6D_6) of [(^{Mes}BIAN)Co(*cyclo*-P$_5$Cy$_2$)] (**3c**).

Figure S27. Section of the $^{31}P\{^1H\}$ NMR (400.13 MHz, 300 K, C$_6$D$_6$) of [(^{Mes}BIAN)Co(*cyclo*-P$_5$Cy$_2$)] (**3c**) and schematic representation of the CoP$_5$Cy$_2$ core; experimental (upwards) and simulation (downwards); [Co] = (^{Mes}BIAN)Co.

Table S5. Coupling constants from the iterative fit of the AMM'XX' spin system of [(^{Mes}BIAN)Co(*cyclo*-P$_5$Cy$_2$)] (**3c**).

$^1J_{AX} = {}^1J_{AX'}$	−390.1 Hz	$^2J_{MX'} = {}^2J_{M'X}$	37.5 Hz
$^1J_{MM'}$	−379.0 Hz	$^2J_{AM} = {}^2J_{AM'}$	9.5 Hz
$^1J_{MX} = {}^1J_{M'X'}$	−413.5 Hz	$^2J_{XX'}$	8.0 Hz

Figure S28. UV/vis spectrum of [(^{Mes}BIAN)Co(*cyclo*-P$_5$Cy$_2$)] (**3c**) recorded in THF.

2.5.8 Intermediate [(^{Mes}BIAN)Co(μ-η^4:η^2-P$_5$$iPr_2$)Ga(nacnac)}] (4)
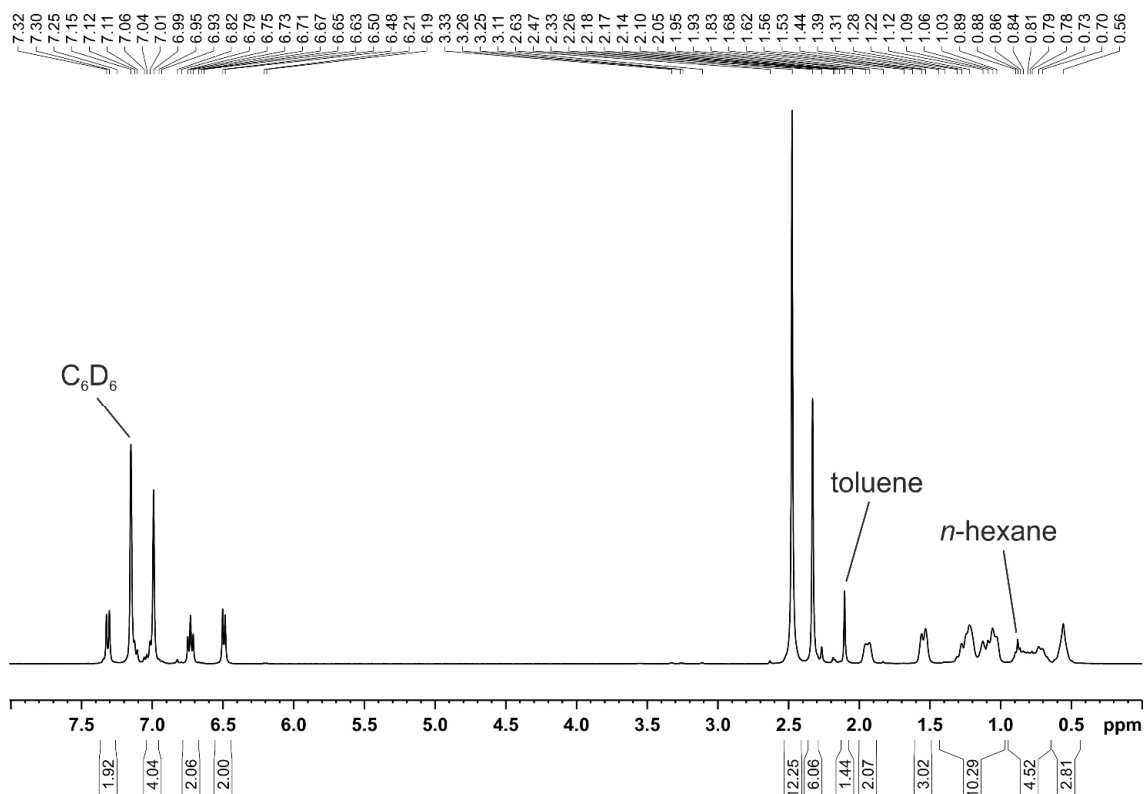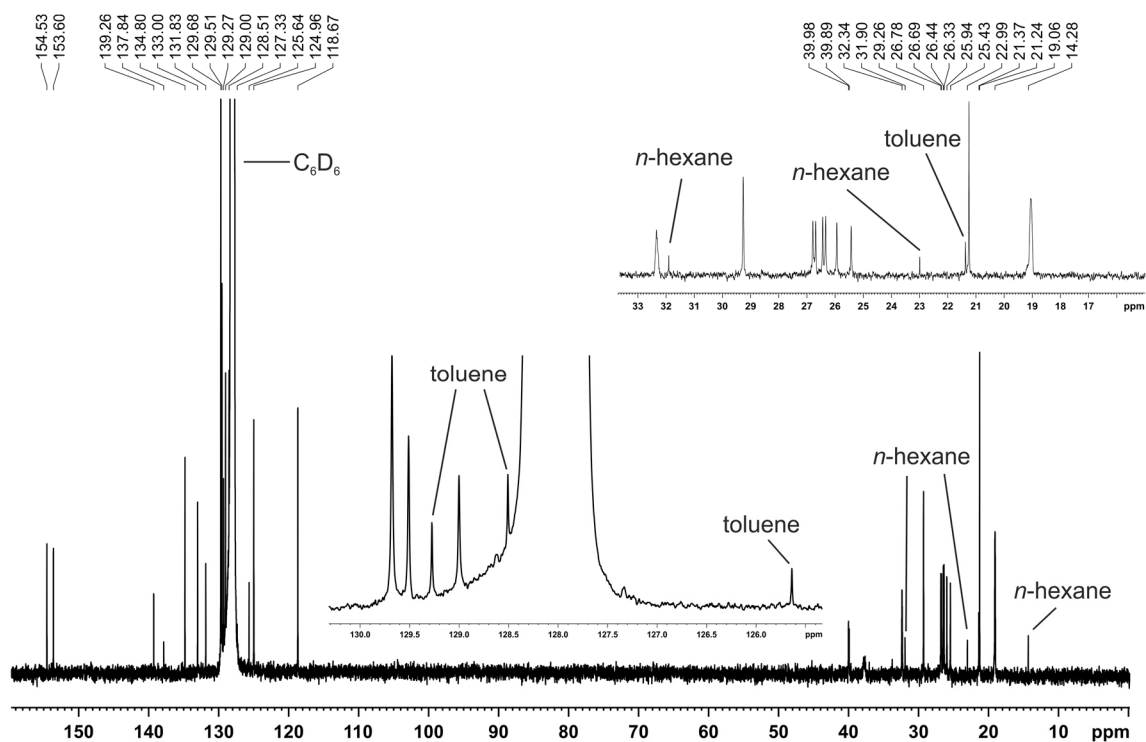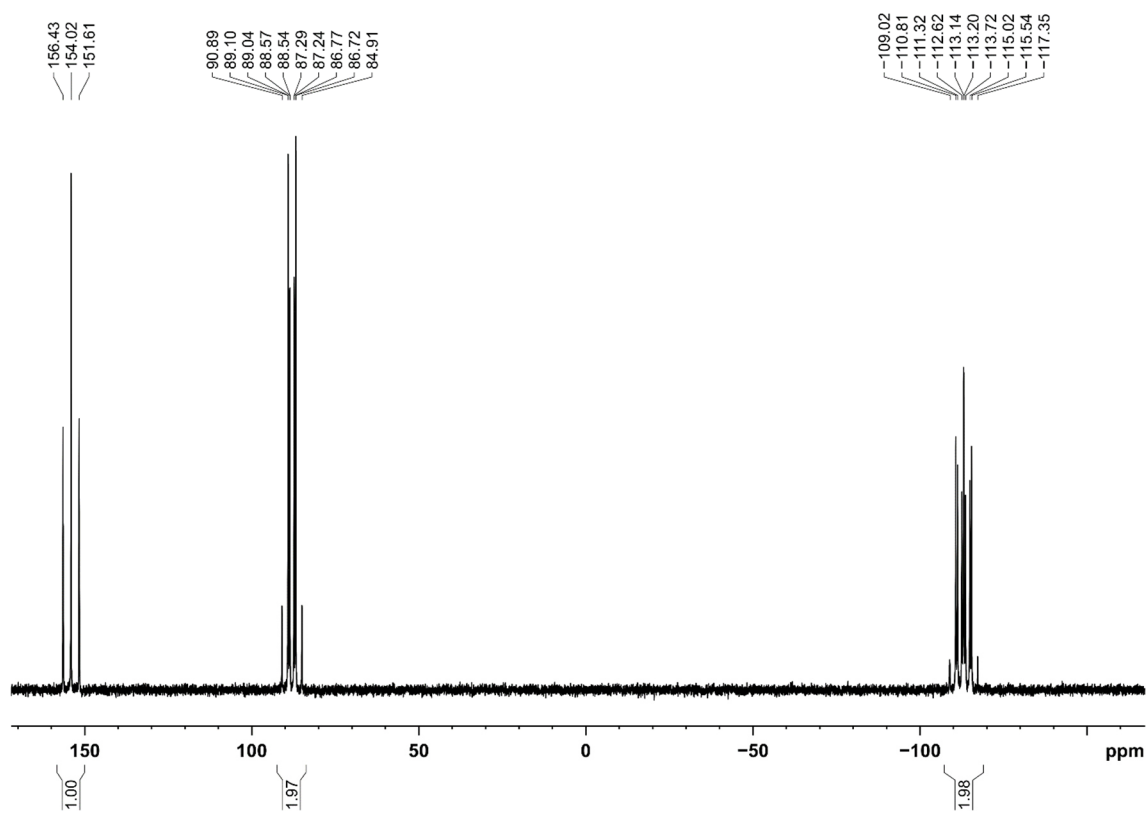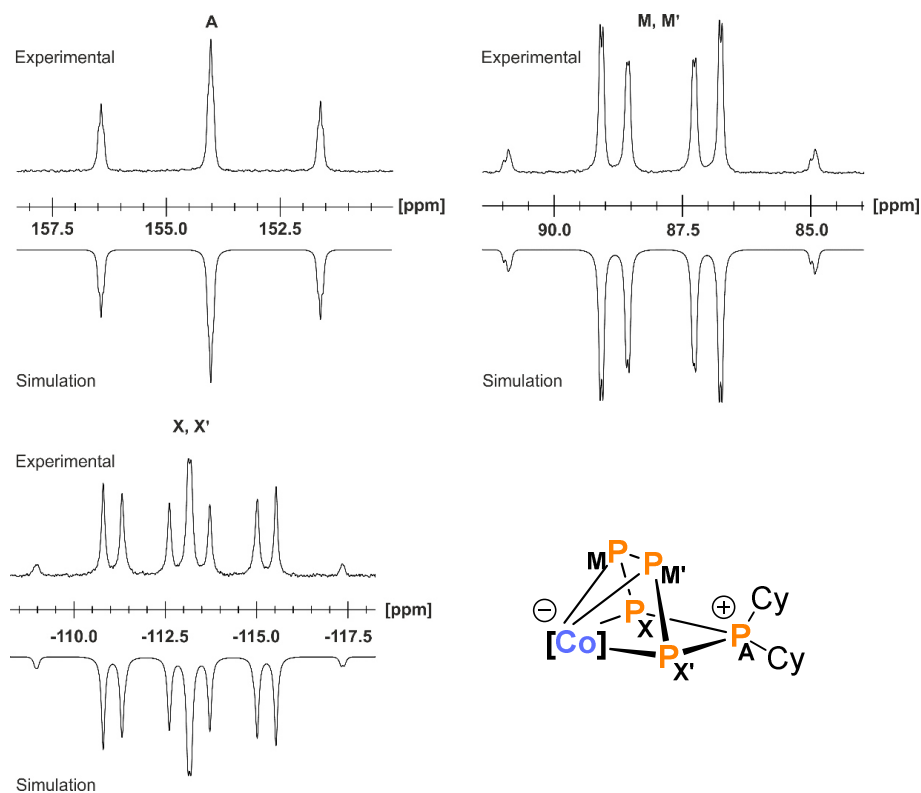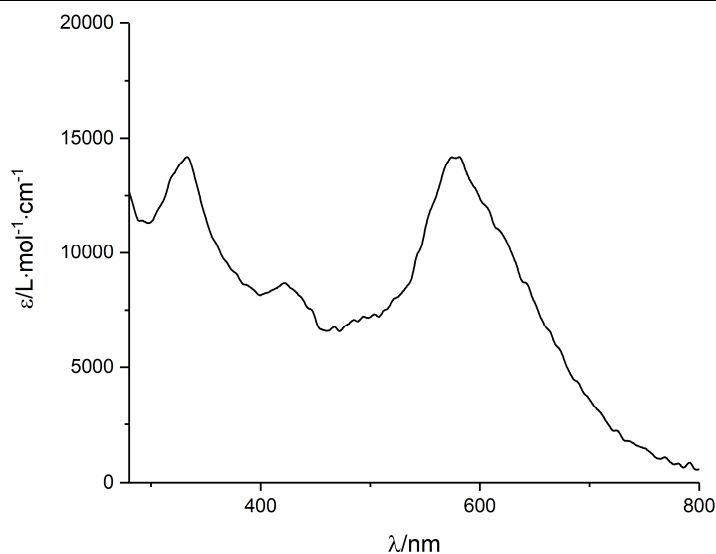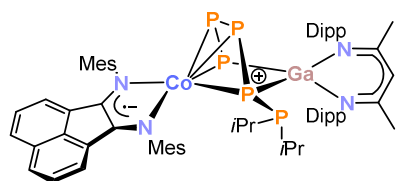
A solution of iPr$_2$PCl in THF (0.38 mL, c = 0.18 mol·L^{-1}, 1.0 equiv.) was added to a dark violet THF solution (10 mL) of [K(dme)$_2${(^{Mes}BIAN)Co(μ-η^4:η^2-P$_4$)Ga(nacnac)}] (2) (85 mg, 0.07 mmol, 1.0 equiv.) and stirred for 30 minutes. Volatiles were removed in *vacuo* and the remaining violet residue was extracted with 20 mL *n*-hexane. Violet crystals of 4 suitable for single X-ray diffraction formed during storage at −30 °C in the course of two days.

The instability of compound 4 in solution prevented its further characterization. 4 readily transform to compound 3a in solution (*vide infra*).

2.5.9   Synthesis of [(^{Mes}BIAN)Co(μ-η^4:η^1-P$_5$*t*Bu)GaCl(nacnac)] (5)
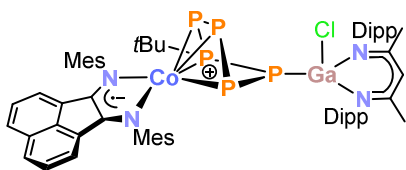
A solution of *t*BuPCl$_2$ in THF (2.0 mL, c = 0.12 mol·L^{-1}, 1.0 equiv.) was added to a dark violet THF solution (15 mL) of [K(dme)$_2${(^{Mes}BIAN)Co(μ-η^4:η^2-P$_4$)Ga(nacnac)}] (**2**) (300 mg, 0.24 mmol, 1.0 equiv.). The mixture turned greyish-blue and was stirred for two days at room temperature. Subsequently, all volatiles were removed in *vacuo*. The remaining dark solid was redissolved in toluene (10 mL, greyish-blue solution) and filtered through a P4 frit. The ^{1}H NMR spectrum (400.13 MHz, 300 K, THF-d_8) of the raw product shows the signals of the main product **5** and signals assigned to an unidentified paramagnetic impurity [δ / ppm = 48.6 (br), 41.4, 18.9, 6.5 (br), 1.3, −6.1 (br), −8.2, −16.6 (br)]. The paramagnetic impurity was removed by recrystallizing the raw product six times from concentrated toluene solution at −30 °C. According to the ^{1}H NMR spectrum, the isolated compound subsequently only contained traces of the paramagnetic impurity. Based on the ^{1}H NMR data, 0.74 toluene solvate molecules per formula unit were present after evacuating the solid for 5 h at room temperature. Crystals suitable for single X-ray diffraction were obtained by slow evaporation of fluorobenzene solution over the course of three weeks.

Yield: 18.4 mg (6%).

m.p. 255 °C (decomposition to black oil).

UV/vis: (THF, λ_{max} / nm, ε_{max} / L·mol^{-1}·cm^{-1}): 348 (30000), 421 (12000), 612 (15500).

^{1}H NMR (400.13 MHz, 300 K, THF-d_8): δ / ppm = 7.63 (d, *J* = 8.0, 2H, C*H*$_{BIAN}$), 6.98 (m, 2H, C*H*$_{BIAN}$), 7.32 – 7.03 (m, 6H, C*H*$_{Dipp}$), 7.01 – 6.96 (m, 2H C*H*$_{BIAN}$), 6.96 – 6.90 (m, 4H, C*H*$_{Mes}$), 6.19 (d, $^3J_{HH}$ = 6.2 Hz, 2H, C*H*$_{BIAN}$), 5.15 (s, 1H, C*H*$_{nacnac}$), 3.24 – 3.05 (m, 3H, C*H*(CH$_3$)$_2$), 2.77 (sept, $^3J_{HH}$ = 6.8 Hz, 2H, C*H*(CH$_3$)$_2$), 2.41 (s, 6H, C*H*$_{3(Mes)}$), 2.21 (s, 6H, C*H*$_{3(Mes)}$), 1.92 (s, 6H, C*H*$_{3(Mes)}$) 1.77 (s, 3H, C*H*$_{3(nacnac)}$), 1.73 (s, 3H, C*H*$_{3(nacnac)}$), 1.55 (d, $^3J_{HH}$ = 6.7 Hz, 3H, CH(C*H*$_3$)$_2$), 1.45 (d, $^3J_{HH}$ = 6.6 Hz, 3H, CH(C*H*$_3$)$_2$), 1.36 (d, $^3J_{HH}$ = 6.8 Hz, 3H, CH(C*H*$_3$)$_2$), 1.18 – 1.12 (m, 9H, CH(C*H*$_3$)$_2$), 1.00 (m, 6H, CH(C*H*$_3$)$_2$), 0.89 (d, $^3J_{HP}$ = 15.5 Hz, 9H, C(CH$_3$)$_3$).

^{13}C{^{1}H} (100.61 MHz, 300 K, THF-d_8): δ / ppm = 170.3 (C$_{nacnac}$), 170.0 (C$_{nacnac}$), 156.3 (C$_{BIAN}$), 153.2 (C$_{Mes}$), 146.1 (C$_{Dipp}$), 145.6 (C$_{Dipp}$), 143.4 (C$_{Dipp}$), 143.3 (C$_{Dipp}$), 143.3 (C$_{Dipp}$), 141.8 (C$_{BIAN}$), 141.3 (C$_{Dipp}$), 138.4 (C$_{BIAN}$), 134.8 (C$_{Mes}$), 133.4 (C$_{BIAN}$), 133.3 (C$_{BIAN}$), 132.2 (C$_{BIAN}$), 129.5 (CH$_{Mes}$), 129.3 (CH$_{Mes}$), 128.9 (CH$_{BIAN}$), 128.8 (CH$_{BIAN}$), 128.7 (CH$_{BIAN}$), 128.3 (CH$_{Dipp}$), 126.2 (CH$_{Dipp}$), 126.0 (CH$_{Dipp}$), 125.9 (CH$_{Dipp}$), 125.4 (CH$_{Dipp}$), 125.3 (CH$_{BIAN}$), 125.2 (CH$_{BIAN}$), 124.8 (CH$_{Dipp}$), 118.8 (CH$_{BIAN}$) 97.1 (CH$_{nacnac}$), 40.6 (*C*(CH)$_3$), 33.2 (C(*C*H)$_3$), 30.6 (*C*H(CH$_3$)$_2$), 30.2 (*C*H(CH$_3$)$_2$), 28.4 (*C*H(CH$_3$)$_2$), 28.2 (*C*H(CH$_3$)$_2$), 27.3 (CH(*C*H$_3$)$_2$) 27.6 (CH(*C*H$_3$)$_2$), 26.0 (CH(*C*H$_3$)$_2$), 25.7 (CH(*C*H$_3$)$_2$), 25.5 (CH(*C*H$_3$)$_2$), 25.3 (CH(*C*H$_3$)$_2$), 24.4 (CH(*C*H$_3$)$_2$), 23.9 (CH(*C*H$_3$)$_2$), 23.8 (CH$_{3(nacnac)}$), 23.7 (CH$_{3(nacnac)}$), 23.6 (CH$_{3(Mes)}$), 21.2 (CH$_{3(Mes)}$), 19.5 (CH$_{3(Mes)}$), 19.5 (CH$_{3(Mes)}$), 19.1 (CH$_{3(Mes)}$) 19.2 (CH$_{3(Mes)}$).

^{31}P{^{1}H} NMR (161.98 MHz, 300 K, THF-d_8): (ABEMX) spin system δ / ppm = 70.6 (m, 2P), 50.5 (m, 1P), 13.6 (m, 1P), −64.7 (m, 1P), ^{31}P{^{1}H} NMR (161.98 MHz, 213 K, THF-d_8): (ABEMX) spin system δ / ppm = 70.3 (m, 1P), 66.0 (m, 1P), 48.4 (m, 1P), 12.0 (m, 1P), −66.8 (m, 1P).

Elemental analysis calcd. for C$_{63}$H$_{78}$ClCoGaN$_4$P$_5$ · (C$_4$H$_{10}$O$_2$)$_2$ · (C$_7$H$_8$)$_{0.74}$ (Mw = 1278.5 g·mol^{-1}): C 64.05, H 6.62, N 4.38; found C 64.79, H 6.61, N 4.46. According to

^{1}H NMR spectroscopy the compound contains 0.74 molecules toluene per formula unit after drying under vacuum (10^{−3} mbar). The elemental analysis showed a higher C-value than expected for this composition indicating varying concentrations of the solvate.
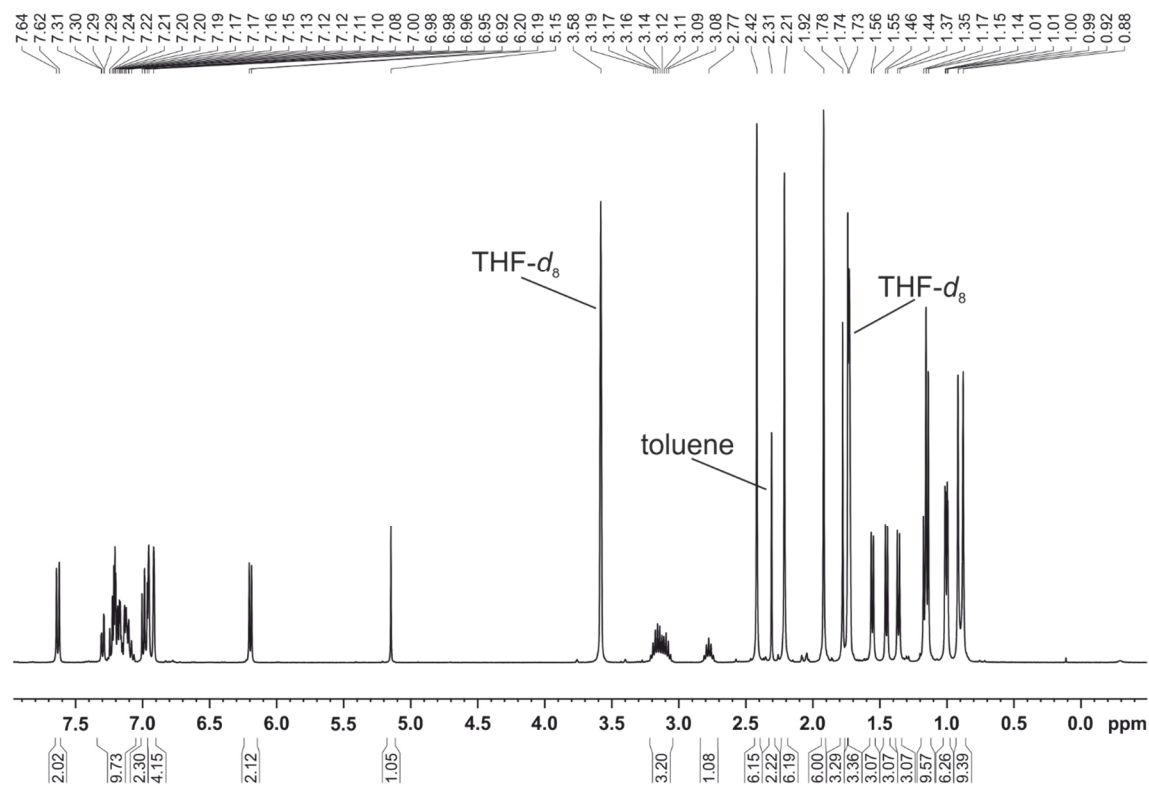
Figure S29. ^{1}H NMR spectrum (400.13 MHz, 300 K, THF-d_8) of [(^{Mes}BIAN)Co(μ-η^4:η^1-P$_5t$Bu)GaCl(nacnac)] (**5**).
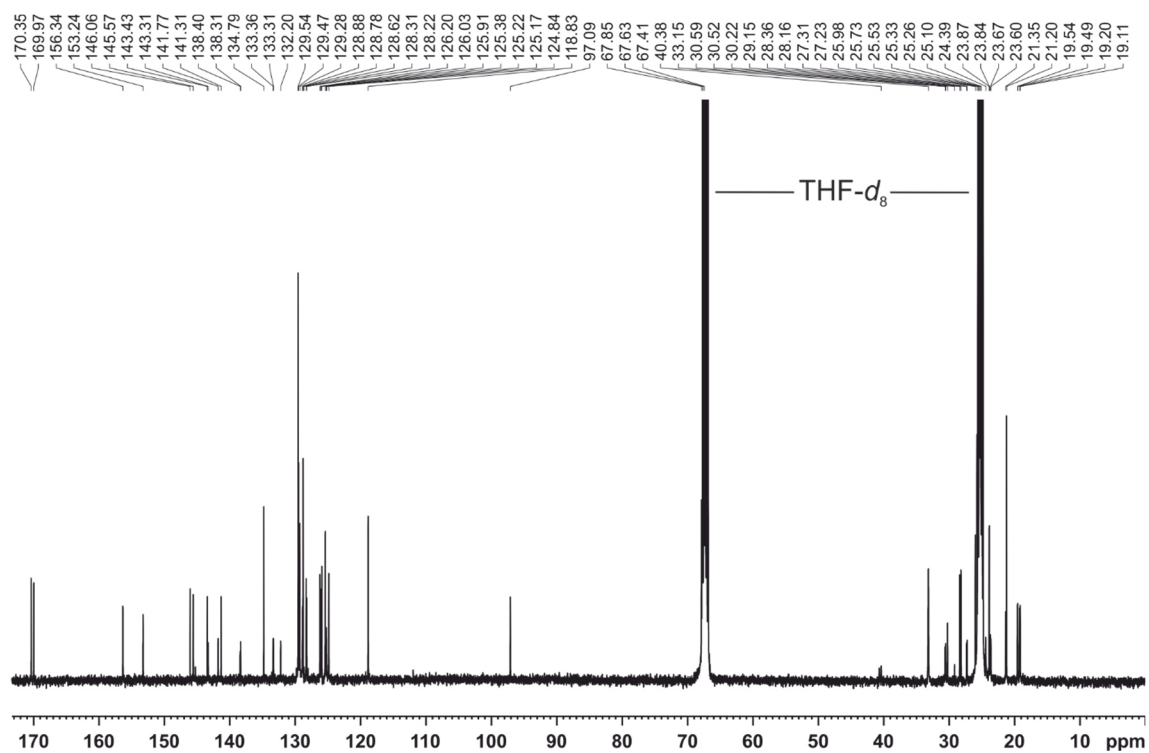
Figure S30. $^{13}\text{C}\{^1\text{H}\}$ NMR spectrum (100.61 MHz, 300 K, THF-d_8) of [($^{\text{Mes}}$BIAN)Co(μ-η^4:η^1-P$_5t$Bu)GaCl(nacnac)] (**5**).
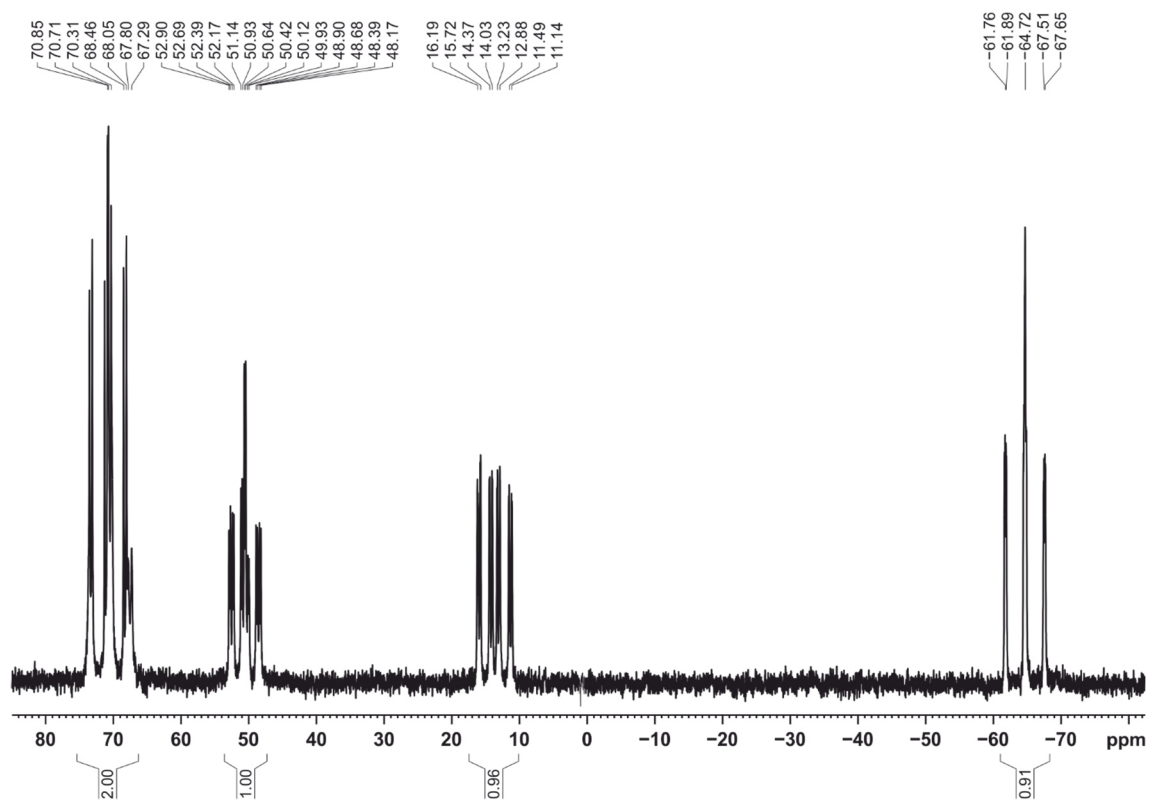
Figure S31. $^{31}\text{P}\{^1\text{H}\}$ NMR spectrum (161.98 MHz, 300 K, THF-d_8) of [($^{\text{Mes}}$BIAN)Co(μ-η^4:η^1-P$_5t$Bu)GaCl(nacnac)] (**5**).
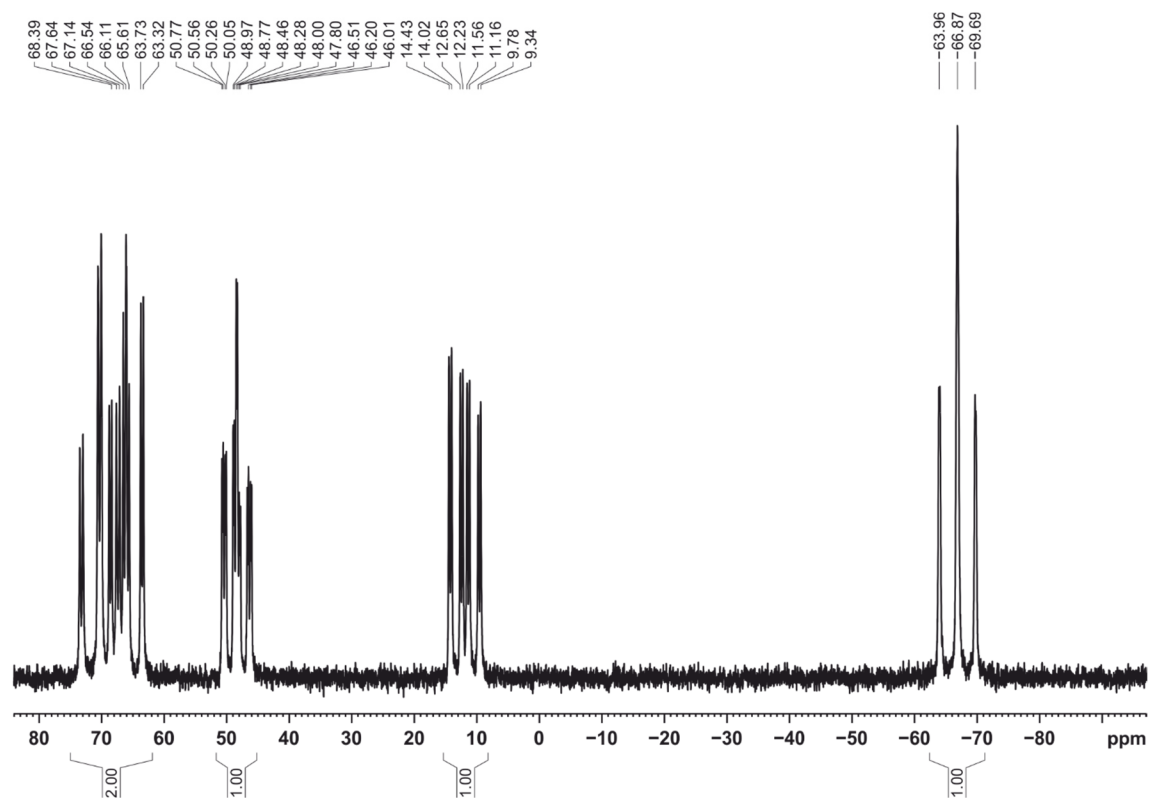
Figure S32. ^{31}P{^{1}H} NMR spectrum (161.98 MHz, 213 K, THF-d_8) of [(^{Mes}BIAN)Co(μ-η^4:η^1-P$_5t$Bu)GaCl(nacnac)] (**5**).
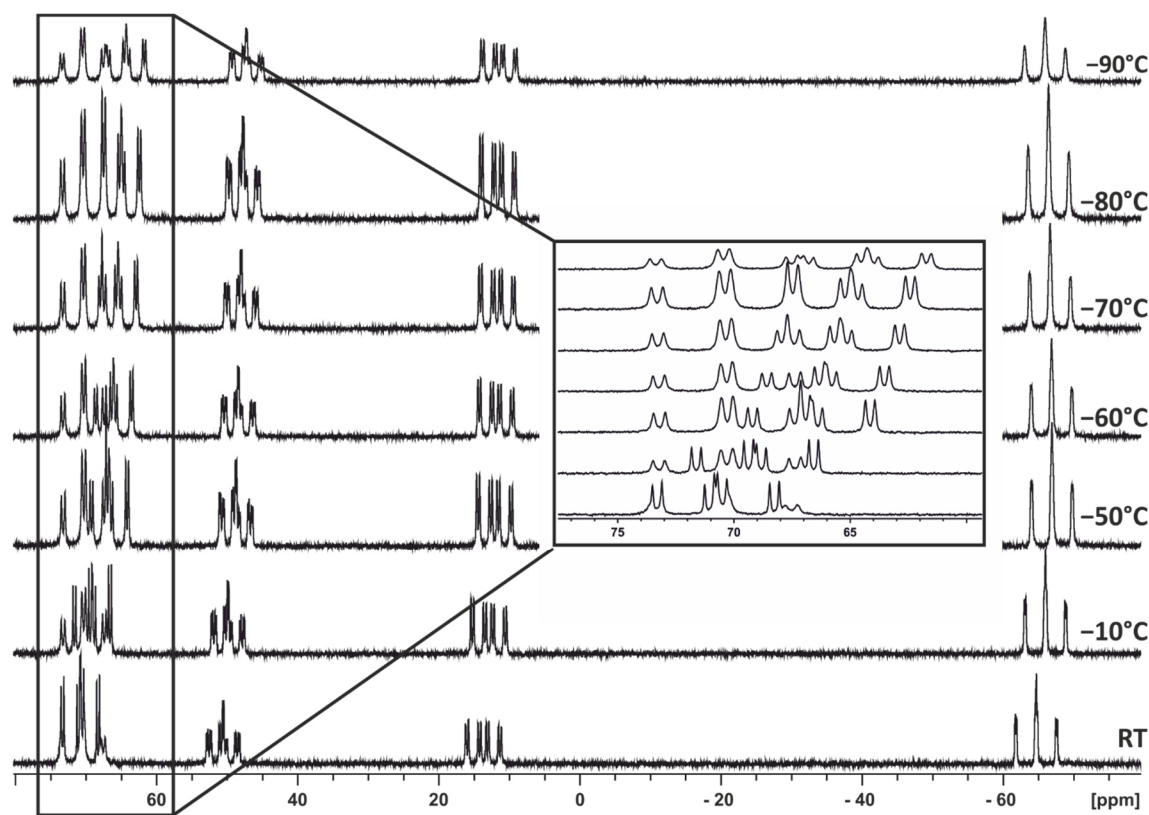
Figure S33. VT-^{31}P{^{1}H} NMR spectrum (161.98 MHz, THF-d_8) of [(^{Mes}BIAN)Co(μ-η^4:η^1-P$_5t$Bu)GaCl(nacnac)] (**5**); inset section from 77.0 ppm to 60.0 ppm.
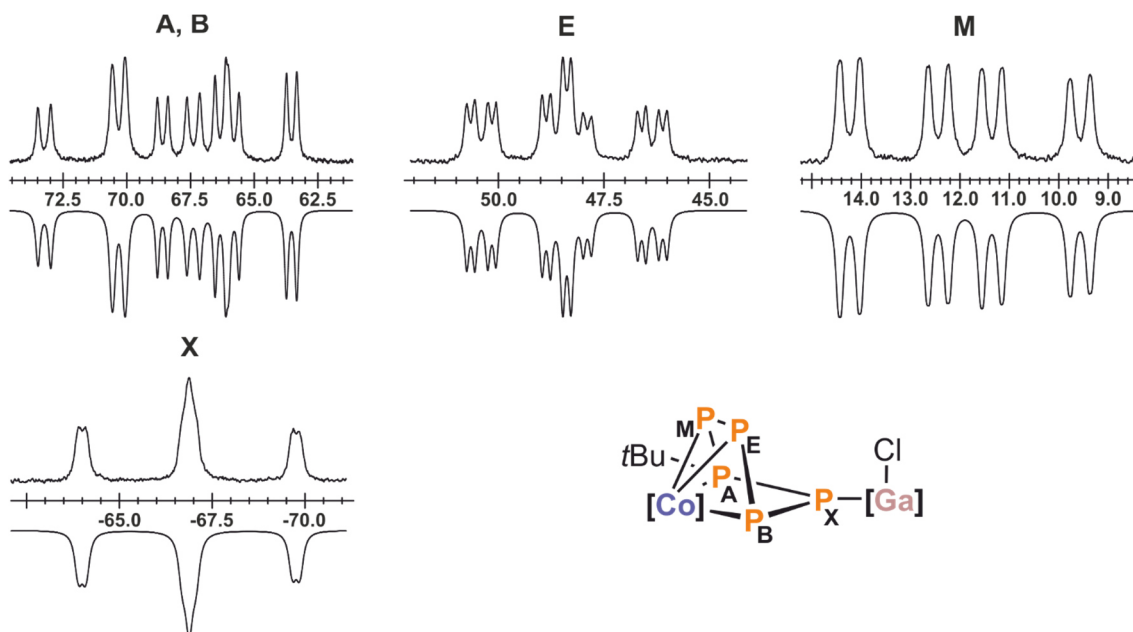
Figure S34. Section of the $^{31}P\{^1H\}$ NMR (400.13 MHz, 213 K, THF-d_8) of [(^{Mes}BIAN)Co(μ-η^4:η^1-P$_5$$t$Bu)GaCl(nacnac)] (**5**) and schematic representation of the CoP$_5$$t$BuGa core; experimental (upwards) and simulation (downwards); [Co] = (^{Mes}BIAN)Co, [Ga] = (nacnac)Ga.

Table S6. Coupling constants from the iterative fit of the ABEMX spin system of [(^{Mes}BIAN)Co(μ-η^4:η^1-P$_5$$t$Bu)GaCl(nacnac)] (**5**) at 213 K.

$^1J_{AM}$	−466.3 Hz	$^2J_{AE}$	81.8 Hz
$^1J_{AX}$	−481.4 Hz	$^2J_{ABM}$	8.2 Hz
$^1J_{BX}$	−455.1 Hz	$^2J_{BM}$	67.7 Hz
$^1J_{BE}$	−367.0 Hz	$^2J_{EX}$	33.7 Hz
$^1J_{EM}$	−291.6 Hz	$^2J_{MX}$	12.2 Hz

Figure S35. UV/vis spectrum of [(^{Mes}BIAN)Co(μ-η^4:η^1-P$_5t$Bu)GaCl(nacnac)] (**5**) recorded in THF.

2.5.10 ^{31}P NMR reaction monitoring

In a glovebox 40 mg (0.032 mmol; 1.0 equiv.) [K(dme)$_2$\{(^{Mes}BIAN)Co(μ-η^4:η^2-P$_4$)Ga(nacnac)\}] (**2**) were dissolved in 0.4 mL of THF-d_8 after which 4.85 mg (0.032 mmol; 1.0 equiv.) iPr$_2$PCl in 0.2 mL THF-d_8 was slowly added under stirring. After 5 minutes the reaction mixture was transferred into a J. Young valve NMR tube and the first NMR measurements started 5 minutes later. ^{1}H, ^{31}P\{^{1}H\} and ^{31}P NMR measurements were performed after every hour in the course of six hours. After that, the intermediate time was extended to 4 hours and the measurements continued for 102 hours. Throughout the reaction monitoring the NMR tube was kept spinning with 20 Hz to obtain a homogeneous solution.

2.5.11 VT ^{31}P NMR reaction monitoring

In a glovebox 25 mg (0.02 mmol; 1.0 equiv.) [K(dme)$_2$\{(^{Mes}BIAN)Co(μ-η^4:η^2-P$_4$)Ga(nacnac)\}] (**2**) were dissolved in 0.4 mL of THF-d_8 after which 3 mg (0.02 mmol; 1.0 equiv.) iPr$_2$PCl in 0.2 mL THF-d_8 was slowly added while stirring. After 5 minutes the reaction mixture was transferred into a J. Young valve NMR tube and the first NMR measurements started 5 minutes later. ^{1}H and ^{31}P\{^{1}H\} NMR measurements were performed in a temperature range from 240 K to 329 K. After every hour the temperature was increased by 10 K. Due to the boiling point of THF (339 K), 329 K was the highest temperature achievable. Throughout the measurement the NMR tube was kept spinning with 20 Hz to obtain a homogeneous solution.

Figure S36. $^{31}P\{^1H\}$ VT NMR monitoring of the reaction of **2** dissolved in THF-d_8 with iPr$_2$PCl in a 1:1 ratio; resonances marked with ● are assigned to product [(^{Mes}BIAN)Co(η^4-P$_5$iPr$_2$)] (**3a**) whereas those marked with ▲ (**Int-A**) and ■ (**Int-B**) are assigned to intermediates. The ratio of **Int-A** and **Int-B** was determined by $^{31}P\{^1H\}$ NMR integration.

2.6 X-ray Crystallography

The single-crystal X-ray diffraction data were recorded on an Agilent Technologies SuperNova in case of **2**, **2'**, **3b**, **3c, 5** and on a GV1000 diffractometer in case of **1-dme**, **3a**, and **4** with Cu K$_\alpha$ radiation (λ = 1.54184 Å). Empirical multi-scan[10] and analytical absorption corrections[11],[12] were applied to the data. The structures were solved with SHELXT[13] and least-square refinements on F^2 were carried out with SHELXL.[14] During the refinement of structure **2** the PLATON Squeeze model was applied to one highly disordered DME molecule per formula unit, which was found in a volume of 841.6 Å^3 containing 92.9 electrons.[15]

Compound **4** crystallized as multicrystal in the triclinic space group $P\bar{1}$. Three unit cells were identified. For each unit cell a separate data reduction was performed using the multicrystal/twining data reduction tool as implemented in CrysAlisPro.[12] In case of **4·thf** a solvent mask was calculated and 79.5 electrons were found in a volume of 543.0 Å^3. This is consistent with the presence of one molecule THF per formula unit (80 electrons) using Olex2 Solvent Mask.[16]

CCDC 1861837 (**1-dme**), 1861833 (**2**), 1861832 (**2'**), 1861829 (**3a**), 1861830 (**3b**), 1861831 (**3c**), 1861834 (**4·thf**), 1861835 (**4·*n*-hexane**), 1861836 (**4'·*n*-hexane**), and 1874059 (**5**) contain the supplementary crystallographic data for this paper. These data are provided free of charge by The Cambridge Crystallographic Data Centre.

Figure S37. Solid-state molecular structure of [K(dme)$_4${Co(^{Mes}BIAN)(cod)}] (**1-dme**); hydrogen atoms are omitted for clarity and thermal ellipsoids are drawn at the 40% probability level; selected bond lengths [Å] and angles [°]: C1–C2 1.377(5), C1–N1 1.378(5), C2–N2 1.370(4), C3–C4 1.400(6), C5–C6 1.387(6), N1–Co1–N2 84.18(1), bite angle cod-ligand 90.36(3), torsion angle N1–N2–C$_{34cent}$–C$_{56cent}$ 13.60(2).

Figure S38. Solid-state molecular structure of [K(dme)$_2${(^{Mes}BIAN)Co(μ-η^4:η^2-P$_4$)Ga(nacnac)}] (**2**); hydrogen atoms are omitted for clarity and thermal ellipsoids are drawn at the 40% probability level; selected bond lengths [Å] and angles [°]: P1–P2 2.1198(7), P2–P3 2.1755(8), P3–P4 2.1286(7), P4–Ga1 2.3328(5), P1…P4 3.3073(6), P1–Ga1 2.3179(5), Ga1–N3 1.991(1), Ga1–N4 2.014(2), Co1–P1 2.3514(6), Co1–P2 2.3098(6), Co1–P3 2.3117(5), Co1–P4 2.3961(6), Co1–N1 1.918(2), Co1–N2 1.948(2), N1–C1 1.337(2), N2–C2 1.334(2), C1–C2 1.411(3), K1–P3 3.7168(7), K1–P4 3.3430(6), Ga1–P4–P3 94.85(2), P4–P3–P2 106.97(3), P3–P2–P1 103.92(3), P2–P1–Ga1 97.31(2), P1–Ga1–P4 90.66(2).

Figure S39. Solid-state molecular structure of [K(dme)$_2${(^{Dipp}BIAN)Co(μ-η^4:η^2-P$_4$)Ga(nacnac)}] (**2'**); hydrogen atoms are omitted for clarity. Thermal ellipsoids are drawn at the 40% probability level. Selected bond lengths [Å] and angles [°]: P1–P2 2.130(1), P2–P3 2.176(1), P3–P4 2.125(1), P4–Ga1 2.3350(9), P1…P4 3.263(1), P1–Ga1 2.3301(9), Ga1–N3 1.975(3), Ga1–N4 2.015(3), Co1–P1 2.3730(9), Co1–P2 2.3106(9), Co1–P3 2.3105(9), Co1–P4 2.371(1), Co1–N1 1.944(3), Co1–N2 1.940(3), N1–C1 1.336(4), N2–C2 1.338(4), C1–C2 1.406(5), K1–P1 3.393(1), K1–P2 3.548(1), Ga1–P4–P3 96.59(4), P4–P3–P2 103.86(5), P3–P2–P1 105.71(5), P2–P1–Ga1 94.85(4), P1–Ga1–P4 88.75(3).

Figure S40. Solid-state molecular structure of [(^{Mes}BIAN)Co(*cyclo*-P$_5$*i*Pr$_2$)] (**3a**); hydrogen atoms and solvent molecules are omitted for clarity and thermal ellipsoids are drawn at the 40% probability level; selected bond lengths [Å] and angles [°]: P1–P2 2.1297(2), P2–P3 2.1576(2), P3–P4 2.1297(2), P4–P5 2.1347(2), P5–P1 2.1506(1), P5–C1 1.8423(1), P5–C2 1.8458(1), Co1–P1 2.3720(1), Co1–P2 2.3442(1), Co1–P3 2.3447(2), Co1–P4 2.3595(2), Co1–N1 1.9104(1), Co1–N2 1.9480(1), N1–C3 1.32559(8), N2–C4 1.32069(8), C3–C4 1.4366(1), P1–P2–P3 103.926(5), P2–P3–P4 107.049(5), P3–P4–P5 98.104(6), P4–P5–P1 99.966(5), P5–P1–P2 100.689(5), C1–P5–C2 113.0644(5).

Figure S41. Solid-state molecular structure of [(^{Mes}BIAN)Co(*cyclo*-P$_5$*t*Bu$_2$)] (**3b**); hydrogen atoms and solvent molecules are omitted for clarity and thermal ellipsoids are drawn at the 40% probability level. Selected bond lengths [Å] and angles [°]: P1–P2 2.1572(8), P2–P3 2.1310(9), P3–P4 2.1641(9), P5–P1 2.1634(8), P4–P5 2.1626(8), P5–C1 1.888(3), P5–C2 1.897(3), Co1–P1 2.3327(7), Co1–P2 2.3251(7), Co1–P3 2.3211(7), Co1–P4 2.3459(7), Co1–N1 1.925(2), Co1–N2 1.924(2), N1–C3 1.336(3), N2–C4 1.325(3), C3–C4 1.414(3), P1–P2–P3 103.61(3), P2–P3–P4 104.44(3), P3–P4–P5 100.66(3), P4–P5–P1 94.58(3), P5–P4–P3 101.93(3), C1–P5–C2 111.4(1).

Figure S42. Solid-state molecular structure of [(^{Mes}BIAN)Co(*cyclo*-P₅Cy₂)] (**3c**); hydrogen atoms and solvent molecules are omitted for clarity and thermal ellipsoids are drawn at the 40% probability level; Selected bond lengths [Å] and angles [°]: P1–P2 2.1246(1), P2–P3 2.1566(1), P3–P4 2.1285(2), P4–P5 2.1504(1), P5–P1 2.1561(2), P5–C1 1.8412(1), P5–C2 1.85192(9), Co1–P1 2.3473(1), Co1–P2 2.3385(1), Co1–P3 2.33926(9), Co1–P4 2.3704(2), Co1–N1 1.90439(8), Co1–N2 1.9378(1), N1–C3 1.33410(8), N2–C4 1.32937(5), C3–C4 1.41812(8), P1–P2–P3 104.116(5), P2–P3–P4 106.735(5), P3–P4–P5 97.747(5), P4–P5–P1 99.554(5), P5–P1–P2 99.783(5), C1–P5–C2 106.874(4).

Figure S43. Solid-state molecular structure of [(^{Mes}BIAN)Co(μ-η⁴:η²-P₅iPr₂)Ga(nacnac)}] (**4**); hydrogen atoms are omitted for clarity and thermal ellipsoids are drawn at the 40% probability level; selected bond lengths [Å] and angles [°]: P1–P2 2.122(1), P2–P3 2.159(2), P3–P4 2.164(1), P4–P5 2.239(1), P1–Ga1 2.3320(9), P4–Ga1 2.418(1), Ga1–N1 1.992(3), Ga1–N2 1.974(3), Co1–P1 2.348(2), Co1–P2 2.337(1), Co1–P3 2.306(1), Co1–P4 2.353(1), Co1–N3 1.919(3), Co1-N4 1.963(3), C1–N3 1.335(4), C2–N4 1.323(4), C1–C2 1.422(5), P1–P2–P3 103.59(5), P2–P3–P4 102.46(5), P3–P4–P5 93.59(5), P5–P4–Ga1 133.22(5), P4–Ga1–P1 82.28(3), Ga1–P1–P2 97.13(4).

Figure S44. Solid-state molecular structure of [(^{Mes}BIAN)Co(μ-η^4:η^1-P$_5t$Bu)GaCl(nacnac)] (**5**); hydrogen atoms are omitted for clarity and thermal ellipsoids are drawn at the 40% probability level; selected bond lengths [Å] and angles [°]: P1–P2 2.19903(6), P2–P3 2.14129(5), P3–P4 2.13102(7), P4–P5 2.13310(5), P5–P1 2.14148(6), P1–Ga1 2.34200(6), P5–C3 1.89094(6), Ga1–N1 1.94202(6), Ga1–N2 1.96271(5), Ga1–Cl1 2.20080(5), Co1–P2 2.33156(7), Co1–P3 2.33788(6), Co1–P4 2.37439(6), Co1–P5 2.23375(6), Co1–N3 1.95761(5), Co1–N4 1.90519(4), C1–N3 1.31832(3), C2–N4 1.32622(3), C1–C2 1.42740(3); P1–P2–P3 113.062(2), P2–P3–P4 103.661(2), P3–P4–P5 97.566(2), P4–P5–P1 118.046(2), P5–P1–P2 84.471(2), P4–P5–C3 112.065(2), P4–P5–C3 115.399(2), Ga1–P1–P5 115.834(2), Ga1–P1–P2 112.634(2).

Table S7. Crystallographic data of **1-dme**, **2** and **2'**.

Compound	1-dme	2	2'
Empirical formula	$C_{54}H_{80}CoKN_2O_8$	$C_{67}H_{89}CoGaKN_4O_4P_4$	$C_{77}H_{111}CoGaKN_4O_6P_4$
Formula weight	983.23	1306.05	1480.32
Temperature [K]	123(1)	123(1)	123(1)
Crystal system	triclinic	triclinic	orthorhombic
Space group	P-1	P-1	$P2_12_12_1$
a [Å]	15.3646(3)	15.4512(3)	13.84854(12)
b [Å]	25.7695(5)	16.1163(4)	21.0014(2)
c [Å]	27.6375(4)	16.5636(3)	27.3815(3)
α [°]	105.4393(15)	94.7947(16)	90
β [°]	90.5348(15)	103.1479(16)	90
γ [°]	90.8565(17)	98.1715(18)	90
Volume [Å^3]	10545.7(4)	3946.83(14)	7963.62(13)
Z	8	2	4
ρ_{calc} [g/cm^3]	1.239	1.099	1.235
μ [mm^{-1}]	3.678	3.623	3.668
F(000)	4224.0	1376.0	3144.0
Crystal size [mm^3]	0.1887 × 0.132 × 0.0838	0.3316 × 0.1837 × 0.1439	0.227 × 0.205 × 0.125
Radiation	Cu Kα (λ = 1.54184)	Cu Kα (λ = 1.54184)	Cu Kα (λ = 1.54184)
2Θ range for data collection [°]	6.642 to 147.204	7.072 to 153.024	7.154 to 147.026
Index ranges	-19 ≤ h ≤ 18, -31 ≤ k ≤ 31, -33 ≤ l ≤ 34	-19 ≤ h ≤ 19, -18 ≤ k ≤ 20, -20 ≤ l ≤ 20	-12 ≤ h ≤ 17, -25 ≤ k ≤ 18, -34 ≤ l ≤ 33
Reflections collected	135248	50128	37068
Independent reflections	41065 [R_{int} = 0.0703, R_{sigma} = 0.0655]	16206 [R_{int} = 0.0288, R_{sigma} = 0.0273]	14919 [R_{int} = 0.0347, R_{sigma} = 0.0376]
Data / restraints / parameters	41065/0/2479	16206/0/759	14919/167/936
Goodness-of-fit on F^2	1.010	1.036	1.093
Final R indexes [I>=2σ (I)]	R_1 = 0.0710, wR_2 = 0.1778	R_1 = 0.0380, wR_2 = 0.1075	R_1 = 0.0343, wR_2 = 0.0979
Final R indexes [all data]	R_1 = 0.0997, wR_2 = 0.1999	R_1 = 0.0395, wR_2 = 0.1089	R_1 = 0.0387, wR_2 = 0.1081
Largest diff. peak/hole [e Å^{-3}]	1.54/-0.68	0.89/-0.51	0.53/-0.65
Flack parameter	-	-	-0.0292(17)

Table S8. Crystallographic data of **3a-c**.

Compound	3a	3b	3c
Empirical formula	$C_{39}H_{49}CoN_2P_5$	$C_{41}H_{53}CoN_2P_5$	$C_{45}H_{57}CoN_2P_5$
Formula weight	759.58	787.63	839.70
Temperature [K]	123(1))	123(1)	123(1)
Crystal system	triclinic	triclinic	triclinic
Space group	*P*-1	*P*-1	*P*-1
a [Å]	8.2950(6)	11.5086(6)	11.0975(4)
b [Å]	10.3193(6)	12.6623(6)	12.9085(8)
c [Å]	23.1847(14)	16.1055(8)	16.7384(9)
α [°]	84.114(5)	71.013(4)	68.191(5)
β [°]	82.677(5)	69.473(5)	88.775(4)
γ [°]	80.838(6)	70.661(4)	72.802(4)
Volume [Å³]	1936.4(2)	2015.0(2)	2116.1(2)
Z	2	2	2
ρ_{calc} [g/cm³]	1.303	1.298	1.318
μ [mm⁻¹]	5.648	5.446	5.220
F(000)	798.0	830.0	886.0
Crystal size [mm³]	0.374 × 0.092 × 0.037	0.36 × 0.19 × 0.158	0.167 × 0.074 × 0.046
Radiation	Cu Kα (λ = 1.54184)	Cu Kα (λ = 1.54184)	Cu Kα (λ = 1.54184)
2Θ range for data collection [°]	7.716 to 147.388	7.616 to 148.178	7.678 to 148.1
Index ranges	-9 ≤ h ≤ 10, -12 ≤ k ≤ 11, -27 ≤ l ≤ 28	-13 ≤ h ≤ 14, -15 ≤ k ≤ 15, -19 ≤ l ≤ 20	-13 ≤ h ≤ 11, -15 ≤ k ≤ 14, -20 ≤ l ≤ 20
Reflections collected	11921	13999	19056
Independent reflections	7390 [R_{int} = 0.0460, R_{sigma} = 0.0627]	7873 [R_{int} = 0.0457, R_{sigma} = 0.0477]	8231 [R_{int} = 0.0397, R_{sigma} = 0.0543]
Data / restraints / parameters	7390/30/421	7873/0/455	8231/0/485
Goodness-of-fit on F²	1.018	1.026	1.085
Final R indexes [I>=2σ (I)]	R_1 = 0.0793, wR_2 = 0.2044	R_1 = 0.0544, wR_2 = 0.1467	R_1 = 0.0492, wR_2 = 0.1123
Final R indexes [all data]	R_1 = 0.0902, wR_2 = 0.2164	R_1 = 0.0563, wR_2 = 0.1501	R_1 = 0.0601, wR_2 = 0.1164
Largest diff. peak/hole [e Å⁻³]	2.01/-0.88	1.02/-0.70	0.56/-0.38

Table S10. Crystallographic data of **5**.

Compound	**5**
Empirical formula	$C_{75}H_{88}ClCoF_2GaN_4P_5$
Formula weight	1402.44
Temperature [K]	123 (1)
Crystal system	triclinic
Space group	*P*-1
a [Å]	11.8741(3)
b [Å]	12.4783(3)
c [Å]	24.9702(6)
α [°]	89.008(2)
β [°]	77.087(2)
γ [°]	78.673(2)
Volume [Å^3]	3534.63(15)
Z	2
ρ_{calc} [g/cm^3]	1.318
μ [mm^{-1}]	4.115
F(000)	1468.0
Crystal size [mm^3]	0.402 × 0.36 × 0.197
Radiation	Cu Kα (λ = 1.54184)
2Θ range for data collection [°]	7.228 to 148.414
Index ranges	-14 ≤ h ≤ 14, -15 ≤ k ≤ 15, -31 ≤ l ≤ 29
Reflections collected	28770
Independent reflections	13997 [R_{int} = 0.0329, R_{sigma} = 0.0378]
Data / restraints / parameters	13997/0/831
Goodness-of-fit on F^2	1.037
Final R indexes [I>=2σ (I)]	R_1 = 0.0444, wR_2 = 0.1162
Final R indexes [all data]	R_1 = 0.0461, wR_2 = 0.1179
Largest diff. peak/hole [e Å^{-3}]	1.85/-0.60

2.7   Theoretical investigations

Prior to the calculation of the phosphorus chemical shielding σ_{calcd} the electronic structure of the compounds **2**, **3b,** and **4** were analyzed with respect to the redox-active BIAN ligand. Benchmark studies were performed on a truncated model complex **3'** (Figure S45) using the Gaussian09 program package (Revision E.01).[17]

Figure S45. Representation of the truncated model complex **3'**.

The geometry of **3'** was optimized in the closed-shell singlet configuration on the B3LYP/6-311G(d) level of theory. Subsequently, single point calculations were performed on different possible electronic configurations (Table S11).

Table S11. DFT computed single point energies of different electronic configurations of **3'** on the B3LYP/6-311G(d) level of theory.

	closed-shell singlet (S = 0)	open-shell singlet (S = 0)	triplet (S =1)
Energy (hartree)	−3741.270596	−3741.271997	−3741.246415
S²	0.00	0.6072	2.0353
ΔE (kcal/mol)	0.00	-0.88	15.17

The preliminary benchmark studies revealed that the triplet (S = 1) state is less favored (15.17 kcal/mol) relative to the closed-shell configuration (S = 0). The relative energies of the open-shell singlet configuration to the closed-shell system are close together and differ only by 0.88 kcal/mol, suggesting an open-shell spin state. The single-reference broken symmetry approach only yields an approximate solution, in which an antiferromagnetic coupling between an unpaired electron of the BIAN ligand with an unpaired electron of the cobalt atom is observed (Figure S46). However, DFT is a single reference method and relative energies of species in different spin state configurations are innately troublesome. Due to the very small energy difference of open-shell to closed-shell configuration (0.88 kcal/mol) the true electronic structure of model complex **3'** cannot be sufficiently described using standard DFT methods.[18],[19],[20],[21],[22]

Figure S46. Spin density plot of the open-shell singlet state calculated at the uB3LYP/6-311G(d) level of theory (Isosurface value 0.004). Mulliken spin densities: Co 0.83, BIAN −0.64.

Multi-reference approaches, such as CASSCF, are able to describe the electronic structure of open-shell singlet configurations more precise. However, such large systems present in compounds **2**, **3a**, and **4** are currently too expensive to optimize with these multi-reference methods.[18],[19],[20],[21],[22]

Thus, we decided to optimize the full systems **2**, **3a**, and **4** in a closed-shell singlet configuration, well knowing that the obtained electronic state is only an approximation. The meta-hybrid functional TPSSh together with split basis sets (def2-QZVP for Co, N, P, Ga; and def2-SVP for C, H) were employed. The optimized structures are in good agreement with the single-crystal X-ray diffraction measurements and the nature of the stationary points was further verified by numerical frequency analyses.

2.6.1 Calculation of ^{31}P NMR chemical shielding

Even though the closed shell configuration of compounds **2**, **3a**, and **4** does not represent the true electronic structure we calculated the phosphorus chemical shielding σ_{calcd} using the Amsterdam Density Functional program package.[23] The pre-optimized structures were supplied to ADF, optimized at the PBE-D3BJ/TZP level of theory and subsequently the ^{31}P chemical shielding was calculated by ADF's EPR/NMR program. The obtained values can be transformed to chemical shifts δ relative to a suitable reference system. The ^{31}P NMR reference compound 85% aqueous phosphoric acid was used as a reference system as complex **3a** has shown to be inappropriate for the Ga containing complexes **2** and **4**.

The theoretical magnetic shielding of 85% aqueous H_3PO_4 can barely be assigned and other chemical compounds for which gas-phase NMR data are available have to be used (PH$_3$ δ_g = 266.1 ppm). The calculated phosphorus chemical shielding σ_{calcd} can be converted into chemical shifts by this relationship:[24]

$$\delta(\text{s,calc}) = \sigma(\text{PH}_3, \text{calc}) - \sigma(\text{s, calc}) - 266.1 \text{ ppm}$$

$\sigma(\text{PH}_3, \text{calc})$ is the theoretical magnetic shielding of PH$_3$ calculated at the PBE-D3BJ/TZP level of theory using ADF (σ_{calcd} = 584.9).

*^{31}P NMR chemical shielding of **3a***

At first, the phosphorus chemical shieldings σ_{calcd} for **3a** were calculated to show that the ^{31}P chemical shielding in the closed-shell configurations give the same trend as those observed experimentally (Table S12). The experimental ^{31}P NMR spectrum of **3a** displays a symmetric splitting pattern in solution. Thus, the geometry of **3a** was optimized once in a C_s constrained symmetry and once without any symmetry constraint. The resulting C_s symmetric complex **3a^{Cs}** is about 1 kcal/mol less favored to the unsymmetrical geometry resemble the XRD data.

Table S12. PBE-D3BJ/TZP ^{31}P NMR chemical shieldings σ_{calcd} and chemical shifts δ_{calcd} [ppm] of complex **3a** and the C_S symmetry constrained complex **3a^{Cs}**; [Co] = (^{Mes}BIAN)Co.

	3a		**3a^{Cs}**		**Experimental Values**
	σ_{calcd}	δ_{calcd}	σ_{calcd}	δ_{calcd}	δ_{exp}
P(5) MM'	243.27	75.5	222.3	96.5	88.6
P(4) MM'	202.79	116.0	222.4	96.4	88.6
P(3) XX'	458.34	−139.6	467.3	−148.5	−111.4
P(2) XX'	464.82	−146.0	467.3	−148.5	−111.4
P(1) A	143.00	175.8	137.7	181.1	161
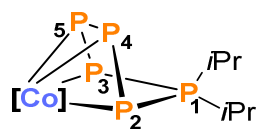
By comparing the theoretical values with the experimental ones, we conclude, that the ^{31}P NMR calculated chemical shifts represent the right trend and can be employed to further investigate compounds **2** and **4**.

^{31}P NMR chemical shielding of 4

The calculated chemical ^{31}P NMR chemical shieldings σ_{calcd} and chemical shifts δ_{calcd} for compound **4** are given in Table S13. Chemical shifts were referenced either to 85% aqueous phosphoric acid or were referenced internally to phosphorus atom P2.

Table S13. PBE-D3BJ/TZP ^{31}P NMR chemical shieldings σ_{calcd} and chemical shifts δ_{calcd} [ppm] of complex **4**; [Co] = (^{Mes}BIAN)Co; [Ga] = (nacnac)Ga.

	4			**Experimental Values**
	σ_{calcd}	δ_{calcd}[a]	δ_{calcd}[b]	δ_{exp}
P(1)	273.5	45.2	21.6	15.0
P(2)	378.2	−59.4	−83.0	−83.0
P(3)	202.2	116.6	93.0	88.1
P(4)	198.8	120.0	96.4	88.1
P(5)	187.6	131.2	107.6	81.1

[a] Referenced to 85% aqueous phosphoric acid; [b] P2 used as reference chemical shift (δ_{ref} = 295.2 ppm).
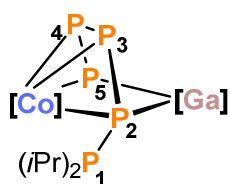
The theoretically obtained phosphorus chemical shifts resemble a similar trend like it is observed for intermediate **Int-1** in the ^{31}P NMR reaction monitoring experiment (Figure S47). Thus, we conclude, that the phosphorus chemical shifts of intermediate **Int-1** are likely assigned to compound **4**.
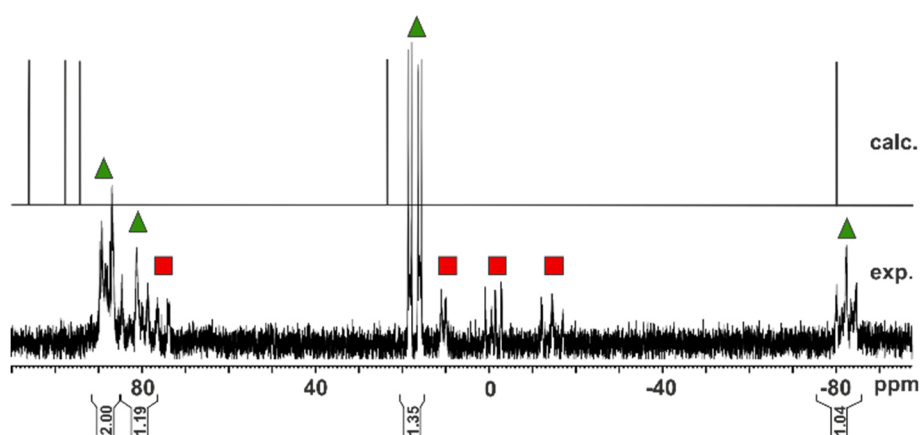
Figure S47. Section of ^{31}P{^{1}H} NMR spectrum of crystalline **4** in C$_6$D$_6$; resonances marked with ▲ (**Int-1**) and ■ (**Int-2**) are assigned to the intermediates (bottom); calculated ^{31}P NMR chemical shifts of **4** referenced internally to P2 (top).

^{31}P NMR chemical shielding of 2

In order to properly assign the P atoms in compounds **2** and **2'** the ^{31}P NMR chemical shieldings of anion **2** were calculated. The trend of calculated and experimental chemical shifts were compared and the high-field shifted signal can clearly be assigned to the Ga-bound phosphorus atoms.

Table S14. PBE-D3BJ/TZP ^{31}P NMR chemical shieldings σ_{calcd} and chemical shifts δ_{calcd} [ppm] of anion **2'**; [Co] = ^{Mes}BIAN)Co; [Ga] = (nacnac)Ga.

	2		**Experimental Values**
	σ_{calcd}	δ_{calcd}	δ_{exp}
P(1) XX'	417.4	−98.6	−125.4
P(4) XX'	418.5	−99.7	−125.4
P(2) AA'	194.6	124.2	74.0
P(3) AA'	243.0	75.8	74.0
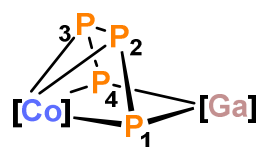
2.8 References of Supporting Information

[1]   (a) K. Jonas, R. Mynott, C. Krüger, J. C. Sekutowski and Y.-H. Tsay, *Angew. Chem. Int. Ed. Engl.* **1976**, *15*, 767; *Angew. Chem.* **1976**, *88*,808; (b) K.Jonas, US patent 4169845, **1979**.

[2]   S. Pelties, T. Maier, D. Herrmann, B. d. Bruin, C. Rebreyend, S. Gärtner, I. G. Shenderovich and R. Wolf, *Chem. Eur. J.* **2017**, *23*, 6094.

[3]   G. Prabusankar, A. Doddi, C. Gemel, M. Winter and R. A. Fischer, *Inorg. Chem.* **2010**, *49*, 7976.

[4]   M. Gasperini, F. Ragaini and S. Cenini, *Organometallics* **2002**, *21*, 2950.

[5]   P. Li, B. Lü, C. Fu and S. Ma, *Adv. Synth. Catal.* **2013**, *355*, 1255.

[6]   (a) A. A. Naiini, Y. Han, M. Akinc and J. G. Verkade, *Inorg. Chem.* **1993**, *32*, 5394; (b) M. Fild, O. Stelzer, R. Schmutzler and G. O. Doak, *Inorg. Synth.* **1973**, *14*, 4.

[7]   Y. Liu, B. Ding, D. Liu, Z. Zhang, Y. Liu and W. Zhang, *Res. Chem. Intermed.* **2017**, *43*, 4959.

[8]   R. K. Harris, E. D. Becker, S. M. Cabral de Menezes, R. Goodfellow and P. Granger, *Magn. Reson. Chem.* **2002**, *40*, 489.

[9]   P. H. M. Budzelaar, *gNMR for Windows (5.0.6.0)*, NMR Simulation Program, **2006**.

[10]   (a) SCALE3ABS, CrysAlisPro, Aglient Technologies Inc. Oxford and GB **2015**; (b) G. M. Sheldrick, SADABS, Bruker AXS, Madison and USA **2007**.

[11]   R. C. Clark, J. S. Reid, *Acta Crystallogr. A* **1995**, *51*, 887.

[12]   CrysAlisPro, version 171.39.37b, Agilent Technologies Inc., Oxford and GB, **2017**.

[13]   G. M. Sheldrick, *Acta Cryst.* **2015**, *A17*, 3.

[14]   G. M. Sheldrick, *Acta Cryst.* **2015**, *C71*, 3.

[15]   A. L. Spek, Acta Cryst. **2009**, *D65*, 148.

[16]   O. V. Dolomanov, L. J. Bourhis, R. J. Gildea, J. A. K. Howard and H. Puschmann, *J. Appl. Cryst.* **2009**, *42*, 339.

[17]   Gaussian 09, Revision E.01, M. J. Frisch, G. W. Trucks, H. B. Schlegel, G. E. Scuseria, M. A. Robb, J. R. Cheeseman, G. Scalmani, V. Barone, G. A. Petersson, H. Nakatsuji, X. Li, M. Caricato, A. Marenich, J. Bloino, B. G. Janesko, R. Gomperts, B. Mennucci, H. P. Hratchian, J. V. Ortiz, A. F. Izmaylov, J. L. Sonnenberg, D. Williams-Young, F. Ding, F. Lipparini, F. Egidi, J. Goings, B. Peng, A. Petrone, T. Henderson, D. Ranasinghe, V. G. Zakrzewski, J. Gao, N. Rega, G. Zheng, W. Liang, M. Hada, M. Ehara, K. Toyota, R. Fukuda, J. Hasegawa, M. Ishida, T. Nakajima, Y. Honda, O. Kitao, H. Nakai, T. Vreven, K. Throssell, J. A. Montgomery, Jr., J. E. Peralta, F. Ogliaro, M. Bearpark, J. J. Heyd, E. Brothers, K. N. Kudin, V. N. Staroverov, T. Keith, R. Kobayashi, J. Normand, K. Raghavachari, A. Rendell, J. C. Burant, S. S. Iyengar, J. Tomasi, M. Cossi, J. M. Millam,

M. Klene, C. Adamo, R. Cammi, J. W. Ochterski, R. L. Martin, K. Morokuma, O. Farkas, J. B. Foresman, and D. J. Fox, Gaussian, Inc., Wallingford CT **2009**.

[18] P. Milko, M. A. Iron, *J. Chem. Theory Comput.* **2014**, *10*, 220.

[19] T. Zell, P. Milko, K. L. Fillman, Y. Diskin-Posner, T. Bendikov, M. A. Iron, G. Leitus, Y. Ben-David, M. L. Neidig and D. Milstein, *Chem. Eur. J.* **2014**, *20*, 4403.

[20] S. C. Bart, K. Chłopek, E. Bill, M. W. Bouwkamp, E. Lobkovsky, F. Neese, K. Wieghardt and P. J. Chirik, *J. Am. Chem. Soc.* **2006**, *128*, 13901.

[21] P. H. M. Budzelaar, B. d. Bruin, A. W. Gal, K. Wieghardt and J. H. van Lenthe, *Inorg. Chem.* **2001**, *40*, 4649.

[22] C. Lichtenberg, M. Adelhardt, T. L. Gianetti, K. Meyer, B. d. Bruin and H. Grützmacher, *ACS Catal.* **2015**, *5*, 6230.

[23] (a) ADF 2017, SCM, Theoretical Chemistry, Vrije Universiteit, Amsterdam, The Netherlands, http://www.scm.com; (b) C. Fonseca Guerra, J. G. Snijders, G. te Velde and E. J. Baerends, *Theor. Chem. Acc.* **1998**, *99*, 391; (c) G. te Velde, F. M. Bickelhaupt, E. J. Baerends, C. Fonseca Guerra, S. J. A. van Gisbergen, J. G. Snijders and T. Ziegler, *J. Comput. Chem.* **2001**, *22*, 931.

[24] (a) C. van Wüllen, *Phys. Chem. Chem. Phys.* **2000**, *2*, 2137; (b) C. J. Jameson, A. de Dios and A. Keith Jameson, *Chem. Phys. Lett.* **1990**, *167*, 575.

Chapter 3   Iron-Gallium and Cobalt-Gallium Tetraphosphido Complexes

Abstract: The synthesis and characterization of two heterobimetallic complexes [K(18-crown-6){(η^4-C$_{14}$H$_{10}$)Fe(μ-η^4:η^2-P$_4$)Ga(nacnac)}] (**1**, C$_{14}$H$_{10}$ = anthracene) and [K(dme)$_2${(η^4-C$_{14}$H$_{10}$)Co(μ-η^4:η^2-P$_4$)Ga(nacnac)}] (**2**) with strongly reduced P$_4$ units is reported. Compounds **1** and **2** are prepared by reaction of the gallium(III) complex [(nacnac)Ga(η^2-P$_4$)] (nacnac = CH[CMeN(2,6-iPr$_2$C$_6$H$_3$)]$_2$) with bis(anthracene)ferrate(1–) and -cobaltate(1–) salts. The molecular structures of **1** and **2** were determined by X-ray crystallography and feature a P$_4$ chain that binds to the transition metal atom *via* all four P atoms and to the gallium atom *via* the terminal P atoms. Multinuclear NMR studies on **2** suggest that the molecular structure is preserved in solution.
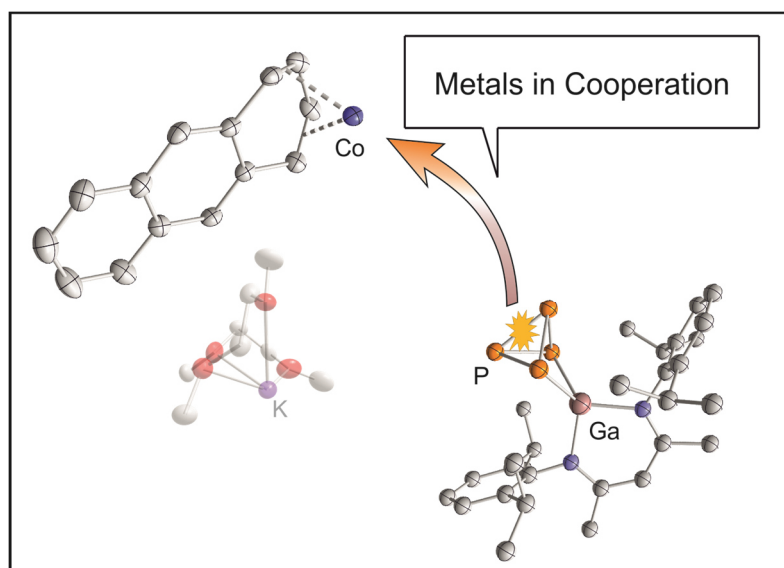
3.1   Introduction

Since the discovery of the first transition metal complex of white phosphorus (P_4) by Ginsberg and Lindsell in the 1970s,[1] an extensive coordination chemistry has emerged for the P_4 molecule.[2] In numerous cases, the use of low-oxidation state metal complexes lead to the formation of coordinated P_n units with two to six P atoms ($n = 2$–6).[2] Thereby, the size of the phosphorus framework is mainly dictated by the electronic requirements of the metal atom. While formally anionic, these P_n units are typically not very reactive, although selected reports in literature show that functionalization of transition metal polyphosphides are feasible with electrophiles[3],[4] and, as shown by more recent literature, with nucleophiles.[5],[6]

The use of two electronically distinct metal atoms can generate strongly reduced P_n fragments. However, such heterodinuclear complexes are relatively scarce. Some relevant examples are shown in Figure 1.[5],[7] [{Cp*Co}{Cp″(CO)Ta}(μ-$\eta^{2:2}$-P_2)$_2$] (**A**, Cp* = C_5Me_5, Cp″= C_5H_3{1,3-tBu$_2$}) was synthesized by Scherer and co-workers by reaction of [Cp″CO)$_2$Ta(η^4-P_4)] with [Cp*Co(η^2-C_2H_4)$_2$],[8] while the related complex [{Cp*Fe}{Cp″Ta}(μ-$\eta^{4:3}$-P_5)] (**B**) is formed by cothermolysis of two sandwich compounds [Cp*Fe(η^5-P_5)] and [Cp″Ta(CO)$_4$].[9] Peruzzini and co-workers described the insertion of platinum(0) complexes into polyphosphido ligands.[10] Among other examples, such reactions resulted in complexes **C** and **D** shown in Figure 1. Akbayeva reported insertions into a P−P bond of η^1-P_4 complexes of ruthenium(II) and iron(II).[11]

Particularly relevant to the work described in this manuscript is a report by Driess and co-workers on heterodinuclear compound **E**, which was synthesized from the silylene-activated P_4 ligand [(nacnac′)Si(η^2-P_4)] (nacnac′ = CH[(C=CH$_2$)CMe][N(2,6-iPr$_2$C$_6$H$_3$)]$_2$) and the nickel(I) species [{nacnac}Ni)$_2$·toluene] (nacnac = CH[CMeN(2,6-iPr$_2$C$_6$H$_3$)]$_2$) and [({nacnac″}Ni)$_2$·toluene] (nacnac″ = CH[CMeN(2,6-Et$_2$C$_6$H$_3$)]$_2$).[12] These complexes feature a [Si(μ,$\eta^{2:2}$-P_4)Ni] core, where the [(nacnac′)Si(η^2-P_4)] ligand is side-on coordinated to a tetrahedral nickel(I) center. Significantly, a reductive P−P bond cleavage does not occur in this case.
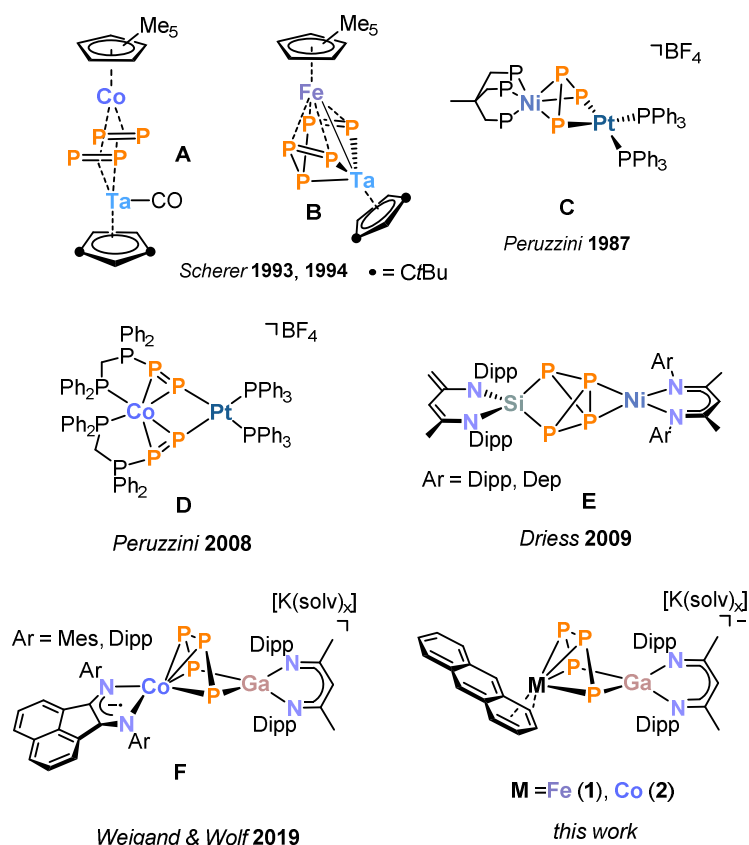
Figure 1. Selected examples of heterodinuclear transition metal tetraphosphido complexes.

We recently reported the synthesis of a related cobalt-gallium compound [K(dme)$_2${(^{Mes}BIAN)Co(μ-η^4:η^2-P$_4$)Ga(nacnac)}] (**F**) containing the α-diimine ligand bis(mesitylimino)acenaphthenediimine (^{Mes}BIAN).[4] Complex **F** is formed by reaction [K(Et$_2$O){(^{Mes}BIAN)Co(η^4-1,5-cod)}][13] and the previously reported gallium tetraphosphido complex [(nacnac)Ga(η^2-P$_4$)]. The latter compound is readily accessible by reaction [(nacnac)Ga^I] with P$_4$.[14],[15] In contrast to the structures of the aforementioned Ni compounds **E**, a highly reduced *catena*-P$_4^{4-}$ unit resulting from the oxidative addition of a P–P bond to cobalt is observed in the structure of complex **F**. Reactions with chlorophosphanes R$_2$PCl afford pentacyclic *cyclo*-P$_5$R$_2$ ligands (see chapter 2 of this thesis). Such a route thus offers the possibility to prepare new organofunctionalized polyphosphorus ligands in the coordination sphere of transition metal atoms.

3.2   Results and Discussion

Building on this initial work, we subsequently investigated whether the range of accessible heterobimetallic phosphorus compounds can be expanded by using related transition metallates. Here, we describe the synthesis and structural characterization of [K(18-crown-6){(η^4-C$_{14}$H$_{10}$)Fe(μ-η^4:η^2-P$_4$)Ga(nacnac)}] (**1**) and [K(dme)$_2${(η^4-C$_{14}$H$_{10}$)-Co(μ-η^4:η^2-P$_4$)Ga(nacnac)}] (**2**). These compounds show a similar M(μ-P$_4$)Ga motif as compound **F**, but feature a distinct ancillary ligand at the transition metal center.

Expanding on the initial synthesis of **F** from $[K(Et_2O)\{(BIAN)Co(\eta^4\text{-}1,5\text{-cod})\}]$[13] and $[(nacnac)Ga(\eta^2\text{-}P_4)]$,[14],[15] similar reactions of bis(anthracene) complexes $[K(18\text{-crown-}6)(thf)_2][Fe(\eta^4\text{-}C_{14}H_{10})_2]$[16],[17] and $[K(dme)_2][Co(\eta^4\text{-}C_{14}H_{10})_2]$[17],[18] were examined according to Scheme 1. Such complexes are useful sources of "naked" Fe$^-$ and Co$^-$ anions due to the presence of labile anthracene ligands.[16],[18],[19]
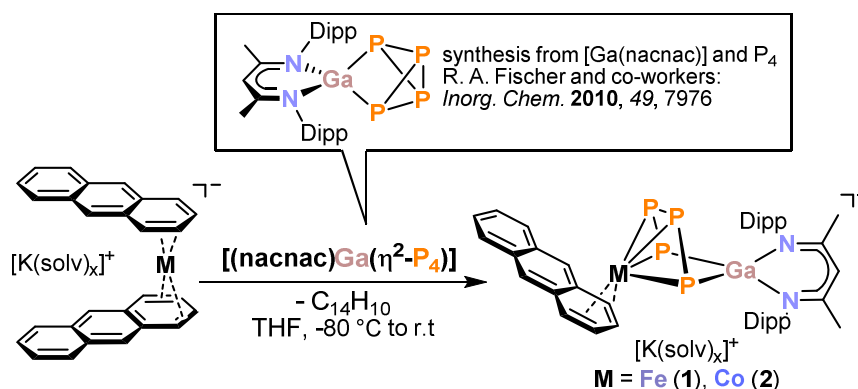
Scheme 1. Synthesis of **1** and **2**; reagents and conditions for **1**: $[K(18\text{-crown-}6)\{(\eta^4\text{-}C_{14}H_{10})Fe(\mu\text{-}\eta^4:\eta^2\text{-}P_4)Ga(nacnac)\}]$, for **2**: $[K(dme)_2\{(\eta^4\text{-}C_{14}H_{10})Co(\mu\text{-}\eta^4:\eta^2\text{-}P_4)Ga(nacnac)\}]$.

Slow addition of a yellow solution of $[(nacnac)Ga(\eta^2\text{-}P_4)]$ (one equiv.) to a cooled rust-colored solution of $[K(18\text{-crown-}6)(thf)_2][Fe(\eta^4\text{-}C_{14}H_{10})_2]$ affords a brownish-yellow solution. After work-up, dark crystals of **1** suitable for X-ray diffraction analysis can be obtained by slow diffusion of *n*-hexane into a concentrated DME solution of the crude product. Solid **1** is readily soluble in polar coordinating solvents such as DME and THF, and it is highly sensitive toward oxygen and moisture. Unfortunately, all attempts to isolate **1** as a pure compound were unsuccessful until now. Resonances of residual free anthracene are found in ^{1}H NMR spectra, while the C, H, N combustion analysis gave variable results, which strongly deviated from the values expected for pure **1**. Nevertheless, the molecular structure of **1** was confirmed by single-crystal diffraction (XRD) analysis.

Complex **1** crystallizes in space group *P*-1 with two formula units per cell. The molecular structure is depicted in Figure 2. An ion-separated structure is observed where the potassium cation is coordinatively saturated by one molecule 18-crown-6 and one DME molecule. The anion shows a bridging P_4 chain that binds to the iron center with all four P atoms, while only the terminal P atoms coordinate the gallium atom. As a result of the coordination by two P atoms and a nacnac ligand, the gallium atom adopts a nearly ideal tetrahedral geometry with a twist angle of 87.57°. The P−P bond lengths are all shorter than typical P–P single bonds. Notably, the terminal P−P bonds (P1−P2 2.1166(6) Å and P3−P4 2.1131(7) Å) are significantly shorter than the internal P−P bond (P2−P3 2.1801(7) Å), while the distance between the terminal P atoms (P1–P4 3.5473(6) Å) is long. The dihedral angle (P1–P2–P3–P4 2.62°) shows that these bonds are nearly co-planar, while the P1−P2−P3 and P2−P3−P4 angles are almost identical (108.75(3)° and 108.93(3)°, respectively). The anthracene ligand is η^4-coordinated to the iron center and

shows the typical long-short-long pattern for the C−C bonds of transition-metal-coordinated anthracene molecules (C1−C2 1.4138(3) Å, C2−C3 1.409(3) Å, C3−C4 1.421(3) Å). Based on Fe–C and C–C distances, the coordination mode of the anthracene ligand seems identical with that in the starting material [K(18-crown-6)(thf)$_2$][Fe(η^4-C$_{14}$H$_{10}$)$_2$].[16]

Cobalt complex **2** can be synthesized in a similar manner as **1** by adding a THF solution of [(nacnac)Ga(η^2-P$_4$)] to a solution of [K(dme)$_2$][Co(η^4-C$_{14}$H$_{10}$)$_2$] in THF. ^{31}P{^{1}H} NMR monitoring of the reaction revealed the selective formation of **2** as the sole P-containing species. As a result, this compound was isolated purely and is fully characterized. Released anthracene can be removed by extraction of the crude product with diethyl ether and *n*-hexane, and subsequent crystallization from DME/*n*-hexane affords **2** as thin, dark-violet plates, which were suitable for single-crystal XRD. Due to the elaborate work-up procedure, the yield of isolated compound is modest (22%). Nevertheless, multinuclear NMR spectra and elemental analysis confirm the purity of the isolated complex.

Notably, the same compound **2** is formed as the major product even when an excess of bis(anthracene)cobaltate is employed in the reaction. Apparently, a substitution of the second anthracene ligand does not occur.

Complex **2** likewise crystallizes in space group *P*-1 with two formula units per cell, and the molecular structure is shown in Figure 2. In case of **2**, an ion-contact structure is observed. The K1–P2 (3.298(1) Å) distance is considerably shorter than the sum of the van der Waals radii (4.63 Å),[20] while it is slightly longer than the sum of the covalent radii (3.10 Å).[21] Furthermore, the potassium cation interacts with the anthracene ligand (K1–C5 3.370(2) Å, K1–C6 3.175(2) Å) and two DME molecules. The structure of the Co(μ-P$_4$)Ga core is nevertheless similar to that of **1**. The bridging P$_4$ unit is essentially in a syn conformation with a dihedral angle P1–P2–P3–P4 of 2.37°. The P$_4$ chain displays short terminal P−P bonds (P1−P2 2.1095(9) Å and P3−P4 2.1057(9) Å), while the internal P2−P3 bond (2.1825(9) Å) is closer to a single bond. The anthracene ligand coordinates to cobalt in an η^4-fashion. The C–C distances (C1−C2 1.4138(3) Å, C2−C3 1.413(4) Å, C3−C4 1.426(4) Å) indicate that there is considerable back-bonding between cobalt and anthracene similar to the structure of **1**.
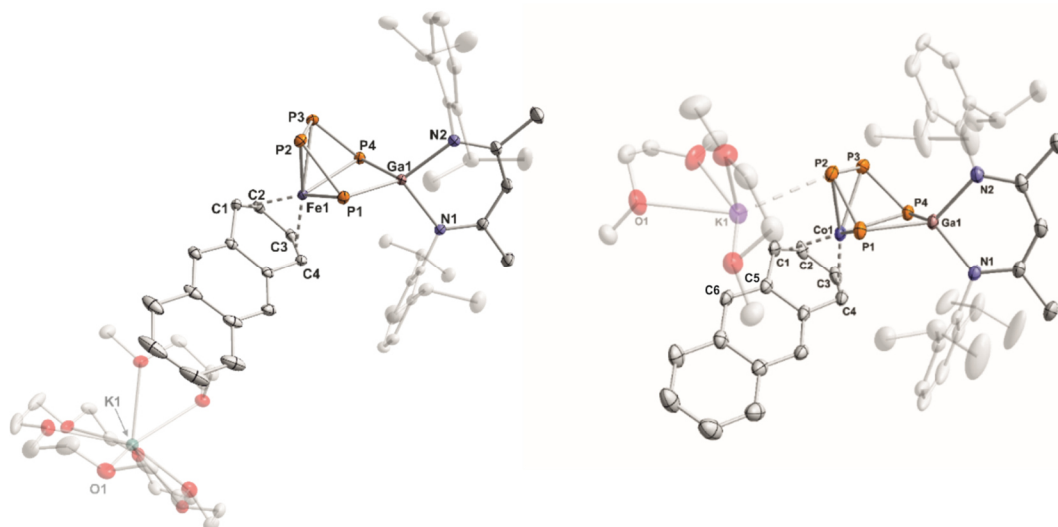
Figure 2. Solid-state molecular structures of **1** (left) and **2** (right). Hydrogen atoms and some disordered parts are omitted for clarity; thermal ellipsoids are drawn at the 40% probability level. Selected bond lengths [Å] and angles [°] for **1**: P1−P2 2.1166(6), P2−P3 2.1801(7), P3−P4 2.1131(7), P1···P4 3.5473(6), Ga1−P1 2.3383(5), Ga1−P4 2.3307(5), Ga1−N1 2.018 (1), Ga1−N2 2.015(1), Fe1−P1 2.3879(5), Fe1−P2 2.3344(5), Fe1−P3 2.3368(7), Fe1−P4 2.3568(5), Fe1−C1 2.128(2), Fe1−C2 2.065(2), Fe1−C3 2.057(2), Fe1−C4 2.112(2), C1−C2 1.4138(3), C2−C3 1.409(3), C3−C4 1.421(3); P1−P2−P3 108.75(3), P2−P3−P4 108.94(3), P3−P4−Ga1 101.36(2), P4−Ga1−P1 98.89(2), Ga1−P1−P2 100.54(2), C4−Fe1−P1 97.07(5), C1−Fe1−P2 97.49(5), C2−Fe1−P3 101.14(5), C3−Fe1−P4 95.34(5); for **2**: P1−P2 2.1095(9), P2−P3 2.1825(9), P3−P4 2.1057(9), P1···P4 3.4509(8), Ga1−P1 2.3512(6), Ga1−P4 2.3297(6), Ga1−N1 1.993(2), Ga1−N2 2.008(2), Co1−P1 2.3635(7), Co1−P2 2.2922(7), Co1−P3 2.3368(7), Co1−P4 2.4108(7), Co1−C1 2.187(2), Co1−C2 2.026(2), Co1−C3 2.001(2), Co1−C4 2.82(2), C1−C2 1.4138(3), C2−C3 1.413(4), C3−C4 1.426(4), K1−P1 3.5646(9), K1−P2 3.2981(8); P1−P2−P3 109.13(3), P2−P3−P4 105.88(3), P3−P4−Ga1 101.3(3), P4−Ga1−P1 94.99(2), Ga1−P1−P2 98.41(3), C4−Co1−P1 113.18(7), C1−Co1−P2 126.01(8), C2−Co1−P3 121.78(8), C3−Co1−P4 104.08(7) K1 − C5 3.370(2) Å, K1 − C6 3.175(2) Å.

In addition to complex **F**, only a few structures with P_4 fragments sandwiched between two metal atoms have been reported.[13],[22] The most closely related compound appears to be [(Cp^RRh)(μ-η^4:η^2-P_4){Rh(CO)Cp^R}] (Cp^R = η^5-C_5Me_4Et) reported by Scherer and co-workers.[23] It is noteworthy that Roesky, Konchenko, Scheer, and co-workers synthesized a trinuclear samarium-cobalt complex [($Cp'''Co$)$_2$(μ_3-η^2:η^2:η^2-P_4)SmCp^*_2] (Cp^* = η^5-C_5Me_5, Cp''' = η^5-1,2,4-tBu$_3C_5H_2$), which shows a similar structure motif.[24]

The ^{1}H NMR spectrum of the isolated crystals of **2** dissolved in THF-d_8 displays five multiplets for coordinated anthracene with an integral ratio of 2:2:2:2:2. The chemical shifts of these resonances are in the range δ = 6.90 ppm to 2.69 ppm, which is common for anthracene coordinated to a transition metal center.[18],[25] The observed high-field shift of the anthracene signals is explained by π-donation from the metal atom to the π-acceptor ligand, which reduces the aromaticity of anthracene.[18] Two chemically distinct 2,6-diisopropylphenyl groups are observed in accordance with the single-crystal X-ray structure, which are also discernible in the $^{13}C\{^1H\}$ NMR spectrum. The $^{31}P\{^1H\}$ NMR spectrum shows two higher order multiplets in a 1:1 ratio at δ = 89.2 ppm and δ = −94.7 ppm, which can be assigned to an AA'XX' spin system shown in Figure 3. The AA'XX' spin pattern observed is in line with a C_2 symmetrical P_4 moiety. The high-field shifted multiplet at δ = −94.7 ppm can be tentatively assigned to the terminal phosphorus atoms bound to the gallium atom based on the larger line broadening and DFT calculations

on the related compound **F**.[4] Conversely, the signal at δ = 89.2 ppm ($\tau_{1/2}$ = 10.64 Hz) can be assigned to the internal phosphorus atoms. The $^1J_{AX}$ coupling constant is larger in magnitude than the $^1J_{AA'}$ coupling constant ($^1J_{AA'} - {}^1J_{AX}$ = 126.2 Hz). This is in agreement with a putative partial double bond character of the terminal P–P bonds as suggested by the crystallographically obtained P–P distances (*vide supra*). The previously reported diimine complex **F** displays a similar AA'XX' pattern in the ^{31}P{^{1}H} NMR spectrum with $^1J_{AX}$ = −450.5 Hz and $^1J_{AA'}$ = −380.2 Hz.[4] Nevertheless, it is noteworthy that the magnitude of the $^1J_{AX}$ coupling constant of **2** is about 45 Hz higher than that of compound **F** ($^1J_{AX} = {}^1J_{A'X'}$ = −450.5 Hz), while the $^1J_{AA'}$ constants are similar (**2**: $^1J_{AA'} = {}^1J_{A'A}$ = −370.6 Hz; **F**: $^1J_{AA'} = {}^1J_{A'A}$ = −380.5 Hz).[4] The large difference of the $^1J_{AX}$ coupling constant might be caused by the shorter terminal P–P bonds in **2**. The $^2J_{PP}$ coupling constant is small ($^2J_{AX'} = {}^2J_{A'X}$ = 4.9 Hz) and similar to those of **F** ($^2J_{AX'} = {}^2J_{A'X}$ = 6.6 Hz).[4] Remarkably, complex **2** shows a rather large $^3J_{PP}$ coupling constant $^3J_{XX'} = {}^3J_{X'X}$ = −52.2 Hz compared to that determined in compound **F** ($^3J_{XX'} = {}^3J_{X'X}$ = −7.2 Hz), which might be explained by the more co-planar alignment of the P atoms of the P$_4$ chain of **2**.[4] Overall, the multinuclear NMR spectra of **2** are in full agreement with the molecular structure observed in solid-state.
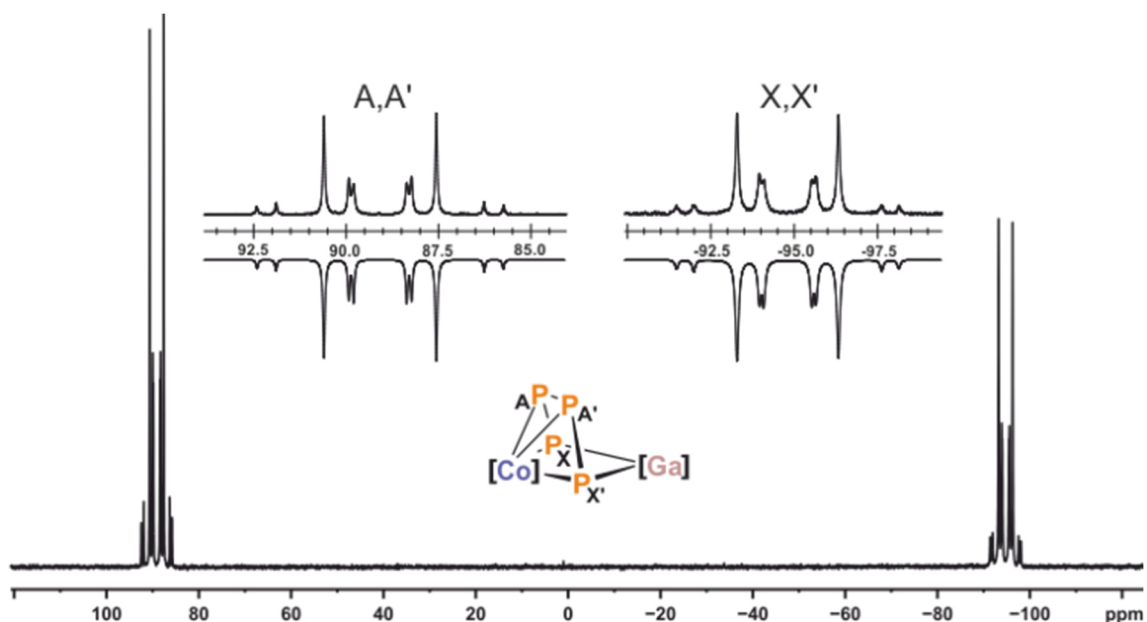
Figure 3. ^{31}P{^{1}H} NMR spectrum of compound **2** (121.49 MHz, 300 K, THF-d_8) with nuclei assigned to an AA′XX′ spin system; insets: expanded spectrum (upwards) and simulated spectrum (downwards); δ(P$_{AA'}$) = 89.2 ppm, δ(P$_{XX'}$) = −94.7 ppm, $^1J_{AA'} = {}^1J_{A'A}$ = −370.6 Hz, $^1J_{AX} = {}^1J_{A'X'}$ = −496.8 Hz, $^2J_{AX'} = {}^2J_{A'X}$ = 4.9 Hz, $^3J_{XX'} = {}^3J_{X'X}$ = −52.2 Hz; [Co] = (η^4-C$_{14}$H$_{10}$)Co, [Ga] = (nacnac)Ga.

The UV-Vis spectrum of **2** was recorded in THF solution (see Figure S5 of the Supporting Information). The spectrum shows two very strong absorption bands in the UV region at 301 nm (ε = 42000 L·mol^{-1}·cm^{-1}) and 356 nm (ε = 39000 L·mol^{-1}·cm^{-1}), with the latter absorption tailing far into the visible region. The visible part shows a broad absorption at 524 nm. It is notable that the UV-Vis spectrum of **F** is similar in the UV region, while

additional intense bands observed for **F** at 553 nm and 658 nm can be presumably assigned to charge transfer transitions involving the BIAN ligand.[4]

3.3   Conclusion

In summary, heterodinuclear complexes with a strongly reduced P_4 unit have been synthesized by oxidative P–P bond addition of $[(\text{nacnac})\text{Ga}(\eta^2\text{-}P_4)]$ with low-valent ferrate(–I) and cobaltat(–I) anions. The molecular structures of the resulting complexes **1** and **2** feature an $\eta^4{:}\eta^2$-bridging P_4 chain between the transition metal atom and the gallium atom. Although bridging polyphosphide ligands are generally quite common in homodinuclear complexes,[2],[22] this precise structural motif is rare, which underlines the flexible coordination behavior of polyphosphido ligands. In future work, substitution of the labile anthracene ligand in such complexes could enable the further derivatization of the P_4 ligand. In addition, it is noteworthy that polyphosphorus complexes containing the [Ga(nacnac)] moiety have recently emerged as promising platforms for the construction of extensive P_n frameworks.[4],[15] Therefore, the complexes reported herein and related species might become a suitable starting point for further transformations leading to structurally novel species.

3.4   Notes and References

[1]   A. P. Ginsberg, W. E. Lindsell, *J. Am. Chem. Soc.* **1971**, *93*, 2082.

[2]   (a) M. Peruzzini, L. Gonsalvi, A. Romerosa, *Chem. Soc. Rev.* **2005**, *34*, 1038 (b) M. Scheer, G. Balázs, A. Seitz, *Chem. Rev.* **2010**, *110*, 4236; (c) M. Caporali, L. Gonsalvi, A. Rossin, M. Peruzzini, *Chem. Rev.* **2010**, *110*, 4178; (d) B. M. Cossairt, N. A. Piro, C. C. Cummins, *Chem. Rev.* **2010**, *110*, 4164.

[3]   (a) G. Capozzi, L. Chiti, M. Di Vaira, M. Peruzzini, P. Stoppioni, *J. Chem. Soc., Chem. Commun.* **1986**, 1799; (b) B. M. Cossairt, M.-C. Diawara, C. C. Cummins, *Science* **2009**, *323*, 602; (c) A. E. Seitz, M. Eckhardt, A. Erlebach, E. V. Peresypkina, M. Sierka, M. Scheer, *J. Am. Chem. Soc.* **2016**, *138*, 10433; (d) M. Piesch, S. Reichl, M. Seidl, G. Balázs, M. Scheer, *Angew. Chem. Int. Ed.* **2019**, *58*, 16563; *Angew. Chem.* **2019**, *131*, 16716.

[4]   C. G. P. Ziegler, T. M. Maier, S. Pelties, C. Taube, F. Hennersdorf, A. W. Ehlers, J. J. Weigand, R. Wolf, *Chem. Sci.* **2019**, *110*, 4178.

[5]   Selected recent examples, see: (a) S. Pelties, D. Herrmann, B. d. Bruin, F. Hartl, R. Wolf, *Chem. Commun.* **2014**, *50*, 7014; (b) C. C. Mokhtarzadeh, A. L. Rheingold, J. S. Figueroa, *Dalton Trans.* **2016**, *45*, 14561; (c) E. Mädl, G. Balázs, E. V. Peresypkina, M. Scheer, *Angew. Chem. Int. Ed.* **2016**, *55*, 7702; *Angew. Chem.* **2016**, *128*, 7833; (d) F. Dielmann, A. Timoshkin, M. Piesch, G. Balázs, M. Scheer, *Angew. Chem. Int. Ed.* **2017**, *56*, 1671; *Angew. Chem.* **2017**, *129*, 1693; (e) C. Chan, A. E. Carpenter, M. Gembicky, C. E. Moore, A. L. Rheingold, J. S. Figueroa, *Organometallics* **2019**, *38*, 1436; (f) C. M. Hoidn, T. M. Maier, K. Trabitsch, J. J. Weigand, R. Wolf, *Angew. Chem. Int. Ed.* **2019**, *58*, 18931*; Angew. Chem.* **2019**, *131*, 19107.

[6]   (a) P. Barbaro, M. Di Vaira, M. Peruzzini, S. Seniori Costantini, P. Stoppioni, *Chem. Eur. J.* **2007**, *13*, 6682; (b) E. Mädl, M. V. Butovskii, G. Balázs, E. V. Peresypkina, A. V. Virovets, M. Seidl, M. Scheer, *Angew. Chem. Int. Ed.* **2014**, *53*, 7643; *Angew. Chem.* **2014**, *126*, 7774.

[7]   (a) M. Di Vaira, P. Stoppioni, *Polyhedron* **1994**, *13*, 3045; (b) M. Detzel, T. Mohr, O. J. Scherer, G. Wolmershäuser, *Angew. Chem. Int. Ed. Engl.* **1994**, *33*, 1110; *Angew. Chem.* **1994**, *106*, 1142; (c) O. J. Scherer, T. Mohr, G. Wolmershäuser, *J. Organomet. Chem.* **1997**, *529*, 379; (d) M. Caporali, M. Di Vaira, M. Peruzzini, S. Seniori Costantini, P. Stoppioni, F. Zanobini, *Eur. J. Inorg. Chem.* **2010**, *2010*, 152; (e) V. Mirabello, M. Caporali, V. Gallo, L. Gonsalvi, A. Ienco, M. Latronico, P. Mastrorilli, M. Peruzzini, *Dalton Trans.* **2011**, *40*, 9668; (f) M. Piesch, F. Dielmann, S. Reichl, M. Scheer, *Chem. Eur. J.* **2020**, *26*, 1518; (g) M. Scheer, M. Piesch, C. Graßl*, Angew. Chem. Int. Ed.* **2020**, *59*, 7154; *Angew. Chem.* **2020**, *132*, 7220.

[8]   O. J. Scherer, R. Winter, G. Wolmershäuser, *Z. Anorg. Allg. Chem.* **1993**, *619*, 827.

[9]   M. Detzel, T. Mohr, O. J. Scherer, G. Wolmershäuser, *Angew. Chem. Int. Ed. Engl.* **1994**, *33*, 1110.

[10]   (a) M. Di Vaira, P. Stoppioni, M. Peruzzini, *Polyhedron* **1987**, *6*, 351; (b) M. Caporali, P. Barbaro, L. Gonsalvi, A. Ienco, D. Yakhvarov, M. Peruzzini, *Angew. Chem. Int. Ed.* **2008**, *47*, 3766; *Angew. Chem.* **2008**, *120*, 3826.

[11]   D. N. Akbayeva, *Russ. J. Coord. Chem.,* **2007**, *33*, 661.

[12]   Y. Xiong, S. Yao, E. Bill, M. Driess, *Inorg. Chem.* **2009**, *8*, 7522.

[13]   S. Pelties, T. Maier, D. Herrmann, B. de Bruin, C. Rebreyend, S. Gärtner, I. G. Shenderovich, R. Wolf, *Chem. Eur. J.* **2017**, *23*, 6094.

[14]   G. Prabusankar, A. Doddi, C. Gemel, M. Winter, R. A. Fischer, *Inorg. Chem.* **2010**, *49*, 7976.

[15]   (a) F. Hennersdorf, J. J. Weigand, *Angew. Chem. Int. Ed.* **2017**, *56*, 7858; *Angew. Chem.* **2017**, *129*, 7966; (b) F. Hennersdorf, J. Frötschel, J. J. Weigand, *J. Am. Chem. Soc.* **2017**, *139*, 14592.

[16]   W. W. Brennessel, R. E. Jilek, J. E. Ellis, *Angew. Chem. Int. Ed.* **2007**, *46*, 6132; *Angew. Chem.* **2007**, *119*, 6244.

[17]   P. P. Power (ed.), *Inorg. Synth. Vol. 37*, chapter 4.8., pp. 67–77. W. W. Brennessel J. E. Ellis in P. P. Power (ed.), *Inorg. Synth. Vol. 37*, chapter 4.8., pp. 76.

[18]   (a) W. W. Brennessel, J. V. G. Young, J. E. Ellis, *Angew. Chem. Int. Ed.* **2002**, *41*, 1211; *Angew. Chem.* **2002**, 114, 1259; (b) W. W. Brennessel, J. E. Ellis, *Inorg. Chem.* **2012**, *51*, 9076.

[19]   (a) J. E. Ellis, *Inorg. Chem.* **2006**, *45*, 3167; (b) R. Wolf, A. W. Ehlers, J. C. Slootweg, M. Lutz, D. Gudat, M. Hunger, A. L. Spek, K. Lammertsma, *Angew. Chem. Int. Ed.* **2008**, *47*, 4584; *Angew. Chem.* 2008, *120*, 5660; (c) R. Wolf, J. C. Slootweg, A. W. Ehlers, F. Hartl, B. de Bruin, M. Lutz, A. L. Spek, K. Lammertsma, *Angew. Chem. Int. Ed.* **2009**, *48*, 3104; *Angew. Chem.* **2009**, *121*, 3150; (d) R. Wolf, N. Ghavtadze, K. Weber, E.-M. Schnöckelborg, B. d. Bruin, A. W. Ehlers, K. Lammertsma, *Dalton Trans.* **2010**, *39*, 1453.

[20]   S. Alvarez, *Dalton Trans.* **2013**, *42*, 8617.

[21]   B. Cordero, V. Gómez, A. E. Platero-Prats, M. Revés, J. Echeverría, E. Cremades, F. Barragán, S. Alvarez, *Dalton Trans.* **2008**, 2832.

[22]   (a) O. J. Scherer, G. Berg, G. Wolmershäuser, *Chem. Ber.* **1995**, *128*, 635; (b) O. J. Scherer, S. Weigel, G. Wolmershäuser, *Chem. Eur. J.* **1998**, *4*, 1910; (c) V. A. Miluykov, O. G. Sinyashin, P. Lönnecke, E. Hey-Hawkins, *Mendeleev Commun.* **2003**, *13*, 212; (d) W. W. Seidel, O. T. Summerscales, B. O. Patrick, M. D. Fryzuk, *Angew. Chem. Int. Ed.* **2008**, *48*, 115; *Angew. Chem.* **2008**, *121*, 121; (e) S. Yao, Y. Xiong, C. Milsmann, E. Bill, S. Pfirrmann, C. Limberg, M. Driess, *Chem. Eur. J.* **2010**, *16*, 436; (f) C. Schwarzmaier, M. Bodensteiner, A. Y. Timoshkin, M. Scheer, *Angew. Chem. Int. Ed.* **2014**, *53*, 290; (g) S.

Yao, N. Lindenmaier, Y. Xiong, S. Inoue, T. Szilvási, M. Adelhardt, J. Sutter, K. Meyer, M. Driess, *Angew. Chem. Int. Ed.* **2015**, *54*, 1250; *Angew. Chem.* **2015**, *127*, 1266; (h) S. Yao, T. Szilvási, N. Lindenmaier, Y. Xiong, S. Inoue, M. Adelhardt, J. Sutter, K. Meyer, M. Driess, *Chem. Commun.* **2015**, *51*, 6153; (i) F. Spitzer, C. Graßl, G. Balázs, E. M. Zolnhofer, K. Meyer, M. Scheer, *Angew. Chem. Int. Ed.* **2016**, *55*, 4340; *Angew. Chem.* **2016**, *128*, 4412; (j) U. Chakraborty, J. Leitl, B. Mühldorf, M. Bodensteiner, S. Pelties, R. Wolf, *Dalton Trans.* **2018**, *47*, 3693.

[23] O. J. Scherer, M. Swarowsky, H. Swarowsky, G. Wolmershäuser, *Angew. Chem. Int. Ed. Engl.* **1988**, *27*, 694; *Angew. Chem.* **1988**, *100*, 738

[24] T. Li, N. Arleth, M. T. Gamer, R. Köppe, T. Augenstein, F. Dielmann, M. Scheer, S. N. Konchenko, P. W. Roesky, *Inorg. Chem.* **2013**, *52*, 14231.

[25] P. Büschelberger, D. Gärtner, E. Reyes-Rodriguez, F. Kreyenschmidt, K. Koszinowski, A. Jacobi von Wangelin, R. Wolf, *Chem. Eur. J.* **2017**, *23*, 3139.

3.5 Supporting Information (SI)

3.5.1 General Procedures

All manipulations were performed under an atmosphere of dry argon using standard Schlenk techniques or a MBraun UniLab glovebox. Solvents were dried and degassed with a MBraun SPS800 solvent-purification system. THF, diethyl ether, and toluene were stored over molecular sieves (3Å). *n*-Hexane was stored over a potassium mirror. 1,2-Dimethoxyethane (DME) was stirred over K/benzophenone, distilled, and stored over molecular sieves (3Å). Deuterated tetrahydrofuran was purchased from Sigma-Aldrich and used as received. The starting materials [(nacnac)Ga(η^2-P$_4$)],[1] [K(18-crown-6)(thf)$_2$]Fe(η^4-C$_{14}$H$_{10}$)$_2$],[2],[3] and [K(dme)$_2$][Co(η^4-C$_{14}$H$_{10}$)$_2$],[3],[4] were prepared according to previously reported procedures.

NMR Spectroscopy: NMR spectra were recorded on Bruker Avance 300 and Avance 400 spectrometers at 300 K and internally referenced to residual solvent resonances (δ(TMS) = 0.00 ppm, ^{1}H, ^{13}C; δ(H$_3$PO$_4$)(85%) = 0.00 ppm, ^{31}P, externally). Chemical shifts (δ) are reported in ppm. Coupling constants (*J*) are reported in Hz. For compounds, which give rise to a higher order spin system in the ^{31}P{^{1}H} NMR spectrum, the resolution enhanced ^{31}P{^{1}H} NMR spectrum was transferred to the software gNMR, version 5.0, by Cherwell Scientific.[5] The full line shape iteration procedure of gNMR was applied to obtain the best match of the fitted to the experimental spectrum. ^{1}*J*(^{31}P^{31}P) coupling constants were set to negative values and all other signs of the coupling constants were obtained accordingly. The assignment of the ^{13}C signals was deduced from the cross-peaks in 2D correlation experiments (HMBC, HSQC).

Elemental analysis: Elemental analyses were determined by the analytical department of the University of Regensburg with a Micro Vario Cube (Elementar).

UV/vis spectroscopy: UV/vis spectra were recorded on an Ocean Optics Flame spectrometer.

3.5.2 Synthesis of [K(18-crown-6){(η^4-C$_{14}$H$_{10}$)Fe(μ-η^4:η^2-P$_4$)Ga(nacnac)}] (1)
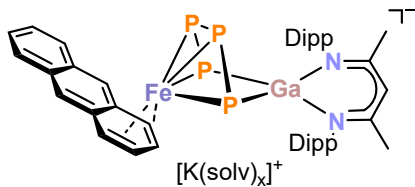
A yellow solution of [(nacnac)Ga(η^2-P$_4$)] (12 mg, 0.018 mmol, 1.0 equiv.) in THF (2 mL) was slowly added to a rust-colored solution of [K(18-crown-6)(thf)$_2$][Fe(η^4-C$_{14}$H$_{10}$)$_2$] (15.7 mg, 0.018 mmol, 1 equiv.) in THF (2 mL). The reaction mixture was stirred for 24 h at room temperature. Volatiles were removed under reduced pressure and the residual brown solid was washed with 8 mL *n*-hexane. The crude product was dissolved in 4 mL DME and filtered through a Whatman glass filter (pore size: 0.1 µm). Crystals suitable for X-ray diffraction were obtained by diffusion of *n*-hexane into the concentrated filtrate of the crude product at room temperature. ^{1}H NMR spectra of isolated samples of paramagnetic **1** show resonances of residual free anthracene. In addition, inconsistent and variable elemental analyses indicate the presence of large quantities of other unknown impurities. Unfortunately, all attempts to purify **1** by fractional crystallization have been unsuccessful so far.

3.5.3 Synthesis of [K(dme)$_2${(η^4-C$_{14}$H$_{10}$)Co(μ-η^4:η^2-P$_4$)Ga(nacnac)}] (2)
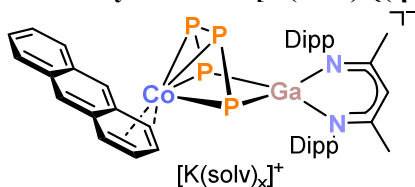
[K(dme)$_2$][Co(η^4-C$_{14}$H$_{10}$)$_2$] (199 mg, 0.315 mmol, 1.0 equiv.) was dissolved in THF (20 mL), resulting in a deep-violet solution, and a yellow solution of [(nacnac)Ga(η^2-P$_4$)] (200 mg, 0.315 mmol, 1.0 equiv.) in 40 mL THF was slowly added at –80 °C. The reaction mixture was allowed to warm to room temperature while stirring. Volatiles were removed in *vacuo* and the remaining solid was washed with diethyl ether (20 mL) and *n*-hexane (40 mL). The brownish residue was redissolved in DME and filtered through a P4 glass frit. The dark red-brown filtrate was concentrated in *vacuo* and layered with *n*-hexane (35 mL). Pure [K(dme)$_2${(η^4-C$_{14}$H$_{10}$)Co(μ-η^4:η^2-P$_4$)Ga(nacnac)}] (**2**) was isolated as dark violet thin plates after storage at room temperature for five days. Based on ^{1}H NMR spectroscopy and C,H,N analysis, **2** contains 1.9 molecules of DME per formula unit after drying under vacuum (10^{-3} mbar) for several hours.

Yield: 86 mg (22%).

^{1}H NMR (400.13 MHz, 300 K, THF-d_8): δ / ppm = 7.49 (br m, 3H, CH$_{Dipp}$), 6.99 (m, 1H, CH$_{Dipp}$), 6.93 (m, 2H, CH$_{Dipp}$), 6.90 (m, 2H, CH$_{(anth)}$), 6.74 (m, 2H,CH$_{(anth)}$), 5.84 (s, 2H, CH$_{(anth)}$), 5.59 (m, 2H, CH$_{(anth)}$), 4,82 (s, 1H, CH$_{(nacnac)}$), 3.96 (sept, $^3J_{HH}$ = 6.8 Hz, 2H, C*H*(CH$_3$)$_{2(nacnac)}$), 3.44 (s, 7.6H DME), 3.27 (s, 11H, DME), 2.88 (sept, $^3J_{HH}$ = 6.8 Hz, 2H, C*H*(CH$_3$)$_{2(nacnac)}$), 2.62 (m, 2H, CH$_{(anth)1,4}$), 1.79 (s, 3H, (s, 3H, CH$_{3(nacnac)}$), 1.53 (d, $^3J_{HH}$ = 6.8 Hz, 6H, CH(C*H$_3$*)$_{2(nacnac)}$), 1.50 (s, 3H, CH$_{3(nacnac)}$), 1.38 (d, $^3J_{HH}$ = 6.8 Hz, 6H, CH(C*H$_3$*)$_{2(nacnac)}$), 1.25 (d, $^3J_{HH}$ = 6.8 Hz, 6H, CH(C*H$_3$*)$_{2(nacnac)}$), 0.94 (d, $^3J_{HH}$ = 6.8 Hz, 6H, CH(C*H$_3$*)$_{2(nacnac)}$).

^{13}C{^{1}H} NMR (100.61 MHz, 300 K, THF-d_8): δ / ppm = 168.0 (N*C*CH$_3$CH$_{(nacnac)}$), 165.0 (N*C*CH$_3$CH$_{(nacnac)}$), 145.5 (C$_{(anth)}$), 145.1 (C$_{(Dipp)}$), 145.0 (C$_{(Dipp)}$), 144.1 (C$_{(Dipp)}$), 143.2 (C$_{(Dipp)}$), 133.3 (C$_{(anth)}$), 127.0 (C$_{Dipp}$), 126.2 (CH$_{(Dipp)}$), 125.8 (C$_{(anth)}$), 125.6 (CH$_{(Dipp)}$), 123.9 (CH$_{(Dipp)}$), 123.1 (C$_{(anth)}$), 113.5 (C$_{(anth)}$), 95.8 (CH$_{(nacnac)}$), 83.9 (C$_{(anth)}$), 72.6 (DME), 58.8 (DME), 56.4 (C$_{(anth)}$), 29.3 (*C*H(CH$_3$)$_{2(Dipp)}$), 28.7 (*C*H(CH$_3$)$_{2(Dipp)}$), 26.1 (CH(*C*H$_3$)$_{2(Dipp)}$), 25.9 (CH(*C*H$_3$)$_{2(Dipp)}$), 25.1 (CH(*C*H$_3$)$_{2(Dipp)}$), 24.6 (CH$_{3(Dipp)}$), 24.5 (CH$_{3(Dipp)}$).

^{31}P{^{1}H} NMR (161.98 MHz, 300 K, THF-d_8): (AA'XX') spin system δ / ppm = 89.2 (m, 2P$_P$), −94.7 (m, 2P$_{Ga}$).

UV/vis: (THF, λ$_{max}$ / nm, ε$_{max}$ / L·mol^{-1}·cm^{-1}): 301 (42000), 356 (39000), 524sh (8200).

Elemental analysis calcd. for $C_{51}H_{71}CoGaKN_2O_4P_4$ · $(C_4H_{10}O_2)_{1.9}$ (Mw = 1058.78 g·mol^{-1}): C 57.40, H 6.66, N 2.65; found C 57.51, H 6.52; N 2.59.
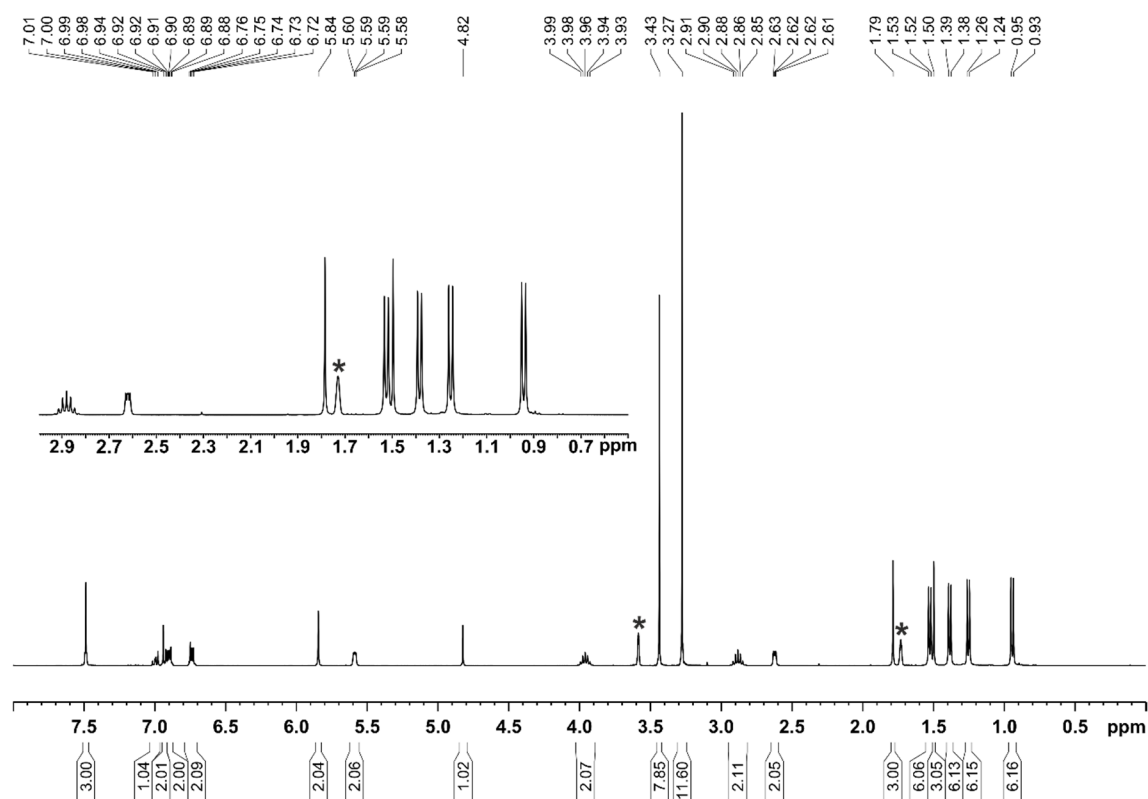
Figure S1. ^{1}H NMR spectrum (400 MHz, 300 K, THF-d_8) of $[K(dme)_2\{(\eta^4\text{-}C_{14}H_{10})Co(\mu\text{-}\eta^4\text{:}\eta^2\text{-}P_4)Ga(^{Dipp}nacnac)\}]$ (**2**). * THF-d_8.
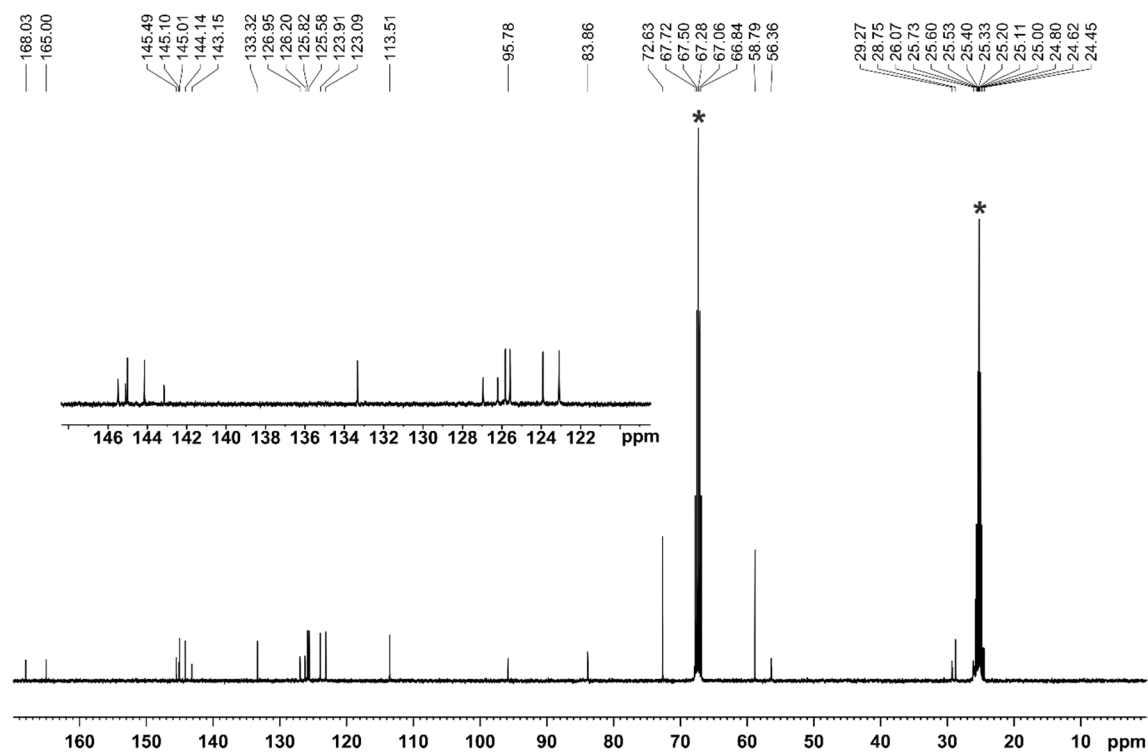
Figure S2. $^{13}C\{^1H\}$ NMR spectrum (100.61 MHz, 300 K, THF-d_8) of $[K(dme)_2\{(\eta^4\text{-}C_{14}H_{10})Co(\mu\text{-}\eta^4\text{:}\eta^2\text{-}P_4)Ga(^{Dipp}nacnac)\}]$ (**2**). * THF-d_8.
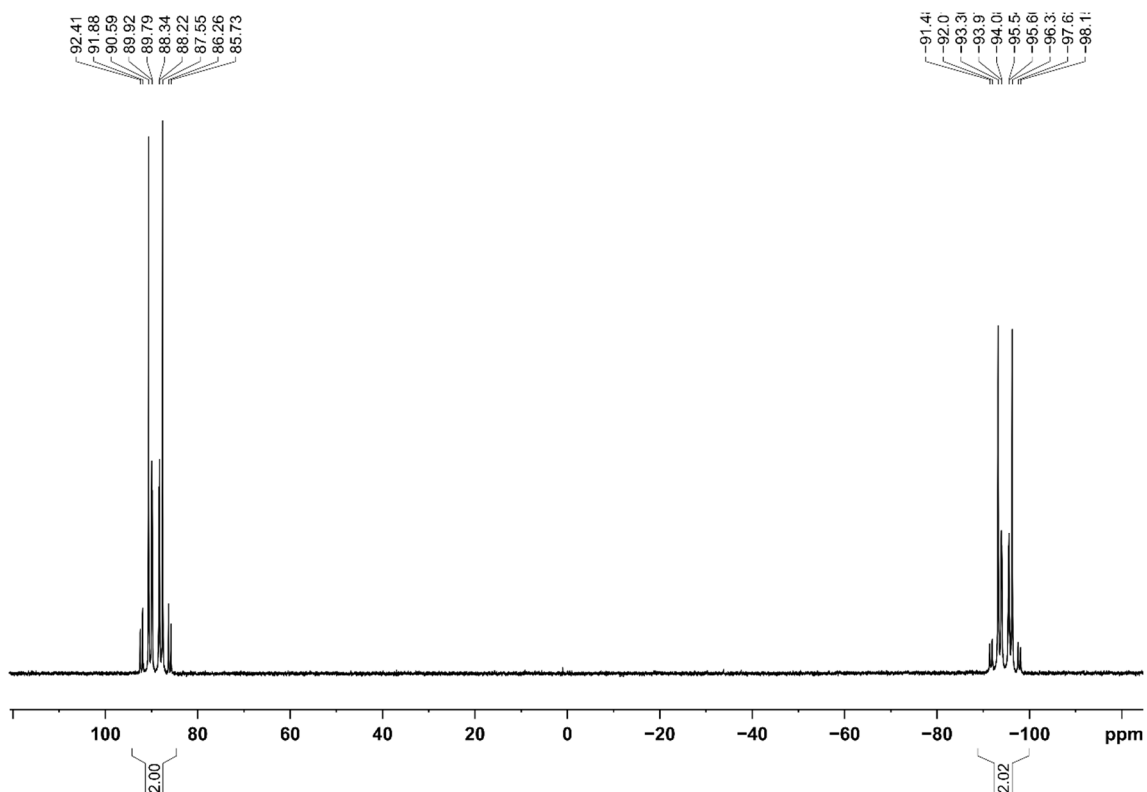
Figure S34. $^{31}P\{^1H\}$ NMR spectrum (121.49 MHz, 300 K, THF-d_8) of [K(dme)$_2$\{(η^4-C$_{14}$H$_{10}$)Co(μ-η^4:η^2-P$_4$)Ga(^{Dipp}nacnac)\}] (**2**).
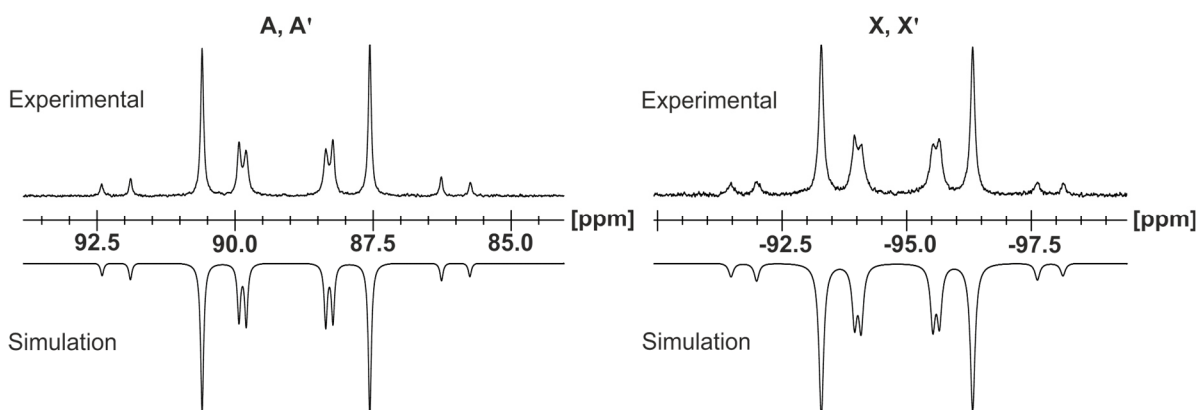
Figure S4. Section of the $^{31}P\{^1H\}$ NMR (400.13 MHz, 300 K, THF-d_8) of **2**; experimental (upwards) and simulation (downwards).

Table S1. Coupling constants from the iterative fit of the AA'XX' spin system and schematic representation of the CoP$_4$Ga core of [K(dme)$_2$\{(η^4-C$_{14}$H$_{10}$)Co(μ-η^4:η^2-P$_4$)Ga(nacnac)\}] (**2**); [Co] = (anth)Co, [Ga] = (nacnac)Ga.

$^1J_{AA'} = {}^1J_{A'A}$	−370.6 Hz	$^2J_{AX'} = {}^2J_{A'X}$	4.9 Hz	
$^1J_{AX} = {}^1J_{A'X'}$	−496.8 Hz	$^3J_{XX'} = {}^3J_{X'X}$	−52.2 Hz	
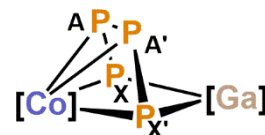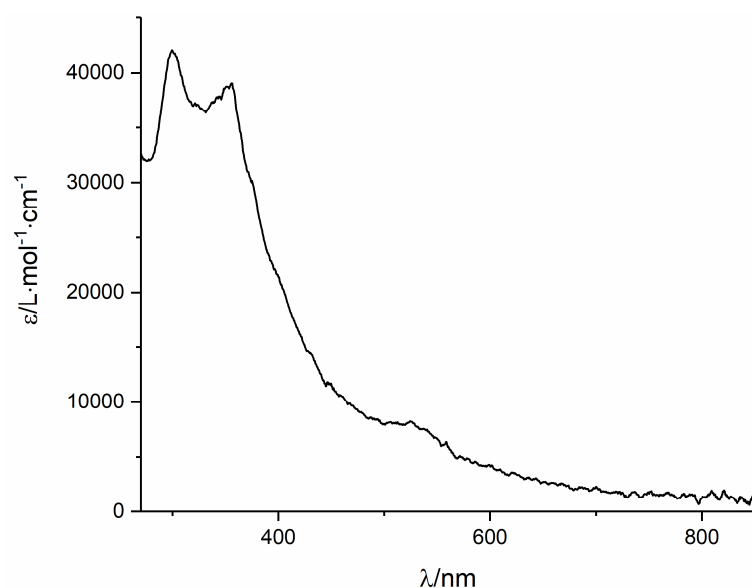
Figure S5. UV/vis spectrum of $[K(dme)_2\{(\eta^4\text{-}C_{14}H_{10})Co(\mu\text{-}\eta^4:\eta^2\text{-}P_4)Ga(^{Dipp}nacnac)\}]$ (**2**) recorded in THF.

3.6   X-ray Crystallography

Crystallographic data were recorded on an Oxford Diffraction Gemini R Ultra with Atlas S2 CCD detector for **1** and an Agilent GV1000 diffractometer with a Titan S2 CCD detector for **2**. In both cases, Cu-K_α radiation (λ = 1.54184 Å) was used. Crystals were selected under mineral oil, mounted on micromount loops and quench-cooled using an Oxford Cryosystems open flow N_2 cooling device. Either semi-empirical multi-scan absorption corrections[6] or analytical ones[7] were applied to the data. Using Olex2,[8] the structures were solved with SHELXT[9] using intrinsic phasing and refined with SHELXL[10] using least squares refinement on F^2. The hydrogen atoms were located in idealized positions and refined isotropically with a riding model. Crystallographic data for the structures in this paper have been deposited with the Cambridge Crystallographic Data Centre, CCDC, 12 Union Road, Cambridge CB21EZ, UK. Copies of these data can be obtained free of charge (http://www.ccdc.cam.ac.uk) on quoting the depository number: CCDC 1972352 for **1** and 1972351 for **2**.

3.6.1   Refinement   of   the   solid-state   molecular   structure   of $[K(dme)_2\{(\eta^4\text{-}C_{14}H_{10})Co(\mu\text{-}\eta^4:\eta^2\text{-}P_4)Ga(nacnac)\}]$ (2)

One of two DME solvate molecules, coordinated to the potassium counterion in the solid-state molecular structure of **2** had to be split into two parts and was successfully refined without the need of any additional restraints or constraints. During the refinement, one of the diisopropylphenylgroups of the [Ga(nacnac)] backbone had to be split into two parts and a Simu was applied to restrain the U_{ij} components. A rather strong distorted *n*-hexane molecule was masked using the Olex2 solvent mask. A solvent mask was calculated and 42 electrons were found in a volume of 174 Å^3 in two voids per unit cell. This is consistent with the presence of $0.5[C_6H_{14}]$ per asymmetric unit which accounts for 50 electrons per unit cell.

Table S1. Crystallographic data for compounds **1** and **2**.

Compound	1	2
Empirical formula	$C_{66}H_{102}FeGaKN_2O_{10}P_4$	$C_{51}H_{71}CoGaKN_2O_4P_4$
Formula weight	1372.04	1067.72
Temperature [K]	123(1)	123.01(10)
Crystal system	triclinic	triclinic
Space group	P-1	P-1
a [Å]	12.8013(4)	10.9891(2)
b [Å]	12.8477(3)	12.0239(2)
c [Å]	22.8788(6)	21.5532(3)
α [°]	95.470(2)	90.3270(10)
β [°]	99.362(2)	92.4990(10)
γ [°]	105.796(2)	104.3790(10)
Volume [Å³]	3533.66(17)	2755.63(8)
Z	2	2
ρ_{calc} [g/cm³]	1.290	1.287
μ [mm⁻¹]	3.933	5.059
F(000)	1456.0	1120.0
Crystal size [mm³]	0.573 × 0.272 × 0.202	0.46 × 0.16 × 0.057
Radiation	Cu Kα (λ = 1.54184)	Cu Kα (λ = 1.54184)
2Θ range for data collection [°]	7.23 to 133.694	7.592 to 147.664
Index ranges	-15 ≤ h ≤ 15, -15 ≤ k ≤ 14, -27 ≤ l ≤ 19	-13 ≤ h ≤ 13, -14 ≤ k ≤ 14, -26 ≤ l ≤ 24
Reflections collected	51666	71275
Independent reflections	12403 [R_{int} = 0.0334, R_{sigma} = 0.0246]	11035 [R_{int} = 0.0509, R_{sigma} = 0.0286]
Data / restraints / parameters	12403/0/781	11035/318/742
Goodness-of-fit on F^2	1.030	1.056
Final R indexes [I>=2σ (I)]	R_1 = 0.0314, wR_2 = 0.0807	R_1 = 0.0394, wR_2 = 0.1016
Final R indexes [all data]	R_1 = 0.0325, wR_2 = 0.0816	R_1 = 0.0437, wR_2 = 0.1051
Largest diff. peak/hole [e Å⁻³]	0.71/-0.45	0.67/-0.80

101

3.7 References of Supporting Information

[1] G. Prabusankar, A. Doddi, C. Gemel, M. Winter, R. A. Fischer, *Inorg. Chem.* **2010**, *49*, 7976.

[2] W. W. Brennessel, R. E. Jilek, J. E. Ellis, *Angew. Chem. Int. Ed.* **2007**, *46*, 6132; *Angew. Chem.* 2007, *119*, 6244.

[3] P. P. Power (ed.), *Inorg. Synth. Vol. 37*, chapter 4.8., pp. 67. W. W. Brennessel J. E. Ellis in P. P. Power (ed.), *Inorg. Synth. Vol. 37*, chapter 4.8., pp. 76.

[4] (a) W. W. Brennessel, J. V. G. Young, J. E. Ellis, *Angew. Chem. Int. Ed.* **2002**, *41*, 1211; *Angew. Chem.* **2002**, 114, 1259; (b) W. W. Brennessel, J. E. Ellis, *Inorg. Chem.* **2012**, *51*, 9076.

[5] P. H. M. Budzelaar, *gNMR for Windows (5.0.6.0), NMR Simulation Program* **2006**.

[6] (a) SCALE3ABS, CrysAlisPro, Aglient Technologies Inc. Oxford, GB **2015**; (b) G. M. Sheldrick, SADABS, Bruker AXS, Madison, USA **2007.**

[7] R. C. Clark, J. S. Reid, *Acta Crystallogr. A* **1995**, *51*, 887.

[8] O. V. Dolomanov, L. J. Bourhis, R. J. Gildea, J. A. K. Howard, H. Puschmann, *J. Appl. Cryst.* **2009**, *42*, 339.

[9] G. M. Sheldrick, *Acta Cryst.* **2015**, *A17*, 3.

[10] G. M. Sheldrick, *Acta Cryst.* **2015**, *C71*, 3.

Chapter 4   An unusual $Ni_2Si_2P_8$ cluster formed by complexation and thermolysis

Abstract: $[LSi(\eta^2\text{-}P_4)]$ (L = CH[C(Me)N(Dipp)][C(CH₂)N(2,6-iPr₂C₆H₃)]) forms well-defined 1:1 and 2:1 complexes with N-heterocyclic carbene nickel fragments. The unusual cluster compound $[(IPr)Ni_2P_8(SiL)_2]$ (IPr = 1,3-bis(2,6-diisopropylphenyl)imidazolin-2-ylidene) is selectively formed from $[(IPr)Ni(\mu\text{-}\eta^{2:2}\text{-}P_4)SiL]$ by thermolysis.

4.1 Introduction

Nickel phosphides are of interest in material science and industry due to their favorable magnetic[1] and catalytic properties and their potential in hydrogen evolution reactions (HER),[2] water splitting,[3] hydrodenitrogenation, and hydrodesulfuration reactions.[4],[5] Doping nickel phosphides with different transition metal elements is a common approach to modify their electro- and photocatalytic activity.[6] Including main group elements, such as sulfur, has been shown to improve the catalytic activity of nickel phosphides in HER.[7] Although promising, the synthesis of such metal phosphides remains challenging[5],[8] and contemporary methods require sensitive and toxic phosphine precursors (e.g. P(SiMe₃)₃), special additives (e.g. tri-*n*-octylphosphine, oleylamine) and high temperatures.[9],[10],[11] A possible alternative is the mild thermolysis of carefully designed transition metal polyphosphido complexes,[12] which can be accessed by the direct activation of white phosphorus (P₄). The use of nickel(0) complexes already dates back to 1979, when Sacconi and co-workers reported the synthesis of a monohapto P₄ complex [(κ^3-P,P,P-NP₃)Ni(η^1-P₄)] [(NP₃ = tris(2-diphenylphosphinoethyl)amine)].[13] Since then, several other groups have shown that Ni⁰ sources are suitable reagents for the targeted synthesis of nickel polyphosphido compounds.[10],[14],[15],[16],[17]

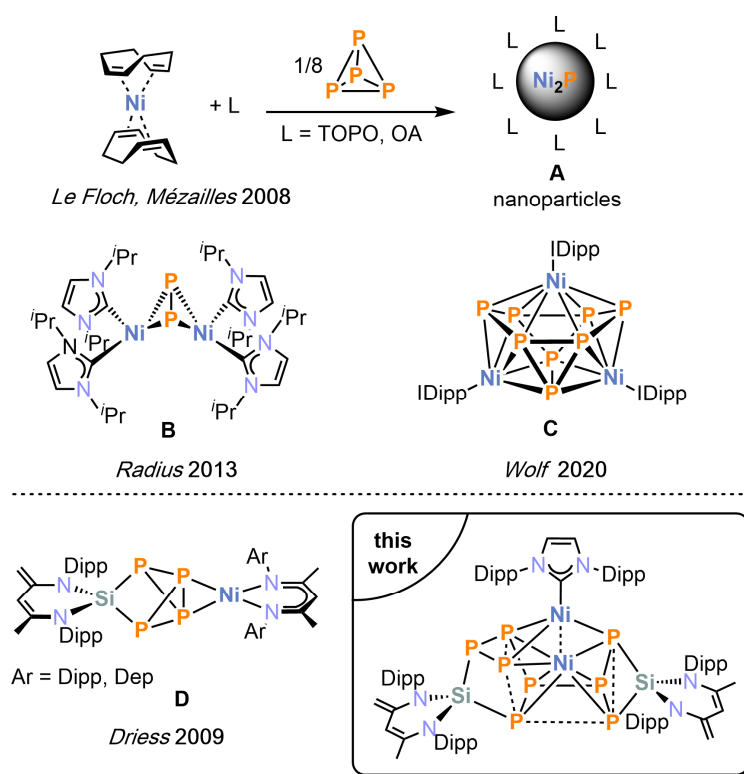**Figure 1.** Examples of P₄ activation by Ni⁰ precursors (top); heterodinuclear silicon-nickel polyphosphido complexes (bottom).

Le Floch and Mézailles prepared Ni₂P nanoparticles directly by reacting [Ni(cod)₂] (cod = 1,5-cyclooctadiene) with P₄ in the presence of TOPO (tri-*n*-octylphosphine oxide) (Figure 1, **A**)[10] and Radius and co-workers accessed the P₂ complex [{Ni(Im*i*Pr₂)₂}₂(μ,$\eta^{2:2}$-P₂)] (Figure 1, **B**,

Im*i*Pr₂ = 1,3-bis(*iso*-propyl)imidazolin-2-ylidene).[16] More recently, our group described the aggregation of P₄ using (NHC)Ni complexes leading to novel di- and trinuclear complexes (see e.g. Figure 1, **C**).[17] Molecular main-group doped nickel phosphide complexes were reported by Driess in 2009 (Figure 1, **D**).[18] This type of complex is obtained from [LSi(η^2-P₄)][19] (L = CH[(C=CH₂)CMe][N(2,6-iPr₂C₆H₃)]₂) and [(L'Ni)₂·toluene] (L' = CH[CMeN(2,6-iPr₂C₆H₃)]₂) and [(L″}Ni)₂·toluene] (L″ = CH[CMeN(2,6-Et₂C₆H₃)]₂). The molecular structures of these complexes feature an intact SiP₄ unit coordinating to the Ni^I center.[18] We reasoned that reactions with a more reductive Ni⁰ precursor could lead to P–P bond cleavage and subsequent aggregation of the resulting intermediates. Herein, we report the preparation of (NHC)Ni⁰ complexes with the silatetraphosphapentane [LSi(η^2-P₄)]. Mild thermolysis of one of the complexes affords an unusual Ni₂Si₂P₈ cluster by the nickel-mediated dimerization of two [LSi(η^2-P₄)] units.

4.2 Results and Discussion

Vinyltrimethylsilane complexes [(NHC)Ni(η^2-vtms)₂] (NHC = IPr, IMes, vtms = Me₃SiCH=CH₂) were selected as well-proven "(NHC)Ni⁰" equivalents and reacted with [LSi(η^2-P₄)] in a 1:1 and 1:2 stoichiometry in toluene at −50 °C.[19],[20] Using two equivalents of [LSi(η^2-P₄)], [(NHC)Ni{(μ-$\eta^{2:2}$-P₄)SiL}₂] **1a** (NHC = IPr) and **1b** (NHC = IMes) are isolated as red powders in 50% and 26% yield, respectively (Scheme 1).
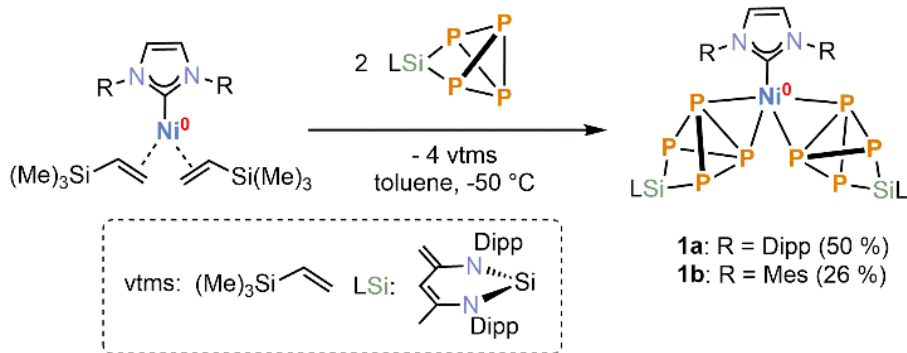
Scheme 1. Synthesis of [(NHC)Ni{(μ-$\eta^{2:2}$-P₄)SiL}₂] (NHC = IPr (**1a**), NHC = IMes (**1b**)).

A single-crystal X-ray diffraction (XRD) study revealed that both compounds are isostructural and therefore only **1a** will be discussed here (Figure 2). The molecular structure shows two [LSi(η^2-P₄)] ligands side-on coordinated to the bridging [(IPr)Ni] unit. The P–P bond distances of the coordinated P atoms (P3–P4 2.2686(6) Å, P7–P8 2.4749(7) Å) are considerably longer than the corresponding P–P bond length in [LSi(η^2-P₄)] (2.159(2) Å), although similar to complex **D** (2.351(3) Å).[18],[19] This might be explained by a significant back-donation of electron density from the Ni⁰ center. The Ni–P distances (av. 2.2744 Å) in **1a** lie in a similar range to those of **D** (av. 2.266 Å).[18]
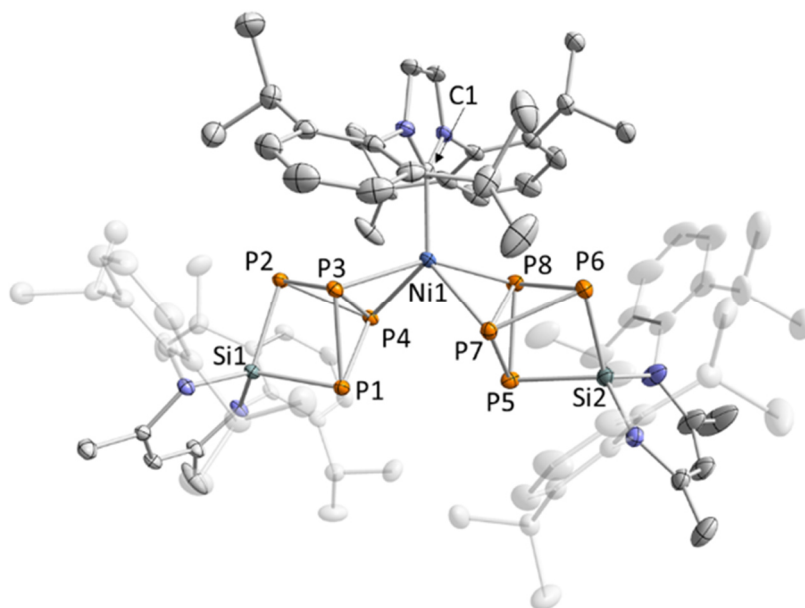
Figure 2. Solid-state molecular structure of **1a**. Hydrogen atoms and solvate molecules are omitted for clarity; thermal ellipsoids are drawn at the 40% probability level; selected bond lengths [Å] for **1a**: P1–P3 2.2651(6), P1–P4 2.2511(7), P2–P3 2.2565(7), P2–P4 2.2724(7), P3–P4 2.2686(6), Si1–P1 2.2512(8), Si1–P2 2.2422(7), Ni1–P3 2.2923(8), Ni1–P4 2.2674(8), P5–P7 2.2451(6), P5–P8 2.2603(7), P6–P7 2.2714(9), P6–P8 2.2607(7), P7–P8 2.4749(7), Si2–P5 2.2475(9), Si2–P6 2.2455(6), Ni1–P7 2.2657(6), Ni1–P8 2.2847(7), Ni1–C1 1.9761(16); bond distances and angles of derivatives **1b** are presented in the SI (see Fig. S25, SI).

The $^{31}P\{^1H\}$ NMR spectra of **1a** (Figure S5, SI) shows two very broad resonances at δ = –234.3 ppm and 190.6 ppm with an integral ratio of 1:1, which do not resolve at differing temperatures, suggesting a fluxional behavior in solution (Figure S7, S8, SI). Complex **1b** shows comparatively sharper multiplets at δ = –236.4 ppm and 194.2 ppm in the $^{31}P\{^1H\}$ NMR spectrum (Figure S11, S13, S14, SI). Despite the broad resonances observed in the ^{31}P NMR spectra, both **1a** and **1b** give rise to well-resolved ^1H NMR spectra (Figures S3 and S9, SI), which indicate a symmetric structure. The ^{29}Si NMR spectrum of **1a** reveals a very broad signal at δ = –50.5 ppm ($\nu_{1/2}$ = 90 Hz), whereas **1b** displays a broad pseudo-triplet resonance at δ = –51.1 ppm which is slightly shifted to higher field compared to the starting material [LSi(η^2-P₄)] (δ = –40.4 ppm).[19]

The reaction with equimolar amounts of [(IPr)Ni(η^2-vtms)₂] and [LSi(η^2-P₄)] in toluene at room temperature results in the selective formation of a new species [(IPr)Ni(μ-$\eta^{2:2}$-P₄)SiL] (**2**). After filtration and recrystallization from *n*-hexane, **2** was isolated as red crystalline blocks (Scheme 2).
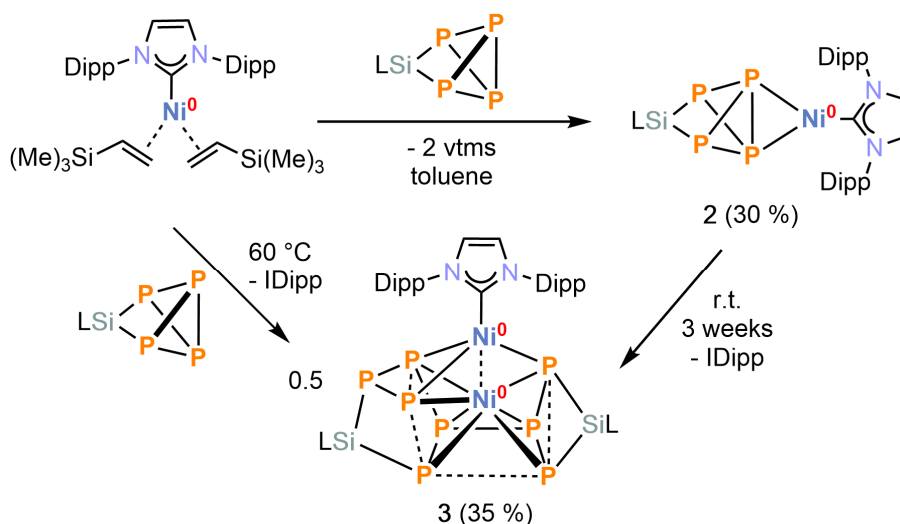
Scheme 2. Synthesis of [(IPr)Ni(μ-η²-P₄)SiL] (**2**) and [(IPr)NiP₈{SiL}₂] (**3**).

The solid-state molecular structure is presented in Figure 3a and reveals a heterodinuclear [Si(μ-η²:²-P₄)Ni] core which resembles Driess Ni^I complex **D**.[18] Similar to complexes **1a,b** and **D** the conformation of the side-on coordinated [(L)Si(η²-P₄)] moiety remains untouched except for the nickel coordinated P3–P4 bond (2.389(6) Å) which is about 0.23 Å longer than in the starting material [LSi(η²-P₄)] and even slightly elongated compared to the related compound **D** (2.335(4) Å).[18],[19] Interestingly, the Ni–P distances (Ni1–P3 2.151(6) Å, Ni1–P4 2.1223(10) Å) are considerably shorter than those observed in complex **D** (Ni1–P3 2.255(4) Å, Ni1–P4 2.277(2) Å).[18] This might be explained by significant back-donation of electron density from the Ni center toward the phosphorus framework. The bonding-situation was investigated by means of natural bond orbital analysis (NBO) of the optimized structure of **2**, calculated at the PBE/def2-TZVP level of theory (see the SI). Looking at the composition of the constructed orbitals five occupied $3d^{10}$ orbitals together with five two-center-two-electron P–P bonds were found, suggesting the presence of nickel in its formal oxidation state zero (Figure S29 and S30, SI). By looking more closely, a strong interaction of a filled Ni(d) orbital with the antibonding σ* orbital of the P3–P4 bond can be observed with a donor-acceptor stabilization energy of 36.5 kcal · mol^{-1} (Figure 3b). This supports the notion that there is strong back-donation of the nickel center, which is more pronounced in the Ni^0 complex **2** than in the Ni^I compound **D**.[18] The ^{31}P{^{1}H} NMR spectrum of **2** dissolved in C₆D₆ at room temperature shows three chemically different ^{31}P nuclei resonating at δ(P$_A$) = –155.1 ppm, δ(P$_B$) = –138.0 ppm, and δ(P$_X$) = 147.3 ppm. The two signals shifted to higher field are each split into a doublet of triplets (^1J(P$_A$,P$_X$) = –114.2 Hz, ^1J(P$_A$,P$_B$) = –25.6 Hz) while the low-field shifted signal δ(P$_X$) shows a pseudo triplet (^1J(P$_X$,P$_A$) = –114.2 Hz, ^1J(P$_X$,P$_B$) = –114.1 Hz), giving rise to an ABX₂ spin system (Figure S17). Upon coordination of the [(NHC)Ni] fragment the resonances P$_A$ and P$_B$ are shifted to lower field compared to the starting

material[19] and to other comparable diamagnetic [LM(η²-P₄)] (M = Ga,[21] Ge,[22] Zr, Hf[23]) type complexes with a tricyclo[3.1.0]pentane-like structure. The coordination of the nickel atom is also reflected in the $^1J(P_A,P_B)$ coupling constant ($^1J(P_A,P_B)$ = –25.6 Hz) which is about 162.4 Hz smaller in magnitude than in the non-coordinated case ($^1J(P_A,P_B)$ = –188.0 Hz). The recorded ^{29}Si NMR spectrum of **2** in C_6D_6 reveals a broad resonance at δ = –37.1ppm.
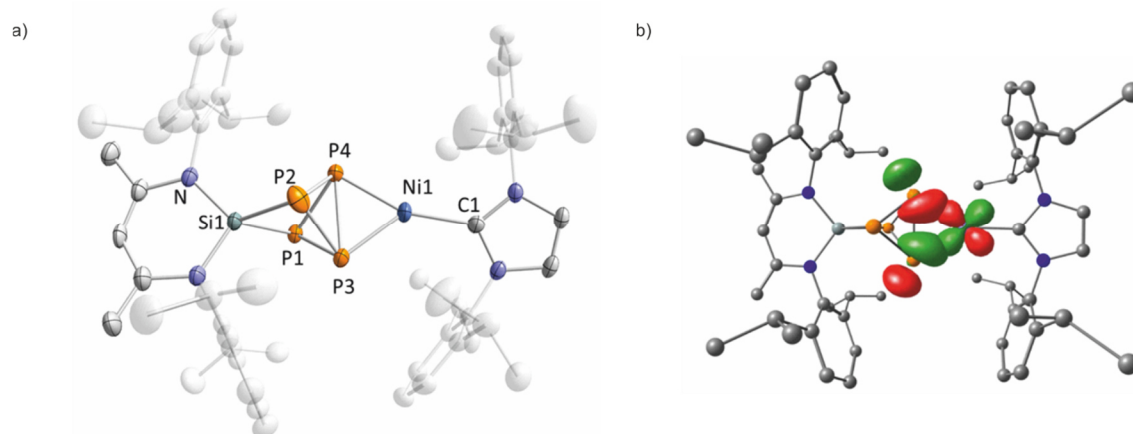

Figure 3. a) Solid-state molecular structure of **2**. Hydrogen atoms and disorder are omitted for clarity; thermal ellipsoids are drawn at the 40% probability level. Selected bond lengths [Å] and angles [°] for **2** (in case of disorder bond lengths and angles were derived from the part with highest occupancy): P1–P3 2.265(6), P1–P4 2.244(6), P2–P3 2.186(11), P2–P4 2.2469(14), P3–P4 2.389(6), Si1–P1 2.249(5), Si1–P2 2.2235(14), Ni1–P3 2.151(6), Ni1–P4 2.1223(10), Ni1–C1 1.930(3); P1–P3–P2 87.2(3), P1–P4–P2 86.25(16), P3–P1–P4 64.0(2), P3–P2–P4 65.20(18), P3–Ni1–P4 67.97(18), C1–Ni1–P3 132.00(19), C1–Ni1–P4 159.79(11); b) Natural bond orbitals representing the back-bonding of an occupied Ni d-orbital into the antibonding orbital of the coordinated P−P bond. Ni(d) → σ* (P3–P4) 36.5 kcal · mol⁻¹. Surface isovalue = 0.07. H atoms have been omitted for clarity.

It is noteworthy that complex **2** can only be accessed using the more sterically demanding [(IPr)Ni(η²-vtms)₂] complex. Conducting the same reaction with the less sterically demanding [(IMes)Ni(η²-vtms)₂] the exclusive formation of **1b** was observed. Compound **2** slowly decomposes in solution and over the course of three weeks gives rise to a ^{31}P{^{1}H} NMR spectrum with two new ABCDEMSX spin systems, which are assigned to [(IPr)Ni₂P₈(SiL)₂] (**3**, vide infra). The clean formation of **3** can also be achieved by heating the reaction of [(IPr)Ni(η²-vtms)₂] and [LSi(η²-P₄)] to 60 °C, circumventing the isolation of **2**. Significant amounts of co-crystallized IPr were removed *via* sublimation (95 °C and 1 · 10⁻⁵ mbar). Subsequent recrystallization from toluene layered with *n*-hexane afforded compound **3** as brown crystals in a 35% yield. The structure of **3** shows an unusual asymmetrical Si₂Ni₂P₈ cluster with strongly varying P–P distances (range 2.1702(8) Å − 3.4219(8) Å). The phosphorus atoms P1, P3, P8, and P6 are aligned in a plane (torsion angle ⪦ 1.8°) and coordinated by the central Ni1 atom. This plane is fused to a P₃ ring (P2, P4, and P5) with one large P4···P5 distance of 2.5499(9) Å. In addition, this unit is connected to a second P₃ ring (P6, P7, and P8) *via* a P–P single bond (P3–P7 2.1702(8) Å). The P₈ framework is stabilized by two LSi moieties. Each silicon atom is connected to two phosphorus atoms. The whole framework is capped by a [(IPr)Ni] fragment connected to

three P atoms (P4, P5, and P7). The Ni1–Ni2 distance (2.4126(4) Å) also deserves to be commented on. This value is consistent with an estimated value of 2.48 Å received from the covalent radius of a single nickel atom (1.24 Å).[24] While covalent metal-metal bonds are common for nickel(I) complexes,[25] only a few related dinickel(0) complexes have been described with Ni^0–Ni^0 distances ranging from 2.437 to 2.572 Å.[26],[27] A notable example is the isonitrile complex [Ni₂(μ-CNMe)(CNMe)₂(μ-PPh₂CH₂PPh₂)₂] reported by Kubiak and co-workers with a Ni–Ni separation of 2.572(1) Å.[27]
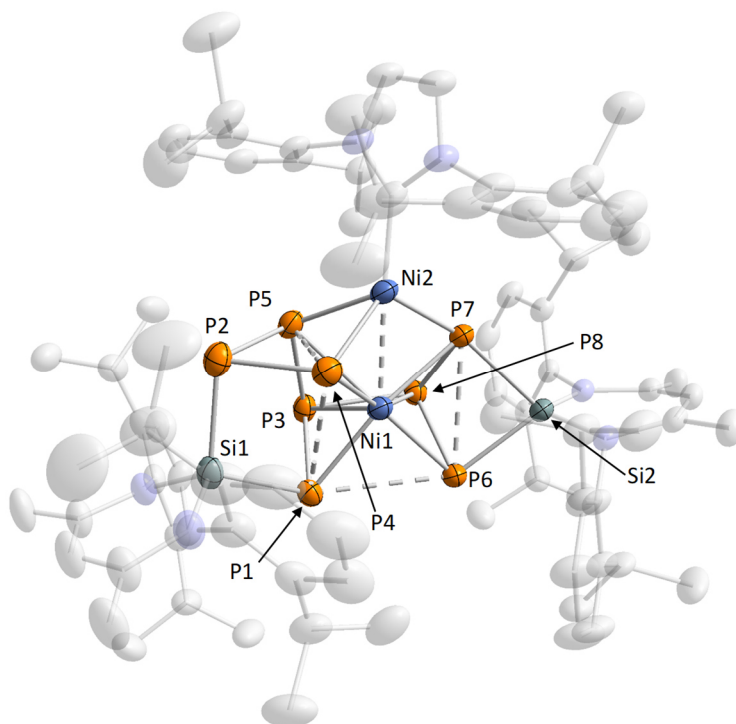

Figure 4. Solid-state molecular structure of **3**. Hydrogen atoms and disorder are omitted for clarity; thermal ellipsoids are drawn at the 40% probability level; selected bond distances [Å] and angles [°] for **3**: P1–P3 2.1702(8), P1⋯P4 3.4219(8), P1⋯P6 3.0176(7), P2–P4 2.2160(9), P2–P5 2.1704(10), P4⋯P5 2.5499(9), P3–P8 2.4018(7), P6⋯P7 2.1946(7), P7–P8 2.3083(7), Si1–P1 2.2539(8), Si1–P2 2.2832(11), Si2–P6 2.2265(7), Si2–P7 2.2709(7), Ni1⋯Ni2 2.4126(4), Ni1–P1 2.2717(6), Ni1–P3 2.4280(6), Ni1–P6 2.3132(6), Ni1–P8 2.4143(6), Ni2–P4 2.1983(8), Ni2–P5 2.2448(6), Ni2–P7 2.1811(7); P1–P3–P8 98.26(3), P3–P8–P6 97.79(3), P3–P1–P6 82.91(2), P3–P1–P4 84.04(3), P1–P4–P5 68.31(2), P4–P5–P3 104.92(4), P2–P4–P5 53.63(3), P4–P5–P2 55.29(3), P5–P2–P4 71.08(3), P5–P3–P8 95.97(3), P3–P8–P7 107.97(3), P6–P8–P7 79.88(3), P8–P7–P6 48.896(18), P7–P6–P8 51.23(2), P4–P1–P6 85.977(19), P1–P6–P7 96.32(2), P1–Ni1–P4 98.25(3), P3–Ni1–P5 56.10(2), P6–Ni1–P7 79.0 (2), P8–Ni–P7 59.00(2).

In order to investigate the bonding situation in more detail, the electronic structure was analyzed by calculating intrinsic bond orbitals (IBOs)[28] at the PBE/def2-TZVP level of theory. A truncated model of **3′** (with *i*Pr of **3** replaced by Me groups) was used for the calculations. The composition of the IBOs suggests a $3d^{10}$ configuration for the two Ni atoms. Seven two-center-two-electron P−P bonds, four doubly occupied IBOs involving the Si−P bonds and additionally, three three-center-two-electron bonds were calculated. An IBO corresponding to a two-center-two-electron bond was not found. However, one of the multicenter bonds (see Figure S33, SI) suggests a Ni1⋯Ni2 interaction. The presence of a weak Ni–Ni bond is also supported by the calculated Mayer bond order of 0.3. The short Ni1⋯Ni2 distance might thus mainly be explained by the constraint alignment of the

core of the cluster and additional significant contributions of the multicenter bonds. Multinuclear NMR spectra of **3** suggest the presence of two isomers in solution in an approximate ratio of 3:1 due to the asymmetric L ligand. It is worth noting a similar ratio was found in the solid-state, in the disorder of the diketiminate ligand (L) backbone (see Figure S28, SI). As a result, the ^1H, ^{13}C NMR spectra are complex but confirm the presence of all molecular components. The ^{29}Si NMR spectrum shows two broad resonances at δ = −3.9 ppm and 60.8 ppm. However, the $^{31}P\{^1H\}$ NMR spectrum is particularly informative, showing two ABCDEMSX spin systems independent of temperature (see Figure 5 and Figures S23, S24, SI). To aid in assigning the signals, ^{31}P and ^{29}Si NMR chemical shieldings were calculated for the main isomer (see Table S3, S4, SI) of the slightly truncated model cluster **3′** at the TPSS/pcSseg-2 level of theory. Complex **2** was chosen as a reference system and the resonances of the $^{31}P\{^1H\}$ NMR spectrum (Figure 5) were assigned according to the calculation, allowing for the iterative fitting of the $^{31}P\{^1H\}$ NMR spectrum of **3** (see the SI). DFT-calculated $J(^{31}P,^{31}P)$ coupling constants were used as an initial starting point for the fitting procedure (see Table S1, SI). Five large $^1J(^{31}P,^{31}P)$ coupling constants (−204.2 to −409.7 Hz) and one unexpectedly small $^1J(^{31}P,^{31}P)$ coupling constant of −7.5 Hz between nuclei P_A and P_B was derived. The small $^1J(P_A,P_B)$ (−7.5 Hz) coupling constant might be explained by the relatively long distance of the nuclei P_A and P_B observed by X-ray crystallography (P3–P8 2.4018(7) Å). Notably, a rather large coupling constant of 218.1 Hz between nuclei P_D and P_M is observed despite the long P–P distance (P1···P6 3.0176(7) Å) deduced from the solid-state structure. We reason this finding as a through space coupling as observed also in other polyphosphorus compounds.[29]
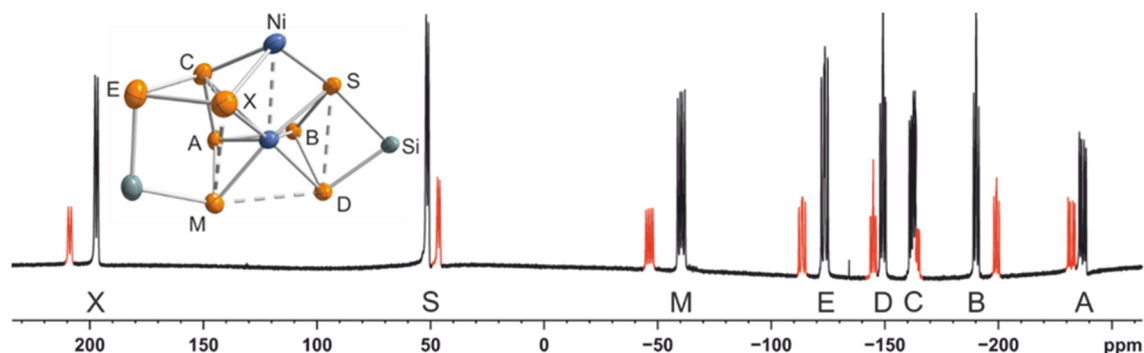
Figure 5. $^{31}P\{^1H\}$ NMR spectrum of cluster **3** in C_6D_6 at room temperature with nuclei assigned to the ABCDEMSX spin system; two isomers are present in solution (signals color-coded in black and red, assigned based on integration); Chemical shifts for isomer A: δ / ppm = −237.1 (P_A), −190.3 (P_B), −162.2 (P_C), −149.2 (P_D), −123.5 (P_E), −60.5 (P_M), 51.3 (P_S), 191.1(P_X); Isomer B: δ / ppm −232.2 (P_A), −199.3 (P_B), −164.8 (P_C), −145.0 (P_D), −113.7 (P_E), −46.5 (P_M), 46.4 (P_S), 208.8 (P_X); DFT-calculated and simulated coupling constants are presented in the SI (see Table S1, SI); Insets: representation of the core of the cluster; thermal ellipsoids are drawn at the 40% probability level.

4.3 Conclusion

In summary, we have shown that the (NHC)Ni synthon [(NHC)Ni(η^2-vtms)$_2$] (NHC = IPr, IMes, vtms = Me$_3$SiCH=CH$_2$) effects an unusual dimerisation of [LSi(η^2-P$_4$)] to form an uncommon Ni$_2$P$_8$Si$_2$ cluster **3**. Additionally, the classical (NHC)Ni complexes **1a,b** and **2** have been isolated alongside. Such Ni complexes show great potential as starting materials for the synthesis of ternary phosphorus clusters such as compound **3** as they are well-defined and conveniently prepared. Derivatization reactions of the cluster core **3** through the substitution of the diketiminate ligands L may further enhance the diversity of this class of cluster molecules. An extension of the synthetic methodology reported here and the use of **3** and related clusters as single source precursors for phosphorus-based materials will be of significant future interest.

4.4 Notes and References

[1] V. Jourdain, E. T. Simpson, M. Paillet, T. Kasama, R. E. Dunin-Borkowski, P. Poncharal, A. Zahab, A. Loiseau, J. Robertson and P. Bernier, *J. Phys. Chem. B* **2006**, *110*, 9759.

[2] (a) H. Li, G. Li and Z. Liu, *ACS Omega* **2019**, *4*, 2075; (b) A. Parra-Puerto, K. L. Ng, K. Fahy, A. E. Goode, M. P. Ryan and A. Kucernak, *ACS Catal.* **2019**, *9*, 11515; (c) Z. Sun, M. Zhu, M. Fujitsuka, A. Wang, C. Shi and T. Majima, *ACS Appl. Mater. Interfaces* **2017**, *9*, 30583; (d) Y. Shi and B. Zhang, *Chem. Soc. Rev.* **2016**, *45*, 1529.

[3] G. Zhang, G. Wang, Y. Liu, H. Liu, J. Qu and J. Li, *J. Am. Chem. Soc.* **2016**, *138*, 14686.

[4] (a) S. T. Oyama, T. Gott, H. Zhao and Y.-K. Lee, *Catal. Today* **2009**, *143*, 94; (b) I. I. Abu and K. J. Smith, *Appl. Catal., A* **2007**, *328*, 58; (c) S. Yang, C. Liang and R. Prins, *J. Catal.* **2006**, *237*, 118; (d) Y. Shu and S. T. Oyama, *Chem. Commun.*, **2005**, 1143; (e) S.T. Oyama, *J. Catal.* **2003**, *216*, 343; (f) R. Prins, G. Pirngruber and T. Weber, *Chimia* **2001**, *55*, 791.

[5] S. L. Brock, S. C. Perera and K. L. Stamm *Chem. Eur. J.* **2004**, *10*, 3364.

[6] (a) Z. Jin, P. Li, X. Huang, G. Zeng, Y. Jin, B. Zheng, D. Xiao, *J. Mater. Chem. A* **2014**, *2*, 18593; (b) Y. Li, X. Jiang, Z. Miao, J. Tang, Q. Zheng, F. Xie, D. Lin, *ChemCatChem* **2019**, *12*, 917; (c) H.-W. Man, C.-S. Tsang, M. Meng-Jung Li, J. Mo, B. Huang, L. Yoon Suk Lee, Y.-C. Leung, K.-Y. Wong, S. Chi Edman Tsang, *Appl. Catal. B Environ.* **2019**, *242*, 186; (d) S. Anantharaj, S. Rao Ede, K. Sakthikumar, K. Karthick, S. Mishra, S. Kundu *ACS Catal.* **2016**, 6, 12, 8069.

[7] J. Chang, K. Li, Z. Wu, J. Ge, C. Liu, W. Xing, *ACS appl. mater. inter.* **2018**, *10*, 26303.

[8] M. Shatruk in *Fundamentals and applications of phosphorus nanomaterials*, *Vol. 6*, (ed. H.-F. Ji), American Chemical Society, Washington, DC **2019**, S. 103–134.

[9] (a) K. L. Stamm, J. C. Garno, G.-y. Liu and S. L. Brock, *J. Am. Chem. Soc.* **2003**, *125*, 4038; (b) S. C. Perera, G. Tsoi, L. E. Wenger and S. L. Brock, *J. Am. Chem. Soc.* **2003**, *125*, 13960.

[10] S. Carenco, I. Resa, X. Le Goff, P. Le Floch and N. Mézailles, *Chem. Commun.* **2008**, 2568.

[11] (a) A. E. Henkes, Y. Vasquez and R. E. Schaak, *J. Am. Chem. Soc.* **2007**, *129*, 1896, (b) R.-K. Chiang and R.-T. Chiang, *Inorg. Chem.* **2007**, *46*, 369.

[12] (a) T. Grell, D. M. Yufanyi, A. K. Adhikari, M.-B. Sárosi, P. Lönnecke and E. Hey-Hawkins, *Pure Appl. Chem.* **2019**, *91*, 103; (b) A. Kırcalı Akdag, P. Lönnecke and E. Hey-Hawkins, *Z. Anorg. Allg. Chem.* **2014**, *640*, 271.

[13] P. Dapporto, S. Midollini and L. Sacconi, *Angew. Chem., Int. Ed. Engl.* **1979**, *18*, 469; *Angew. Chem.* **1979**, *91, 510.*

[14] Selected examples of P₄ activation using Ni^II sources: (a) M. Di Vaira, S. Midollini and L. Sacconi, *J. Am. Chem. Soc.* **1979**, *101*, 1757; (b) M. Di Vaira, C. A. Ghilardi, S. Midollini and L. Sacconi, *J. Am. Chem. Soc.* **1978**, 100, 2550.

[15] Selected examples of P$_4$ activation using Ni^I sources: (a) S. Pelties, D. Herrmann, B. d. Bruin, F. Hartl and R. Wolf, *Chem. Commun.* **2014**, *50*, 7014; (b) S. Yao, Y. Xiong, C. Milsmann, E. Bill, S. Pfirrmann, C. Limberg and M. Driess, *Chem. Eur. J.* **2010**, *16*, 436; (c) O. J. Scherer, J. Braun, P. Walther and G. Wolmershäuser, *Chem. Ber.* **1992**, *125*, 2661; (d) O. J. Scherer, J. Braun and G. Wolmershäuser, *Chem. Ber.* **1990**, *123*, 471; (e) O. J. Scherer, T. Dave, J. Braun and G. Wolmershäuser, *J. Organomet. Chem.* **1988**, *350*, C20.

[16] B. Zarzycki, T. Zell, D. Schmidt and U. Radius, *Eur. J. Inorg. Chem.* **2013**, *2013*, 2051.

[17] G. Hierlmeier, P. Coburger, N. P. van Leest, B. de Bruin and R. Wolf, *Angew. Chem. Int. Ed.* **2020***, 59*, 14148*; Angew. Chem.* **2020***, 132*, 14252.

[18] Y. Xiong, S. Yao, E. Bill and M. Driess, *Inorg. Chem.* **2009**, *48*, 7522.

[19] Y. Xiong, S. Yao, M. Brym and M. Driess, *Angew. Chem. Int. Ed.* **2007**, *46*, 4511; *Angew. Chem.* **2007***,119*, 4595.

[20] (a) M. R. Elsby, J. Liu, S. Zhu, L. Hu, G. Huang and S. A. Johnson, *Organometallics* **2019**, *38*, 436; (b) M. R. Elsby and S. A. Johnson, *J. Am. Chem. Soc.* **2017**, *139*, 9401.

[21] G. Prabusankar, A. Doddi, C. Gemel, M. Winter and R. A. Fischer, *Inorg. Chem.* **2010**, *49*, 7976.

[22] J. W. Dube, C. M. E. Graham, C. L. B. Macdonald, Z. D. Brown, P. P. Power and P. J. Ragogna, *Chem. Eur. J.* **2014**, *20*, 6739.

[23] O. J. Scherer, M. Swarowsky, H. Swarowsky and G. Wolmershäuser, *Angew. Chem. Int. Ed. Engl.* **1988**, *27*, 694; *Angew. Chem.* **1988**, *100*, 738.

[24] B. Cordero, V. Gómez, A. E. Platero-Prats, M. Revés, J. Echeverría, E. Cremades, F. Barragán, S. Alvarez, *Dalton Trans.* **2008**, 2832.

[25] R. H. Duncan Lyngdoh, H. F. Schaefer, R. B. King, *Chem. Rev.* **2018**, *118*, 11626.

[26] (a) A. Kempter, C. Gemel, T. Cadenbach and R. A. Fischer, *Organometallics* **2007**, *26*, 4257; (b) O. Serrano, E. Hoppe, J. C. Fettinger and P. P. Power, *J. Organomet. Chem.* **2011**, *696*, 2217; (c) A. Seifert and G. Linti, *Inorg. Chem.* **2008**, *47*, 11398.

[27] D. L. DeLaet, P. E. Fanwick and C. P. Kubiak, *Organometallics* **1986**, *5*, 1807.

[28] G. Knizia, *J. Chem. Theory Comput.* **2013**, *9*, 4834.

[29] For representative examples, see: (a) C. Taube, K. Schwedtmann, M. Noikham, E. Somsook, F. Hennersdorf, R. Wolf and J. J. Weigand, *Angew. Chem. Int. Ed.* **2020**, *59*, 3585; *Angew. Chem.* **2020**, *132*, 3613. (b) P. Coburger, P. Bielytskyi, D. Williamson, E. Rys, A. Kreienbrink, P. Lönnecke, J. Matysik and E. Hey-Hawkins, *Chem. Eur. J.* **2019**, *25*, 11456; (c) H. C. E. McFarlane and W. McFarlane, *Polyhedron* **1999**, *18*, 2117; (d) H. C. E. McFarlane and W. McFarlane, *Polyhedron* **1988**, *7*, 1875.

4.5 Supporting Information (SI)

4.5.1 General Procedures

All manipulations were performed under an atmosphere of dry argon using standard Schlenk techniques or a MBraun UniLab glovebox. Solvents were dried and degassed with a MBraun SPS800 solvent-purification system. THF, diethyl ether, and toluene were stored over molecular sieves (3 Å). *n*-Hexane was stored over a potassium mirror. Deuterated solvents (C_6D_6, tol-d_8, THF-d_8) were stirred over potassium, distilled, degassed, and stored over molecular sieves (3 Å). The starting materials [(IPr)Ni(η^2-$H_2C=CHSiMe_3$)$_2$] (IPr = 1,3-bis(2,6-diisopropylphenyl)imidazolin-2-ylidene), [IMes)Ni(η^2-$H_2C=CHSiMe_3$)$_2$] (1,3-bis(2,4,6-trimethylphenyl)imidazolin-2-ylidene), LSi and [LSi(η^2-P_4)] were prepared according to previously reported procedures.[1],[2],[3],[4] The synthesis of [LSi(η^2-P_4)] (L = CH[C(Me)N(Dipp)][C(CH₂)N(Dipp), Dipp = 2,6-*i*Pr₂C₆H₃) published by Driess and co-workers was slightly modified as described below.

NMR Spectroscopy: NMR spectra were measured on a Bruker AVANCE III HD Nanobay (^1H (400.13 MHz), ^{13}C (100.61 MHz), ^{19}F (376.50 MHz), ^{29}Si (79.50 MHz), ^{31}P (161.98 MHz)) 400 MHz UltraShield or on a Bruker AVANCE III HDX, 500 MHz Ascend (^1H (500.13 MHz), ^{13}C (125.75 MHz), ^{19}F (470.59 MHz), ^{29}Si (99.36 MHz), ^{31}P (202.45 MHz)). All ^{13}C NMR spectra were exclusively recorded with composite pulse decoupling. Reported numbers assigning atoms in the ^{13}C spectra were indirectly deduced from the cross-peaks in 2D correlation experiments (HMBC, HSQC). Chemical shifts were referenced to δ_{TMS} = 0.00 ppm (^1H, ^{13}C), δ_{CFCl3} = 0.00 ppm (^{19}F), δ_{TMS} = 0.00 ppm (^{29}Si) and $\delta_{H3PO4(85\%)}$ = 0.00 ppm (^{31}P). Chemical shifts (δ) are reported in ppm. Coupling constants (J) are reported in Hz.

For compounds, which give rise to a higher order spin system in the $^{31}P\{^1H\}$ NMR spectrum, the resolution enhanced $^{31}P\{^1H\}$ NMR spectrum was transferred to the software gNMR, version 5.0, by Cherwell Scientific.[5] The full line shape iteration procedure of gNMR was applied to obtain the best match of the fitted to the experimental spectrum. $^1J(^{31}P^{31}P)$ coupling constants were set to negative values and all other signs of the coupling constants were obtained accordingly.

In a glovebox, 20 mg of the respective compound were dissolved in 0.4 mL of deuterated solvent (tol-d_8 or THF-d_8). The solution was transferred into a *J. Young* valve NMR tube. ^1H and ^{31}P NMR measurements were performed in a temperature range from 240 K to 360 K. Throughout the measurement the NMR tube was kept spinning at 20 Hz to obtain a homogeneous solution.

Elemental analysis: Elemental analyses were determined by the analytical department of the University of Regensburg with a Micro Vario Cube (Elementar).

4.5.2 Modified Procedure for the Synthesis of [LSi(η²-P₄)]
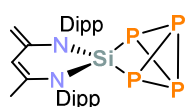
The synthesis of LSi and [LSi(η²-P₄)] was performed according to a published procedure of Driess and co-workers.[3],[4] However, the synthesis of [LSi(η²-P₄)] was modified in order to prevent the formation of significant amounts of [{LSi}₂(μ-η²:²-P₄)]. Silylene LSi (6.29 g, 14.1 mmol, 1.0 equiv.) was dissolved in toluene (75 mL). This solution was added dropwise via a dropping funnel to a clear solution of white phosphorus (1.75 g, 14.1 mmol, 1.0 equiv.) dissolved in toluene (30 mL) at 60 °C. The reaction mixture was additionally stirred for 18 h at 60 °C. ^{31}P{^{1}H} NMR monitoring subsequently showed the selective formation of [LSi(η²-P₄)]. Next, the solution was concentrated in *vacuo* to 25 mL. Crystals of [LSi(η²-P₄)] were obtained after storage at −30 °C over a period of 2 days.

Yield: 6.1 g (76%).

NMR spectroscopic data agree with those reported by Driess and co-workers.[4]

^{1}H NMR (400.13 MHz, 300 K, C₆D₆): δ / ppm = 1.21 (d, $^3J_{HH}$ = 6.7 Hz, 6 H, Dipp: CH*Me₂*), 1.37 (d, $^3J_{HH}$ = 6.7 Hz, 6 H, Dipp: CH*Me₂*), 1.46 (s, 3 H, L: NC*Me*), 1.51 (d, $^3J_{HH}$ = 6.8 Hz, 6 H, Dipp: CH*Me₂*), 1.54 (d, $^3J_{HH}$ = 6.8 Hz, 6 H, Dipp: CH*Me₂*), 3.32 (s, 1 H, L: NCC*H₂*), 3.61 (sept, $^3J_{HH}$ = 6.8 Hz, 2 H, Dipp-IPr: C*H*Me₂), 3.70 (sept, $^3J_{HH}$ = 6.7 Hz, 2 H, Dipp-IPr: C*H*Me₂), 3.91 (s, 1 H, L: NCC*H₂*), 5.21 (s, 1 H, L: γ-C*H*), 6.98-7.36 (m, 6 H, Dipp: 2,6-*i*Pr₂C₆*H₃*).

^{31}P{^{1}H} NMR (161.98 MHz, 300 K, C₆D₆): δ / ppm = ABX₂ δ(P$_A$) = –348.0 (dt, ^1J(P$_A$,P$_X$) = –146.8 Hz, ^1J(P$_B$,P$_X$) = –188.0 Hz, 1P), δ(P$_B$) = –342.4(dt, ^1J(P$_B$,P$_X$) = –144.7 Hz, ^1J(P$_A$,P$_B$) = –188.0 Hz 1P), δ(P$_X$) = 131.9 (dd, ^1J(P$_X$,P$_A$) = 146.8 Hz, ^1J(P$_X$,P$_B$) = –144.7Hz, 2P) ^{29}Si satellites: ^1J(Px,Si) =31.5 Hz.
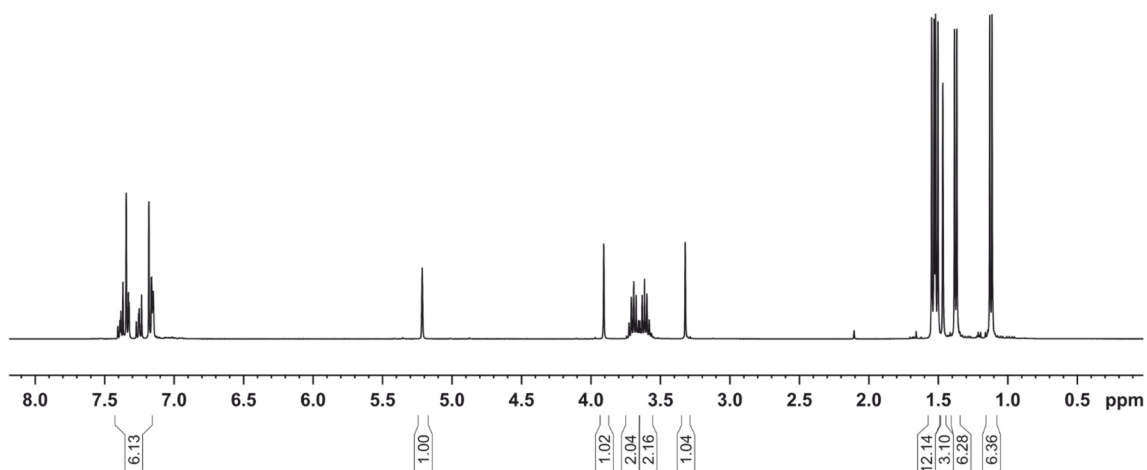

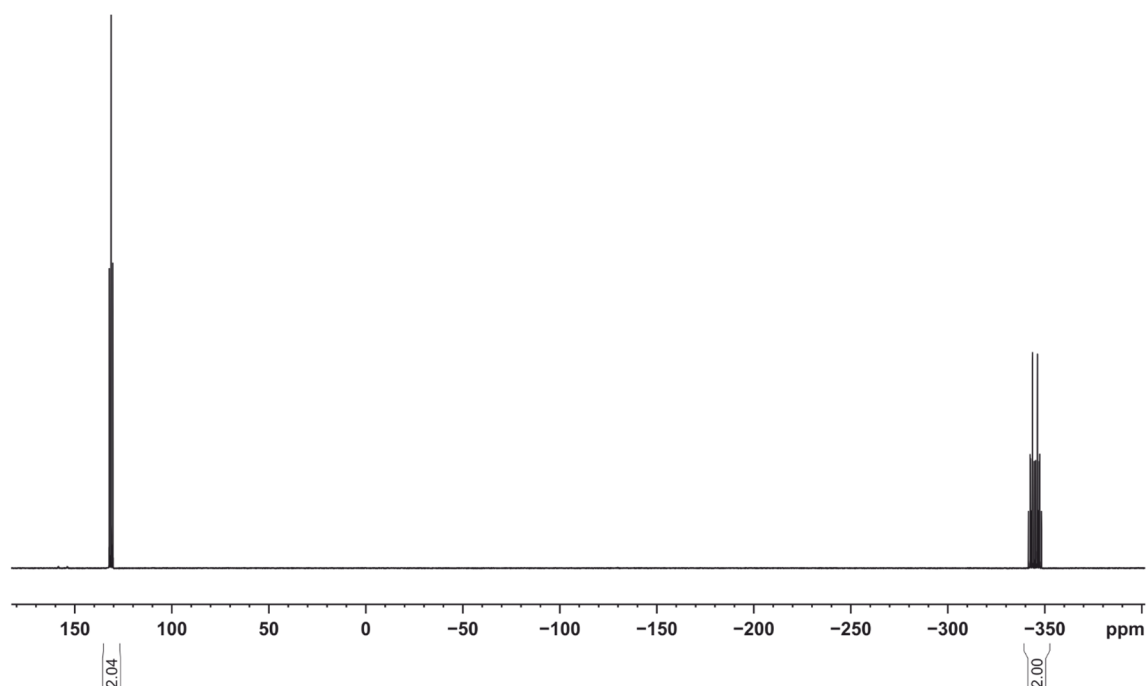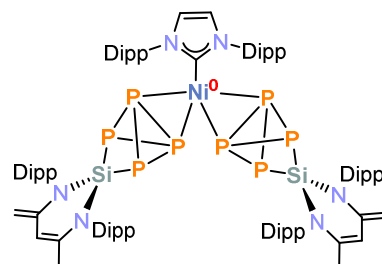**Figure S1.** ^{1}H NMR spectrum (400 MHz, 300 K, C₆D₆) of [LSi(η²-P₄)].

Figure S2. $^{31}P\{^1H\}$ NMR spectrum (161.98 MHz, 300 K, C_6D_6) of [LSi(η^2-P$_4$)].

4.5.3 Synthesis of [(IPr)Ni{(μ-η²:²-P₄)SiL}₂] (1a)

A yellow solution of [(IPr)Ni(η^2-H$_2$C=CHSiMe$_3$)$_2$] (286 mg, 0.44 mmol, 1.0 equiv.) in 10 mL toluene was added to a pale-yellow solution of [LSi(η^2-P$_4$)] (500 mg, 0.88 mmol, 2.0 equiv.) in 20 mL toluene at −50 °C. The reaction mixture was stirred for 18 h. Upon warming to room temperature, the color changed from yellow to burgundy. Volatiles were removed in *vacuo*, and the resulting violet solid was redissolved in toluene and filtered through a glass frit (pore size P4). The filtrate was concentrated in *vacuo* and stored at −30 °C. Storage for 2 days resulted in the precipitation of **1a** as a violet, microcrystalline powder. According to the ^1H NMR spectrum the isolated product contains 1.7 toluene solvate molecules per formula unit after drying in *vacuo* (10^{-3} mbar) at 60 °C for 3 hours. Crystals suitable for single-crystal X-ray diffraction analysis were obtained by slow diffusion of *n*-hexane into a concentrated toluene solution of **1a**.

Yield: 377 mg (50%).

^1H NMR (400.13 MHz, 300 K, C_6D_6): δ / ppm = 0.90 (d, $^3J_{HH}$ = 7 Hz, 12 H, Dipp: CH*Me₂*), 1.04 (d, $^3J_{HH}$ = 7 Hz, 12 H, Dipp-IPr: CH*Me₂*), 1.23 (d, $^3J_{HH}$ = 7 Hz, 12 H, Dipp: CH*Me₂*), 1.44 (s, 6 H, L: NC*Me*), 1.44 (d, $^3J_{HH}$ = 7 Hz, 12 H, Dipp: CH*Me₂*), 1.51 (d, $^3J_{HH}$ = 7 Hz, 12 H, Dipp: CH*Me₂*), 1.53 (d, $^3J_{HH}$ = 7 Hz, 12 H, Dipp: CH*Me₂*), 2.95 (sept, $^3J_{HH}$ = 7 Hz, 4 H, Dipp-IPr: C*H*Me₂), 3.25 (s, 2 H, L: NCC*H₂*), 3.67 (sept, $^3J_{HH}$ = 7 Hz, 8 H, Dipp: C*H*Me₂), 3.89 (s, 2 H, L: NCC*H₂*), 5.17 (s, 2 H, L: γ-C*H*), 6.43 (s, 2 H, IPr: *H*C=C*H*), 6.82 (s, 4 H, IPr: Ar-*H*), 7.22-7.47 (m, 12 H, Dipp: 2,6-*i*Pr₂C₆*H₃*).

$^{13}C\{^1H\}$ NMR (125.75 MHz, 300 K, C_6D_6): δ / ppm = 21.9 (L: NC*Me*), 24.10 (Dipp: CH*Me₂*), 28.8 (Dipp: CH*Me₂*), 25.3 (Dipp: CH*Me₂*), 25.4 (Dipp: CH*Me₂*), 25.8 (Dipp: CH*Me₂*), 27.3 (Dipp: CH*Me₂*), 28.0 (Dipp: *C*HMe₂), 28.8 (Dipp: *C*HMe₂), 29.2 (Dipp: *C*HMe₂), 86.6 (L: NC*C*H₂), 103.4 (L: γ-*C*H), 122.9 (IPr: H*C*=*C*H), 123.9 (Dipp, *C*H), 124.6 (Dipp, *C*H), 124.7 (Dipp, *C*H),

125.3 (Dipp, *C*H), 128.2 (Dipp, *C*H), 129.0 (Dipp, *C*H), 129.5 (Dipp, *C*H), 136.6 (Dipp), 137.2 (Dipp), 137.5 (Dipp), 140.2 (L: N*C*Me), 145.4 (Dipp), 147.8 (L: NC*C*H₂), 148.0 (Dipp), 148.4 (Dipp). The signal of the quaternary carbon atom of the IPr ligand could not be detected in the ^{13}C{^{1}H} NMR spectrum.

^{31}P{^{1}H} NMR (161.98 MHz, 300 K, C₆D₆): δ / ppm = –234.3 (br, 4 P), 190.6 (br, 4 P).

^{29}Si NMR (99.36 MHz, 300 K, C₆D₆): δ / ppm = –50.5 (br).

Elemental analysis calcd. for $C_{85}H_{116}N_6NiP_8Si_2 \cdot 1.7\ C_7H_8$ (Mw = 1741.20 g·mol^{-1}): C 66.84, H 7.50, N 4.83; found C 67.20, H 7.46, N 4.80.
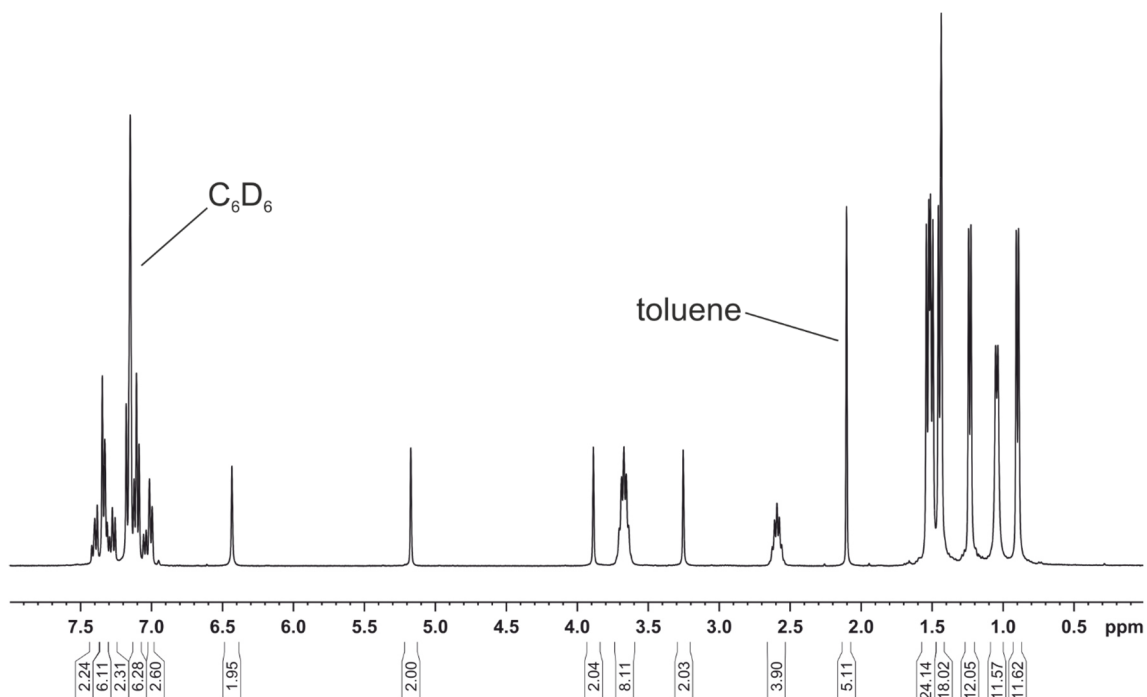

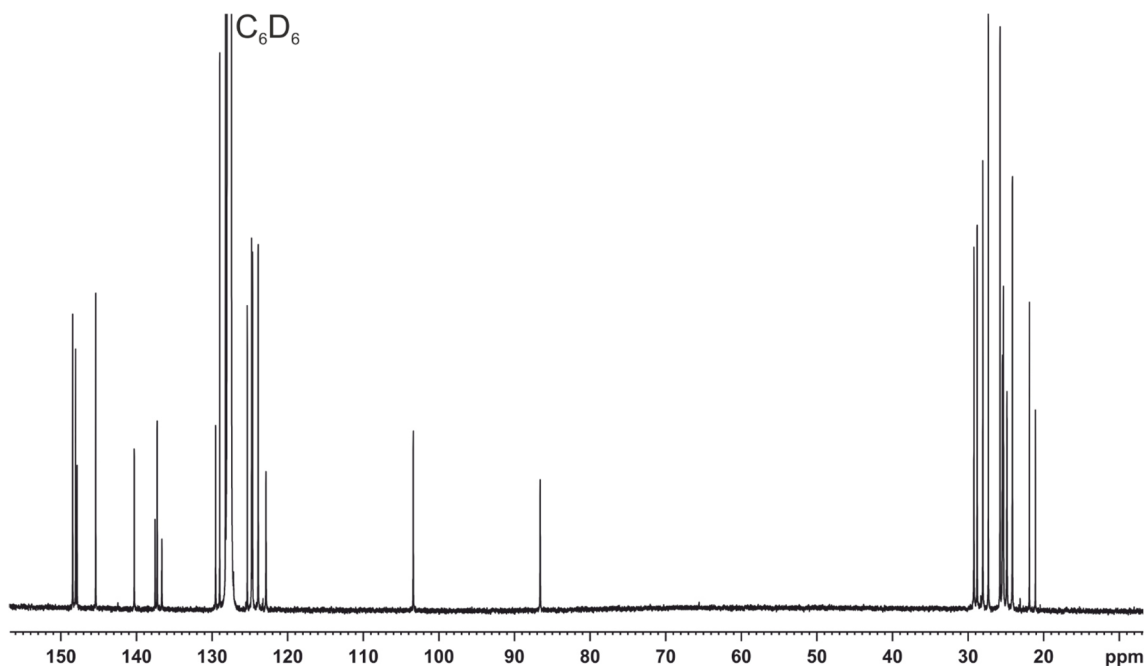**Figure S3.** ^{1}H NMR spectrum (400 MHz, 300 K, C₆D₆) of [(IPr)Ni{(μ-η$^{2:2}$-P₄)SiL}₂] (**1a**).

Figure S4. ^{13}C{^{1}H} NMR spectrum (125.75 MHz, 300 K, C₆D₆) of [(IPr)Ni{(μ-η$^{2:2}$-P₄)SiL}₂] (**1a**).
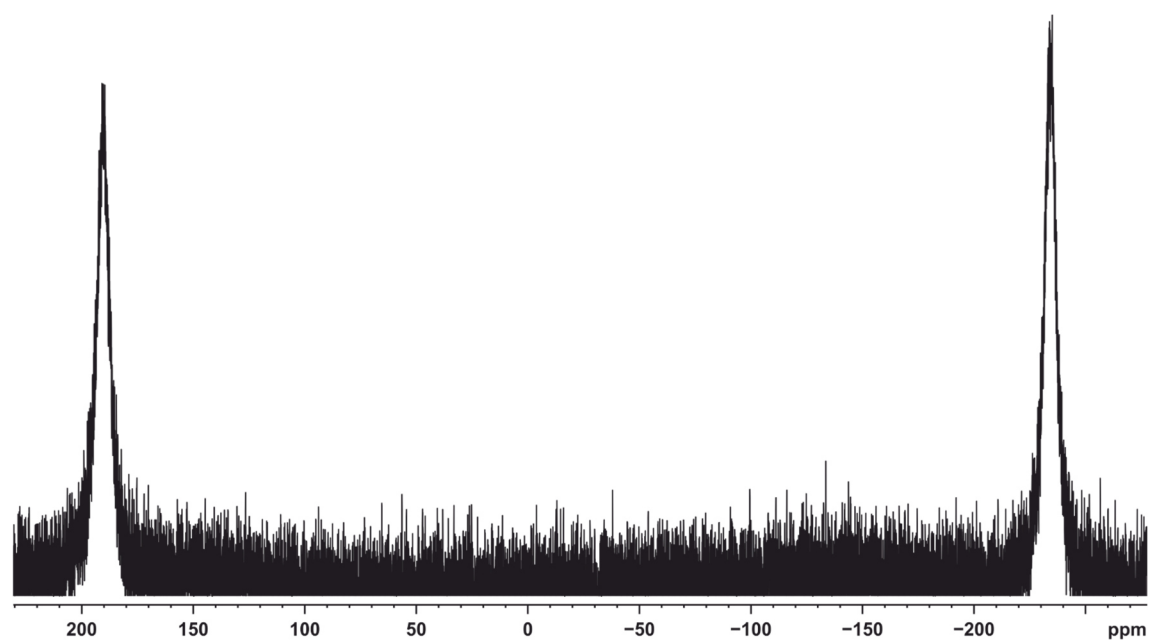
Figure S5. ^{31}P{^{1}H} NMR spectrum (161.98 MHz, 300 K, C$_6$D$_6$) of [(IPr)Ni{(μ-η$^{2:2}$-P$_4$)SiL}$_2$] (**1a**).
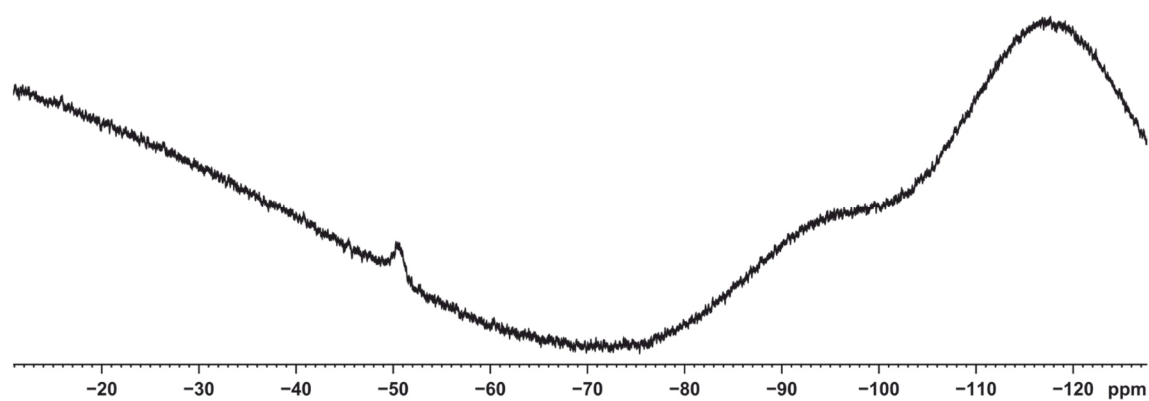
Figure S6. ^{29}Si NMR spectrum (99.36 MHz, 300 K, C$_6$D$_6$) of [(IPr)Ni{(μ-η$^{2:2}$-P$_4$)SiL}$_2$] (**1a**).

Figure S7. VT ^{31}P{^{1}H} NMR spectra of [(IPr)Ni{(μ-η$^{2:2}$-P$_4$)SiL}$_2$] (**1a**) in tol-d_8. The sample used for the VT ^{31}P{^{1}H} NMR experiments shows a minor impurity which resonates at –153.0 ppm. Upon heating to 350 K complex **1a** thermolyses to form cluster compound **3**.
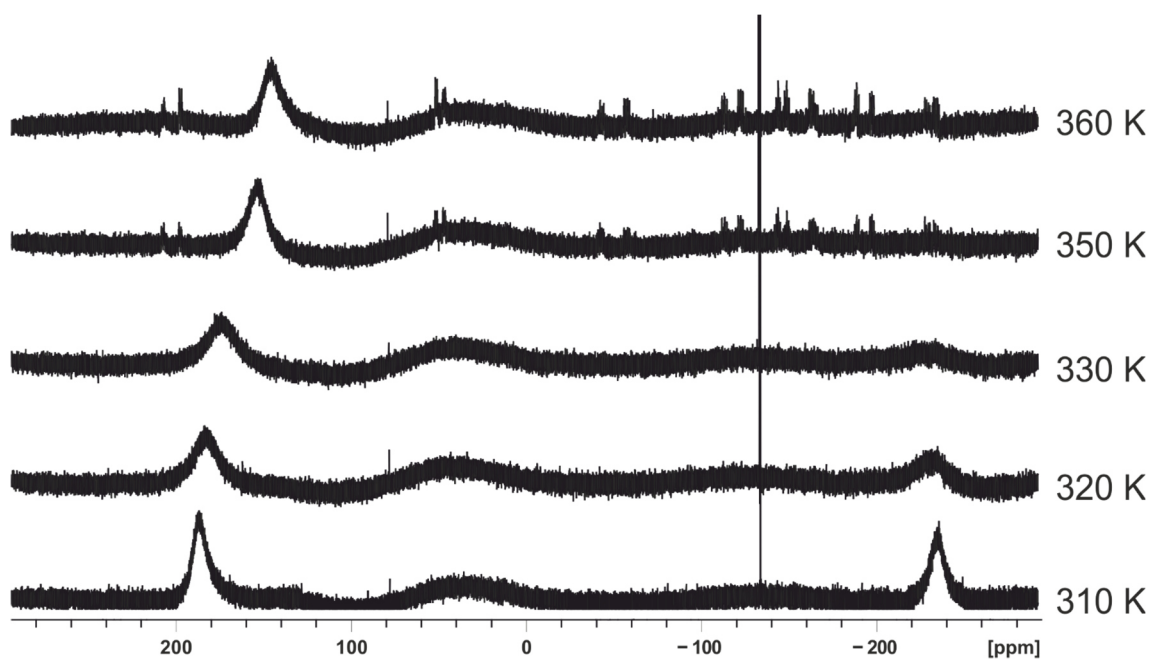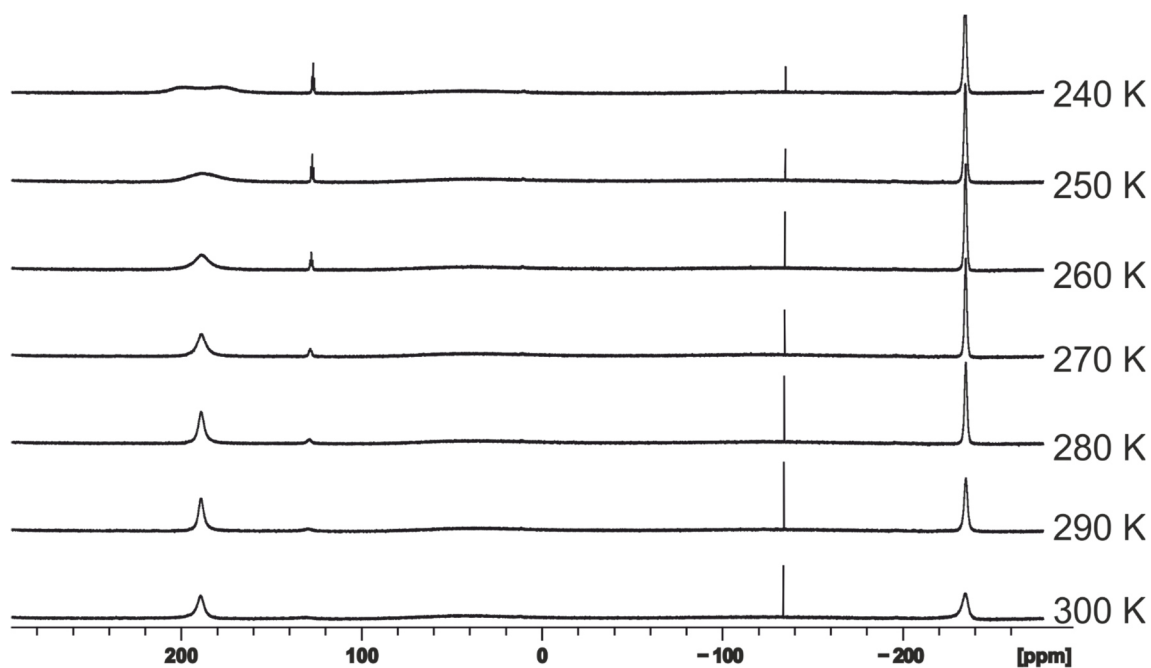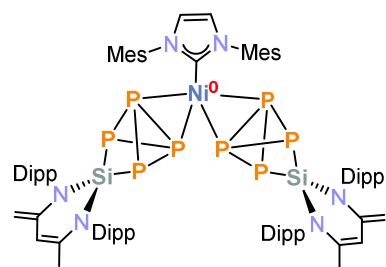

Figure S8. VT ^{31}P{^{1}H} NMR spectra of [(IPr)Ni{(μ-η$^{2:2}$-P$_4$)SiL}$_2$] (**1a**) in tol-d_8. The sample used for the VT ^{31}P{^{1}H} NMR experiments shows some minor impurities which resonate at –153.0 ppm as well as small amounts of [LSi(η^2-P$_4$)].

119

4.5.4   Synthesis of [(IMes)Ni{(μ-η$^{2:2}$-P$_4$)SiL}$_2$] (1b)

A yellow solution of [(IMes)Ni(η^2-H$_2$C=CHSiMe$_3$)$_2$] (0.91 g, 1.60 mmol, 1.0 equiv.) in 20 mL toluene was added to a pale-yellow solution of [LSi(η^2-P$_4$)] (1.81 g, 3.20 mmol, 2.0 equiv.) in 30 mL toluene at −50 °C. The reaction mixture was stirred for 18 h. Upon warming to room temperature, the color changed from yellow to burgundy red. Volatiles were removed in *vacuo*, and the resulting violet solid was redissolved in toluene and filtered through a glass frit (pore size P4). The filtrate was concentrated in *vacuo* and stored at −30 °C. After 2 days, a violet microcrystalline precipitate of **1b** had formed. According to the ^{1}H NMR spectrum, the isolated product contains 0.21 toluene solvate molecules per formula unit after drying in *vacuo* (10^{-3} mbar) over 5 hours. Crystals suitable for single-crystal X-ray diffraction analysis were obtained by slow evaporation of a concentrated solution of **1b** dissolved in *n*-hexane.

Yield: 620 mg (26%).

^{1}H NMR (400.13 MHz, 300 K, C$_6$D$_6$): δ / ppm = 1.19 (d, $^3J_{HH}$ = 7 Hz, 12 H, Dipp: CH*Me₂*), 1.44 (d, $^3J_{HH}$ = 7 Hz, 12 H, Dipp: CH*Me₂*), 1.48 (s, 6 H, L: NC*Me*), 1.52 (d, $^3J_{HH}$ = 7 Hz, 24 H, Dipp: CH*Me₂*), 1.75 (s, 12 H, IMes: *o*-Ar-*Me*), 2.43 (s, 6 H, IMes: *p*-Ar-*Me*), 3.28 (s, 2 H, L: NCC*H₂*), 3.60 (sept, $^3J_{HH}$ = 7 Hz, 4 H, Dipp: C*H*Me₂), 3.66 (sept, $^3J_{HH}$ = 7 Hz, 4 H, Dipp: C*H*Me₂), 3.91 (s, 2 H, L: NCC*H₂*), 5.21 (s, 2 H, L: γ-C*H*), 6.12 (s, 2 H, IMes: *H*C=C*H*), 6.82 (s, 4 H, IMes: Ar-*H*), 7.22-7.47 (m, 12 H, Dipp: 2,6-*i*Pr$_2$C$_6$*H₃*).

^{13}C{^{1}H} NMR (100.61 MHz, 300 K, C$_6$D$_6$): δ / ppm = 19.1 (IMes: *o*-C$_6$H$_2$*Me₃*), 21.3 (IMes: *p*-C$_6$H$_2$*Me₃*), 22.1 (L: NC*Me*), 24.8 (Dipp: CH*Me₂*), 25.3 (Dipp: CH*Me₂*), 26.0 (Dipp: CH*Me₂*), 27.7 (Dipp: CH*Me₂*), 29.0 (Dipp: *C*HMe₂), 29.4 (Dipp: *C*HMe₂), 86.6 (L: NC*C*H₂), 103.2 (L: γ-*C*H), 121.5 (IMes: H*C*=*C*H), 124.6 (Ar: *C*H), 124.8 (Ar: *C*H), 129.2 (Ar: *C*H), 136.1 (Ar), 136.7 (Ar), 137.4 (Ar), 137.5 (Ar), 137.7 (Ar), 140.7 (L: N*C*Me), 148.3 (L: N*C*CH₂), 148.7 (Ar), 149.2 (Ar). The quaternary carbon atom of the IMes ligand could not be detected in the ^{13}C{^{1}H} NMR spectrum.

^{31}P{^{1}H} NMR (161.98 MHz, 300 K, C$_6$D$_6$): δ / ppm = −236.4 (m, 4 P), 194.2 (m, 4 P).

^{29}Si NMR (99.36 MHz, 300 K, THF-*d₈*): δ / ppm = −52.1 (broad pseudo-triplet).

Elemental analysis calcd. for C$_{79}$H$_{104}$N$_6$NiP$_8$Si$_2$ · 0.21 C$_7$H$_8$ (Mw = 1519.73 g·mol^{-1}): C 63.43, H 7.00, N 5.56; found C 63.60, H 7.01, N 5.53.
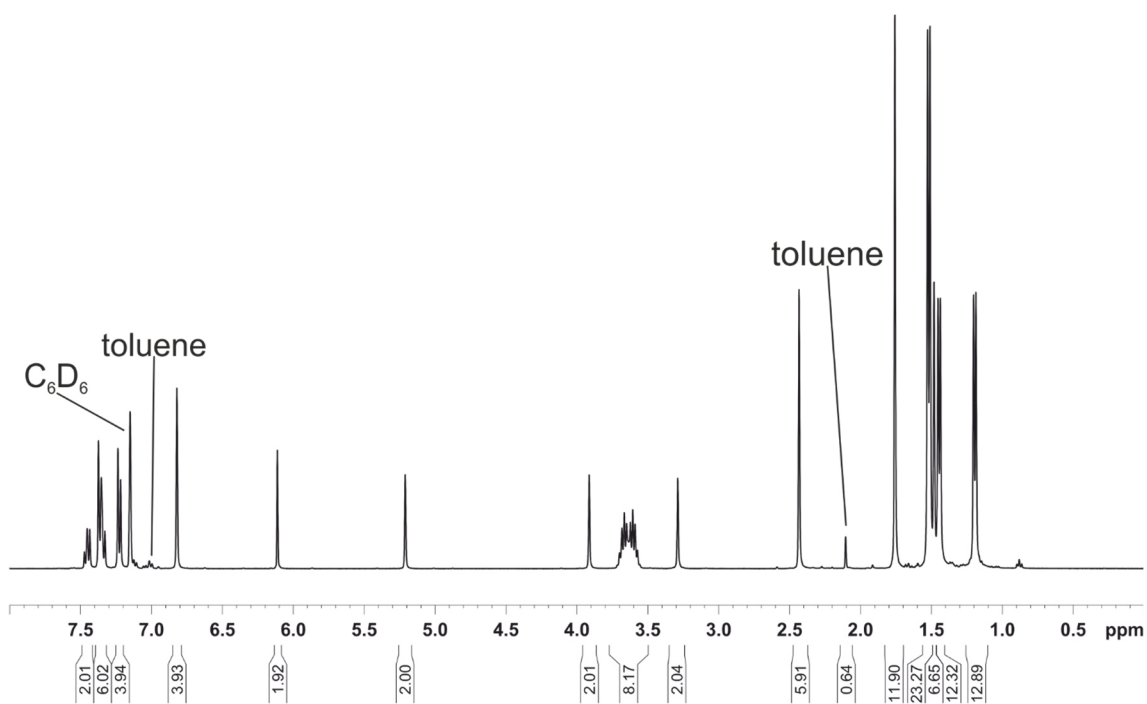
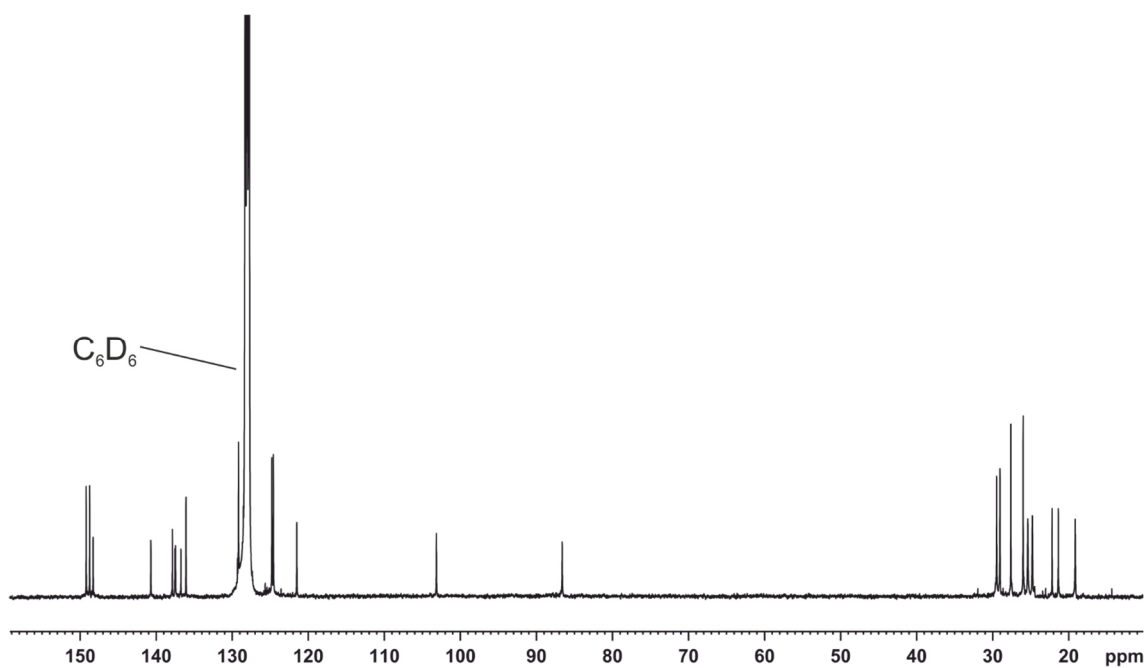**Figure S9.** ^{1}H NMR spectrum (400 MHz, 300 K, C_6D_6) of [(IMes)Ni{(μ-$\eta^{2:2}$-P$_4$)SiL}$_2$] (**1b**).

Figure S10. ^{13}C{^{1}H} NMR spectrum (100.61 MHz, 300 K, C_6D_6) of [(IMes)Ni{(μ-$\eta^{2:2}$-P$_4$)SiL}$_2$] (**1b**).

Figure S11. $^{31}P\{^1H\}$ NMR spectrum (161.98 MHz, 300 K, C_6D_6) of [(IMes)Ni$\{(\mu\text{-}\eta^{2:2}\text{-}P_4)SiL\}_2$] (**1b**).

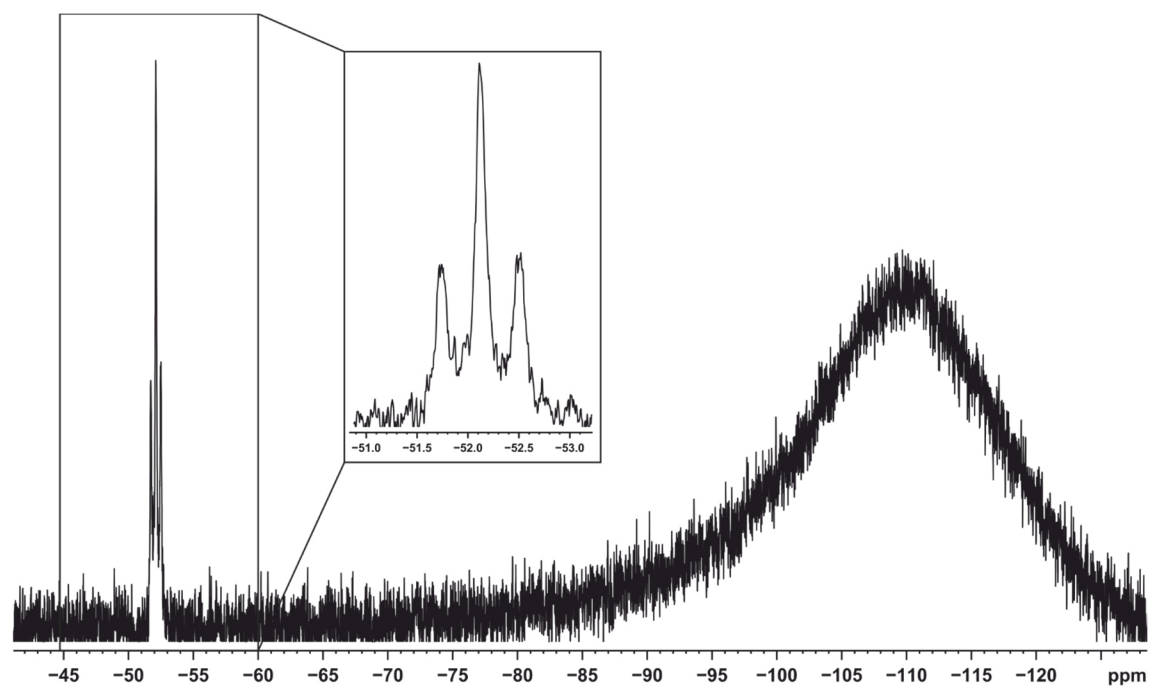**Figure S12.** ^{29}Si NMR spectrum (99.36 MHz, 300 K, THF-d_8) of [(IMes)Ni$\{(\mu\text{-}\eta^{2:2}\text{-}P_4)SiL\}_2$] (**1b**).

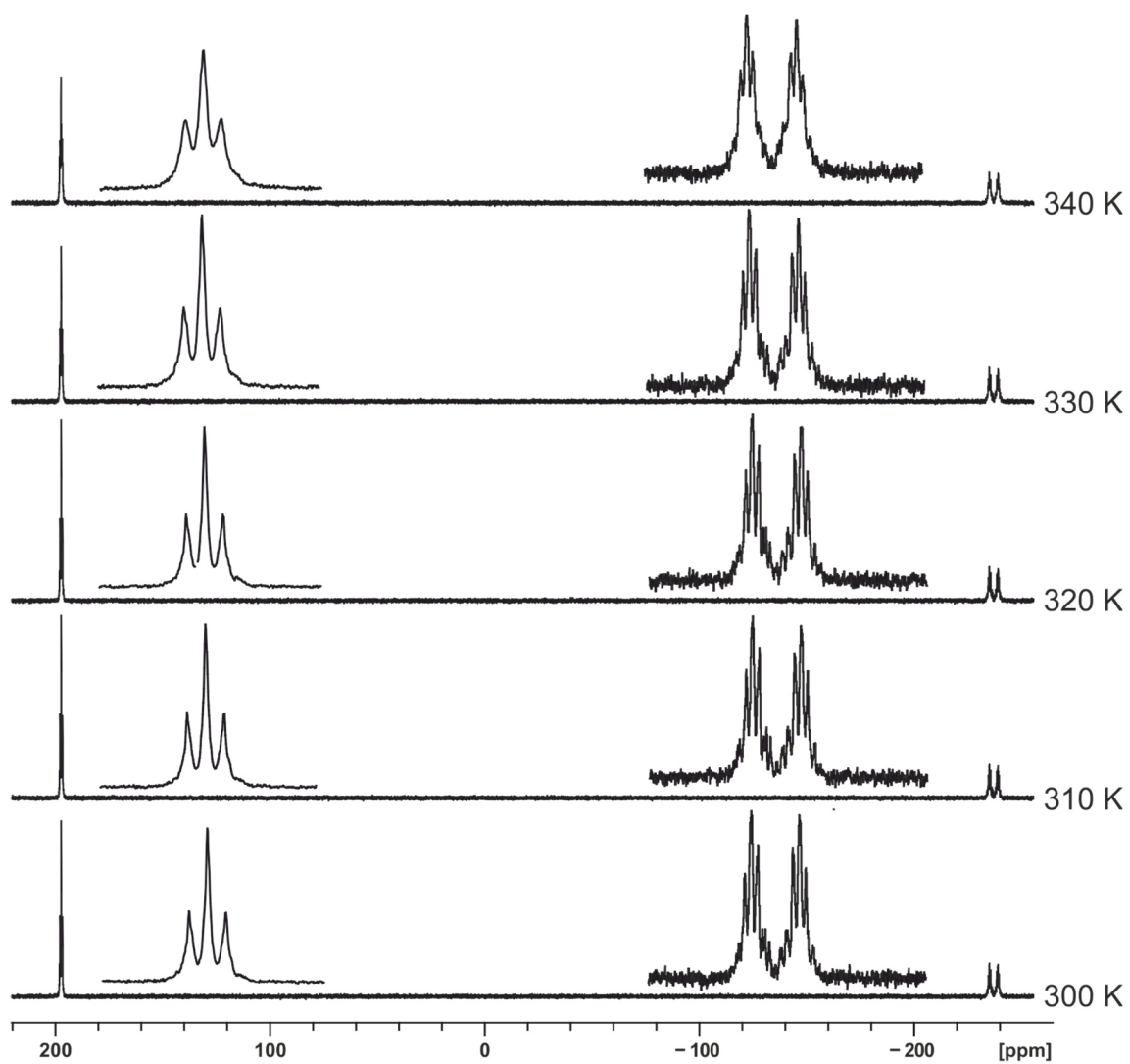**Figure S13.** VT $^{31}P\{^{1}H\}$ NMR spectra of [(IMes)Ni{(μ-η$^{2:2}$-P₄)SiL}₂] (**1b**) in tol-d_8.
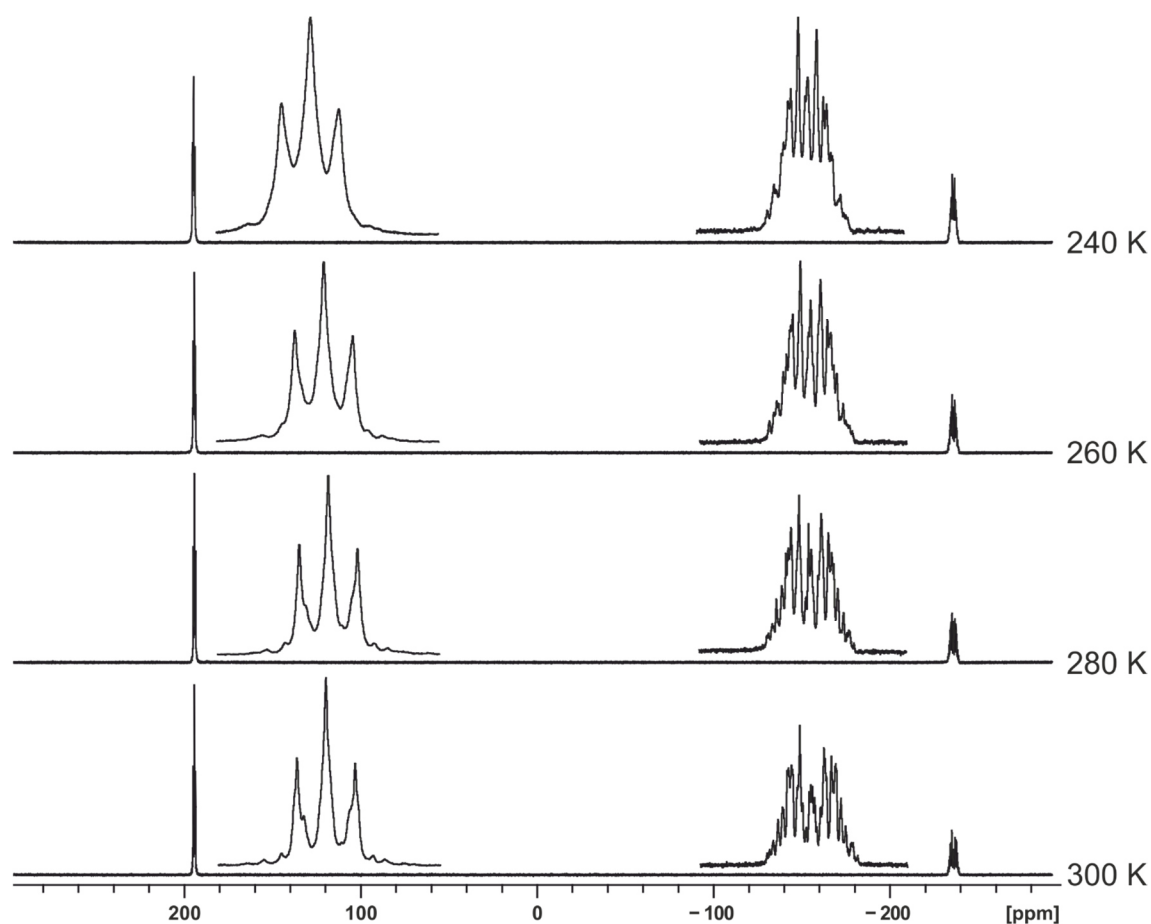
Figure S14. VT ^{31}P{^{1}H} NMR spectra of [(IMes)Ni{(μ-η$^{2:2}$-P$_4$)SiL}$_2$] (**1b**) in THF-d_8.

4.5.5 Synthesis of [(IPr)Ni(μ-η$^{2:2}$-P$_4$)SiL] (2)
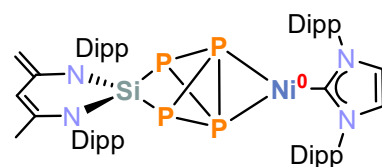
A pale-yellow solution of [LSi(η^2-P$_4$)] (432.6 mg, 0.77 mmol, 1.0 equiv.) in toluene (15 ml) was added dropwise to a yellow solution of [(IPr)Ni(η^2-H$_2$C=CHSiMe$_3$)$_2$] (500 mg, 0.77 mmol, 1.0 equiv.) in toluene (15 ml) at room temperature. The reaction mixture was stirred for 18 h at room temperature, whereupon the color changed to brown. Volatiles were removed in *vacuo* and the brown residue was extracted with *n*-hexane (60 mL) using a glass frit (pore size P4). The filtrate was concentrated to 25 mL. Storage at −30 °C for 2 days gave **2** as an analytically pure, microcrystalline powder. According to the ^{1}H NMR spectrum the isolated product contains 0.36 *n*-hexane solvate molecules per formula unit after drying in *vacuo* (10^{-3} mbar) over period of 3 hours. Crystals suitable for single-crystal X-ray diffraction analysis were obtained by slow evaporation of a concentrated solution of **2** dissolved in *n*-hexane.

N.B. Complex **2** is unstable in solution and converts slowly into compound **3** at room temperature.

Yield: 240 mg (30%).

^{1}H NMR (400.13 MHz, 300 K, C$_6$D$_6$): δ / ppm = 1.02 (d, $^3J_{HH}$ = 7 Hz, 12 H, Dipp: CH*Me$_2$*), 1.14 (d, $^3J_{HH}$ = 7 Hz, 6 H, Dipp: CH*Me$_2$*), 1.42 (d, $^3J_{HH}$ = 7 Hz, 18 H, Dipp: CH*Me$_2$*), 1.49 (m, 12 H, Dipp: CH*Me$_2$* and 3 H L: NC*Me*), 2.57 (sept, $^3J_{HH}$ = 7 Hz, 4 H, Dipp-IPr: C*H*Me$_2$), 3.25 (s, 1 H, L: NCC*H$_2$*), 3.73 (sept, $^3J_{HH}$ = 7 Hz, 2 H, Dipp: C*H*Me$_2$), 3.79 (sept, $^3J_{HH}$ = 7 Hz, 2 H, Dipp:

CHMe$_2$), 3.89 (s, 1 H, L: NCCH_2), 5.26 (s, 1 H, L: γ-CH), 6.16 (s, 2 H, IPr: HC=CH), 6.98-7.35 (m, 12 H, Dipp: 2,6-iPr$_2$C$_6$$H_3$).

^{13}C{^{1}H} NMR (100.61 MHz, 300 K, C$_6$D$_6$): δ / ppm = 21.8 (L: NCMe), 23.9 (Dipp: CHMe_2), 24.6 (Dipp: CHMe_2), 25.6 (Dipp: CHMe_2), 27.2 (Dipp: CHMe_2), 28.5 (IPr: CHMe$_2$), 28.6 (L: CHMe$_2$), 29.0 (L: CHMe$_2$), 85.6 (L: NCCH$_2$), 102.8 (L: γ-CH), 121.6 (IPr: HC=CH), 123.7 (Dipp, CH), 124.2 (Dipp, CH), 124.4 (Dipp, CH), 130.0 (Dipp, CH), 135.1 (Dipp), 137.3 (Dipp), 137.6 (Dipp), 140.3 (L: NCMe), 145.3 (Dipp), 148.1 (L: NCCH$_2$), 148.5 (Dipp). The quaternary carbon atom of the IPr ligand could not be detected in the ^{13}C{^{1}H} NMR spectrum.

^{31}P{^{1}H} NMR (161.98 MHz, 300 K, C$_6$D$_6$): ABX$_2$ spin system; δ / ppm ABX$_2$ δ(P$_A$) = −155.1 (dt, ^1J(P$_A$,P$_X$) = −114.2 Hz, ^1J(P$_A$,P$_B$) = −25.6 Hz), δ(P$_B$) = −138.0 (dt, ^1J(P$_B$,P$_X$) = −114.1 Hz, ^1J(P$_A$,P$_B$) = −25.6 Hz), δ(P$_X$) = 147.3 (dd, ^1J(P$_X$,P$_A$) = −114.2 Hz, ^1J(P$_X$,P$_B$) = −114.1 Hz).

^{29}Si NMR (99.36 MHz, 300 K, C$_6$D$_6$): δ / ppm = −37.1 (br).

Elemental analysis calcd. for C$_{56}$H$_{76}$N$_4$NiP$_4$Si · 0.36 C$_6$H$_{14}$ (Mw = 1046.95 g·mol^{-1}): C 66.72, H 7.80, N 5.35; found C 66.91, H 7.40, N 5.38.

Figure S15. ^{1}H NMR spectrum (400 MHz, 300 K, C$_6$D$_6$) of [(IPr)Ni(μ-η$^{2:2}$-P$_4$)SiL] (**2**).
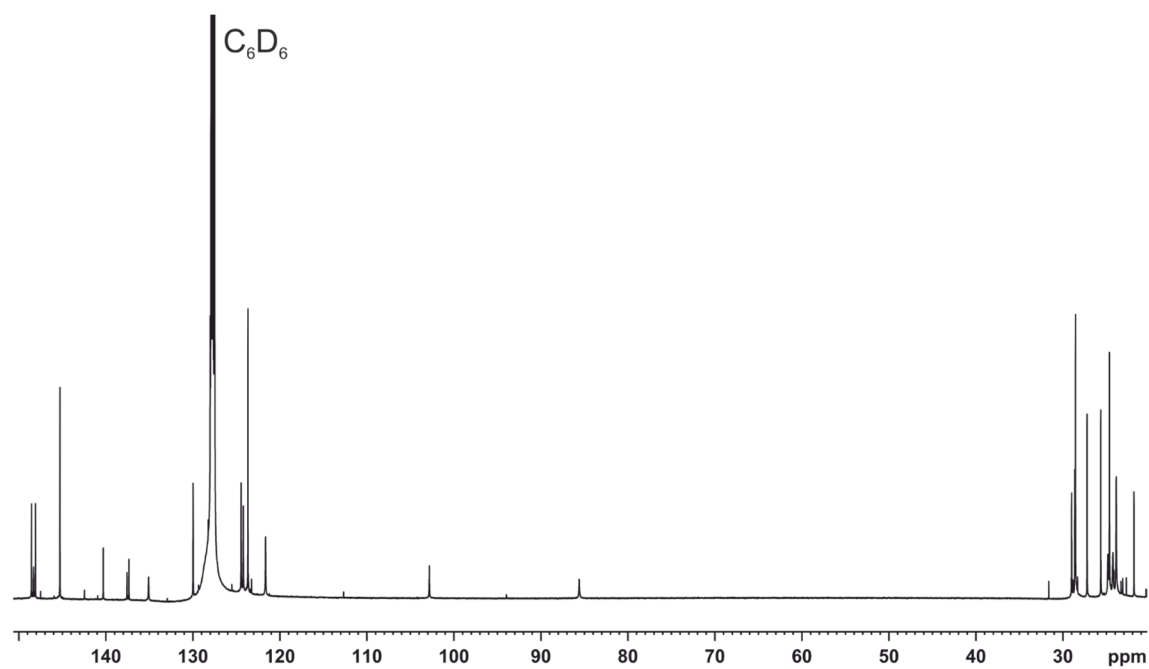
Figure S16. $^{13}C\{^1H\}$ NMR spectrum (125.75 MHz, 300 K, C₆D₆) of [(IPr)Ni(μ-η$^{2:2}$-P₄)SiL] (**2**).

Figure S17. $^{31}P\{^1H\}$ NMR spectrum (161.98 MHz, 300 K, C₆D₆) of [(IPr)Ni(μ-η$^{2:2}$-P₄)SiL] (**2**).

126

Figure S18. ^{29}Si NMR spectrum (99.36 MHz, 300 K, C_6D_6) of [(IPr)Ni(μ-$η^{2:2}$-P_4)SiL] (**2**).

4.5.6 Synthesis of [(IPr)Ni₂P₈(SiL)₂] (3)

A pale-yellow solution of [LSi($η^2$-P_4)] (217.2 mg, 0.38 mmol, 1.0 equiv.) in toluene (15 ml) was added dropwise to a yellow solution of [(IPr)Ni($η^2$-H_2C=CHSiMe₃)₂] (247.8 mg, 0.38 mmol, 1.0 equiv.) in toluene (15 ml) at room temperature. The reaction mixture was stirred for 18 h at 60 °C, whereupon the color changed to brown. Volatiles were removed in *vacuo* and the remaining brown solid was transferred to a sublimation apparatus. Free carbene IPr, was removed by vacuum sublimation (95 °C, 1·10⁻⁵ mbar). The residual solid was redissolved in toluene (60 mL) and filtered through a glass frit (pore size P4). The solution was concentrated to a volume of 15 mL. Layering the concentrated toluene solution with *n*-hexane gave brownish crystals of **3** after one week. Crystals suitable for single-crystal X-ray diffraction analysis were obtained by slow evaporation of a concentrated *n*-hexane solution of **3**.

Yield: 110 mg (35%).

N.B. Two isomers (labeled A and B) were detected in the NMR spectra and by single-crystal X-ray diffraction experiments. These isomers cannot be separated and are assigned *via* their respective integrations in the ^1H and $^{31}P\{^1H\}$ NMR spectra (major isomer: A, minor isomer: B).

^1H NMR (400.13 MHz, 300 K, C_6D_6): signals of isomers A and B partly overlap strongly; δ / ppm = 0.09 (m, Dipp: CH*Me₂*), 0.59 (d, Isomer B, Dipp: CH*Me₂*), 0.67 (d, Isomer B, Dipp: CH*Me₂*), 0.75 (d, Isomer A, Dipp: CH*Me₂*), 0.85–1.65 (m, Dipp: CH*Me₂* overlap with L: NC*Me*), 1.71 (d, Isomer B, Dipp: CH*Me₂*), 1.75 (d, Isomer A, Dipp: CH*Me₂*), 1.86 (d, Isomer A, Dipp: CH*Me₂*); (integrals fit to the 78 expected hydrogen atoms); 1.97 (m, Dipp: C*H*Me₂), 2.34 (sept, Isomer B, Dipp: C*H*Me₂), 2.48 (sept, Isomer A, Dipp: C*H*Me₂), 2.62 (m, Isomer A, Dipp: C*H*Me₂), 2.67 (m, Isomer B, Dipp: C*H*Me₂), 2.74 (sept, Isomer A, Dipp: C*H*Me₂), 2.85 (sept, Isomer B, Dipp: C*H*Me₂), 3.23 (m, Dipp: C*H*Me₂), 3.60 (sept, Isomer B, Dipp: C*H*Me₂), 3.66–3.90 (m, Dipp: C*H*Me₂), 4.11 (sept, Isomer A, Dipp: C*H*Me₂); (integrals fit to the 12 expected hydrogen atoms of the Dipp: C*H*Me₂ groups); 3.33 (s, Isomers A,B, L: NCC*H₂*), 3.37 (s, Isomer A, L: NCC*H₂*), 3.39 (s, Isomer B, L: NCC*H₂*), 3.92 (s, Isomer B, L: NCC*H₂*), 3.97 (s, Isomer A, L: NCC*H₂*), 4.00 (s, Isomer B, L: NCC*H₂*), 4.03 (s, Isomer A, L: NCC*H₂*); (integrals fit to the 4 expected hydrogen atoms of the L: NCC*H₂* moiety); 5.35 (s, Isomer A, L: γ-C*H*), 5.39 (s, Isomer B, L: γ-C*H*), 5.42 (s, Isomer B, L: γ-C*H*); integrals fit to the 2 expected hydrogen atoms of the L: γ-C*H* moiety); 6.34 (m, IPr: *H*C=C*H*), 6.50 (m, IPr: *H*C=C*H*); (integrals fit to the 2 expected hydrogen atoms of

the IPr: H*C*=C*H* backbone); 6.84–7.37 (m, Dipp: 2,6-*i*Pr₂C₆*H₃*); (integrals fit to the 18 expected hydrogen atoms of the Dipp: 2,6-*i*Pr₂C₆*H₃* group).

^{13}C{^{1}H} NMR (100.61 MHz, 300 K, C₆D₆): δ / ppm = 21.6, 21.7, 22.2, 22.3, 22.5, 22.5, 23.1, 23.2, 23.6, 23.7, 23.8, 23.9, 23.9, 24.3, 24.3, 24.4, 24.6, 24.7, 25.1, 25.3, 25.4, 25.4, 25.5, 25.7, 25.9, 26.0, 26.2, 26.4, 26.5, 26.6, 26.7, 26.9, 27.0, 27.1, 27.3, 27.4, 27.7, 27.8, 27.9, 28.0, 28.1, 28.1, 28.2, 28.3, 28.4, 28.7, 28.8, 28.9, 28.9, 29.0, 29.2, 29.4, 29.5 (Dipp: *C*HMe₂, Dipp: CH*Me₂*, and L: NC*Me*), 87.4, 90.6 (L: NC*C*H₂ Isomer B), 89.4, 90.6 (L: NC*C*H₂, Isomer A), 103.1, 109.4 (L: γ-*C*H, Isomer B), 106.4, 108.6 (L: γ-*C*H, Isomer A), 123.4, 123.7, 123.8, 123.9, 123.9, 124.1, 124.1, 124.2, 124.3, 124.5, 124.9, 125.0, 125.1, 128.2, 128.2, 128.3, 128.3, 129.0, 130.2, 130.3, 130.8 (Dipp, *C*H), 126.0 (IPr: H*C*=*C*H, Isomer B), 126.3 (IPr: H*C*=*C*H, Isomer A), 126.5 (IPr: H*C*=*C*H, Isomer B), 126.7 (IPr: H*C*=*C*H, Isomer B), 140.6 (L: N*C*Me, Isomer B), 140.7 (L: N*C*Me, Isomer A), 141.6 (L: N*C*Me Isomer A), 141.8 (L: N*C*Me, Isomer B), 147.6, 147.7, 148.3, 148.4 (L: N*C*CH₂), 135.9, 136.2, 136.6, 136.9, 137.0, 137.0, 137.3, 137.9, 137.9, 138.1, 138.3, 138.5, 145.1, 145.4, 145.4, 145.6, 146.7, 146.8, 147.0, 147.1, 147.2, 147.9, 148.6, 148.8, 148.9, 149.1, 149.2, 149.5, 149.5, 149.5 (Dipp), 187.4 (IPr: N*C*N, Isomer A), 187.8 (IPr: N*C*N, Isomer B).

^{31}P{^{1}H} NMR (161.98 MHz, 300 K, C₆D₆): ABCDEMSX spin system: Isomer A: –237.1 (m, P_A), –190.3 (m, P_B), –162.2 (m, P_C), –149.2 (m, P_D), –123.5 (m, P_E), –60.5 (m, P_M), 51.3 (m, P_S), 191.1 (m, P_X); Isomer B: –232.2 (m, P_A), –199.3 (m, P_B), –164.8 (m, P_C), –145.0 (m, P_D), –113.7 (m, P_E), –46.5 (m, P_M), 46.4 (m, P_S), 208.8 (m, P_X).

^{29}Si NMR (99.36 MHz, 300 K, C₆D₆): δ / ppm = –3.9 (br), 60.8 (br).

Elemental analysis calcd. for $C_{85}H_{116}N_6Ni_2P_8Si_2$ (Mw = 1643.25 g·mol^{-1}): C 62.13, H 7.12, N 5.11; found C 62.86, H 7.09, N 5.08. The deviation in the carbon content might be explained by small amounts of residual carbene IPr.
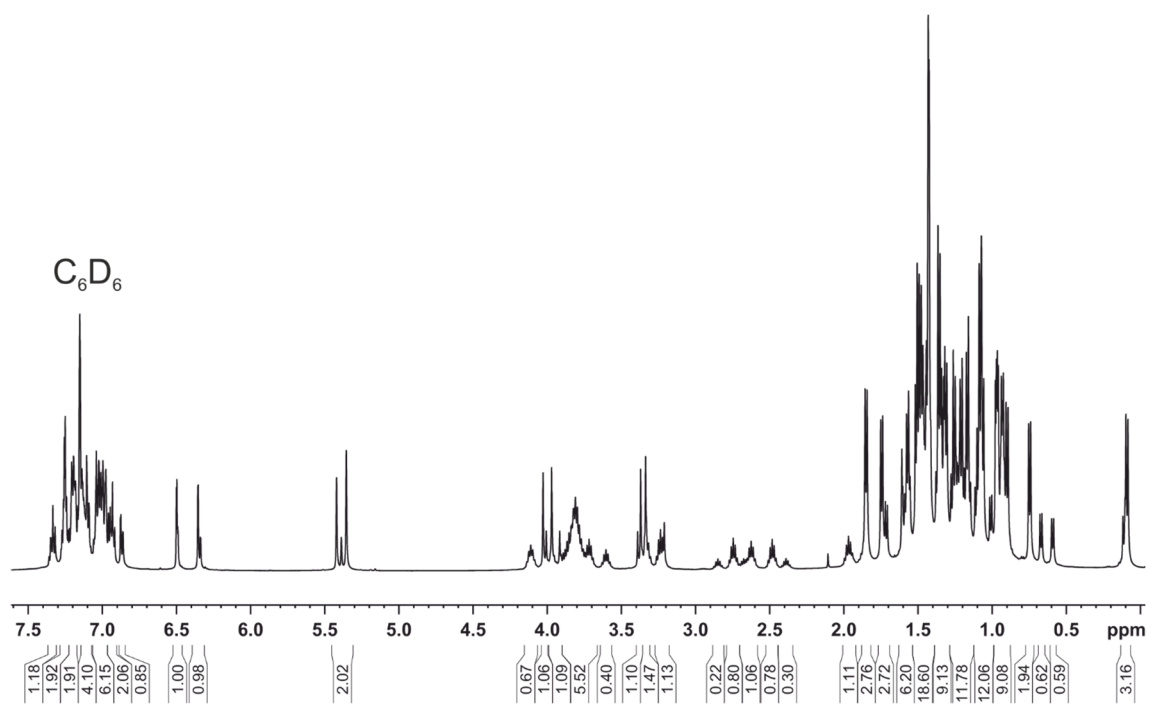

Isomer A   Isomer B
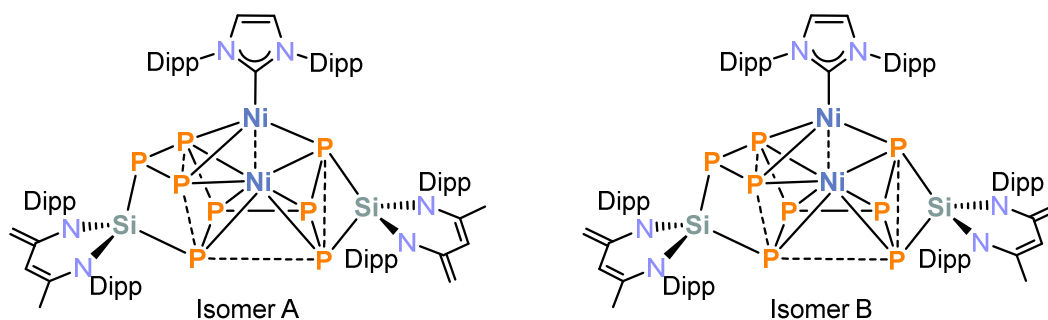
Figure S19. ^{1}H NMR spectrum (400 MHz, 300 K, C$_6$D$_6$) of [(IPr)Ni$_2$P$_8$(SiL)$_2$] (**3**).
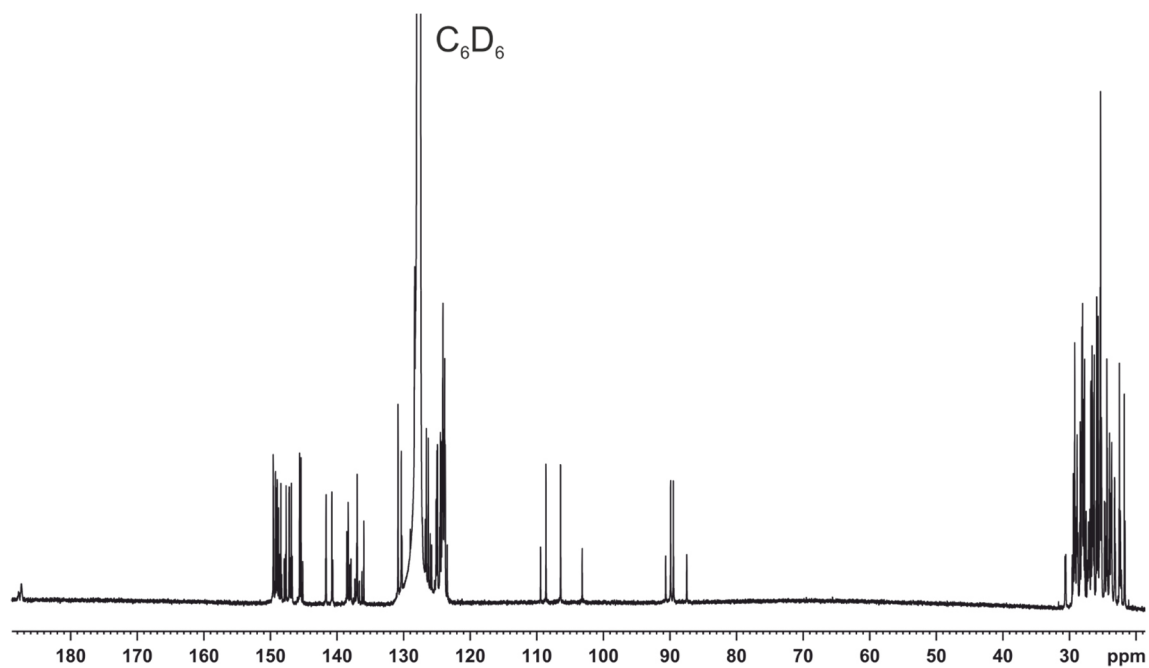

Figure S20. ^{13}C{^{1}H} NMR spectrum (125.75 MHz, 300 K, C$_6$D$_6$) of [(IPr)Ni$_2$P$_8$(SiL)$_2$] (**3**).
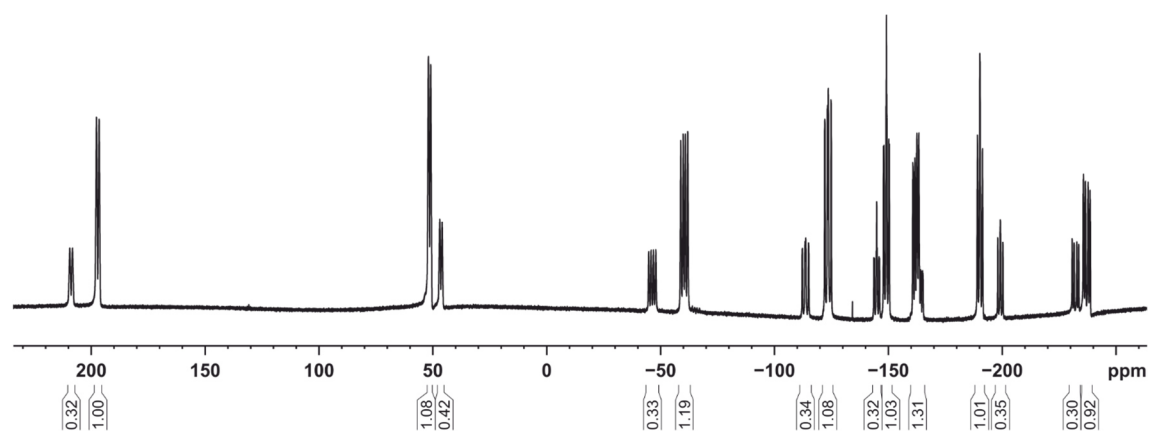
Figure S21. ³¹P{¹H} NMR spectrum (202.45 MHz, 300 K, C₆D₆) of [(IPr)Ni₂P₈(SiL)₂] (**3**).
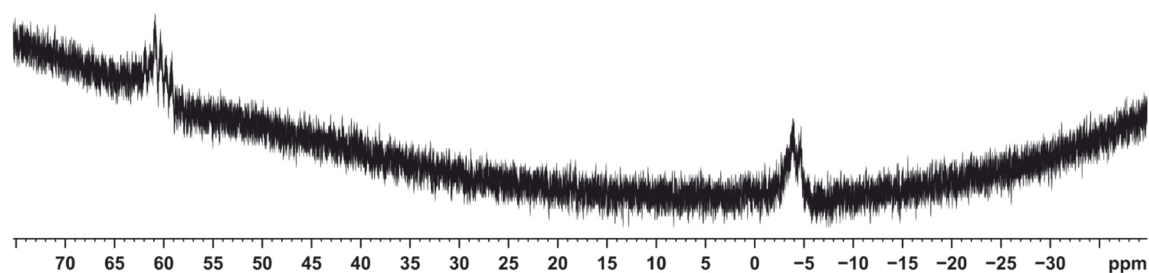
Figure S22. ²⁹Si NMR spectrum (99.36 MHz, 300 K, C₆D₆) of [(IPr)Ni₂P₈(SiL)₂] (**3**).
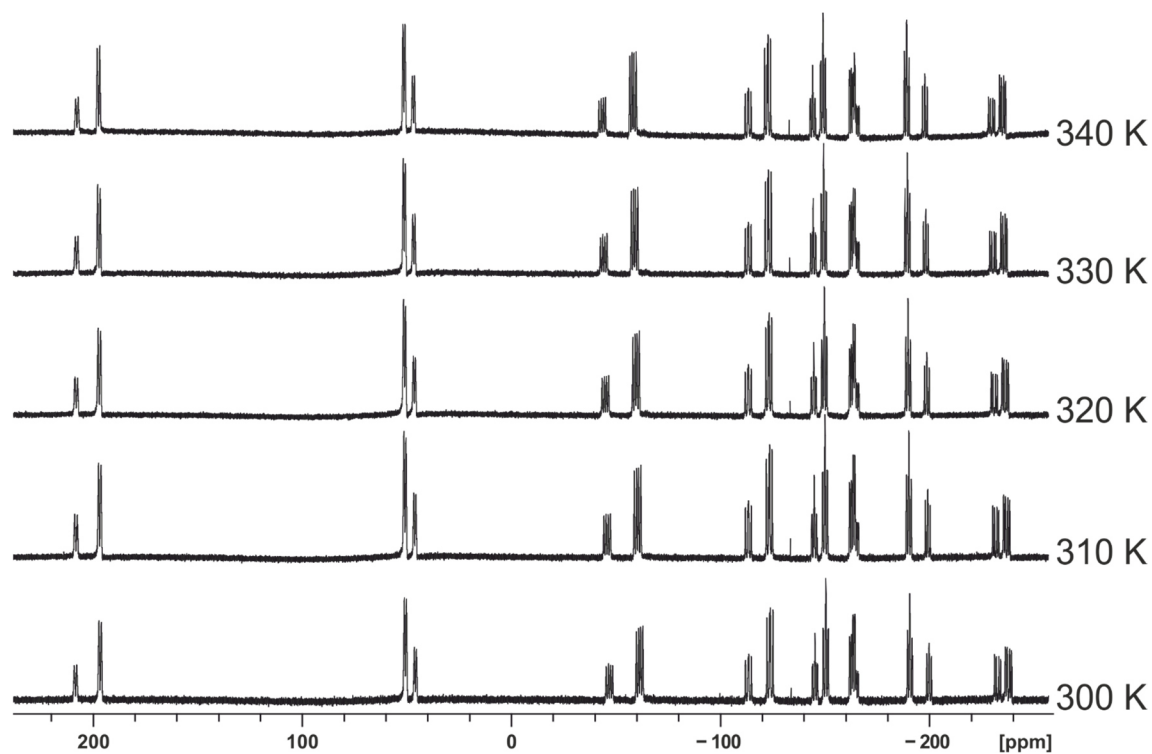
Figure S23. VT ³¹P{¹H} NMR spectra of [(IPr)Ni₂P₈(SiL)₂] (**3**) in tol-*d₈*.
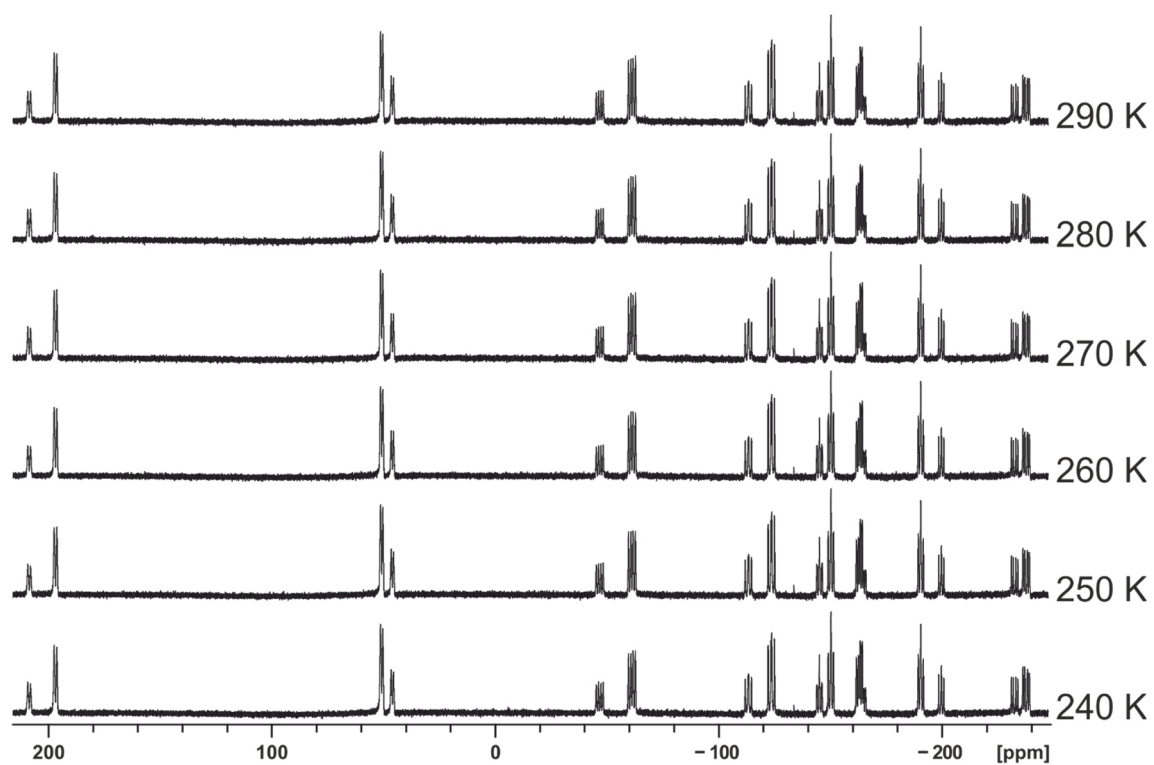
Figure S24. VT ^{31}P{^{1}H} NMR spectra of [(IPr)Ni$_2$P$_8$(SiL)$_2$] (**3**) in tol-d_8.

Table S1. Calculated $J(^{31}P,^{31}P)$ coupling constants (TPSS/pcSseg-2 level of theory) and $J(^{31}P,^{31}P)$ coupling constants obtained by an iterative fitting procedure using the calculated $J(^{31}P,^{31}P)$ coupling constants as starting point. $J(^{31}P,^{31}P)$ coupling constants are given in Hz. Extended signals (upwards) and simulations (downwards) with a representation of the core of the cluster **3**; thermal ellipsoids are drawn at the 40% probability level (bottom).

Assignment of nuclei	Calculated $J(^{31}P,^{31}P)$	Iterative fitting $J(^{31}P,^{31}P)$	Assignment of nuclei	Calculated $J(^{31}P,^{31}P)$	Iterative fitting $J(^{31}P,^{31}P)$
AB	-9.2	-7.5	BC	-6.2	-14.1
AC	-162.4	-175.8	BD	-248.2	-247.9
AD	-7.1	-13.8	BE	--	--
AE	0.3	28.0	BM	-11.7	-26.8
AM	-388.0	-409.7	BS	-198.9	-204.2
AS	20.8	35.2	BX	33.7	32.2
AX	11.9	17.1	DE	--	--
CD	-7.1	-8.0	DM	201.8	218.1
CE	-294.0	-325.3	DS	43.0	49.3
CM	19.7	19.9	DX	23.0	14.1
CS	26.5	20.9	MS	20.3	35.1
CX	73.1	48.1	MX	39.6	28.0
EM	-40.4	-13.0	SX	61.0	45.2
ES	--	--			
EX	-233.6	-241.6			

Note on the fitting procedure: The silicon-phosphorus coupling constants were not included in the simulation due to the rather broad signals observed in the experimental $^{31}P\{^1H\}$ NMR spectra.
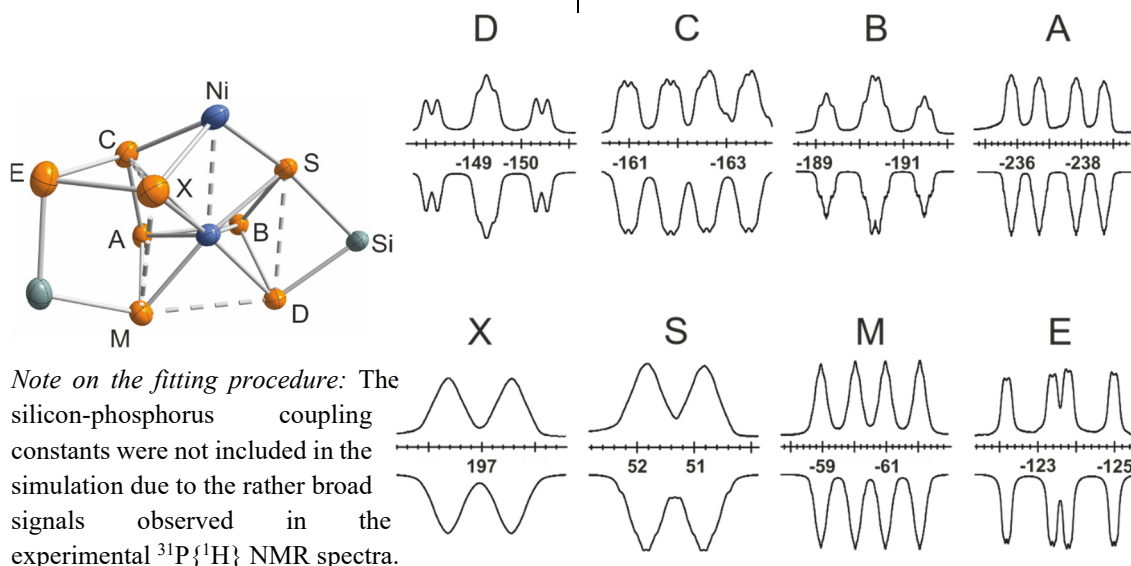
4.6 X-ray Crystallography

Crystallographic data were recorded on a Super Nova with a Mikrofocus Cu anode and an Atlas CCD Detector. In all cases, Cu-K$_\alpha$ radiation (λ = 1.54184 Å) was used. Crystals were selected under mineral oil, mounted on micromount loops and quench-cooled using an Oxford Cryosystems open flow N$_2$ cooling device. The diffraction pattern was indexed and the total number of runs and images was based on the strategy calculation from the program CrysAlisPro (Rigaku, V1.171.40.18b, 2018). The unit cell was refined using CrysAlisPro (Rigaku, V1.171.40.18b, 2018). Either semi-empirical multi-scan absorption corrections[6] or analytical[7] ones were applied to the data. Using Olex2,[8] the structures were solved with SHELXT[9] using intrinsic phasing and refined with SHELXL[10] using least squares refinement on F^2. The hydrogen atoms were located in idealized positions and refined isotropically with a riding model. Crystallographic data for the structures in this paper have been deposited with the Cambridge Crystallographic Data Centre, CCDC, 12 Union Road, Cambridge CB21EZ, UK. Copies of these data can be obtained free of charge (http://www.ccdc.cam.ac.uk) on quoting the depository number: 2009284 (**1a**), 2009285 (**1b**), 2009286 (**2**), 2009287 (**3**).

4.6.1 Refinement of the solid-state molecular structure of [(IPr)Ni{(μ-η$^{2:2}$-P$_4$)SiL}$_2$] (1a)
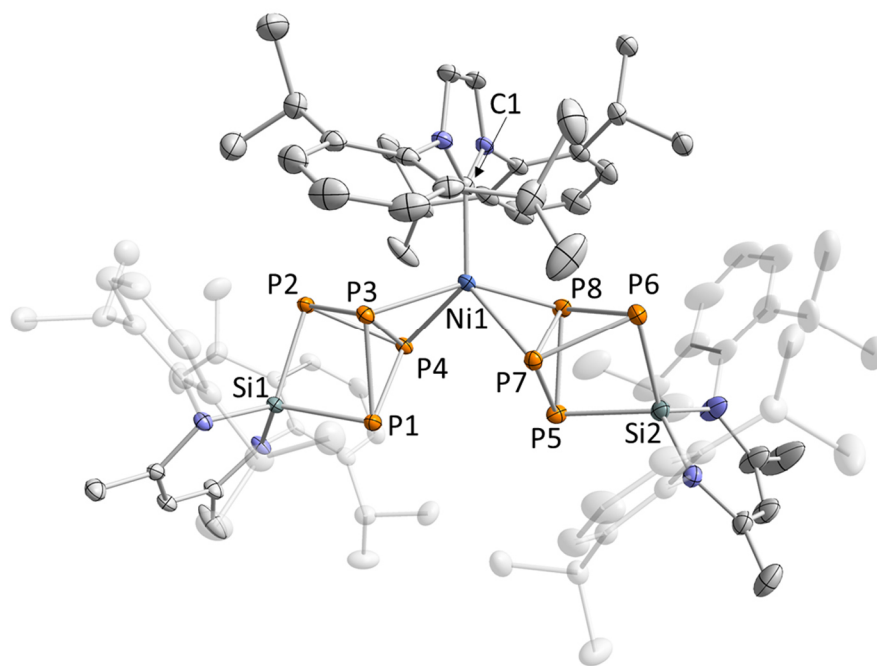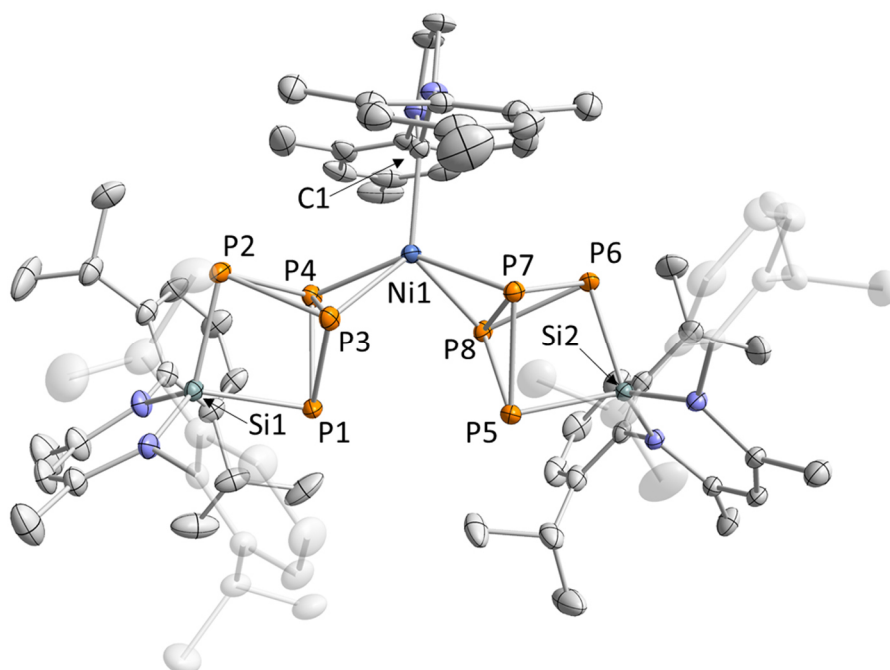

Figure S25. Solid-state molecular structure of **1a**. Hydrogen atoms and solvate molecules are omitted for clarity; thermal ellipsoids are drawn at the 40% probability level. Selected bond lengths [Å] and angles [°] for **1a**: P1–P3 2.2651(6), P1–P4 2.2511(7), P2–P3 2.2565(7), P2–P4 2.2724(7), P3–P4 2.2686(6), Si1–P1 2.2512(8), Si1–P2 2.2422(7), Ni1–P3 2.2923(8), Ni1–P4 2.2674(8), P5–P7 2.2451(6), P5–P8 2.2603(7), P6–P7 2.2714(9), P6–P8 2.2607(7), P7–P8 2.4749(7), Si2–P5 2.2475(9), Si2–P6 2.2455(6), Ni1–P7 2.2657(6), Ni1–P8 2.2847(7), Ni1–C1 1.9761(16); P1–P3–P2 86.95(3), P1–P4–P2 86.90(3), P3–P1–P4 59.54(2), P3–P2–P4 60.12(6), P3–Ni1–P4 59.67(2), P5–P7–P6 86.95(3), P5–P8–P6 86.85(2), P7–P5–P8 60.65(2), P7–P6–P8 60.26(2), C1–Ni1–P3 105.87(5), C1–Ni1–P4 131.99(5), C1–Ni1–P7 128.92(5), C1–Ni1–P8 104.22(6).

4.6.2 Refinement of the solid-state molecular structure of [(IMes)Ni{(μ-η²:²-P₄)SiL}₂] (1b)

Figure S26. Solid-state molecular structure of **1b**. Hydrogen atoms and solvate molecules are omitted for clarity; thermal ellipsoids are drawn at the 40% probability level. Selected bond lengths [Å] and angles [°] for **1b**: P1–P3 2.2589(6), P1–P4 2.2685(7), P2–P3 2.2652(7), P2–P4 2.2417(7), P3–P4 2.2553(7), Si1–P1 2.2457(7), Si1–P2 2.2300(6), Ni1–P3 2.2610(7), Ni1–P4 2.2531(7), P5–P7 2.2539(6), P5–P8 2.2352(8), P6–P7 2.2594(8), P6–P8 2.2659(7), P7–P8 2.2561(7), Si2–P5 2.2473(8), Si2–P6 2.2362(6), Ni1–P7 2.2775(6), Ni1–P8 2.2482(6), Ni1–C1 1.957(2); P1–P3–P2 87.07(2), P1–P4–P2 87.40(3), P3–P1–P4 59.76(2), P3–P2–P4 60.05(2), P3–Ni1–P4 59.95(2), P5–P7–P6 86.97(2), P5–P8–P6 87.26(3), P7–P5–P8 60.24(2), P7–P6–P8 59.81(2), C1–Ni1–P3 124.23(7), C1–Ni1–P4 105.57(7), C1–Ni1–P7 112.80(7), C1–Ni1–P8 126.99(7).

4.6.3 Refinement of the solid-state molecular structure of [(IPr)Ni(μ-η²:²-P₄)SiL] (2)
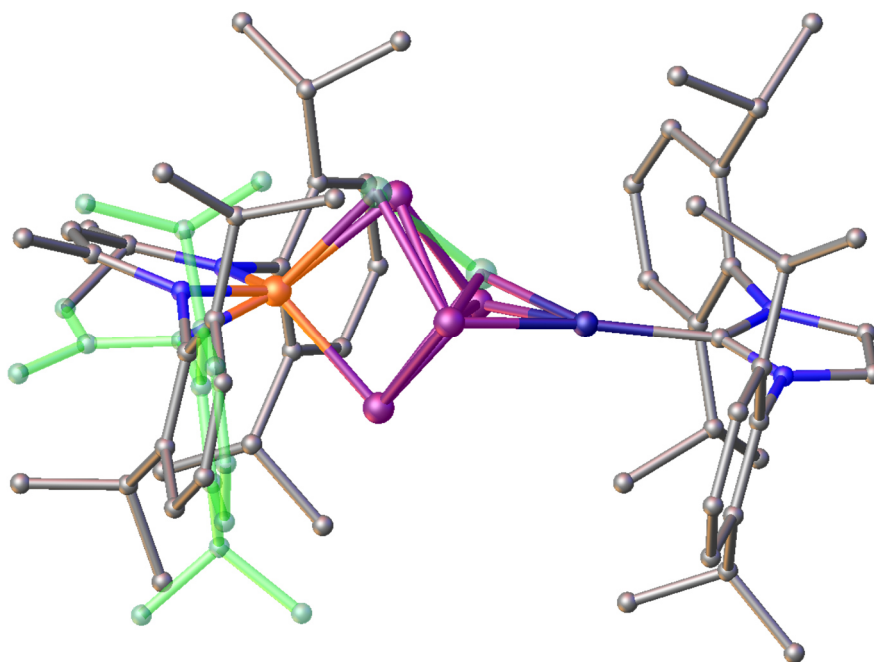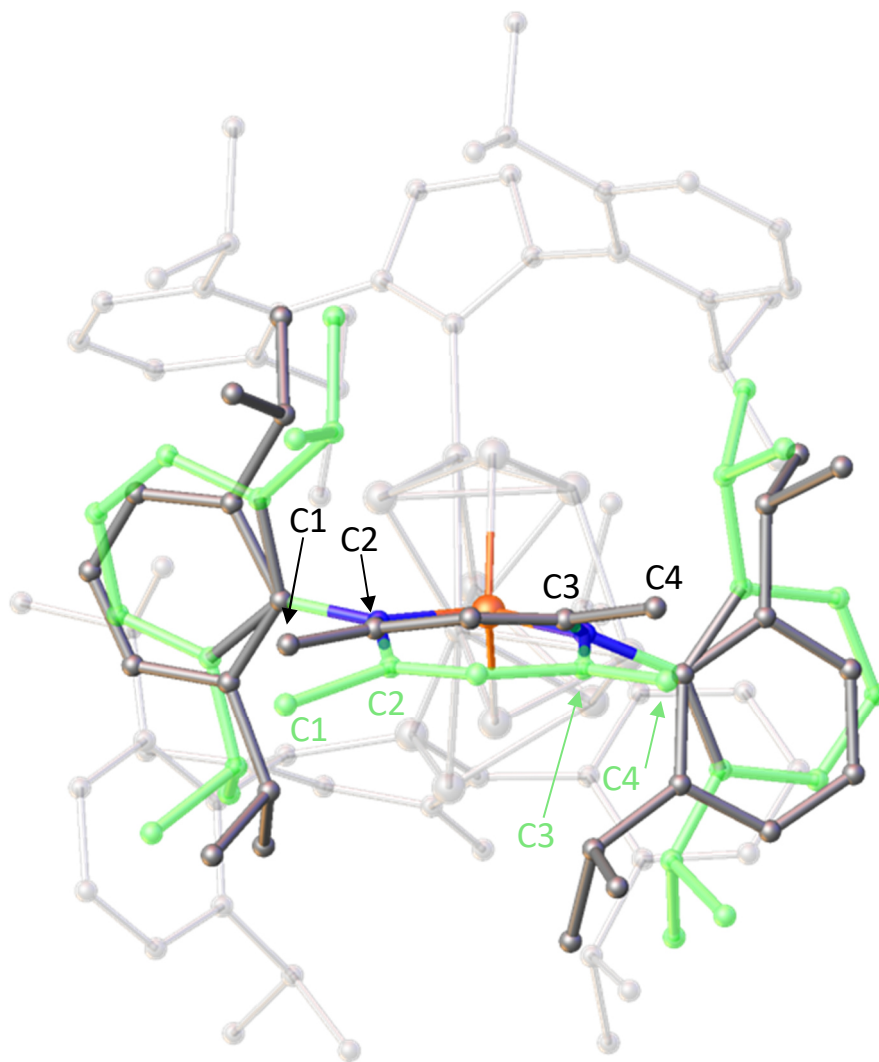

Figure S27. Ball and stick representation of the solid-state molecular structure of **2**. Hydrogen atoms are omitted for clarity. Disordered part is highlighted in green (PART 2).

The asymmetric unit of the solid-state molecular structure of **2** is disordered over two positions. The occupancy distribution of the backbone of the [LSi] ligand was refined to 82:18 and restrained with a SIMU. Additionally, an AFIX66 was applied to the phenylring of the disordered diisopropylphenly group. The bridging P_4 unit is also disordered over two positions with crystallographic occupancies of 70:30. The anisotropic displacement factors were restrained with a SIMU.

4.6.4 Refinement of the solid-state molecular structure of [(IPr)Ni₂P₈(SiL)₂] (3)

Figure S28. Ball and stick representation of the solid-state molecular structure of **3**. Hydrogen atoms are omitted for clarity. Disordered part is highlighted in green (PART 2). Selected bond distances [Å] of Part 1: C1–C2 1.350(9), C3–C4 1.473(7); Selected bond distances [Å] of Part 2 (highlighted in green): C1–C2 1.57(3), C3–C4 1.36(2).

The asymmetric unit of the solid-state molecular structure of **3** is disordered over two positions. The occupancy distribution of the backbone of the [LSi] ligand was refined to 73:27 and restrained with a SIMU. Additionally, an AFIX66 was applied to the phenyl ring of the disordered diisopropyphenly group. The disorder of the LSi moiety is likely caused by the presence of two isomers of **3**, which differ in the relative orientation of the C=C double bond in the ligand backbone (Figure S28). A solvent mask was calculated, and 366 electrons were found in a volume of 2140 Å³ in 2 voids per unit cell. This is consistent with the presence of two *n*-hexane solvent molecules per asymmetric unit, which account for 400 electrons per unit cell.

**Table S2.** Crystallographic data for compounds **1a**, **1b**, **2**, and **3**.

| Compound	1a	1b	2	3
Empirical formula	$C_{91}H_{130}N_6NiP_8Si_2$	$C_{85}H_{118}N_6NiP_8Si_2$	$C_{56}H_{76}N_4NiP_4Si$	$C_{85}H_{116}N_6Ni_2P_8Si_2$
Formula weight	1670.65	1586.50	1015.88	1643.19
Temperature [K]	123.00(10)	123.00(10)	123.00(10)	123.00(10)
Crystal system	monoclinic	monoclinic	orthorhombic	monoclinic
Space group	P2₁/c	P2₁/c	Pbca	P2₁/c
a [Å]	23.6231(4)	17.4813(3)	17.4645(3)	23.3638(5)
b [Å]	13.31130(10)	22.9979(3)	15.4359(3)	16.0951(3)
c [Å]	30.4842(5)	22.0196(3)	42.6490(6)	27.7549(6)
α [°]	90	90	90	90
β [°]	105.741(2)	97.889(2)	90	107.229(2)
γ [°]	90	90	90	90
Volume [Å³]	9226.4(2)	8768.8(2)	11497.3(3)	9968.7(4)
Z	4	4	8	4
ρ_{calc} [g/cm³]	1.203	1.202	1.174	1.095
μ [mm⁻¹]	2.213	2.303	2.020	2.217
F(000)	3576.0	3384.0	4336.0	3488.0
Crystal size [mm³]	0.304 × 0.112 × 0.051	0.372 × 0.081 × 0.027	0.32 × 0.107 × 0.088	0.192 × 0.114 × 0.057
Radiation	Cu Kα (λ = 1.54184)	Cu Kα (λ = 1.54184)	Cu Kα (λ = 1.54184)	Cu Kα (λ = 1.54184)
2Θ range for data collection [°]	7.292 to 148.682	7.182 to 146.22	6.542 to 147.986	6.668 to 148.204
Index ranges	-29 ≤ h ≤ 28, -16 ≤ k ≤ 10, -37 ≤ l ≤ 37	-21 ≤ h ≤ 16, -28 ≤ k ≤ 26, -24 ≤ l ≤ 27	-21 ≤ h ≤ 20, -18 ≤ k ≤ 16, -52 ≤ l ≤ 52	-28 ≤ h ≤ 28, -19 ≤ k ≤ 14, -34 ≤ l ≤ 34
Reflections collected	55783	41046	46160	58661
Independent reflections	18506 [R_{int} = 0.0253, R_{sigma} = 0.0258]	16774 [R_{int} = 0.0293, R_{sigma} = 0.0362]	11392 [R_{int} = 0.0388, R_{sigma} = 0.0307]	19509 [R_{int} = 0.0257, R_{sigma} = 0.0254]
Data / restraints / parameters	18506/6/1033	16774/146/984	11392/468/769	19509/654/1183
Goodness-of-fit on F²	1.015	1.018	1.137	1.029
Final R indexes [I>=2σ (I)]	R₁ = 0.0334, wR₂ = 0.0816	R₁ = 0.0390, wR₂ = 0.0939	R₁ = 0.0664, wR₂ = 0.1626	R₁ = 0.0446, wR₂ = 0.1149
Final R indexes [all data]	R₁ = 0.0397, wR₂ = 0.0854	R₁ = 0.0518, wR₂ = 0.1021	R₁ = 0.0759, wR₂ = 0.1680	R₁ = 0.0533, wR₂ = 0.1215
Largest diff. peak/hole [e Å⁻³]	0.50/-0.51	0.53/-0.59	0.70/-0.62	0.78/-0.35

4.7 Theoretical investigations

All calculations were performed with the ORCA program package[11] and were conducted in the gas phase. The RI[12] approximation was used for GGA calculations whereas the RIJCOSX[13] approximation was used for hybrid-DFT calculations. Geometry optimizations have been carried out at the PBE/def2-TZVP[14],[15],[16] level of theory and the nature of stationary point was confirmed by a numerical frequency analysis. For compound **3**, a model **3′** in which the *iso*-propyl substituents of at the diisopropylphenyl moieties have been truncated to methyl groups. The higher occupied part of the single X-ray crystal structure was chosen as initial geometry for **3′**.

4.7.1 NBO Analysis of complex 2

An NBO (version 6.0)[17] analysis was carried out using the Gaussian 09 program package[18] (using the ORCA PBE singlet geometry and using the def2-TZVP basis). The donor properties of the nickel atom in complex **2** were quantified in a second order perturbation theory analysis.

112

113

114

115
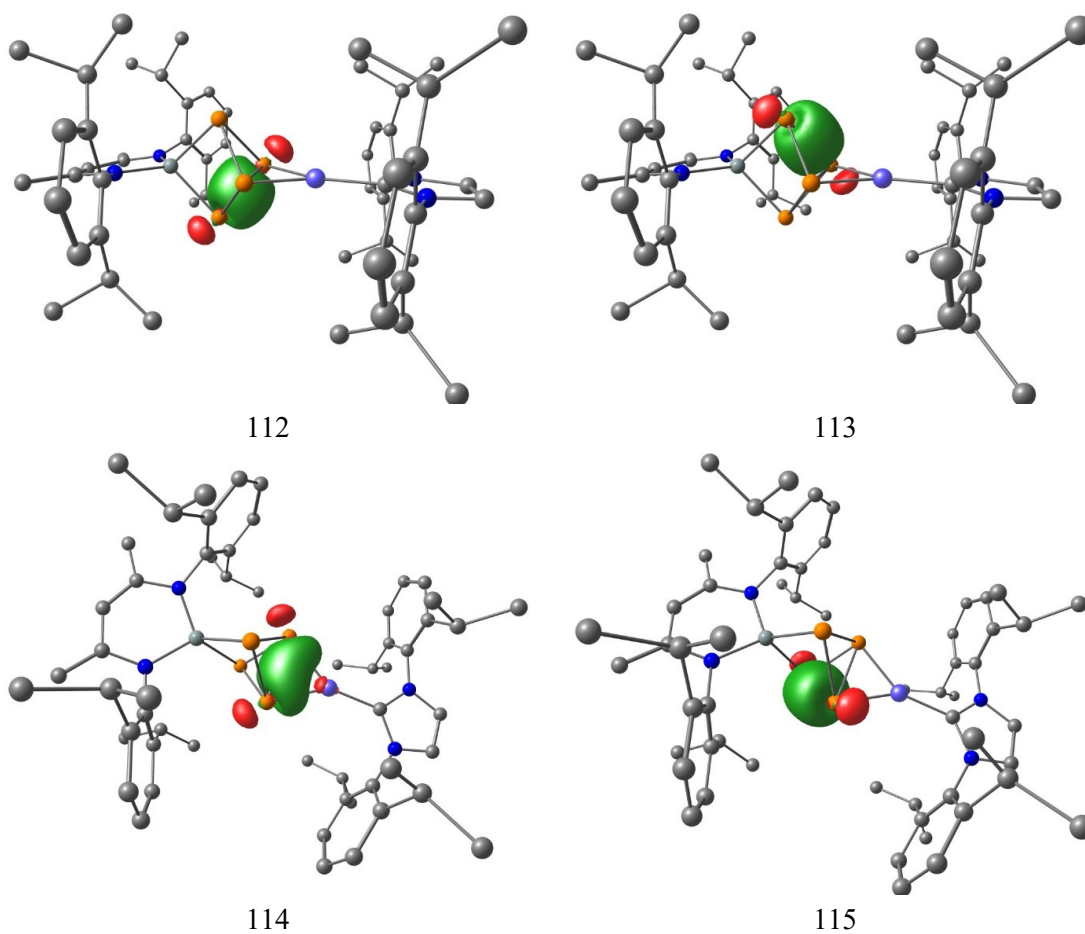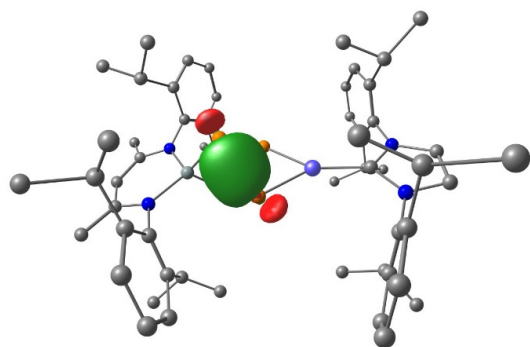
116

Figure S 29. Natural bond orbitals of **2** showing five P–P bonds. Surface isovalue = 0.07. H atoms have been omitted for clarity.
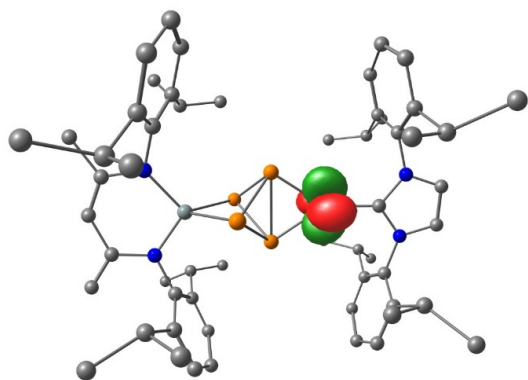
95
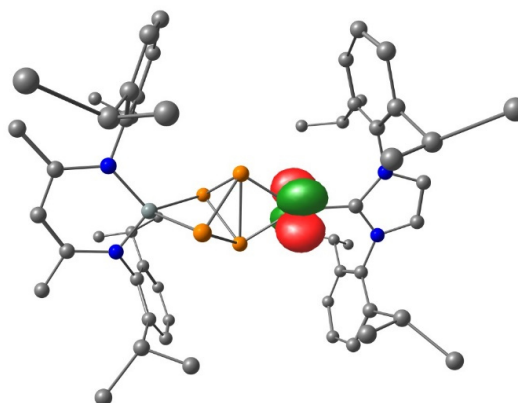
96
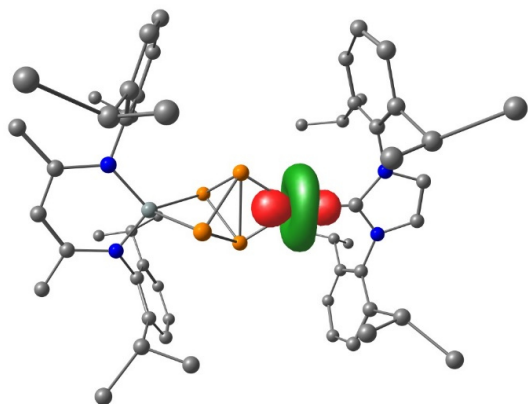
97
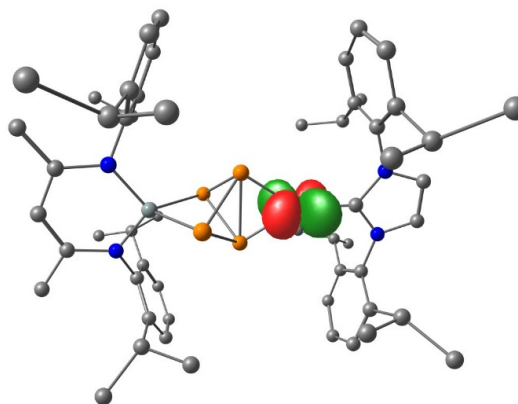
98
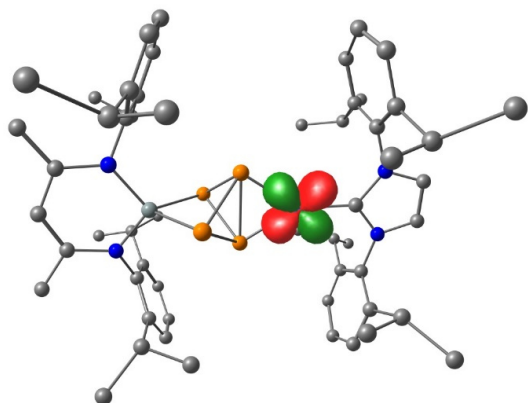
99

Figure S30. Natural bond orbitals of **2** showing five occupied Ni 3d-orbitals. Surface isovalue = 0.05. H atoms have been omitted for clarity.
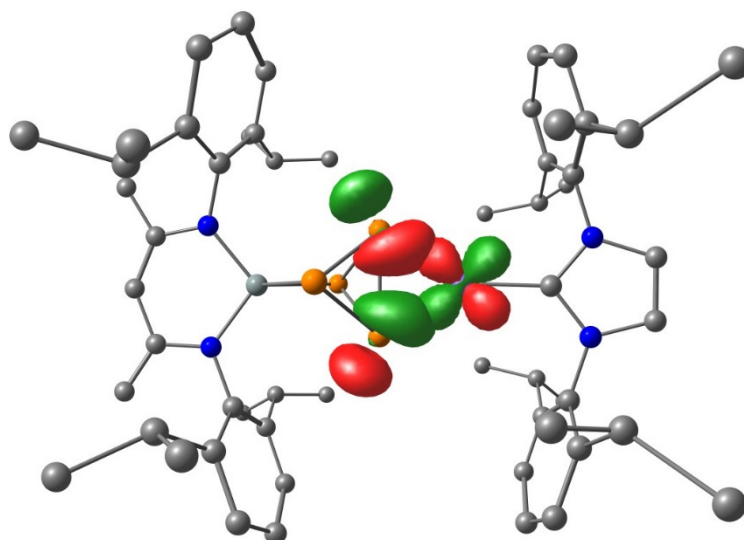
Figure S31. Natural bond orbitals representing the back-bonding of an occupied Ni d-orbital into the antibonding orbital of the coordinated P−P bond. Ni(d) → σ* (P1–P2) 36.5 kcal · mol⁻¹. Surface isovalue = 0.07. H atoms have been omitted for clarity.

4.7.2 Intrinsic bond orbital analysis of compound 3′

Intrinsic bond orbitals (IBO) have been calculated from the occupied PBE orbitals according to Knizia *et al*.[19] To investigate the bonding interactions within the cluster we analyzed the composition and shape of the IBOs. IBOs with a Ni contribution higher than 70% were assigned to be occupied 3d orbitals. This guarantees that only significant interactions are considered. Orbitals with low Ni contributions 71% to 73% may be explained by a significant back-donation of electron density from the Ni atoms to the electron-deficient cluster.
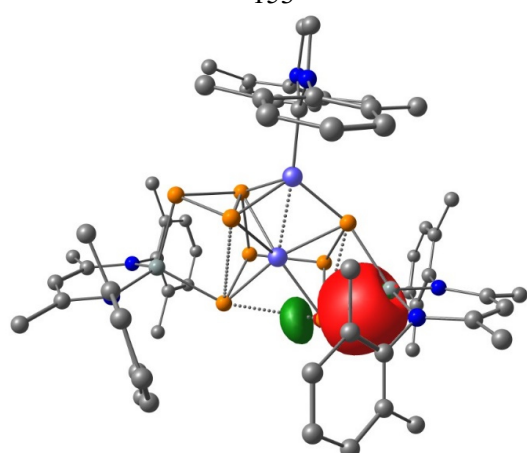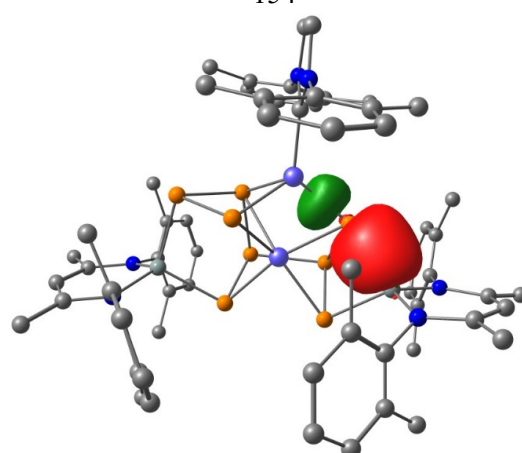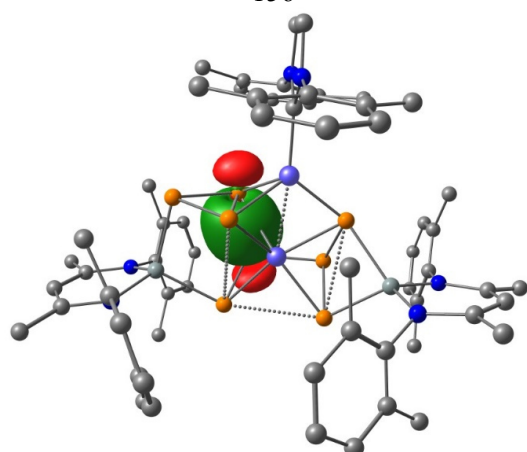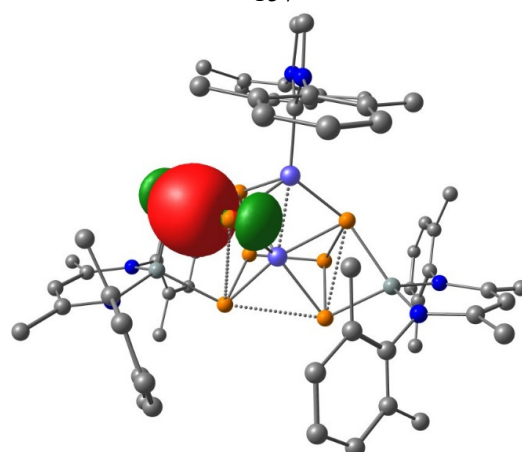

150   152
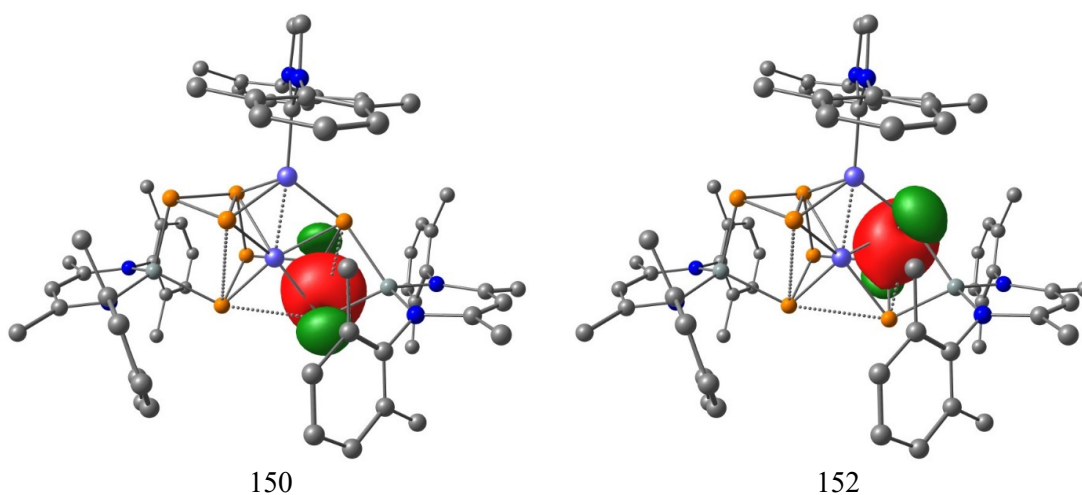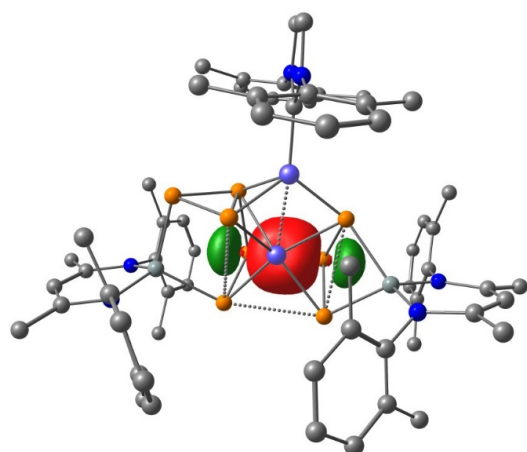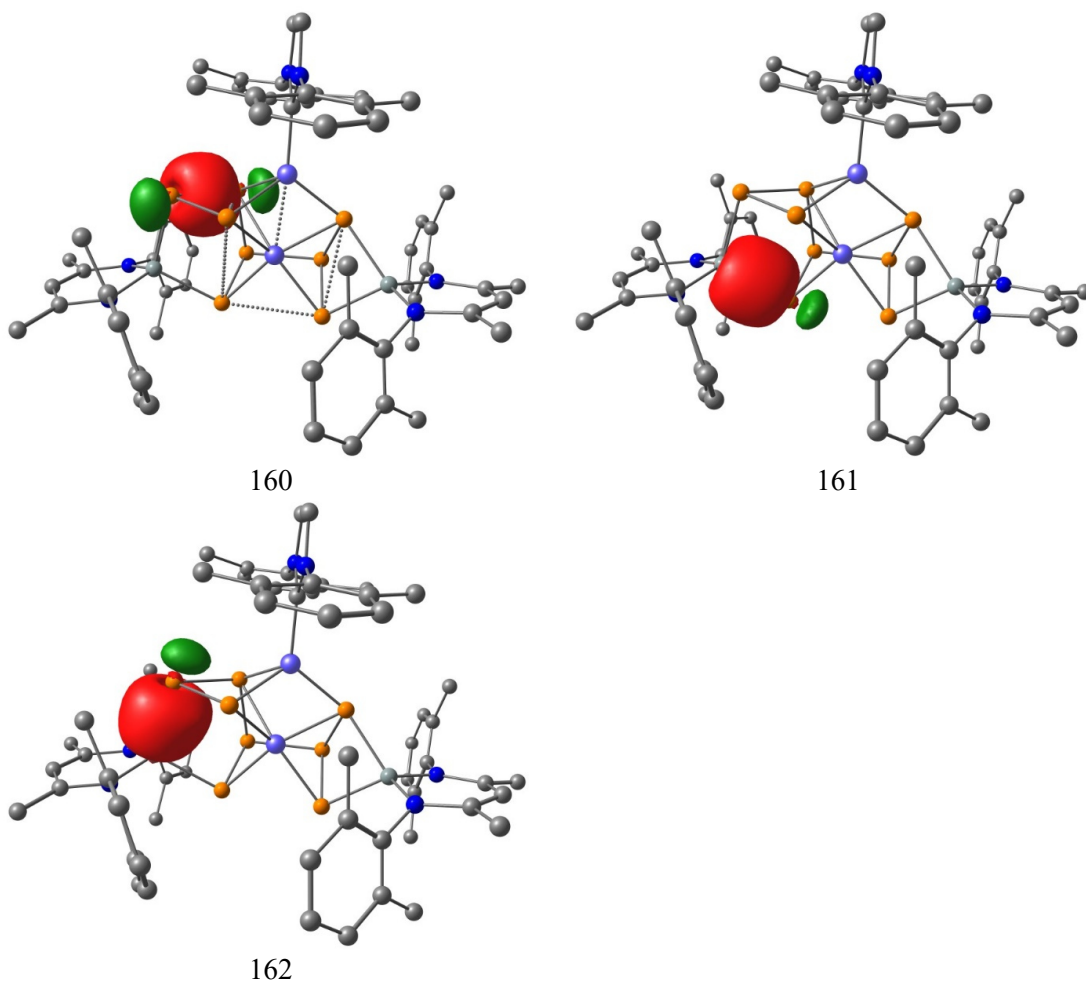
153

154

156
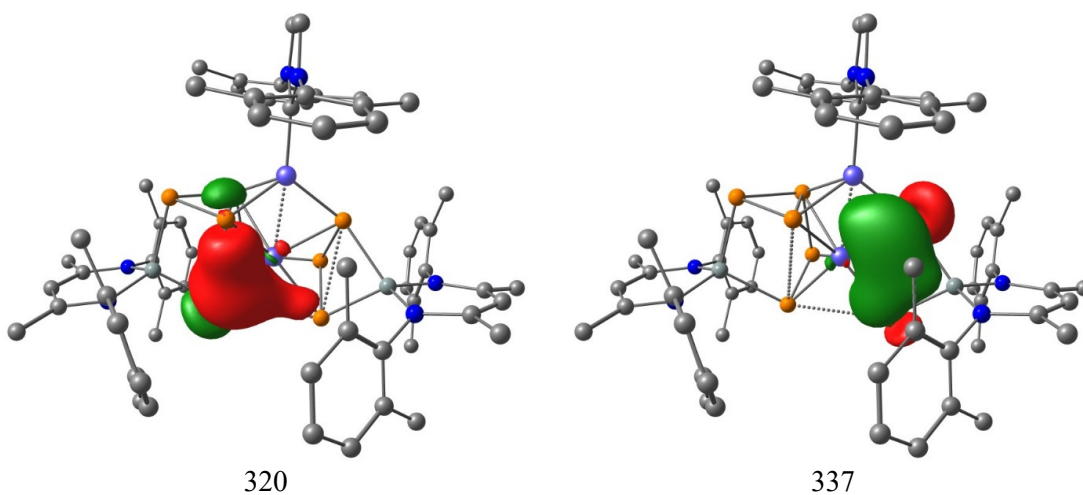
157

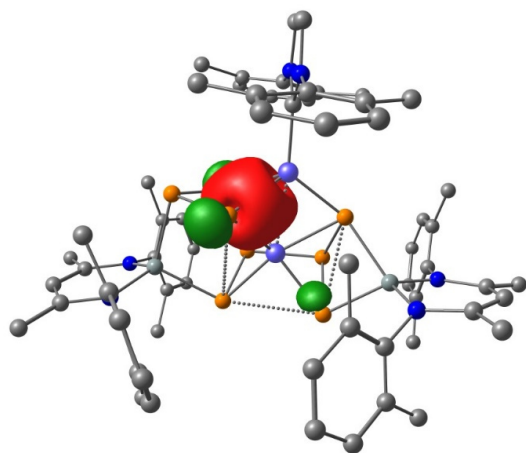158

159

160

161

162
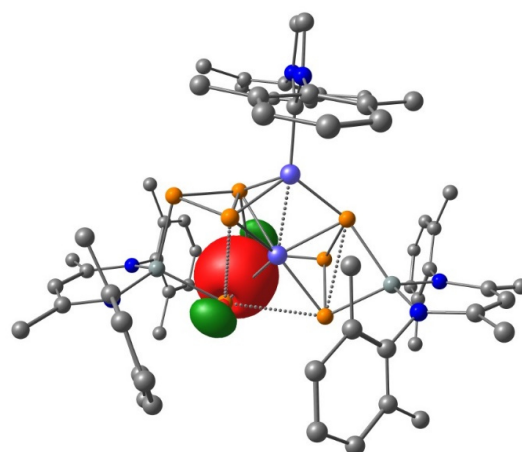
Figure S32. Intrinsic bond orbitals of **3′** showing 2-center-2-electron bonding interactions between the cluster atoms. Surface isovalue = 0.05. H atoms have been omitted for clarity.
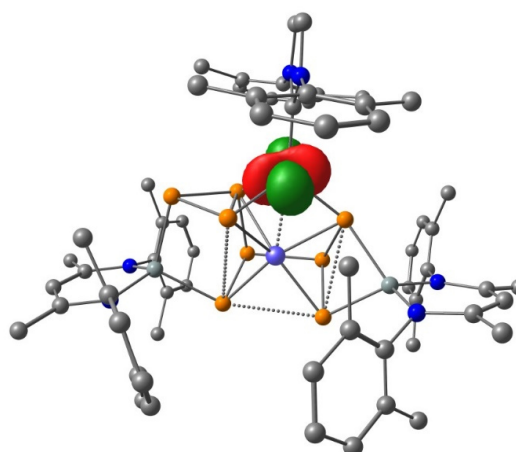

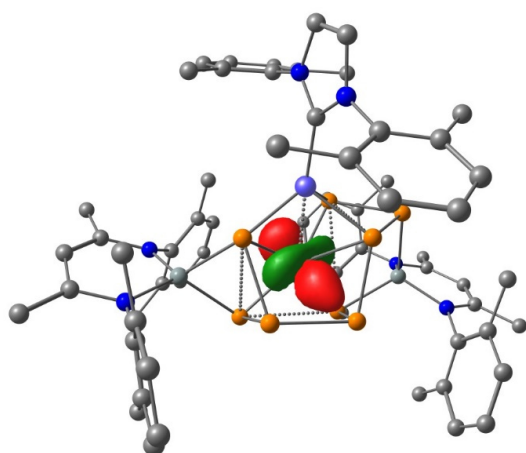320

337

339

Figure S33. Intrinsic bond orbitals of **3′** multicenter bonding interactions between the cluster atoms. Surface isovalue = 0.05. H atoms have been omitted for clarity.
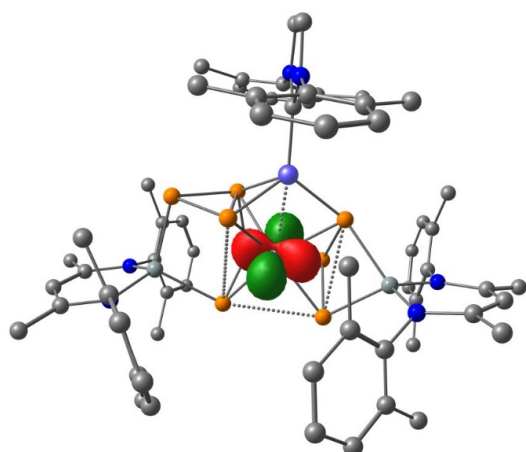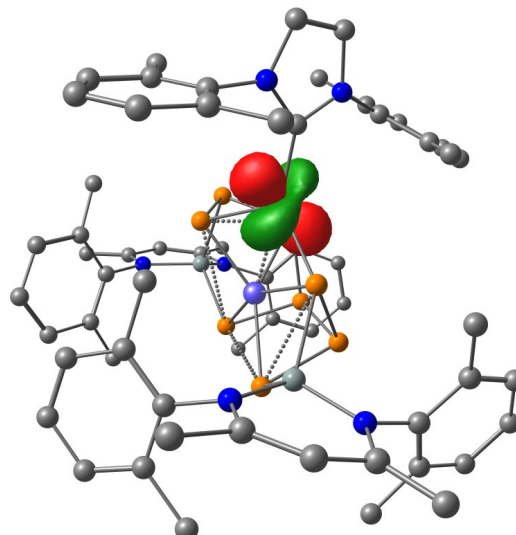
9 (96% Ni)

19 (96% Ni)

144 (93% Ni)

145 (94% Ni)

146 (91% Ni)   147 (89% Ni)

148 (86% Ni)   149 (81% Ni)

155 (71% Ni)   319 (73% Ni)
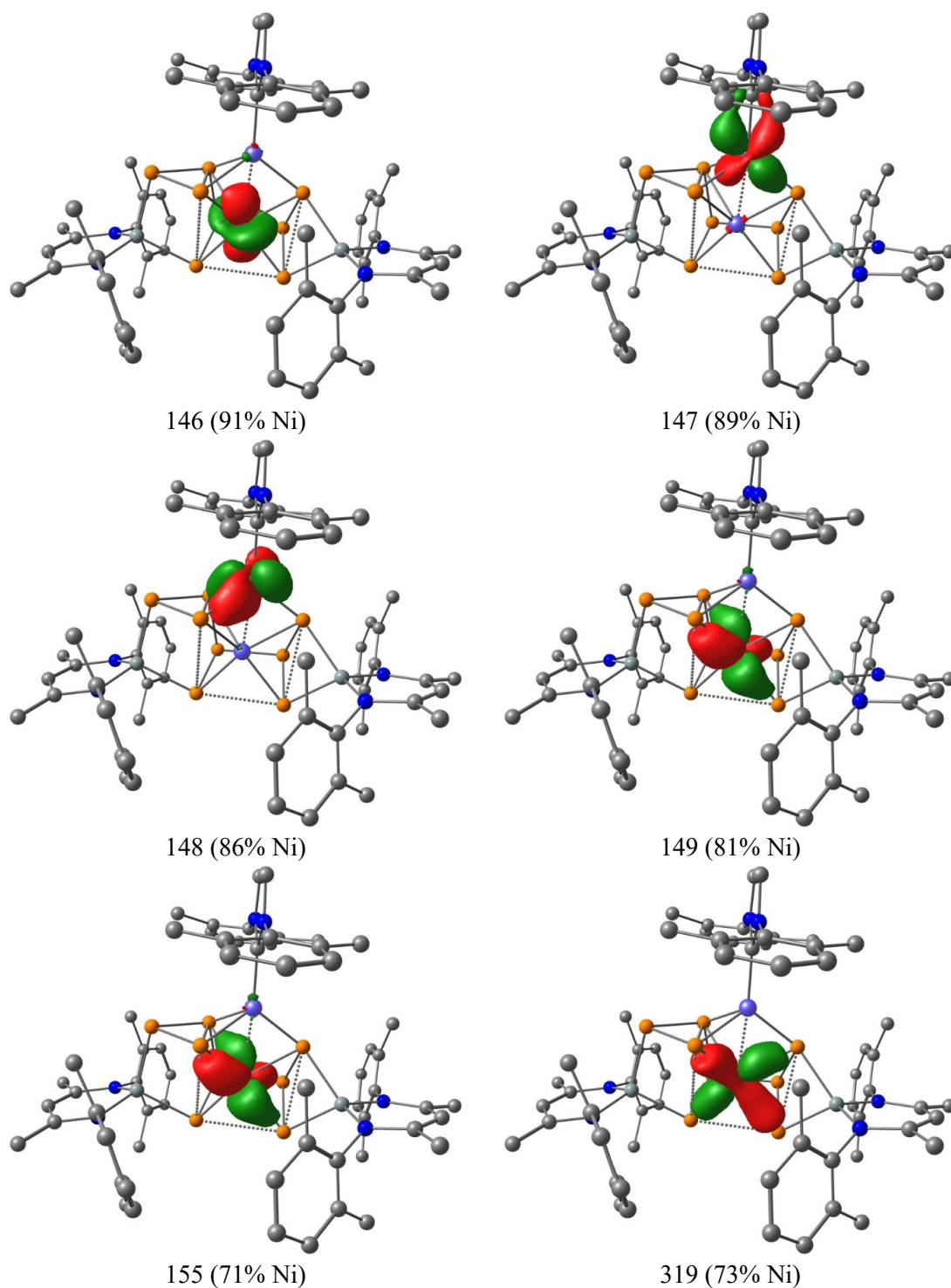
Figure S34. Intrinsic bond orbitals of **3′** showing the filled 3d-orbitals at the Ni atoms (highest contribution of a single Ni atom is given in parentheses). Surface isovalue = 0.05. H atoms have been omitted for clarity.

4.7.3 Calculation of ^{31}P NMR shieldings

The chemical shielding constants of the optimized geometries of complexes **2** and **3′** and were calculated at the TPSS/pcSseg-2 level of theory.[20],[21] Calculated coupling constants are given in Table S1, *vide supra*.

Table S3. Calculated chemical shielding constants and chemical shifts of **3′**. Complex **2** was used as reference. Representation and assignment of ^{31}P nuclei of core of **3** (bottom).

assignment of the ^{31}P	isotropic shielding constant	calculated chemical shift [ppm]	experimental chemical shift [ppm]	absolute deviation from the experimental values
A	545.167	-233.5	-236.7	3.2
B	504.562	-192.9	-189.8	3.1
C	444.44	-132.7	-161.4	28.7
D	439.386	-127.7	-148.5	20.8
E	396.255	-84.5	-122.8	38.3
M	361.048	-49.3	-59.7	10.4
S	244.308	67.4	51.9	15.5
X	87.693	224.0	197.7	26.3

Table S4. Calculated chemical shielding constants and chemical shifts of **3′**. Complex **2** was used as reference. Representation and assignment of ^{29}Si nuclei of core of **3** (bottom).

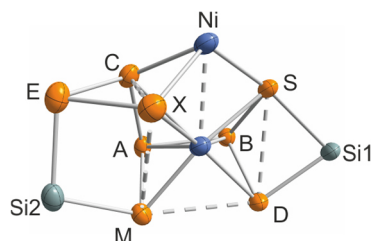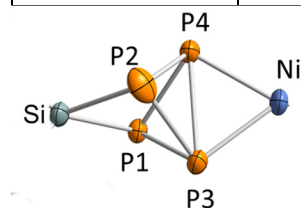| assignment of the ^{29}Si	isotropic shielding constant	calculated chemical shift [ppm]	experimental chemical shift [ppm]	absolute deviation from the experimental values
Si1	360.958	-8.6	-3.9	4.7
Si2	294.852	57.5	60.8	3.3

Table S5. Calculated chemical shielding constants and chemical shifts of reference system **2**. Representation and assignment of ^{31}P nuclei of core of **2** (bottom).

assignment of the ^{31}P and ^{29}Si nuclei	isotropic shieling constant	calculated chemical shift [ppm]	experimental chemical shift [ppm]	absolute deviation from the experimental values
P1	148.7	163.0	147.3	15.7
P2	164.4	reference	147.3	0.0
P3	468.6	-156.9	-138.0	18.9
P4	489.2	-177.5	-155.1	22.4

Cartesian coordinates of the optimized gas phase geometry of the complex **2** (PBE/def2-TZVP, S= 0)

Ni	7.04674659858483	7.77380192561013	25.95004525916821
Si	9.42411136763949	11.42440432603290	27.44306874250845
P	8.29946996869168	9.45075309790504	25.41415003450989
P	7.30926338697802	11.04394117932097	26.71892808243584
P	9.87052737160240	9.23777923580356	27.04900529004216
P	7.67347323011013	8.97533710856267	27.62965200103657
N	5.84922695366098	5.75176064802026	24.11778150849454
N	5.36411844088936	5.33073450702456	26.17438532961149
N	9.60749592260333	11.96471264953618	29.11203950327963
C	6.38289110092842	6.36728542874326	22.92736274254545
C	6.04850881715092	6.23071115646047	25.39145269493477
N	10.36787462879715	12.61455122053654	26.52261729076772
C	9.11287071446023	11.11817375469191	30.17672998871487
C	4.76625181760074	4.33514696075697	25.41435950134098
H	4.18416293411810	3.53786615127133	25.86121274172554
C	4.20939508725900	6.12937023187050	28.18579955735599
C	5.07278745140863	4.60108286833123	24.11440234801167
H	4.81196562060927	4.08237736441493	23.19948512523417
C	5.27784417229504	5.41097488690136	27.61226967408099
C	7.78790913578659	11.28553847182430	30.65544427914755
C	9.98458258368918	10.16791337470641	30.76867640046171
C	7.65046091938277	5.95902220779767	22.46566746386945
C	5.61132015229006	7.34547993387679	22.26815157107801
C	6.26224895774307	4.76345643040253	28.38560170007807
C	4.15142874990748	6.19192304705052	29.58395702351892
H	3.34253377309090	6.74874085400559	30.06063889217476
C	10.84116367450554	12.27231560087542	25.19626341104923
C	10.09372905174045	12.62770729566998	24.04382244090683
C	6.83132649541612	12.33791699109498	30.10740513094145
H	7.26485303460718	12.72912994040556	29.17448613389487
C	3.15983877987073	6.84676642668255	27.34974134185663
H	3.34132753958628	6.59927628205284	26.29327123552740
C	10.60357282003821	12.27416298010641	22.78614217149041
H	10.03737256908611	12.53961767489080	21.89096807548109
C	4.25512333531782	7.80486543600117	22.78245693247280
H	3.98523501295557	7.16978609903067	23.63922151538369
C	6.15164871736355	7.92115107552500	21.11100343863953
H	5.58377774226253	8.68811145700852	20.58097507535985
C	7.40181288869809	7.53858137613724	20.63152612383822
H	7.80513510366215	8.00322194859336	19.72985489407803
C	7.35427520910689	10.46897790717632	31.70896410484486

H	6.33648352960505	10.58411117278380	32.08649868349347
C	11.44147366014708	10.00836686514950	30.35051891765110
H	11.57486694887234	10.54875538411912	29.40108215544419
C	7.42474582810610	4.00192317279300	27.76616190822924
H	7.28470088262652	3.99897952900270	26.67503069088615
C	6.15392255801080	4.85956778254312	29.77889782878109
H	6.90545677408554	4.37818470886738	30.40744517776874
C	8.49294251418387	4.91993363637269	23.19040341889643
H	7.90264968392212	4.53480550997056	24.03495215852408
C	5.11220149299702	5.56615512246403	30.37408072274598
H	5.05114605867821	5.63342914716831	31.46182733172065
C	8.14057265657534	6.56808754268500	21.30328638695589
H	9.12282852914336	6.28080706249976	20.92339564518143
C	5.44563466797540	11.75983332797894	29.77714196686681
H	5.51480513244075	10.88210209936972	29.12005020867641
H	4.83366188450083	12.51818795516508	29.26670397153446
H	4.90535130390895	11.46216685766984	30.68875891336959
C	3.29488398542191	8.37242205470351	27.48939582917828
H	3.12526718727548	8.69427275584627	28.52803233011637
H	2.55638720503239	8.88309986136633	26.85310497367524
H	4.29858481663437	8.70804180706345	27.18994006030849
C	9.49526898845027	9.37848653473254	31.81753932946239
H	10.15381625159499	8.64167547739911	32.28140474045884
C	10.82913541571979	13.80141695940076	27.12551853171590
C	10.72263985179429	14.04896793408987	28.45837833951209
H	11.09166642714970	15.01322572594295	28.80595306894586
C	1.73604543835990	6.37898748113144	27.69153473225489
H	1.62852385553816	5.29105125086285	27.57182777165266
H	1.00581351603025	6.86977606866229	27.03115336337875
H	1.46507193272365	6.63019020394768	28.72774031736320
C	12.08020577568777	11.58729376464960	25.07217839917595
C	8.19309418725749	9.52167077003963	32.28656540120505
H	7.83331314563806	8.89702386061514	33.10680113826626
C	10.19318952935727	13.19378730800493	29.50226012166081
C	7.45723227782609	2.53609166996639	28.22857889003978
H	7.63030535895950	2.45796862056095	29.31223215080509
H	8.27154849865334	1.99554179434384	27.72363337457938
H	6.51257324409347	2.02018641281702	28.00272350428594
C	3.15289972850787	7.63942828475675	21.72401391916899
H	3.33306494166397	8.27959981995375	20.84763578718469
H	2.17665884256201	7.92280436188335	22.14450441938026
H	3.08451865929907	6.60011268472058	21.37099908713245

C 11.81250202318032 11.60111096322915 22.65232872045299

H 12.18883218929098 11.33871681417808 21.66157527737224

C I0.28069135059773 13.58636392219894 30.80422783542227

H 9.90967794380501 12.98481104066564 31.62967820408744

H 10.74867848466252 14.54075403127510 31.03794040583599

C 4.32544211809824 9.25340462567534 23.29466090966079

H 5.07703579847075 9.35336358859830 24.09159852637888

H 3.35082198909228 9.56523544366330 23.69940143891304

H 4.59346218352376 9.94955001585516 22.48545852209750

C 8.78208933815535 13.40459944627531 24.09170487891562

H 8.51652716516465 13.54725163311247 25.15058189427233

C 6.68527937141103 13.52287673032717 31.08083066858746

H 6.25772360595811 13.18926112333750 32.03948654980739

H 6.00943000160389 14.28145419325505 30.65697040849183

H 7.65508936591891 13.99751383769784 31.27950490227369

C 12.54148126623332 11.26591205416322 23.78954071778429

H 13.49277147673968 10.74189769780036 23.68033330326424

C 8.76136896051179 4.70697499650055 28.05099133136878

H 8.75195309996339 5.73872072125784 27.67008297392830

H 9.58958835260579 4.16819667001430 27.56645857250148

H 8.97045543521860 4.74568263543164 29.13067392399838

C 11.83683691676567 8.54202662884754 30.11653571238368

H 11.81558286050051 7.96161592242921 31.05132301108179

H 12.86309893667626 8.48761148109309 29.72295395132302

H 11.17114665099683 8.05142704953892 29.39271120707231

C 11.42166172728207 14.85782698318099 26.23199554629149

H 12.15825283369421 14.45035309165515 25.52605807001256

H 11.90821823951117 15.62868279687893 26.84114182071805

H 10.64095633901779 15.34489043072409 25.62919488044285

C 7.63039275763056 12.64797559233364 23.40746202133334

H 7.80728100427441 12.55478354257603 22.32495913030391

H 6.68486902884901 13.19366798909799 23.54413851861556

H 7.50312638392482 11.63749861358009 23.81593532598957

C 12.94846729058941 11.23122295148325 26.27498592218447

H 12.32515709516953 11.32566162789137 27.17718431340966

C 12.38523964115773 10.65354860495738 31.38307203845021

H 12.15620892874765 11.71868274655352 31.52025611247923

H 13.43144708257245 10.56406883283751 31.05206057319552

H 12.29679198908787 10.15066022887030 32.35891332980808

C 8.83133073390235 3.72553964540709 22.28365437627571

H 7.92289878395933 3.25165520913920 21.88400372541036

H 9.39322075145881 2.96639473090724 22.84775750316009

H 9.45334744504199 4.03047208632862 21.42893222698349

C 9.76504487951549 5.55413872484442 23.77727307859755

H 10.41244288360918 5.95789046325067 22.98428460885519

H 10.34450959374235 4.80374887734251 24.33587461740527

H 9.51498221139763 6.37680698332211 24.46296987550628

C 8.91768027335686 14.79226816551053 23.43575359058903

H 9.73514994580703 15.38513191289205 23.86614029760136

H 7.98347843792312 15.36142590796928 23.55443662017678

H 9.11395550365062 14.69632028482400 22.35694735754071

C 13.47665343777078 9.78923903275437 26.22505581741856

H 12.66109613503967 9.06343785399141 26.10016555434891

H 14.00167710229958 9.55120011846136 27.16227202648466

H 14.19546420931568 9.64507866793052 25.40441939569680

C 14.12327356349195 12.21565507962175 26.42698869124569

H 14.77287317526423 12.18752403541831 25.53838991983670

H 14.73430942375266 11.94684898422087 27.30180298386289

H 13.77865928454108 13.24891808004947 26.56409384296799

Cartesian coordinates of the optimized gas phase geometry of the complex **3′** (PBE/def2-TZVP, S= 0)

Ni 3.46992935601479 8.24848891114341 9.42394021291902

Ni 3.99945139093572 6.50413538060208 7.81811191628061

P 5.43802409058460 8.25154506453334 10.81854611458549

P 4.56181039361306 10.19398197523525 10.12900378103278

P 5.54958207834036 7.89532214133878 8.52478539023505

P 3.33021560240204 7.25291596799215 11.61208141382603

P 1.95928025350554 8.86440610564872 11.03495165267339

P 1.98769244389277 7.42772188551576 7.94189049390136

Si 6.19775518786027 10.08590306182417 8.59125307813643

P 3.03811412892156 5.85559703933306 9.76398130776037

P 0.92025785582594 5.92504414723546 9.19025352326131

Si 0.17882377280012 7.45958588247207 10.74315362369082

N 7.91835691136872 10.25101080937710 8.92771041929245

N 5.94524775562550 11.25223961616107 7.29714716796257

N 4.66270746557256 3.82708029602057 6.80730040053223

N 4.07596441236421 5.11155268750884 5.17535444381488

N -0.35251256947311 6.66204958938008 12.23807110575826

N -1.29048766039089 8.27048312199405 10.19762943542857

C 8.31791876215020 11.58999752164214 6.90637987306788

H 9.07811065361695 11.99787788315683 6.24062275214401

C 8.46995513236494 9.54734096977946 10.06072947224468

C 8.41850732214850 10.14485981765447 11.33799795865046

C 7.02052353217213 11.76020526796878 6.54140873502059

C	8.83136311988285	10.97134402647939	8.11676136638077
C	9.09648379431490	8.29609648385081	9.86572197145038
C	0.59330717355261	6.24718152304036	13.24823486824612
C	4.24541542037167	5.11406528264357	6.53988442820260
C	9.23017649433681	7.69380439232699	8.49454867978549
C	8.95374378505459	9.44243518335806	12.42662673714601
H	8.91282618198720	9.89631145122093	13.41935567285490
C	6.23209553027205	3.45777588130764	8.65390979784171
C	7.82446842625212	11.51180187477121	11.54056434766739
C	4.75190712244003	3.06648520350602	5.64842953918348
H	5.07137626116299	2.03136095612851	5.66637540030904
C	4.95153557134074	3.27184783908229	8.10583029077409
C	4.67381425801164	11.93522382423819	7.20672519774513
C	3.79740810554365	10.09089671976678	5.70179203765313
C	3.62862511544296	11.38745500039146	6.43741015413357
C	4.51808828244569	13.16731328547652	7.88106781833575
C	3.95368536175127	2.51328847600257	8.74443684317723
C	10.15018805741364	11.09117702214225	8.43348286001411
H	10.58200493106136	10.66035181404718	9.33369022313237
H	10.80527804408264	11.65039034260954	7.76844484192579
C	5.62995568083753	13.75078999678194	8.71054878756912
C	9.61742947626346	7.63063666538721	10.98178195452914
H	10.09746987434477	6.65928147867487	10.84070639227881
C	7.29262794536191	4.23569304484085	7.92611455156622
C	4.38250295988599	3.87313081377325	4.62163354441219
H	4.31235356914549	3.69032967516730	3.55604010975853
C	9.54093092563170	8.19154042396075	12.25590838523667
H	9.95148870577263	7.65753030730043	13.11489551556647
C	6.07969841438344	6.89122444809674	4.12343559984853
C	4.62413512064707	7.03901158143874	3.77238671840387
C	6.67478491544051	12.52114129048097	5.29008933549736
H	6.03559606193510	11.92592305600115	4.61970485788666
H	7.59072527664939	12.79422201731720	4.75266357292929
H	6.11826788859180	13.44391998797047	5.51510292173181
C	3.64511908779630	6.20750560649312	4.34459931835980
C	1.15935235455759	4.95560535240541	13.22238696962057
C	2.39458607186821	5.49241429409397	15.25072136878633
H	3.10374913623561	5.20005762632715	16.02727208478739
C	-1.21612280510547	9.26236963658676	9.14958375256752
C	3.29582837186696	13.84095649922917	7.76737146036496
H	3.16711592908399	14.79396409043817	8.28581294765775
C	2.59311045753372	2.32254487166951	8.13159780676526

C	6.48994547192097	2.88761348009227	9.90736192896030
H	7.47377242313162	3.02935069673223	10.35915813251260
C	4.26319594510477	1.95477300325269	9.99084843530459
H	3.50238357319896	1.36781719083663	10.50967556851989
C	-1.03179468548414	10.61634839596460	9.50637024378026
C	5.51551335074401	2.14617496275781	10.57243229047188
H	5.73544953256485	1.70965844509765	11.54825649134192
C	2.41922431262970	12.09011272293929	6.36026656945946
H	1.59983868982583	11.66461285029849	5.77786349200931
C	0.89631454803634	7.15149012284907	14.29440353330113
C	2.06516285027838	4.60255385424746	14.23433185020166
H	2.51037228716587	3.60473931955749	14.21768348938735
C	4.19520542240781	8.01481158277493	2.86403736927009
H	4.93676923932244	8.67088541225609	2.40350684306077
C	2.27583026016973	6.32767560265333	4.04812682956313
C	1.25466761212881	5.41410808978077	4.66784854790697
C	2.84464004111743	8.15781525009766	2.54991897634044
H	2.52945865068256	8.92444367679069	1.83982122321137
C	1.89527713093682	7.32761398590185	3.14354248102227
H	0.83721158213261	7.44407557938107	2.90019761689878
C	0.82178510769384	3.93851590248659	12.16398542738922
C	2.25091620106568	13.30729027860133	7.01549041450496
H	1.30151845586896	13.84116781025367	6.94271298256785
C	-1.72042470434779	6.44993458202417	12.49964356624129
C	1.80507814327490	6.75611462177416	15.28132143365424
H	2.04786869126308	7.45314343971763	16.08652737360059
C	-0.93985225427282	11.04451266990933	10.94605473939897
C	0.25969690744747	8.51315515010991	14.35534313277780
C	-2.59081454318014	7.97805547463608	10.68160412866780
C	-1.38911377740464	9.88185067102083	6.82008083132104
H	-1.55997330463528	9.59947014010445	5.77841780869356
C	-1.43515128790326	8.88649103549922	7.80590651907534
C	-2.71115957882509	7.02078273725284	11.76450247425228
H	-3.73453055014770	6.77017460781433	12.04101618740744
C	-0.99087367204020	11.57573775780120	8.48700498031152
H	-0.84273121591943	12.62392711324315	8.75601296938574
C	-2.07170841448027	5.54610134518581	13.65108738112157
H	-1.64435790915826	4.53931644101767	13.52781771919434
H	-3.16139721163083	5.45496691124431	13.72855733393954
H	-1.68749932922261	5.93449241835319	14.60675035804782
C	-3.70910825104113	8.57583043642078	10.18340425816843
H	-3.68220856058039	9.31321641000346	9.38529691728951

H -4.67659520159823	8.32161813766952	10.61180758215770
C -1.15889781328493	11.21451815060678	7.15215154745067
H -1.13514720923045	11.97729647095877	6.37110058298687
C -1.77466307405937	7.47151145707219	7.42023655320214
H 0.62173628417346	9.15711206884774	13.53714131902252
H -0.83471707132173	8.46271643196355	14.25623957787775
H 0.50142095432538	9.00934873518965	15.30439710877910
H 0.63253564178636	2.95624010848339	12.62263759965502
H -0.05763890736069	4.22228080401074	11.57422343357774
H 1.66186545903586	3.80981327140906	11.46170250884641
H -0.89031368637709	6.81483483441701	7.43749601707643
H -2.51776761927018	7.03949533388831	8.10497005964896
H -2.18501466243520	7.44433917636976	6.40146435960109
H 0.01683901703649	10.74382437024811	11.40165630010324
H -1.01635205326333	12.13713665045987	11.02465534283358
H -1.74519643547853	10.59397118406766	11.54402352927781
H 7.47879952172722	3.82745625602253	6.92084682239098
H 6.99143417092665	5.28678966120053	7.79868304024160
H 8.23718560525024	4.21543395685742	8.48402289617946
H 2.64922138466736	1.85941231339860	7.13491167666725
H 1.97074965363167	1.68168716698461	8.76887473843228

H 2.07338769990181	3.28640933030244	8.01206989547824
H 1.44422903935501	4.35927093474100	4.41557887291643
H 1.27057107778604	5.49123891338691	5.76584661567284
H 0.24582942331580	5.67065562311349	4.32096648911068
H 6.68587038447577	7.62613354203288	3.57906392766407
H 6.24172952309925	7.04084869010975	5.20215204641253
H 6.46063455790751	5.88755080289535	3.87964476819556
H 8.18020213759558	12.21903198872817	10.77789660253789
H 6.72360278643056	11.48639542475399	11.47640558123149
H 8.08913385273479	11.90330131241577	12.53179051235173
H 9.78295599231105	6.74611235222298	8.54107384876029
H 8.24504339294198	7.49215333194355	8.04465042577434
H 9.76160535229059	8.37690451841043	7.81491001202126
H 6.54618298432566	13.91542056621985	8.12295081211379
H 5.32289191242751	14.71045972550698	9.14625665362460
H 5.90838238567164	13.07780603005748	9.53672435315346
H 4.69595423186427	10.09605714597483	5.06768118333333
H 3.91037642877044	9.24432623798799	6.39767471911179
H 2.92751097040386	9.88572031999116	5.06597393068944

4.8   References of Supporting Information

[1]   M. R. Elsby and S. A. Johnson, J. Am. Chem. Soc. **2017**, *139*, 9401.

[2]   (a) M. R. Elsby, J. Liu, S. Zhu, L. Hu, G. Huang and S. A. Johnson, *Organometallics*, **2019**, *38*, 436; (b) D. Wang, X. Leng, S. Ye and L. Deng, *J. Am. Chem. Soc.* **2019**, *141*, 7731.

[3]   M. Driess, S. Yao, M. Brym, C. van Wüllen and D. Lentz, *J. Am. Chem. Soc*. **2006**, *128*, 9628.

[4]   Y. Xiong, S. Yao, M. Brym and M. Driess, *Angew. Chem. Int. Ed.* **2007**, *46*, 4511; *Angew. Chem.*, **2007**, *119*, 4595.

[5]   P. H. M. Budzelaar, *gNMR for Windows (5.0.6.0), NMR Simulation Program* **2006**.

[6]   (a) SCALE3ABS, CrysAlisPro, Aglient Technologies Inc. Oxford, GB, **2015**; (b) G. M. Sheldrick, SADABS, Bruker AXS, Madison, USA, **2007**.

[7]   R. C. Clark, J. S. Reid, *Acta Crystallogr. A*, **1995**, *51*, 887.

[8]   O. V. Dolomanov, L. J. Bourhis, R. J. Gildea, J. A. K. Howard, H. Puschmann, *J. Appl. Cryst.* **2009**, *42*, 339.

[9]   G. M. Sheldrick, *Acta Cryst.* **2015**, *A17*, 3.

[10]   G. M. Sheldrick, *Acta Cryst.* **2015**, *C71*, 3.

[11]   F. Neese, *Wiley Interdiscip. Rev. Comput. Mol. Sci.* **2012**, *2*, 73.

[12]   F. Weigend, *Phys. Chem. Chem. Phys.* **2002**, *4*, 4285.

[13]   F. Neese, F. Wennmohs, A. Hansen, U. Becker, *Chem. Phys.* **2009**, *356*, 98.

[14]   Perdew, Burke and Ernzerhof, *Phys. Rev. Lett.* **1996**, *77*, 3865.

[15]   F. Weigend, R. Ahlrichs, *Phys. Chem. Chem. Phys.* **2005**, *7*, 3297.

[16]   F. Weigend, *Phys. Chem. Chem. Phys.* **2006**, *8*, 1057.

[17]   E. D. Glendening, C. R. Landis, F. Weinhold, *J. Comput. Chem.* **2013**, *34*, 1429.

[18]   Gaussian 09, Revision E.01, M. J. Frisch, G. W. Trucks, H. B. Schlegel, G. E. Scuseria, M. A. Robb, J. R. Cheeseman, G. Scalmani, V. Barone, G. A. Petersson, H. Nakatsuji, X. Li, M. Caricato, A. Marenich, J. Bloino, B. G. Janesko, R. Gomperts, B. Mennucci, H. P. Hratchian, J. V. Ortiz, A. F. Izmaylov, J. L. Sonnenberg, D. Williams-Young, F. Ding, F. Lipparini, F. Egidi, J. Goings, B. Peng, A. Petrone, T. Henderson, D. Ranasinghe, V. G. Zakrzewski, J. Gao, N. Rega, G. Zheng, W. Liang, M. Hada, M. Ehara, K. Toyota, R. Fukuda, J. Hasegawa, M. Ishida, T. Nakajima, Y. Honda, O. Kitao, H. Nakai, T. Vreven, K. Throssell, J. A. Montgomery, Jr., J. E. Peralta, F. Ogliaro, M. Bearpark, J. J. Heyd, E. Brothers, K. N. Kudin, V. N. Staroverov, T. Keith, R. Kobayashi, J. Normand, K. Raghavachari, A. Rendell, J. C. Burant, S. S. Iyengar, J. Tomasi, M. Cossi, J. M. Millam, M. Klene, C. Adamo, R. Cammi, J. W. Ochterski, R. L. Martin, K. Morokuma, O. Farkas, J. B. Foresman, and D. J. Fox, Gaussian, Inc., Wallingford CT, **2009**.

[19]   G. Knizia, *J. Chem. Theory Comput.* **2013**, *9*, 4834.

[20]   J. Tao, J. P. Perdew, V. N. Staroverov and G. E. Scuseria, *Phys. Rev. Lett.* **2003**, *91*, 146401.

[21]   F. Jensen, *J. Chem. Theory Comput.* **2015**, *11*, 132.

Chapter 5 Coordination Studies of a Silabicyclotetraphosphane Towards the "Carbon-Free" Sandwich Complex $[Co(\eta^4\text{-}P_4)_2]^-$

Abstract: Heterometallic polyphosphido complexes $[K(thf)][Co\{(\mu\text{-}\eta^4\text{:}\eta^2\text{-}P_4)Si(nacnac')\}_2]$ (**1**, nacnac' = $CH[C(Me)N(Dipp)][C(CH_2)N(2,6\text{-}iPr_2C_6H_3)])$) and $[Li(diox)_2]_2[Fe\{(\mu\text{-}\eta^4\text{:}\eta^2\text{-}P_4)Si(nacnac')\}_2]$ (**2**) were synthesized by reacting $[(nacnac')Si(\eta^2\text{-}P_4)]$ with metallates $[K(thf)_{0.2}][Co(\eta^4\text{-}1,5\text{-}cod)_2]$ and $[Li(dme)]_2[Fe(\eta^4\text{-}1,5\text{-}cod)_2]$ (1,5-cod = 1,5-cyclooctadiene). While the formation of **1** is selective, several by-products were observed for the reaction forming **2**, including $[Li(diox)_3]_2[P_8\{Si(nacnac')\}]$ (**3**). The reactivity of **1** was studied aiming at protonation reactions and the elimination of [Si(nacnac')] ligands. Protonation of **1** with Brookhart's acid affords the neutral complex $[Co\{(\mu\text{-}\eta^4\text{:}\eta^2\text{-}P_4)Si(nacnac)\}_2][B(Ar^F)_4]$ (**5**, nacnac = $CH[CMeN(2,6\text{-}iPr_2C_6H_3)]_2$). Reaction of $[Me_4N]F$ with **1** led to the fragmentation of one silatetraphosphacyclopentadiene ligand, affording the *cyclo*-P_3 complex $[Me_4N]_2[(\eta^3\text{-}P_3)Co(\mu\text{-}\eta^4\text{:}\eta^2\text{-}P_4)Si(nacnac')]$ (**6**) and the hexacoordinated tetrafluorosilicate $[Me_4N][(nacnac)SiF_4]$ (**7**). Both compounds were identified by a single-crystal XRD experiment. The [Si(nacnac')] moiety is selectively eliminated upon treating **1** with benzoic acid, yielding the *cyclo*-P_4 complex $[(\eta^4\text{-}P_4)Co(\mu\text{-}\eta^4\text{:}\eta^2\text{-}P_4)Si(nacnac)]$ (**8**) in good yield. Subsequent treatment of complex **8** with KOPh results in a new species, which was characterized by multinuclear NMR spectroscopy, ESI mass spectrometry, and UV/VIS spectroscopy supported by TDDFT calculations. These data suggest the formation of a "carbon-free" sandwich compound $[K(18\text{-}crown\text{-}6)][(\eta^4\text{-}P_4)_2Co]$ (**9**).
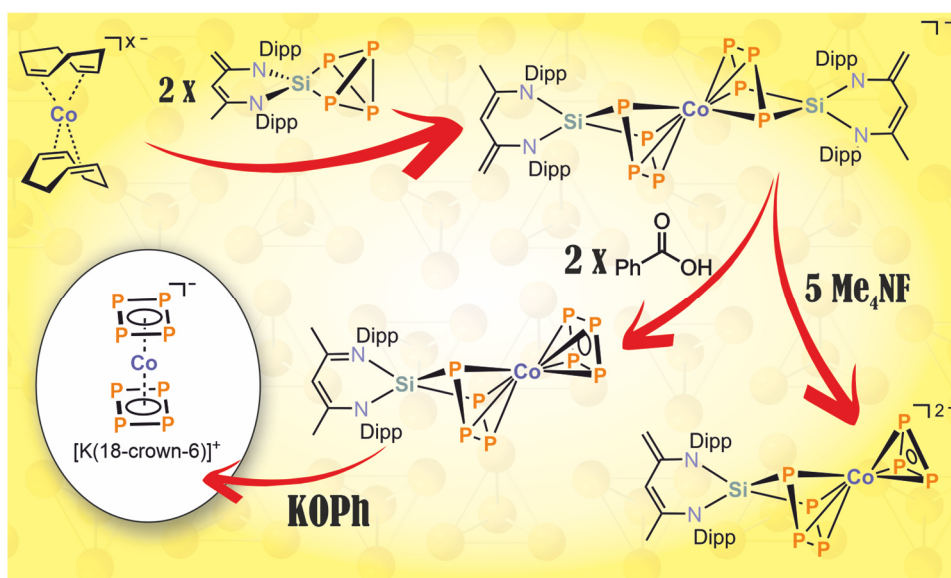
Christoph G. P. Ziegler synthesized and characterized all compounds reported in this chapter. Clemens Taube performed $^{31}P\{^1H\}$ NMR monitoring experiments. Jan. J. Weigand and Robert Wolf conceived the project and directed the investigations.

5.1 Introduction

The discovery of ferrocene, [Cp₂Fe] (Cp = C₅H₅), has been a landmark in organometallic chemistry. Since this breakthrough, innummerable sandwich complexes have been reported, which have found a large array of uses as synthetic buildingblock, catalyst, and are for example useful in medicine, or in other applications.[1],[2] Due to the diagonal relationship between phosphorus and carbon in the periodic table, it is possible to formally substitute CH units in metallocenes by electronically equivalent (isolobal) P atoms.[3] In seminal work, Baudler and co-workers in 1988 illustrated this concept by the synthesis of the first all-phosphorus analogue of Cp⁻, the pentaphosphacyclopentadienide P_5^- anion, which was trapped by FeCl₂ in presence of LiC₅Me₅ yielding the heteroleptic sandwich complex [Cp*Fe(η⁵-P₅)] (**A**, Cp* = η⁵-C₅Me₅, Scheme 1). The putative synthesis of decaphosphaferrocene, [Fe(P₅)₂], was also proposed based on IR spectroscopic data, but its existence could not be further substantiated.[4],[5] Instead, reactions of the P_5^- anion, which appears to be fairly stable as a dilute solution in THF solvent, result in high molecular weight solids.[4]

Nearly 15 years later, Ellis and co-workers described the preparation of the purely inorganic metallocene [(η⁵-P₅)₂Ti]²⁻ (**B**) by reaction of the highly reduced titanate [Ti(η⁴-C₁₀H₈)₃]²⁻ (C₁₀H₈ = naphthalene) with white phosphorus (P₄).[2] Based on this seminal result, it is tempting to speculate that related "carbon-free" bis(tetraphosphacyclobutadiene) complexes of type [M(P₄)]ˣ ought to exist as well. This hypothesis is further supported by the well-known chemistry of heteroleptic tetraphosphacyclobutadiene complexes.[6] In addition, the synthesis of a variety of homoleptic diphosphacyclobutadiene compounds has been reported. The first example of such a complex, [Ni(P₂C₂tBu₂)₂] (**D**), was prepared by Regitz and co-workers in early 1990 by the reduction of the Niᴵ precursor [Ni(acac)₂] (acac = acetylacetonate) with *n*-butyllithium *via* the subsequent cyclodimerization of *tert*-butylphosphaalkyne (*t*Bu−C≡P, *t*Bu = tert-butyl).[7] Later, Lammertsma and co-workers investigated the reaction of bis(anthracene)metallates [M(η⁴-C₁₄H₁₀)₂]⁻ (M = Fe, Co; C₁₄H₁₀ = anthracene) with phosphaalkynes such as *t*Bu−C≡P, *t*Pent−C≡P, and Ad−C≡P (*t*Pent = *tert*-pentyl, Ad = adamantyl) and the respective homoleptic bis(1,3-diphosphacyclobutadiene) complexes [M(P₂C₂R₂)₂]⁻ (**E**; M = Fe, Co) were isolated.[8]

Recently, Scheer and co-workers presented the first oligonuclear metal complexes of a bis(tetraphosphacyclobutadiene) sandwich complex. The [{(Cp‴Fe(CO)₂)₂(μ₃-η¹:¹:⁴-P₄)}₂Fe][PF₆]₂, (**F**, Cp‴ = 1,2,4-*t*Bu₃C₅H₂) features two formally aromatic, albeit metal-substituted *cyclo*-P₄ ligands which act as 6π-electron donors. This remarkable compound was obtained by the isomerization of the P₄-butterfly complex [{Cp‴Fe(CO)₂}₂(μ-η¹:¹-P₄)] observed upon its reaction with [Fe(MeCN)₆][PF₆]₂.[9] The preparation of the cobalt analogue [{(Cp‴Fe(CO)₂)₂(μ₃-η¹:¹:⁴-P₄)}₂Co][SbF₆]₃ by a similar route was reported soon afterwards.[10]

To date, a variety of heteroleptic *cyclo*-P$_4$ complexes are accessible by early[11] and late transition metals,[12],[13],[14],[15] commonly prepared by the direct reaction of white phosphorus with suitable L$_n$M precursors. Nonetheless, only two examples are known with cobalt.[12],[13] In 2017, the neutral [Cp'''Co(η^4-P$_4$)] complex was synthesized by Scheer and co-workers by the reaction of a 14-valence electron [Cp'''Co] metal fragment with P$_4$. However, this compound is unstable in solution and tends to dimerize to form two isomeric P$_8$ complexes.[12] More recently, our group showed that the reaction of a low-valent phenanthrene diimine cobaltate anion with P$_4$ yields the mononuclear *cyclo*-P$_4$ complex [(PHDI)Co(η^4-P$_4$)]$^-$ (**C**, PHDI = bis(2,6-diisopropylphenyl)phenanthrene-9,10-diimine).[13] By contrast, compound **C** is stable in solution and has turned out to be a suitable precursor for the targeted functionalization of the *cyclo*-P$_4$ unit into diorgano substituted pentaphosphido fragments.[13]
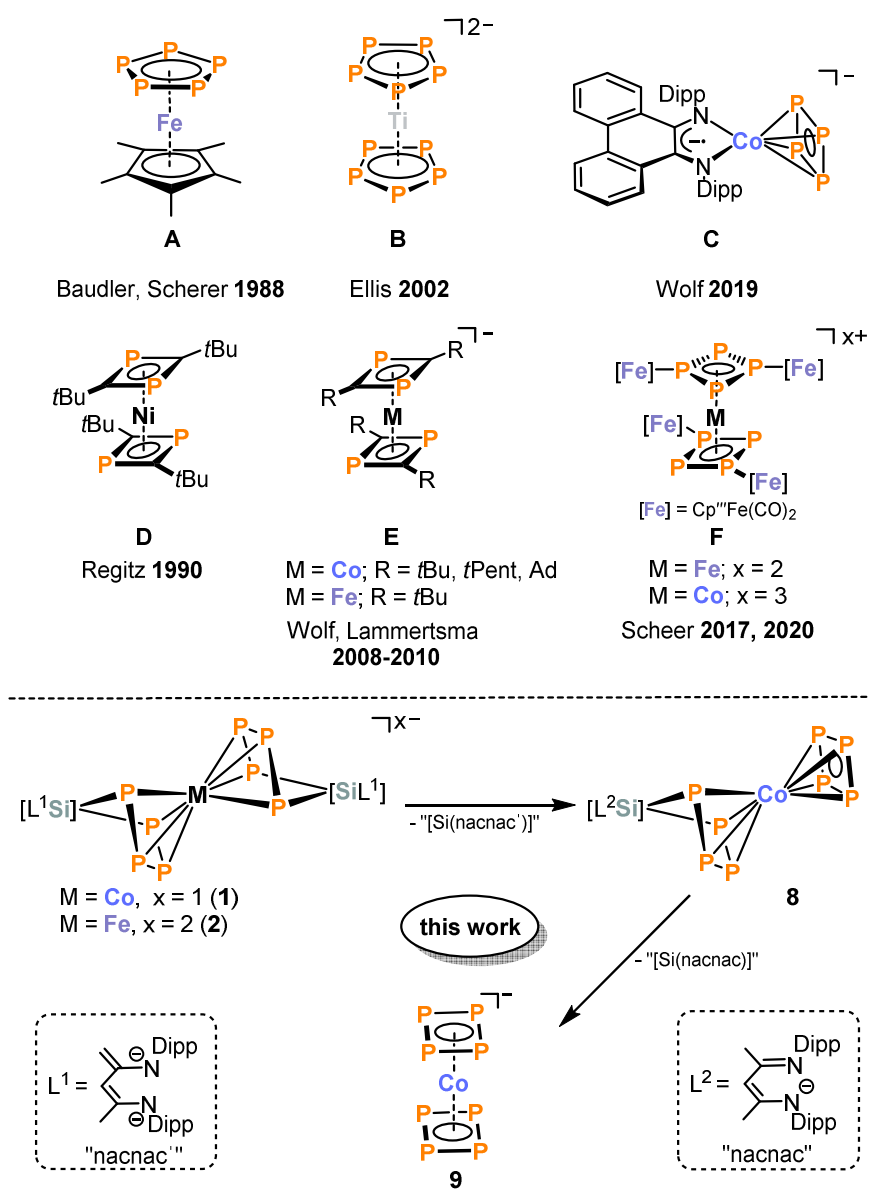
Figure 1. Examples of hetero- and homoleptic inorganic sandwich complexes.

Further investigations in the Wolf group targeted the direct reaction of white phosphorus with the bis(cyclooctadiene) cobaltate $[K(thf)_{0.2}][Co(\eta^4\text{-}1,5\text{-cod})_2]$ (1,5-cod = cyclooctadiene). However, numerous attempts only resulted in the decomposition of the starting materials. Due to this negative result, a more stable P_4 synthon was sought which might enable a more controlled reaction with the highly reactive cobaltate. Building on our previous investigations with $[(\text{nacnac})Ga(\eta^2\text{-}P_4)],$[16],[17] (nacnac = $CH[CMeN(2,6\text{-}i\text{Pr}_2C_6H_3)]_2$; see chapters 2 and 3 of this thesis) we turned towards the group 14 analogue $[(\text{nacnac}')Si(\eta^2\text{-}P_4)]$[18] (nacnac' = $CH[(C{=}CH_2)CMe][N(2,6\text{-}i\text{Pr}_2C_6H_3)]_2)$. Here we show that the simple reaction of $[K(thf)_{0.2}][Co(\eta^4\text{-}1,5\text{-cod})_2]$ with $[(\text{nacnac}')Si(\eta^2\text{-}P_4)]$ affords the heterometallic polyphosphido sandwich complex $[K(thf)][Co\{(\mu\text{-}\eta^4{:}\eta^2\text{-}P_4)Si(\text{nacnac}')\}_2]$ (**1**). The subsequent elimination of the [Si(nacnac')] fragments enables access to highly unusual *cyclo*-P_4 sandwich complexes, including the desired purely inorganic sandwich compound $[Co(P_4)_2]^-$.

5.2   Results and Discussion

The reactions of metallates $[K(thf)_{0.2}][Co(\eta^4\text{-}1,5\text{-cod})_2]$[19] and $[Li(dme)]_2[Fe(\eta^4\text{-}1,5\text{-cod})_2]$[20] with $[(\text{nacnac}')Si(\eta^2\text{-}P_4)]$[18] are shown in Scheme 1. Addition of $[K(thf)_{0.2}][Co(\eta^4\text{-}1,5\text{-cod})_2]$ (two equiv.) to a solution of $[(\text{nacnac}')Si(\eta^2\text{-}P_4)]$ in THF at low temperature (−80 °C) affords $[K(thf)][Co\{(\mu\text{-}\eta^4{:}\eta^2\text{-}P_4)Si(\text{nacnac}')\}_2]$ (**1**), which is identified by three multiplets ($\delta = -77.8, 127.7, 140.8$ ppm) in the $^{31}P\{^1H\}$ NMR spectrum in THF. $^{31}P\{^1H\}$ NMR monitoring of the reaction indicates that **1** is the only spectroscopically detectable P-containing product. Complex **1** was subsequently isolated in a moderate yield of 44% by crystallization from THF/*n*-hexane.

The analogous iron complex $[Li(diox)_2]_2[Fe\{(\mu\text{-}\eta^4{:}\eta^2\text{-}P_4)Si(\text{nacnac}')\}_2]$ (**2**) can be synthesized in a similar manner. However, $^{31}P\{^1H\}$ NMR monitoring of the reaction mixture revealed that this reaction is less selective and the formation of several other polyphosphorus species is visible (Figure S6, SI). Several attempts to separate these compounds were unsuccessful so far, as the reaction mixture tends to form poorly soluble brown oils when layering with less polar solvents. Nevertheless, a mixture of yellow and orange crystals was obtained from 1,4-dioxane/*n*-hexane, which were identified by X-ray crystallography as $[Li(diox)_2]_2[Fe\{(\mu\text{-}\eta^4{:}\eta^2\text{-}P_4)Si(\text{nacnac}')\}_2]$ (**2**) and a remarkable by-product $[Li(diox)_3]_2[P_8\{Si(\text{nacnac}')\}]$ (**3**), respectively.

A single-crystal X-ray diffraction (XRD) analysis of **1**, which was recrystallized from DME/*n*-hexane for better quality crystals, and **2** revealed that both complexes are structurally similar (see section 5.6.2, SI). The metal ion is sandwiched between two η^4-coordinated silatetraphosphacyclopentadiene rings (Figure 2). The phosphorus atoms form a bridging P_4 chain each coordinating to the metal center with all four P atoms, while only the terminal P atoms coordinate the silicon atom. As a result, the $[M\{(\mu\text{-}\eta^4{:}\eta^2\text{-}P_4)Si\}_2]$

(M = Co, Fe) units are in a syn conformation with a dihedral angle of P1–P2–P3–P4 of 1.18 ° for **1** and 1.71° for **2**. The terminal P–P bonds (for **1**: P1–P2 2.133(2) Å, P3–P4 2.127(2) Å) are shorter than the internal P–P bond (for **1**: P2–P3 2.162(2) Å) and the distance between the terminal P atoms (for **1**: P1–P4 3.275(2) Å) is too large for there to be any appreciable bond. The potassium counter ion in **1** is saturated by the coordination of three DME molecules in a distorted octahedral fashion. In contrast, the two lithium counter ions in **2** are each coordinated by one P atom of the [Fe{(μ-η⁴:η²-P₄)Si}₂] unit and additionally by 1,4-dioxane molecules forming a 3D-coordination-polymer (Li1–P4 2.588(5) Å, Li2–P1 2.642(4) Å, cf. the sum of the van-der-Waals radii of Li and P: 3.61 Å).[21] While the presence of the nacnac′ ligand in its deprotonated, dianionic form is clearly identified in **2** by the bond distances of the conjugated C–C π-bonds and by the exocyclic C–C double (C1–C2 1.364(3) Å, C9–C10 1.370(3) Å) and C–C single bonds (C4–C5 1.484(3) Å, C6–C7 1.490(3) Å) the C1–C2 and C4–C5 bond distances in **1** are nearly identical (C1–C2 1.453(6) Å, C4–C5 1.421(7) Å). This is explained by the comparatively poor quality of the crystal and an orientational disorder, which is common for this type of ligand (see section 5.6.1, SI).[18],[22] It is noteworthy that multinuclear NMR spectroscopy on the isolated complex **1** proves the β-diketiminate ligand is present in its dianionic form (*vide infra*).
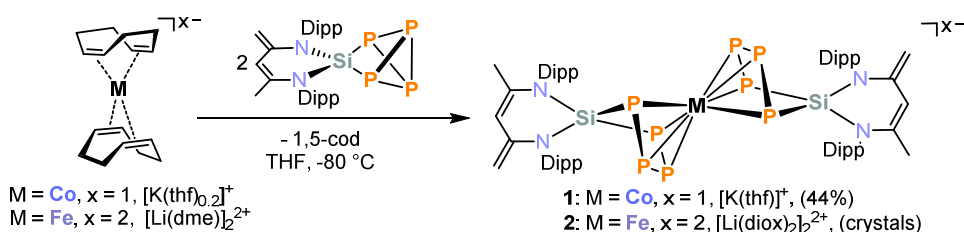
Scheme 1. Synthesis of [K(thf)][Co{(μ-η⁴:η²-P₄)Si(nacnac′)}₂] (**1**) and [Li(diox)₂]₂[Fe{(μ-η⁴:η²-P₄)Si(nacnac′)}₂] (**2**); reagents and conditions for **1**: [K(thf)₀.₂][Co(η⁴-1,5-cod)₂], for **2**: [Li(dme)]₂[Fe(η⁴-1,5-cod)].

Interestingly, such heterodinuclear inorganic sandwich complexes are scarce. The most closely related compound is [Cp*Fe(η⁴-P₄)Si(PhC(N*t*Bu)₂)] reported by Scheer and Roesky and co-workers very recently.[23] This species was obtained by the extrusion of a P atom and the consecutive insertion of a silylene into the *cyclo*-P₅ ring of [Cp*Fe(η⁴-P₅)], forming a silatetraphosphacyclopentadiene ligand with P−P bond distances in the range of 2.139(1) Å – 2.160(2) Å.[23] Similar anionic cobalt-gallium and iron-gallium compounds were reported by our group earlier, all displaying analogue [Co(μ-P₄)Ga] cores with alternating short-long-short bond distances of the P₄ units (2.1057(9) Å – 2.1825(9) Å).[16],[17] These structures of **1** and **2** are also reminiscent of a dizirconium complex of Fryzuk and co-workers[24] and of some neutral diiron complexes with *catena*-P₄ chains reported by the groups of Scherer,[25] Miluykov[26] and Walter.[27]

As already indicated, the reaction of $[Li(dme)]_2[Fe(\eta^4\text{-}1,5\text{-}cod)_2]$ with two equivalents $[(nacnac')Si(\eta^2\text{-}P_4)]$ is unselective and several P-containing by-products were formed, rendering the separation and isolation of the main product **2** difficult. One of these by-products tends to co-crystallize with **2** as orange crystals and was identified as $[Li(diox)_3]_2[P_8\{Si(nacnac')\}]$ (**3**).
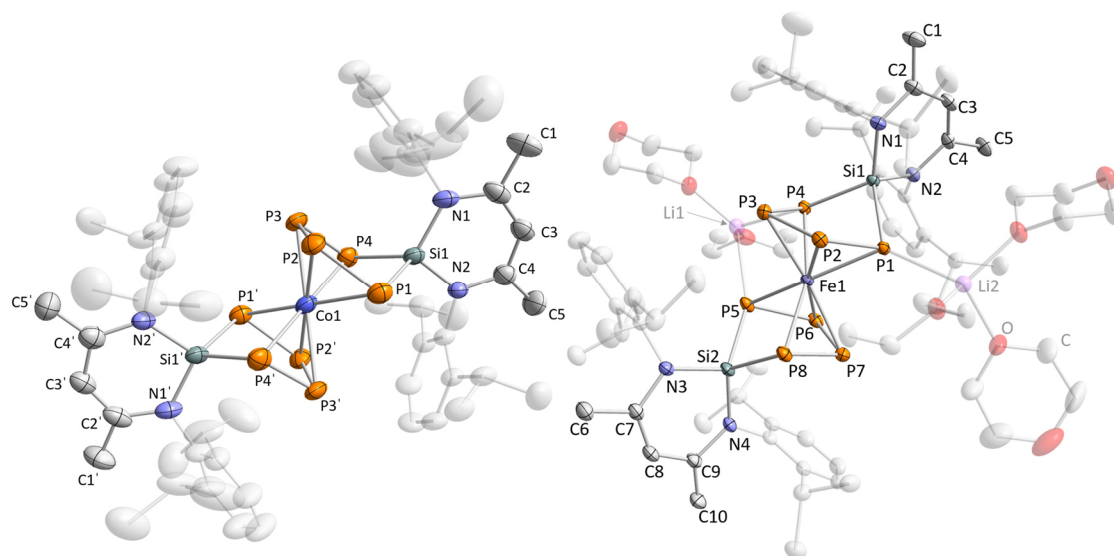
Figure 2. Solid-state molecular structure of **1** (left) and **2** (right). For **1** hydrogen atoms, counterion, solvate molecules, and disorders are omitted for clarity. For **2** hydrogen atoms, solvate molecules, and disorders are omitted for clarity; thermal ellipsoids are drawn at the 40% probability level. The crystal of **1** contains a second crystallographically independent molecule with very similar structural parameters; only one of these molecules is shown; selected bond lengths [Å] and angles [°] for **1** (in case of disorder bond lengths and angles were derived from the part with highest occupancy): P1–P2 2.133(2), P1–P4 3.275(2), P2–P3 2.162(2), P3–P4 2.127(2), Si1–P1 2.233(2), Si1–P4 2.222(1), Co1–P1 2.404(1), Co1–P2 2.309(1), Co1–P3 2.332(1), Co1–P4 2.391(1), C1–C2 1.453(6), C4–C5 1.421(7), P1–P2–P3 105.49(7), P2–P3–P4 104.79(6), P3–P4–Si1 100.67(6), P2–P1–Si1 100.40(6), P1–Si1–P4 94.64(6); selected bond lengths [Å] and angles [°] for **2**: P1–P2 2.1277(7), P1–P4 3.1678(7), P2–P3 2.1730(7), P3–P4 2.1424(7), P5–P6 2.1361(8), P5–P8 3.2093(7), P6–P7 2.1801(7), P7–P8 2.1234(8), S1–P1 2.2370(6), Si1–P4 2.2471(6), Si2–P5 2.2489(7), Si2–P8 2.2244(7), Fe1–P1 2.4083(5), Fe1–P2 2.3343(5), Fe1–P3 2.3199(7), Fe1–P4 2.3899(5), Fe1–P5 2.3951(5), Fe1–P6 2.3222(6), Fe1–P7 2.3247(7), Fe1–P8 2.4414(6), C1–C2 1.364(3), C4–C5 1.484(3), C6–C7 1.490(3), C9–C10 1.370(3), Li1–P4 2.588(5), Li2–P1 2.642(4), P1–P2–P3 104.58(3), P2–P3–P4 102.36(3), P3–P4–Si1 98.17(3), P2–P1–Si1 96.78(3), P1–Si1–P4 89.90(2), P5–P6–P7 101.77(3), P6–P7–P8 106.20(3), P7–P8–Si2 96.78(3), P6–P5–Si2 99.23(3), P5–Si2–P8 91.69(3).

The solid-state molecular structure of **3** is depicted in Figure 3. The structure shows a nortricyclic P_7 core with a single P atom bound to the P_7 cage. The basal phosphorus atoms (P4, P5, P6) form a nearly equilateral triangle (P–P 2.2066(7) Å – 2.2295(7) Å; internal angles 59.56(2)° – 60.59(2)°) and are connected to the equatorial P atoms (P1, P2, P3). These three atoms are additionally bound to the apical P atom (P7). One of the equatorial P atoms (P2) is connected to the phosphorus atom (P8) outside the P_7 cage *via* a bridging [Si(nacnac')] fragment, while the other equatorial P atoms (P1, P3) are coordinated by Li⁺ ions (P1–Li2 2.595(4) Å, P3–Li1 2.650(3) Å, cf. the sum of the van-der-Waals radii of Li and P: 3.61 Å).[21] The shortest P–P bonds are found within the core and are those of the P atoms coordinated to lithium (P1–P7 2.1434(7) Å, P1–P4 2.1787(7) Å and P3–P6 2.2158(7) Å), while the remaining P–P bonds (2.1903(6) Å – 2.2295(7) Å) are

significantly longer. Several anionic and neutral P_x^{n-} compounds with a nortricyclic P_7 framework are known in literature.[28] In addition, such a P_8 framework was observed for [(nacnac)GaBr]$_2$P$_8$ synthesized by Weigand and co-workers by reaction of white phosphorus with [Ga(nacnac)].[29] A very similar anionic analogue [{(Me$_3$Si)$_3$Si}$_2$P$_8$]$^-$ was presented by Hopkins, Wright and co-workers in 2007. This anion was synthesized by reacting [K(18-crown-6)][(Me$_3$Si)$_3$Si] with P$_4$.[30]
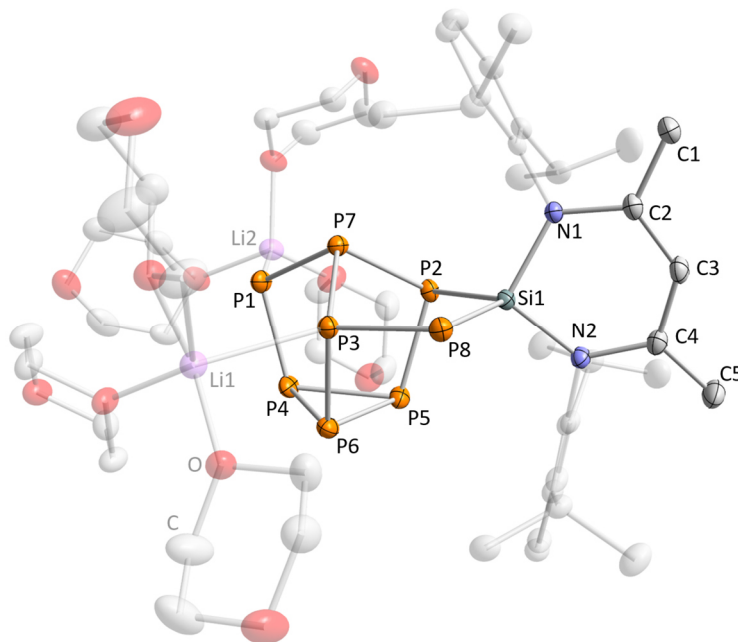
Figure 3. Solid-state molecular structure of **3**. Hydrogen atoms and solvate molecules are omitted for clarity; thermal ellipsoids are drawn at the 40% probability level. Selected bond lengths [Å] and angles [°]: P1–P7 2.1434(7), P2–P7 2.1903(6), P3–P7 2.2091(7), P5–P2 2.2104(6), P6–P3 2.2158(7), P4–P1 2.1787(7), P4–P5 2.2295(7), P5–P6 2.2066(7), P4–P6 2.2132(7), P3–P8 2.1599(6), P1–P2 3.3437(6), P1–P3 3.3734(7), P3–P2 3.2877(6), P2–P8 3.6566(5), P2–Si1 2.2832(5), P8–Si1 2.1978(6), P1–Li2 2 2.595(4), P3–Li1 2.650(3), C1–C2 1.466(3), C4–C5 1.383(3), P1–P7–P2 100.98 (3), P3–P7–P1 101.60(3), P3–P7–P2 96.72(2), P4–P5–P6 59.85(2), P5–P6–P5 60.59(2), P6–P4–P5 59.56(2), P2–Si1–P8 109.37(2), P1–P2–P3 61.15(1), P2–P3–P1 60.25(1), P3–P1–P2 58.61(1).

Despite many attempts, it was not possible to isolate/separate complexes **2** and **3** in a pure form. Therefore, subsequent discussions and reactivity studies focus exclusively on **1**, which was fully characterized by C, H, N combustion analysis and multinuclear NMR spectroscopy. The ^{1}H NMR spectrum of **1** shows broad signals, which nevertheless confirm the presence of all molecular components. Despite the broad resonances observed in the ^{1}H NMR spectrum, the ^{13}C{^{1}H}, and the ^{29}Si NMR spectra (see Figures S3 and S5, SI) are well-resolved and particularly informative, because they clearly indicate the presence of two isomers in solution due to the asymmetric nacnac′ β-diketiminate ligand. This was also found in an unusual Ni$_2$Si$_2$P$_8$ cluster capped by two [Si(nacnac′)] fragments described in Chapter 4 of this thesis (*vide supra*).[22] The presence of a symmetric and an asymmetric isomer is indicated by the ^{29}Si NMR spectrum, which shows three triplet resonances in a 1:2:1 integral ratio. The signal with the highest intensity at δ = 19.5 ppm (^1J(^{31}P^{29}Si) = 112.1 Hz) can be assigned to the symmetrical isomer, whereas the two remaining triplets at δ = 16.0 ppm (^1J(^{31}P^{29}Si) = 106.5 Hz) and δ = 25.7 ppm (^1J(^{31}P^{29}Si) =

119.1 Hz) can be assigned to the unsymmetrical isomer (see section 5.5.2, Figure S5, SI). As a result, the $^{31}P\{^{1}H\}$ NMR spectrum (see Figures S4, SI) of **1** is complex showing three multiplets resonating at $\delta = -77.8$ ppm, 127.7ppm, and 140.8 ppm with an integral ratio of 2:2:4. These signals arise from the overlapping multiplets of the two isomers, which are expected to show unsymmetrical ABCD spin systems. Unfortunately, it was not possible to determine the J_{PP} coupling constants by an iterative fit of the $^{31}P\{^{1}H\}$ NMR spectrum due to the severe overlap of the resonances.

Initial reactivity studies of **1** focused on reactions with phosphorus electrophiles, such as alkyl/arylchlorophosphanes, which have been shown to be suitable reagents for the targeted synthesis of 1,1-diorganopentaphosphido ligands *via* a P–P condensation reaction.[16] However, these reactions resulted in the formation of intractable products. Reviewing related literature reveals that the unsaturated backbone of the nacnac′ β-diketiminate ligand of [Si(nacnac′)] seems to have a high affinity toward electrophiles as highlighted in several reports from Driess and co-workers.[31] Especially relevant is the protonation of [Si(nacnac′)] by [H(OEt₂)₂][B(C₆F₅)₄] which affords a remarkable silyliumylidene cation [Si(nacnac)]⁺.[31],[32] Bearing this in mind, the reaction of [(nacnac′)Si(η²-P₄)] toward Brønsted acids was initially investigated. The 1:1 reaction of [(nacnac′)Si(η²-P₄)] with [H(OEt₂)₂][BArF₄] (BArF₄ = tetrakis[3,5-bis(trifluoromethyl)phenyl]borate) at low temperatures (−60 °C) proceeds selectively according to ^{31}P NMR monitoring. After work-up, yellow needles of [(nacnac)Si(η²-P₄)][BArF₄] (**4**) suitable for XRD analysis were isolated in pure form in 36% yield (Scheme 2).
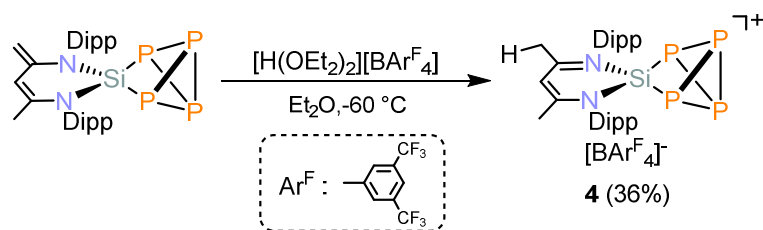
Scheme 2. Synthesis of [(nacnac)Si(η²-P₄)][BArF₄] (**4**) by protonation of [(nacnac′)Si(η²-P₄)] with Brookhart's acid.
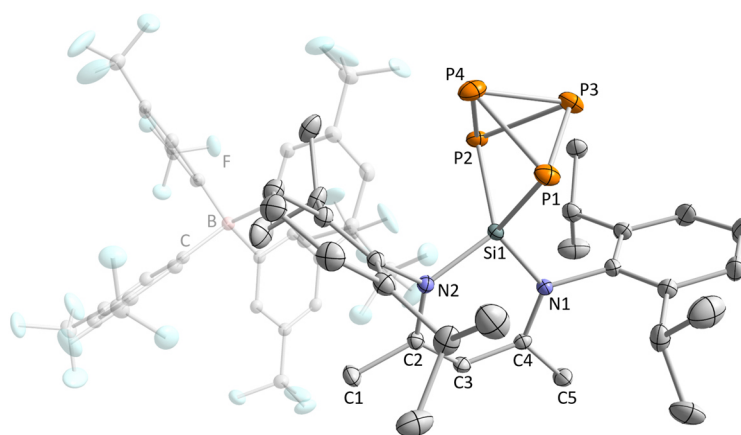
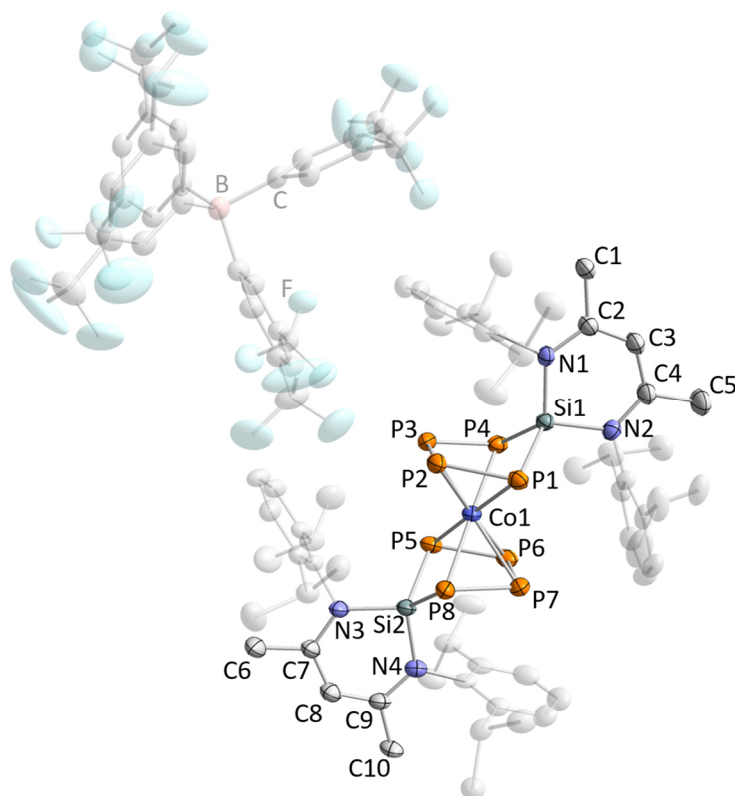**Figure 4.** Solid-state molecular structure of **4**. Hydrogen atoms are omitted for clarity; thermal ellipsoids are drawn at the 40% probability level. Selected bond lengths [Å] and angles [°]: P1–P3 2.23779(6), P1–P4 2.23358(6), P3–P4 2.15550(5), P2–P3 2.24812(8), P2–P4 2.23980(6), P1–P2 3.13510(9), Si1–P1 2.21887(7), Si1–P2 2.21669(6), C1–C2 1.50014(5), C4–C5 1.49710(3), P1–P3–P4 61.09(2), P3–P4–P1 61.27(2), P4–P1–P3 57.64(2), P2–P4–P3 61.49(2), P4–P3–P2 61.10(2), P3–P2–P4 57.41(2), P1–P4–P2 88.98(2), P1–P3–P2 88.67(3).

The molecular structure of **4** is depicted in Figure 4 and consists of a separated ion pair (shortest Si−F distance: 3.503(2) Å). The P₄ ligand is η²-coordinated to the silicon atom forming a tricyclic SiP₄ core. As expected, the P–P bond distances are in a similar range (2.155(5) Å − 2.2398(6) Å) as in the starting material [(nacnac′)Si(η²-P₄)] (2.159(2) Å − 2.235(2) Å)[18] and to other comparable [LM(η²-P₄)] (M = Ga,[33] Ge)[34] species with a tricyclo[3.1.0]pentane-like structure. The six membered C₃N₂Si skeleton is nearly planar (dihedral angle N1−C4−C2−N2 0.9(1)°) and bond lengths and N1−Si1−N2 angle (99.78(6)°) are almost identical with those observed in [(nacnac)Si][B(C₆F₅)₄] which was reported by Driess and co-workers.[32] The same is true for the exocyclic C1–C2 and C4–C5 bond distances (C1–C2 1.50014(5) Å, C4–C5 1.49710(3) Å) which lie in a typical range of C−C single bonds indicating the protonation of the former nacnac′ backbone.[35],[36]

The ¹H, ¹³C{¹H}, ³¹P{¹H}, and ²⁹Si NMR spectra of **4** are in line with the solid-state molecular structure and confirm the presence of a formally monoanionic β-diketiminate ligand. Compared to the related complex [(nacnac)Si][B(C₆F₅)₄] the p$_\pi$–p$_\pi$ donor–acceptor interaction between the π-electron system of the β-diketiminato ligand and the Si atom seems to be less pronounced which can be explained by the additional Si bound P₄ unit. This is further reflected in the ¹H NMR spectrum of **4** (Figure S7, SI) in which the resonance of the γ-C*H* atom (δ = 5.92 ppm) is more shielded than in the related compound [(nacnac)Si][B(C₆F₅)₄] (δ = 6.79 ppm).[32] Similar to previously reported complexes [LM(η²-P₄)] (cf. examples with M = Ga,[33] Zr, Hf)[37] the ³¹P{¹H} NMR spectrum shows a symmetric A₂X₂ spin system with two chemically inequivalent ³¹P nuclei resonating at δ(P$_A$) = –336.6 ppm and δ(P$_X$) = 92.5 ppm (Figure S9, SI). Each signal splits into a triplet with a ¹*J*(P$_A$,P$_X$) coupling constant of −173 Hz. The ²⁹Si satellites are well resolved and can be observed at the low field shifted P$_X$ atom (δ(P$_X$) = 92.5 ppm) with a ¹*J*(P$_X$,Si)

coupling constant of 56 Hz. This is consistent with the ^{29}Si NMR spectrum of **4**, which shows the corresponding triplet resonating at $\delta = -39.9$ ppm (Figure S12, SI). The chemical shift of the silicon atom is nearly identical to the starting material [(nacnac′)Si(η²-P₄)] ($\delta = -40.4$ ppm). However, the ^1J(P,Si) coupling constant differs and is about 24 Hz smaller in magnitude.[18]

We then turned our attention to the inorganic sandwich complex **1** and its reactivity towards Brønsted acids. While strong acids such as HCl lead to the formation of insoluble particles, the reaction with two equivalents of [H(OEt₂)₂][BArF₄] at −60 °C yielded the formation of the desired protonated complex [Co{(μ-η⁴:η²-P₄)Si(nacnac)}₂][B(Ar^F)₄] (**5**) as analytically pure crystals in a yield of 36% (Scheme 3).
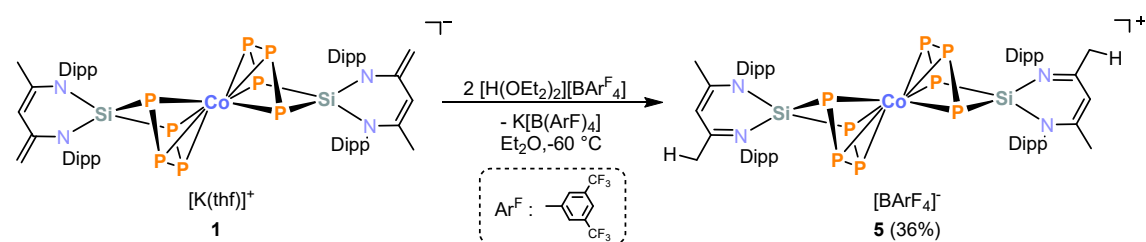
Scheme 3. Synthesis of [Co{(μ-η⁴:η²-P₄)Si(nacnac)}₂][BAr^{F}₄] (**5**) by protonation of [K(thf)][Co{(μ-η⁴:η²-P₄)Si(nacnac′)}₂] (**1**) with two equivalents of Brookhart's acid.

Complex **5** crystallizes in the space group P-1 and its molecular structure is depicted in Figure 5 (see section 5.6.4). The main structural motif of **5** is reminiscent of the anionic complexes **1** and **2** showing a similar [Co{(μ-η⁴:η²-P₄)Si}₂] core. The bridging *catena*-P₄ fragment binds to the cobalt center with all four P atoms, while only the terminal P atoms are connected to the [Si(nacnac)] fragment. Like in **1** and **2** the P−P bond distances of **5** are alternating in a short-long-short pattern with short terminal P–P bonds (range 2.129(2) Å – 2.135(2) Å) and elongated internal P–P distances (P2–P3 2.166(2) Å, P6–P7 2.156(2) Å). The C−C bonds in **5** are all in the expected range of C−C single bonds (1.497(8) Å − 1.511(7) Å). This additionally confirms the successful protonation of the nacnac′ backbone.

Figure 5. Solid-state molecular structure of **5**. Hydrogen atoms, solvate molecules, and disorder are omitted for clarity; thermal ellipsoids are drawn at the 40% probability level. The crystal of **5** contains three crystallographically independent molecules with very similar structural parameters; only one of these molecules is shown; selected bond lengths [Å] and angles [°] (in case of disorder bond lengths and angles were derived from the part with highest occupancy): P1–P2 2.133(2), P1–P4 3.335(2), P2–P3 2.166(2), P3–P4 2.135(2), P5–P6 2.129(2), P5–P8 3.347(2), P6–P7 2.156(2), P7–P8 2.134(2), S1–P1 2.203(2), Si1–P4 2.204(2), Si2–P5 2.214(2), Si2–P8 2.213(2), Co1–P1 2.407(1), Co1–P2 2.315(1), Co1–P3 2.311(1), Co1–P4 2.382(1), Co1–P5 2.397(1), Co1–P6 2.315(1), Co1–P7 2.312(1), Co1–P8 2.387(1), C1–C2 1.501(7), C4–C5 1.497(8), C6–C7 1.503(7), C9–C10 1.511(7), P1–P2–P3 105.81(7), P2–P3–P4 105.96(7), P3–P4–Si1 95.86(7), P2–P1–Si1 96.34(7), P1–Si1–P4 98.35(7), P5–P6–P7 105.88(7), P6–P7–P8 106.54(7), P7–P8–Si2 97.72(7), P6–P5–Si2 98.54(7), P5–Si2–P8 98.23(7).

^{1}H NMR spectroscopy on **5** was performed in CD$_2$Cl$_2$ avoiding an undesirable overlap of the solvent signals. The ^{1}H NMR spectrum of complex **5** is in line with the solid-state molecular structure and two single resonances at δ = 1.78 ppm and 2.10 ppm with the correct integral ratio are observed for the exocyclic CH$_3$ groups of the β-diketiminate backbone. The ^{31}P{^{1}H} NMR spectrum shows two resonances at δ(A) = –90.4 ppm and δ(X) = 138.9 ppm in a 1:1 integral ratio. With regard to literature, it is likely that the multiplet at low frequency (–90.4 ppm) can be assigned to the terminal P atoms (P$_x$) of the P$_4$ chain, whereas the multiplet at high frequency can be assigned to the internal P atoms (Figure 6).[16],[17],[23] An iterative fitting procedure was successful for a symmetric AA′A″A‴XX′X″X‴ spin system and revealed the J_{PP} coupling constants (see Figure 6, Figure S15 and Figure S19, SI). The $^1J_{PP}$ coupling constants of heterodinuclear *catena*-P$_4$ complexes are commonly large in magnitude,[16],[17],[23] and this is also observed in compound **5** with $^1J_{PP}$ coupling constants ranging from −464.0 Hz to −381.3 Hz. The $^2J_{PP}$ (16.9 Hz−21.8 Hz) and $^3J_{PP}$ (−16.7 Hz − −5.3 Hz) coupling constants are rather small and similar to those found in the related complex [Cp*Fe(η^4-P$_4$)Si(PhC(NtBu)$_2$)].[23] This is in

line with the constrained alignment of the P atoms in the P_4 chain observed in the solid-state structure, causing an antiparallel orientation of the lone pairs.[16],[38] Notably, the two [(nacnac)Si(μ-P_4)] ligands seem to interact with each other as the iterative fit only converges to reasonable results if J_{PP} coupling is allowed through the cobalt ion or through space (range from −36.2 Hz − 49.2 Hz, see the SI for details). Several reports for such a long-range J_{PP} coupling of polyphosphorus compounds are found in literature.[22],[39] Due to the complexity of the ${}^{31}P\{{}^1H\}$ NMR spectrum and the broadened signals the commonly small contribution of the ${}^{29}Si$ satellites were not observed and thus excluded in the iterative fitting procedure. However, the ${}^{29}Si$ NMR spectrum of **5** in CD_2Cl_2 reveals the expected triplet resonance at $\delta = 21.2$ ppm. This is in accordance with the signals observed in the related complex **1** ($\delta = 16.0, 19.5, 25.7$ ppm). The ${}^1J({}^{31}P{}^{29}Si)$ coupling constant is 144 Hz and in a similar range to **1** and appears to be nearly identical to the closely related complex [Cp*Fe(η⁴-P_4)Si(PhC(NtBu)₂)] for which a ${}^1J({}^{31}P{}^{29}Si)$ coupling constant of 145.5 Hz has been reported. Interestingly, the ${}^{29}Si$ resonance in [Cp*Fe(η⁴-P_4)Si(PhC(NtBu)₂)] is shifted approximately 20 ppm to the lower field, which is mainly accounted to the different ligand system connected to the Si center.[23]
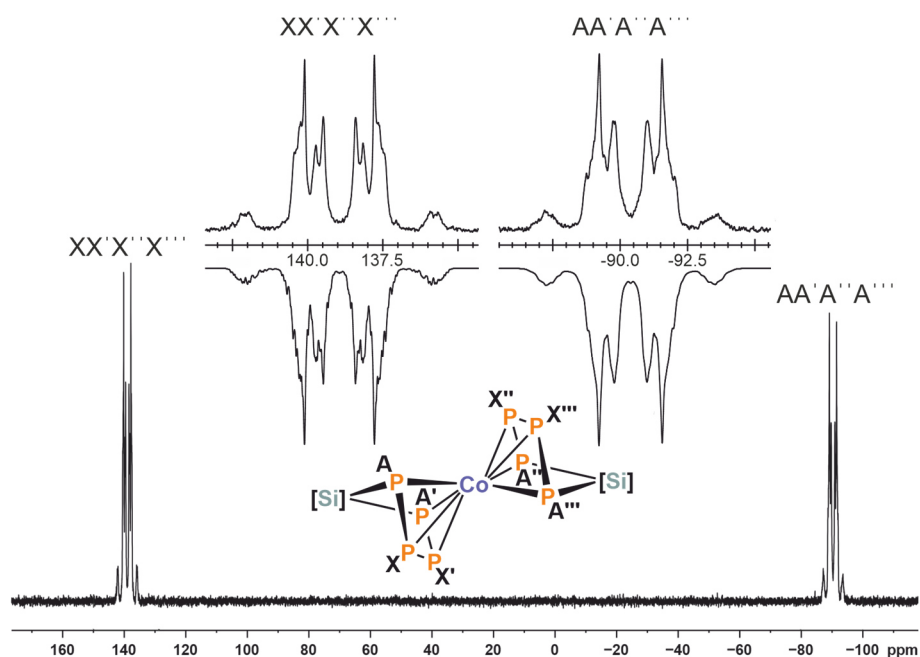
Figure 6. ${}^{31}P\{{}^1H\}$ NMR spectrum of compound **5** with nuclei assigned to AA′A″A‴XX′X″X‴ spin system; insets: extended signals (upwards) and simulations (downwards); selected $\delta(P_{AA'A''A'''}) = -90.4$ ppm, $\delta(P_{XX'X''X'''}) = 138.9$ ppm; selected $J({}^{31}P,{}^{31}P)$ coupling constants: ${}^1J_{XX'} = {}^1J_{X'X} = -419.1$ Hz, ${}^1J_{XA} = {}^1J_{A'X} = -464.0$ Hz, ${}^2J_{AX'} = {}^2J_{A'X} = 16.9$ Hz, ${}^3J_{A'A} = {}^3J_{AA'} = -5.6$ Hz, ${}^1J_{X''X'''} = {}^1J_{X'''X''} = -381.3$ Hz, ${}^1J_{X''A''} = {}^1J_{A'''X'''} = -438.7$ Hz, ${}^2J_{A''X'''} = {}^2J_{A'''X''} = 21.8$ Hz, ${}^3J_{A''A''} = {}^3J_{A''A''} = -16.7$ Hz; [Si] = (nacnac)Si.

Having substantial quantities of the inorganic sandwich complexes **1** and **5** in hand, reactions of these compounds were examined in the hope of releasing the [Si(nacnac′)] fragment. Initial reactions were based on the high affinity of fluoride to silicon which is reflected in the large bond dissociation energy of 135 kcal·mol⁻¹.[40] Of the fluorinating

agents used (e.g. [Me$_4$N]F, CsF, KHF$_2$, selectfluor, N-fluorodibenzenesulfonimide (NFSI)) only the reaction with [Me$_4$N]F seemed to be promising. Upon the addition of **1** to a suspension of [Me$_4$N]F in THF a new set of signals appeared in the corresponding ^{31}P$\{^1$H$\}$ NMR spectrum which might tentatively be assigned to an AMM′XX′ spin system. Five equivalents of the fluorine source are necessary to fully consume the starting material (Scheme 4). After extraction of the reaction mixture with fluorobenzene brownish-yellow blocks and colorless needles were obtained after slow evaporation of a concentrated DME solution. A single-crystal X-ray diffraction experiment revealed the molecular structures of [Me$_4$N]$_2$[(η^3-P$_3$)Co(μ-η^4:η^2-P$_4$)Si(nacnac′)] (**6**) and [Me$_4$N][(nacnac)SiF$_4$] (**7**), respectively. It is worth mentioning that performing the same reaction with **5** instead of **1** gives a silent ^{31}P$\{^1$H$\}$ NMR spectrum.
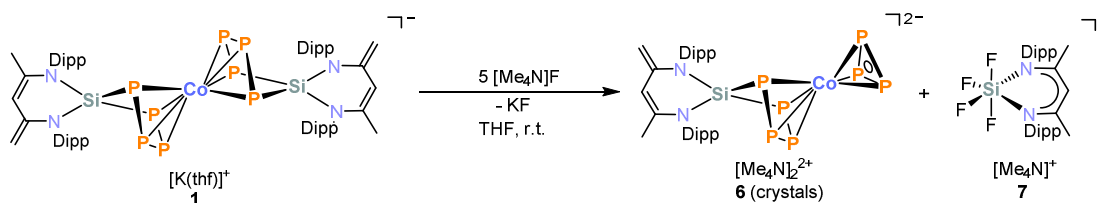
Scheme 4. Synthesis of [Me$_4$N]$_2$[(η^3-P$_3$)Co(μ-η^4:η^2-P$_4$)Si(nacnac′)] (**6**); reagents and conditions for **6**: 5 equiv. [Me$_4$N]F.

The solid-state molecular structures of anions **6** and **7** are depicted in Figure 7. Intriguingly, the molecular structure of complex **6** shows the transition metal ion to be sandwiched between an η^4-coordinated silatetraphosphacyclopentadiene ligand and a *cyclo*-P$_3$ ring. This confirms that the elimination of the [Si(nacnac′)] moiety is in principle possible. Transition metal complexes featuring a *cyclo*-P$_3$ ring are already known[41] and some examples of the targeted fragmentation of polyphosphido complexes leading to *cyclo*-P$_3$ moieties are reported in literature.[13],[42] For instance, our group presented the [3+2] fragmentation of a pentaphosphido cobalt complex with tetraalkylammonium or potassium cyanide resulting in a cyclotriphosphido cobaltate anion [(PHDI)Co(η^3-P$_3$)(CN)]⁻ and 1-cyanodiphosphan-1-ide anions [R$_2$PPCN]⁻ (R = Cy, *t*Bu, Ph, Mes, N(*i*Pr)$_2$).[13] At the same time, Scheer and co-workers published the fragmentation of [Cp′′′Co(η^4-P$_4$)] (Cp′′′ = 1,2,4-*t*Bu$_3$C$_5$H$_2$) with ^{Me}NHC (^{Me}NHC=1,3,4,5-tetramethylimidazol-2-ylidene) yielding the ring contraction product [(^{Me}NHC)$_2$P][Cp′′′Co(η^3-P$_3$)].[42]

The mean P−P (2.159(2) Å) and Co−P (2.271(1) Å) bond lengths in **6** are similar to that of Scheer's [(^{Me}NHC)$_2$P][Cp′′′Co(η^3-P$_3$)] complex (average P−P 2.1588(6) Å, Co−P 2.2651(5) Å)[42] and are slightly elongated compared to the *cyclo*-P$_3$ anion in [(PHDI)Co(η^3-P$_3$)(CN)]⁻ reported by Wolf and co-workers (average P−P 2.1361(8) Å, Co−P 2.300(5) Å).[13] The presence of the *cyclo*-P$_3$ ligand in **6** is also reflected in the corresponding ^{31}P$\{^1$H$\}$ NMR spectrum of the reaction mixture appearing as a singlet at

$\delta = -295.3$ ppm. This fits well to related neutral species such as $[(ArNC)_3Co(\eta^3-P_3)]$ (Ar = 2,6-(Mes)$_2$C$_6$H$_3$, $\delta = -276$ ppm),[43] and $[(CH_3C(CH_2PPh_2)_3)Co(\eta^3-P_3)]$ ($\delta = -278$ ppm),[44] as well as to the anionic compounds $[Cp'''Co(\eta^3-P_3)]^-$ ($\delta = -313$ ppm),[42] and $[(PHDI)Co(\eta^3-P_3)(CN)]^-$ ($\delta = -192$ ppm).[13] The remaining two mulitplets observed in the $^{31}P\{^1H\}$ NMR spectrum of **6** are tentatively assigned to a MM'XX' spin system ($\delta_{MM'} = -117.0$ ppm, $\delta_{XX'} = 54.9$ ppm). It is plausible that the signal resonating at high field can be assigned to the terminal P$_{MM'}$ atoms of η^4-coordinated silatetraphosphacyclopentadiene ligand and the internal P$_{XX'}$ atoms resonate at lower field. This is common and typically observed for related heterodinuclear complexes $[M(\mu-P_4)M']$ (M' = Co, Fe; M = Ga, Si) such as $[Cp^*Fe(\eta^4-P_4)Si(PhC(N\mathit{t}Bu)_2)]$ and supports the assignment of the $^{31}P\{^1H\}$ resonances.[16],[17],[23] The β-diketiminato ligand is present in its doubly deprotonated, dianionic form as the exocyclic C−C bond distances are clearly distinct (C1–C2 1.471(6) Å and C4–C5 1.379(6) Å).

The XRD analysis of the co-crystallized colorless needles confirms the fate of the former [Si(nacnac')] fragment and additionally explains the need for five equivalents of [Me₄N]F. The result of the XRD experiment is depicted in Figure 7 and reveals it is a hexacoordinated fluorosilicate. The central Si atom adopts a close to ideal octahedral geometry with four fluorine atoms and a β-diketiminato ligand. The distances of the four Si−F bonds are of similar magnitude (range 1.669(1) Å – 1.672(2) Å) and are nearly identical with an 8-(dimethylamino)naphthyl) substituted tetrafluorosilicate reported by Corriu and co-workers in 1991.[45] In addition these bond lengths resemble those of SiF_6^{2-} salts.[46] It is noteworthy that the former nacnac' backbone seems to be protonated to form the monoanionic nacnac ligand. This is reflected in the similar C−C bond distances of the exocyclic C1−C2 (1.515(3) Å) and C4−C5 (1.511(2) Å) bond lengths. It is likely that the proton originates from traces of moisture as it is known that ammonium salts are extremely hygroscopic. The Si coordinated β-diketiminato ligand in **7** is slightly folded at the N1−N2 vector with a plane-to-plane angle (plane(N1,Si1,N2) to plane(N1,C2,C3,C4,N2)) by about 27.93(9)°. The Si−N bond distances are approximately 0.2 Å elongated compared to those in related [Si(nacnac)] compounds featuring a monoionic β-diketiminate ligand.[32]
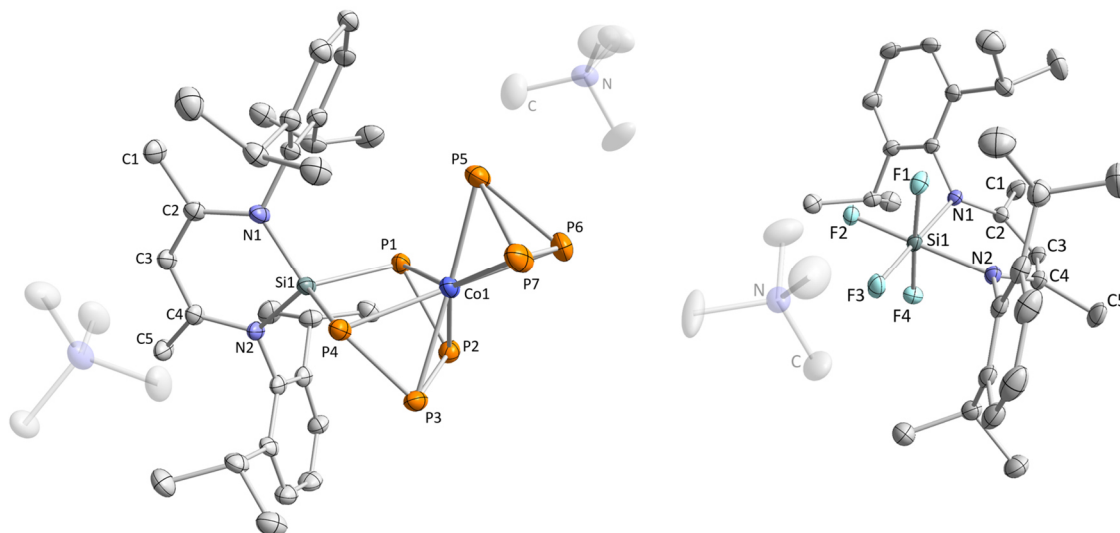
Figure 7. Solid-state molecular structure of **6** (left) and **7** (right). For **6** hydrogen atoms, solvate molecules and disorders are omitted for clarity. For **6** hydrogen atoms and disorders are omitted for clarity; thermal ellipsoids are drawn at the 40% probability level; selected bond lengths [Å] and angles [°] for **6**: P1–P2 2.131(2), P1–P4 3.358(2), P2–P3 2.172(2), P3–P4 2.138(2), P5–P6 2.163(2), P6–P7 2.155(2), P7–P5 2.161(2), C1–C2 1.471(6), C4–C5 1.379(6), Si1–P1 2.226(2), Si1–P4 2.222(2), P1–P2–P3 105.90(6), P2–P3–P4 106.37(6), P3–P4–Si1 99.81(6), P2–P1–Si1 100.07(6), P1–Si1–P4 98.07(6), P5–P6–P7 60.07(5), P6–P7–P5 60.14.(6), P7–P5–P6 59.79(7); selected bond lengths [Å] and angles [°] for **7**: C1–C2 1.515(3), C4–C5 1.511(2), F1–Si1 1.669(1), F2–Si1 1.672(1), F3–Si1 1.672(2), F4–Si1 1.671(1), fold angle: 27.93(9) defined by plane(N1,Si1,N2) and plane(N1,C2,C3,C4,N2).

Compounds **6** and **7** are insoluble in hydrocarbons and diethyl ether and only sparingly soluble in toluene. Due to their similar solubility, the separation and isolation of complexes **6** and **7** in their pure form was unsuccessful.

In summary, this reaction might be considered as a [3+1] fragmentation similar to the NHC-induced ring contraction reactions reported by Scheer and co-workers[42] and the substitution reactions of silylenes in a metal-coordinated polyphosphide.[23] However, the fate of the abstracted phosphorus atom remains unclear.

With some initial success in removing the [Si(nacnac′)] unit, we next explored the reactivity of **1** toward alcohols and carboxylic acids in the hope of utilizing the basicity of the β-diketiminate backbone (*vide supra*) and the oxophilic nature of silicon to selectively remove the [Si(nacnac′)] fragment with *in-situ* generated alkoxides or carboxylates. To do so, a variety of different alcohols (ethanol, phenol, and 2,2,2-trifluoroethanol) and carboxylic acids (trifluoroacetic acid and benzoic acid) was examined. It was found that the pK_a value of the Brønsted acid seems to play a crucial role. While complex **1** does not react with two equivalents of dry ethanol ($pK_a \approx 15$) a stronger acid such as phenol ($pK_a \approx 10$) selectively forms a new P-containing species identified *via* ³¹P{¹H} NMR monitoring. A similar outcome was observed for 2,2,2-trifluoroethanol, trifluoroacetic acid, and benzoic acid. All further investigations were performed using benzoic acid ($pK_a \approx 4$), which is commercially available, easy to handle and not hygroscopic. Complex **1** reacts readily with benzoic acid in a 1:2 stoichiometry at room temperature (Scheme 5)

giving rise to a symmetric AMM′XX′ spin system in the $^{31}P\{^1H\}$ NMR spectrum with an integral ratio of 4:2:2 (Figure 8).
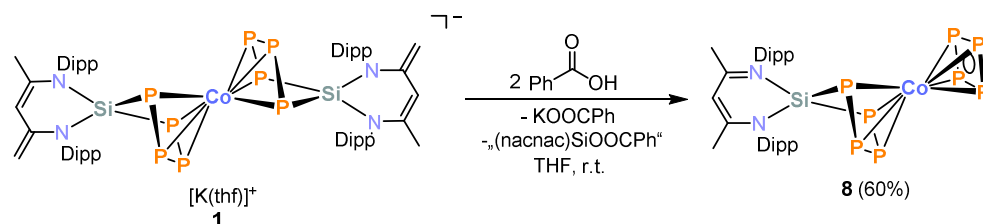
Scheme 5. Synthesis of $[(\eta^4\text{-P}_4)\text{Co}(\mu\text{-}\eta^4{:}\eta^2\text{-P}_4)\text{Si(nacnac)}]$ (**8**); reagents and conditions for **8**: 2 equiv. benzoic acid.

The splitting pattern observed here is very similar to that observed for complex **6**. However, the singlet resonance is shifted to lower field for **8** ($\delta(\text{P}_X) = 175.0$ ppm). With this in mind and considering the integral ratio of the ^{31}P NMR resonances, it is plausible, that an η^4-coordinated silatetraphosphacyclopentadiene ligand and a *cyclo*-P₄ ring is formed, proposed to be the sandwich complex $[(\eta^4\text{-P}_4)\text{Co}(\mu\text{-}\eta^4{:}\eta^2\text{-P}_4)\text{Si(nacnac)}]$ (**8**). The presence of a *catena*-P₄ unit is further supported by the P–P coupling constants obtained by an iterative fit of the $^{31}P\{^1H\}$ NMR spectrum of **8** dissolved in THF-d_8 (see Figure 8 and Figures S24 and S25, SI). As in complex **5** and other comparable heterodinuclear *catena*-P₄ complexes, the $^1J_{PP}$ coupling constants are large in magnitude and range from −444.4 Hz to −394.9 Hz.[16],[17],[23] The similarity of the compounds is also reflected in the rather small $^2J_{PP}$ and $^3J_{PP}$ coupling constants which were fitted to 24.8 Hz and −24.9 Hz, respectively. The nature of the low-field shifted singlet ($\delta(\text{P}_X) = 175.0$ ppm) suggests the presence of a *cyclo*-P₄ ring. Related neutral and anionic *cyclo*-P₄ complexes such as $[\text{Cp}'''\text{Co}(\eta^4\text{-P}_4)]$ ($\delta = 175.2$ ppm),[12] $[(\eta^5\text{-Cp}^{Ar})\text{Fe}(\eta^4\text{-P}_4)]^-$ ($\text{Cp}^{Ar}=\text{C}_5(\text{C}_6\text{H}_4\text{-4-Et})_5$) ($\delta = 114.1$ ppm)[14] and $[(\text{PHDI})\text{Co}(\eta^4\text{-P}_4)]^-$ (**C**, $\delta = 136.5$ ppm)[13] give rise to ^{31}P NMR singlet in a similar chemical shift range.
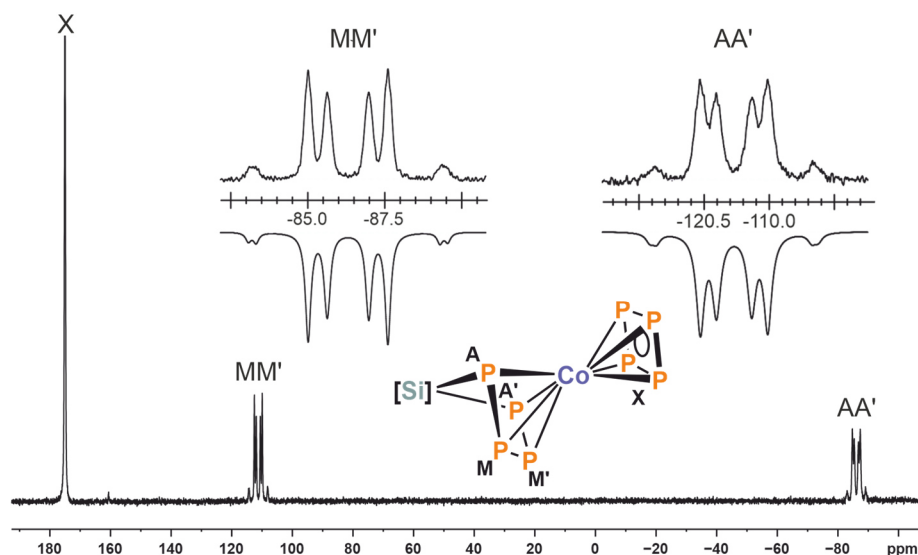
Figure 8. $^{31}P\{^1H\}$ NMR spectrum of compound **8** with nuclei assigned to AA′MM′X spin system; insets: extended signals (upwards) and simulations (downwards); $\delta(P_{AA'}) = -86.1$ ppm, $\delta(P_{MM'}) = 111.2$ ppm, $\delta(P_X) = 175.0$ ppm, $^1J_{XX'} = {}^1J_{X'X} = -394.9$ Hz, $^1J_{MX} = {}^1J_{M'X'} = -444.4$ Hz, $^2J_{MX'} = {}^2J_{M'X} = 24.8$ Hz, $^3J_{MM'} = {}^3J_{M'M} = -24.9$ Hz; [Si] = (nacnac)Si.

Unfortunately, attempts to grow suitable single-crystals for structural characterization by single-crystal X-ray diffraction have remained unsuccessful to date. Compound **8** tends to form microcrystalline powders from various solvent mixtures. The most convenient method to isolate the compound appears to be its precipitation as a brownish powder from THF using a mixture of Et$_2$O/n-hexane (1:3 v:v). As a result, compound **8** can be isolated in a yield of 60%.

The ^1H and ^{13}C NMR spectra of the isolated product were recorded in THF-d_8. These spectra are in line with the suggested structure and display all signals expected for a β-diketiminato substituted silatetraphosphacyclopentadiene ligand. Two singlet resonances at δ = 1.99 ppm and 2.17 ppm with the correct integral ratio are observed for the exocyclic CH$_3$ groups suggesting that the exocyclic C−C double bond present in the starting material **1** is protonated in product **8**. This is further supported by the absence of a negative resonance in the corresponding DEPT 135 spectrum. The γ-C*H* atom of the [Si(nacnac)] unit gives rise to a single resonance which integrates to one at δ = 5.87 ppm and lies in a similar region to that observed in compound **4**. The C, H, N combustion analysis further verified the elemental composition of **8**.

The molecular structure of **8** derived by multinuclear NMR spectroscopy proves that the elimination of the [Si(nacnac′)] moiety with carboxylic acids is indeed possible leading to an unprecedented sandwich complex featuring an η⁴-coordinated silatetraphosphacyclopentadiene ligand and a *cyclo*-P$_4$ ring. Such mononuclear *cyclo*-P$_4$ complexes were once rare species but have flourished over the past decade. While numerous examples with early transition metals (e.g. V, Nb, Ta, Mo) are known,[11] only

a few late transition metal *cyclo*-P_4 complexes have reported to date.[12],[13],[14],[15] As described in the introduction, examples with cobalt are still very rare (see Figure 1, above). Motivated by the synthesis of **8**, the question arose if it is possible to eliminate the second silicon fragment to access the elusive all-inorganic phosphorus analogue bis(cyclobutadiene) sandwich complex. Up to now, examples of "carbon-free" sandwich complexes are extremely limited. Ellis and co-workers reported the isolation of the all-inorganic analogue of the titanocene dianion $[K(18\text{-crown-}6)]_2[Ti(cyclo\text{-}P_5)_2]$ (**B**, Figure 1) in 2002.[2] This remarkable complex was synthesized by treating a naphthalene-stabilized titanate complex with 2.5 equivalents of P_4. Further examples of "carbon-free" all phosphorus sandwich complexes are limited to $[\{(Cp'''Fe(CO)_2)_2(\mu^3\text{-}\eta^{1:1:4}\text{-}P_4)\}_2Fe][PF_6]_2$ and $[\{(Cp'''Fe(CO)_2)_2(\mu^3\text{-}\eta^{1:1:4}\text{-}P_4)\}_2Co][SbF_6]_3$, which were both recently published by Scheer and co-workers.[9],[10]

Inspired by the work of Grützmacher and co-workers, who first synthesized a stable terminal complex of the CP^- (= "cyaphide") anion by selectively eliminating triphenylsilane from a silyl-substituted phosphaalkyne complex with sodium phenoxide,[47] the reaction of complex **8** toward alkoxides was investigated as depicted in Scheme 6. Upon mixing one equivalent potassium phenoxide and 18-crown-6 or [2.2.2]-cryptand with complex **8**, the singlet resonances are observed in the $^{31}P\{^1H\}$ NMR spectrum at $\delta = 238.7$ ppm and $\delta = -225.9$ ppm (the latter signal is very broad, see Figure S26, SI). In contrast to the reaction of **1** with benzoic acid, this reaction proceeds slowly, and the starting material is fully consumed after three days at room temperature. It should be noted that this reaction only proceeds in presence of crown ether. ^1H NMR spectroscopy of the crude reaction mixture shows a singlet clearly assigned to the crown ether molecule and further resonances which might be derived from a yet unidentified β-diketiminate species (see Figure S27, SI). Subsequent work-up involved washing the crude reaction mixture with diethyl ether and toluene followed by extraction of the solid residue with acetonitrile. Only the signals of the crown ether molecule are observed in the ^1H NMR spectrum of the acetonitrile solution (see Figure S32, SI). The corresponding $^{31}P\{^1H\}$ NMR spectrum (Figure S33, SI) still shows the same resonances as before, a sharp singlet at low field as well as a broad signal at high field nearly undistinguishable from the baseline. These NMR data suggest that the "carbon-free" all-phosphorus compound, $[K(18\text{-crown-}6)][Co(\eta^4\text{-}P_4)_2]$ (**9**) might be formed, which may be identified by a singlet at $\delta = 239.3$ ppm in deuterated acetonitrile.
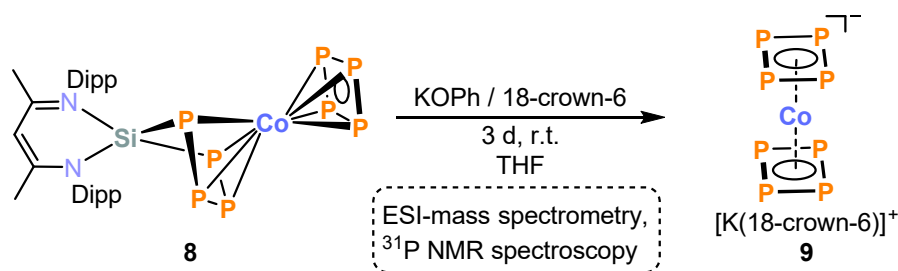
Scheme 6. Synthetic route to the "carbon-free" sandwich complex [K(18-crown-6)][Co(η⁴-P₄)₂] (**9**). The presence of compound **9** was proven by ESI-MS and heteronuclear NMR spectroscopy; reagents and conditions for **9**: 1 equiv. potassium phenolate in presence of crown ether.

Proposing a reliable structure based purely on NMR spectroscopy is inadequate and is further hampered by the lack of comparative literature as the only closely related example is the dianion **B**. The $^{31}P\{^1H\}$ chemical shifts reported for this species range from 60 ppm to 63 ppm, depending on the solvent and counterion.[2] The $^{31}P\{^1H\}$ NMR resonances of related mononuclear *cyclo*-P₄ cobalt complexes such as the starting material **8** (δ = 175.0 ppm), [Cp‴Co(η⁴-P₄)] (δ = 175.2 ppm),[12] and [(PHDI)Co(η⁴-P₄)]⁻ (**C**, δ = 136.5 ppm)[13] lie all in a similar range, however, they are shifted to higher field of up to 100 ppm compared to the signal observed for **9**. Mills and co-workers reported on the reaction of [Th(Cp″)₃] (Cp″ = {C₅H₃(SiMe₃)₂-1,3}) with P₄ yielding the thorium *cyclo*-P₄ complex [{Th(Cp″)₃}₂(μ–η¹:η¹-P₄)] with a μ–η¹:η¹-P₄ binding mode.[48] $^{31}P\{^1H\}$ NMR spectroscopy revealed two triplet resonances at δ = 227.6 ppm and δ = 328.9 ppm, which correlate well with the signal of Korber's elusive 6π aromatic P₄²⁻ anion (δ = 348 ppm).[48],[49] Interestingly, a broad resonance at δ = −246.6 ppm was additionally observed by Mills and co-workers which could not be further assigned even by elaborated NMR spectroscopic investigations.[48]

In order to gain additional proof of the homoleptic octaphosphorus cobalt sandwich complex an electrospray ionization mass spectrometry (ESI-MS) mass spectrum was recorded after work-up of the reaction mixture (see SI for details). The signal of the molecular ion was detected at m/z = 306.7246 when performing the ESI in the negative mode, confirming the molecular composition of the proposed [Co(η⁴-P₄)₂]⁻ anion of **9**. No isotope pattern was observed for this as ^{59}Co and ^{31}P are mononuclidic elements. This signal is the base peak of the ESI-MS spectrum. Some other signals are observed (see SI), however, none of these signals could be assigned to further species or fragments of **9**.

This finding is further supported by comparing the experimental UV/Vis absorption spectrum with a TDDFT calculated at ωB97X-D3/def2-TZVP (including continuum solvation (CPCM) for acetonitrile) level of theory of anion **9** (see SI for details). The shape of the calculated UV/Vis spectrum fits the experimental spectrum recorded of the reaction mixture after work-up in acetonitrile (Figure 9). The spectrum shows two absorption bands in the UV region at 258 nm (ε = 30000 L·mol⁻¹·cm⁻¹) and 296 nm (ε = 21000 L·mol⁻¹·cm⁻¹), with the latter absorption tailing far into the visible region.

According to the TDDFT calculations, the strongly blue-shifted band is dominated by a metal-to-ligand charge transfer (MLCT) while the latter band is mainly accounted for ligand-to-metal charge transfer (LMCT). A weak absorption at 434 nm is additionally predicted by the calculations and can be assigned to d−d transitions. This weak band is presumably obscured by the tailing of the UV bands into the visible region in the experimental spectrum.
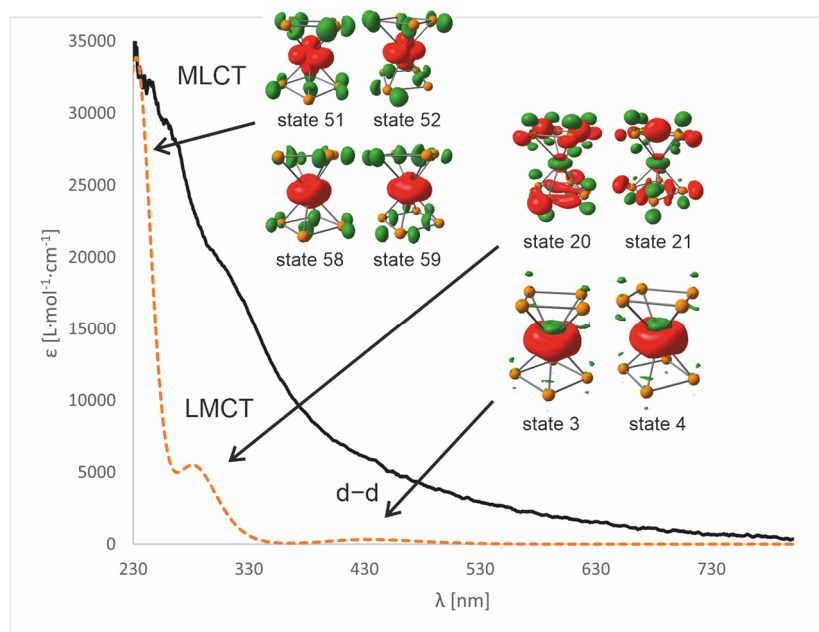
Figure 9. Comparison of experimental (black) and calculated (dotted, orange) absorption spectra of **9** in acetonitrile. Calculated spectrum (60 transitions) was plotted with a full width at half maximum of 5000 cm⁻¹ (scaling factor 1.4). Selected difference densities of singlet transitions; Surface isovalue: 0.003; transitions proceed from red to green.

As of yet unequivocal structural proof of **9** by single-crystal XRD analysis is elusive. Exchanging the cation with tetraphenylphosphoniumchloride or bis(triphenylphosphine)iminium (PPN) chloride should help in the recrystallization of **9**. This will necessitate the use of different solvent systems as exchanging the cation also influences the solubility and stability of such compounds.[2] Nevertheless, summarizing the data, the synthesis of a second example an unsubstituted "carbon-free" sandwich compound [Co(*cyclo*-P₄)₂]⁻ has likely been successful.

The highly unusual structure of this complex motivated an investigation of the electronic structure using the DFT methods in the gas phase (PBE/def2-TZVP level). Geometry optimizations revealed that [Co(*cyclo*-P₄)₂]⁻ anion favors D_{4d} over the D_{4h} symmetry with an energy difference of about 6 kcal mol⁻¹.[10] The π orbitals of tetraphosphacyclobutadiene form symmetry adapted linear combinations of ligand orbitals (SALCs) in a_1, b_2, e_1, e_2, and e_3 symmetry (Figure S39, SI).[50] These ligand group orbitals interact with the metal s, p_z, $p_{x,y}$, and $d_{xz,yz}$ orbitals, respectively. These interactions are confirmed by the MO interaction diagram shown in Figure 10 (a more extensive MO diagram is given in the SI, see Figure S39). It is important to note that there appears to be a significant interaction

between the d_{xz} and d_{yz} metal orbitals and the appropriate ligand π orbitals of $1e_3$ symmetry. Löwdin population analysis of the relevant Kohn-Sham orbitals 62 and 63 contributions are nearly 50% each of metal 3d and ligand π orbitals, respectively. The interactions with other metal orbitals (such as d_{x2-y2} and d_{xy} of e_2 symmetry and d_{z2} of a1 symmetry) appear to be significantly weaker as the relevant Kohn-Sham orbitals are mainly localized on the metal atom (3d orbital contribution >70%). An analogous observation was reported for the related sandwich complex $[\{(Cp'''Fe(CO)_2)_2(\mu^3-\eta^{1:1:4}-P_4)\}_2Fe][PF_6]_2$ by Scheer and co-workers.[9] As a result of the fairly strong (back-)bonding, metal-ligand bonding ought to be described as an intermediate between two cases, i.e. $[Co^{-I}(L^0)_2] \leftrightarrow [Co^{III}(L^{2-})_2]$. A similar observation has been reported for the related homoleptic sandwich complexes $[M(\eta^4-P_2C_2R_2)_2]^-$ (M = Fe, Co).[51]
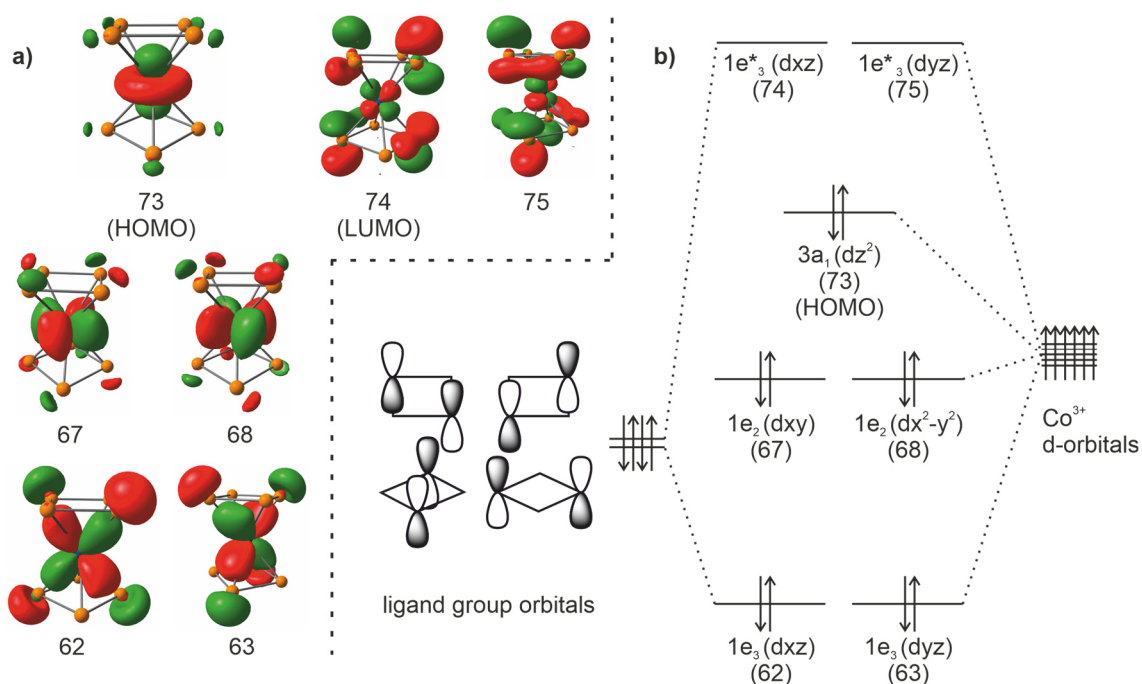
Figure 10. a) Selected Kohn-Sham orbitals of **9** showing d-orbital interactions between the ligand and the Co atom; the hydrogen atoms have been omitted for clarity; surface isovalue=0.05. b) Excerpt of a qualitative d-orbital splitting diagram of **9**; a more extensive MO diagram is given in the Supporting Information (Figure S39).

We were interested in the nature of the *cyclo*-P₄ ligands so the aromaticity was studied by nucleus independent chemical shift (NICS) calculations (see SI for details). The calculated NICS(0) value (−6.4) of complex **9** hints at the presence of formally aromatic *cyclo*-P₄²⁻ ligands (Compare: NICS(0) values of benzene = −8.3, free P₄²⁻ (6.0)[52]). This is comparable to the mononuclear *cyclo*-P₄ complexes [(PhP(CH₂CH₂PCy₂)₂)Fe(η⁴-P₄)] reported by Mézailles and co-workers and to compound **C** studied by our group.[13],[15]

5.3 Conclusion

Reactions of the metallate $[M(\eta^4\text{-}1,5\text{-cod})_2]^-$ (M = Co, Fe) with the SiP_4 compound $[(\text{nacnac}')Si(\eta^2\text{-}P_4)]$ afford inorganic sandwich complexes $[K(thf)][Co\{(\mu\text{-}\eta^4\text{:}\eta^2\text{-}P_4)Si(\text{nacnac}')\}_2]$ (**1**) and iron-silicon $[Li(diox)_2]_2[Fe\{(\mu\text{-}\eta^4\text{:}\eta^2\text{-}P_4)Si(\text{nacnac}')\}_2]$ (**2**). While the cobalt complex **1** is readily accessible by the reaction of $[(\text{nacnac}')Si(\eta^2\text{-}P_4)]$ with $[K(thf)_{0.2}][Co(\eta^4\text{-}1,5\text{-cod})_2]$ the analogous reaction with $[Li(dme)]_2[Fe(\eta^4\text{-}1,5\text{-cod})_2]$ is less selective yielding a mixture of polyphosphorus species. One of the by-products, $[Li(diox)_3]_2[P_8\{Si(\text{nacnac}')\}]$ (**3**), could be identified by single-crystal X-Ray diffraction analysis. The molecular structure shows a dianionic norticyclic P_7 core substituted by the silyl moiety and a single P atom.

Conveniently, complex **1** was accessible in sufficient quantities for reactivity studies. Given the structural similarity of **1** with $[K(dme)_2\{(^{Mes}BIAN)Co(\mu\text{-}\eta^4\text{:}\eta^2\text{-}P_4)Ga(\text{nacnac})\}]$ ($^{Mes}BIAN$ = 1,2-bis(2,4,6-trimethylphenylimino)acenaphthene, see chapter 2 of this thesis),[16] it is surprising that reactions of **1** with alkyl- and arylchlorophosphanes were unsuccessful. Subsequent studies investigated the elimination of the [Si(nacnac′)] fragments in the hope of accessing the "carbon-free" bistetraphosphacyclobutadien sandwich complex $[K(18\text{-crown-}6)][Co(\eta^4\text{-}P_4)_2]$ (**9**). However, reaction of **1** with $[Me_4N]F$ resulted in the unexpected formation of a *cyclo*-P_3 complex $[Me_4N]_2[(\eta^3\text{-}P_3)Co(\mu\text{-}\eta^4\text{:}\eta^2\text{-}P_4)Si(\text{nacnac}')]$ (**6**) and the hexacoordinated tetrafluorosilicate $[Me_4N][(\text{nacnac})SiF_4]$ (**7**). Remarkably, the molecular structure of **6** shows an η^4-coordinated $(\text{nacnac}')SiP_4$ ligand and an η^3-coordinated *cyclo*-P_3 ring. Reactions of **1** with a variety of different alcohols and carboxylic acids afforded a single P-containing product according to $^{31}P\{^1H\}$ NMR spectroscopy. This product was identified as $[(\eta^4\text{-}P_4)Co(\mu\text{-}\eta^4\text{:}\eta^2\text{-}P_4)Si(\text{nacnac})]$ (**8**). Further reacting **8** with potassium phenoxide in the presence of a crown ether presumably affords the bis(tetraphosphacyclobutadiene) sandwich complex $[K(18\text{-crown-}6)][Co(\eta^4\text{-}P_4)_2]$ (**9**), which was characterized by ^1H and ^{31}P NMR spectroscopy and ESI-MS. Current efforts focus on the structural characterization of **9**.

The results of this chapter illustrate that the concept of heterodinuclear P_4 activation and functionalization potentially is a very useful synthetic tool to access unprecedented polyphosphorus compounds. Further derivatization reactions of complex **8** and related species are conceivable, which may afford a multitude of further fascinating polyphosphorus compounds.

5.4   Notes and References

[1]   (a) A. Togni, R. L. Halterman, *Metallocenes. Synthesis, reactivity, applications*, Wiley-VCH, Weinheim, **1998**; (b) P. D. Beer, E. J. Hayes, *Coord. Chem. Rev.* **2003**, *240*, 167; (c) L.-X. Dai, T. Tu, S.-L. You, W.-P. Deng, X.-L. Hou, *Acc. Chem. Res.* **2003**, *36*, 659; (d) D. R. van Staveren, N. Metzler-Nolte, *Chem. Rev.* **2004**, *104*, 5931; (e) D. Astruc, *Eur. J. Inorg. Chem.* **2017**, *2017*, 6.

[2]   E. Urnius, W. W. Brennessel, C. J. Cramer, J. E. Ellis, P. v. R. Schleyer, *Science* **2002**, *295*, 832.

[3]   (a) T. Grell, D. M. Yufanyi, A. K. Adhikari, M.-B. Sárosi, P. Lönnecke, E. Hey-Hawkins, *Pure Appl. Chem.* **2019**, *91*, 103; (b) K. B. Dillon, F. Mathey, J. F. Nixon, *Phosphorus. The carbon copy; from organophosphorus to phospha-organic chemistry*, Wiley, Chichester, **1998**.

[4]   (a) M. Baudler, S. Akpapoglou, D. Ouzounis, F. Wasgestian, B. Meinigke, H. Budzikiewicz, H. Münster, *Angew. Chem. Int. Ed. Engl.* **1988**, *27*, 280; *Angew. Chem.* **1988**, *100*, 288. (b) M. Baudler, T. Etzbach, *Angew. Chem. Int. Ed. Engl.* **1991**, *30*, 580; *Angew. Chem.* **1991**, *103*, 590.

[5]   (a) F. Dielmann, R. Merkle, S.Heinl, M. Scheer, *Z. Naturforsch. B* **2009**, *64b*, 3; (b) O. J. Scherer, T.Hilt, G. Wolmershäuser, *Organometallics* **1998**, *17*, 4110; (c) O. J. Scherer, T.Brück, G. Wolmershäuser, *Chem. Ber.* **1988**, *121*, 935; (d) O. J. Scherer, T.Brück, *Angew. Chem. Int. Ed. Engl.* **1987**, *26*, 59; *Angew. Chem.* **1987**, *99*, 59.

[6]   (a) M. Peruzzini, L. Gonsalvi, A. Romerosa, *Chem. Soc. Rev.* **2005**, *34*, 1038; (b) V. A. Milyukov, Y. H. Budnikova, O. G. Sinyashin, *Russ. Chem. Rev.* **2005**, *74*, 781; (c) B. M. Cossairt, N. A. Piro, C. C. Cummins, *Chem. Rev.* **2010**, *110*, 4164; (d) J. E. Borger, A. W. Ehlers, J. C. Slootweg, K. Lammertsma, *Chem. Eur. J.* **2017**, *49*, 11738; (e) F. Scalambra, M. Peruzzini, A. Romerosa in *Advances in Organometallic Chemistry* (Hrsg.: P. J. Perez), Academic Press, Amsterdam, **2019**, S. 173; (f) C. M. Hoidn, D. J. Scott, R. Wolf, *Chem. Eur. J.* **2020**, *27*, 1886.

[7]   (a) T. Wettling, G. Wolmershäuser, P. Binger, M. Regitz, *J. Chem. Soc., Chem. Commun.* **1990**, 1541; (b) D. Himmel, M. Seitz, M. Scheer, *Z. Anorg. Allg. Chem.* **2004**, *630*, 1220.

[8]   (a) R. Wolf, A. W. Ehlers, J. C. Slootweg, M. Lutz, D. Gudat, M. Hunger, A. L. Spek, K. Lammertsma, *Angew. Chem. Int. Ed.* **2008**, *47*, 4584; *Angew. Chem.* **2008**, *120*, 4660; (b) R. Wolf, J. C. Slootweg, A. W. Ehlers, F. Hartl, B. de Bruin, M. Lutz, A. L. Spek, K. Lammertsma, *Angew. Chem. Int. Ed.* **2009**, *48*, 3104; *Angew. Chem.* **2009**, *121*, 3150; (c) R. Wolf, E.-M. Schnöckelborg, *Chem. Commun.* **2010**, *46*, 2832; (d) R. Wolf, A. W. Ehlers, M. M. Khusniyarov, F. Hartl, B. de Bruin, G. J. Long, F. Grandjean, F. M. Schappacher, R. Pöttgen, J. C. Slootweg, M. Lutz, A. L. Spek, K. Lammertsma, *Chem. Eur. J.* **2010**, *16*, 14322.

[9]   J. Müller, S. Heinl, C. Schwarzmaier, G. Balázs, M. Keilwerth, K. Meyer, M. Scheer, *Angew. Chem. Int. Ed.* **2017**, *56*, 7312; *Angew. Chem.* **2017**, *129*, 7418.

[10]   J. Müller, M. Scheer, *Chem. Eur. J.* **2020**, *27*, 3675.

[11]   (a) O. J. Scherer, J. Vondung, G. Wolmershäuser, *Angew. Chem. Int. Ed. Engl.* **1989***, 28,* 1355; Angew. Chem. **1989**, *101*, 1395; (b) O. J. Scherer, R. Winter, G. Wolmershuser, *Z. Anorg. Allg. Chem.* **1993**, *619*, 827; (c) M. Herberhold, G. Frohmader, W. Milius, *J. Organomet. Chem.* **1996***, 522,* 185; (d) K. A. Mandla, C. E. Moore, A. L. Rheingold, J. S. Figueroa, *Angew. Chem. Int. Ed.* **2019***, 58,* 1779*; Angew. Chem.* **2019**, *131*, 1793; (e) K. A. Mandla, M. L. Neville, C. E. Moore, A. L. Rheingold, J. S. Figueroa, *Angew. Chem. Int. Ed.* **2019***, 58,* 15329*; Angew. Chem.* **2019**, *131*, 15473.

[12]   F. Dielmann, A. Timoshkin, M. Piesch, G. Balázs, M. Scheer, *Angew. Chem. Int. Ed.* **2017**, *56*, 1671; *Angew. Chem.* **2017**, *129*, 1693.

[13]   C. M. Hoidn, T. M. Maier, K. Trabitsch, J. J. Weigand, R. Wolf, *Angew. Chem. Int. Ed.* **2019**, *58*, 18931; *Angew. Chem.* **2019**, *131*, 19107.

[14]   U. Chakraborty, J. Leitl, B. Mühldorf, M. Bodensteiner, S. Pelties, R. Wolf, *Dalton Trans.* **2018**, *47*, 3693.

[15]   A. Cavaillé, N. Saffon-Merceron, N. Nebra, M. Fustier-Boutignon, N. Mézailles, *Angew. Chem. Int. Ed.* **2018**, *57*, 1874; Angew. Chem. **2018**, *130*, 1892.

[16]   C. G. P. Ziegler, T. M. Maier, S. Pelties, C. Taube, F. Hennersdorf, A. W. Ehlers, J. J. Weigand, R. Wolf, *Chem. Sci.* **2019**, *110*, 4178.

[17]   C. G. P. Ziegler, F. Hennersdorf, J. J. Weigand, R. Wolf, *Z. Anorg. Allg. Chem.* **2020**, *93*, 303.

[18]   Y. Xiong, S. Yao, M. Brym, M. Driess, *Angew. Chem. Int. Ed.* **2007**, *46*, 4511; Angew. Chem. **2007**, *119*, 4595.

[19]   (a) K. Jonas, R. Mynott, C. Krüger, J. C. Sekutowski and Y.-H. Tsay, *Angew. Chem. Int. Ed. Engl.*, **1976**, *15*, 767; *Angew. Chem.*, **1976**, *88*,808; (b) K. Jonas, US patent 4169845, **1979**.

[20]   A. Fürstner, R. Martin, H. Krause, G. Seidl, R. Goddard, C. W. Lehmann, *J. Am.Chem. Soc.*, **2008**, *130*, 8773.

[21]   S. Alvarez, *Dalton Trans.* **2013**, *42*, 8617.

[22]   C. G. P. Ziegler, C. Taube, J. A. Kelly, G. Hierlmeier, M. Uttendorfer, J. J. Weigand, R. Wolf, *Chem. Commun.* **2020**, *56*, 14071.

[23]   R. Yadav, T. Simler, S. Reichl, B. Goswami, C. Schoo, R. Köppe, M. Scheer, P. W. Roesky, *J. Am. Chem. Soc.* **2020**, *142*, 1190.

[24]   W. W. Seidel, O. T. Summerscales, B. O. Patrick, M. D. Fryzuk, *Angew. Chem. Int. Ed.* **2008**, *48*, 115; *Angew. Chem.* **2008**, *121*, 121.

[25]   O. J. Scherer, T. Hilt and G. Wolmershäuser, *Organometallics*, **1998**, *17*, 4110.

[26] V. A. Miluykov, O. G. Sinyashin, P. Lönnecke and E. Hey-Hawkins, *Mendeleev Commun.*, **2003**, *13*, 212.

[27] M. D. Walter, J. Grunenberg and P. S. White, *Chem. Sci.*, **2011**, *2*, 2120.

[28] Anionic complexes containing nortricyclic P₇ fragments: (a) W. Hönle, H. G. von Schnering, A. Schmidpeter, G. Burget, Angew. *Chem. Int. Ed.* **1984**, *23*, 817; *Angew. Chem.* **1984**, *96*, 796; (b) G. Fritz, H. W. Schneider, W. Hönle, H. G. von Schnering, *Z. Naturforsch. B* **1988***, 43,* 561.

[29] F. Hennersdorf, J. J. Weigand, *Angew. Chem. Int. Ed.* **2017**, *56*, 7858; *Angew. Chem.* **2017**, *129*, 7966.

[30] W. T. K. Chan, F. García, A. D. Hopkins, L. C. Martin, M. McPartlin, D. S. Wright, *Angew. Chem. Int. Ed.* **2007**, *46*, 3084; Angew. Chem. **2007**, *119*, 3144.

[31] (a) M. Driess, S. Yao, M. Brym, C. van Wüllen, D. Lentz, *J. Am. Chem. Soc.* **2006**, *128*, 9628; (b) S. Yao, M. Brym, C. van Wüllen, M. Driess, *Angew. Chem. Int. Ed.* **2007**, *46*, 4159; *Angew. Chem.* **2007**, *119*, 4237; (c) Y. Xiong, S. Yao, M. Driess, *Organometallics* **2009**, *28*, 1927.

[32] M. Driess, S. Yao, M. Brym, C. van Wüllen, *Angew. Chem. Int. Ed.* **2006**, *45*, 6730; *Angew. Chem.* **2006**, *118*, 6882.

[33] G. Prabusankar, A. Doddi, C. Gemel, M. Winter and R. A. Fischer*, Inorg. Chem.* **2010**, *49*, 7976.

[34] J. W. Dube, C. M. E. Graham, C. L. B. Macdonald, Z. D. Brown, P. P. Power, P. J. Ragogna, *Chem. Eur. J.* **2014**, *20*, 6739.

[35] M. Driess, S. Yao, M. Brym, C. van Wüllen, D. Lentz, *J. Am. Chem. Soc.* **2006**, *128*, 9628.

[36] P. Pyykkö, M. Atsumi, *Chem. Eur. J.* **2009**, *15*, 12770.

[37] O. J. Scherer, M. Swarowsky, H. Swarowsky, G. Wolmershäuser, *Angew. Chem. Int. Ed. Engl.* **1988**, *27*, 694; *Angew. Chem.* **1988**, *100*, 738.

[38] M. Baudler, Y. Aktalay, K.-F. Tebbe and T. Heinlein, *Angew. Chem. Int. Ed. Engl.* **1981**, *20*, 967; *Angew. Chem.*, **1981**, *93*, 1020.

[39] For representative examples, see: (a) H. C. E. McFarlane and W. McFarlane, *Polyhedron*, **1988**, *7*, 1875; (b) P. Coburger, P. Bielytskyi, D. Williamson, E. Rys, A. Kreienbrink, P. Lönnecke, J. Matysik and E. Hey-Hawkins, *Chem. Eur. J.* **2019**, *25*, 11456; (c) H. C. E. McFarlane and W. McFarlane, *Polyhedron*, **1999**, *18*, 2117; (c) C. Taube, K. Schwedtmann, M. Noikham, E. Somsook, F. Hennersdorf, R. Wolf and J. J. Weigand, *Angew. Chem. Int. Ed.* **2020**, *59*, 3585*; Angew. Chem.* **2020**, *132*, 3613.

[40] *Bond Energies. In Encyclopedia of Inorganic and Bioinorganic Chemistry, R. A. Scott (Ed.),* Wiley, **2011**.

[41] For representative examples, see: (a) C. Bianchini, C. Mealli, A. Meli, L. Sacconi, *Inorg. Chim. Acta* **1979**, *37*, L543-L544; (b) M. Di Vaira, C. A. Ghilardi, S. Midollini, L. Sacconi,

J. Am. Chem. Soc. **1978**, *100*, 2550; (c) M. Di Vaira, L. Sacconi, P. Stoppioni, *J. Organomet. Chem.* **1983**, *250*, 183; (d) G. Capozzi, L. Chiti, M. Di Vaira, M. Peruzzini, P. Stoppioni, *J. Chem. Soc., Chem. Commun.* **1986**, 1799; (e) O. J. Scherer, T. Dave, J. Braun, G. Wolmershäuser, *J. Organomet. Chem.* **1988**, *350*, C20-C24; (f) F. H. Stephens, M. J. A. Johnson, C. C. Cummins, O. P. Kryatova, S. V. Kryatov, E. V. Rybak-Akimova, J. E. McDonough, C. D. Hoff, *J. Am. Chem. Soc.* **2005**, *127*, 15191; (g) B. M. Cossairt, M.-C. Diawara, C. C. Cummins, *Science* **2009**, *323*, 602; (h) D. Tofan, B. M. Cossairt, C. C. Cummins, *Inorg. Chem.* **2011**, *50*, 12349; (i) B. Pinter, K. T. Smith, M. Kamitani, E. M. Zolnhofer, B. L. Tran, S. Fortier, M. Pink, G. Wu, B. C. Manor, K. Meyer et al., *J. Am. Chem. Soc.* **2015**, *137*, 15247; (j) E. Mädl, G. Balázs, E. V. Peresypkina, M. Scheer, *Angew. Chem. Int. Ed.* **2016**, *55*, 7702; *Angew. Chem.* **2016**, *128*, 7833; (k) C. M. Hoidn, T. M. Maier, K. Trabitsch, J. J. Weigand, R. Wolf, *Angew. Chem. Int. Ed.* **2019**, *58*, 18931; *Angew. Chem.* **2019**, *131*, 19107; (l) M. Piesch, S. Reichl, M. Seidl, G. Balázs, M. Scheer, *Angew. Chem. Int. Ed.* **2019**, *58*, 16563; *Angew. Chem.* **2019**, *131*, 16716; (m) M. Scheer, C. Riesinger, L. Dütsch, G. Balazs, M. Bodensteiner, *Chem. Eur. J.* **2020**.

[42] M. Piesch, S. Reichl, M. Seidl, G. Balázs, M. Scheer, *Angew. Chem. Int. Ed.* **2019**, *58*, 16563; *Angew. Chem.* **2019**, *131*, 16716.

[43] C. Chan, A. E. Carpenter, M. Gembicky, C. E. Moore, A. L. Rheingold, J. S. Figueroa, *Organometallics* **2019**, *38*, 1436.

[44] M. Di Vaira, L. Sacconi, P. Stoppioni, *J. Organomet. Chem.* **1983**, *250*, 183.

[45] C. Breliere, F. Carre, R. J. P. Corriu, W. E. Douglas, M. Poirier, G. Royo, M. Wong Chi Man, *Organometallics* **1992**, *11*, 1586.

[46] S. N. Tandura, M. G. Voronkov, N. V. Alekseev in *Topics in Current Chemistry*, *Vol. 131* (Hrsg.: N. V. Alekseev), Springer, Berlin, **1986**, S. 99–189.

[47] J. G. Cordaro, D. Stein, H. Rüegger, H. Grützmacher, *Angew. Chem. Int. Ed.* **2006**, *45*, 6159; *Angew. Chem.* **2006**, *118*, 6305.

[48] A. Formanuik, F. Ortu, R. Beekmeyer, A. Kerridge, R. W. Adams, D. P. Mills, *Dalton Trans.* **2016**, *45*, 2390.

[49] F. Kraus, J. C. Aschenbrenner, N. Korber, *Angew. Chem. Int. Ed.* **2003**, *42*, 4030; *Angew. Chem.* **2003**, *115*, 4162.

[50] (a) R. M. Pitzer, J. D. Goddard, H. F. Schaefer, *J. Am. Chem. Soc.* **1981**, *103*, 5681.; (b) S. Y. Chu, R. Hoffmann, *J. Phys. Chem.* **1982**, *86*, 1289; (c) P. Coburger, R. Wolf, H. Grützmacher, *Eur. J. Inorg. Chem.* **2020**, *2020*, 3580.

[51] R. Wolf, A. W. Ehlers, M. M. Khusniyarov, F. Hartl, B. de Bruin, G. J. Long, F. Grandjean, F. M. Schappacher, R. Pöttgen, J. C. Slootweg, M. Lutz, A. L. Spek, K. Lammertsma, *Chem. Eur. J.* **2010**, *16*, 14322.

[52]   J. O. C. Jiménez-Halla, E. Matito, J. Robles, M. Solà, *J. Organomet. Chem.* **2006**, *691*, 4359.

5.5 Supporting Information (SI)

5.5.1 General Procedures

All manipulations were performed under an atmosphere of dry argon using standard Schlenk techniques or a MBraun UniLab glovebox. Solvents were dried and degassed with a MBraun SPS800 solvent-purification system. *n*-hexane THF, diethyl ether, and toluene were stored over molecular sieves (3 Å). 1,2-dimethoxyethane was stirred over K/benzophenone, distilled, and stored over molecular sieves (3 Å). *n*-Pentane and 1,4-dioxane were stirred over sodium, distilled, and stored over a potassium mirror. Fluorobenzene and MeCN were stirred over CaH_2, distilled, and stored over molecular sieves (3 Å). Deuterated solvents (C_6D_6, tol-d_8, THF-d_8, MeCN-d_3) were stirred over potassium, distilled, degassed, and stored over molecular sieves (3 Å). The starting materials [K(thf)$_{0.2}$][Co(η^4-1,5-cod)$_2$],[1] [Li(dme)]$_2$[Fe(η^4-1,5-cod)$_2$],[2] [(nacnac′)Si(η^2-P$_4$)][3] (nacnac′ = CH[C(Me)N(Dipp)][C(CH$_2$)N(2,6-*i*Pr$_2$C$_6$H$_3$)]), and [H(OEt$_2$)$_2$][BAr$^F_4$][4] (BAr$^F_4$ = tetrakis[3,5-bis(trifluoromethyl)phenyl]borate) were prepared according to previously reported procedures. Benzoic acid was purchased from Sigma Aldrich and used as delivered. Anhydrous tetramethylammonium fluoride was purchased from ABCR and used as delivered.

NMR Spectroscopy: NMR spectra were measured on a Bruker AVANCE III HD Nanobay (^{1}H (400.13 MHz), ^{13}C (100.61 MHz), ^{19}F (376.50 MHz), ^{29}Si (79.50 MHz), ^{31}P (161.98 MHz)) 400 MHz UltraShield or on a Bruker AVANCE III HDX, 500 MHz Ascend (^{1}H (500.13 MHz), ^{13}C (125.75 MHz), ^{19}F (470.59 MHz), ^{29}Si (99.36 MHz), ^{31}P (202.45 MHz)). All ^{13}C NMR spectra were exclusively recorded with composite pulse decoupling. Reported numbers assigning atoms in the ^{13}C spectra were indirectly deduced from the cross-peaks in 2D correlation experiments (HMBC, HSQC). Chemical shifts were referenced to δ_{TMS} = 0.00 ppm (^{1}H, ^{13}C), δ_{CFCl3} = 0.00 ppm (^{19}F), δ_{TMS} = 0.00 ppm (^{29}Si) and $\delta_{H3PO4(85\%)}$ = 0.00 ppm (^{31}P). Chemical shifts (δ) are reported in ppm. Coupling constants (J) are reported in Hz.

For compounds which give rise to a higher order spin system in the ^{31}P{^{1}H} NMR spectrum, the resolution enhanced ^{31}P{^{1}H} NMR spectrum was transferred to the software gNMR, version 5.0, by Cherwell Scientific.[5] The full line shape iteration procedure of gNMR was applied to obtain the best match of the fitted to the experimental spectrum. $^1J(^{31}P^{31}P)$ coupling constants were set to negative values and all other signs of the coupling constants were obtained accordingly.

UV/vis spectra: UV/vis spectra were recorded on an Ocean Optics Flame spectrometer.

Elemental analysis: Elemental analyses were determined by the analytical department of the University of Regensburg with a Micro Vario Cube (Elementar) elemental analyzer.

5.5.2 Synthesis of [K(thf)][Co{(μ-η⁴:η²-P₄)Si(nacnac′)}₂] (1)
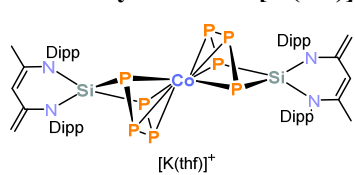
A yellow solution of [K(thf)$_{0.2}$][Co(η⁴-1,5-cod)₂] (433.7 mg, 1.32 mmol, 1.0 equiv.) in THF (30 mL) cooled to −80 °C was added dropwise to a precooled (−80 °C) yellow solution of [(nacnac′)Si(η²-P₄)] (1.50g, 2.64 mmol, 2.0 equiv.) in THF (50 mL). The reaction mixture was stirred for 3 hours at −80 °C and subsequently warmed to room temperature over a period of 16 hours. The resulting brownish-yellow solution was filtered through a glass frit (pore size P4) and the filtrate was concentrated in *vacuo*. Brown block-shaped crystals of **1** were isolated after layering with *n*-hexane at room temperature. The ¹H NMR spectrum of the isolated product contains 1.0 THF solvate molecules per formula unit after drying in *vacuo* (10⁻³ mbar) over a period of 5 hours. Multinuclear NMR spectra reveal the presence of two isomers of **1** (labeled isomer **A** and **B**), which are observed in an approximate 1:1 ratio.

Yield: 760 mg (44%).

¹H NMR (400.13 MHz, 300 K, THF-*d₈*): δ / ppm = 0.95 (12 H, Dipp: CH*Me₂*), 1.14–1.66 (42 H Dipp: CH*Me₂* overlapping with ^{Dipp}nacnac′: NC*Me*), 2.35 (s, 1 H, ^{Dipp}nacnac′: NCC*H₂*), 2.77 (br, 3 H, Dipp: C*H*Me₂ overlapping with ^{Dipp}nacnac′: NCC*H₂*), 2.92 (br, 2 H, Dipp: C*H*Me₂), 3.18 (s, 1 H, ^{Dipp}nacnac′: NCC*H₂*), 3.42 (s, 1 H, ^{Dipp}nacnac′: NCC*H₂*), 3.78 (br, 4 H, Dipp: C*H*Me₂), 4.89 (br, 2 H, ^{Dipp}nacnac′: γ-C*H*), 6.8 – 7.39 (m, 12 H, Dipp: 2,6-*i*Pr₂C₆*H₃*).

¹³C{¹H} NMR (100.61 MHz, 300 K, THF-*d₈*): δ / ppm = 22.9–29.6 (Dipp: CH*Me₂*, ^{Dipp}nacnac′: NC*Me*), 85.0, 85.1, 85.3, 85.5 (4 signals, 2 for each isomer, ^{Dipp}nacnac′: NC*C*H₂), 103.4, 103.5, 103.6, 104.2 (4 signals, 2 for each isomer, ^{Dipp}nacnac′: γ-*C*H), 124.6–127.8 (Dipp: *C*HMe₂), 139.2–148.8 (Dipp: *i*Pr₂*C*H₃, ^{Dipp}nacnac′: N*C*Me), 148.3, 148.4, 149.7, 149.8 (4 signals, 2 for each isomer, ^{Dipp}nacnac′: N*C*CH₂).

³¹P{¹H} NMR (161.98 MHz, 300 K, THF-*d₈*): δ / ppm = −77.8 (m, 4 P), 127.7 (m, 2 P), 140.8 (m, 2 P).

²⁹Si NMR (99.36 MHz, 300 K, THF-*d₈*): δ / ppm = 19.5 (t, ¹*J*(³¹P²⁹Si) = 112.1 Hz, isomer A), 16.0 (t, ¹*J*(³¹P²⁹Si) = 106.5 Hz, isomer B), 25.7 (t, ¹*J*(³¹P²⁹Si) = 119.1 Hz, isomer A).

Elemental analysis calcd. for C₅₈H₆₀CoKN₄P₈Si₂ · 1.0 C₄H₈O (Mw = 1307.40 g·mol⁻¹): C 56.96, H 6.48, N 4.20; found C 56.95, H 6.78, N 4.20.

NMR spectroscopy indicates the presence of isomers in solution. Specifically, observed in the ¹³C{¹H} and ²⁹Si NMR spectra. The ¹H NMR spectrum gives rise to broad signals presumed to arise from two plausible stereoisomers depicted in Figure S1.
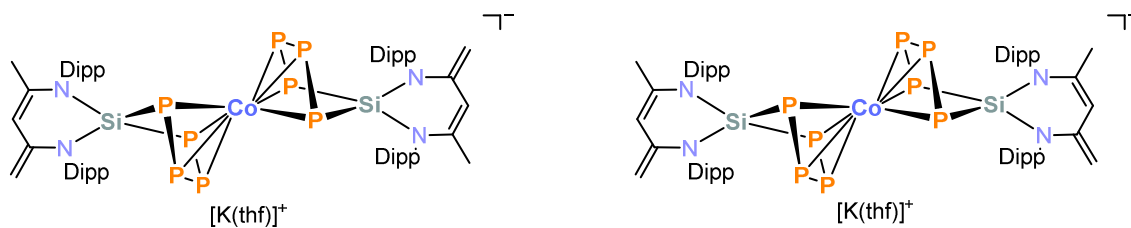
Figure S1. Plausible isomers of [K(thf)][Co{(μ-η⁴:η²-P₄)Si(nacnac′)}₂] (**1**).
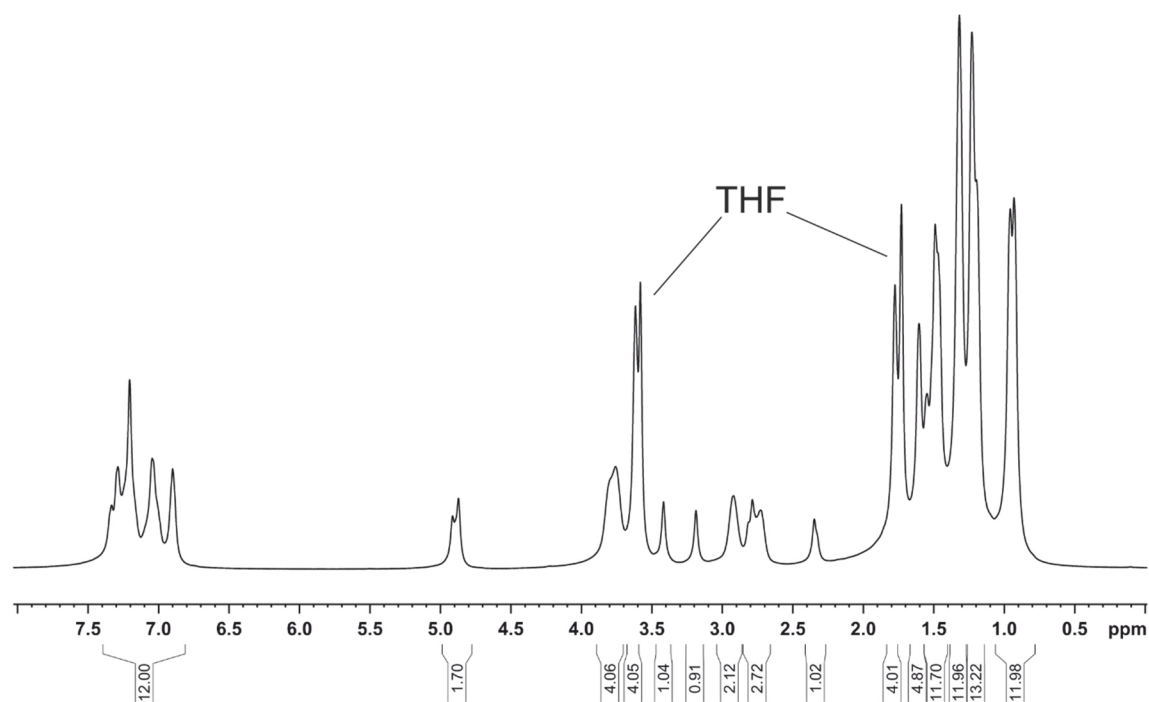
Figure S2. ^{1}H NMR spectrum (400 MHz, 300 K, THF-d$_8$) of [K(thf)][Co{(μ-η^4:η^2-P$_4$)Si(nacnac′)}$_2$] (**1**).
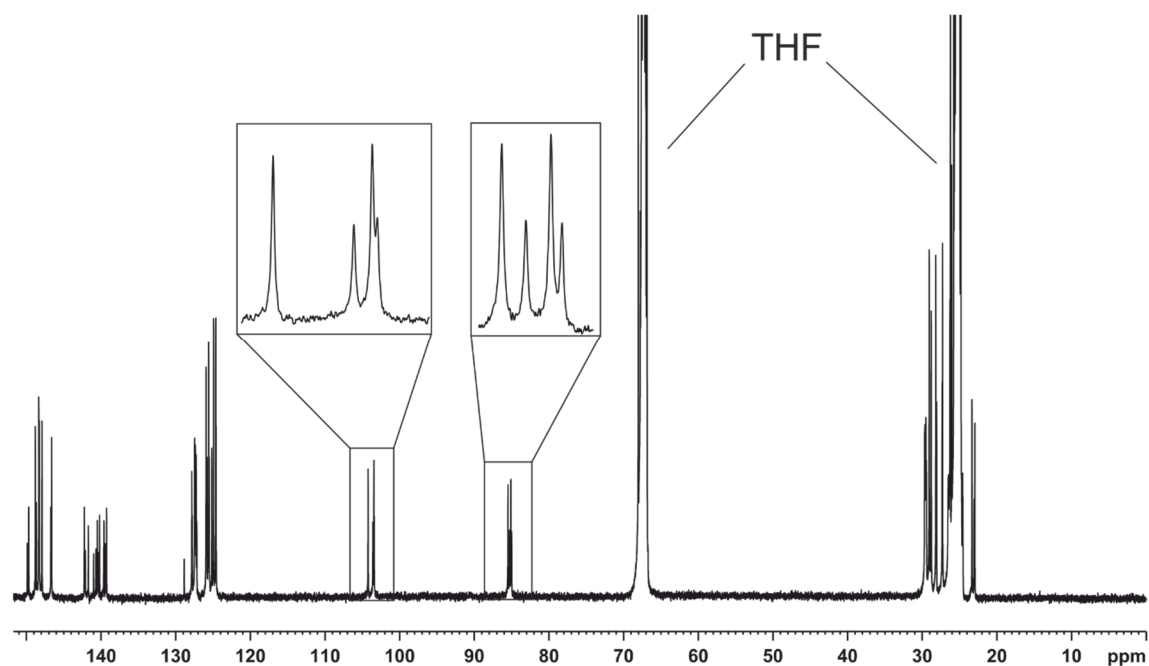
Figure S3. ^{13}C{^{1}H} NMR spectrum (100.61 MHz, 300 K, THF-d_8) of [K(thf)][Co{(μ-η^4:η^2-P$_4$)Si(nacnac′)}$_2$] (**1**).

Figure S4. ^{31}P{^{1}H} NMR spectrum (161.98 MHz, 300 K, THF-d$_8$) of [K(thf)][Co{(μ-η^4:η^2-P$_4$)Si(nacnac′)}$_2$] (**1**).

Figure S5. ^{29}Si NMR spectrum (99.36 MHz, 300 K, THF-d_8) of [K(thf)][Co{(μ-η^4:η^2-P$_4$)Si(nacnac′)}$_2$] (**1**).
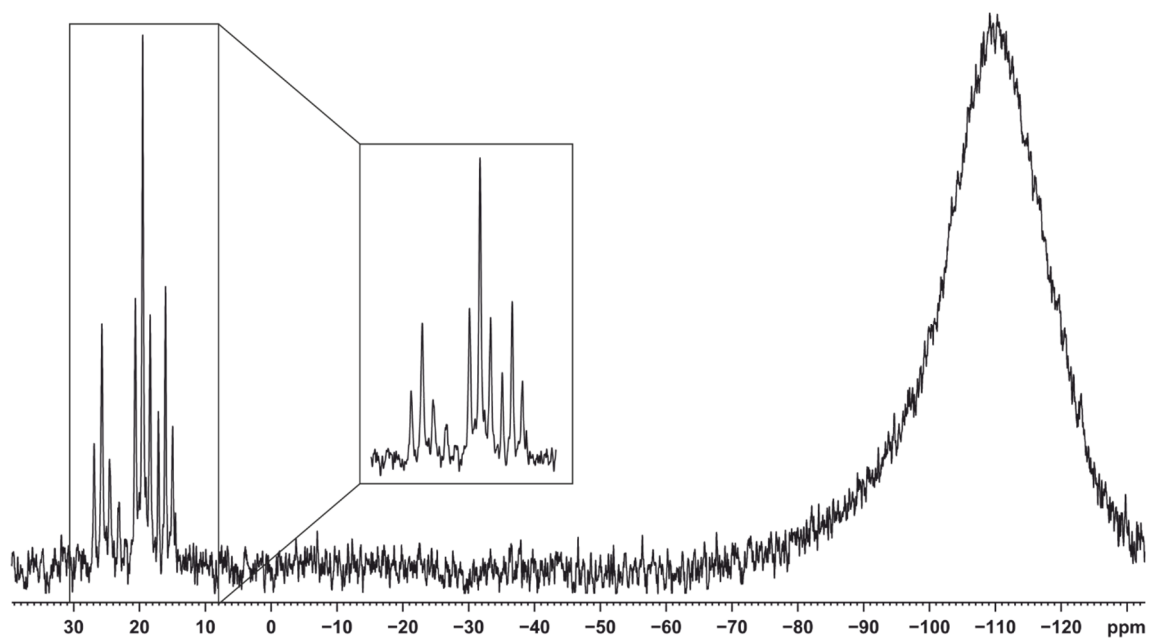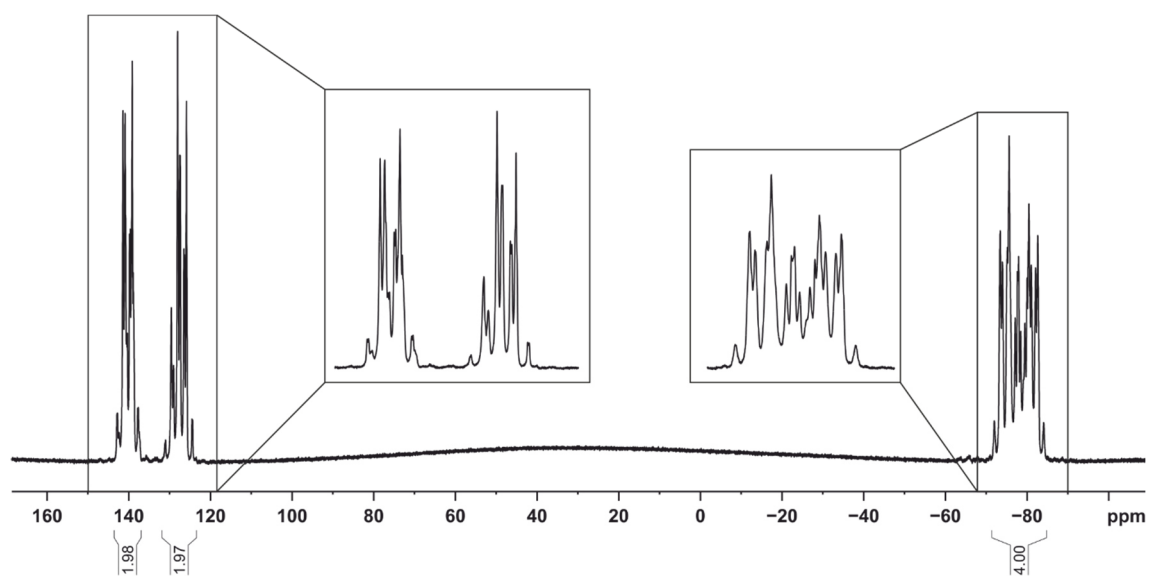
5.5.3 Synthesis of [Li(diox)₂]₂[Fe{(μ-η⁴:η²-P₄)Si(nacnac′)}₂] (2) and [Li(diox)₃]₂[P₈{Si(nacnac′)}] (3)
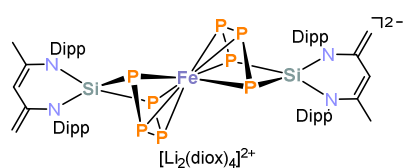
A greenish-yellow solution of $[Li(dme)]_2[Fe(\eta^4\text{-}1,5\text{-cod})_2]$ (82 mg, 0.18 mmol, 1.0 equiv.) in THF (30 mL) cooled to −80 °C was added dropwise to a precooled (−80 °C) yellow solution of $[(nacnac')Si(\eta^2\text{-}P_4)]$ (200 mg, 0.36 mmol, 2.0 equiv.) in THF (50 mL). The reaction mixture was stirred for an additional 3 hours at −80 °C and subsequently warmed to room temperature over a period of 16 hours. The resulting brown solution was filtered through a glass frit (pore size P4) and the filtrate was concentrated in *vacuo* to complete dryness. The remaining brown solid was redissolved in 1,4-dioxane and layered with *n*-hexane. After one week at room temperature, **2** co-crystallized with **3** as yellow prisms.
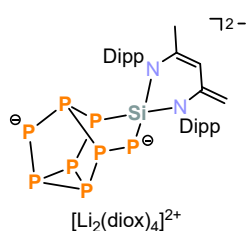
Note: As indicated by the $^{31}P\{^1H\}$ NMR spectrum of the reaction mixture (see Figure S6) the formation of $[Li(diox)_2]_2[Fe\{(\mu\text{-}\eta^4\text{:}\eta^2\text{-}P_4)Si(nacnac')\}_2]$ (**2**) is less selective than the formation of $[K(thf)][Co\{(\mu\text{-}\eta^4\text{:}\eta^2\text{-}P_4)Si(nacnac')\}_2]$ (**1**) described in section 5.5.2. Therefore, the full characterization of **2** was hampered by the presence of the by-product **3**. All attempts to recrystallize **2** from different solvents remained unsuccessful, as the reaction mixture tends to form hardly soluble brown oils. Further attempts to crystallize **2** by the addition of 12-crown-4 or TMEDA were unsuccessful as well. After refinement of the solid-state molecular structure of **2** the molecular formula consists of $C_{79}H_{123}FeK_{0.153}Li_{1.847}N_4O_9P_8Si_2$. It remains unclear where the potassium ion originates from. Several attempts have been made to crystallize **2** as a pure lithium salt, which unfortunately were unsuccessful so far (see section 5.6.2).

It is noteworthy that **2** might form two stereoisomers **A** and **B** similar to those observed for **1** (see Figure S1 and Figure S6).

$^{31}P\{^1H\}$ NMR (161.98 MHz, 300 K, THF-d_8): δ / ppm = –164.2 (m, 4 P, Isomer A), –157.2 (m, 4 P, Isomer B). 12.7 (m, 4 P, Isomer A), 9.0 (m, 4 P, Isomer B); *Assignment of the signals is based on integration. Plausible stereoisomers similar to those observed for [K(thf)][Co{(μ-η⁴:η²-P₄)Si(nacnac')}₂] (1) (see Figure S1 and Figure S6).*
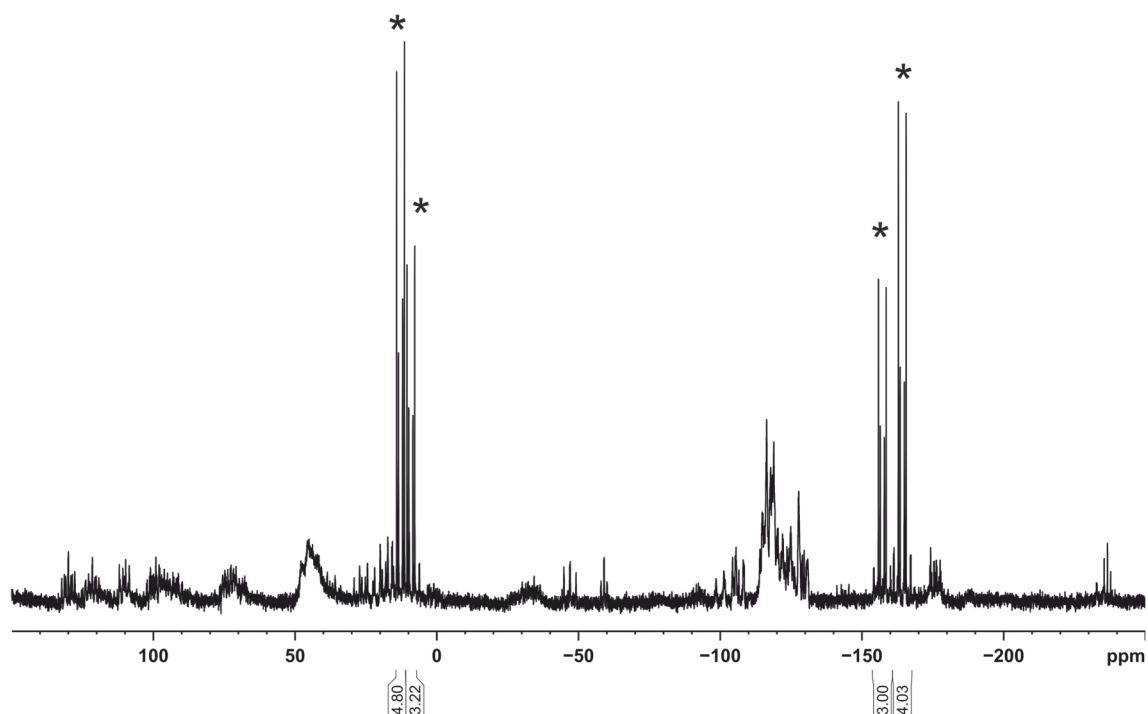
Figure S6. $^{31}P\{^1H\}$ NMR spectrum (161.98 MHz, 300 K, THF-d_8) of the reaction mixture. Signals marked with * might be assigned to $[Li(diox)_2]_2[Fe\{(\mu\text{-}\eta^4\text{:}\eta^2\text{-}P_4)Si(nacnac')\}_2]$ (**2**). Assignment of the signals is based on integration.

5.5.3 Synthesis of [(nacnac)Si(η²-P₄)][BArᶠ₄] (4)
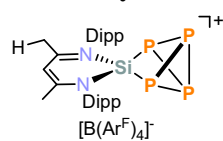
A colorless Et₂O (10 mL) solution of [H(OEt₂)₂][BArᶠ₄] (445 mg, 0.44 mmol, 1.0 equiv.) cooled to −60 °C was added dropwise to a −60 °C precooled yellow solution of [(nacnac′)Si(η²-P₄)] (250 mg, 0.44 mmol, 1.0 equiv.) in Et₂O (10 mL). The yellow reaction mixture was stirred and warmed to room temperature over a period of 16 hours. In the meantime, an orange precipitate formed which was removed by filtration via a teflon filter cannula. The yellow filtrate was concentrated in *vacuo* and stored at −35 °C. After two days yellow crystalline needles were isolated in 36% yield. ¹H NMR spectrum of the isolated product contains 0.25 Et₂O solvate molecules per formula unit after drying in *vacuo* (10⁻³ mbar) over a period of 3 hours.

Note: If necessary, **4** can be washed with *n*-hexane and small portions of cold Et₂O. Compound **4** is unstable in THF and forms a rubbery polymer which was not further investigated.

Yield: 232 mg (36%).

^1H NMR (400.13 MHz, 300 K, CD₂Cl₂): δ / ppm = 1.24 (d, $^3J_{HH}$ = 6.7 Hz, 12 H, Dipp: CH*Me₂*), 1.53 (d, $^3J_{HH}$ = 6.7 Hz, 12 H, Dipp: CH*Me₂*), 2.18 (s, 6 H, ^{Dipp}nacnac: NCC*H₃*), 2.99 (sept, $^3J_{HH}$ = 6.7 Hz, 4 H, Dipp: C*H*Me₂), 5.92 (s, 1 H, ^{Dipp}nacnac: γ-C*H*), 7.55 – 7.60 (m, 6 H, Dipp: 2,6-*i*Pr₂C₆*H₃*), 7.70 – 7.73 (m, 12 H, BArᶠ₄).

$^{13}C\{^1H\}$ NMR (100.61 MHz, 300 K, CD₂Cl₂): δ / ppm = 24.5 (Dipp: CH*Me₂*), 24.7 (^{Dipp}nacnac: NC*C*H₃), 25.8 (^{Dipp}nacnac: N*C*CH₃, 30.4 (Dipp: *C*HMe₂), 104.2 (^{Dipp}nacnac: γ-*C*H), 117.9 (s, BArᶠ₄), 123.7 (Dipp, *C*H), 126.4 (Dipp, *C*H), 127.3 (Dipp, *C*H), 129.3 (qd, $^1J_{FC}$ = 35 Hz, BArᶠ₄), 132.4 (Dipp), 133.3 (Dipp), 135.2 (s, BArᶠ₄), 145.4 (Dipp), 162.2 (1:1:1:1 q, $^1J_{BC}$ = 50 Hz, BArᶠ₄), 174.3 (^{Dipp}nacnac: N*C*CH₂).

$^{31}P\{^{1}H\}$ NMR (161.98 MHz, 300 K, CD$_2$Cl$_2$): A$_2$X$_2$ spin system δ / ppm A$_2$X$_2$ δ(P$_A$) = –336.6 (t, ^{1}J(P$_A$,P$_X$) = 173 Hz, 2 P), δ(P$_X$) = 92.5 (t, ^{1}J(P$_X$,P$_A$) = 137 Hz, 2 P); ^{29}Si satellites: ^{1}J(P$_X$,Si) = 56 Hz).

$^{19}F\{^{1}H\}$ NMR (376 MHz, 300 K, CD$_2$Cl$_2$): δ / ppm = –62.5 (s, BAr$^F_4$).

$^{11}B\{^{1}H\}$ NMR (128 MHz, 300 K, CD$_2$Cl$_2$): δ / ppm = –6.4 (s, BAr$^F_4$).

^{29}Si NMR (99.36 MHz, 300 K, CD$_2$Cl$_2$): δ / ppm = –39.9 (br t, ^{1}J(P$_X$,Si) = 56 Hz).

Elemental analysis calcd. for C$_{29}$H$_{41}$N$_2$P$_4$Si 0.25 C$_4$H$_{10}$O (Mw = 1451.39 g·mol^{-1}): C 51.31, H 3.85, N 1.93; found C 51.93, H 3.76, N 1.80.
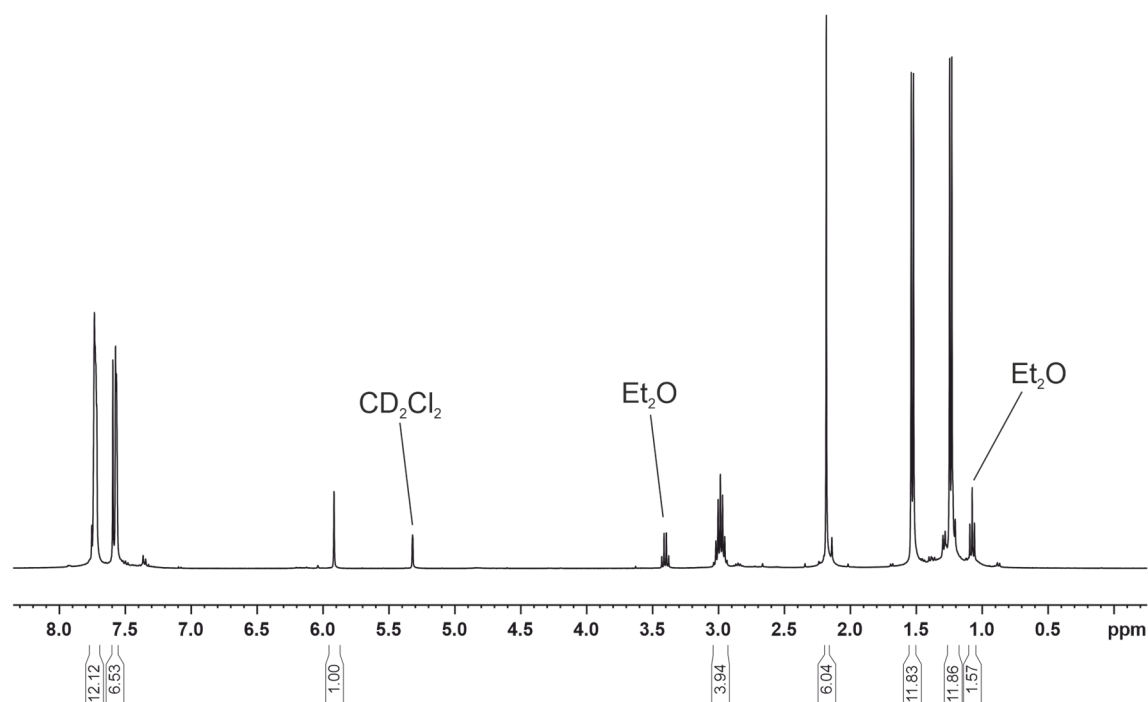
Figure S7. ^{1}H NMR-spectrum (400 MHz, 300 K, CD$_2$Cl$_2$) of [(nacnac)Si(η^2-P$_4$)][BAr$^F_4$] (**4**).
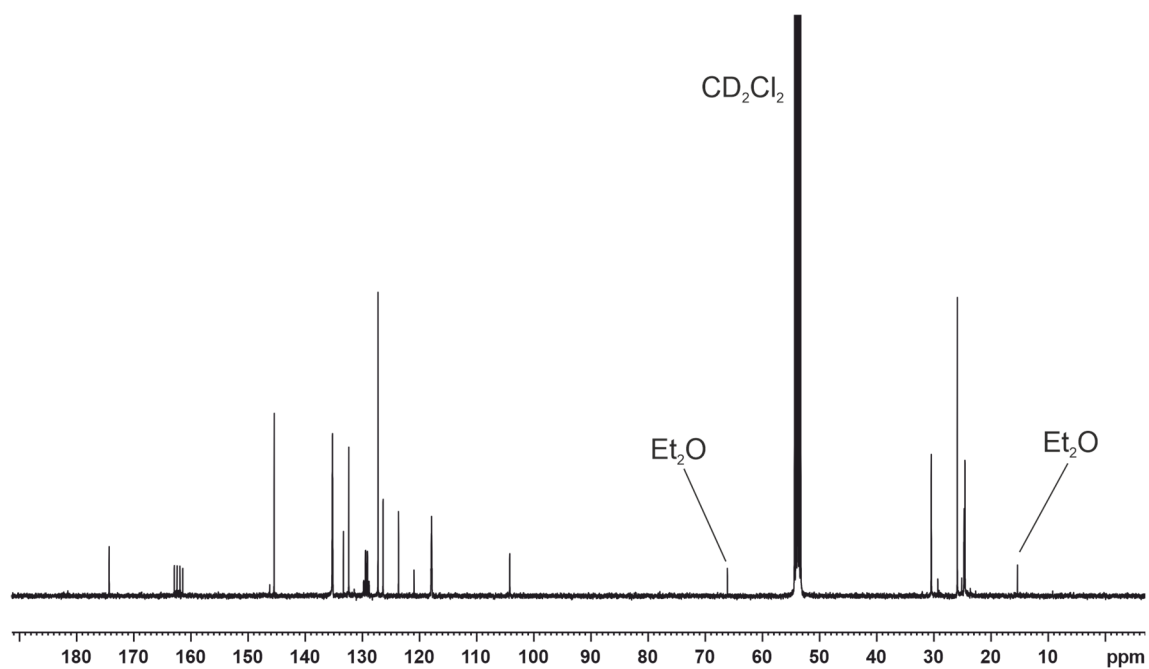
Figure S8. $^{13}C\{^1H\}$ NMR spectrum (100.61 MHz, 300 K, CD$_2$Cl$_2$) of [(nacnac)Si(η^2-P$_4$)][BAr$^F_4$] (**4**).
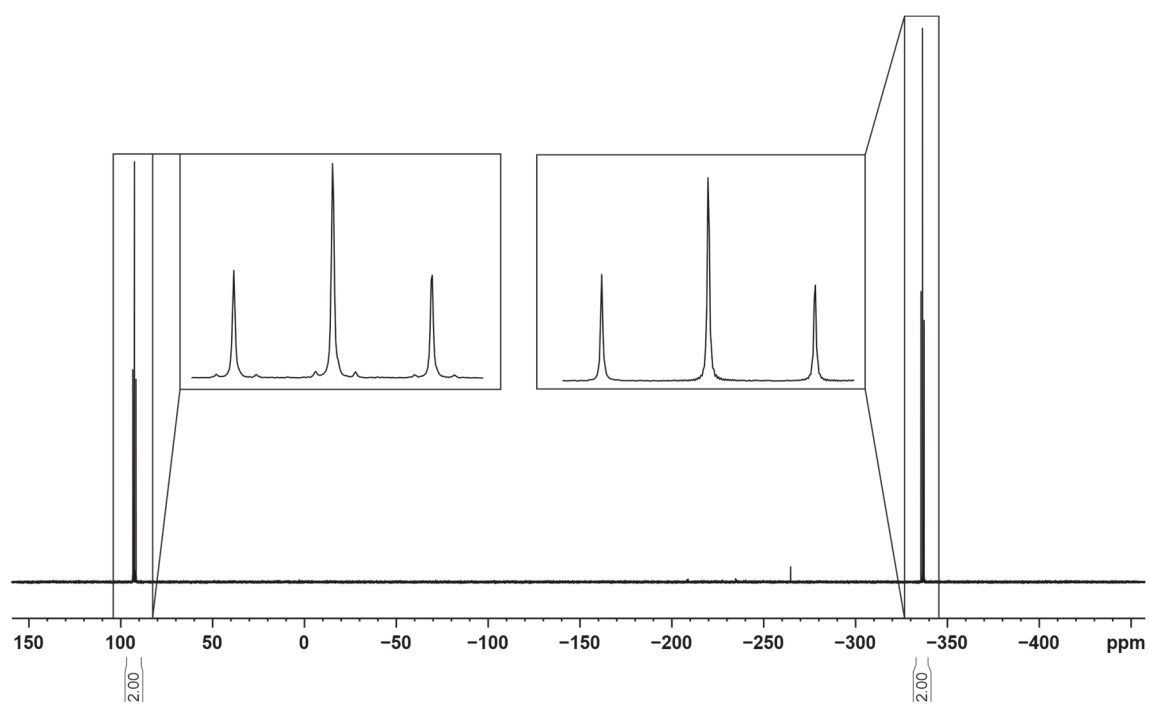
Figure S9. $^{31}P\{^1H\}$ NMR spectrum (161.98 MHz, 300 K, CD$_2$Cl$_2$) of [(nacnac)Si(η^2-P$_4$)][BAr$^F_4$] (**4**).

185
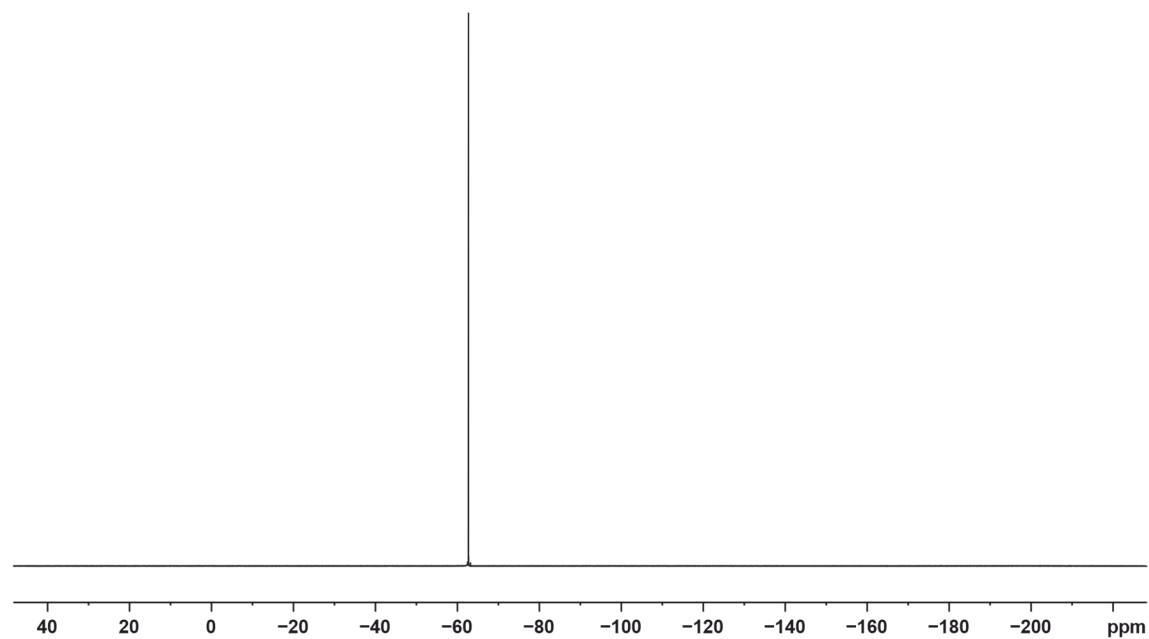
Figure S10. $^{19}F\{^{1}H\}$ NMR spectrum (376 MHz, 300 K, CD₂Cl₂) of [(nacnac)Si(η²-P₄)][BArᶠ₄] (**4**).
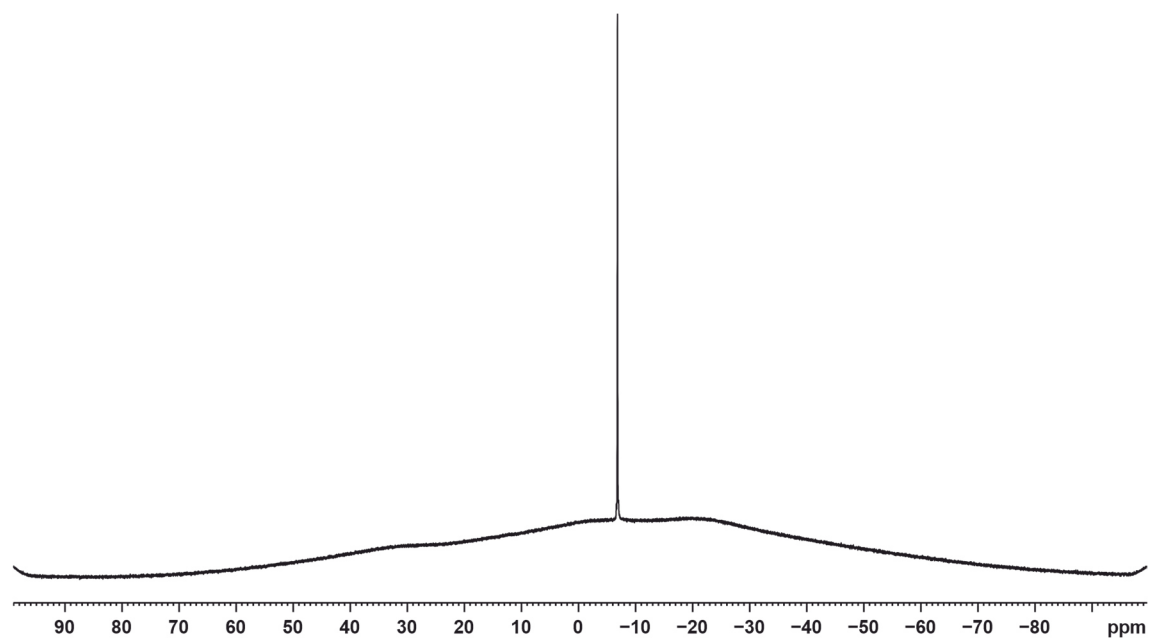
Figure S11. $^{11}B\{^{1}H\}$ NMR spectrum (128 MHz, 300 K, CD₂Cl₂) of [(nacnac)Si(η²-P₄)][BArᶠ₄] (**4**).
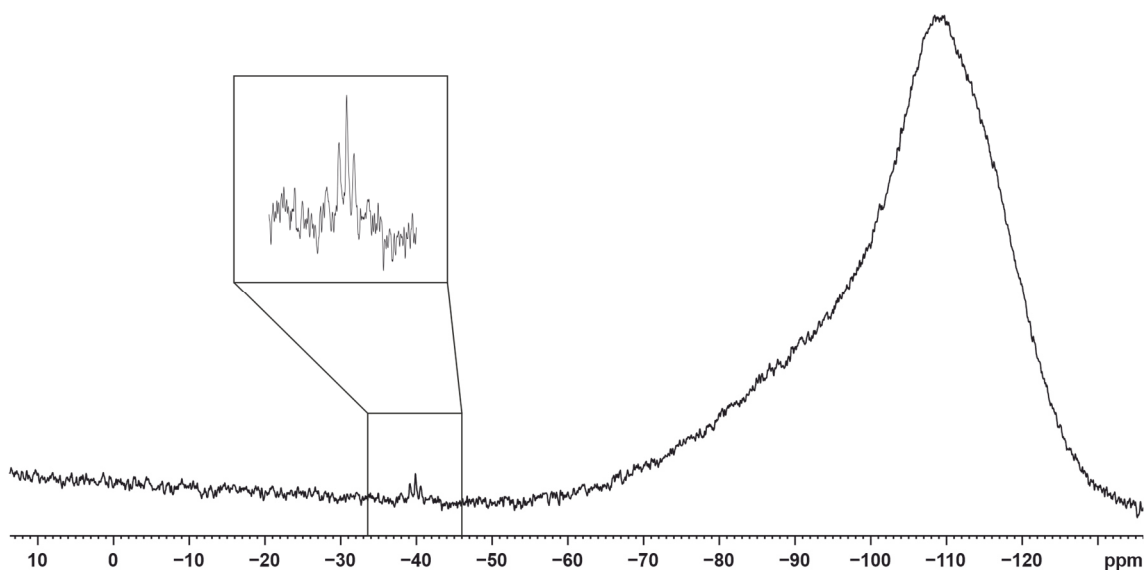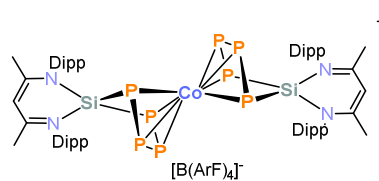
Figure S12. ^{29}Si NMR spectrum (99.36 MHz, 300 K, CD$_2$Cl$_2$) of [(nacnac)Si(η^2-P$_4$)][BAr$^F_4$] (**4**).

5.5.4   Synthesis of [Co{(μ-η⁴:η²-P₄)Si(nacnac)}₂][BArF₄] (5)

A colorless solution of [H(OEt$_2$)$_2$][BAr$^F_4$] (500 mg, 0.50 mmol, 2.0 equiv.) in Et$_2$O (20 mL) was added dropwise to a precooled (−60 °C) solution of [K(thf)][Co{(μ-η^4:η^2-P$_4$)Si(nacnac')}$_2$] (**1**) (332 mg, 0.25 mmol, 1.0 equiv.) in Et$_2$O (20 mL). The reaction mixture was stirred and warmed to room temperature over a period of 16 hours. The resulting brownish-yellow solution was filtered through a glass frit (pore size P4) and the solvent was removed in *vacuo*. The resulting brownish residue was redissolved in Et$_2$O. THF (2 mL) was added dropwise to increase the solubility of the crude product. After layering with *n*-hexane block-shaped brown crystals of [Co{(μ-η^4:η^2-P$_4$)Si(nacnac)}$_2$][B(Ar^F)$_4$] (**5**) were isolated after two days in 36% yield. A ^{1}H NMR spectrum of the isolated product shows 0.56 Et$_2$O solvate molecules per formula unit after drying in *vacuo* (10^{-3} mbar) over a period of 3 hours.

Yield: 187 mg (36%).

^{1}H NMR (400.13 MHz, 300 K, CD$_2$Cl$_2$): δ / ppm = 0.90 (d, $^3J_{HH}$ = 6.7 Hz, 12 H, Dipp: CH*Me₂*), 1.20 (d, $^3J_{HH}$ = 6.7 Hz, 12 H, Dipp: CH*Me₂*), 1.35 (d, $^3J_{HH}$ = 6.7 Hz, 12 H, Dipp: CH*Me₂*), 1.54 (d, $^3J_{HH}$ = 6.7 Hz, 12 H, Dipp: CH*Me₂*), 1.78 (s, 6 H, ^{Dipp}nacnac: NCC*H₃*), 2.10 (s, 6 H, ^{Dipp}nacnac: NCC*H₃*), 2.24 (sept, $^3J_{HH}$ = 6.7 Hz, 4 H, Dipp: C*H*Me₂), 3.30 (sept, $^3J_{HH}$ = 6.7 Hz, 4 H, Dipp: C*H*Me₂), 5.52 (s, 1 H, ^{Dipp}nacnac: γ-C*H*), 7.24 (d, $^3J_{HH}$ = 7.9 Hz, 4 H, Dipp: 2,6-*i*Pr$_2$C$_6$*H₃*), 7.46 (t, $^3J_{HH}$ = 7.9 Hz, 2 H, Dipp: 2,6-*i*Pr$_2$C$_6$*H₃*), 7.56 (m, br, 3 H, BAr$^F_4$), 7.59 (m, 6 H, Dipp: 2,6-*i*Pr$_2$C$_6$*H₃*), 7.72 (m, br, 9 H, BAr$^F_4$).

^{13}C{^{1}H} NMR (100.61 MHz, 300 K, CD$_2$Cl$_2$): δ / ppm = 24.3 (Dipp: CH*Me₂*), 25.1 (^{Dipp}nacnac: NCC*C*H₃), 25.3 (Dipp: CH*Me₂*), 25.5 (Dipp: CH*Me₂*), 26.5 (Dipp: CH*Me₂*), 29.3 (Dipp: *C*HMe₂), 29.8 (Dipp: *C*HMe₂), 101.5 (^{Dipp}nacnac: γ-*C*H), 117.9 (BAr$^F_4$), 120.9 (Dipp), 123.6 (Dipp), 126.3 (Dipp *C*H), 126.9 (Dipp *C*H), 127.4 (Dipp *C*H), 129.3 (qd, $^1J_{CF}$ = 35 Hz, BAr$^F_4$), 130.5 (Dipp, *C*H), 130.8 (Dipp, *C*H), 134.3 (Dipp), 135.2 (BAr$^F_4$), 136.1 (Dipp), 143.8 (Dipp), 145.3 (Dipp), 162.2 (1:1:1:1 q, $^1J_{BC}$ = 50 Hz, BAr$^F_4$), 169.9 (^{Dipp}nacnac: N*C*CH₂), 174.5 (^{Dipp}nacnac: N*C*CH₂).

187

^{31}P{^{1}H} NMR (161.98 MHz, 300 K, CD$_2$Cl$_2$): AA'A''A'''XX'X''X''' spin system δ / ppm
AA'A''A'''XX'X''X''' δ(P$_{AA'A''A'''}$) = –90.4 (m, 4 P), δ(P$_{XX'X''X'''}$) = 138.9 (m, 4 P).

^{19}F{^{1}H} NMR (376 MHz, 300 K, CD$_2$Cl$_2$): δ / ppm = –62.8 (s, BAr$^F_4$).

^{11}B{^{1}H} NMR (128 MHz, 300 K, CD$_2$Cl$_2$): δ / ppm = –6.9 (s, BAr$^F_4$).

^{29}Si NMR (99.36 MHz, 300 K, CD$_2$Cl$_2$): δ / ppm = 21.2 (t, br, ^1J(P,Si) = 144 Hz).

Elemental analysis calcd. for C$_{90}$H$_{94}$CoF$_{24}$N$_4$P$_8$Si$_2$ · 0.56 C$_4$H$_{10}$O (Mw = 2050.62 g·mol^{-1}):
C 52.96, H 4.80, N 2.68; found C 52.83, H 4.71, N 2.51.
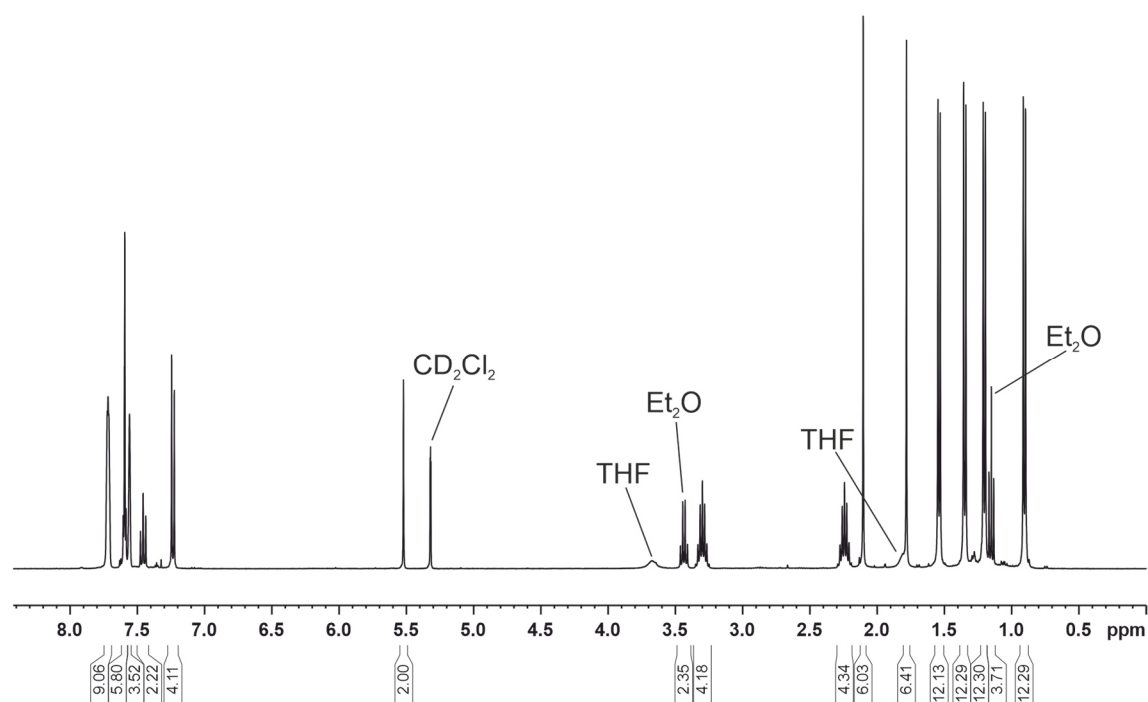
Figure S13. ^{1}H NMR spectrum (400 MHz, 300 K, CD$_2$Cl$_2$) of [Co{(μ-η^4:η^2-P$_4$)Si(nacnac)}$_2$][BAr$^F_4$] (**5**).
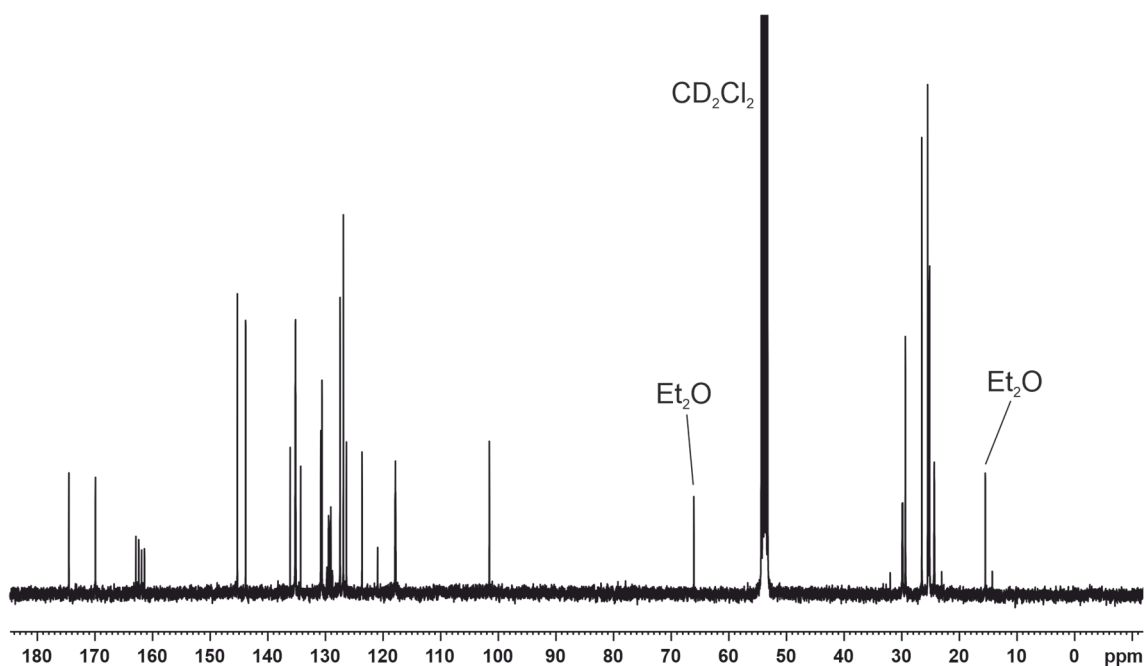
Figure S14. $^{13}C\{^1H\}$ NMR spectrum (100.61 MHz, 300 K, CD_2Cl_2) of $[Co\{(\mu-\eta^4:\eta^2-P_4)Si(nacnac)\}_2][BAr^F_4]$ (**5**).
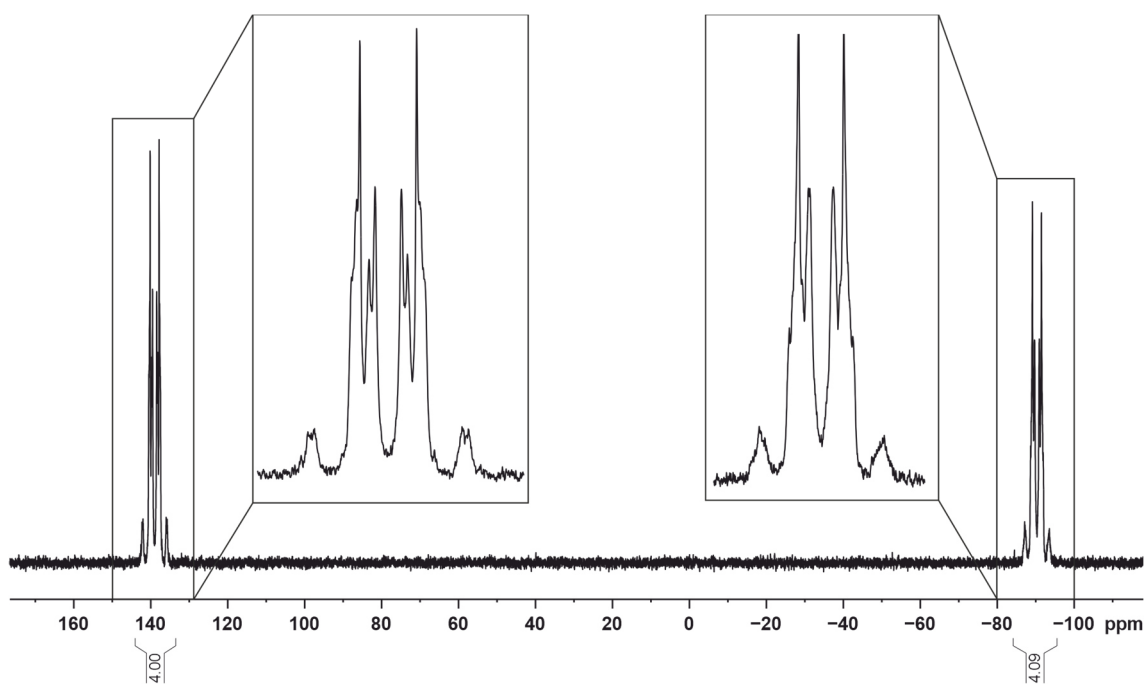
Figure S15. $^{31}P\{^1H\}$ NMR spectrum (161.98 MHz, 300 K, CD_2Cl_2) of $[Co\{(\mu-\eta^4:\eta^2-P_4)Si(nacnac)\}_2][BAr^F_4]$ (**5**).
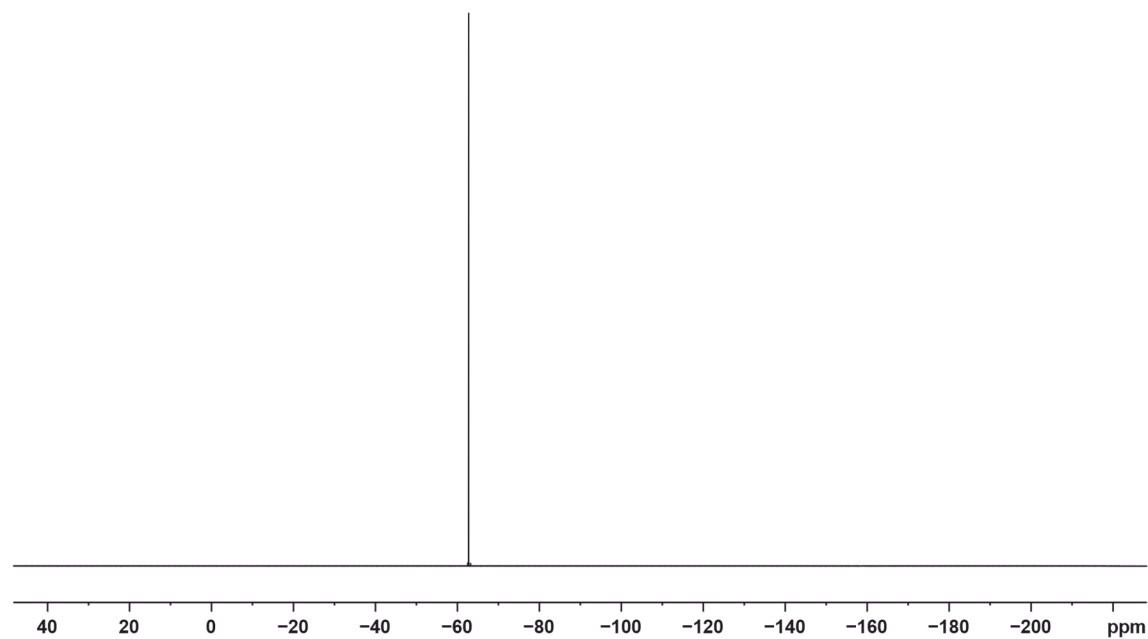
Figure S16. $^{19}F\{^1H\}$ NMR spectrum (376 MHz, 300 K, CD₂Cl₂) of [Co{(μ-η⁴:η²-P₄)Si(nacnac)}₂][BAr^{F}₄] (**5**).
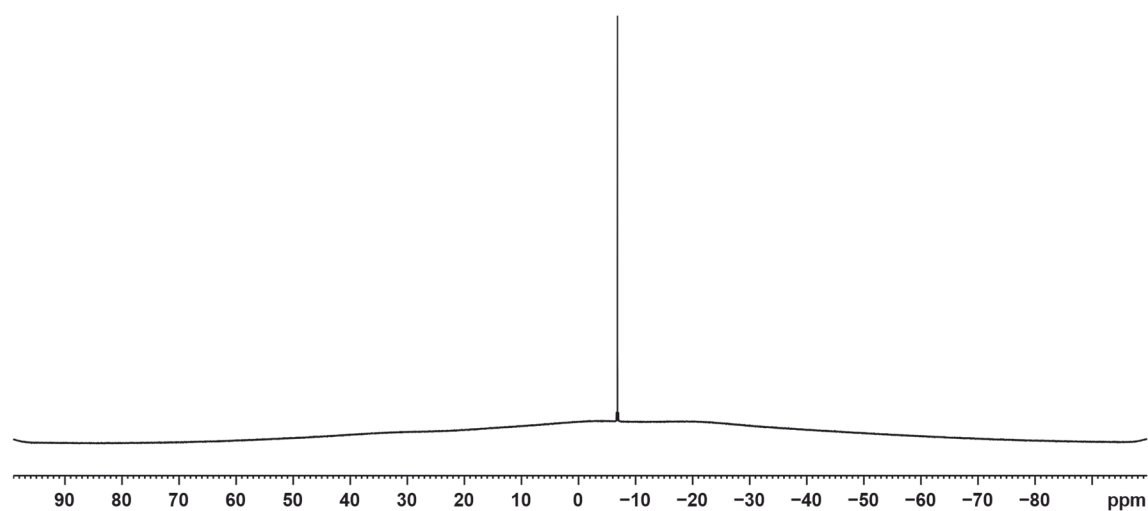
Figure S17. $^{11}B\{^1H\}$ NMR spectrum (128 MHz, 300 K, CD₂Cl₂) of [Co{(μ-η⁴:η²-P₄)Si(nacnac)}₂][BAr^{F}₄] (**5**).
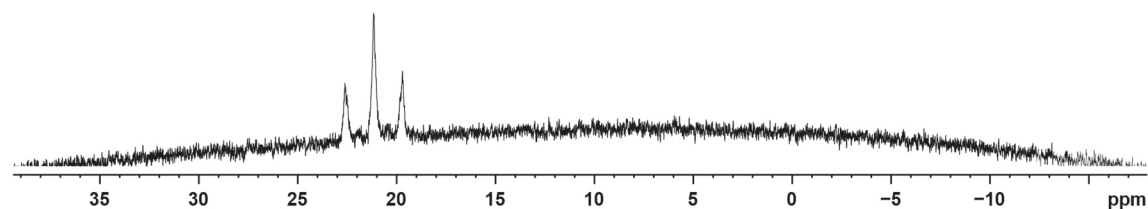
Figure S18. ^{29}Si NMR spectrum (99.36 MHz, 300 K, CD₂Cl₂) of [Co{(μ-η⁴:η²-P₄)Si(nacnac)}₂][BAr^{F}₄] (**5**).
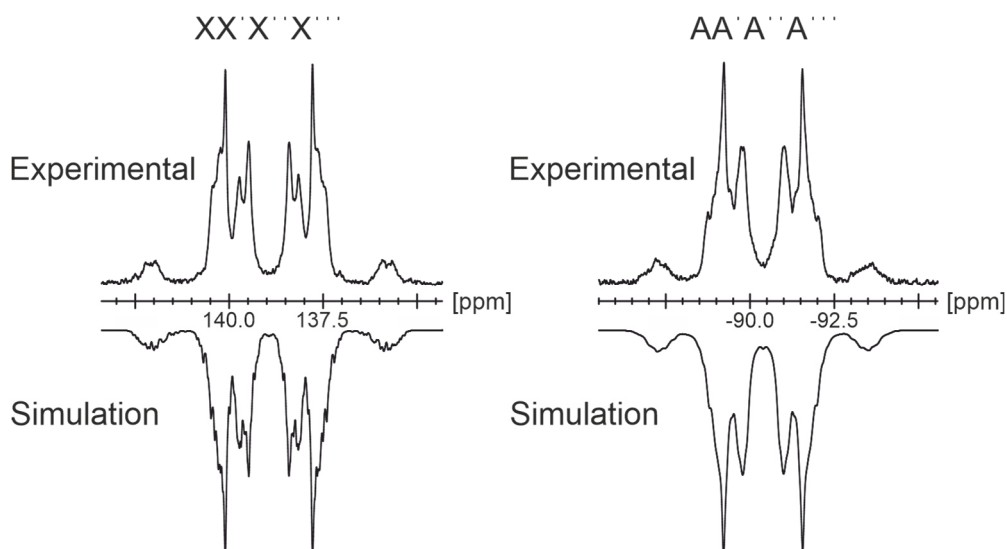
Figure S19. Section of the ^{31}P{^{1}H} NMR (161.98 MHz, 300 K, CD$_2$Cl$_2$) spectrum of [Co{(μ-η^4:η^2-P$_4$)Si(nacnac)}$_2$][BAr$^F_4$] (**5**) experimental (upwards) and simulation (downwards).

Table S1. J(^{31}P,^{31}P) coupling constants obtained by an iterative fitting procedure for an AA′A″A‴XX′X″X‴ spin system. Coupling constants are given in Hz. Schematic representation of the [Co{(μ-η^4:η^2-P$_4$)Si}$_2$] core of [Co{(μ-η^4:η^2-P$_4$)Si(nacnac)}$_2$][BAr$^F_4$] (**5**); [Si] = (nacnac)Si.

Assignment of nuclei	Iterative fitting J(^{31}P,^{31}P)	Assignment of nuclei	Iterative fitting J(^{31}P,^{31}P)
XX′ = X′X	−419.1	XX″ = X′X‴	−36.2
X″X‴ = X‴X″	−381.3	XX‴ = X′X″	−31.9
XA = A′X′	−464.0	X″A = A′X‴	37.2
X′A = A′X	16.9	X‴A = A′X″	0.8
A′A = AA′	−5.7	A″X = AX‴	49.2
A″X″ = A″X‴	−438.7	A″X′ = A‴X	15.8
A″X‴ = A‴X″	21.8	A″A = A‴A′	42.2
A‴A″ = A″A‴	−16.7	A″A′ = A‴A	0.2
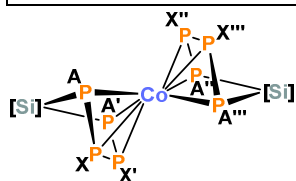
Note on the fitting procedure: The silicon-phosphorus coupling constants were not included in the simulation due to the rather broad signals observed in the experimental ^{31}P{^{1}H} NMR spectra.

5.5.5   Synthesis of [Me₄N]₂[(η³-P₃)Co(µ-η⁴:η²-P₄)Si(nacnac′)] (6) and [Me₄N][(nacnac)SiF₄] (7)
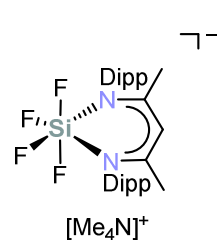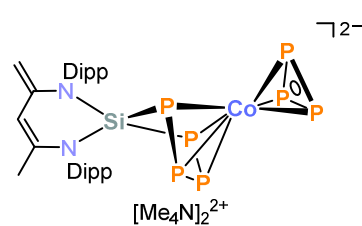
A brownish-yellow solution of [K(thf)][Co{(µ-η⁴:η²-P₄)Si(nacnac′)}₂] (**1**) (80 mg, 0.062 mmol, 1.0 equiv.) in THF (5 mL) was added dropwise to a suspension of [Me₄N]F in THF (5 mL). The reaction mixture was stirred for 24 h at room temperature. Volatiles were removed in *vacuo* and the brownish solid residue was extracted with fluorobenzene. Compound [Me₄N]₂[(η³-P₃)Co(µ-η⁴:η²-P₄)Si(nacnac′)] (**6**) co-crystallizes with the hexacoordinated fluorosilicate [Me₄N][(nacnac)SiF₄] (**7**) from a concentrated DME solution over a period of 2 days at room temperature. Due to the similar solubility of **6** and **7** all attempts to remove by-product **7** were unsuccessful so far.

Note: The reaction only proceeds to completion when five equivalents of [Me₄N]F are present.

^{31}P{^{1}H} NMR (161.98 MHz, 300 K, THF-d_8): δ / ppm = –295.3 (s, 3 P), –117.0 (m, 2 P), 54.9 (m, 2 P).

^{19}F{^{1}H} NMR (376 MHz, 300 K, CD₂Cl₂): δ / ppm = –109.4 (s), 120.2 (s). *Signals might be assigned to the by-product [Me₄N][(nacnac)SiF₄] (**7**).*
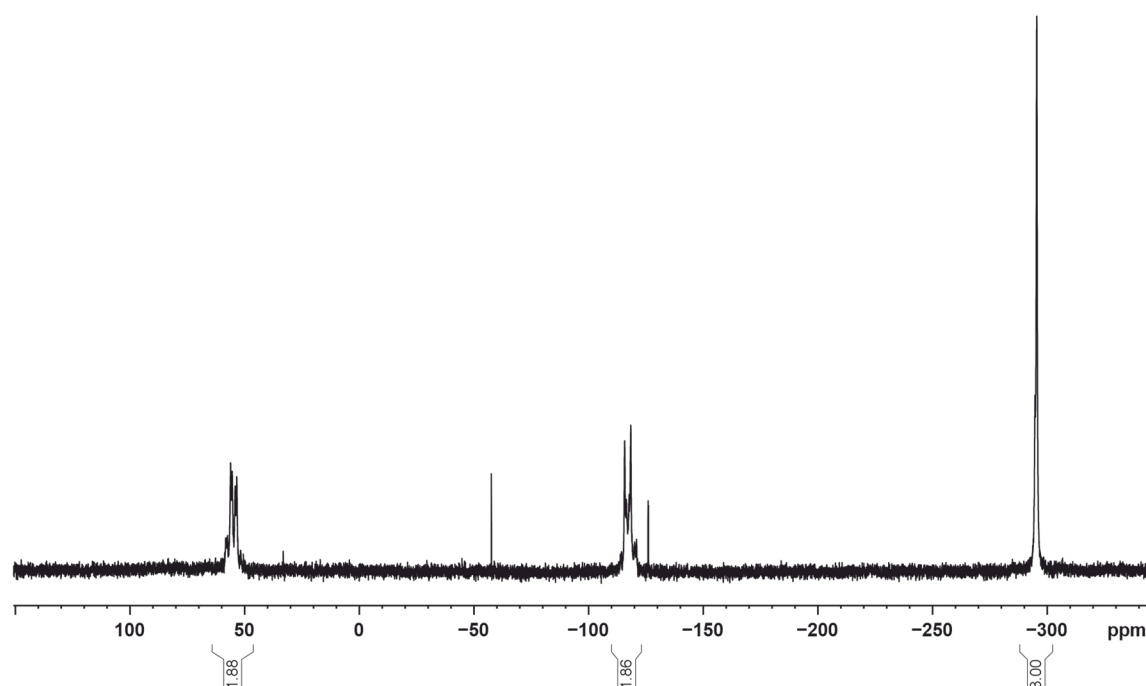
Figure S20. ^{31}P{^{1}H} NMR spectrum (161.98 MHz, 300 K, THF-d_8) of the reaction mixture.
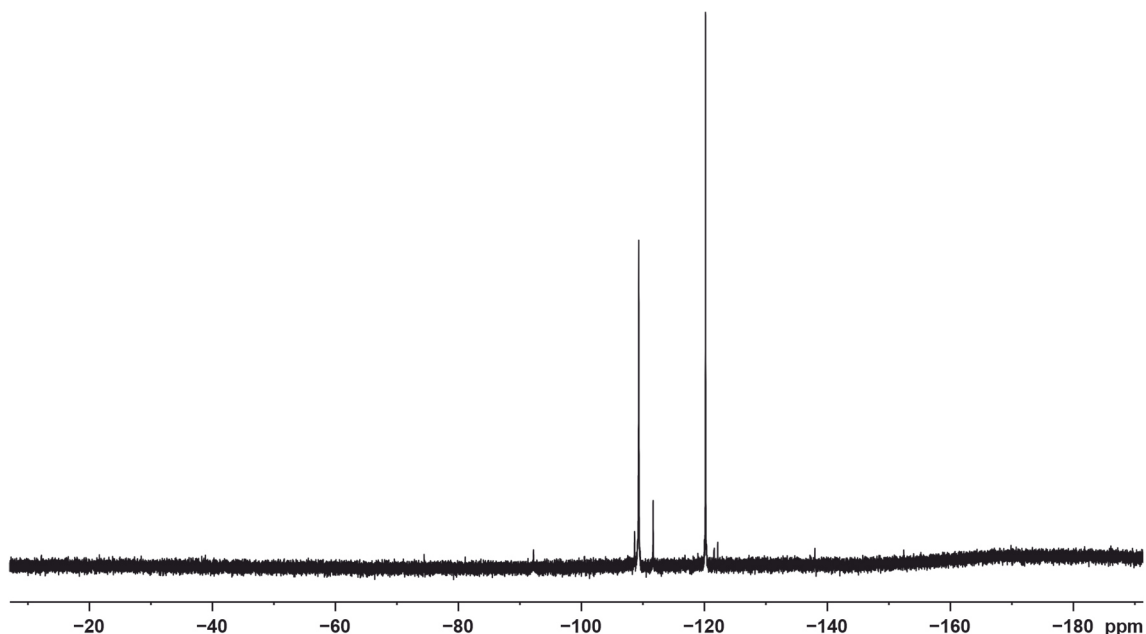
Figure S21. ^{19}F{^{1}H} NMR spectrum (376 MHz, 300 K, THF-d_8) of the reaction mixture.

5.5.6 Synthesis of [(η^4-P$_4$)Co(μ-η^4:η^2-P$_4$)Si(nacnac)] (8)
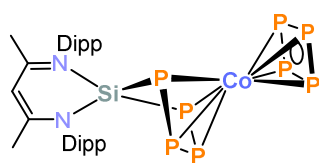
A colorless THF solution (5 mL) of benzoic acid (45.4 mg, 0.372 mmol, 2.0 equiv.) was added to a brownish-yellow THF (10 mL) solution of [K(thf)][Co{(μ-η^4:η^2-P$_4$)Si(nacnac′)}$_2$] (**1**) (230 mg, 0.186 mmol, 1.0 equiv.) at room temperature and stirred for 3 h. Diethyl ether (20 mL) and *n*-hexane (60 mL) were added to the reaction mixture while stirring whereupon a brown powder precipitated. The precipitate was collected on a glass frit (pore size P4). The crude product was washed with a mixture of Et$_2$O/*n*-hexane (10 mL:20 mL v:v) and then washed again with a mixture of Et$_2$O/*n*-hexane (20 mL:20 mL v:v). The brown solid was dried in *vacuo* (10^{-3} mbar) for 3 h and compound [(η^4-P$_4$)Co(μ-η^4:η^2-P$_4$)Si(nacnac)] (**8**) was isolated as brown powder in 60% yield. ^{1}H NMR spectrum of the isolated product contains 0.21 Et$_2$O and 0.17 *n*-hexane solvate molecules per formula unit after drying in *vacuo* (10^{-3} mbar) over a period of 3 hours.

Note: All attempts to grow crystals suitable for a single-crystal X-ray diffraction experiment were unsuccessful so far. However, the presence of [(η^4-P$_4$)Co(μ-η^4:η^2-P$_4$)Si(nacnac)] (**8**) was confirmed by heteronuclear NMR experiments and CHN analysis.

Yield: 88 mg (60%).

^{1}H NMR (400.13 MHz, 300 K, THF-d_8): δ / ppm = 1.09 (d, $^3J_{HH}$ = 6.7 Hz, 6 H, Dipp: CH*Me$_2$*), 1.26 (d, $^3J_{HH}$ = 6.7 Hz, 6 H, Dipp: CH*Me$_2$*), 1.47 (d, $^3J_{HH}$ = 6.7 Hz, 6 H, Dipp: CH*Me$_2$*), 1.67 (d, $^3J_{HH}$ = 6.7 Hz, 6 H, Dipp: CH*Me$_2$*), 1.99 (s, 3 H, ^{Dipp}nacnac: NCC*H$_3$*), 2.17 (s, 3 H, ^{Dipp}nacnac: NCC*H$_3$*), 2.90 (sept, $^3J_{HH}$ = 6.7 Hz, 2 H, Dipp: C*H*Me$_2$), 3.70 (sept, $^3J_{HH}$ = 6.7 Hz, 4 H, Dipp: C*H*Me$_2$), 5.87 (s, 1 H, ^{Dipp}nacnac: γ-C*H*), 7.35 – 754 (m, 6 H, Dipp: 2,6-*i*Pr$_2$C$_6$*H$_3$*).

^{13}C{^{1}H} NMR (100.61 MHz, 300 K, THF-d_8): δ / ppm = 25.1 (Dipp: CH*Me$_2$*), 25.1 (^{Dipp}nacnac: NCC*H$_3$*), 25.3 (^{Dipp}nacnac: NCC*H$_3$*), 25.6 (Dipp: CH*Me$_2$*), 25.9 (Dipp: CH*Me$_2$*), 26.2 (Dipp: CH*Me$_2$*), 102.0 (^{Dipp}nacnac: γ-*C*H), 123.6 (Dipp, *C*H), 125.9 (Dipp), 126.9 (Dipp, *C*H), 127.1

(Dipp, CH), 130.7(Dipp, CH), 130.9 (Dipp, CH), 136.0 (Dipp), 138.6 (Dipp), 145.1 (Dipp,), 146.1 (Dipp,), 170.1 (^{Dipp}nacnac: NCCH₂), 174.9 (^{Dipp}nacnac: NCCH₂).

$^{31}P\{^1H\}$ NMR (161.98 MHz, 300 K, THF-d_8): AMM′XX′ spin system δ / ppm AMM′XX′ δ(P$_{AA'}$) = –86.1 (m, 2 P), δ(P$_{MM'}$) = 111.2 (m, 2 P), δ(P$_X$) = 175.0 (s, 4 P).

Elemental analysis calcd. for C₂₉H₄₁CoN₂P₈Si · 0.21 C₄H₁₀O · 0.17 C₆H₁₄ (Mw = 782.69 g·mol⁻¹): C 47.36, H 5.86, N 3.58; found C 48.06, H 4.98, N 2.80. The small deviation of the CHN analysis is explained by minor impurities presumably of a nacnac derived species which can also be observed in the ¹H NMR spectrum (see Figure S22).
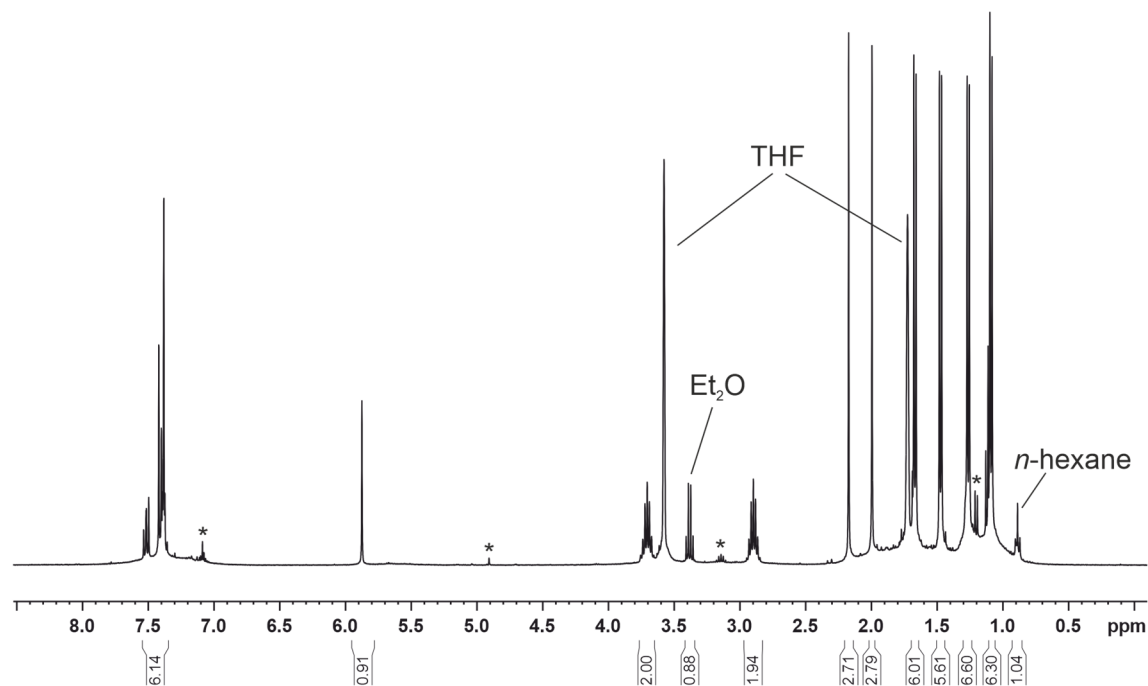
Figure S22. ¹H NMR spectrum (400 MHz, 300 K, THF-d_8) of [(η⁴-P₄)Co(μ-η⁴:η²-P₄)Si(nacnac)] (**8**). Minor impurities are marked with *.
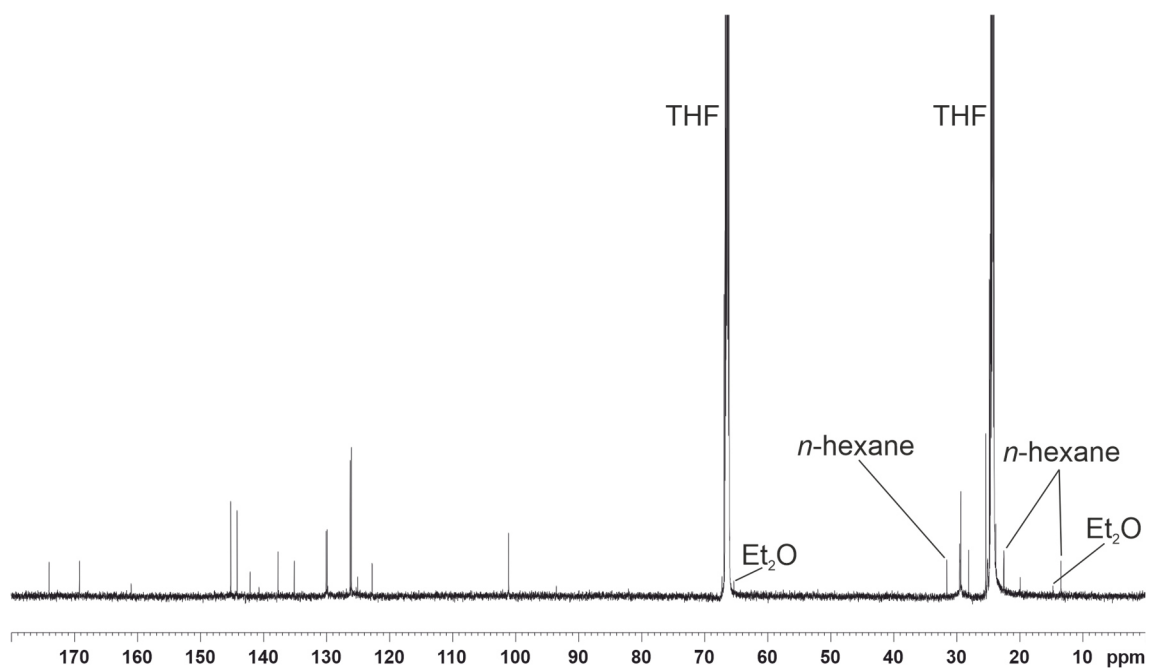
Figure S23. ^{13}C{^{1}H} NMR spectrum (150.88 MHz, 300 K, THF-d_8) of [(η^4-P$_4$)Co(μ-η^4:η^2-P$_4$)Si(nacnac)] (**8**).
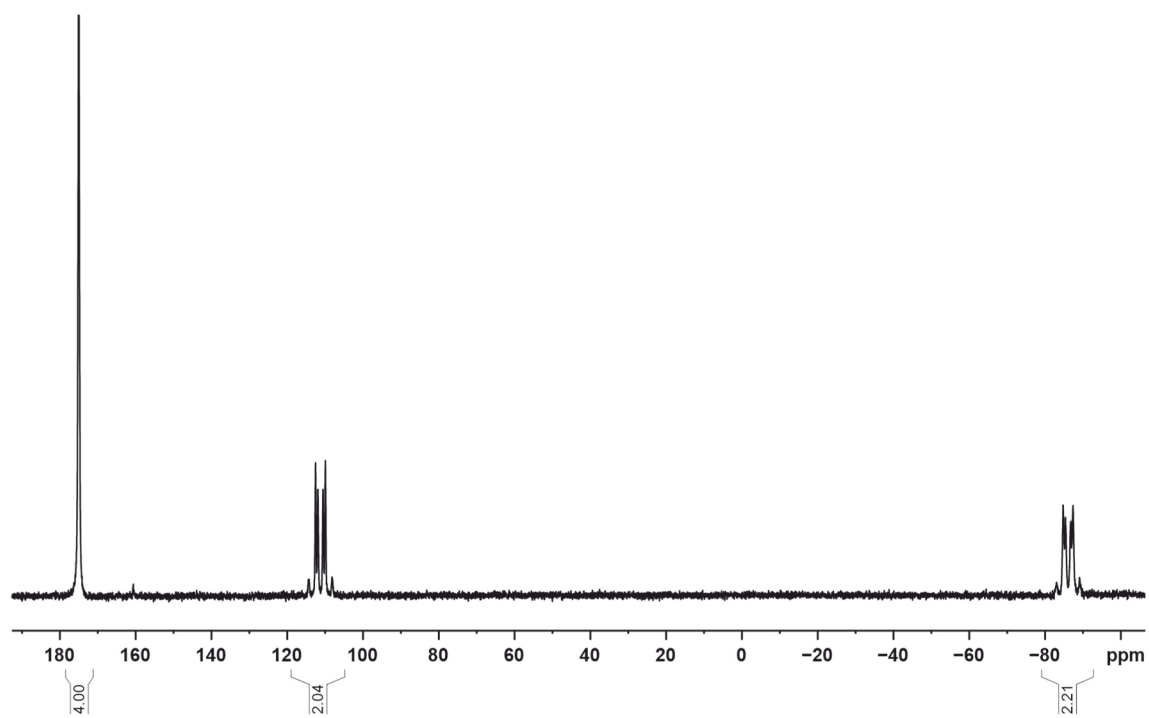
Figure S24. ^{31}P{^{1}H} NMR spectrum (161.98 MHz, 300 K, THF-d_8) of [(η^4-P$_4$)Co(μ-η^4:η^2-P$_4$)Si(nacnac)] (**8**).
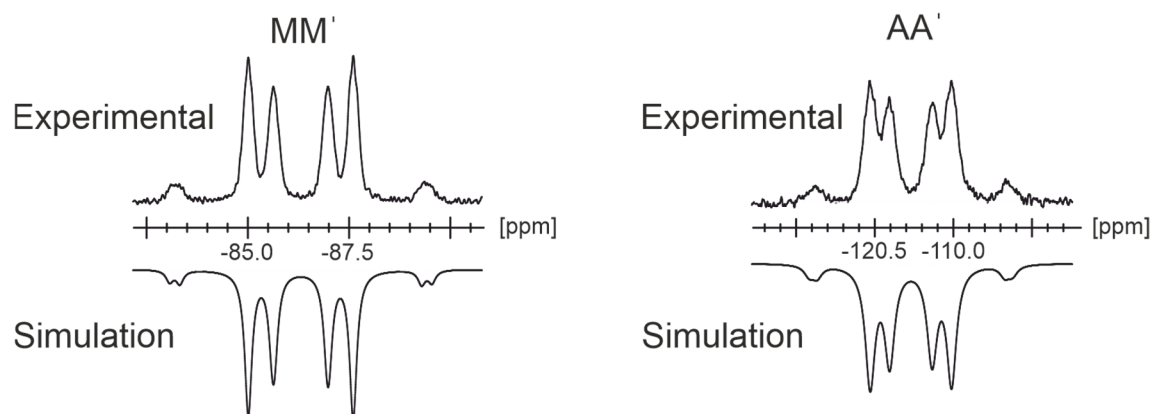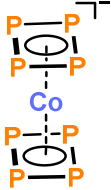
Figure S25. Section of the $^{31}P\{^1H\}$ NMR (161.98 MHz, 300 K, THF-d_8) spectrum of $[(\eta^4\text{-}P_4)Co(\mu\text{-}\eta^4{:}\eta^2\text{-}P_4)Si(nacnac)]$ (**8**) experimental (upwards) and simulation (downwards).

Table S2. $J(^{31}P,^{31}P$ coupling constants from the iterative fit of the AA′MM′X spin system and schematic representation of the [(cyclo-P₄)CoP₄Si] core of $[(\eta^4\text{-}P_4)Co(\mu\text{-}\eta^4{:}\eta^2\text{-}P_4)Si(nacnac)]$ (**8**); [Si] = (nacnac)Si.

$^1J_{XX'} = {}^1J_{X'X}$	−394.9 Hz	$^2J_{MX'} = {}^2J_{M'X}$	24.8 Hz
$^1J_{MX} = {}^1J_{M'X'}$	−444.4 Hz	$^3J_{MM'} = {}^3J_{M'M}$	−24.9 Hz
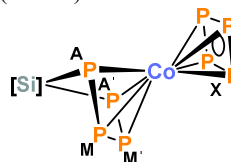
5.5.7 Synthesis of [K(18-crown-6)][Co(η⁴-P₄)₂] (9)

A THF solution (1 mL) of 18-crown-6 (5 mg, 0.02 mmol, 1.0 equiv.) was added to a THF solution (2 mL) of potassium phenolate (2.5 mg, 0.02 mmol, 1.0 equiv.) at room temperature and stirred for 5 minutes. This mixture was then added to a brownish THF solution of [(η⁴-P₄)Co(μ-η⁴:η²-P₄)Si(nacnac)] (**8**) at room temperature and stirred for additional 3 days. The solvent was removed in *vacuo* and the remaining brown solid was washed with Et₂O (3 x 3 mL) and toluene (1 mL). After drying in *vacuo,* the brown residue was extracted with MeCN (filtration through a Whatman glass microfiber filter). All attempts to grow crystals of [K(18-crown-6][Co(η⁴-P₄)₂] (**9**) suitable for a single-crystal X-ray diffraction experiment were unsuccessful so far.

Note: According to ³¹P{¹H} NMR monitoring the formation of **9** can be accelerated by heating the reaction mixture to 45 °C for 1 day. However, this is accompanied by lower selectivity. The reaction was also performed in a completely analogous manner using [2.2.2]cryptand instead of [K(18-crown-6].

¹H NMR (400.13 MHz, 300 K, MeCN-*d₃*): δ / ppm = 3.51 (s, 24 H, 18-crown-6).

³¹P{¹H} NMR (161.98 MHz, 300 K, MeCN-*d₃*): δ / ppm = 239.3 ppm (s).

UV/Vis: (MeCN, λ_max / nm, ε_max / L·mol⁻¹·cm⁻¹): 258 (30000), 296 (21000).

Note: The UV/Vis spectrum was recorded after the described work-up of the reaction mixture. The purity of this sample was only verified by NMR spectroscopy. The UV/Vis spectrum should be remeasured once **9** is isolated and characterized in its pure form.
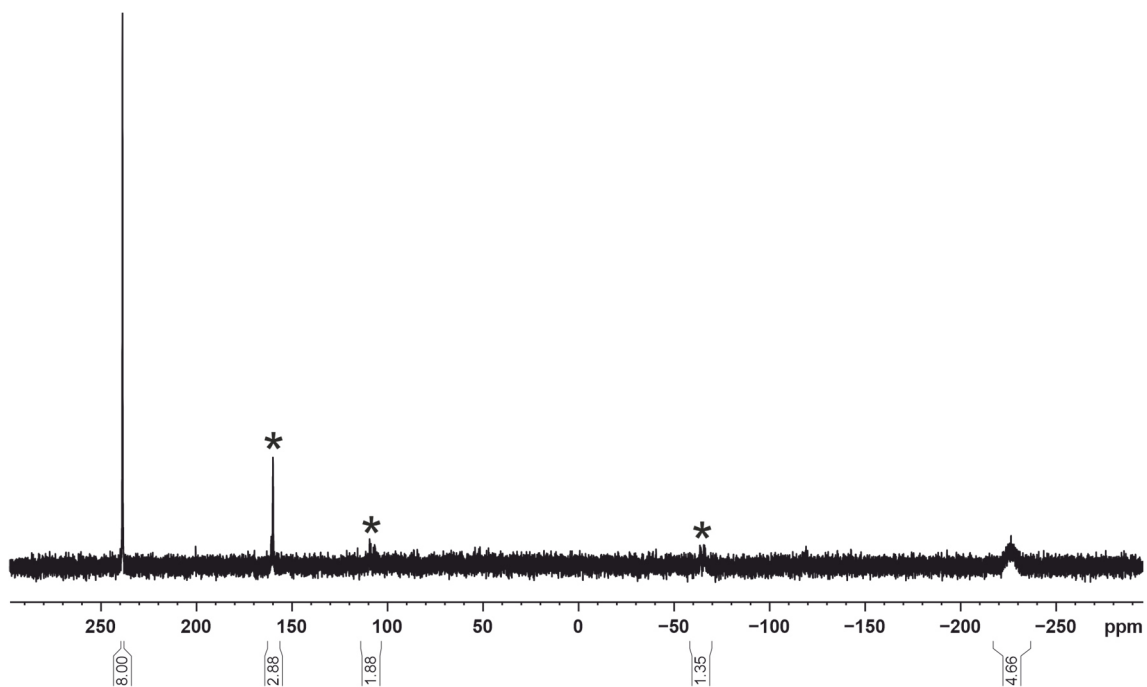

Figure S26. ³¹P{¹H} NMR spectrum (161.98 MHz, 300 K, THF-d₈) of the reaction of [(η⁴-P₄)Co(μ-η⁴:η²-P₄)Si(nacnac)] (**8**) with potassium phenolate in presence of [18-crown-6] after 3 days at room temperature. Signals marked with * can be assigned to unreacted [(η⁴-P₄)Co(μ-η⁴:η²-P₄)Si(nacnac)] (**8**).
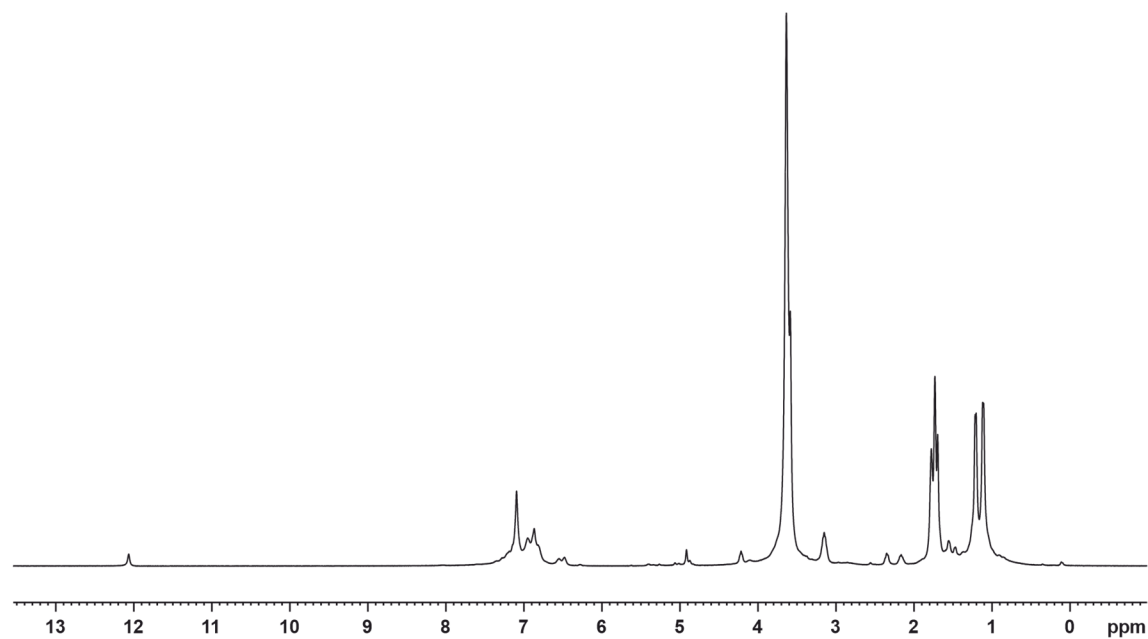
Figure S27. ^{1}H NMR spectrum (400 MHz, 300 K, THF-d_8) of the reaction of [(η^4-P$_4$)Co(μ-η^4:η^2-P$_4$)Si(nacnac)] (**8**) with potassium phenolate in presence of [18-crown-6] after 3 days at room temperature.

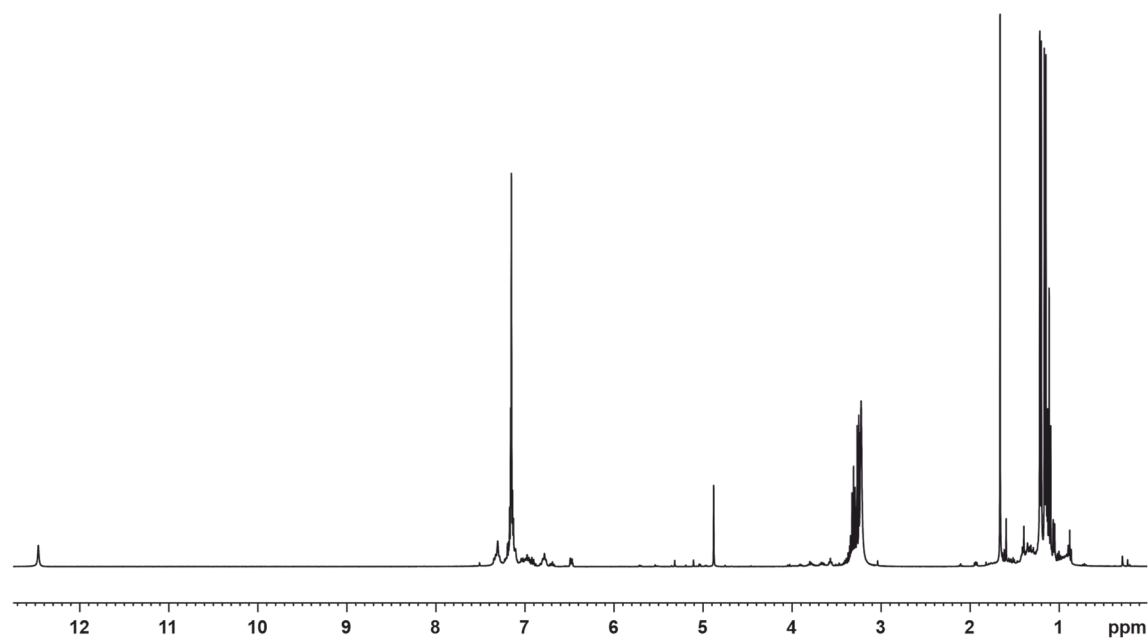**Figure S28.** ^{1}H NMR spectrum (400 MHz, 300 K, C$_6$D$_6$) of the Et$_2$O washing solution of the reaction of [(η^4-P$_4$)Co(μ-η^4:η^2-P$_4$)Si(nacnac)] (**8**) with potassium phenolate in presence of [18-crown-6]. The absence of a P-containing species was confirmed by ^{31}P{^{1}H} NMR spectroscopy.
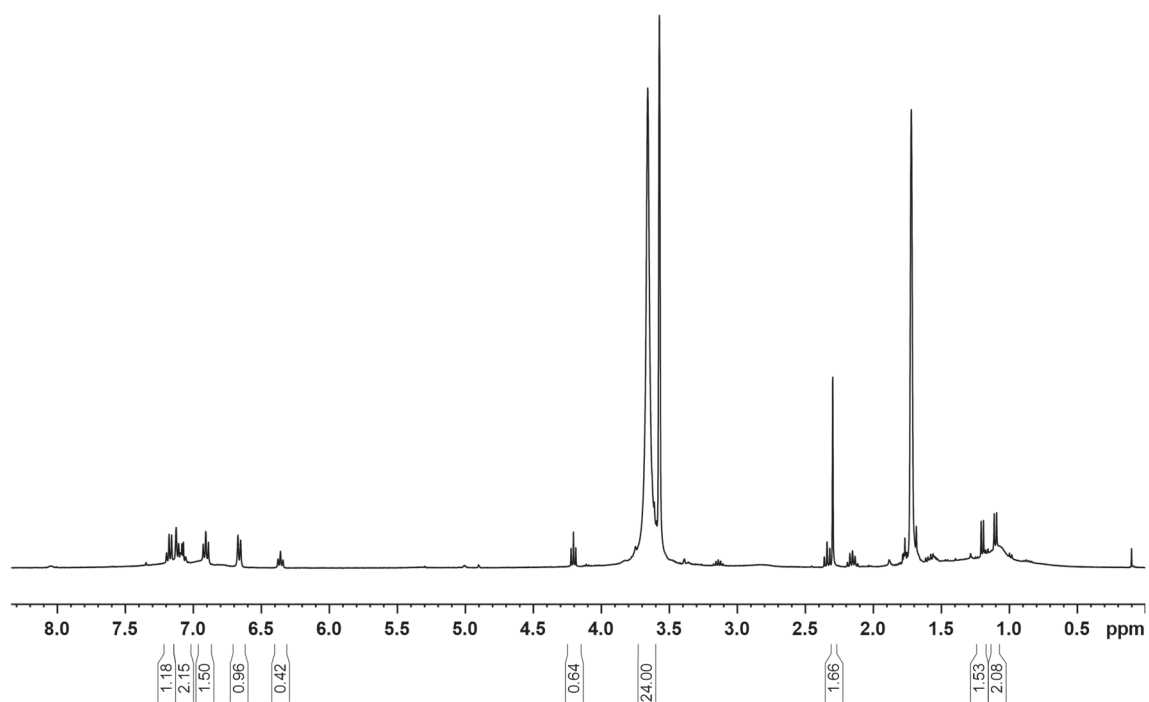
Figure S29. ^{1}H NMR spectrum (400 MHz, 300 K, THF-d$_8$) of the solid residue of the reaction of [(η^4-P$_4$)Co(μ-η^4:η^2-P$_4$)Si(nacnac)] (**8**) with potassium phenolate in presence of [18-crown-6] after washing with Et$_2$O and toluene.
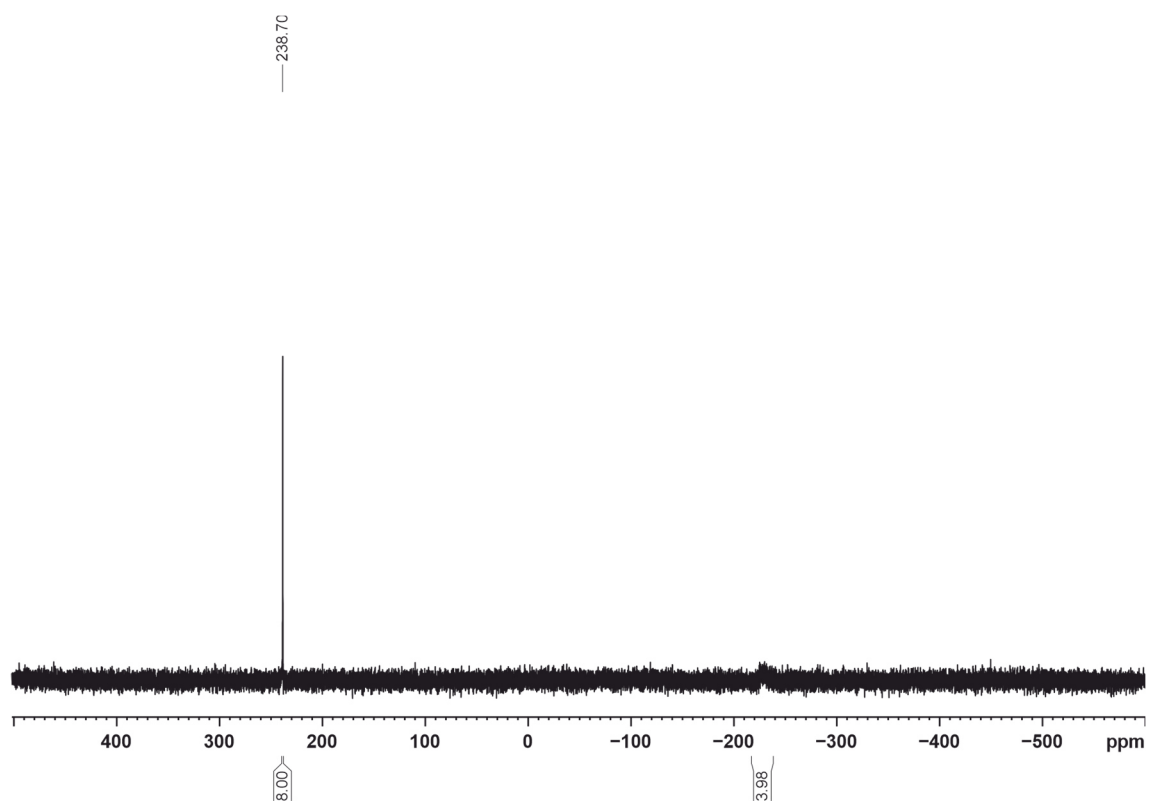
Figure S30. ^{31}P{^{1}H} NMR spectrum (161.98 MHz, 300 K, THF-d$_8$) of the solid residue of the reaction of [(η^4-P$_4$)Co(μ-η^4:η^2-P$_4$)Si(nacnac)] (**8**) with potassium phenolate in the presence of [18-crown-6] after washing with Et$_2$O and toluene.
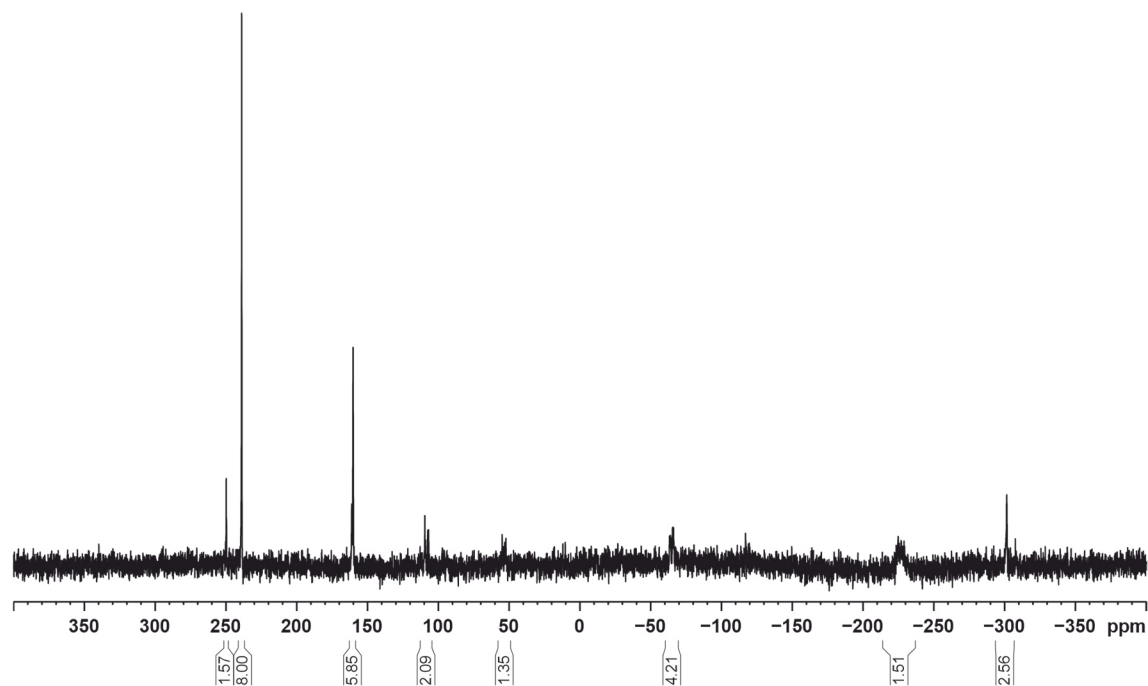
Figure S31. ^{31}P{^{1}H} NMR spectrum (161.98 MHz, 300 K, THF-d$_8$) of the reaction of [(η^4-P$_4$)Co(μ-η^4:η^2-P$_4$)Si(nacnac)] (**8**) with potassium phenolate in presence of [18-crown-6] after 1 day at 45 °C.
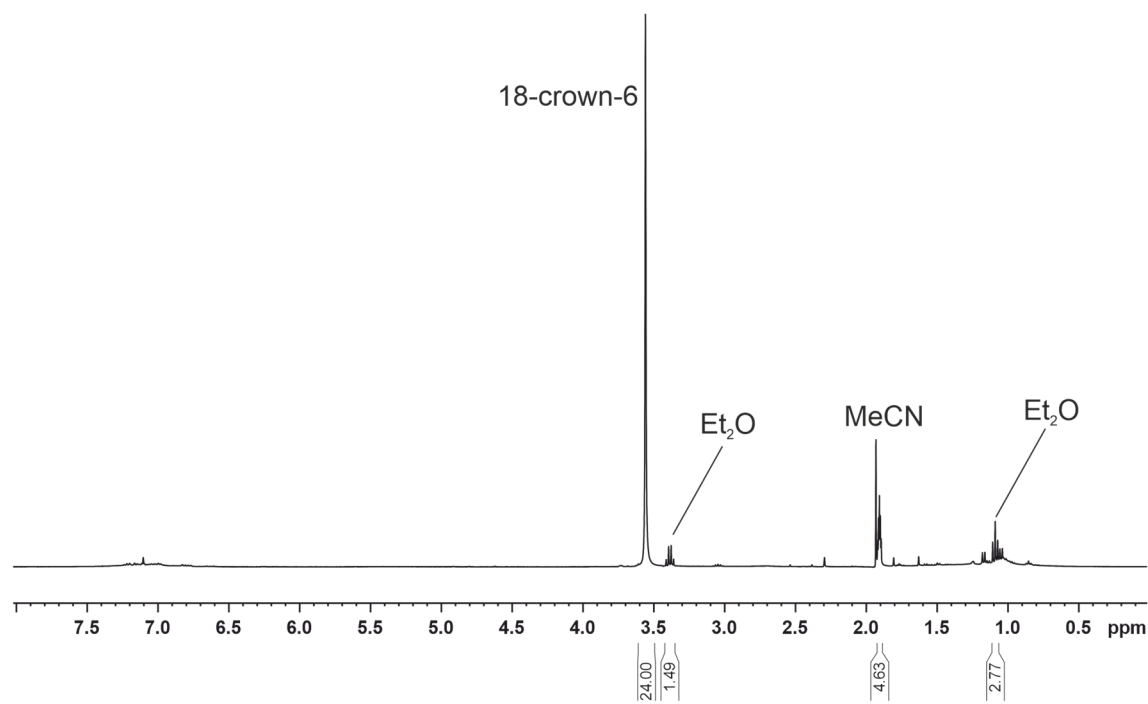
Figure S32. ^{1}H NMR spectrum (400 MHz, 300 K, MeCN-d$_3$) of the reaction of [(η^4-P$_4$)Co(μ-η^4:η^2-P$_4$)Si(nacnac)] (**8**) with potassium phenolate and [18-crown-6] after 1 day at 45 °C and work-up. Work-up involved washing of the crude product with Et$_2$O and toluene and subsequent extraction with MeCN.

Figure S33. ^{31}P{^{1}H} NMR spectrum (161.98 MHz, 300 K, MeCN-d_3) of the reaction of [(η⁴-P₄)Co(μ-η⁴:η²-P₄)Si(nacnac)] (**8**) with potassium phenolate and [18-crown-6] after 1 day at 45 °C and work-up. Work-up involved washing of the crude product with Et₂O and toluene and subsequent extraction with MeCN.
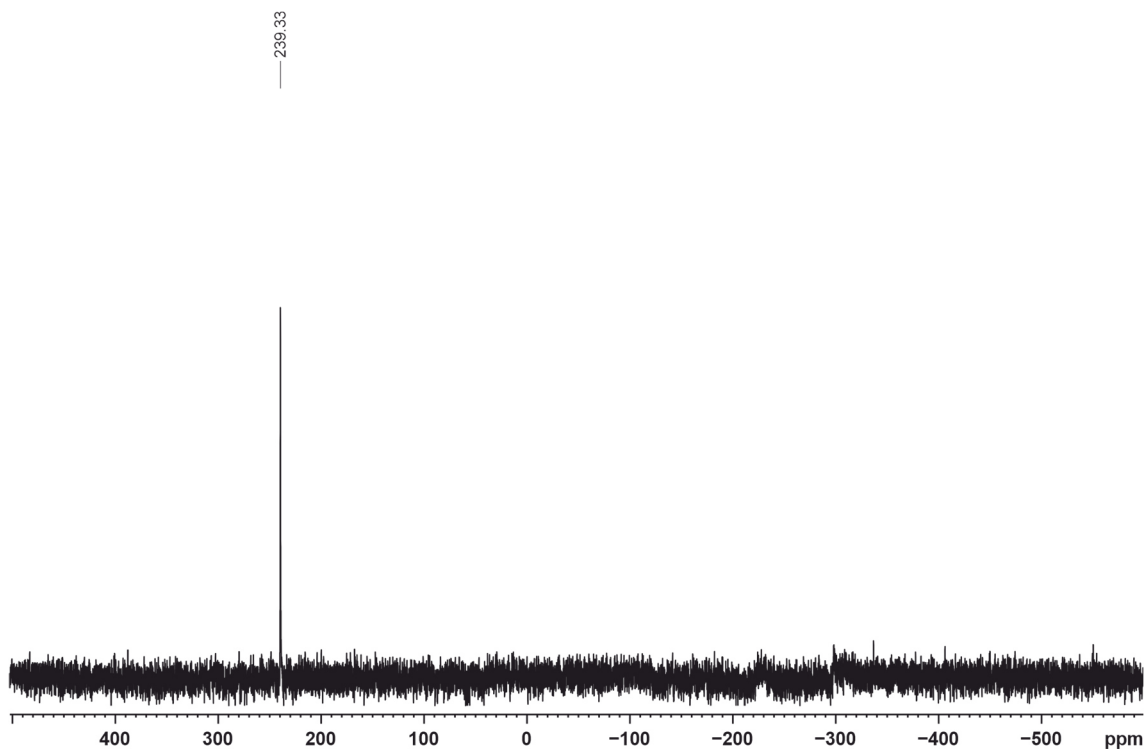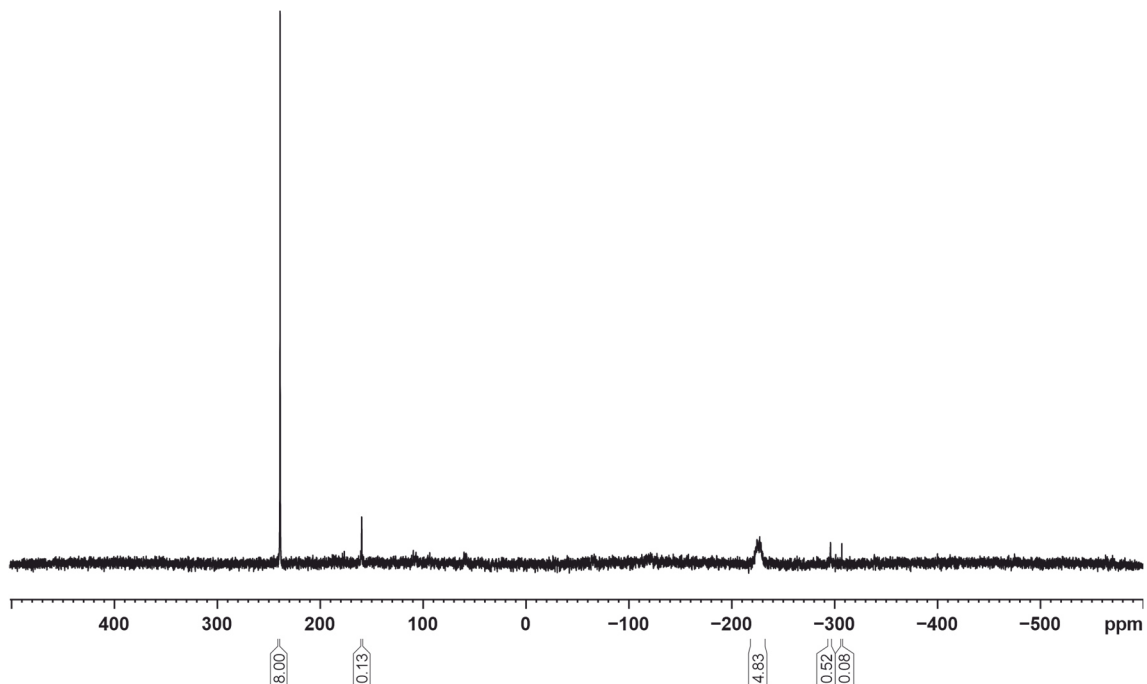

Figure S34. ^{31}P{^{1}H} NMR spectrum (161.98 MHz, 300 K, THF-d_8) of the reaction of [(η⁴-P₄)Co(μ-η⁴:η²-P₄)Si(nacnac)] (**8**) with potassium phenolate in presence of [2.2.2]cryptand.

5.5.7 Mass spectrometric investigation of the reaction of [(η⁴-P₄)Co(μ-η⁴:η²-P₄)Si(nacnac)] (8) with potassium phenolate in presence of 18-crown-6

In an argon atmosphere, a THF solution of 18-crown-6 (5 mg, 0.02 mmol, 1.0 equiv.) was added to a THF solution of potassium phenolate (2.5 mg, 0.02 mmol, 1.0 equiv.) at room temperature and stirred for 5 minutes. This mixture was then added to a brownish THF solution of [(η⁴-P₄)Co(μ-η⁴:η²-P₄)Si(nacnac)] (**8**) at room temperature and stirred for additional 3 days. The solvent was removed in *vacuo* and the remaining brown solid was washed with Et₂O (3 x 3 mL) and toluene (1 mL). After drying in *vacuo,* the remaining brown solid was extracted with MeCN and filtered through a Whatman glass microfiber filter. The reaction mixture was diluted to a concentration of approximately $1 \cdot 10^{-5}$ mol·L⁻¹ and injected into the ESI-MS spectrometer *via* a Hamilton syringe. The sample was analyzed by ESI in negative mode using a fragmentation potential of 120V. Mass spectrometry was performed by the analytical department of the University of Regensburg with an Agilent Q-TOF 6540 UHD mass spectrometer. The obtained mass spectrum suggests the presence of [(η⁴-P₄)₂Co]⁻ (the anion of compound **9**, calculated m/z = 306.7233).
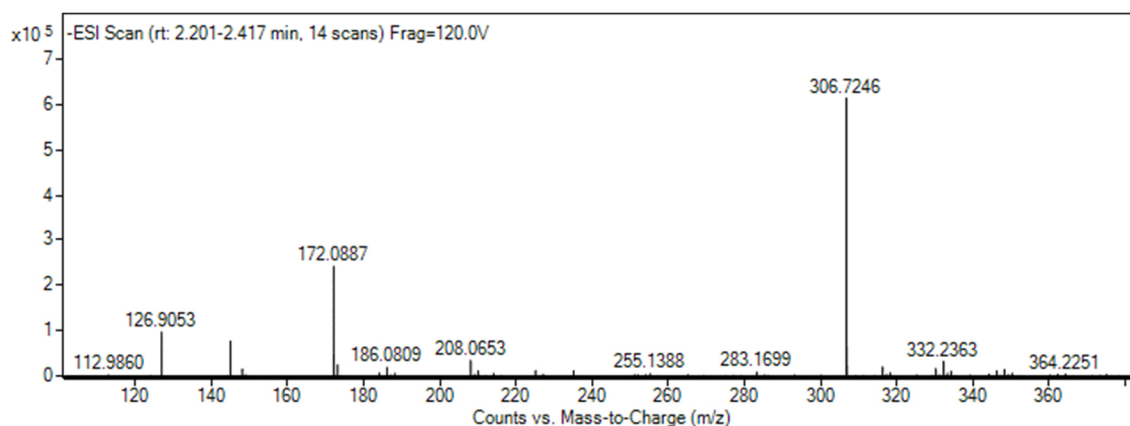

Figure S35. ESI-MS spectrum (rt 2.201-2.417, 14 scans) Frag = 120V.

5.6   X-ray Crystallography

Crystallographic data were recorded on a Super Nova with a Mikrofocus Cu anode and an Atlas CCD Detector (**1**, **2**, **3**, **4**), or on a GV1000 with a TitanS2 detector (**5**) or a XtaLAB Synergy R, DW system with HyPix-Arc 150 detector (**6**, **7**). In all cases, Cu-K$_\alpha$ radiation (λ = 1.54184 Å) was used except for **5** which was measured using Cu-K$_\beta$ radiation (λ = 1.39222 Å). Crystals were selected under mineral oil, mounted on micromount loops and quench-cooled using an Oxford Cryosystems open flow N$_2$ cooling device. The diffraction pattern was indexed and the total number of runs and images was based on the strategy calculation from the program CrysAlisPro (Rigaku, V1.171.41_64.93a, 2020). The unit cell was refined using the same program. Either semi-empirical multi-scan absorption corrections[6] or analytical[7] ones were applied to the data. Using Olex2,[8] the structures were solved with SHELXT[9] using intrinsic phasing and refined with SHELXL[10] using least squares refinement on F^2. The hydrogen atoms were located in idealized positions and refined isotropically with a riding model.

5.6.1   Refinement of the solid-state molecular structure of [K(dme)₃][Co{(μ-η⁴:η²-P₄)Si(nacnac′)}₂] (1-dme)
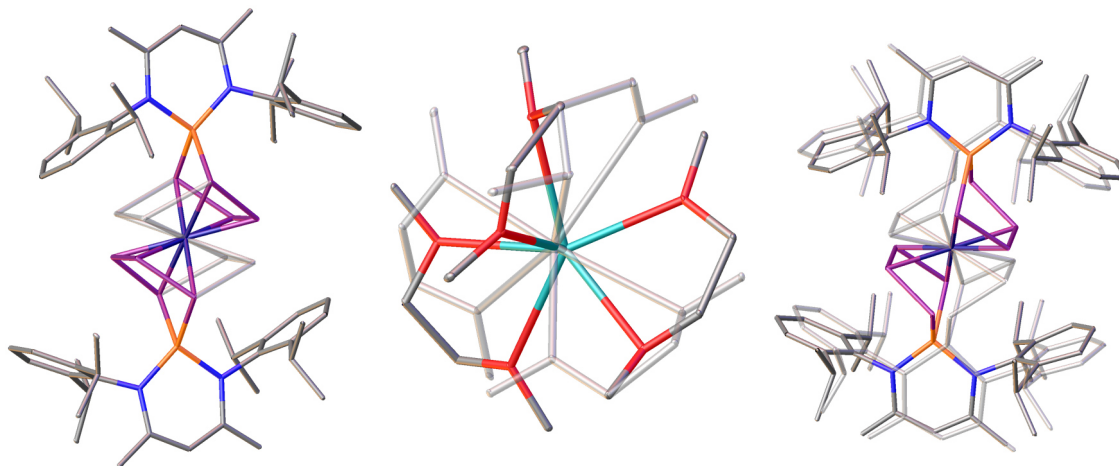
Figure S36. Wire/Stick representation of extracts of the grown solid-state molecular structure of **1-dme**. Hydrogen atoms are omitted for clarity. Transparent parts depict disorders (PART 2).

Several crystallization efforts only afforded weakly diffracting crystals. All tested crystals showed disorder in the phosphorus framework as well as in the counter ion. Addition of crown ethers did not lead to an improvement of the disorders. The best quality crystals were formed by crystallizing **1** from a concentrated solution of DME layered with *n*-hexane. **1-dme** crystallizes in the triclinic space group P-1 with one cation and two times half of the anionic molecule in the asymmetric unit. Disorder of the DME molecules around the potassium cation was treated with strong restraints (SIMU, DFIX) to model a chemically sensible coordination of the potassium cation. Disorder of the phosphorus framework was treated with the SIMU restraint. One of the [Si(nacanc′)] moieties was additionally split into two parts to maintain a reasonable connectivity to the *catena*-P₄ moiety. The modeled disorders are presented in Figure S36. Due to the heavy disorder of the solid-state molecular structure of **1-dme** structural parameters must be considered carefully, especially within the phosphorus framework.

5.6.2 Refinement of the solid-state molecular structure of [Li(diox)₂]₂[Fe{(μ-η⁴:η²-P₄)Si(nacnac′)}₂] (2)
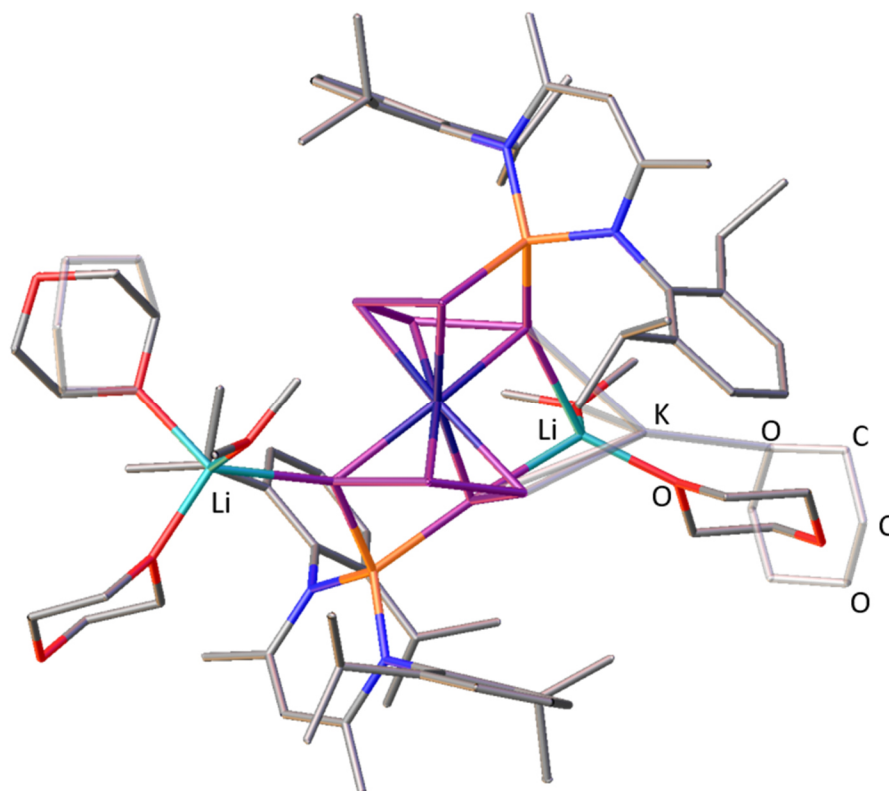

Figure S37. Wire/Stick representation of the solid-state molecular structure of **2**. Hydrogen atoms and solvate molecules are omitted for clarity. Transparent parts depict disorders (PART 2).

Several crystallization efforts afforded only weakly diffracting crystals. **2** crystallizes in the triclinic space group P-1 with one molecule of **2** in the asymmetric unit. High residual electron density close to the disordered 1,4-dioxane solvate molecule could be assigned to a potassium atom with a crystallographic occupancy of 0.153. After refinement of the solid-state molecular structure of **2** the molecular formula consists of $C_{79}H_{123}FeK_{0.153}Li_{1.847}N_4O_9P_8Si_2$. It remains unclear where the potassium ion originates from. Several attempts have been made to crystallize **2** as a pure lithium salt which however were unsuccessful so far (see 5.5.3 for further details).

The Li/K counter ions are coordinated by three 1,4-dioxane solvate molecules forming a coordination polymer in the solid-state. This likely explains that crystallization of **2** was only successful from a saturated 1,4-dioxane solution of **2** layered with *n*-hexane (see section 5.5.3). The distance of the coordinating disordered 1,4-dioxane solvate molecule to the potassium cation is 2.776(14) Å, which is in the typical range of K–O distances.[11] In comparison, the Li–O distances are significantly shorter and range from 1.929(5) Å to 1.975(4) Å. During the refinement a disorder of a 1,4-dioxane molecule was resolved by splitting the solvate molecule into two parts. Atomic displacement parameters (ADPs) were restrained with SIMU.

5.6.3 Refinement of the solid-state molecular structure of [(nacnac)Si(η²-P₄)][B(ArF)₄] (4)

[(nacnac)Si(η²-P₄)][B(ArF)₄] (**4**) crystallizes in the triclinic space group P-1 with one cation and one anion in the asymmetric unit. Only one CF_3 group of [B(ArF)₄] shows a weak disorder which was resolved by splitting this group into two parts and the ADPs were restrained with a RIGU.

5.6.4 Refinement of the solid-state molecular structure of [Co{(μ-η⁴:η²-P₄)Si(nacnac)}₂][B(ArF)₄] (5)
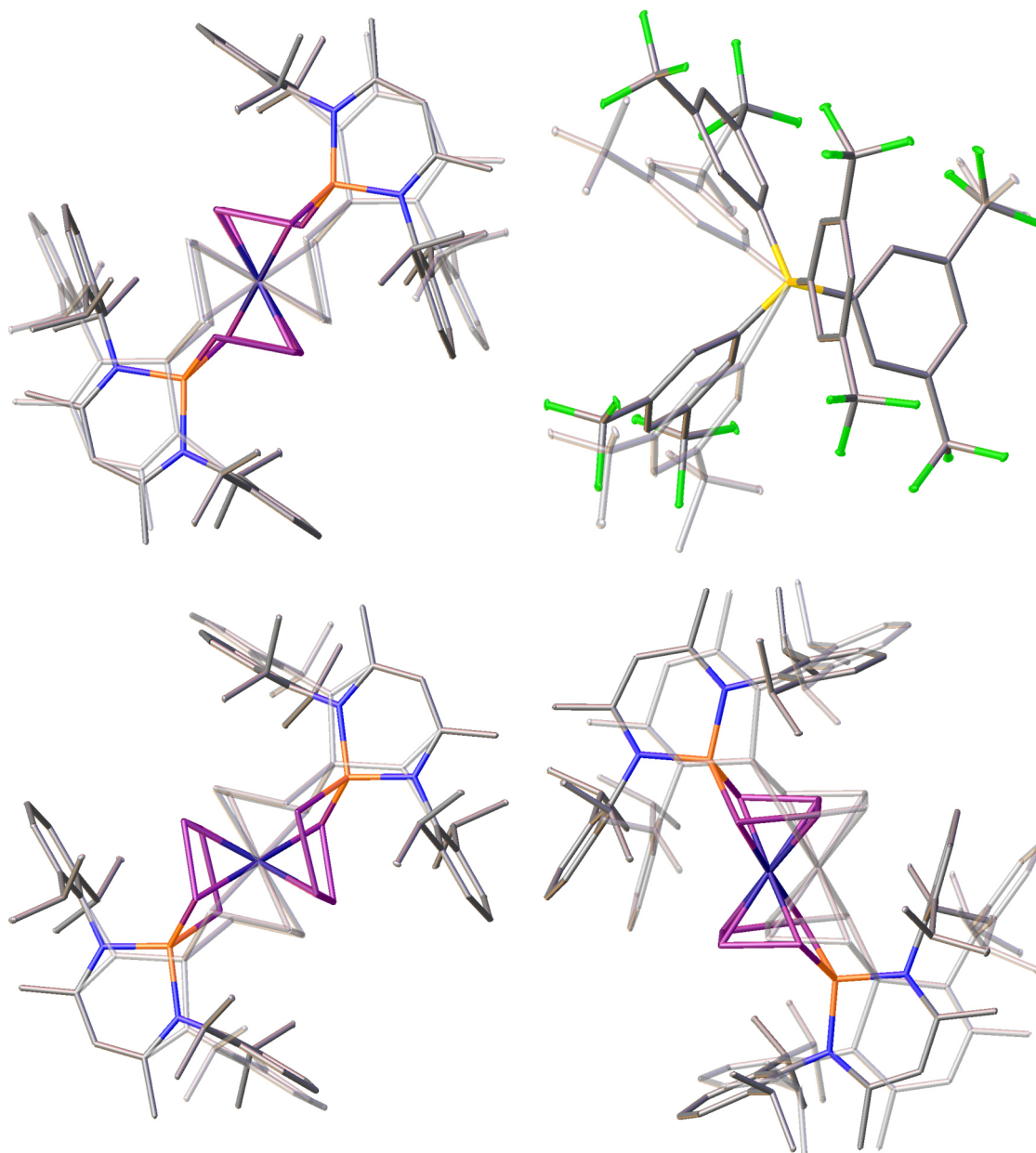
Figure S38. Wire/Stick representation of extracts of the grown solid-state molecular structure of **5**. Hydrogen atoms are omitted for clarity. Transparent parts depict disorders (PART 2).

Several crystallization efforts only afforded weakly diffracting crystals. All tested crystals showed disorder in the phosphorus framework and in the counterion. **5** crystallizes in the triclinic space group P-1 with two cations and one and two half anions in the asymmetric unit. Disorder of the phosphorus framework was treated with the SIMU restraint. The [Si(nacnac′)] backbone was additionally split into two parts and rather strong restraints were applied (SIMU, SADI) to

maintain a chemically reasonable connectivity to the *catena*-P_4 moiety. Additionally, one of the $[B(Ar^F)_4]$ counter ions was disordered and was split into two parts and the ADPs were restrained with a SIMU. The modeled disorder is presented in Figure S38. Due to the heavy disorder of the solid-state molecular structure of **5** structural parameters must be considered carefully, especially within the phosphorus framework.

5.6.5 Refinement of the solid-state molecular structure of $[Me_4N]_2[(\eta^3\text{-}P_3)Co(\mu\text{-}\eta^4{:}\eta^2\text{-}P_4)Si(nacnac')]$ (6)

$[Me_4N]_2[(\eta^3\text{-}P_3)Co(\mu\text{-}\eta^4{:}\eta^2\text{-}P_4)Si(nacnac')]$ (**6**) crystallizes in the monoclinic space group $P2_1/c$ with one anion and two cations in the asymmetric unit. One of the $[Me_4N]^+$ cations shows a weak disorder which was treated with a split model and restraints (SIMU). Residual electron density (1.33) is located around the anion which could not be refined to a chemically sensible solution.

5.6.6 Refinement of the solid-state molecular structure of $[Me_4N][(nacnac)SiF_4]$ (7)

$[Me_4N][(nacnac)SiF_4]$ (**7**) crystallizes in the monoclinic space group $C2/c$ with one cation and one anion in the asymmetric unit. The $[Me_4N]^+$ cation shows a weak disorder which was treated with a split model. No restraints or constraints were applied.

Table S3. *Crystallographic data for compounds **1-dme**, **2**, **3**, and **4**.*

Compound	1-dme	2	3	4
Empirical formula	$C_{140}H_{220}Co_2K_2N_8O_{12}P_{16}Si_4$	$C_{79}H_{123}FeK_{0.153}Li_{1.847}N_4O_9P_8Si_2$	$C_{65}H_{112}Li_2N_2O_{18}P_8Si$	$C_{61}H_{53}BN_2F_{24}SiP_4$
Formula weight	3011.17	1666.03	1498.28	1432.83
Temperature [K]	123.01(10)	123.00(10)	123.01(10)	123.01(10)
Crystal system	triclinic	triclinic	triclinic	triclinic
Space group	P-1	P-1	P-1	P-1
a [Å]	15.1112(6)	12.3548(2)	13.2002(3)	12.6367(3)
b [Å]	15.9506(6)	16.1038(3)	14.1944(3)	16.0923(4)
c [Å]	20.0778(8)	23.8944(4)	22.3759(4)	18.4919(5)
α [°]	90.376(3)	97.716(2)	86.812(2)	64.773(2)
β [°]	110.837(4)	96.0260(10)	88.468(2)	71.615(2)
γ [°]	115.288(4)	111.088(2)	69.391(2)	80.884(2)
Volume [Å³]	4016.9(3)	4334.64(14)	3918.06(15)	3226.86(15)
Z	2	2	2	2
ρ_{calc} [g/cm³]	1.245	1.276	1.270	1.475
μ [mm⁻¹]	4.315	3.705	2.336	2.253
F(000)	1600.0	1773.0	1598.0	1456.0
Crystal size [mm³]	0.411 × 0.342 × 0.2	0.149 × 0.1 × 0.092	0.494 × 0.154 × 0.107	0.515 × 0.243 × 0.14
Radiation	Cu Kα (λ = 1.54184)	Cu Kα (λ = 1.54184)	Cu Kα (λ = 1.54184)	Cu Kα (λ = 1.54184)
2Θ range for data collection [°]	6.772 to 152.716	6.462 to 148.026	7.154 to 151.98	7.374 to 148.416
Index ranges	-15 ≤ h ≤ 18, -20 ≤ k ≤ 19, -24 ≤ l ≤ 25	-12 ≤ h ≤ 15, -19 ≤ k ≤ 20, -29 ≤ l ≤ 29	-16 ≤ h ≤ 16, -14 ≤ k ≤ 17, -28 ≤ l ≤ 27	-15 ≤ h ≤ 12, -19 ≤ k ≤ 19, -23 ≤ l ≤ 22
Reflections collected	33164	67403	28755	26471
Independent reflections	16364 [R_{int} = 0.0485, R_{sigma} = 0.0496]	17274 [R_{int} = 0.0301, R_{sigma} = 0.0238]	15603 [R_{int} = 0.0159, R_{sigma} = 0.0215]	12782 [R_{int} = 0.0142, R_{sigma} = 0.0159]
Data / restraints / parameters	16364/1490/1368	17274/222/1067	15603/0/874	12782/36/876
Goodness-of-fit on F²	1.028	0.857	1.034	1.021
Final R indexes [I>=2σ (I)]	R1 = 0.0847, wR2 = 0.2395	R1 = 0.0396, wR2 = 0.0996	R1 = 0.0428, wR2 = 0.1176	R1 = 0.0332, wR2 = 0.0840
Final R indexes [all data]	R1 = 0.0949, wR2 = 0.2535	R1 = 0.0433, wR2 = 0.1025	R1 = 0.0454, wR2 = 0.1199	R1 = 0.0349, wR2 = 0.0854
Largest diff. peak/hole [e Å⁻³]	0.84/-0.63	0.75/-0.4	0.81/-0.73	0.65/-0.45

Table S4. *Crystallographic data for compounds **5**, **6**, and **7**.*

Compound	**5**	**6**	**7**
Empirical formula	$C_{180}H_{188}B_2Co_2F_{48}N_8P_{16}Si_4$	$C_{45}H_{84}CoN_4O_4P_7Si$	$C_{33}H_{53}F_4N_3Si$
Formula weight	4122.73	1048.97	595.87
Temperature [K]	123.00(10)	100.01(10)	100.00(10)
Crystal system	triclinic	monoclinic	monoclinic
Space group	P-1	P21/c	C2/c
a [Å]	20.9843(4)	18.8574(2)	31.2868(7)
b [Å]	22.1475(4)	17.9151(2)	12.9849(3)
c [Å]	23.1120(4)	16.5178(2)	16.5639(4)
α [°]	90.379(2)	90	90
β [°]	104.781(2)	93.9700(10)	96.470(2)
γ [°]	109.328(2)	90	90
Volume [Å³]	9751.6(3)	5566.85(11)	6686.3(3)
Z	2	4	8
ρ_{calc} [g/cm³]	1.404	1.252	1.184
μ [mm⁻¹]	2.712	4.853	1.015
F(000)	4232.0	2240.0	2576.0
Crystal size [mm³]	0.391 × 0.116 × 0.102	0.321 × 0.236 × 0.137	0.26 × 0.07 × 0.05
Radiation	Cu Kβ (λ = 1.39222)	Cu Kα (λ = 1.54184)	Cu Kα (λ = 1.54184)
2Θ range for data collection [°]	4.188 to 131.856	4.698 to 143.118	5.686 to 145.67
Index ranges	-27 ≤ h ≤ 27, -28 ≤ k ≤ 29, -30 ≤ l ≤ 30	-22 ≤ h ≤ 22, -21 ≤ k ≤ 20, -19 ≤ l ≤ 19	-36 ≤ h ≤ 37, -15 ≤ k ≤ 3, -20 ≤ l ≤ 19
Reflections collected	169023	52367	18219
Independent reflections	44588 [Rint = 0.0479, Rsigma = 0.0486]	10624 [R_{int} = 0.0461, R_{sigma} = 0.0304]	6088 [R_{int} = 0.0313, R_{sigma} = 0.0295]
Data / restraints / parameters	44588/3190/3669	10624/36/611	6088/0/415
Goodness-of-fit on F²	1.015	1.075	1.063
Final R indexes [I>=2σ (I)]	R1 = 0.0851, wR2 = 0.2323	R1 = 0.0746, wR2 = 0.2066	R1 = 0.0481, wR2 = 0.1289
Final R indexes [all data]	R1 = 0.1155, wR2 = 0.2603	R1 = 0.0812, wR2 = 0.2106	R1 = 0.0528, wR2 = 0.1321
Largest diff. peak/hole [e Å⁻³]	1.28/-0.52	1.33/-0.69	0.49/-0.28

5.7 **Theoretical investigations**

All calculations were performed with the ORCA program package[12] and were conducted in the gas phase. The RI[13] approximation was used for GGA calculations whereas the RIJCOSX[14] approximation was used for hybrid-DFT calculations. Geometry optimizations have been carried out at the PBE/def2-TZVP[15],[16],[17] level of theory and the nature of the stationary point was confirmed by frequency analysis.

5.7.1 **Calculation of the qualitative molecular orbital scheme**

The performed DFT calculations on **9** indicated that the D_{4d} symmetry is favored over the D_{4h} symmetry. Optimizing the geometry by starting with a D_{4h} symmetrized molecule ends in the D_{4d} symmetric geometry. However, a single point energy calculation at the PBE/def2-TZVP level of theory of the constrained D_{4h} symmetry reveals only a small barrier about 6 kcal·mol^{-1}.

The PBE functional was used to analyze the electronic structure of **9**. For the qualitative molecular orbital scheme, the canonical Kohn-Sham orbitals were evaluated (Figure S39). For the d orbital splitting only large contributions of >= 50% (Loewdin population analysis) were considered. Thus, a minor contribution of the 3dz^2 orbital was neglected in the qualitative molecular orbital scheme (Figure S40). Symmetry and characters presented in the MO scheme are derived from a character table for the point group D_{4d}.
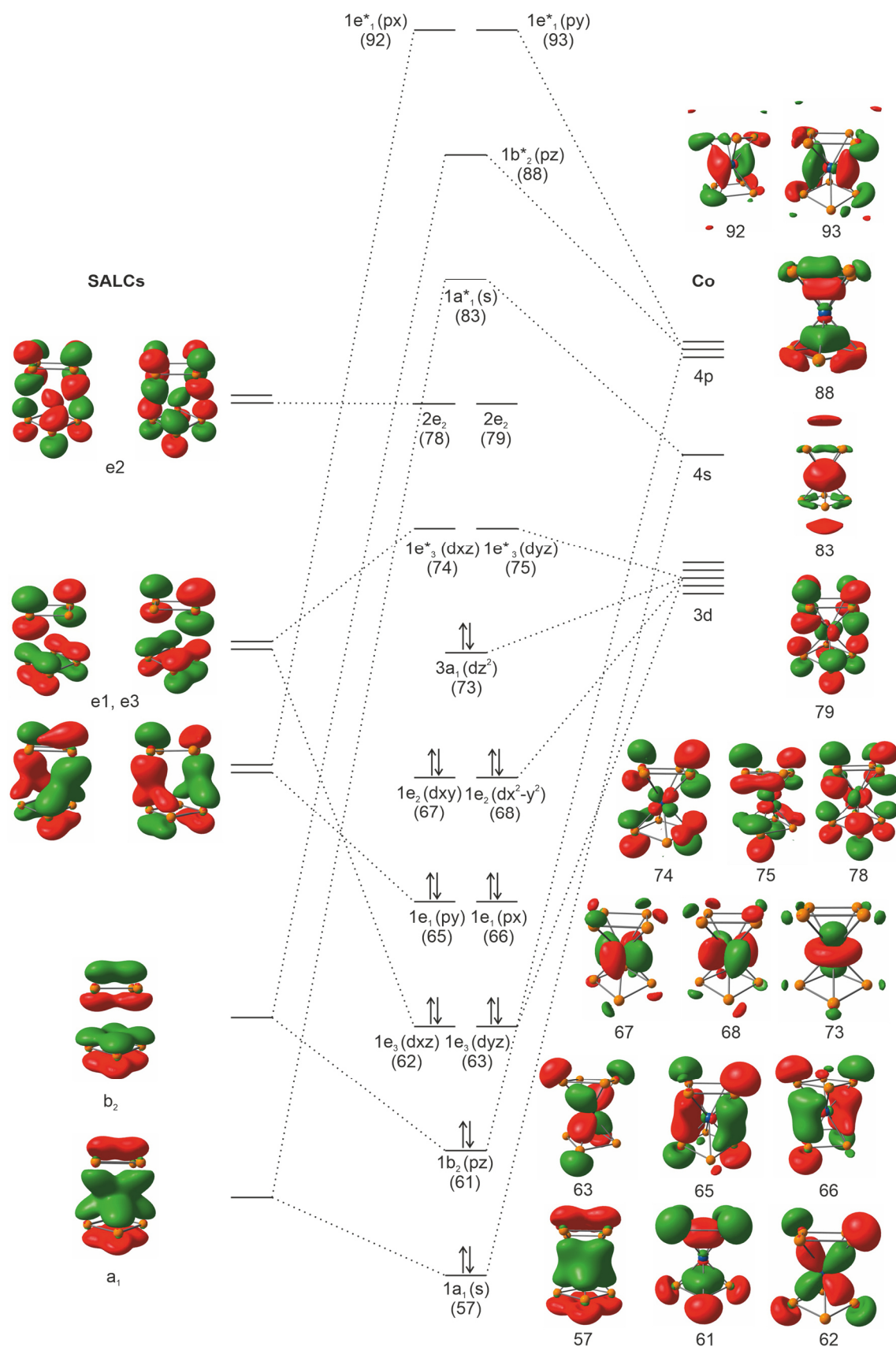
Figure S39. Qualitative molecular orbital scheme of **9** for a D$_{4d}$ symmetry and corresponding Kohn-Sham orbitals (surface isovalue = 0.05).

58   89

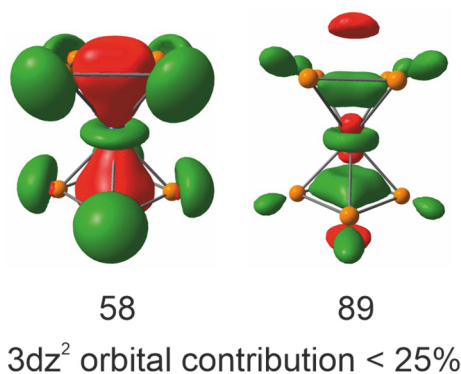3dz^2 orbital contribution < 25%

Figure S40. Selected Kohn-Sham orbitals of **9** showing a weak d orbital interaction of the z^2 level of the Co atom with the lone pairs of the ligand. Orbital contribution derived by Loewdin population analysis; surface isovalue = 0.05.

5.7.2   TDDFT Calculations on anion 9

To get further insight into the absorption spectra of **9** TDDFT (time-dependent density functional theory) calculations were carried out at the ωB97X-D3/def2-TZVP level of theory. A conductor-like polarizable continuum model (CPCM) for acetonitrile was used for the calculation of the UV/Vis spectra. The overall shapes of the theoretical spectra are in agreement with the experiment. This allowed identifying the nature of the transitions by analyzing the difference densities.

Table S5. Comparison of the most significant calculated singlet transitions of **9**.

state	9		
	λ [nm]	f$_{osc.}$	character
3	434.1	0.0027	d−d
4	434.1	0.0027	d−d
20	302.0	0.00747	LTMCT
21	302.0	0.00747	LTMCT
24	280.4	0.0804	d−d
38	246.7	0.0032	d−d
39	246.6	0.0032	d−d
51	235.0	0.0169	MTLCT
52	235.0	0.0169	MTLCT
53	233.7	0.4171	d−d
58	224.8	0.0668	MTLCT
59	224.8	0.0669	MTLCT

Table S6. Selected difference densities of singlet transitions; Surface isovalue: 0.003; transitions proceed form red to green.

3

4

20

21

24

38

39

51

52

53

58

59
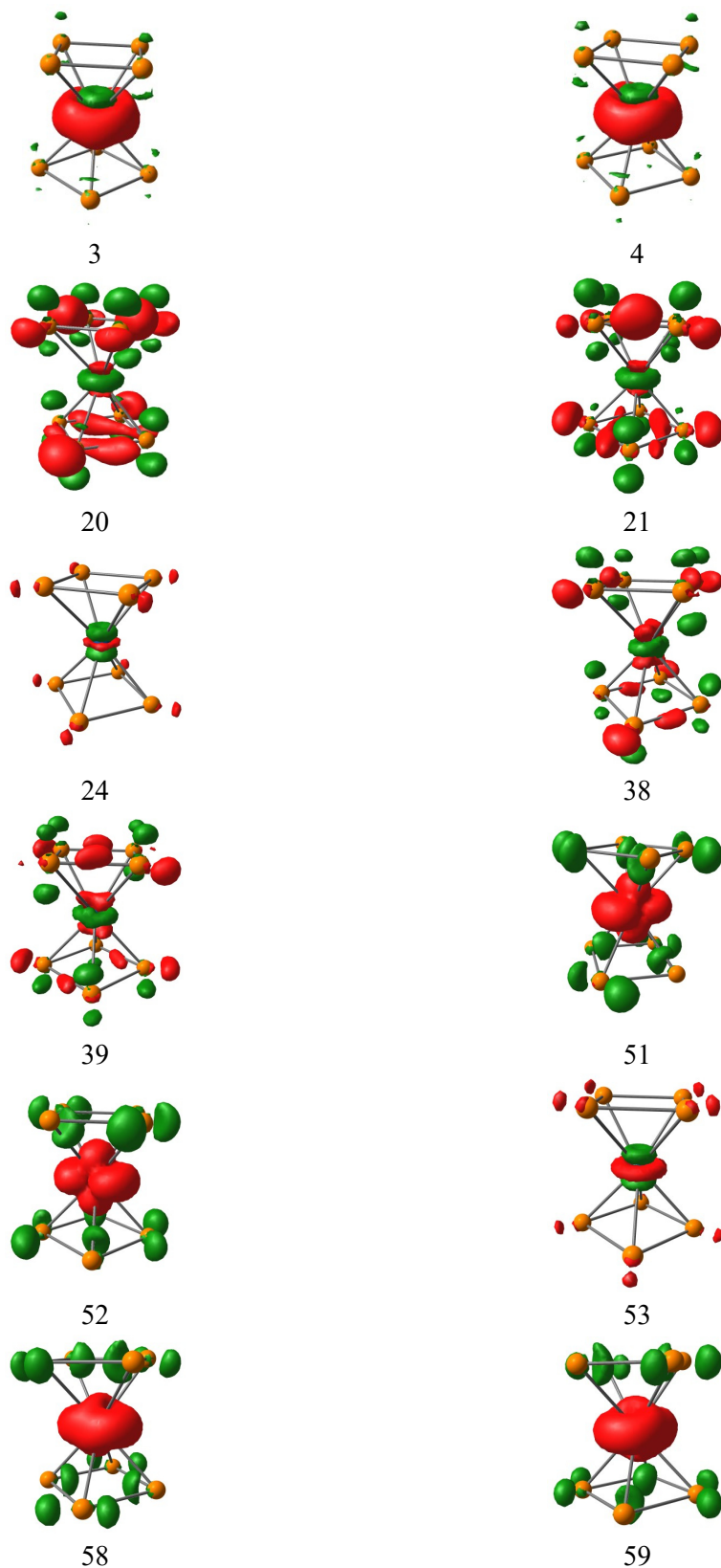
5.7.3   Calculation of the NICS values

Density functional theory (DFT) studies at the TPSS/pcSseg-2[18],[19] level of theory gave further insight into the nature of the *cyclo*-P_4 unit in anion **9**. The nucleus independent chemical shift (NICS) was calculated to study the aromaticity of the *cyclo*-P_4 ligand.[20] The chemical shielding constants were calculated using the GIAO approach as implemented in ORCA. Comparing the NICS(0) values of benzene (−8.3) and the free P_4^{2-} (6.0), the NICS(0) value for complex **9** (−6.4) suggests an aromatic character of the *cyclo*-P_4 ligands.

Cartesian coordinates of the optimized gas phase geometry of the complex **9** (PBE/def2-TZVP, S= 0, D$_{4d}$ symmetry)

Co 0.00000000762576   -0.00000000350190 -0.00000000151481
P   0.59397994112194   1.43400058759910   1.69615640221606
P -1.43400058238968   0.59397994022568   1.69615639905160
P   1.43400057524675   -0.59397994287164   1.69615642832522
P   0.59397994610561   -1.43400058373629 -1.69615641610502
P -0.59397994132802   1.43400058647060 -1.69615639085719
P -0.59397994373922   -1.43400058589359   1.69615640929915
P -1.43400058664449   -0.59397994142223 -1.69615640023244
P   1.43400058400135   0.59397994313027 -1.69615643018256

5.8 References of Supporting Information

[1] (a) K. Jonas, R. Mynott, C. Krüger, J. C. Sekutowski and Y.-H. Tsay, *Angew. Chem. Int. Ed. Engl.*, **1976**, *15*, 767; *Angew. Chem.*, **1976**, *88*, 808; (b) K. Jonas, US patent 4169845, **1979**.

[2] A. Fürstner, R. Martin, H. Krause, G. Seidl, R. Goddard, C. W. Lehmann, *J. Am.Chem. Soc.*, **2008**, *130*, 8773.

[3] (a) C. G. P. Ziegler, C. Taube, J. A. Kelly, G. Hierlmeier, M. Uttendorfer, J. J. Weigand, R. Wolf, *Chem. Commun.* **2020**, *56*, 14071; (b) M. Driess, S. Yao, M. Brym, C. van Wüllen and D. Lentz, *J. Am. Chem. Soc.*, **2006**, *128*, 9628.

[4] M. Brookhart, B. Grant, A. F. Volpe, Jr., *Organometallics*, **1992**, *11*, 3920.

[5] P. H. M. Budzelaar, *gNMR for Windows (5.0.6.0), NMR Simulation Program* **2006**.

[6] (a) SCALE3ABS, CrysAlisPro, Aglient Technologies Inc. Oxford, GB, **2015**; (b) G. M. Sheldrick, SADABS, Bruker AXS, Madison, USA, **2007**.

[7] R. C. Clark, J. S. Reid, *Acta Crystallogr. A*, **1995**, *51*, 887.

[8] O. V. Dolomanov, L. J. Bourhis, R. J. Gildea, J. A. K. Howard, H. Puschmann, *J. Appl. Cryst.*, **2009**, *42*, 339.

[9] G. M. Sheldrick, *Acta Cryst.*, **2015**, *A17*, 3.

[10] G. M. Sheldrick, *Acta Cryst.*, **2015**, *C71*, 3.

[11] (a) B. Cordero, V. Gómez, A. E. Platero-Prats, M. Revés, J. Echeverría, E. Cremades, F. Barragán, S. Alvarez, *Dalton Trans.* **2008**, 2832; (b) S. Alvarez, *Dalton Trans.* **2013**, *42*, 8617.

[12] F. Neese, *Wiley Interdiscip. Rev. Comput. Mol. Sci.*, **2012**, *2*, 73.

[13] F. Weigend, *Phys. Chem. Chem. Phys.*, **2002**, *4*, 4285.

[14] F. Neese, F. Wennmohs, A. Hansen, U. Becker, *Chem. Phys.*, **2009**, *356*, 98.

[15] Perdew, Burke and Ernzerhof, *Phys. Rev. Lett.*, **1996**, *77*, 3865.

[16] F. Weigend, R. Ahlrichs, *Phys. Chem. Chem. Phys.*, **2005**, *7*, 3297.

[17] F. Weigend, *Phys. Chem. Chem. Phys.*, **2006**, *8*, 1057.

[18] J. Tao, J. P. Perdew, V. N. Staroverov and G. E. Scuseria, *Phys. Rev. Lett.*, **2003**, *91*, 146401.

[19] F. Jensen, *J. Chem. Theory Comput.*, **2015**, *11*, 132.

[20] P. von Ragué Schleyer, C. Maerker, A. Dransfeld, H. Jiao, N. J. R. van Eikema Hommes, *J. Am. Chem. Soc.* **1996**, *118*, 6317.

Chapter 6 Summary and Conclusion

6.1   Heterobimetallic activation and functionalization of white phosphorus

This introductory chapter reviews and explains the concept of heterobimetallic activation and functionalization of white phosphorus (P_4). The chapter is categorized into subunits giving an overview of the current state of the research field. After a brief introduction concerning the relevance of phosphorus chemistry, this chapter first gives a detailed description and definition of the concept. Heterobimetallic P_4 activation and functionalization is subdivided into variations, which are based on the use of two d-block elements, a d-block element, and a f-block element, and the combination of d-block and p-block elements. The results obtained with these approaches are described. It is concluded that the concept of heterobimetallic P_4 activation still needs to be further developed in particular with respect to subsequent functionalization of the presented heterometallic polyphosphorus complexes.

6.2   Construction of alkyl-substituted pentaphosphido ligands in the coordination sphere of cobalt[1]

This chapter describes a new strategy for the synthesis of polyphosphido complexes, which uses heterobimetallic complexes derived from P_4 as a tool for the construction of more extended P_n units. The heterobimetallic tetraphosphido complexes $[K(dme)_2\{(BIAN)Co(\mu-\eta^4{:}\eta^2{-}P_4)Ga(nacnac)\}]$ (**2-2**, BIAN = 1,2-bis(2,4,6-trimethylphenylimino)acenaphthene (^{Mes}BIAN); **2-2′**, BIAN = 1,2-bis(2,6-diisopropyl-phenylimino)acenaphthene (^{Dipp}BIAN); nacnac = CH[CMeN(2,6-iPr$_2$C$_6$H$_3$)]$_2$) were synthesised by the reaction of $[K(Et_2O)\{(BIAN)Co(\eta^4{-}1{,}5{-}cod)\}]$ (**2-1**, BIAN = ^{Mes}BIAN; **2-1′**, BIAN = ^{Dipp}BIAN) with $[(nacnac)Ga(\eta^2{-}P_4)]$. Single-crystal X-ray diffraction (XRD) revealed that these complexes show similar molecular structures. Moreover, reactivity studies of **2-2** with phosphorus electrophiles such as dialkylchlorophosphanes were performed. The stoichiometric reaction of **2-2** with R_2PCl (R = iPr, tBu, and Cy) led to the formation of rare organo-substituted pentaphosphido complexes $[(^{Mes}BIAN)Co(\eta^4{-}P_5R_2)]$ (**2-3a**, R = iPr; **2-3b**, R = tBu; **2-3c**, R = Cy) which were isolated in moderate yields (26 to 31%). XRD studies reveal an η^4-coordinated *cyclo*-P_5R_2 ligand in an envelope conformation. $^{31}P\{^1H\}$ NMR monitoring of the reaction of **2-2** with iPr$_2$PCl led to the observation of two intermediary species. One of them could be identified by a single-crystal XRD analysis as $[(^{Mes}BIAN)Co(\mu-\eta^4{:}\eta^2{-}P_5iPr_2)Ga(nacnac)]$ (**2-4**). Intermediate **2-4** shows an almost planar P_5 chain which coordinates to cobalt *via* four unsubstituted P atoms and to the [Ga(nacnac)] moiety *via* the 1,4-positions of the P_5 chain.

Furthermore, a related, monosubstituted organopentaphosphido cobalt complex $[(^{Mes}BIAN)Co(\mu-\eta^4{:}\eta^1{-}P_5tBu)GaCl(nacnac)]$ (**2-5**) was isolated by reacting dichloroalkylphosphane tBuPCl$_2$ with **2-2**, albeit in a low yield of 6%. The molecular structure of **2-5** was determined by XRD analysis and features an $\eta^4{:}\eta^1$-coordinated *cyclo*-P_5tBu ligand similar to the dialkyl-substituted ligands in

2-3a-c. This chapter provides proof of principle that heterobimetallic complexes such as **2-2** may enable the targeted construction of a range of new metal-coordinated polyphosphorus frameworks by P–P condensation.
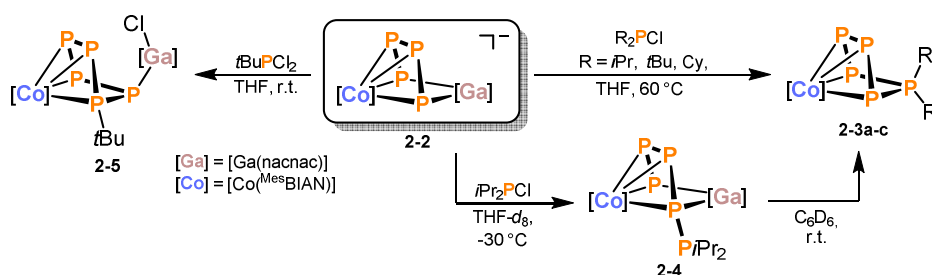

Figure 1. Functionalization of the heterobimetallic tetraphosphido complex **2-2** with chlorophosphanes.

6.3 Iron-gallium and cobalt-gallium tetraphosphido complexes[2]

This chapter describes the synthesis and characterization of two heterobimetallic complexes featuring a strongly reduced P_4 unit as well as a labile anthracene ligand.

Complexes $[K(18\text{-crown-6})\{(\eta^4\text{-}C_{14}H_{10})Fe(\mu\text{-}\eta^4\text{:}\eta^2\text{-}P_4)Ga(nacnac)\}]$ (**3-1**, $C_{14}H_{10}$ = anthracene) and $[K(dme)_2\{(\eta^4\text{-}C_{14}H_{10})Co(\mu\text{-}\eta^4\text{:}\eta^2\text{-}P_4)Ga(nacnac)\}]$ (**3-2**) were synthesised by an oxidative P–P addition of $[(nacnac)Ga(\eta^2\text{-}P_4)]$ (nacnac = $CH[CMeN(2,6\text{-}iPr_2C_6H_3)]_2$) with the low-valent metallates bis(anthracene)ferrate(1–) and -cobaltate(1–). A single-crystal X-ray diffraction experiment reveals that both complexes **3-1** and **3-2** consist of an $\eta^4\text{:}\eta^2$-bridging P_4 chain between the transition metal atom and the gallium atom. While all attempts to isolate the extremely air and moisture sensitive complex **3-1** as a pure compound were unsuccessful its cobalt analogue **3-2** was isolated in 22% crystalline yield. Multinuclear NMR spectroscopic investigations on **3-2** suggest that the molecular structure observed in the solid-state is preserved in solution. The heterodinuclear complexes reported in this chapter might be a suitable starting point for further derivatizations especially by the targeted substitution of the labile anthracene ligand.
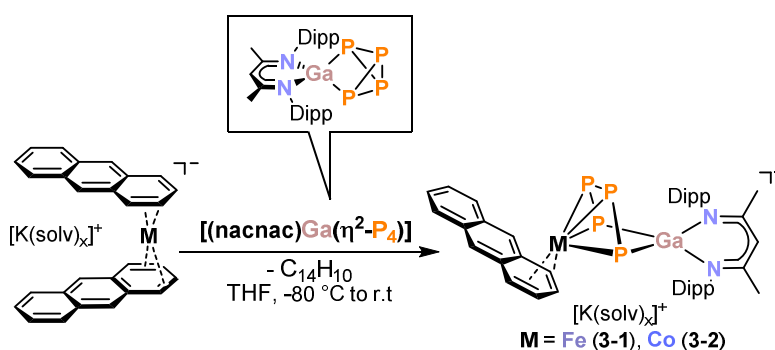

Figure 2. Synthesis of iron-gallium and cobalt-gallium tetraphosphido complexes **3-1** and **3-2**.

6.4   An unusual $Ni_2Si_2P_8$ cluster formed by complexation and thermolysis[3]

This chapter describes the synthesis of well-defined 1:1 and 2:1 complexes of $[LSi(\eta^2\text{-}P_4)]$ (L = $CH[C(Me)N(Dipp)][C(CH_2)N(2,6\text{-}iPr_2C_6H_3)])$ with N-heterocyclic carbene nickel fragments. In addition, the unusual $Ni_2Si_2P_8$ cluster was isolated and characterized.

The reaction of the nickel(0) equivalent $[(NHC)Ni(\eta^2\text{-vtms})_2]$ (NHC = IDipp, IMes; vtms = $Me_3SiCH=CH_2$) with the P_4-activation product $[LSi(\eta^2\text{-}P_4)]$ yielded different coordination compounds, depending on the stoichiometry used. The complexes $[(NHC)Ni\{(\mu\text{-}\eta^{2:2}\text{-}P_4)Si(L)\}_2]$ (**4-1a**, NHC = 1,3-bis(2,6-diisopropylphenyl)imidazolin-2-ylidene (IDipp); **4-1b**, NHC = 1,3-bis(2,4,6-trimethylphenyl)imidazolin-2-ylidene (IMes)) were obtained after reaction of the Ni^0 precursor with two equivalents of $[LSi(\eta^2\text{-}P_4)]$. In case of the sterically more encumbered IDipp substituent, the analogue reaction in 1:1 ratio afforded the heterodinuclear compound $[(IDipp)Ni(\mu\text{-}\eta^{2:2}\text{-}P_4)Si(L)]$ (**4-2**). In solution, compound **4-2** decomposes slowly, dimerizing to the unusual $Ni_2Si_2P_8$ cluster $[(IDipp)Ni_2P_8\{Si(L)\}_2]$ (**4-3**). The unusual structure of the cluster was determined by single-crystal X-ray diffraction and shows strongly varying P−P bond distances. Quantum chemical calculations gave insight into the electronic structure of **4-3** and suggest the presence of two formal nickel(0) centers. Derivatization reactions of the cluster core **4-3** through the substitution of the diketiminate ligands L may further enhance the diversity of this class of cluster molecules. An extension of the synthetic methodology reported here and the use of **4-3** and related clusters as single source precursors for phosphorus-based materials will be of significant future interest.
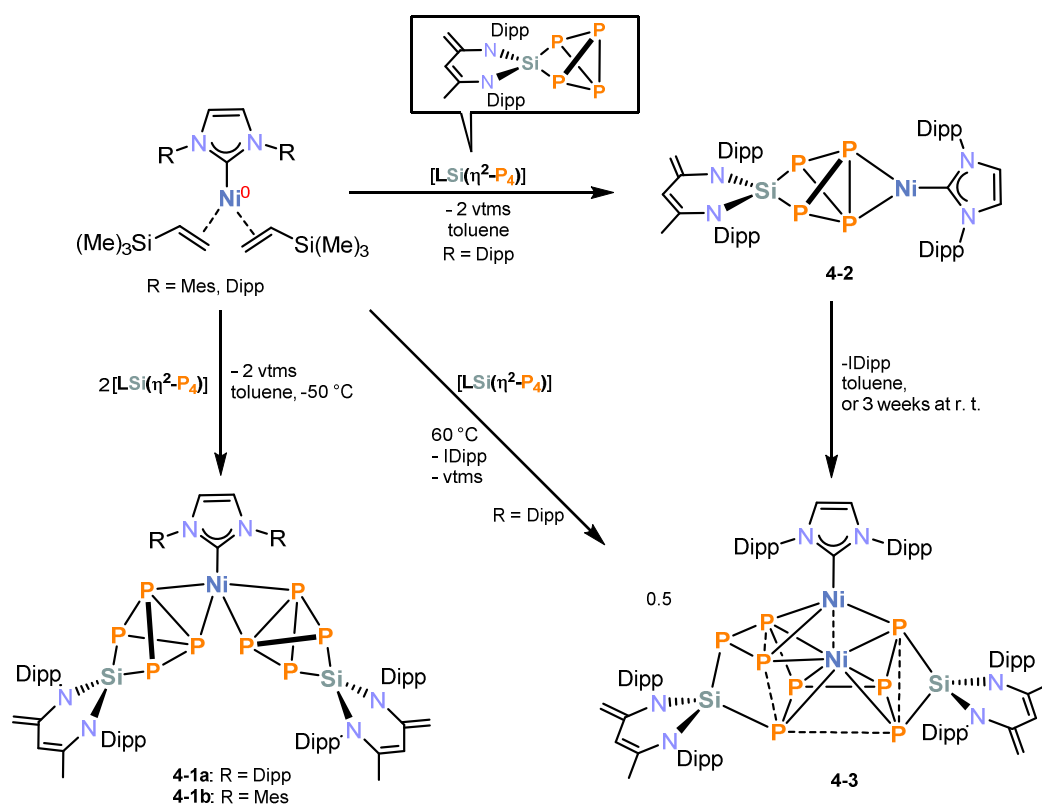

Figure 3. Synthesis of Ni^0 complexes with bridging butterfly-P_4 ligands, and thermolysis to yield an unusual $Ni_2Si_2P_8$ cluster.

6.5 Coordination Studies of a silabicyclotetraphosphane towards the "carbon-free" sandwich complex $[Co(\eta^4\text{-}P_4)_2]^-$

Combining the expertise gained from the previous chapters, this final chapter especially focuses on on the potential of the heterobimetallic P_4 activation approach for the synthesis of novel phosphorus compounds. The chapter reports the synthesis of novel sandwich complexes $[K(thf)][Co\{(\mu\text{-}\eta^4{:}\eta^2\text{-}P_4)Si(nacnac')\}_2]$ (**5-1**) and $[Li(diox)_2]_2[Fe\{(\mu\text{-}\eta^4{:}\eta^2\text{-}P_4)Si(nacnac')\}_2]$ (**5-2**) by reaction of the P_4 activation product $[(nacnac')Si(\eta^2\text{-}P_4)]$ (nacnac' = $CH[C(Me)N(Dipp)][C(CH_2)N(2,6\text{-}iPr_2C_6H_3)$ with metallates $[K(thf)_{0.2}][Co(\eta^4\text{-}1,5\text{-}cod)_2]$ and $[Li(dme)]_2[Fe(\eta^4\text{-}1,5\text{-}cod)_2]$ (1,5-cod = 1,5-cyclooctadiene). While the formation of **5-1** proceeds selectively, the formation of several by-products in the reaction with the Fe complex demonstrates the challenges that may be associated with the heterobimetallic P_4 activation approach. Nevertheless, complex **5-2** as well as one by-product $[Li(diox)_3]_2[P_8\{Si(nacnac')\}]$ (**5-3**) could be structurally characterized by single-crystal X-ray diffraction (XRD) analysis. The solid-state molecular structure of **5-3** shows an unusual dianionic nortricyclic P_7 core with a single P atom bound *exo* to the P_7 cage.

Reactivity studies of **5-1** revealed the apparent Brønsted basic character of the $[Si(nacnac')]$ ligand, which had previously been demonstrated for the starting material $[(nacnac')Si(\eta^2\text{-}P_4)]$. While protonation of **5-1** with Brookhart's acid affords the salt $[(nacnac)Si(\eta^2\text{-}P_4)][B(Ar^F)_4]$ (**5-4**, nacnac = $CH[CMeN(2,6\text{-}iPr_2C_6H_3)]_2$), the metal complex $[Co\{(\mu\text{-}\eta^4{:}\eta^2\text{-}P_4)Si(nacnac)\}_2][B(Ar^F)_4]$ (**5-5**) can be synthesized in an analogous manner.

Targeting the elimination of the $[Si(nacnac')]$ ligand, the reaction of **5-1** with five equivalents of the fluoride source $[Me_4N]F$ was pursued. An unexpected fragmentation of one of the silatetraphosphacyclopentadiene ligands was observed to afford the *cyclo*-P_3 complex $[Me_4N]_2[(\eta^3\text{-}P_3)Co(\mu\text{-}\eta^4{:}\eta^2\text{-}P_4)Si(nacnac')]$ (**5-6**), which co-crystallizes with $[Me_4N][(nacnac)SiF_4]$ (**5-7**).

In order to circumvent the fragmentation of the polyphosphido ligand, the investigations were extended to include a variety of alcohols and carboxylic acids. According to heteronuclear NMR spectroscopic studies, such reactions afford the new *cyclo*-P_4 complex $[(\eta^4\text{-}P_4)Co(\mu\text{-}\eta^4{:}\eta^2\text{-}P_4)Si(nacnac)]$ (**5-8**) as major product. Complex **5-8** can be isolated as a brown powder in a good yield of 60%. This allowed further reactivity studies, which especially focused on the elimination of the $[Si(nacnac)]$ ligand. ^1H and ^{31}P NMR spectra and ESI-MS suggest that the reaction of **5-8** with potassium phenoxide in the presence of 18-crown-6 affords $[K(18\text{-}crown\text{-}6)][Co(\eta^4\text{-}P_4)_2]$ (**5-9**), which features two 'naked' cyclo-P_4 ligands. This complex is the second example of an entirely "carbon-free" transition metal sandwich compound. Further investigations are necessary to determine the solid-state molecular structure of **5-9**. Nevertheless, the synthesis of **5-9** illustrates the outstanding potential of the heterobimetallic P_4 activation and functionalization approach for the synthesis of highly unusual polycyclophosporus compounds.

Figure 4. Synthesis and reactivity studies of the heterodinuclear tetraphosphido complex **5-1**. Synthetic route to the "carbon-free" sandwich complex [K(18-crown-6)][Co(η^4-P$_4$)$_2$] (**5-9**).

6.6   Conclusion

Although the coordination chemistry of P$_4$ is well studied, the use of two chemically distinct metal atoms for the activation and functionalization of P$_4$ is underexplored. The results of this thesis clearly illustrate the advantages of using two distinct metal or metalloid atoms to generate reactive polyphosphido complexes that can be used to generate unique polyphosphorus compounds. As illustrated in chapter 2 of this thesis, mono- and diorgano-substituted pentaphosphido ligands were obtained as a new class of ligands. Mechanistic investigations help to understand the pathway of their formation. Furthermore, an unusual Ni$_2$P$_8$Si$_2$ cluster was obtained under mild conditions. This complex might be suitable as a single source precursor for phosphorus-based materials. The synthetic potential of heterobimetallic activation and functionalization of white phosphorus is furthermore demonstrated by the synthesis of reactive heterodinuclear inorganic sandwich complexes, which were used for the targeted synthesis of a rare "carbon-free" sandwich complex [K(18-crown-6)][Co(η^4-P$_4$)$_2$] (**5-9**). The results of this thesis show that heterobimetallic P$_4$ activation and functionalization is a promising strategy for the synthesis of highly unusual phosphorus compounds, and it is hoped that the considerable potential of this approach will give rise to many further fascinating discoveries in the future.

6.7 References

[1] C. G. P. Ziegler, T. M. Maier, S. Pelties, C. Taube, F. Hennersdorf, A. W. Ehlers, J. J. Weigand, R. Wolf, *Chem. Sci.* **2019**, *110*, 4178.

[2] C. G. P. Ziegler, F. Hennersdorf, J. J. Weigand, R. Wolf, *Z. Anorg. Allg. Chem.* **2020**, *93*, 303.

[3] C. G. P. Ziegler, C. Taube, J. A. Kelly, G. Hierlmeier, M. Uttendorfer, J. J. Weigand, R. Wolf, *Chem. Commun.* **2020**, *56*, 14071.

Chapter 7   Acknowledgement

Eidesstattliche Erklärung

Ich erkläre hiermit an Eides statt, dass ich die vorliegende Arbeit ohne unzulässige Hilfe Dritter und ohne Benutzung anderer als der angegebenen Hilfsmittel angefertigt habe; die aus anderen Quellen direkt oder indirekt übernommenen Daten und Konzepte sind unter Angabe des Literaturzitats gekennzeichnet. Die Arbeit wurde bisher weder im In-noch im Ausland in gleicher oder ähnlicher Form einer anderen Prüfungsbehörde vorgelegt.

_____

Christoph Ziegler